

General Disclaimer

One or more of the Following Statements may affect this Document

- This document has been reproduced from the best copy furnished by the organizational source. It is being released in the interest of making available as much information as possible.
- This document may contain data, which exceeds the sheet parameters. It was furnished in this condition by the organizational source and is the best copy available.
- This document may contain tone-on-tone or color graphs, charts and/or pictures, which have been reproduced in black and white.
- This document is paginated as submitted by the original source.
- Portions of this document are not fully legible due to the historical nature of some of the material. However, it is the best reproduction available from the original submission.

BOEING DOCUMENT
NO. D5-17142

SPACE TUG AEROBRAKING STUDY

VOLUME II OF II TECHNICAL VOLUME

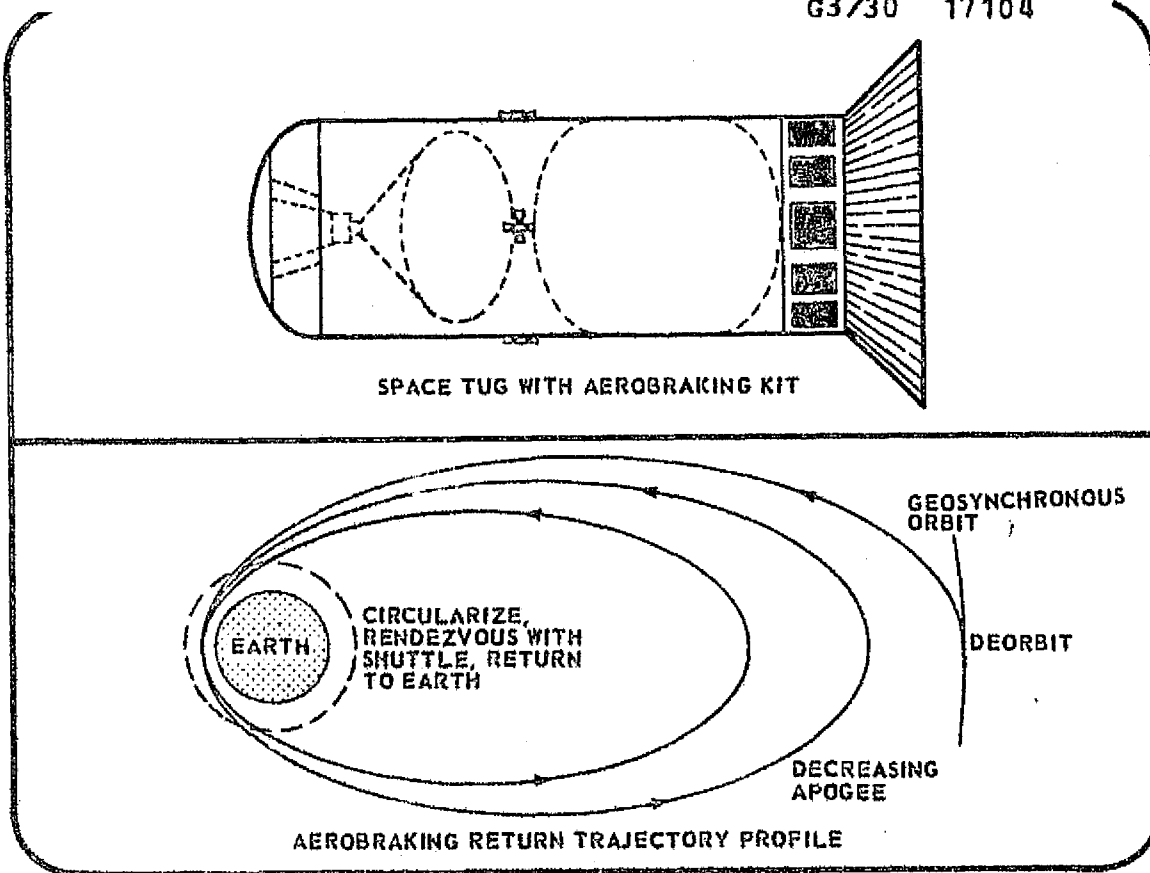
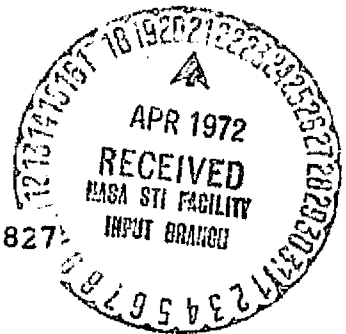
(NASA-CR-124057) SPACE TUG AEROBRAKING
STUDY. VOLUME 2: TECHNICAL Final
Report (Boeing Co., Huntsville, Ala.)
519 p HC \$28.00

CSSL 22A

G3/30

Unclas
17104

N73-18827



PREPARED UNDER
CONTRACT NASO-27501

BY THE **BOEING** COMPANY
HUNTSVILLE, ALABAMA

D5-17142

FINAL REPORT

SPACE TUG AEROBRAKING STUDY

VOLUME II OF II
TECHNICAL VOLUME

PREPARED BY: Charles J. Corso
C. J. CORSO

APPROVED BY: J. W. Allen
J. W. ALLEN

Ch Eyer
C. L. EYER

Joseph W. Monroe
JOSEPH W. MONROE

PREPARED UNDER CONTRACT NAS8-27501
FOR
NATIONAL AERONAUTICS AND SPACE ADMINISTRATION
GEORGE C. MARSHALL SPACE FLIGHT CENTER
MARSHALL SPACE FLIGHT CENTER, ALABAMA 35812

APRIL 12, 1972

D5-17142

THE BOEING COMPANY
SATURN/APOLLO/SKYLAB DIVISION
HUNTSVILLE, ALABAMA

PRECEDING PAGE BLANK NOT FILMED

D5-17142

REVISIONS			
REV. SYM.	DESCRIPTION	DATE	APPROVED

ABSTRACT

The feasibility and practicality of employing an aerobraking trajectory for return of the reusable Space Tug from geosynchronous and other high energy missions was investigated. The aerobraking return trajectory modes from high orbits employ transfer ellipses which have low perigee altitudes wherein the earth's sensible atmosphere provides drag to reduce the Tug descent delta velocity requirements and thus decrease the required return trip propulsive energy. An aerobraked Space Tug, sized to the Space Shuttle payload capability and dimensional constraints, can accomplish 95 percent of the geosynchronous missions with a single Shuttle/Tug launch per mission. Orbital assembly and/or orbital propellant transfer operations are not required. The same size Space Tug using conventional trajectory modes cannot deliver any payload to the geosynchronous orbit.

Aerodynamics, aerothermodynamics, trajectory, guidance and control, configuration concepts, materials, weights and performance parameters were identified. Sensitivities to trajectory uncertainties, atmospheric anomalies and re-entry environments were determined. New technology requirements and future studies required to further enhance the aerobraking potential were identified.

KEY WORDS

Space Tug
Aerobraking
Return trajectories
Synchronous missions
Orbit-to-Orbit Shuttle (OOS)
Earth-to-Orbit Shuttle (EOS)

Space Tug Kits
Flare Concepts
Heat Shield Concepts
Propulsion modules
Astrionics modules
Aerodynamic drag

D5-17142

FOREWORD

This Technical Volume is one of two volumes presenting the results of a study to investigate the feasibility of an aerobraking trajectory mode for return of the reusable Space Tug from geosynchronous equatorial orbit. The Executive Summary Volume presents a brief outline of the objectives, summarizes the results and gives conclusions and recommendations of this study. This Technical Volume presents the detailed technical results.

The Boeing Company performed this study at the Boeing-Huntsville facility for the NASA Marshall Space Flight Center, Huntsville, Alabama. The NASA/MSFC Technical Monitor was Thomas W. Barrett, Advanced Systems Analysis Office, Vehicle Systems Group. Subcontractor to The Boeing Company for the navigation requirements impact on the astrionic module was the International Business Machine Corporation, Huntsville facility.

CONTENTS

PARAGRAPH		PAGE
	REVISIONS	ii
	ABSTRACT	iii
	FOREWORD	iv
	CONTENTS	v
	LIST OF FIGURES	x
	ABBREVIATIONS AND ACRONYMS	xx
	SECTION I - INTRODUCTION	1-1
1.0	GENERAL	1-1
1.1	STUDY OBJECTIVES AND APPROACH	1-2
1.2	BACKGROUND	1-9
	SECTION II - SUMMARY	
2.0	CONCLUSIONS AND RECOMMENDATIONS	2-1
2.1	SUMMARY OF TECHNICAL STUDY RESULTS	2-4
2.1.1	Aerodynamics Analysis	2-4
2.1.1.1	Aerodynamics Conclusions	2-8
2.1.2	Configurations	2-8
2.1.2.1	Configuration Conclusions	2-14
2.1.3	Trajectory Analysis	2-14
2.1.3.1	Trajectory Conclusions	2-16
2.1.4	Control Analysis	2-18
2.1.4.1	Control Conclusions	2-18
2.1.5	Thermal Analysis	2-21
2.1.5.1	Thermal Conclusions	2-24
2.1.6	Astrionics Analysis	2-24
2.1.6.1	Astrionics Conclusions	2-29
2.1.7	Materials	2-30
2.1.7.1	Materials Conclusions	2-30
2.1.8	Weights	2-31
2.1.8.1	Weights Conclusions	2-34
2.2	SUMMARY OF SENSITIVITY ANALYSIS RESULTS	2-38
2.2.1	Sensitivities of Payloads and Temperatures for Tug Configurations for Standard Atmosphere	2-38
2.2.2	Sensitivities of Payloads and Temperatures for Tug Configurations for Atmospheric Perturbations and Navigation Errors	2-41
2.2.3	Conventional/Aerobraking Tug Performance Comparison	2-43
2.2.4	Sensitivity Conclusions	2-46

CONTENTS (Continued)

PARAGRAPH		PAGE
	SECTION III - GROUND RULES, GUIDELINES AND ASSUMPTIONS	
3.0	GENERAL	3-1
3.1	OVERALL SPACE TUG	3-1
3.2	PROPULSION MODULE	3-2
3.3	ASTRIONICS MODULE	3-3
	SECTION IV - PERFORMANCE AND TRADE STUDIES	
4.0	GENERAL	4-1
4.1	AERODYNAMIC ANALYSIS	4-1
4.1.1	Basic Tug Aerodynamic Analysis	4-4
4.1.1.1	Drag Data	4-4
4.1.1.2	Static Stability Data	4-7
4.1.1.3	Nose Pressure Distribution	4-11
4.1.2	Flared Tug Configuration Analysis	4-14
4.1.2.1	Flow Field and Flare Sizing Analysis	4-14
4.1.2.2	Flare Selection Rationale	4-16
4.1.2.3	Flared Tug Drag Characteristics	4-25
4.1.2.4	Static Stability Analysis	4-26
4.1.2.5	Pressure Coefficient Distribution Data	4-31
4.2	AEROBRAKING CONFIGURATION CONCEPTS	4-38
4.2.1	Conventional Trajectory Space Tug Configuration	4-39
4.2.2	Aerobraking Kit Elements	4-41
4.2.2.1	Aft Heat Shield	4-43
4.2.2.2	Sidewall Thermal Protection System	4-55
4.2.2.3	Aerodynamic Flare	4-57
4.2.2.4	Payload Adapter	4-63
4.2.3	Configuration Design Options and Recommendations	4-65
4.3	TRAJECTORY ANALYSIS	4-67
4.3.1	Analytical Model	4-67
4.3.1.1	Assumptions and Groundrules	4-69
4.3.2	Preliminary Trajectory Analysis	4-70
4.3.3	Final Trajectory Analysis	4-70
4.3.4	Dispersed Atmosphere Effects	4-87
4.3.4.1	Trajectory Correction Techniques	4-91
4.3.4.2	Dispersed Atmosphere Effects on Inertial Velocity	4-117
4.3.5	Lunar, Solar and Earth Harmonics Perturbations	4-123

CONTENTS (Continued)

PARAGRAPH		PAGE
4.4	CONTROL ANALYSIS	4-125
4.4.1	Control Methods	4-125
4.4.2	Atmospheric Effects on Control	4-127
4.4.3	Astrionics Effect on Control Requirements	4-130
4.4.4	Control Options	4-130
4.4.5	Results	4-131
4.5	THERMAL ANALYSIS	4-139
4.5.1	Analytical Methods	4-139
4.5.1.1	Assumptions	4-140
4.5.2	Heating Rates	4-140
4.5.3	Equilibrium Temperatures	4-140
4.5.4	Thermal Protection System Requirements	4-156
4.5.4.1	Heat Shield Dome	4-156
4.5.4.2	Flare Structure	4-156
4.5.4.3	Sidewall Area	4-156
4.5.4.4	Thermal Protection System Weights	4-163
4.6	ASTRIONICS ANALYSIS	4-163
4.6.1	Introduction	4-163
4.6.2	Astrionic System Study Groundrules and Guidelines	4-166
4.6.3	Astrionic System Analysis Summary and Observations	4-167
4.6.3.1	Astrionic System Aerobraking Weight Deltas	4-167
4.6.3.2	Navigation Analysis	4-167
4.6.3.3	Radiation Impacts Analysis	4-169
4.6.3.4	Observations and Conclusions	4-169
4.6.4	Navigation Accuracy Analysis	4-171
4.6.4.1	Introduction	4-171
4.6.4.2	Navigation Sensors	4-172
4.6.4.3	Analytical Tools	4-174
4.6.4.4	Synchronous Orbit Navigation Uncertainty Analysis	4-174
4.6.4.5	Aerobraking Descent Orbit Navigation Accuracy Analysis	4-175
4.6.4.6	Trajectory Correction Burn Uncertainty Analysis	4-192
4.6.4.7	Aerobraking Navigation Uncertainty Analysis Sensitivities	4-195
4.6.5	Astrionic System Configuration	4-200
4.6.5.1	Astrionic System Configuration Description	4-202
4.6.5.2	Weight and Power Summary	4-202
4.6.6	Redundancy Analysis	4-202
4.6.6.1	Redundancy Study Assumptions	4-207
4.6.6.2	Analytic Programs	4-207
4.6.6.3	Reliability Enhancement/Coverage	4-207
4.6.6.4	Nominal Mission without Aerobraking	4-208
4.6.6.5	Aerobraking Redundancy Impacts	4-209
4.6.6.6	Redundancy Analysis Observations	4-209

CONTENTS (Continued)

PARAGRAPH		PAGE
4.6.7	Power-Weight Impacts	4-211
4.6.7.1	Space Tug Power Requirements	4-211
4.6.7.2	Aerobraking Weight Deltas	4-211
4.6.8	Astrionic System Radiation Impacts	4-211
4.6.8.1	External Radiation Environments	4-213
4.6.8.2	Internal Radiation Environments	4-213
4.6.8.3	Electronic Device Effects	4-215
4.6.8.4	Observations	4-218
4.6.9	New Technology Implications	4-219
4.6.9.1	Redundancy Implementation	4-219
4.6.9.2	Navigation Sensor Integration	4-219
4.6.9.3	Navigation and Guidance Analyses	4-220
4.6.10	Follow-On Study Effort	4-220
4.6.10.1	Astrionic System Configuration Analysis	4-220
4.6.10.2	Redundancy Analysis	4-220
4.6.10.3	Navigation Timeline Analysis	4-221
4.6.10.4	Advanced Sensor Systems	4-221
4.6.10.5	Updating Capability versus Control Requirements	4-221
4.6.10.6	Radiation Analysis	4-221
4.6.10.7	Astrionic System New Technology Component Analysis	4-221
4.7	Aerobraking Kit Materials Selection	4-222
4.7.1	Materials Groundrules and Criteria	4-222
4.7.2	Thermal Environments of Aerobraking Kit Elements	4-223
4.7.3	Materials Selection	4-226
4.7.3.1	Aft Heat Shield Materials Selection	4-244
4.7.3.2	Sidewall Insulation	4-244
4.7.3.3	Flare Materials Selection	4-245
4.7.3.4	Payload Adapter Materials Selection	4-245
4.7.4	Options and Recommendations	4-246
4.8	WEIGHTS AND MASS PROPERTIES	4-246
4.8.1	Mass Properties Summary	4-246
4.8.2	Structural Weights	4-246
4.8.2.1	Aft Heat Shield	4-254
4.8.2.2	Flared Skirt	4-254
4.8.2.3	Payload Adapter/Flared Skirt Support	4-254
4.8.3	Thermal Protection System Weight	4-254
4.8.4	Astrionics System Weight	4-256
4.8.5	Control System Weight	4-256
4.8.6	Total Tug Weight	4-256
5.0	SENSITIVITY ANALYSES	5-1
5.1	PAYLOAD/AEROBRAKING PERFORMANCE OPTIMIZATION	5-1
5.1.1	General Parametric Results	5-3
5.1.1.1	Inert Weight and Delta Velocity Effects	5-3
5.1.1.2	RCS Isp Effects	5-7
5.1.1.3	Circularization Altitude and EOS Rendezvous Effects	5-12
5.1.1.4	General Parametric Conclusions	5-20

CONTENTS (Continued)

PARAGRAPH		PAGE
5.1.2	Specific Payload Capability Assessment	5-20
5.1.2.1	Delta Velocity Budgets	5-24
5.1.2.2	Basic (No Flare) Configurations	5-27
5.1.2.3	30° Flare Configuration	5-30
5.1.2.4	45° Flare Configuration	5-34
5.1.2.5	60° Flare Configuration	5-34
5.1.2.6	Configuration Payload Comparison	5-34
5.2	ATMOSPHERIC PERTURBATION AND NAVIGATION ERROR SENSITIVITIES	5-47
5.2.1	Effects on Nominal Perigee Altitudes	5-47
5.2.2	Payload Sensitivities	5-53
5.2.3	Perturbation Summary and Conclusions	5-56
5.3	AEROBRAKING/CONVENTIONAL TRAJECTORY TUG COMPARISONS	5-59
5.3.1	Conventional Trajectory Tug Size Comparison	5-59
5.3.2	Sensitivities to Performance Parameters	5-61
5.3.2.1	Mass Fraction	5-61
5.3.2.2	Specific Impulse	5-63
5.3.2.3	Delta Velocity	5-63
5.4	SENSITIVITY ANALYSIS CONCLUSIONS AND RECOMMENDATIONS	5-63
	LIST OF REFERENCES	1
APPENDICES		
A	TWO PASS AEROBRAKING SPACE TUG ANALYSIS	A-1
B	BRIEF DESCRIPTION OF KALMAN FILTERING	B-1
C	ANALYSIS PROGRAMS	C-1
D	NAVIGATION COMPONENTS	D-1
E	RECOMMENDED AEROBRAKING FOLLOW-ON ACTIVITIES	E-1
F	TWO PASS LIGHT WEIGHT LARGE FLARE	F-1

LIST OF FIGURES

FIGURE		PAGE
1.1.0.0-1	Aerobraking Feasibility Study Logic	1-3
1.1.0.0-2	Conventional Tug (Starting Point)	1-4
1.1.0.0-3	Selected Space Tug Aerobraking Configuration Concepts (1st Phase)	1-6
1.1.0.0-4	Selected Space Tug Aerobraking Configuration Concepts (Add-On Activity)	1-7
1.1.0.0-5	Space Tug Aerobraking Study Schedule	1-8
1.2.0.0-1	Comparison of Conventional and Aerobraking Trajectory Profiles	1-10
1.2.0.0-2	Payload Potential for Space Tug Aerobraking	1-12
2.0.0.0-1	Geosynchronous Payload Capability of Aerobraked Tug	2-2
2.1.1.0-1	Drag Coefficients (30°, 45° and 60° Flares)	2-5
2.1.1.0-2	Drag Coefficients (Basic, Short 60° Flare and Large Nose Flare)	2-6
2.1.2.0-1	Baseline Radiative Aft Heat Shield	2-9
2.1.2.0-2	Baseline Flare Concept (60° Flare)	2-11
2.1.2.0-3	Short 60° Flare Concept	2-12
2.1.2.0-4	Large Nose Flare Concept	2-13
2.1.3.0-1	Space Tug Aerobraking Return Time from Synchronous Orbit	2-15
2.1.3.0-2	Space Tug Aerobraking Return from Synchronous Orbit (With Dispersed Atmosphere)	2-17
2.1.4.0-1	RCS Propellant Consumption	2-19
2.1.5.0-1	Comparison of Maximum Equilibrium Temperatures	2-20
2.1.5.0-2	Maximum Equilibrium Temperatures	2-22
2.1.5.0-3	Maximum Equilibrium Temperatures for Basic and 60° Flare Configurations - Nominal and (+) Density Atmosphere	2-23
2.1.6.0-1	Radial Perigee Position Uncertainties (Basic Tug Configuration)	2-26
2.1.6.0-2	Navigation Update History	2-27
2.1.6.0-3	Orbital Correction Burn, Delta Velocity RCS Fuel Consumption, and Radial Perigee Position Error	2-28
2.1.8.0-1	Aft Heat Shield Weight Vs. Number of Passes	2-32
2.1.8.0-2	Flare Weight Vs. Number of Passes	2-33
2.1.8.0-3	Thermal Protection System Weight Vs. Number of Passes	2-35
2.1.8.0-4	Astrionics System Weight Vs. Number of Passes	2-36
2.1.8.0-5	Total Tug Weight Vs. Number of Passes	2-37
2.2.0.0-1	H-33 Configuration External H2 Tank Orbiter (Alternate Mission Capability)	2-39
2.2.1.0-1	Synchronous Round Trip Payload Vs. Number of Passes (200 N.M. Recovery)	2-40
2.2.2.0-1	Round Trip Payload Vs. Number of Passes (Depart and Recover at 200 N.M.)	2-42
2.2.2.0-2	Atmospheric Anomaly and Navigation Error Effect on Round Trip Payload (10 Pass Mission)	2-44

LIST OF FIGURES (Continued)

FIGURE		PAGE
2.2.3.0-1	Round Trip Payload Capabilities of Conventional and Aerobraked Tugs	2-45
4.0.0.0-1	Performance and Trade Study Logic	4-2
4.1.1.0-1	Basic (No Flare) Configuration	4-5
4.1.1.1-1	Drag Bridging Scheme Illustration	4-8
4.1.1.1-2	Final Basic (No Flare) Tug Drag Characteristics	4-9
4.1.1.1-3	Preliminary Basic (No Flare) Tug Drag Characteristics	4-10
4.1.1.2-1	Basic (No Flare) Tug Static Stability Characteristics	4-12
4.1.1.3-1	Basic (No Flare) Pressure Coefficient Distribution	4-13
4.1.1.3-2	Maximum Local Pressure Profile (Basic-No Flare)	4-17
4.1.2.0-1	Flare Sizing Study - Simplified Technical Approach	4-18
4.1.2.1-1	Ellipsoid Nose Bow Shock Profile	4-19
4.1.2.1-2	Embedded Flow Field Characteristics	4-20
4.1.2.1-3	Parametric Flare Drag Characteristics	4-21
4.1.2.1-4	Parametric Flare Static Stability Characteristics	4-21
4.1.2.2-1	Flared Tug Configuration(s) Geometry	4-22
4.1.2.2-2	Preliminary Variation of Time to Decay with Respect to Ballistic Coefficient ($W/C_D A$)	4-24
4.1.2.2-3	C_D and $W/C_D A$ Range for Aerobraked Space Tug Configurations	4-24
4.1.2.3-1	Drag Coefficients for Selected Flared Configurations	4-27
4.1.2.3-2	Drag Coefficients For Optional Flared Configurations	4-28
4.1.2.4-1	Coefficient Of Normal Force Slope For Flared Configurations	4-29
4.1.2.4-2	Center Of Pressure For Flared Configurations	4-30
4.1.2.5-1	Local Pressure Coefficients Over Heat Shield And Cylinder (Flared Configurations)	4-32
4.1.2.5-2	Local Pressure Coefficients Over Flares	4-33
4.1.2.5-3	Maximum Local Pressure On Heat Shield Nose	4-35
4.1.2.5-4	Maximum Local Pressure At Outer Edge Of Flare	4-36
4.1.2.5-5	Maximum Local Pressure Profile (30 Pass Mission-Flared Configurations)	4-37
4.2.1.0-1	Conventional Space Tug Configuration	4-40
4.2.2.1-1	Aft Heat Shield	4-45/4-46
4.2.2.1-2	Internal Cap Heat Shield Concept	4-48
4.2.2.1-3	Clam Shell Aft Heat Shield Concept	4-49
4.2.2.1-4	Single Pivot Point - Total Elliptical Dome Retraction Concept	4-50
4.2.2.1-5	Double Pivot Point - Clam Shell Concept	4-52
4.2.2.1-6	Single Pivot Point - One Piece Cap Concept	4-53
4.2.2.1-7	Single Pivot Point - Clam Shell Concept	4-54
4.2.2.1-8	Payload End Heat Shield Concept	4-56
4.2.2.2-1	Sidewall Insulation - 60 Degree Flare Space Tug Configuration - 30 Pass (5 Day Mission)	4-58

LIST OF FIGURES (Continued)

FIGURE		PAGE
4.2.2.3-1	Baseline Flare Concept	4-59/60
4.2.2.3-2	Alternate Flare Concept	4-62
4.2.2.4-1	Payload Adapter Concept For Flared Aerobraking Tug Concepts	4-64
4.3.1.0-1	Mission Profile	4-68
4.3.2.0-1	Preliminary Trajectory Data	4-71
4.3.3.0-1	Initial Perigee Altitude	4-72
4.3.3.0-2	Tug Aerobraking Return Time From Synchronous Orbit	4-74
4.3.3.0-3	Apogee Altitude Decay	4-75
4.3.3.0-4	Apogee Altitude Decay	4-76
4.3.3.0-5	Perigee Altitude Decay	4-77
4.3.3.0-6	Perigee Altitude Decay	4-78
4.3.3.0-7	Maximum Dynamic Pressure	4-79
4.3.3.0-8	Maximum Dynamic Pressure	4-80
4.3.3.0-9	Maximum Dynamic Pressure	4-81
4.3.3.0-10	Maximum Inertial Velocity Per Pass - Basic (No Flare) Configuration	4-82
4.3.3.0-11	Maximum Inertial Velocity Per Pass - 60° Flare Tug Configuration	4-83
4.3.3.0-12	Comparison of Free Space and Re-Entry Times (Basic - No Flare Configuration)	4-86
4.3.3.0-13	Comparison of Free Space and Re-Entry Times (60° Flare)	4-88
4.3.4.0-1	Summer Atmospheric Density Dispersions	4-89
4.3.4.0-2	Winter Atmospheric Density Dispersions	4-90
4.3.4.0-3	Time to Lower Apogee to 270 N.M.	4-92
4.3.4.1-1	Accumulated Trajectory Correction Delta Velocity for Impulse at Atmosphere Exit	4-94
4.3.4.1-2	Vacuum Perigee Altitude at Atmosphere Exit	4-95
4.3.4.1-3	Apogee Altitude at End of Pass	4-96
4.3.4.1-4	Accumulated Trajectory Correction Delta Velocity for Impulse at Apogee	4-97
4.3.4.1-5	Vacuum Perigee Altitude at Atmosphere Exit	4-98
4.3.4.1-6	Apogee Altitude at End of Pass	4-99
4.3.4.1-7	Final Pass and Apogee Error for Impulse at Apogee	4-101
4.3.4.1-8	Final Pass and Apogee Error for Impulse at Apogee	4-102
4.3.4.1-9	Increase in Delta Velocity to Go to 270 N.M. for Impulse at Exit	4-103
4.3.4.1-10	Increase in Delta Velocity to Go to 270 N.M. for Impulse at Apogee	4-104
4.3.4.1-11	Maximum Dynamic Pressure for Basic Tug Impulse at Exit (10 Pass)	4-105
4.3.4.1-12	Maximum Dynamic Pressure for Basic Tug Impulse at Exit (30 Pass)	4-106
4.3.4.1-13	Maximum Dynamic Pressure for Basic Tug Impulse at Exit (60 Pass)	4-107

LIST OF FIGURES (Continued)

FIGURE		PAGE
4.3.4.1-14	Maximum Dynamic Pressure for Large Flare Tug Impulse at Exit (10 Pass)	4-108
4.3.4.1-15	Maximum Dynamic Pressure for Large Flare Tug Impulse at Exit (30 Pass)	4-109
4.3.4.1-16	Maximum Dynamic Pressure for Large Flare Tug Impulse at Exit (60 Pass)	4-110
4.3.4.1-17	Maximum Dynamic Pressure for Basic Tug Impulse at Apogee (10 Pass)	4-111
4.3.4.1-18	Maximum Dynamic Pressure for Basic Tug Impulse at Apogee (30 Pass)	4-112
4.3.4.1-19	Maximum Dynamic Pressure for Basic Tug Impulse at Apogee (60 Pass)	4-113
4.3.4.1-20	Maximum Dynamic Pressure for Large Flare Impulse at Apogee (10 Pass)	4-114
4.3.4.1-21	Maximum Dynamic Pressure for Large Flare Impulse at Apogee (30 Pass)	4-115
4.3.4.1-22	Maximum Dynamic Pressure for Large Flare Impulse at Apogee (60 Pass)	4-116
4.3.4.2-1	Elapsed Time Trend from Maximum Inertial Velocity to Perigee (First Pass)	4-118
4.3.4.2-2	Sensitivity of First Pass Inertial Velocity to Atmosphere - Basic Tug (No Flare) Configuration	4-119
4.3.4.2-3	Sensitivity of First Pass Inertial Velocity to Atmosphere (60° Flare Configuration)	4-120
4.3.5.0-1	Vacuum Perigee History of the First Pass of a Ten Pass Mission	4-121
4.3.5.0-2	Time to Lower Apogee to 270 n.m.	4-123
4.3.5.0-3	Altitude Time History of the First Pass of a Ten Pass Trajectory	4-124
4.4.1.0-1	RCS System Limit - Cycle Under Worst Case Influence of Aero-Moment	4-126
4.4.1.0-2	Phase Plane Trajectory Showing Tug Oscillations From Time Tug Enters Atmosphere Until It Passes Max Q	4-128
4.4.2.0-1	Pitch Axis Propellant Consumption Due to the Aero-Moment for the Basic Tug	4-129
4.4.5.0-1	Pitch Axis Propellant Consumption Due to Limit Cycling for the Basic and 60° Flare Tugs	4-132
4.4.5.0-2	Roll Axis Propellant Consumption Due to Limit Cycling for the Basic Tug	4-133
4.4.5.0-3	Roll Axis Propellant Consumption Due to Limit Cycle for the Space Tug With 60° Flare	4-134
4.4.5.0-4	RCS Propellant Consumed For the Basic Tug During Change of Orbit Period	4-135
4.4.5.0-5	RCS Propellant Consumed for Tugs With Flares During Change of Orbit Period	4-136

LIST OF FIGURES (Continued)

FIGURE		PAGE
4.4.5.0-6	Effects of Atmospheric Density on RCS Propellant Consumption for the Basic Tug	4-137
4.4.5.0-7	Effects of Atmospheric Density on RCS Propellant Consumption for the 60° Flare Tug	4-138
4.5.2.0-1	Maximum Heating Rates - Basic Configuration	4-141
4.5.2.0-2	Maximum Heating Rates - 30° Flare Con- figuration	4-142
4.5.2.0-3	Maximum Heating Rates - 45° Flare Con- figuration	4-143
4.5.2.0-4	Maximum Heating Rates - 60° Flare Con- figuration	4-144
4.5.2.0-5	Comparison of Maximum Heating Rate	4-145
4.5.2.0-6	Heating Rate Distribution - 10 Pass Basic Configuration	4-146
4.5.2.0-7	Heating Rate Distribution - 10 Pass 30° Flare Configuration	4-147
4.5.2.0-8	Heating Rate Distribution - 10 Pass 45° Flare Configuration	4-148
4.5.2.0-9	Heating Rate Distribution - 10 Pass 60° Flare Configuration	4-149
4.5.2.0-10	Maximum Heating Rates for Basic and 60° Flare Configurations - Normal and (+) Density Atmosphere	4-150
4.5.3.0-1	Maximum Equilibrium Temperatures - Basic Configuration	4-151
4.5.3.0-2	Maximum Equilibrium Temperatures - 30° Flare Configuration	4-152
4.5.3.0-3	Maximum Equilibrium Temperatures - 45° Flare Configuration	4-153
4.5.3.0-4	Maximum Equilibrium Temperatures - 60° Flare Configuration	4-154
4.5.3.0-5	Comparison of Maximum Equilibrium Tempera- tures	4-155
4.5.3.0-6	Maximum Equilibrium Temperatures for Basic and 60° Flare Configurations - Nominal and (+) Density Atmosphere	4-157
4.5.4.3-1	Space Tug Sidewall Cross-Section	4-158
4.5.4.3-2	Space Tug Sidewall Insulation Thickness - Basic Configuration	4-159
4.5.4.3-3	Space Tug Sidewall Insulation Thickness - 30° Flare Configuration	4-160
4.5.4.3-4	Space Tug Sidewall Insulation Thickness - 45° Flare Configuration	4-161
4.5.4.3-5	Space Tug Sidewall Insulation Thickness - 60° Flare Configuration	4-162
4.5.4.4-1	Space Tug Sidewall Thermal Protection System Weights	4-164

LIST OF FIGURES (Continued)

FIGURE		PAGE
4.6.1.0-1	Astrionic Study Approach	4-165
4.6.3.1-1	Astrionic System Aerobraking Weight Delta Summary	4-168
4.6.3.2-1	Perigee Navigation Position Uncertainty Summary	4-170
4.6.4.2-1	Typical Navigation Sensor Characteristics	4-173
4.6.4.4-1	Synchronous Orbit Analysis	4-176
4.6.4.5-1	Navigation Update History	4-179
4.6.4.5-2	Navigation Position Uncertainties (10 day - 60 Pass)	4-181
4.6.4.5-3	RCS Perigee Position Uncertainty (Basic Tug Configurations - 60 Pass)	4-182
4.6.4.5-4	RCS Apogee Position Uncertainties (Basic Tug Configuration)	4-183
4.6.4.5-5	Radial Perigee Position Uncertainties (Basic Tug Configuration)	4-184
4.6.4.5-6	RSS Apogee Position Uncertainties (Flared Tug Configuration)	4-186
4.6.4.5-7	Radial Perigee Position Uncertainties (Flared Tug Configuration)	4-187
4.6.4.5-8	One Pass Navigation Position Uncertainties	4-188
4.6.4.5-9	One Pass Mission Apogee Altitude as a Function of Delta Deboost Velocity (Basic Tug Configuration)	4-190
4.6.4.6-1	Deboost Burn Uncertainty Analysis	4-193
4.6.4.6-2	Orbital Correction Burn, ΔV RCS Fuel Consumption, and Radial Perigee Position Uncertainty	4-194
4.6.4.6-3	Radial Position Uncertainty as a Function of Corrective Burn Timing	4-196
4.6.4.7-1	Effects on Navigation Due to Variation of Navigation Update Rate During Landmark Tracking Prior to Perigee	4-197
4.6.4.7-2	Effects of Navigation Due to Variation of Navigation Update Rate During Landmark Tracking after Perigee	4-198
4.6.4.7-3	RSS Navigation Position for Various Navi- gation Update Sample Rates	4-199
4.6.4.7-4	Second Apogee RSS Position Uncertainty Vs. Time of Reinitialization of Kalman Filter	4-201
4.6.5.1-1	Tug Astrionic System Configuration	4-203
4.6.5.2-1	Nominal Mission Weight and Power	4-204/205
4.6.5.2-2	Weight and Power Summary	4-206
4.6.6.1-1	Failure Rates of Critical Components	4-208
4.6.6.5-1	Aerobraking Redundancy Weight Impacts	4-210
4.6.7.2-1	Aerobraking Power Weight Deltas	4-212
4.6.8.1-1	Summary of External and Internal Van Allen Radiation Environments for Three Proposed Mission Profiles	4-214

LIST OF FIGURES (Continued)

FIGURE		PAGE
4.6.8.2-1	Prescribed Shielding Configuration	4-216
4.6.8.2-2	Electron and Bremsstrahlung Dose/Unit Fluence for a Van Allen Electron Fluence	4-217
4.7.1.0-1	Materials Selection Criteria	4-224
4.7.2.0-1	Comparison of Maximum Equilibrium Temperatures	4-225
4.7.2.0-2	RL-10A-3-8 Engine Maximum Allowable Temperature Limits for Non-Operating Engine	4-227
4.7.3.0-1	Material Properties	4-228/240
4.7.3.0-2	Radiative Material Properties	4-241/242
4.7.3.0-3	Strength to Density Properties of High Temperature Structural Materials	4-243
4.8.1.0-1	Space Tug Mass Properties	4-247
4.8.2.0-1	Aft Heat Shield Materials Summary	4-248
4.8.2.0-2	Aft Heat Shield Weight Vs. Number of Passes	4-249
4.8.2.0-3	Flare Weight Vs. Number of Passes	4-250
4.8.2.0-4	Payload Adapter Weight Vs. Number of Passes	4-251
4.8.2.0-5	Weight Summary - Payload Adapter/Flared Skirt Support	4-252
4.8.2.0-6	Total Structural Weight Vs. Number of Passes	4-253
4.8.3.0-1	Thermal Protection System Weight Vs. Number of Passes	4-255
4.8.4.0-1	Astrionics System Weight Vs. Number of Passes	4-257
4.8.5.0-1	Reaction Control System Weight Vs. Number of Passes	4-258
4.8.6.0-1	Total Tug Weight Vs. Number of Passes	4-259
5.1.0.0-1	Conventional (Non-Aerobraking) Space Tug Configuration	5-2
5.1.1.1-1	Effect of Aerobraking Modification Weights on Round Trip Payload	5-4
5.1.1.1-2	Effect of Aerobraked Return ΔV on Round Trip Payload	5-6
5.1.1.1-3	Effect of Aerobraked Return ΔV on Placement Payload	5-8
5.1.1.1-4	Effect of Aerobraked Return ΔV on Retrieval Payload	5-9
5.1.1.2-1	Atmospheric Entry Weight	5-10
5.1.1.2-2	Initial Weight and Propellant Weight	5-11
5.1.1.2-3	Effect of RCS Usage on Payload	5-13
5.1.1.3-1	Mission Delta Velocity Sensitivity to Final Orbit Altitude	5-14
5.1.1.3-2	Effects of Circularization Altitude on Payload (Light Weight Aerobraking Kit Penalty - 1000 Pounds)	5-16
5.1.1.3-3	Effect of Circularization Altitude on Payload	5-18
5.1.1.3-4	Effect of Tug Recovery Altitude and Recovery Method on Delta Payload	5-19
5.1.2.0-1	Selected Space Tug Aerobraking Configuration Concepts	5-21

LIST OF FIGURES (Continued)

FIGURE		PAGE
5.1.2.0-2	Fully Fueled Weight Statement	5-22
5.1.2.0-3	H-33 Configuration External H ₂ Tank Orbiter (Alternate Mission Capability)	5-23
5.1.2.1-1	Mission Total Delta Velocity Sensitivity to Plane Change Angle and Configuration	5-25
5.1.2.1-2	Payload Sensitivity to Delta Velocity	5-26
5.1.2.1-3	Total Mission Delta Velocity Equivalent Vs. Number of Passes	5-28
5.1.2.2-1	Aerobraking Weight Vs. Number of Passes (Basic - 270-100 n.m. Recovery)	5-29
5.1.2.2-2	Aerobraking Weight Vs. Number of Passes (Basic - Depart and Recover at 200 n.m.)	5-31
5.1.2.3-1	Aerobraking Weight Vs. Number of Passes (30° Flare - 270-100 n.m. Recovery)	5-32
5.1.2.3-2	Aerobraking Weight Vs. Number of Passes (30° Flare - Depart and Recover at 200 n.m.)	5-33
5.1.2.4-1	Aerobraking Weight Vs. Number of Passes (45° Flare - 270-100 n.m. Recovery)	5-35
5.1.2.4-2	Aerobraking Weight Vs. Number of Passes (45° Flare - Depart and Recover at 200 n.m.)	5-36
5.1.2.5-1	Aerobraking Weight Vs. Number of Passes (60° Flare - 270-100 n.m. Recovery)	5-37
5.1.2.5-2	Aerobraking Weight Vs. Number of Passes (60° Flare - Depart and Recover at 200 n.m.)	5-38
5.1.2.6-1	Round Trip Payload Vs. Number of Passes (270 - 100 n.m. Recovery)	5-39
5.1.2.6-2	Round Trip Payload Vs. Number of Passes (De- parture and Recovery at 200 n.m.)	5-40
5.1.2.6-3	Round Trip Payload Vs. Number of Passes (270 - 100 n.m. Recovery)	5-42
5.1.2.6-4	Synchronous Round Trip Payload Vs. Number of Passes	5-43
5.1.2.6-5	Placement Payload Vs. Number of Passes (270 - 100 n.m. Recovery)	5-44
5.1.2.6-6	Retrieval Payload Vs. Number of Passes (Depart and Recover at 200 n.m.)	5-46
5.1.2.6-7	Geosynchronous Payload Capability of Aerobraked Tug	5-48
5.2.1.0-1	Radial Position Uncertainty at Perigee	5-49
5.2.1.0-2	Range of Atmospheric Perturbations	5-51
5.2.1.0-3	Maximum Equilibrium Temperatures Vs. Initial Perigee Error (1st Pass of 30 Pass Mission)	5-52
5.2.2.0-1	Fully Fueled Weight Statements for High Density Atmosphere	5-54
5.2.2.0-2	Round Trip Payload Vs. Number of Passes (Depart and Recover at 200 n.m.)	5-55
5.2.2.0-3	Atmospheric Anomaly and Navigation Error Effect on Round Trip Payload (10 Pass Mission)	5-57

LIST OF FIGURES (Continued)

FIGURE		PAGE
5.3.1.0-1	Payload Capability Comparison - Aerobraked vs. Conventional Tug	5-60
5.3.2.1-1	Comparison of Round Trip Payload Sensitivities to Mass Fraction	5-62
5.3.2.2-1	Comparison of Round Trip Payload Sensitivities to Specific Impulse	5-64
5.3.2.3-1	Comparison of Round Trip Payload Sensitivities to Mission Delta Velocity	5-65
A-1.0.0-1	Selected Space Tug Aerobraking Configuration Concepts (Add-On Activity)	A-3
A-1.0.0-2	Geosynchronous Round Trip Payload	A-4
A-2.1.0-1	Preliminary Flare Configuration/Net Payload Sensitivity Estimate	A-7
A-2.1.1-1	Basic (No Flare) Pressure Coefficient Distribution	A-9
A-2.1.2-1	Short 60° Flared Tug Configuration(s) Geometry	A-10
A-2.1.2-2	Drag Coefficients For Short 60° Flare #1	A-11
A-2.1.2-3	Drag Coefficients For Short 60° Flare #2 (Selected Configuration)	A-12
A-2.1.2-4	Coefficient of Normal Force for Short 60° Flare #2	A-13
A-2.1.2-5	Center of Pressure for Short 60° Flare #2	A-14
A-2.1.2-6	Local Pressure Coefficients Over Short 60° Flare #2	A-15
A-2.1.2-7	Drag Coefficients for Short 60° Flare #3	A-16
A-2.1.3-1	Drag Coefficients for "Ring Tail" Flare	A-18
A-2.1.3-2	Candidate Configurations for $W/C_D A = 2$ PSF	A-19
A-2.1.3-3	Drag Coefficients for Nose Flare (Selected Configuration)	A-20
A-2.2.1-1	Ablative Heat Shield Concept	A-22
A-2.2.3-1	Short 60° Flare Concept	A-24
A-2.2.3-2	Large Nose Flare Concept	A-25
A-2.2.3-3	Large Nose Flare Deployment/Retraction	A-26
A-2.3.1-1	Short 60° Flare Maximum Dynamic Pressure	A-30
A-2.3.1-2	Short 60° Flare Initial Perigee Altitudes	A-29
A-2.3.3-1	Equivalent $W/C_D A$ Values	A-32
A-2.4.0-1	RCS Propellant Consumption	A-34
A-2.5.1-1	Heating Rate Distribution - Basic Configuration (2 Pass)	A-35
A-2.5.1-2	Heating Rate Distribution - 60° Short Flare (2 Pass)	A-36
A-2.5.1-3	Heating Rate Distribution - 60° Short Flare (30 Pass)	A-37
A-2.5.1-4	Heating Rate Distribution - Large Flare (2 Pass)	A-39
A-2.5.2-1	Maximum Equilibrium Temperatures	A-39
A-2.5.3-1	Heat Shield Ablative Material Thickness	A-41
A-2.5.3-2	Space Tug Sidewall Insulation Thickness	A-42
A-2.5.3-3	Thermal Protection System Weight Summary	A-43
A-2.7.0-1	2 Pass Maximum Heating Rates	A-44
A-2.7.0-2	ESA-3560 IIA Properties	A-46
A-2.7.0-3	ESA-3560 IIA Thickness Vs. Heat Input	A-47

LIST OF FIGURES (Continued)

FIGURE		PAGE
A-2.7.0-4	L-605 Cobalt Alloy Material Properties	A-48
A-2.8.0-1	Mass Properties for Add-On Activity	A-50
A-2.8.0-2	Aerobraking Kit Weights	A-51
A-2.8.0-3	Materials Used for Aerobraking Kit Components	A-52
A-2.8.0-4	Total Tug Weight Vs. Number of Passes	A-53
A-3.1.0-1	Atmospheric Density Variations for Space Tug Aerobraking Studies	A-55
A-3.1.0-2	Ten Pass Basic Tug - Target Apogee Vs. Pass Number	A-56
A-3.1.0-3	Final Apogee Error Vs. Number of Passes to 270 n.m.	A-57
A-3.1.0-4	Increase in ΔV to Go to 270 n.m. for Off- Nominal Atmosphere	A-59
A-3.2.0-1	Sensitivity of Total Mission Navigation Error Correction Delta Velocity to Correction Burn Time	A-60
A-3.3.0-1	Fully Fueled Aerobraking Tug Weight Statements	A-62
A-3.3.0-2	Round Trip Payload Capabilities	A-63
A-3.3.0-3	Fully Fueled Weight Statement for 30 Pass Short 60° Flare Tug (#3)	A-65
A-3.3.0-4	Flare Configuration/Net Payload Sensitivity Estimate	A-66
A-3.4.0-1	Round Trip Payload Capabilities of Conventional and Aerobraked Tugs	A-68
A-3.4.0-2	Payload Placement Capabilities of Conventional and Aerobraked Tugs	A-70
A-3.4.0-3	Payload Retrieval Capabilities of Conventional and Aerobraked Tugs	A-71
B-1	Comparison of Least Squares and Maximum Likelihood Estimation	B-1
B-2	Comparison of Straight Position Resets with Kalman Position Resets	B-3
C-1	Autonomous Navigation Modes	C-4
F-1.0.0-1	Light Weight Large Flare Concept	F-3
F-1.0.0-2	Aerobraking Kit Weight Statement for Two Pass Airmat Flared Configuration	F-2
F-1.0.0-3	Candidate Light Weight Large Flare Concepts	F-4
F-2.0.0-1	Round Trip Payload Capabilities	F-5

ABBREVIATIONS AND ACRONYMS

A	Cross-sectional area
ACT	Acquisition, Control and Test (Unit)
AM	Astrionics Module
ANS	Autonomous Navigation Simulation (computer program)
A_R	Reference area (constant @ 154 FT ²)
BITE	Built-In-Test-Equipment
BOM	Basic Operating Memory
CD_0	Zero angle of attack drag coefficient = $\text{Drag}/q_\infty A_R$
C_M	Pitching moment coefficient = $\text{Pitching moment}/q_\infty A_R D_R$
C_{N_α}	Initial normal force coefficient slope = $\partial C_N / \partial \alpha / \alpha=0$
C_p	Local pressure coefficient = $(P_L - P_\infty) / q_\infty$
CP	Total vehicle center of pressure = C_M / C_N @ $\alpha \sim 0$
CPU	Central Processor Unit (computer)
D(D _R)	Tug diameter (14 FT), also deadband
EOS	Earth-to-Orbit Shuttle
FMF	Free Molecular Flow
FOV	Field-of-view
h	Geometric altitude
H ₂	Hydrogen
I	Inertia
Isp	Specific impulse
IBM	International Business Machines Corporation
IMU	Inertial Measurement Unit
IO	Input/Output (computer)
IPEP	Inertial Platform Error Program (computer program)
ITT	International Telephone and Telegraph Company
K	Bridging parameter
K_N	Knudsen Number (assumed herein = $M/\sqrt{R_e}$)
K_R^*	Conversion factor for C_p at max loads
KFT	Kilo feet (thousands of feet)
KLB	Kilopounds (thousands of pounds)
KW(H)	Kilowatt (Hour)
L/D	Lift-to-drag

ABBREVIATIONS AND ACRONYMS (Continued)

r	Radius of vehicle
M	Mach number = V_{∞} / ambient sound speed
MEV	Million electron volts
MHz	Megahertz
MOSFET	Metal-Oxide-Silicon/Field Effect Transistor
MSFN	Manned Space Flight Network
N	Normal (Position), also number of thrusters
\dot{N}	Normal (velocity)
NM	Nautical Mile
O ₂	Oxygen
OMS	On-board maneuvering systems
OOS	Orbit-to-Orbit Shuttle
P	Static pressure
PM	Propulsion Module
PRA	Patrick Reference Atmosphere
q, Q	Dynamic pressure = $1/2 \rho V_{\infty}^2$, also heating rate
R	Bow shock radius = $f(x)$, also gas constant, or radial (position)
\dot{R}	Radial (velocity)
R_e	Reynolds number = $\rho V D / \mu$
RADS(Si)m	Radiation energy deposited in silicon
RCS	Reaction Control System
RE \oplus	Equatorial radius
RMS	Root mean square
RSS	Root sum square
S	Molecular speed ratio = $V / \sqrt{2RT}$
SA	Standard 1962 Atmosphere
Sync	Synchronous
T	Temperature (absolute), also tangential (position/velocity), also time or minimum firing time
TBC	The Boeing Company
TPS	Thermal Protection System
USB	Unified S-Band
USBE	Unified S-Band Equipment

ABBREVIATIONS AND ACRONYMS (Continued)

V	Velocity
W_I	Weight of inerts
W_P	Weight of propellant
W_{PLD}	Weight of payload
$W/C_D A$	Ballistic coefficient
W_t	Weight
X	Axial position coordinate measured from 2:1 ellipsoid nose apex
Y	Vertical position coordinate measured normal to the Tug centerline axis
α	Thermal accommodation coefficient, also angle of attack
γ	Ratio of specific heats
δ	Partial derivative, also flare angle
ΔV	Delta velocity
λ	Mean Free molecular path
λ'	Mass fraction
μ	Coefficient of viscosity
$\mu \oplus$	Gravity constant
ρ	Density
σ	Standard deviation, also Stefan-Boltzman Constant
ϕ	Attitude
$\dot{\phi}$	Attitude rate
$\omega \oplus$	Earth rotation constant
ϵ	Surface emissivity

SUBSCRIPTS

CG	Center of gravity
EQ	Equilibrium
i	Incident flow characteristics
L	Local condition
r	Reflected flow characteristics
s	Conditions behind normal shock
w	Wall surface characteristics
∞	Ambient or free stream characteristics

SECTION I - INTRODUCTION

1.0 GENERAL

This report describes the results of a study to investigate the feasibility and practicality of applying an aerobraking trajectory mode to the Space Tug for return to low earth orbit from geosynchronous orbit. This return scheme will reduce the overall mission delta velocity requirements and will allow for a smaller propulsion module to accomplish these missions. The Space Tug, consisting of the smaller propulsion module coupled with the astronics module, payload adapter and payload, will conform with the Space Shuttle dimensional and weight capabilities and will be able to perform almost all (~ 95 percent) of the proposed geosynchronous missions with a single Shuttle/single Space Tug launch per mission. No orbital assembly and/or orbital propellant transfer operations would be required. The aerobraking Space Tug concept will provide an economical ground based Space Tug system.

The Space Tug is one of the new hardware elements required to support the Integrated Space Program. It must interface with the Space Shuttle, Space Station, Nuclear Shuttle, Orbiting Propellant Stations, Satellites and other payloads. In operating with these elements, it must operate in both a manned and unmanned mode, over a wide range of missions. These missions include low earth orbital resupply, earth orbital operations, geosynchronous, lunar orbit, lunar surface, translunar and interplanetary.

The versatility requirements necessitate that the Space Tug have different modules and/or kits to provide flexibility without imposing undue performance penalties on the basic Space Tug. This study defined the special aerobraking kit elements and assessed their impact on the Space Tug performance.

As the study was limited in scope, it was not possible to analyze all of the mission implications, operational modes, environmental effects and design options. However, the major factors were identified and their influence defined. No major problems appear to exist in applying the aerobraking re-entry trajectory mode to the Space Tug.

Additional Space Tug study activities are required to bring the Aerobraking Space Tug missions, mission modes and configuration options to the same level of knowledge as the other Space Tug conceptual study options. Principle follow-on activities should include: Mission analyses, operational modes, economic analyses, payload/Tug interfaces, Shuttle/Tug interfaces, more detailed Space Tug aerobraking design studies and impact of the aerobraking modes on the advanced technology Space Tug configurations.

In performing this study, areas where new technology is required were also determined. Principle follow-on technical activities required include: Aerodynamics and aerothermodynamics studies, materials and structural concepts, drag configuration concepts, and astronics and control systems.

1.0- (Continued)

This report is divided into five sections: This Section I - Introduction, Section II - Summary, Section III - Groundrules, Guidelines and Assumptions, Section IV - Performance and Trade Results, and Section V - Sensitivity Analysis. In addition, there are six appendices: Appendix A - Two Pass Aerobraking Space Tug Analysis, Appendix B - Brief Description of Kalman Filtering, Appendix C - Analysis Programs, Appendix D - Navigation Components, Appendix E - Recommended Aerobraking Follow-On Activities, and Appendix F - Two Pass Light Weight Large Flare. The Appendix A activities present the results of the contract add-on study.

1.1 STUDY OBJECTIVES AND APPROACH

The objective of this study was to determine the feasibility of applying an aerobraking trajectory mode to the Space Tug for return from geosynchronous orbit. This objective was achieved by:

- o Defining sensitivities of Tug weights to various re-entry environments
- o Defining sensitivity of re-entry environments to trajectory anomalies
- o Determining sensor and sensor accuracy requirements
- o Determining position and velocity update requirements
- o Developing astrionics reliability weight and performance requirements
- o Defining the impact of the radiation environment on the astrionics systems
- o Determining representative inert weight penalties associated with aerobraking (i.e., thermal and aerodynamics)
- o Comparing required Space Tug gross weights for equal payloads for conventional and aerobraking trajectories
- o Determining scar weights for aerobraking kit modifications
- o Identifying the new technology implications of the aerobraking concept
- o Identifying the follow-on Tug aerobraking activities

To accomplish these objectives, the study logic as shown in Figure 1.1.0.0-1 was followed. The first phase of the study was directed towards maximizing the payload potential of the Aerobraked Tug. The second phase add-on activity was directed towards identifying the payload capability with the minimum mission duration.

The Space Tug configuration developed by The Boeing Company for NASA/MSFC under a prior study (Reference 1.1.0.0-1) consisted of a propulsion module, an astrionics module and a payload adapter which, when combined with the payload, matched the former Space Shuttle cargo limit of 54,000 pounds. For this study, the current Space Shuttle cargo limit of 65,000 pounds was used to update the Space Tug. The propulsion module was increased to reflect this change (as shown in the propulsion module weights in Figure 1.1.0.0-2). The astrionics module was updated to reflect Shuttle-era technology. This updating reduced the astrionics weight from 2526 pounds to 1960 pounds. The other modules and kits were unchanged in the

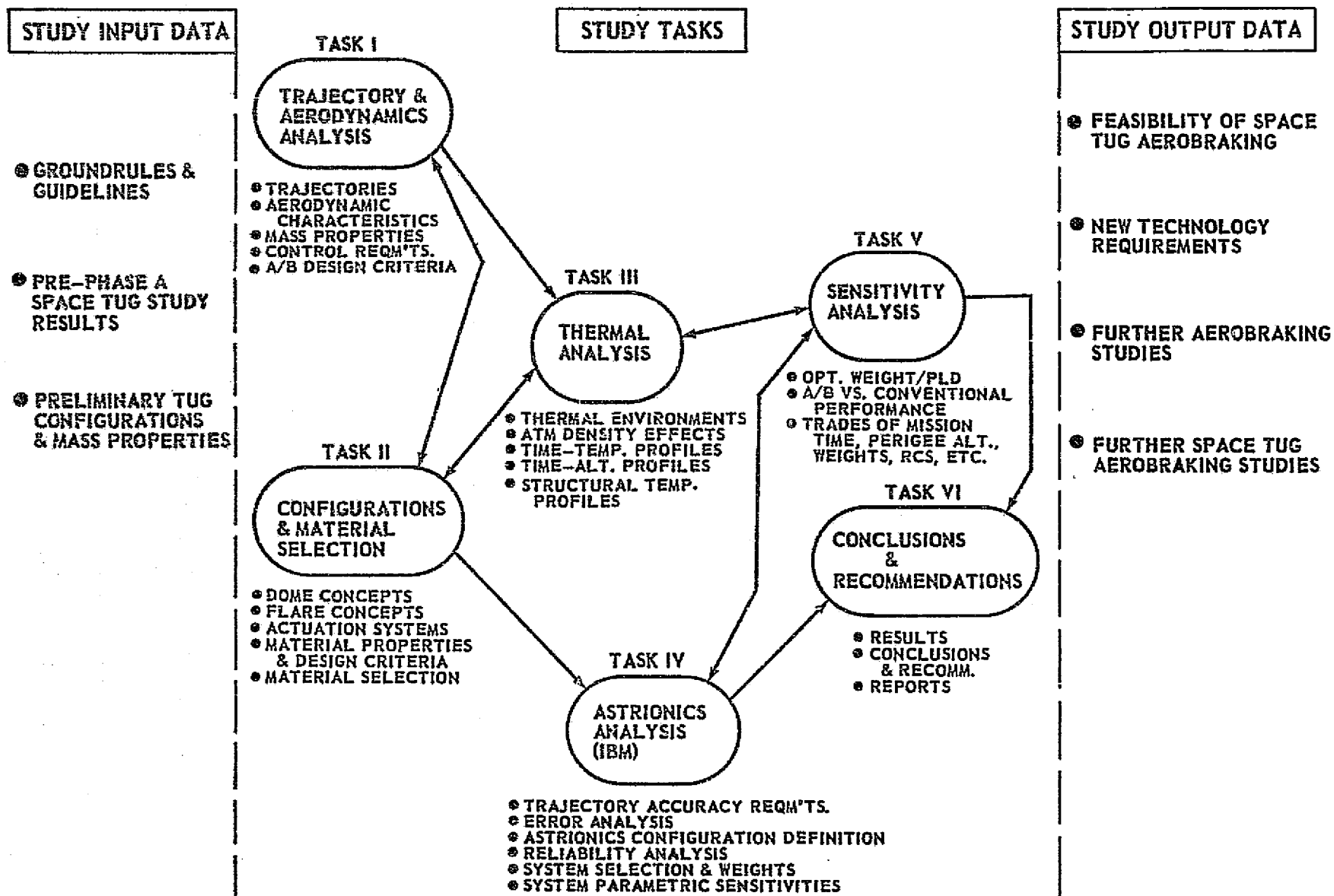
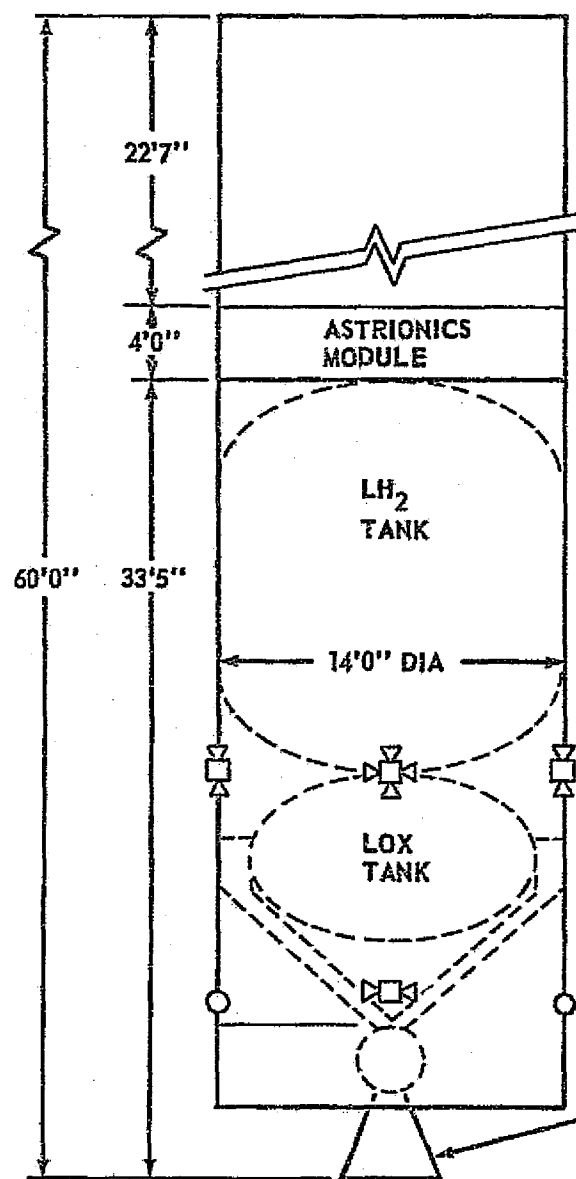


FIGURE 1.1.0.0-1: AEROBRAKING FEASIBILITY STUDY LOGIC



WEIGHT ESTIMATE (LBS)

● PROPULSION MODULE		50,868
● PROPELLANT	45,000	
● INERTS	5,868	
● ENGINE	639	
● PROP/MECH	801	
● THERMO/MICRO	573	
● STRUCTURE	2912	
● CONT. & RESID.	943	
● ASTRIONICS MODULE		1,960
● ELECTRICAL	515	
● AVIONICS	842	
● STRUCTURE	300	
● THERMAL	303	
● PAYLOAD ADAPTER		200
TOTAL SPACE TUG WEIGHT		53,028
MASS FRACTION		0.849
SPECIFIC IMPULSE (SEC)		460

FIGURE 1.1.0.0-2: CONVENTIONAL TUG (STARTING POINT)

1.0 (Continued)

baseline Space Tug configuration.

From this uprated Space Tug configuration, six aerobraking configuration concepts were selected (Figure 1.1.0.0-3 - 1st phase and Figure 1.1.0.0-4 - 2nd phase). These aerobraking concepts were based on nozzle end first re-entry and employed a 2:1 elliptical domed heat shield mounted over the engine as an aft end radiative or ablative thermal protection system. In addition to the aft heat shield, five of the six selected aerobraking configurations reduced the ballistic coefficient by increasing the aerodynamic drag with a flare. Five different flare lengths and four different angles were selected to examine the vehicle static stability and drag characteristics. Aerodynamics, trajectory and control analyses were performed on these configurations. The aerodynamic analyses provided (1) airloads data for determining pressure loads on the structure, (2) drag data for determining trajectory characteristics, and (3) stability data for determining reaction control system requirements. Thermal environmental data was generated which were used to define and select materials and provide design criteria for the aerobraking kit elements. The trajectory data provided input data to the astrionics analysis to permit accuracy and navigation error evaluation, redundancy requirements, sensor systems definition and selection, astrionics module configuration update, and weights. The impact of the structural modifications, thermal protection system requirements, astrionics system modifications and reaction control systems weights as a function of mission duration was defined. Trades of mission time, perigee altitude, weights, operational modes, etc., were performed. The results of the above activities were assessed and conclusions and recommendations were developed.

A majority of the study activity was directed to determining the aerodynamics, astrionics and thermal aspects of the aerobraking analyses. A small portion of the study effort was directed toward conceptual designs. The design activity was only performed in sufficient depth to define the feasibility and weights associated with each concept. Performance analysis show that the round trip payload capability is traded pound for pound with aerobraking kit inerts. Therefore, lightweight aerobraking designs are a necessary follow-on study activity.

The study approach used in the first phase was to determine the feasibility of the aerobraking mode and to determine the mission duration which would maximize the payload capability of the Tug in performing a round trip geosynchronous mission. The second phase (add-on activity) determined the impact of two pass short duration missions on the payload capability.

The task and milestone schedule is shown in Figure 1.1.0.0-5. The first phase of the study was of four months duration with two months for final documentation and presentations. The second phase (add-on activity) was of two months duration with one-half month for documentation. The study flow and major milestones are identified from the Task I, Performance and Aerodynamic Analyses, through the Task VI, Reports, Conclusions and Recommendations.

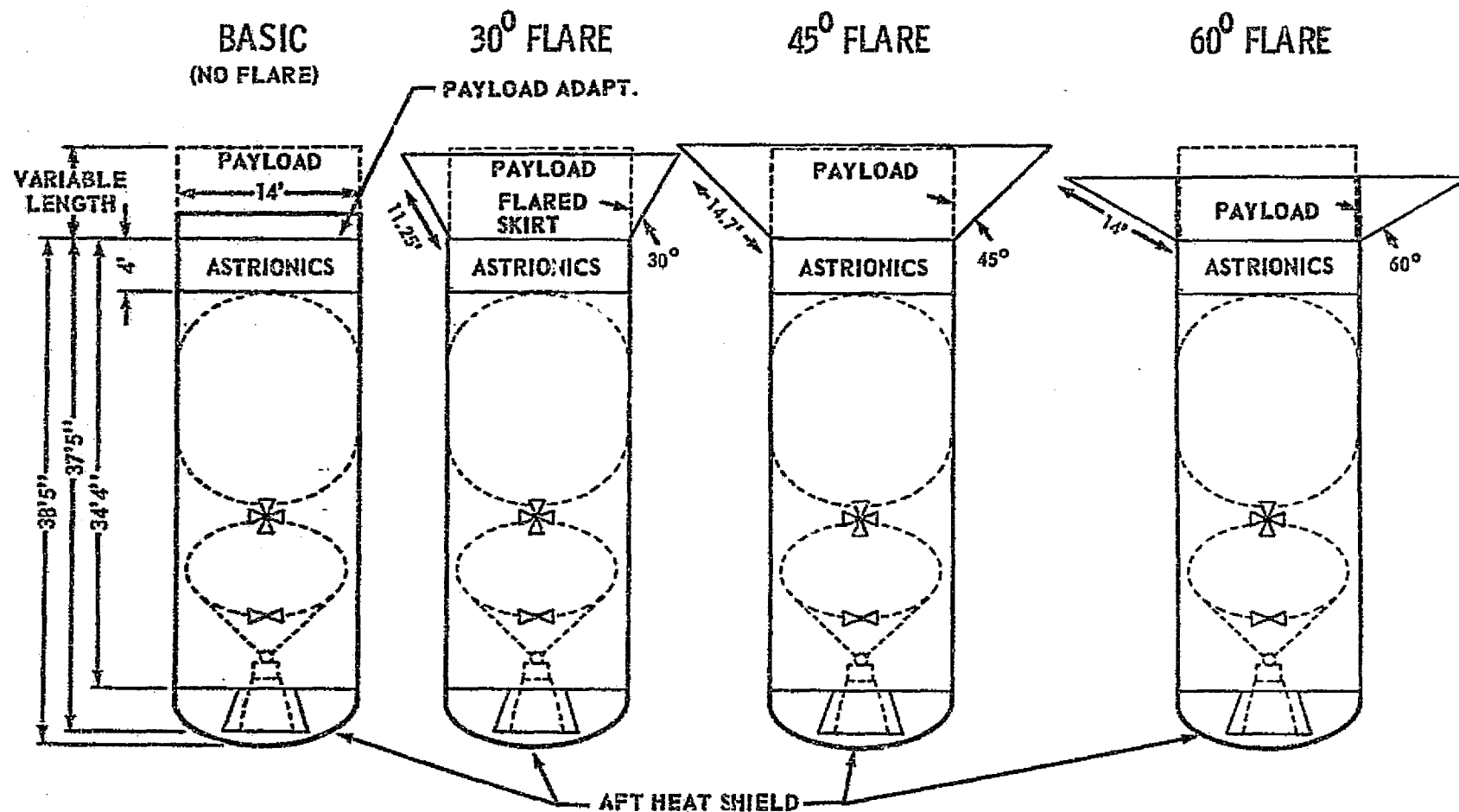


FIGURE 1.1.0.0-3: SELECTED SPACE TUG AEROBRAKING CONFIGURATION CONCEPTS (1ST PHASE)

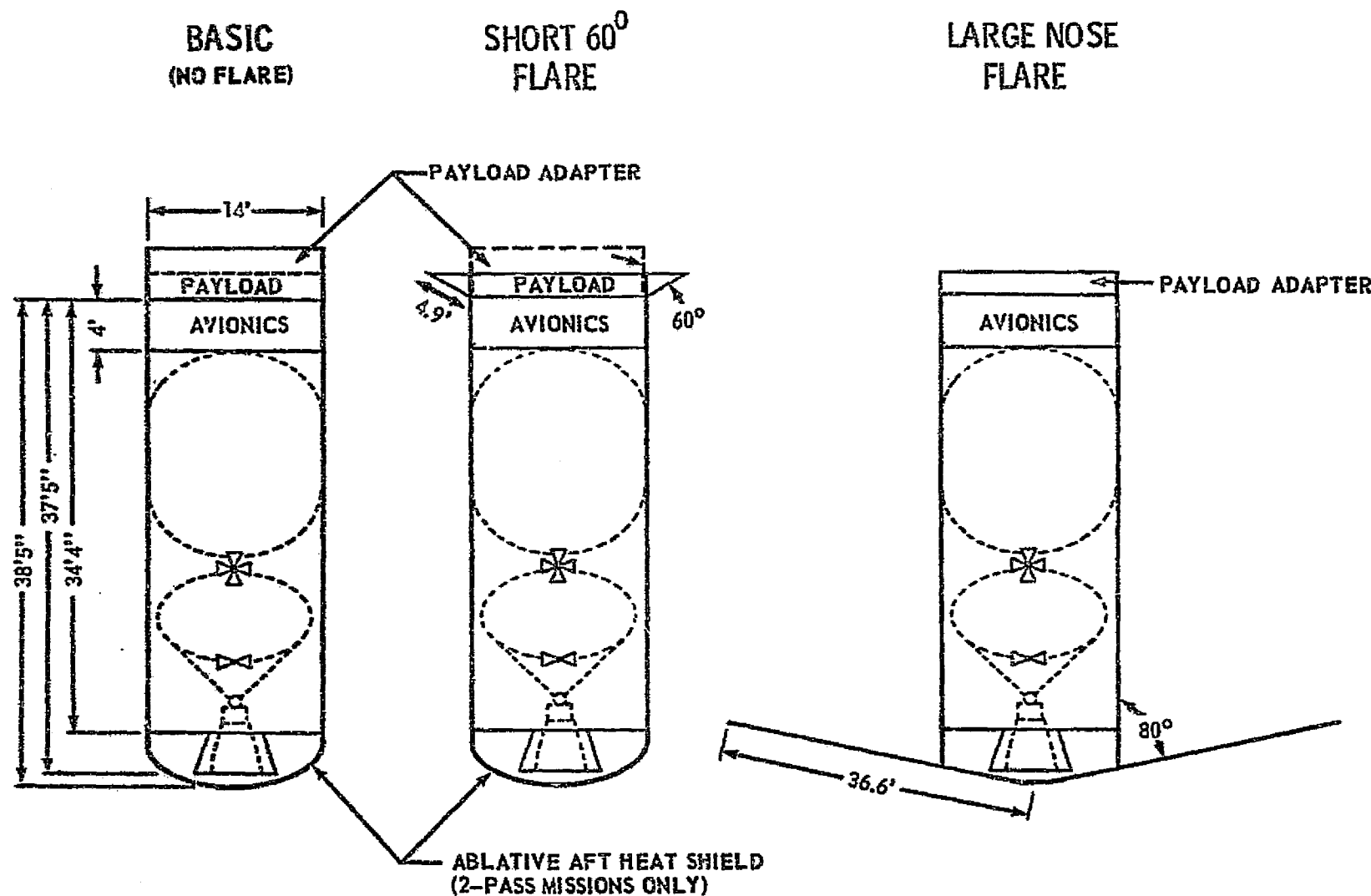


FIGURE 1.1.0.0-4: SELECTED SPACE TUG AEROBRAKING CONFIGURATION CONCEPTS (ADD-ON ACTIVITY)

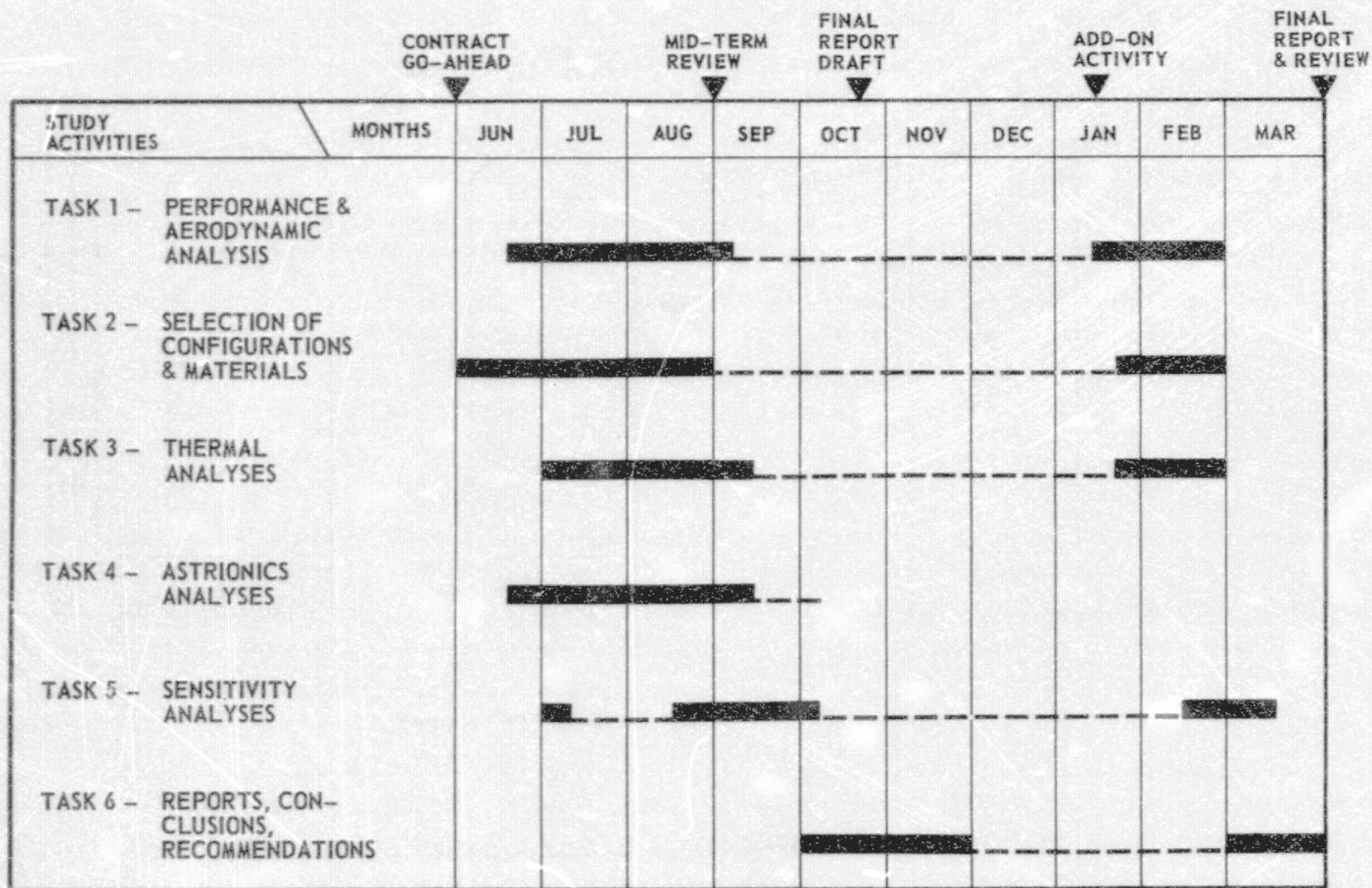


FIGURE 1.1.0.0-5: SPACE TUG AEROBRAKING STUDY SCHEDULE

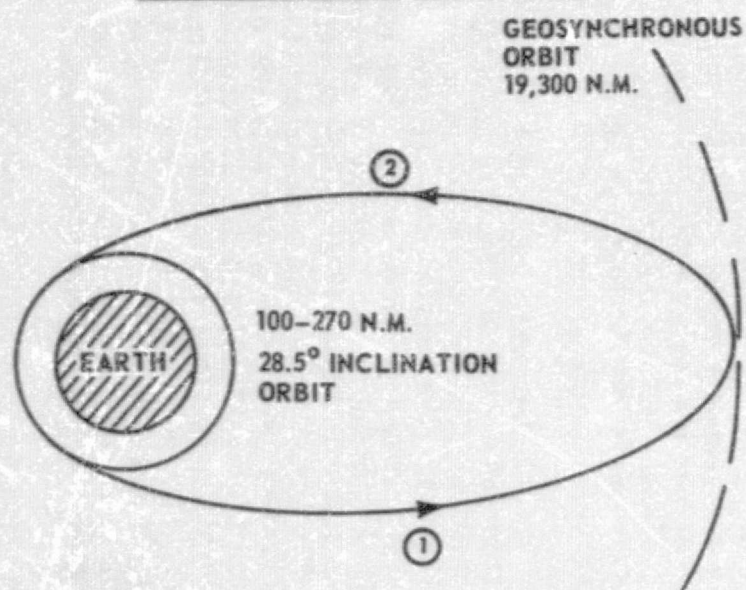
1.2 BACKGROUND

The previous Pre-Phase A studies of the Space Tug have shown that to accomplish the geosynchronous missions and other high energy earth orbital type missions, it is necessary to use either a very large single stage Space Tug or complex multi-stage Space Tugs (two stages or stage plus drop tanks). The large single stage Tug would not meet the Shuttle constraint of 15 foot diameter by 60 foot length and 65,000 pounds payload capability to 100 n.m./28.5° orbit. Similarly, the multistage Tug configurations cannot meet the Shuttle constraints. The multi-stage Tug operational mode would either deliver the stages in two or more launches or deliver the unfueled (or partially fueled) Tug to the departure orbit followed by a delivery of fuel and payloads in a second Shuttle flight. Both approaches would necessitate multi-Shuttle missions and assembly and/or refueling operations in orbit for the accomplishment of a single Space Tug mission. Neither approach is compatible with the desired ground based Shuttle/Tug mode of operation wherein the Shuttle would deliver the Tug and its payload to the departure orbit in a single launch. The Shuttle then could return to earth or wait on orbit until the Space Tug and the replaced payload are recovered from the geosynchronous orbit.

An attractive alternative mode which would reduce the propulsive delta velocity requirements and thereby reduce the size of the propulsion module stage is the use of an aerobraking trajectory for the return mode. Figure 1.2.0.0-1 illustrates the conventional trajectory profile versus the aerobraked trajectory profile. The conventional profile uses two ascent delta velocity burns to (1) leave the departure orbit, and (2) to plane change and circularize at synchronous orbit. These ascent velocities total to approximately 14,100 feet per second. A 400 feet per second additional allowance provides for rendezvous and docking at synchronous orbit. The descent trajectory also uses two burns, one burn to depart from synchronous orbit and the second burn to circularize at low earth orbit. Similarly, a 400 feet per second allowance is required to rendezvous and dock with the Shuttle. Thus the total delta velocity requirements for the conventional trajectory mode is 29,000 feet per second for the geosynchronous round trip mission.

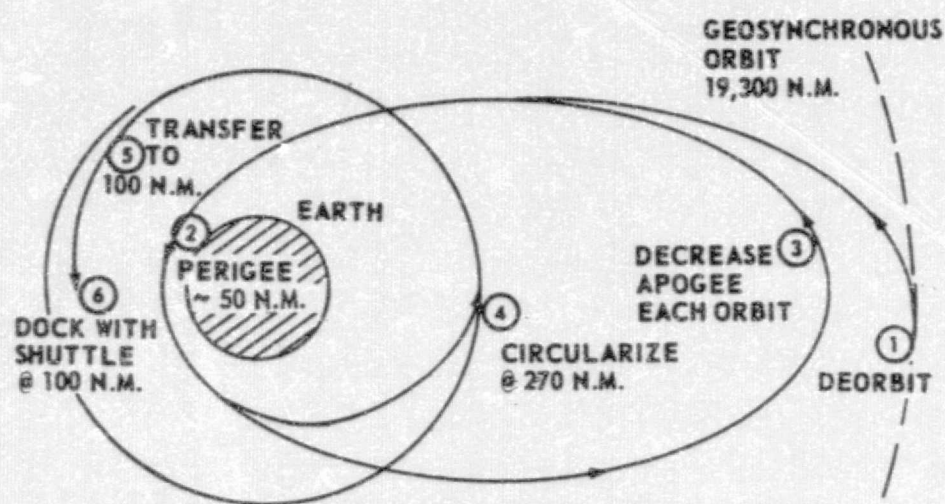
The aerobraking trajectory profile has the same ascent velocity (14,100 feet per second) and the same rendezvous and docking velocity (400 feet per second) requirement. However, the descent mode has a considerably lower delta velocity requirement. The initial deorbit burn from synchronous orbit requires a 5993 feet per second delta velocity. The aerobraking phase is initiated with the Tug entering the atmosphere, proceeding to a low perigee altitude, where some of the vehicle energy is reduced by the atmospheric drag. Subsequent passes have lower apogee altitudes and slightly lower perigee altitudes. When the apogee altitude of the last pass is equal to the desired circularization orbit altitude, a second burn circularizes the Tug orbit. For this study, this altitude was selected as 270 n.m. (Lower altitudes, such as 200 n.m., are desirable ways to increase the Tug payload capabilities and may be used.) The Tug then phases with the Shuttle and with two additional delta velocity burns descends to a Shuttle/Tug rendezvous orbit and circularizes. An additional

CONVENTIONAL PROFILE

 ΔV BUDGET

① ASCENT	14,500 FPS
② DESCENT	14,500 FPS

AEROBRAKING RETURN

RETURN ΔV BUDGET RANGE: (30 PASSES)

	MINIMUM	MAXIMUM
① DEORBIT	5993 FT/SEC	5993 FT/SEC
④ CIRCULARIZE	133 @ 100 N.M.	380 @ 270 N.M.
⑤ TRANSFER TO 100 N.M.	-	656
⑥ DOCKING		400
RESERVES	324	1371
TOTAL	6450 FT/SEC	8800 FT/SEC

FIGURE 1.2.0.0-1: COMPARISON OF CONVENTIONAL AND AEROBRAKING TRAJECTORY PROFILES

1.2 (Continued)

400 feet per second provides for Shuttle/Tug rendezvous and docking. Using the aerobraking mode, the return delta velocity requirements may be as low as 6450 feet per second (20,950 feet per second for total round trip delta velocity) or may be as high as 8800 feet per second for the return mode (23,300 feet per second for the total round trip). This total delta velocity range is dependent on the Tug circularization altitude and the selection of the vehicle to perform rendezvous and docking operations. The delta velocity requirements are reduced by 23 to 28 percent of that required by conventional trajectory modes.

The lower delta velocity requirements for the aerobraking return mode will result in a smaller propulsive stage than that required to accomplish a mission using conventional trajectory flight modes. The use of the aerobraking mode is more advantageous in missions requiring payload retrieval or round trip payload where the returning vehicle is heavy than in the case of a placement payload where the Tug returns light (no payload). For the retrieval or round trip payload missions, the Tug propulsive stage required with an aerobraking return mode is only 50 to 60 percent as large as that required using conventional return modes. For a placement mission the aerobraking mode Tug would have to be approximately 80 percent that of the conventional return mode.

Figure 1.2.0.0-2 illustrates the advantages of aerobraking over a conventional trajectory by comparing the round trip payload capability of each trajectory mode. In each example the Space Shuttle 65,000 pound cargo capability is used to capacity. The center two bars reflect the comparison of current state-of-the-art Tug design. The conventional Tug can place under 1000 pounds in equatorial synchronous orbit as compared to 4050 pounds for the aerobraked Tug. The aerobraked Tug's mass fraction (including aerobraking kit components) is only 0.833 as compared to 0.875 for the conventional stage.

The first two bars represent the impact of a low cost Tug using unsophisticated design concepts. The conventional Tug cannot deliver any round trip payload to synchronous orbit. The aerobraked Tug can deliver 3000 pounds with a stage having a mass fraction of 0.85 (the mass fraction including aerobraking kit components is 0.819).

The last two bars represent the impact of the NASA point design. The point design can deliver 3000 pounds of round trip payload with a stage having a mass fraction of .895 and an Isp of 470 seconds. This stage requires a major advancement in the state-of-the-art (1976). An aerobraked stage with the same mass fraction (0.895) and with a propellant loading of 50,300 pounds (so that stage and payload do not exceed 65,000 pounds gross weight) will round trip 6500 pounds payload.

The conclusions that can be drawn from this comparison are:

1. If monetary constraints do not permit the technology to be developed or if the technology does not meet the desired goals, aerobraking

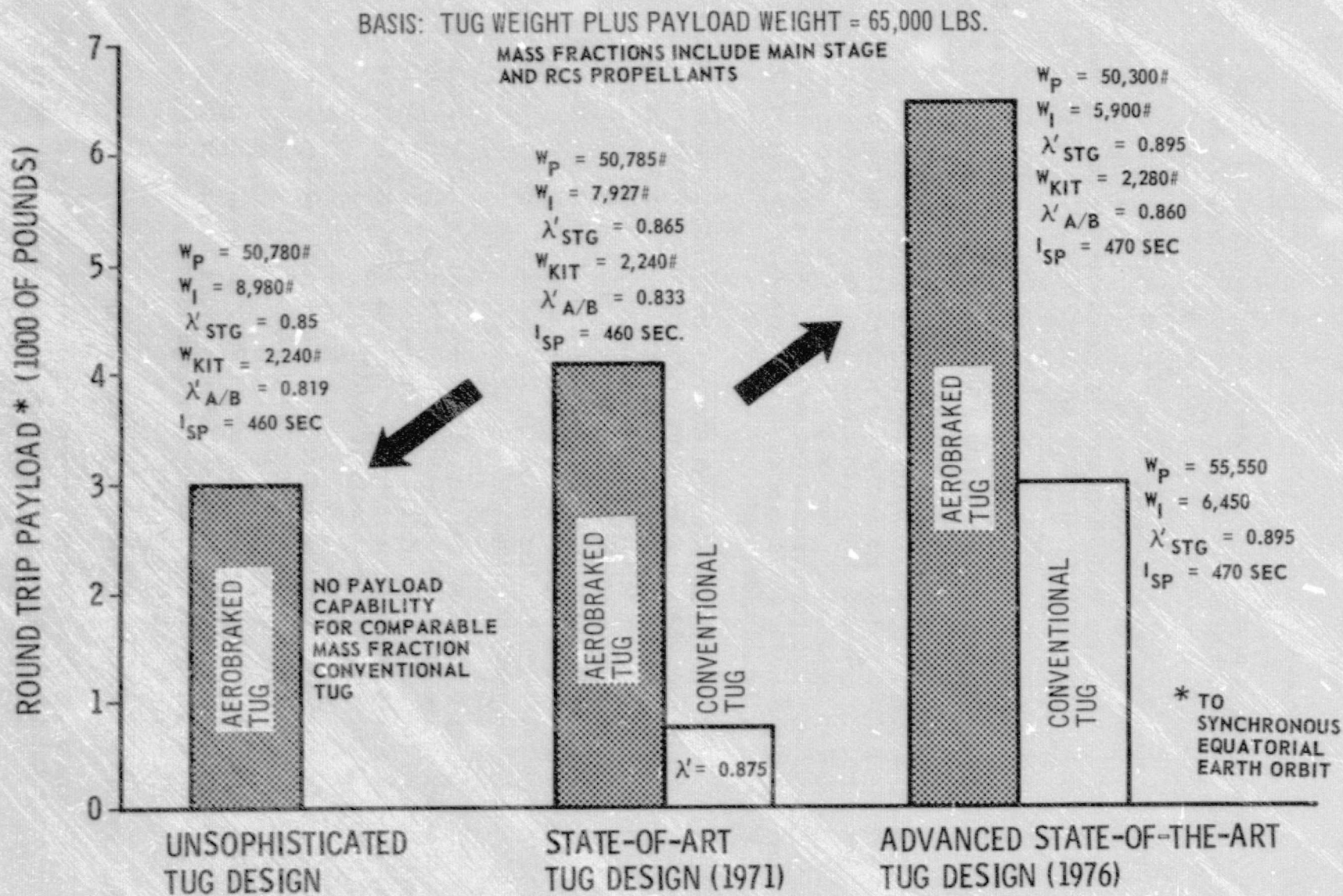


FIGURE 1.2.0.0-2: PAYLOAD POTENTIAL FOR SPACE TUG AEROBRAKING

1.2 (Continued)

will provide a method of achieving the desired payload capability.

2. If the technology is funded and the technology goals are achieved, aerobraking will provide greater payload capability (if required) or can deliver multiple payloads at reduced overall mission costs.

A further advantage of utilizing the aerobraking Tug is that the conventional trajectory Tug is sensitive to variations in mass fraction, specific impulse, and delta velocity. Historical data indicates that inert weights tend to increase with the length of the program development time and improved definition of the configuration during the development phase. This factor coupled with the sensitivity makes a single, large stage Space Tug a high design risk concept. The use of the aerobraking mode would partially decrease this risk as the specific impulse and mass fraction sensitivities impact would be reduced. Further, the options as to which vehicle (Shuttle or Tug) performs the low earth orbit maneuvers offers two additional methods of reducing sensitivities and program risks.

Utilizing the aerobraking return mode will result in longer missions than would be encountered with the conventional mode. If sufficient time is allowed for aerobraking, this trajectory mode can be accomplished with a minimal heating and with little impact on Tug design and structures. However, the longer the mission duration results in increased weight of the electrical power system, increased reaction control system fuel, and with increased weight for the necessary redundancy and reliability requirements of the astronics system. For an aerobraked Space Tug configuration which maximizes the payload capability, it is necessary to define that mission duration in which the combination of decreasing structural and thermal penalties, are minimized. At that mission duration, the payload is maximized. The first phase of this study therefore defined the compromise in return trip time which resulted in the minimum aerobraked weight Tug configuration for each of the selected configurations.

The second phase (add-on activity) minimized the mission duration to two (2) passes (approximately 10 hours). This shorter duration reduced the astronics and control penalties. However, the more rapid return increased the thermal impact on the Aerobraking Tug. The results of the short duration missions on Tug design, performance and payload capability are shown in Appendices A & F. The summary section which follows presents the results of both the first and second phase activities and analyzes these results to define the total study conclusions and recommendations.

SECTION II - SUMMARY

2.0 CONCLUSIONS AND RECOMMENDATIONS

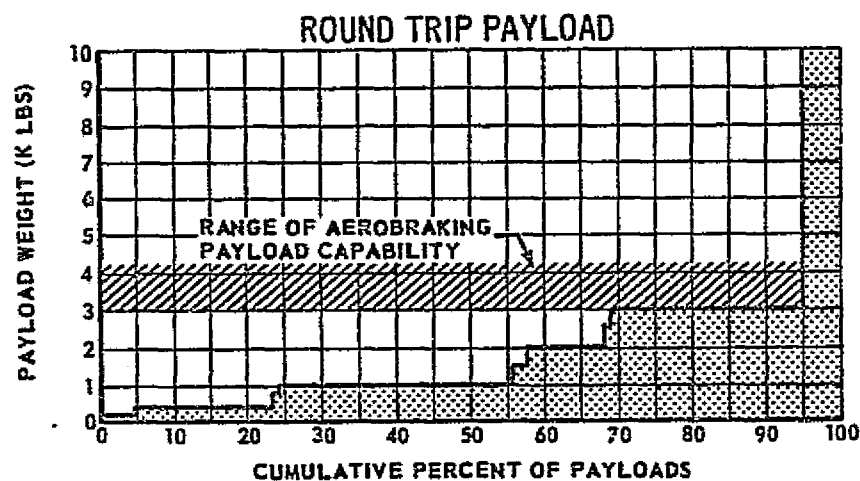
This study investigated the feasibility and practicality of the aerobraking mode for return trajectories of the Space Tug from geosynchronous equatorial orbit. Payloads weighing between 3000 and 4000 pounds can be carried in a round trip mode to and from an equatorial geosynchronous orbit using a Space Tug (exclusive of payload) weighing approximately 55,000 pounds. The aerobraking Space Tug payload capabilities for placement or retrieval missions will be approximately two-and-one-half times the round trip payload. As shown in Figure 2.0.0.0-1, this is sufficient payload capability to perform 95% of the prognosticated round trip geosynchronous missions in a mode wherein a single Shuttle flight can deploy and retrieve the Tug and its round trip payload. The aerobraking mode may also be applied for return from other high energy missions to provide larger payload capabilities than those possible with similar sized Tugs operating with conventional trajectory modes.

The conclusions reached in this study are, due to the limited study scope and time available, preliminary and provide trends rather than detailed data. However, the results present ample justification for the recommendation of further aerobraking study activity and technology programs. Many of the conclusions are subject to re-analysis as the aerobraking technique level of knowledge becomes comparable to conventional trajectory techniques and as the on-going studies further define the Shuttle.

The general study conclusions and recommendations are contained in the subsequent paragraphs. The conclusions for each study discipline are listed at the end of the summary discussion of the particular discipline (Sections 2.1.1 through 2.2). The recommended follow-on activities presented herein are further discussed in Appendix E.

General Conclusions - The general conclusions reached in the study are:

- o The aerobraked Tug's payload capability is maximized by missions having 25 to 35 atmospheric passages during the aerobraking phase. This corresponds to total Tug geosynchronous mission time of from 4 to 7 days. A 5 day mission duration is within the on-orbit capability of the Shuttle and permits a single Shuttle/Tug to accomplish a mission.
- o A one day return mission from geosynchronous orbit can be accomplished in from one to five passes. However, the thermal and pressure environments increase the structural requirements and result in significantly lower payload capability than the longer duration, maximum payload missions.

**BASIS:**

- EOS CAPABILITY ~ H-33 ORBITER
- 287 GEOSYNCHRONOUS MISSIONS
- 30 PASS MISSIONS

CONCLUSIONS:

- 95% OF ALL GEOSYNCHRONOUS MISSIONS CAPTURED

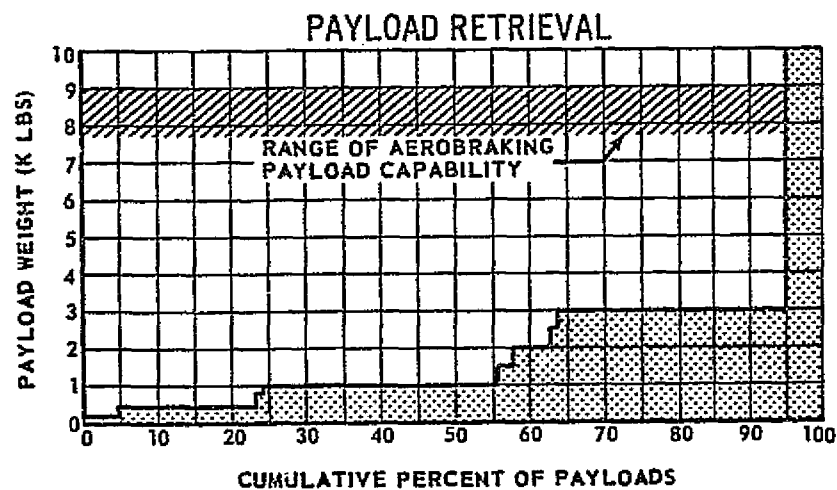
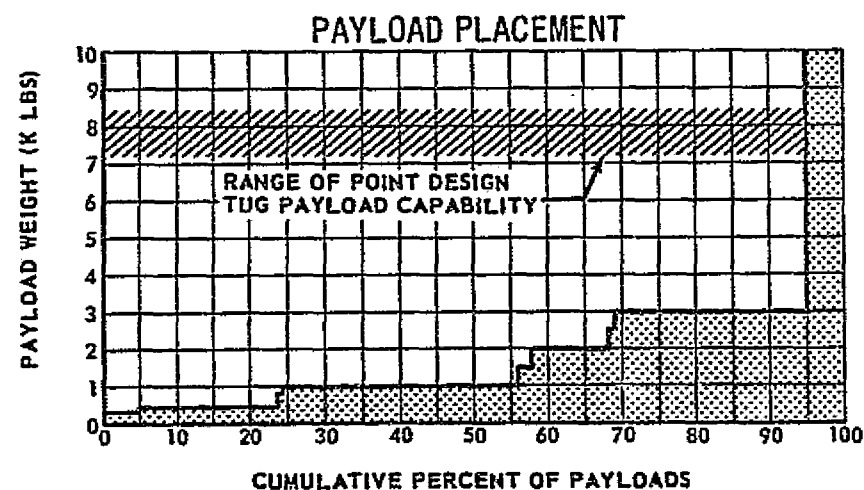


FIGURE 2.0.0.0-1: GEOSYNCHRONOUS PAYLOAD CAPABILITY OF AEROBRAKED TUG

2.0 (Continued)

- o The maximum geosynchronous payload capability of the aerobraked Tug can be obtained by optimizing the departure/recovery orbits and maximizing usage of the Shuttle for Shuttle/Tug interface operations.
- o Comparing the required weights for aerobraked and conventional trajectory Tugs to accomplish comparable payload geosynchronous missions, the aerobraked Tug weight is approximately 55% (retrieval), 65% (round trip), or 80% (placement) that of the conventional Tug.
- o The aerobraking kits for the Space Tug can be designed so that the aerobraked Tug will fit within the Shuttle's cargo bay. The aerobraking kits have a negligible scar weight impact on the conventional trajectory Tug. When the kits are removed, the Tug may be used for its lower energy missions with insignificant reduction in performance.
- o Reducing the ballistic coefficient with a large flare or other large surface area drag devices will permit lower thermal and pressure loads at reentry. Obtaining this large area, however, will reduce the weight available for payload and presents many design problems with packaging in the Shuttle cargo bay, deployment, retraction, astronics visibility and payload rendezvous and docking to the Tug.
- o In general, short duration aerobraking missions will require more complex designs of the aerobraking kit elements and will require technology advances in materials to increase payload capabilities.
- o A radiative heat shield is more desirable than the ablative heat shield as it is lower weight, reusable with minimal and/or no refurbishment and is less complex.
- o The atmospheric anomalies may be overcome by trajectory correction techniques. The thermal effect was less than 100°F.
- o The solar, lunar, and earth harmonics perturbations significantly impact the selection of the target perigee altitudes but have only minor impacts on thermal, aerodynamics, and control parameters. These effects are generally predictable and can be accounted for in pre-mission planning.

Recommendations

The results of this study are indicative of the aerobraking potential. The study did not (1) fully investigate all of the parameters which could potentially increase or reduce the weight aerobraking kits, or (2) examine sufficient aerobraking configuration options, or (3) de-

2.0 (Continued)

fine the operational modes for an optimum performance/cost system. The economic advantages of aerobraking due to fewer required Shuttle launches, however, are obvious and represent a potential for a major reduction in space program costs. These cost savings were not studied and should be assessed in future studies.

More detailed studies should be completed to develop the design and operational detail of the aerobraked Space Tug concept to a level comparable with that of the Space Tug configurations previously investigated or presently under investigation. Such follow-on studies should refine and update the Tug configurations considering the evolving Shuttle era technology, the total mission model, optimal operational modes, Shuttle/Tug/payload interfaces and economic considerations.

The major supporting technology programs should include (1) wind tunnel testing of aerobraking configuration options, (2) investigation of alternative aerobraking kit concepts, (3) further investigation of navigation errors and correction techniques to define guidance laws and targeting, and (4) further identification of potential atmospheric anomalies.

2.1 SUMMARY OF TECHNICAL STUDY RESULTS

The primary approach for this study was to determine the round trip payload capability as a function of the return trip time (number of aerobraking passes) for each of six specified aerobraking adaptations (prior Figures 1.1.0.0-3 and -4) to a baseline Space Tug configuration (prior Figure 1.1.0.0-2). A range of trajectory return times from 0.4 of a day to 11 days (2 to 60 passes) was analyzed. The impact of the various return times were related in terms of the weight of the additional structures, materials, subsystems and expendables required for thermal protection, increased drag, aerodynamic stability, guidance, control, and payload protection. The following subsections summarize the results of the technical studies conducted.

2.1.1 Aerodynamics Analysis

The aerodynamics analysis was conducted to provide the required drag data for trajectory analysis, static stability data for control analysis and aerodynamic loading data for structural analysis. Drag data were developed for each of the six configurations over the continuum, slip flow and free molecular flow regions. The velocities encountered by the aerobraking Tug will range from 20,000 to 35,000 feet per second. As shown in Figures 2.1.1.0-1 and -2, the drag coefficients (at perigee) varied from 1.3 for the basic (no flare) Tug to 44.5 for the large nose flare. At the higher altitudes, the drag coefficients varied from 2.75 to 3.5 for the basic Tug to 59 for the nose flare Tug. The wide range of drag coefficients investigated provided greater than an order of magnitude change in the ballistic

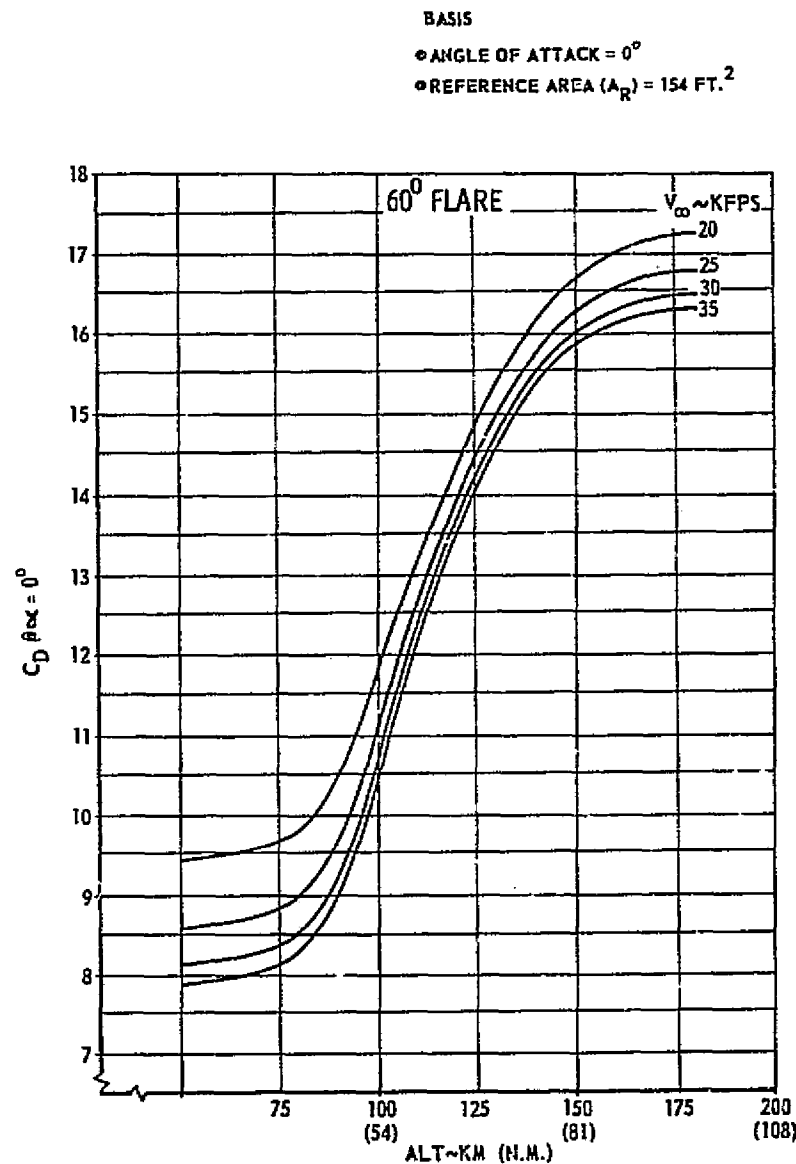
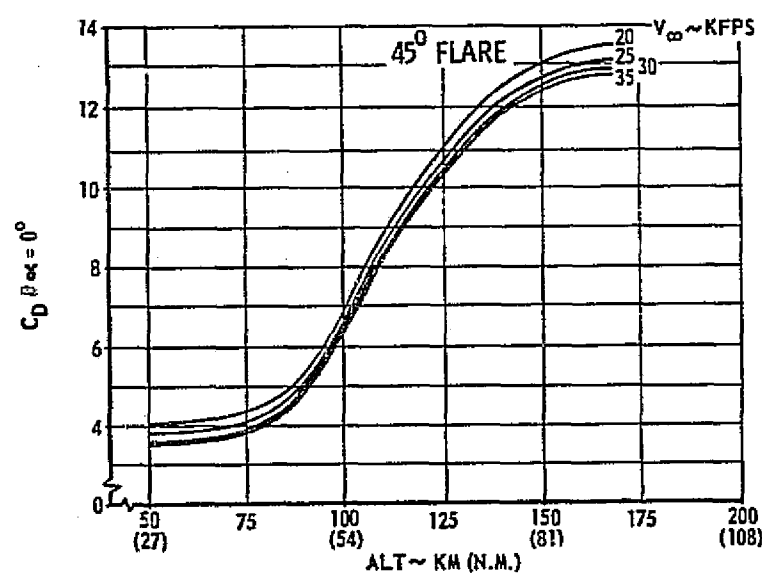
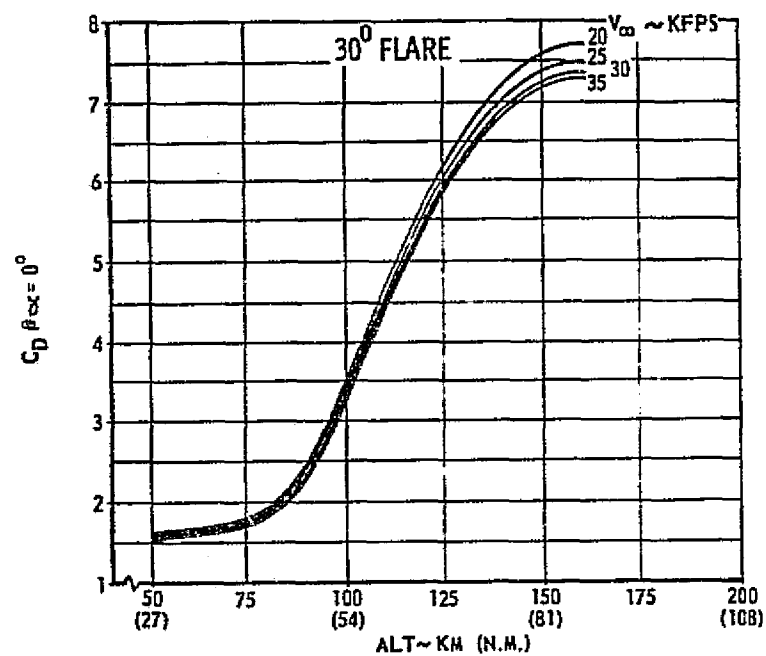


FIGURE 2.1.1.0-1: DRAG COEFFICIENTS (30°, 45° and 60° FLARES)

2-6

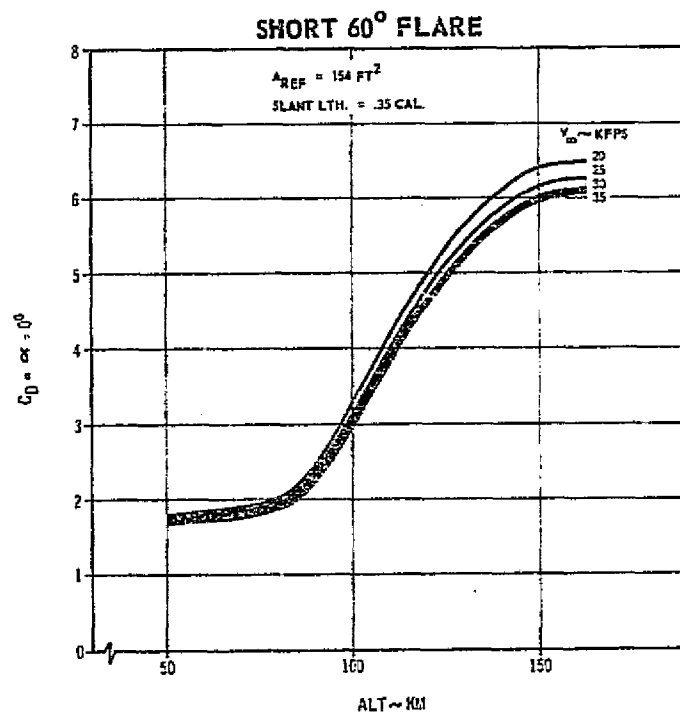
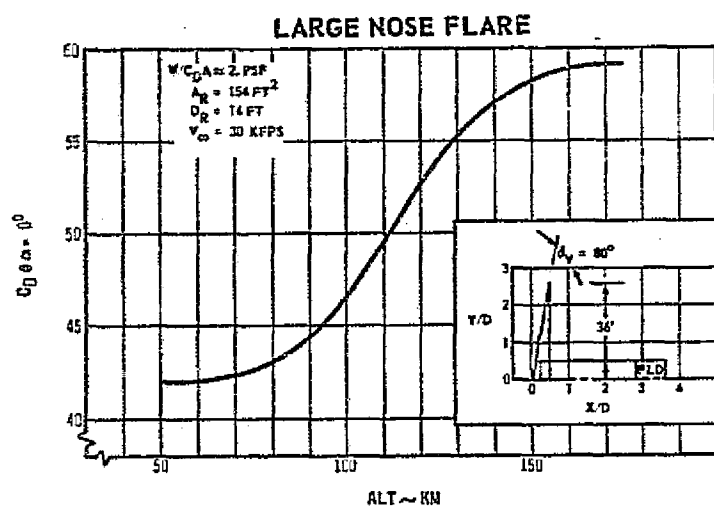
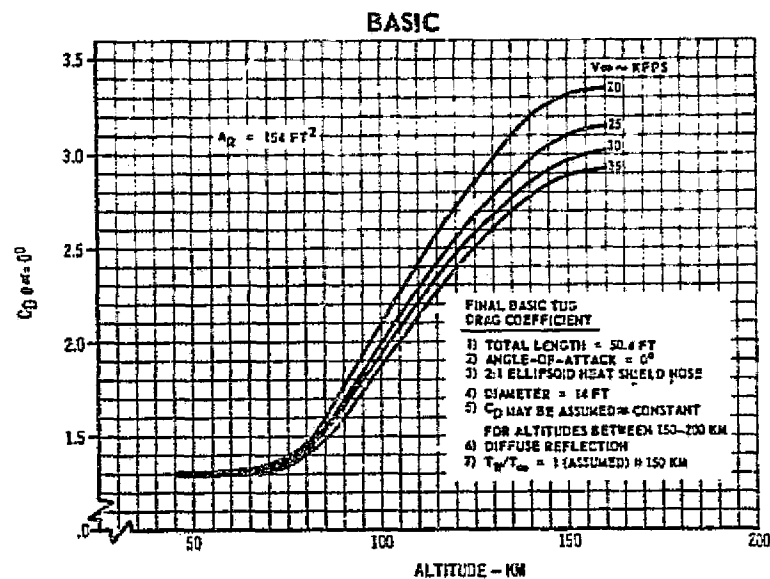


FIGURE 2.1.1.0-2: DRAG COEFFICIENTS (BASIC, SHORT 60° FLARE AND LARGE NOSE FLARE)

D5-17142

2.1.1 (Continued)

coefficient (from approximately 72 for the no flare configuration to approximately 2 for the large nose flare configuration). Thus, a significant change in configuration could be assessed as to its impact on control, thermal, astronics and structural requirements and upon performance and payload capabilities.

The center of pressure and normal force coefficients were determined as a function of altitude and velocity. These data were used for defining the control requirements. At perigee, the basic (no flare) and the short 60° flared Tugs have their centers of pressure located forward of their centers of gravity and therefore are aerodynamically unstable. To offset this instability, the reaction control system will be required to provide a controlling moment. The 30°, 45° and 60° and large nose flared configurations have their centers of pressure located either at the center of gravity or further aft and therefore are stable. The coefficients of normal force were defined over the same altitude and velocity range as the drag coefficients and were used to define the aerodynamic moments of each of the configurations.

The 30° flare is statically stable at 11.25 feet and offers slight improvement in its drag coefficient over the basic Tug. The 45° and 60° flares achieve static stability at approximately the same flare slant length (approximately 9 feet). At flare angles under 45°, the flare slant length required for stability increases rapidly.

The local pressure coefficients were defined for each of the six configurations. These data were then used to determine the local pressure loads at the nose, sidewall and, where applicable, on the flares. The data show an order of magnitude drop in pressure from the heat shield nose to the sidewall. The flare configurations had lower loads than the basic (no flare) configuration and increasing loads with flare angle. Increasing the mission duration, decreased the pressure loads. The basic (no flare) configuration pressure loads were approximately one psi on the heat shield for the two pass mission and decreased to approximately .1 psi for a 60 pass mission. Similar data were developed for the remainder of the configurations.

The short 60° flare (4.9' slant height) has approximately the same drag characteristics as the 30° flare but because of its short length, the configuration is statically unstable. The 60° flare, however, provides a much larger drag coefficient increase over basic flare than the 45° flare does (approximately $C_D = 6.6$ for the 60° flare versus approximately $C_D = 1.9$ for the 45° flare) for the same flare slant height of 14 feet.

2.1.1.1 Aerodynamics Conclusions

- o The basic (no flare) and short 60° flared Tugs have their centers of pressure located forward of their centers of gravity and are unstable. The other flared configurations have their centers of pressure equal to or aft of their centers of gravity and are stable.
- o The pressure loads on the basic (no flare) Tug decrease an order of magnitude from the nose of the heat shield to the cylindrical skirt joint and decrease another near order of magnitude down the length of the Tug.
- o The pressure loads at the end of the steep flare are comparable to the heat shield nose loads and significantly impact the weight of the flare.

2.1.2 Configurations

The prior Figures 1.1.0.0-2, -3 and -4 showed the conventional trajectory Tug configuration and the six aerobraking Tug configurations. The externally mounted aerobraking kits required to modify the conventional to the aerobraking trajectory configurations consist of (1) an aft heat shield, (2) sidewall insulation, (3) a flare (as applicable), and (4) a payload/flare adapter. With these kits installed, the aerobraked Tug will fit within the 15 x 60 feet Shuttle cargo bay. In addition, the reaction control system and the astronics module are impacted. These impacts are discussed in Section 2.1.4 and 2.1.6, respectively.

Aft Heat Shields

Figure 2.1.2.0-1 shows the 2:1 ellipsoidal radiative aft heat shield concept which was designed to provide protection for the aft end of vehicle. It is used on the basic (no flare) configuration, and on the 30°, 45°, short 60° and 60° flared configurations for mission durations of 5-60 passes. The removable cap and its actuation system are also used on the large nose flare for the 2 pass mission. The aft heat shield is composed of a fixed dome section (mounted to the aft skirt of the propulsion module) and a removable cap. The removable cap is emplaced over the engine during the aerobraking phase and during transport of the Tug within the Shuttle's cargo bay. It is rotated outward during normal Tug operation to provide clearance for the main engine exhaust during the main engine burns. The cap is operated by an electric motor driving two gears and is latched and sealed while emplaced.

The ablative aft heat shield is used on the 2 pass basic (no flare) and short 60° flare Tugs. This ablative heat shield is composed of a solid dome (no removable cap). It is actuated similar to the radiative concept described above but the motor and gears are located on the sidewall.

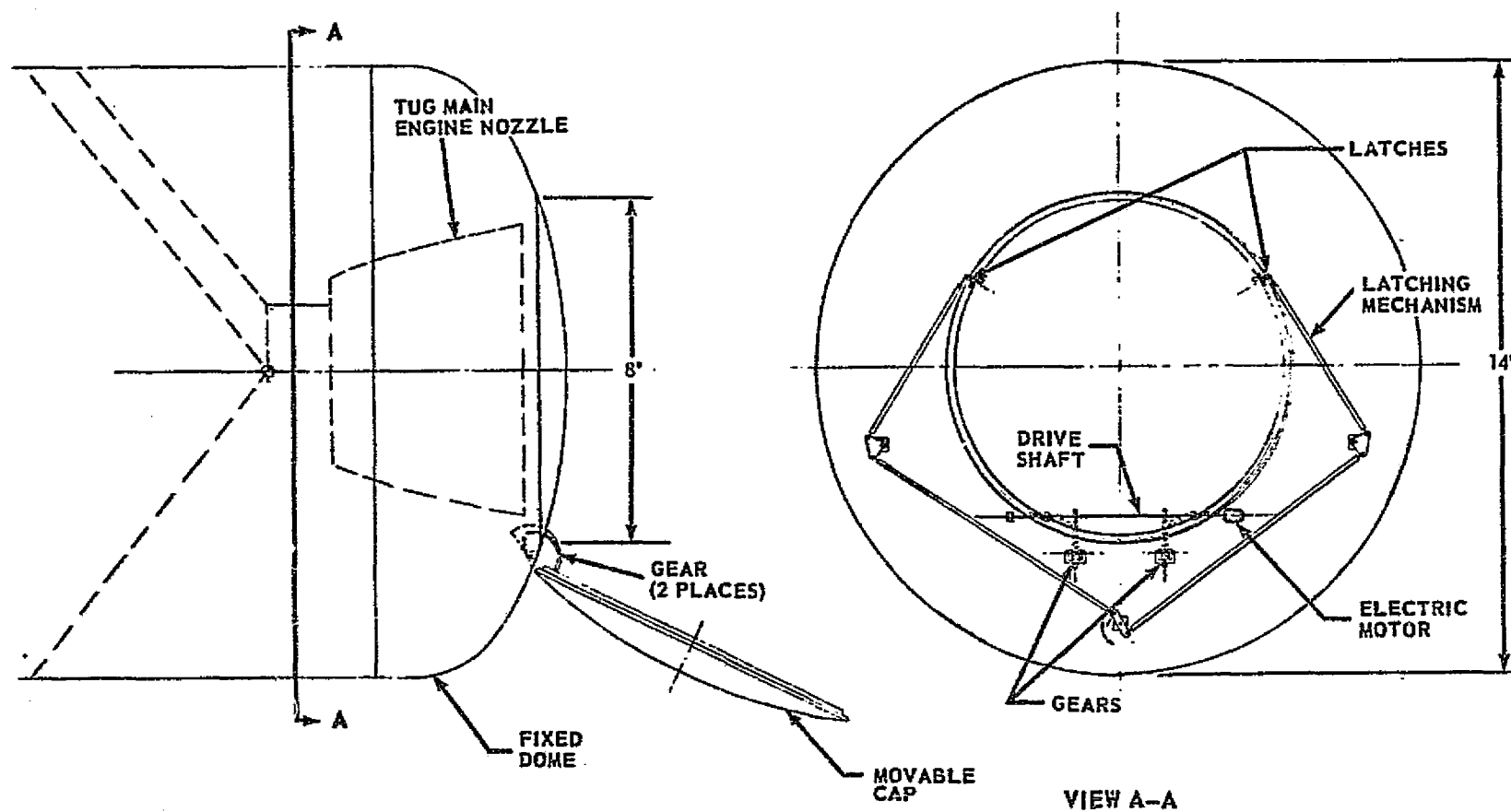


FIGURE 2.1.2.0-1: BASELINE RADIATIVE AFT HEAT SHIELD

2.1.2 (Continued)

Sidewall Insulation

The sidewall insulation covers the Tug's sidewalls (and payload adapter for the no flare and short 60° flare configurations). It is installed over the Tug's aluminum micrometeoroid shield and maintains a 400°F temperature limit at the micrometeoroid shield surface. The insulation consists of a microquartz insulation covered with a titanium or L-605 metallic outer foil.

Flare

The aerodynamic flare kit provides static stability and increased drag for the 30°, 45° and 60° flared configurations. The flare consists of an inconel frame and facing sheet with titanium support struts and a spring/cable actuation system (Figure 2.1.2.0-2). The flare is folded around the vehicle (total diameter approximately 14.5 feet) until after the deorbit burn from geosynchronous orbit. Prior to the first atmospheric passage, the flare is extended by spring hinges and is supported by the struts. After the last atmospheric passage, the cable system retracts the struts and collapses the flare against the Tug sidewall so that the Tug can fit within the Shuttle's cargo bay for return to earth.

The short 60° flare as shown in Figure 2.1.2.0-3 is similar to the larger 30°, 45° and 60° flares in that the same type of panel system is used and the same materials may be used. However, the short flare allows a simpler retraction/actuation system. This system uses threaded rods and followers to elevate the struts and flare. A reversible drive motor, a drive chain and 12 drive sprockets (one per support strut) are used to actuate the rods and followers.

The large flare as shown in Figure 2.1.2.0-4 is unique in that it is located forward of the reentry Tug and is combined with the heat shield into a continuous forward drag flare. The large panels present extremely difficult actuation/retraction problems when coupled with the desirability to fit the Tug with the folded flare into the Shuttle cargo bay. (Appendix F contains data on Light Weight Large Flare.)

Payload/Flare Adapter

The multipurpose integrated payload/flare adapter is used as a payload container, flare mounting fixture and a flare actuation system housing structure. It is an aluminum stiffened structure with a guide cone and guide tubes that assist with the payload docking operations and with payload holddown. The flared configurations have a flare actuation section located within the payload adapter for mounting the cable retraction system. The flare and the aluminum skin of the adapter provide the thermal protection for the payload. Both the basic (no flare) Tug and the short 60° flare Tug configurations have sidewall insulation and an insulated end cap to provide thermal protection for the payload.

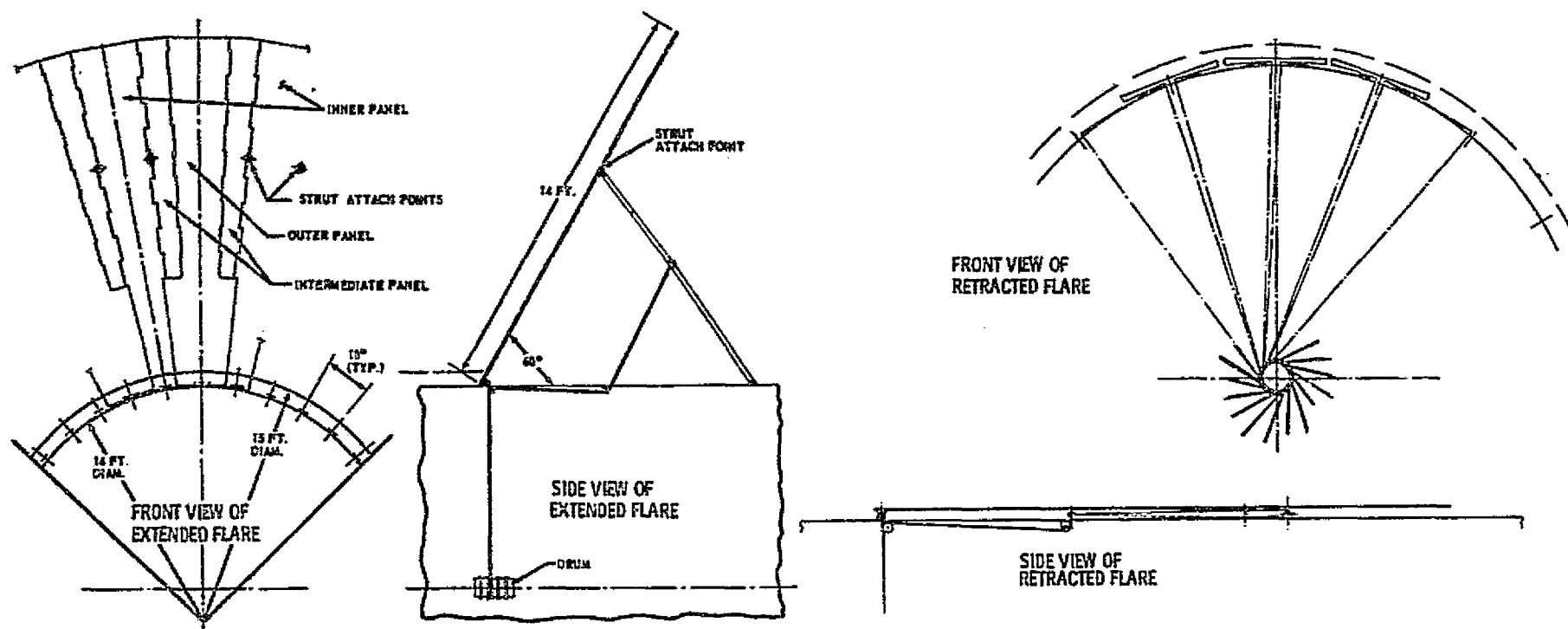


FIGURE 2.1.2.0-2: BASELINE FLARE CONCEPT (60° FLARE)

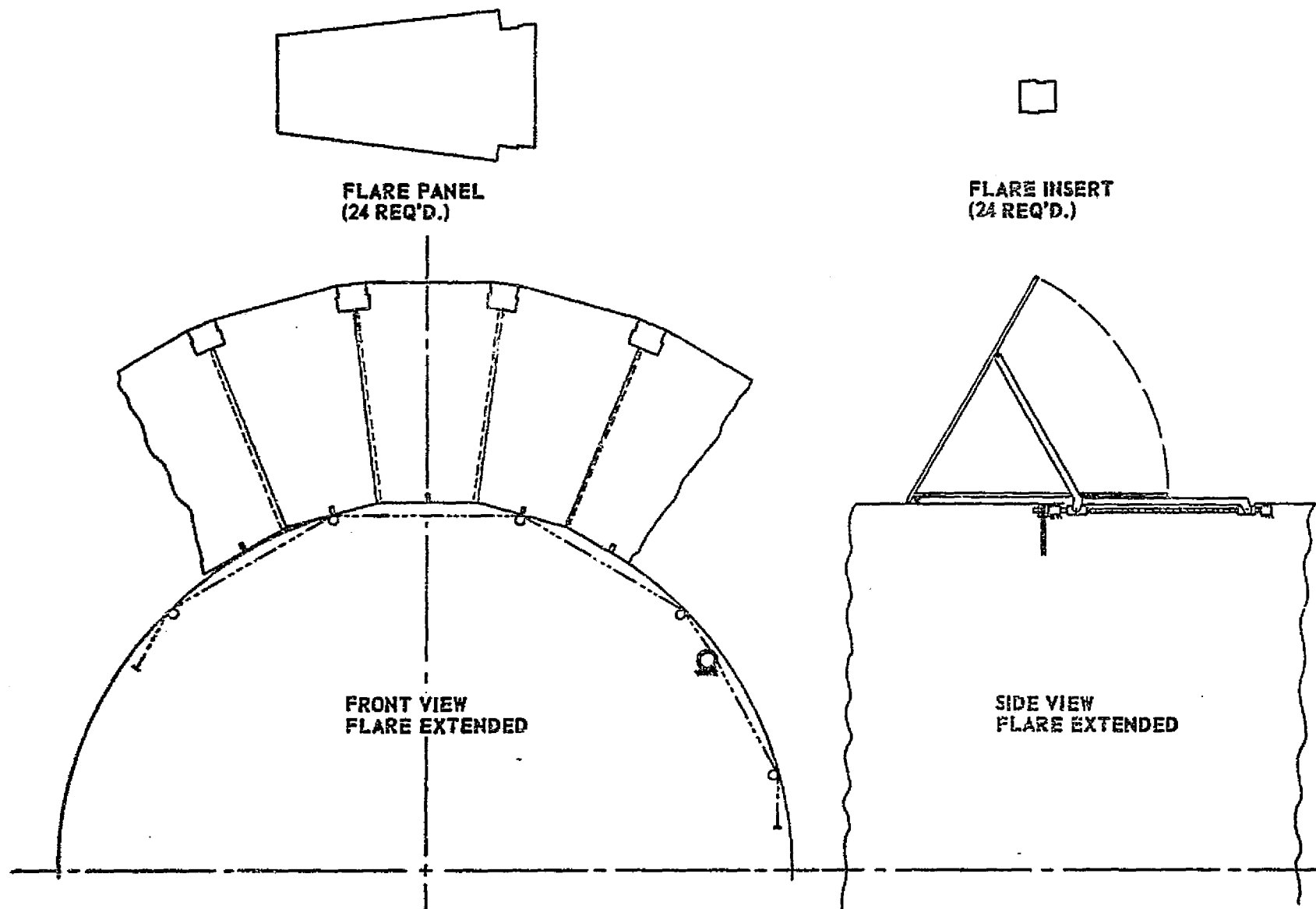


Figure 2.1.2.0-3: SHORT 60° FLARE CONCEPT

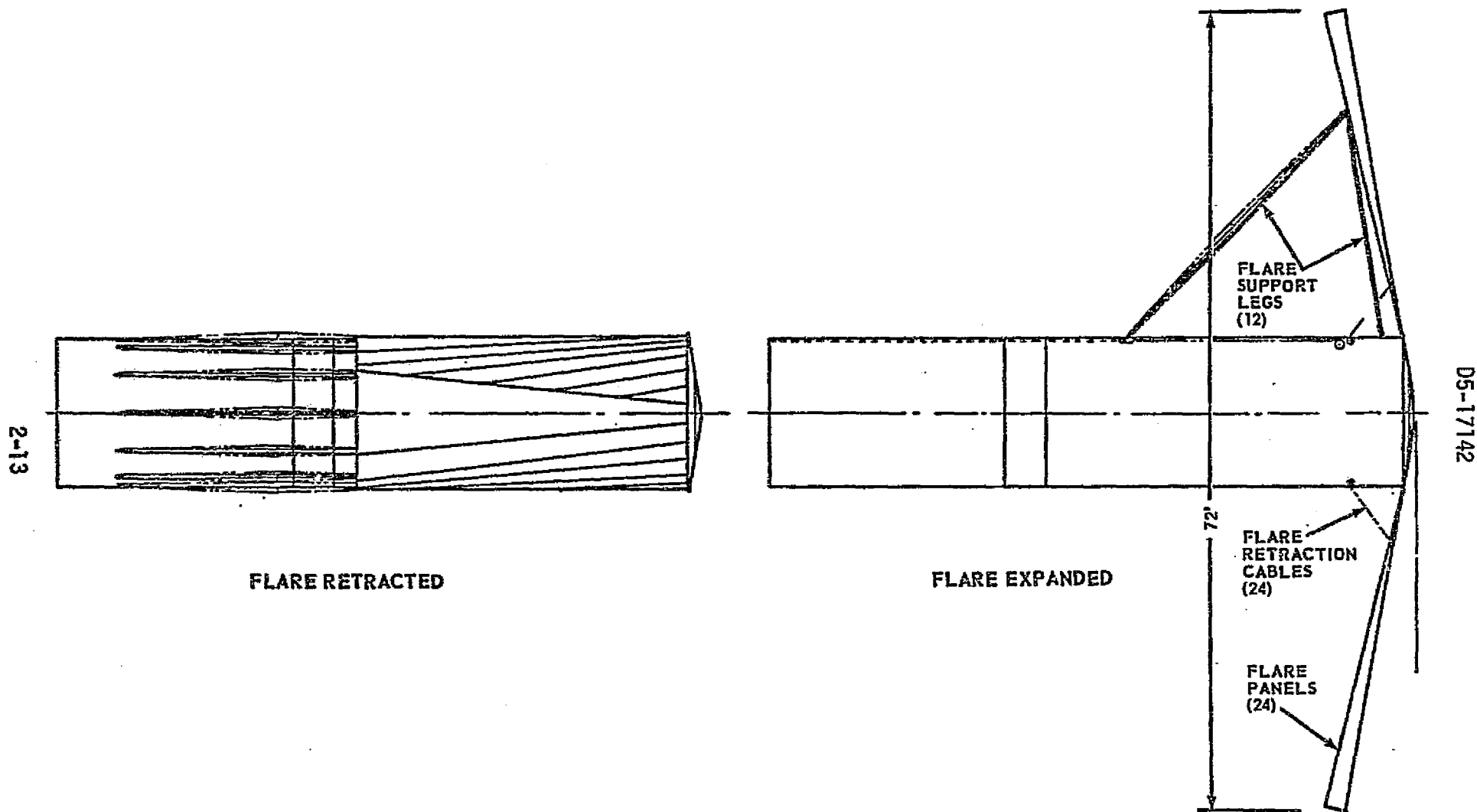


FIGURE 2.1.2.0-4: LARGE NOSE FLARE CONCEPT

2.1.2.1 Configuration Conclusions

- o The Tug's aerobraking kit can be designed to fit (while attached to the Tug) within the Shuttle's 15 x 60 feet cargo bay constraint.
- o Aft-end reentry is preferable to payload-end reentry because of the payload's greater sensitivity to environment. The highest temperatures occur at the reentry end of the vehicle. If the payload were at the reentry end, it would require a heavy complex protection system to accommodate variable length payloads.

2.1.3 Trajectory Analysis

For each of the configurations, trajectory analyses were conducted using the drag coefficient data developed in the aerodynamic analysis. The trajectory scheme used the conventional trajectory profile and delta velocity to leave the earth departure orbit and to achieve geosynchronous orbit. For the return trajectory, the Tug deorbits using an initial target perigee altitude selected for a desired mission return time. Subsequent passes lower apogee altitude significantly while reducing the perigee altitude slightly. When the desired circularization altitude is reached, an engine burn circularizes the orbit.

The return trip time is a direct function of the initial perigee altitude for any fixed ballistic coefficient (configuration weight including payload divided by the product of the configuration frontal area and drag coefficient: $W/C_D A$).

Figure 2.1.3.0-1 shows the relationship of trip time to initial perigee altitude for the various configurations. As shown in the figure, the initial perigee altitude may be higher for the flared configurations for accomplishing the missions in the same return time than that of the non-flared configurations because of the higher drag (lower $W/C_D A$) values obtained with the flared configurations. These higher perigee altitudes will result in lower temperatures and pressure loads than will be encountered with the basic (no flare) configuration.

The impact of atmospheric dispersion was defined for the basic (no flare) and 60° flare Tug configurations. Figure 2.1.3.0-2 presents the initial perigee altitude required for decay to a 270 NM orbit for the 1962 Standard Atmosphere and a constant High Density and constant Low Density Atmospheres. The solid curves of the figure are a result of re-isolation of the initial perigee altitude required to force the trajectory to a final apogee of 270 NM in the presence of the dispersed atmosphere. The data illustrates the range of entry times due to atmospheric dispersions if the vehicle flies an uncorrected trajectory. For example, the flight time of the basic Tug nominal 30 pass trajectory varies from 3.6 days (19 passes) for the more dense atmosphere to 9.6 days (53 passes) for the less dense atmosphere. This large range of potential entry time implies the need for a trajectory correction technique that will significantly reduce this range.

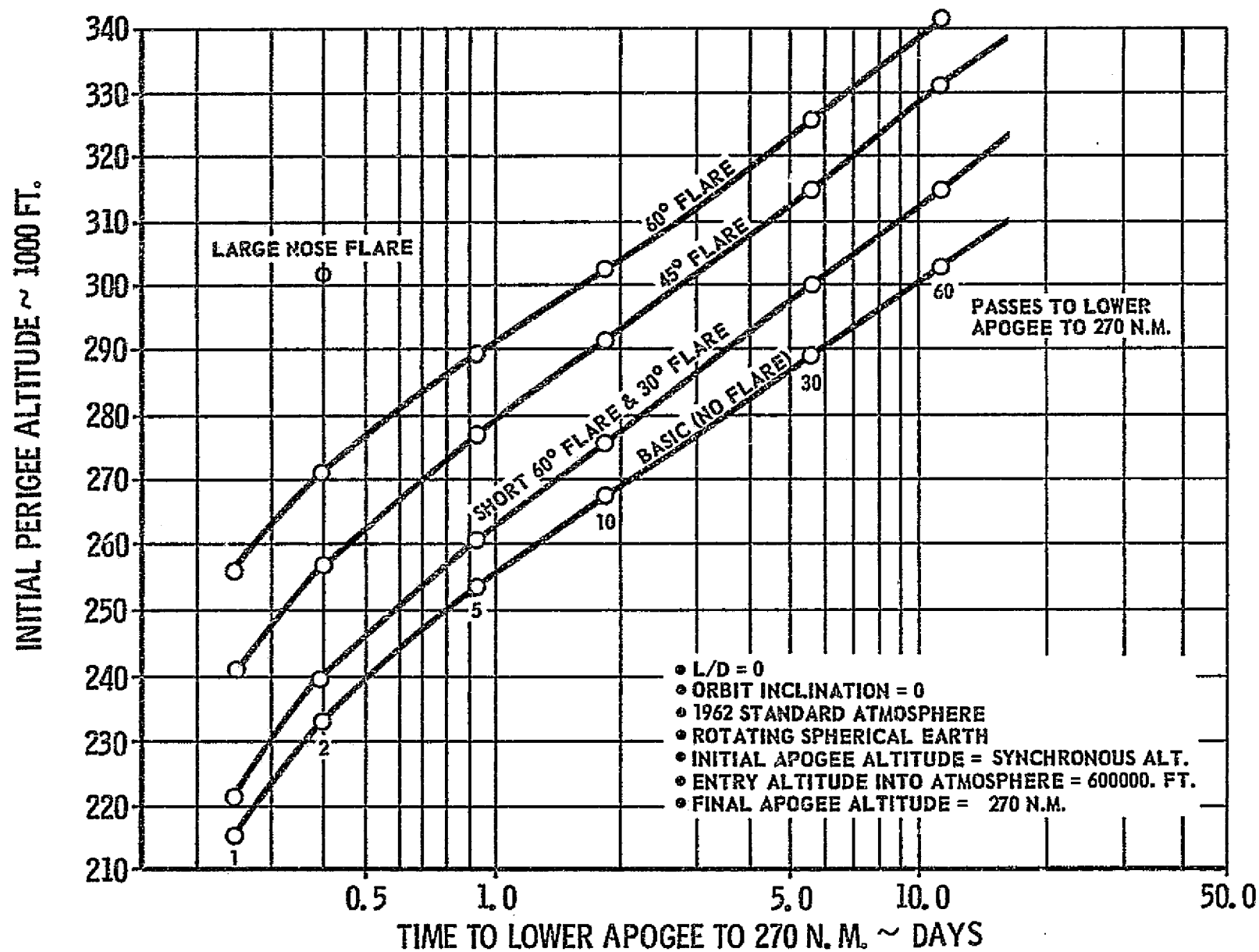


FIGURE 2.1.3.0-1: SPACE TUG AEROBRAKING RETURN TIME FROM SYNCHRONOUS ORBIT

2.1.3 (Continued)

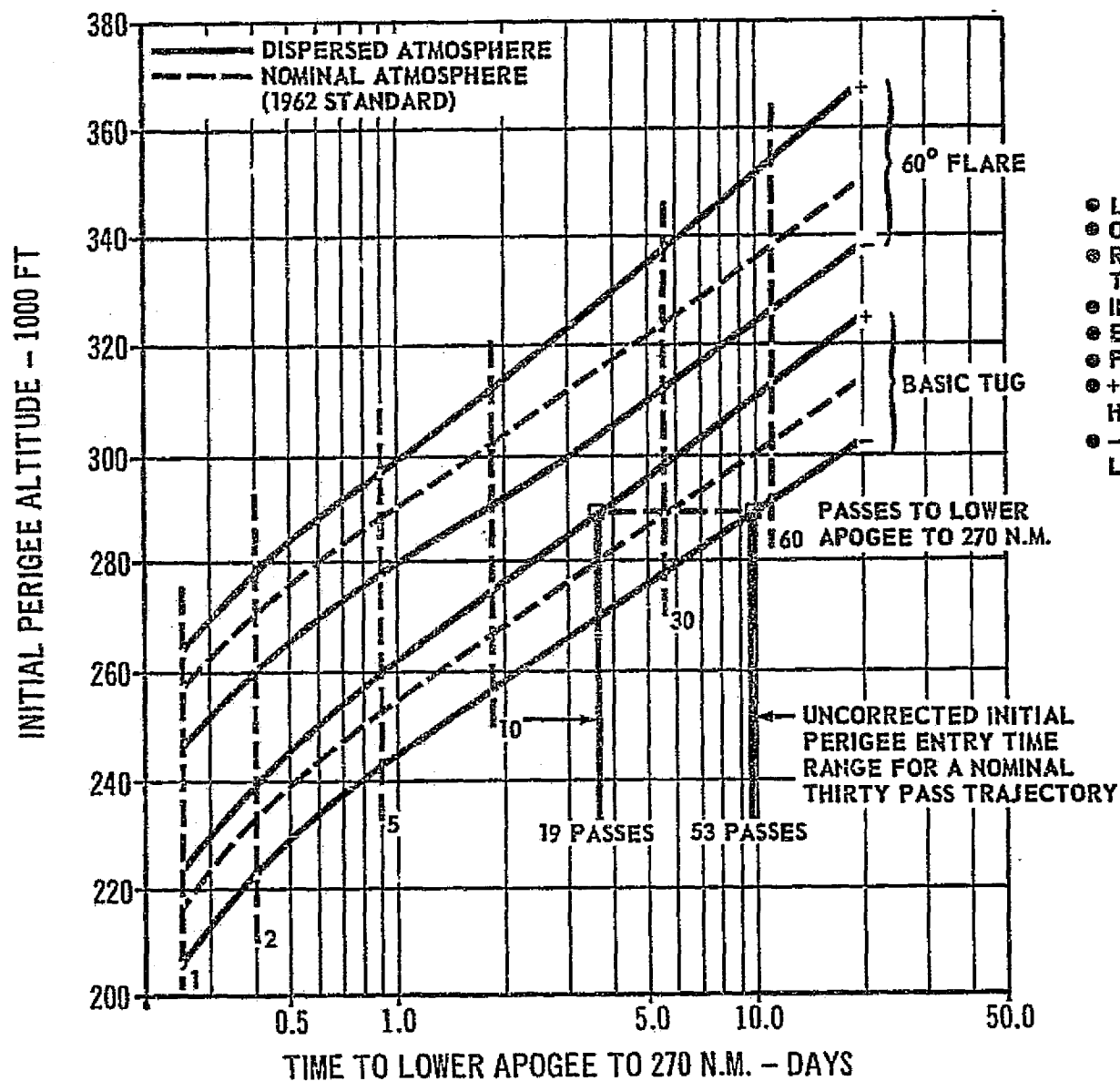
Several techniques were briefly investigated including: (1) impulse at the time of exit from the atmosphere and (2) impulse at apogee and (3) impulse at atmospheric re-entry. It appears that the impulse at atmospheric re-entry technique has greater payload potential as it may combine navigation correction with atmospheric dispersion correction, but this area should be studied in detail in a follow-on study for aerobraking guidance scheme analysis.

The atmospheric dispersion data used in Figure 2.1.3.0-2 to impact mission performance was developed by the NASA early in this study activity and represented a conservative estimate. Updated data for atmospheric dispersion versus time was developed by the NASA. This latter data when applied to the aerobraking analysis indicated that the dispersion effects would be considerably less pronounced (approximately half as severe) as that shown in Figure 2.1.3.0-2.

The impact of lunar, solar and earth harmonic perturbations on the aerobraked Tug trajectory was assessed. Variable initial perigee altitudes will be required for the perturbed environment versus the initial perigee altitude computed using a spherical earth. These perturbations are (1) generally predictable, (2) operationally significant, and (3) have only minor impacts on the thermal, aerodynamic, and control results. The mission planning phase must account for these effects by considering the target perigee altitude to be selected and the phasing required for Shuttle/Tug rendezvous.

2.1.3.1 Trajectory Conclusions

- o The use of aerobraking can reduce the return delta velocity from 5700 to 8050 ft/sec.
- o For a specified mission duration, a lower ballistic coefficient (high drag with flare) will allow higher initial perigee altitudes which result in lower thermal environments and lower pressure loads.
- o The aerobraking Tug is in the sensible atmosphere (600,000 feet altitude) for approximately 3% of the time.
- o Near-constant trip times can be maintained in a dispersed atmosphere by small correction burns prior to each atmospheric passage (approximately 200 ft/sec. total for a 30 pass mission).
- o Lunar, solar, and earth harmonics perturbations require different initial perigees than for the spherical earth but do not significantly change the thermal, air load, and control parameters.



- $L/D = 0$
- ORBIT INCLINATION = 0
- ROTATING SPHERICAL ATMOSPHERE THAT IS INVARIANT WITH TIME
- INITIAL APOGEE ALT = SYNCH. ALT.
- ENTRY ALT. INTO ATMOSPHERE = 600K FT.
- FINAL APOGEE ALT. = 270 N.M.
- + SUMMER, HIGH SOLAR ACTIVITY
HIGHER DENSITY ATMOSPHERE
- - WINTER, LOW SOLAR ACTIVITY
LESS DENSE ATMOSPHERE

FIGURE 2.1.3.0-2: SPACE TUG AEROBRAKING RETURN FROM SYNCHRONOUS ORBIT
 (WITH DISPERSED ATMOSPHERE)

2.1.4 Control Analysis

The control analyses used the center of pressure data and the coefficient of normal force data developed in the aerodynamic studies plus the trajectory data to determine the Tug control requirements. These analyses were directed specifically to define the requirements during aerobraking considering (1) limit cycle requirement, (2) the aeromoment requirements, and (3) directional control requirements.

The requirements for stabilizing the Tug were defined assuming the maintenance of a $\pm 1^\circ$ angle of attack throughout the sensible atmosphere. The basic (no flare) Tug is not aerodynamically stable and required approximately 550 pounds more RCS fuel than the aerodynamically stable flared configurations. The short 60° flare is also unstable and requires approximately 200 pounds more RCS fuel to provide stability. The other flared Tug configurations are statically stable and therefore have significantly lower fuel requirements. Static stability only (no dynamic stability) was investigated.

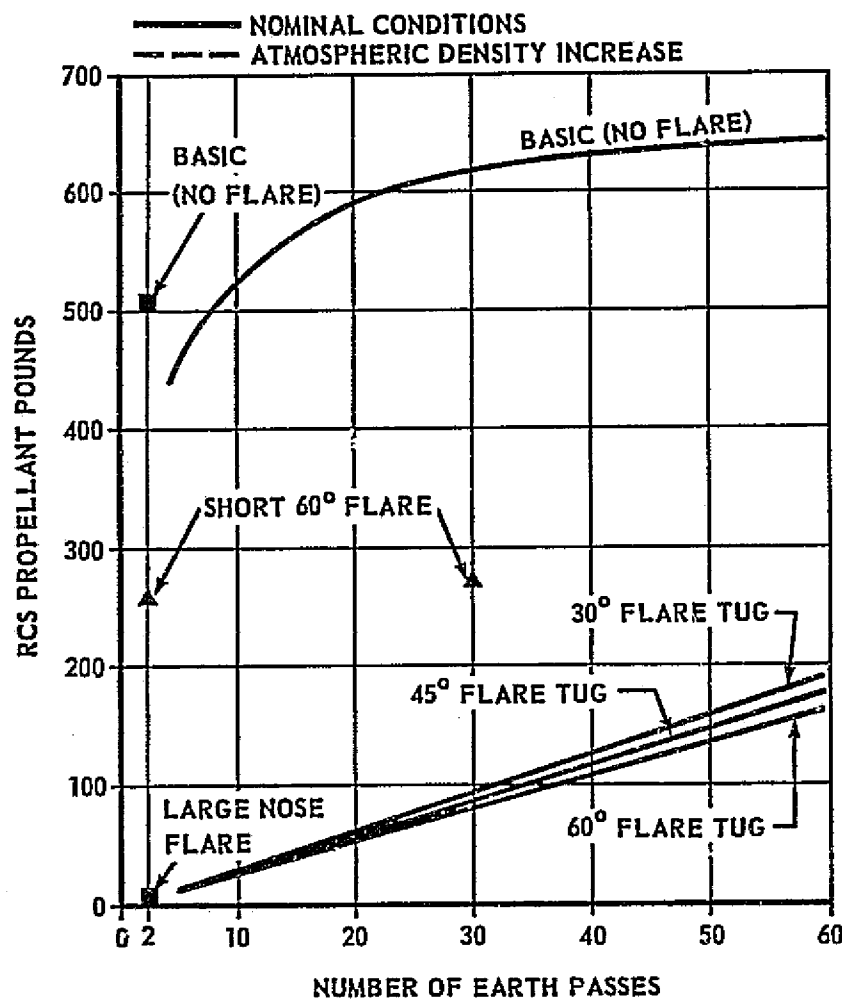
As shown in Figure 2.1.4.0-1, the control propellant requirements increase with mission duration. The RCS fuel requirements are significantly different for the basic Tug and short 60° flare Tug due to their aerodynamic instability. Fuel consumption are tabulated below for a 30 pass mission.

<u>Tug Configuration</u>	<u>RCS Fuel Consumption (Pounds)</u>
Basic (no flare)	620
Short 60° flare	271
30° flare	82
45° flare	80
60° flare	76

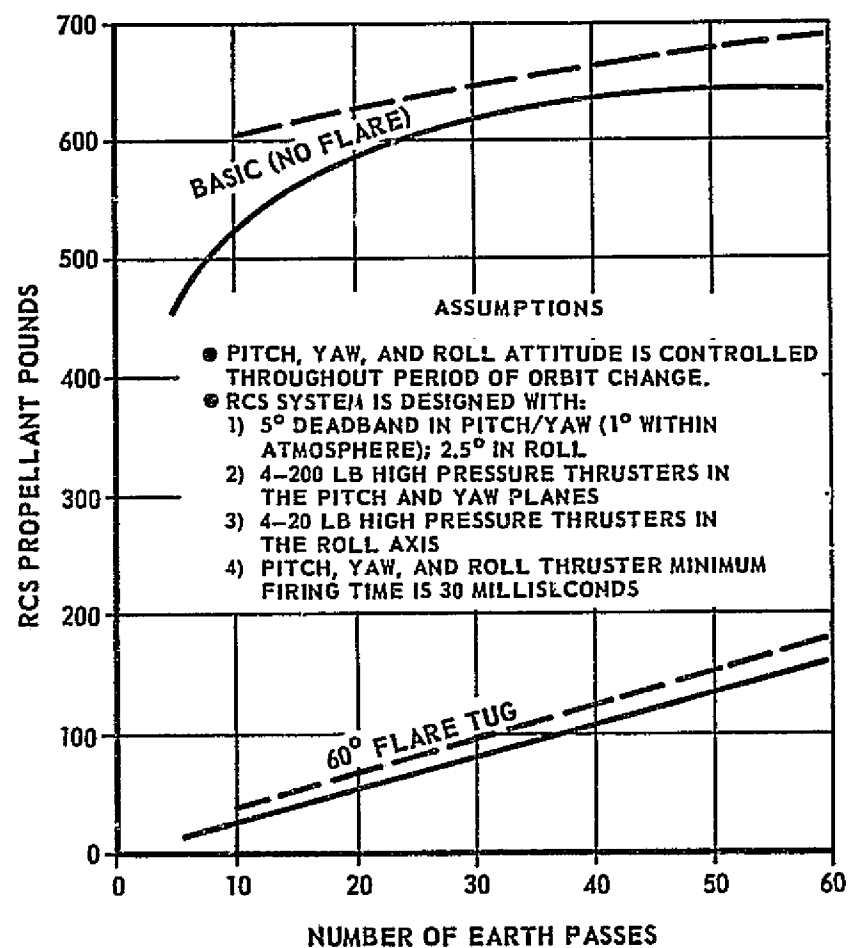
The impact of atmospheric dispersions was assessed for both the basic (no flare) and 60° flared Tugs. The flared Tug requires approximately 15 pounds more fuel and is relatively insensitive to mission duration. The basic (no flare) Tug is sensitive to mission duration and requires approximately 75 pounds additional fuel for a 10 pass mission, approximately 30 pounds additional fuel for a 30 pass mission and approximately 45 pounds additional fuel for a 60 pass mission.

2.1.4.1 Control Conclusions

- o The fuel consumption for the unstable basic Tug is approximately 550 pounds more than that required for the statically stable large flared configurations.
- o The short 60° flare provides some improvement in the static stability properties over the basic Tug. The RCS fuel requirements are 200 pounds more than the stable configurations.

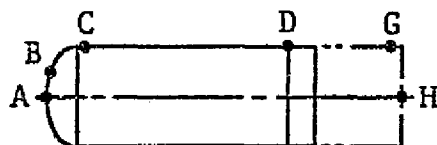


RCS PROPELLANT CONSUMED DURING
CHANGE OF ORBIT PERIOD



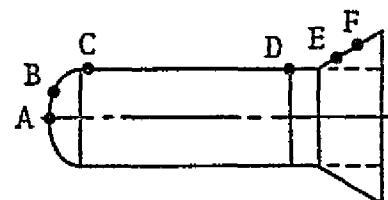
EFFECT OF ATMOSPHERIC DISPERSIONS ON
RCS PROPELLANT CONSUMPTION

FIGURE 2.1.4.0-1: RCS PROPELLANT CONSUMPTION



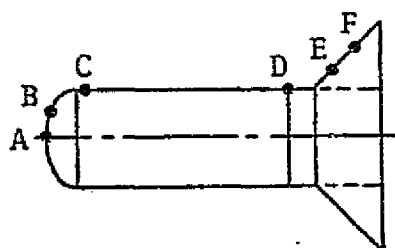
SPACE TUG BASIC CONFIGURATION

TRAJECTORY	MAXIMUM EQUILIBRIUM TEMPERATURES (°F)					
	A	B	C	D	G	H
5 PASS	3320	3175	1585	1120	975	682
10 PASS	2990	2860	1410	987	875	591
30 PASS	2540	2420	1166	797	720	451
60 PASS	2240	2140	1005	676	615	364



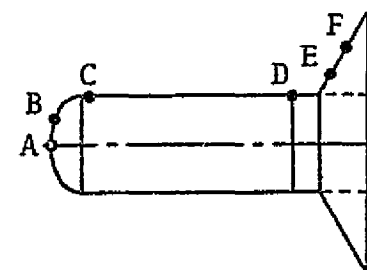
SPACE TUG 30° FLARE CONFIGURATION

TRAJECTORY	MAXIMUM EQUILIBRIUM TEMPERATURES (°F)					
	A	B	C	D	E	F
5 PASS	2940	2800	1382	1082	1272	1293
10 PASS	2630	2520	1215	943	1104	1124
30 PASS	2160	2060	957	753	850	869
60 PASS	1880	1790	809	605	706	729



SPACE TUG 45° FLARE CONFIGURATION

TRAJECTORY	MAXIMUM EQUILIBRIUM TEMPERATURES (°F)					
	A	B	C	D	E	F
5 PASS	2590	2480	1195	927	1037	1085
10 PASS	2309	2205	1040	800	874	919
30 PASS	1886	1798	812	608	635	680
60 PASS	1660	1580	691	507	513	558



SPACE TUG 60° FLARE CONFIGURATION

TRAJECTORY	MAXIMUM EQUILIBRIUM TEMPERATURES (°F)					
	A	B	C	D	E	F
5 PASS	2325	2220	1048	306	943	970
10 PASS	2080	1990	917	697	804	829
30 PASS	1740	1660	733	540	621	648
60 PASS	1512	1467	609	439	503	538

FIGURE 2.1.5.0-1 COMPARISON OF MAXIMUM EQUILIBRIUM TEMPERATURES

2.1.4.1 (Continued)

- o The reaction control system fuel consumption increases with mission duration.
- o To reduce the fuel consumption, it is desirable to have a tight deadband in the sensible atmosphere and then to widen the deadband in the free space environment.
- o Decreasing the minimum impulse time will decrease the fuel consumption (30 milliseconds is considered state-of-the-art).
- o The fuel consumption will increase by 10% to account for the atmospheric dispersions.

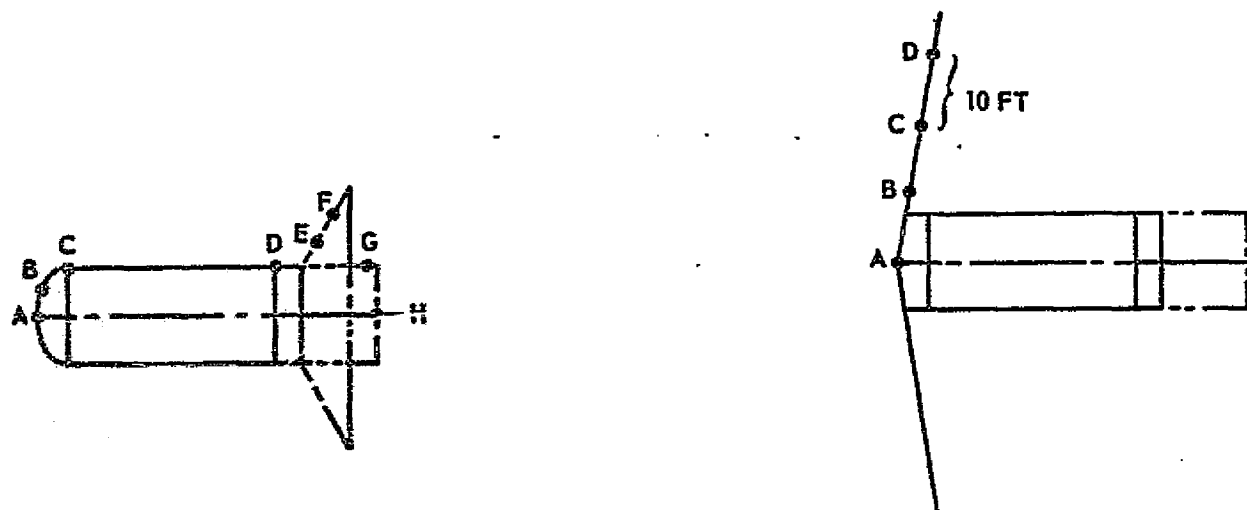
2.1.5 Thermal Analysis

Figure 2.1.5.0-1 shows the maximum equilibrium temperatures, at various points on each of four configurations, as a function of the number of passes required for return. These data were developed assuming thin metallic radiative surfaces. As shown, the maximum temperature decreases with increasing number of passes for the return mission. The maximum temperature for each configuration exists at the stagnation point of the aft heat shield.

Note: The temperatures shown are the surface temperatures of thin films. The effect of heat sink was considered for only (see Section 4.5) the basic configuration. The heat sink effects could reduce the stagnation temperature approximately 300°F for a 30 pass mission if a hot structure is used for the aft heat shield. Because of the anticipated thicknesses of the micrometeoroid shielding and flare material, the temperature of the Tug sidewall and flare will approach the thin film temperatures shown.

Figure 2.5.1.0-2 lists the maximum temperatures encountered on the aerobraking Tug configurations investigated in the add-on activity. The two pass basic Tug and the two pass short 60° flare Tug used ablative heat shields. The 30 pass short 60° flare Tug and the large flared Tug configurations used radiative heat shields and radiative heat shield/flares, respectively. The basic Tug and the short 60° flare Tug configurations will require a TPS for the payload adapter as the temperatures exceed the 300°F payload temperature limit.

Peak heating rates always occur with the first pass and determines the maximum equilibrium temperature. The basic Tug's heating rate is approximately four times greater than the 60° flared Tug. The last pass has lower heating rates but for longer time periods and therefore impacts the insulation requirements. The time in the heating environment is approximately 220 seconds for the first pass and will increase to approximately 800 seconds for the last pass of a 30 pass mission. The heating durations (i.e., time in atmosphere) are relatively insensitive to configuration.



CONFIGURATION	TRAJECTORY	MAXIMUM EQUILIBRIUM TEMPERATURE ($^{\circ}\text{F}$)							
		A	B	C	D	E	F	G	H
BASIC (NO FLARE)	2-PASS	3680	3520	1789	1275	—	—	1170	779
SHORT 60° FLARE	2-PASS	3290	3140	1570	1240	1490	1527	1138	758
SHORT 60° FLARE	30-PASS	2120	2070	980	748	856	889	687	458
LARGE NOSE FLARE	2-PASS	1410	1403	1380	1337	—	—	—	—

FIGURE 2.1.5.0-2: MAXIMUM EQUILIBRIUM TEMPERATURES

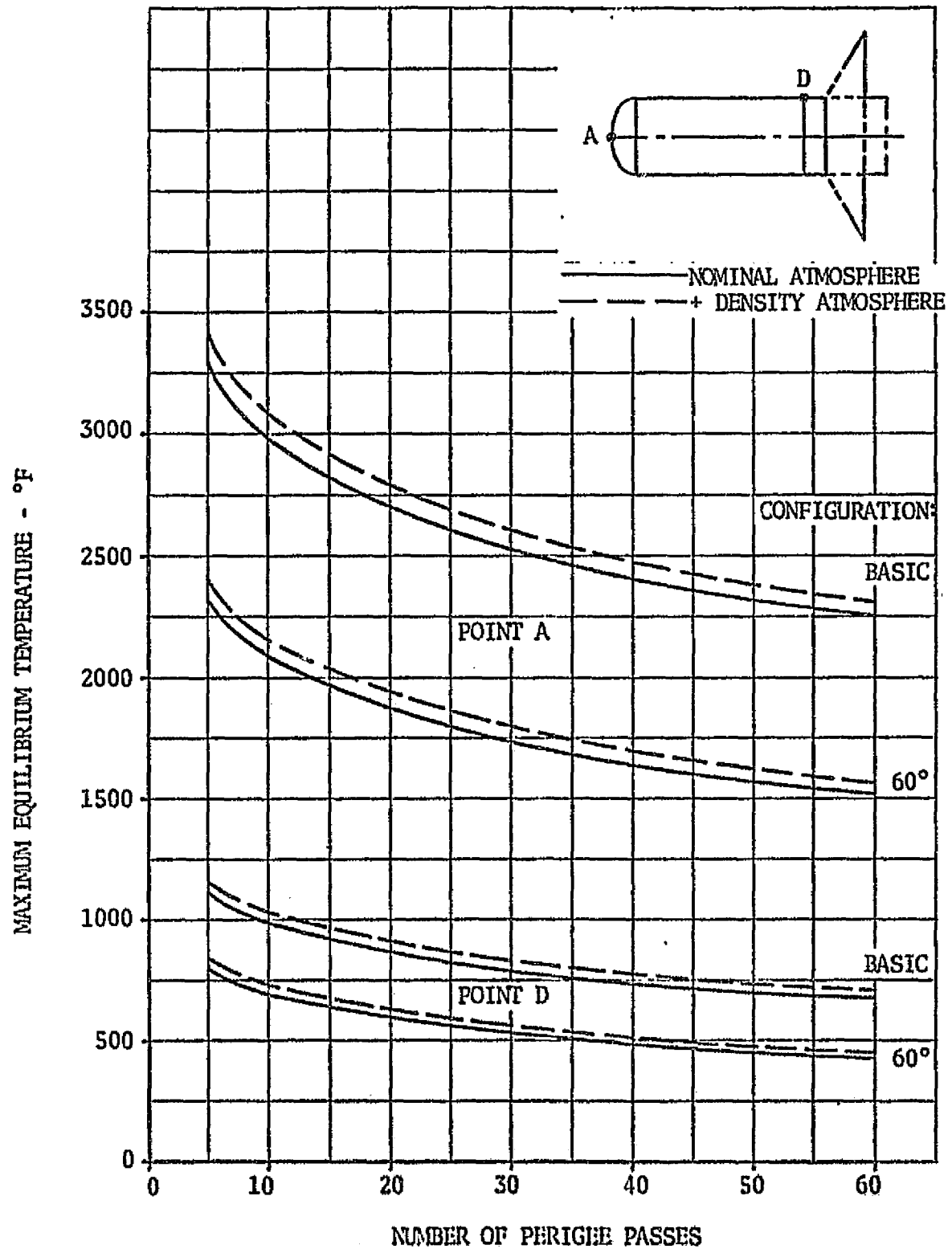


FIGURE 2.1.5.0-3 MAXIMUM EQUILIBRIUM TEMPERATURES FOR BASIC AND 60° FLARE CONFIGURATIONS - NOMINAL AND (+) DENSITY ATMOSPHERE

2.1.5 (Continued)

Similar data was developed for the two pass configurations studied in the add-on activity. The heating rates follow the same trends as shown above. However, the short duration results in considerably higher heating rates for the basic (no flare) Tug-123 BTU/ft²/sec. (first pass of two pass mission) versus 63 BTU/ft²/sec. (first pass of ten pass mission). With the use of the flare, the initial re-entry altitude is higher and therefore lower heating rates are encountered.

Figure 2.1.5.0-3 illustrates the effect of atmospheric dispersions on the basic (no flare) and the 60° flare Tug. Only a minor increase in temperature occurs on the heat shield (approximately 70°F) with the "worst case" atmosphere.

2.1.5.1 Thermal Conclusions

- o Maximum equilibrium temperatures occur on the first pass of the mission and determine the radiative material temperature requirements.
- o Insulation requirements are determined by the last passes of a mission where total heat input is maximum.
- o The flared configurations have lower maximum equilibrium temperatures than does the basic (no flare) configuration (for equal mission durations).
- o Maximum equilibrium temperatures decrease rapidly by increasing the mission duration from 5 to 20 passes. Temperatures decrease at a lesser rate beyond 20 passes.
- o The temperatures on the sidewalls and on the flares are approximately 25-50% of those on the heat shield nose.
- o The constant High Density Atmosphere increases:
 - The maximum heat shield temperatures less than 100°F
 - The maximum flare temperatures by less than 50°F
 - The sidewall insulation weights less than 25 pounds
 - The number of passes by 4 or 5 to maintain temperatures at the level of the Standard Atmosphere.

2.1.6 Astrionics Analysis

The astrionics systems analysis was conducted by the IBM Corporation for The Boeing Company. The astrionics study investigated navigation accuracy analysis, astrionics system configuration, redundancy analysis, weight impact, radiation impact and new technology and follow-on study effort.

2.1.6 (Continued)

The navigation analysis was performed to determine the navigation sensors required for the aerobraking mission and to define the navigation accuracies obtained with these sensor combinations. The IMU, star tracker, landmark tracker, horizon sensor and laser radar were selected as the required navigation sensors. It was determined that the same complement of hardware was required for all aerobraking mission durations, and that only redundant hardware would be added to achieve reliability.

The results of the navigation analysis indicated that the navigation perigee uncertainties were rather insensitive to configurations (no flare or flared Tug). A summary of the perigee uncertainty for the basic configuration is shown in Figure 2.1.6.0-1. This figure shows that the maximum 1σ errors expected for the first pass of 2 to 15 day missions are less than .35 nm and the steady state values are in the order of 0.05 nm. It should also be noted that the navigation perigee uncertainties are generally smaller for the longer duration mission because of the decreased atmospheric perturbations.

Figure 2.1.6.0-2 illustrates the navigation update history. The horizon sensor is used for the high altitude navigation accuracy estimates. At lower altitudes (under 4000 n.m.), the effective operating range of the landmark tracker is reached and this more accurate sensor is used for navigation updates (1800 to 500 seconds before perigee; 300-500 to 1700 seconds after perigee). The star tracker is used to provide attitude update for correction of the platform drift of the IMU system and to improve navigation update accuracy. After the aerobraked Tug has passed through perigee, the Kalman filter is re-initialized because the vehicle has attained a new orbit. Landmark tracker updates after filter re-initialization reduces the post-perigee navigation uncertainties to under one mile (3 sigma).

Figure 2.1.6.0-3 illustrates the position error, delta RCS fuel consumption and delta velocity corrections as functions of first pass correction burn time prior to perigee. The unshaded top portion of the figure represents the perigee errors if a correction burn is made based on relatively limited information (e.g., after horizon sensor updates). A burn at this time would result in a perigee error greater than the expected error with no burn (data point on the border between the shaded and unshaded portions). The shaded bottom portion of the figure represents the perigee errors if a correction burn is based on the more accurate landmark tracker information. Correction burns made after at least 500 seconds of landmark tracking result in relatively small perigee errors.

The impacts of repeated passes through the Van Allen radiation belt for the aerobraking mission do not appear significant at this time. Assuming a vehicle skin thickness of approximately .090 inches of aluminum, no problems appear for times up to 10 days. The 15 day analysis indicates that care must be taken in the selection of silicon

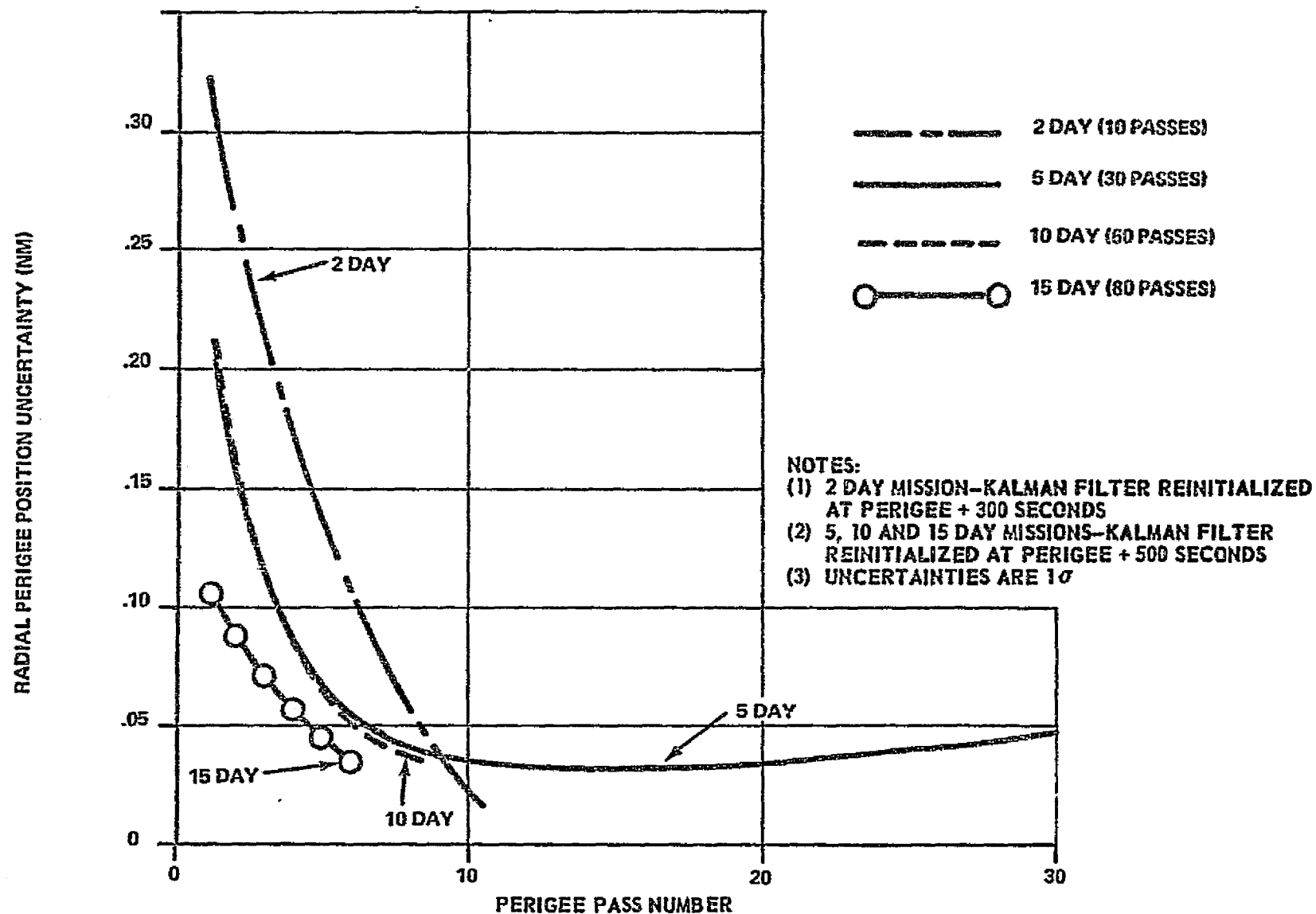


FIGURE 2.1.6.0-1: RADIAL PERIGEE POSITION UNCERTAINTIES (BASIC TUG CONFIGURATION)

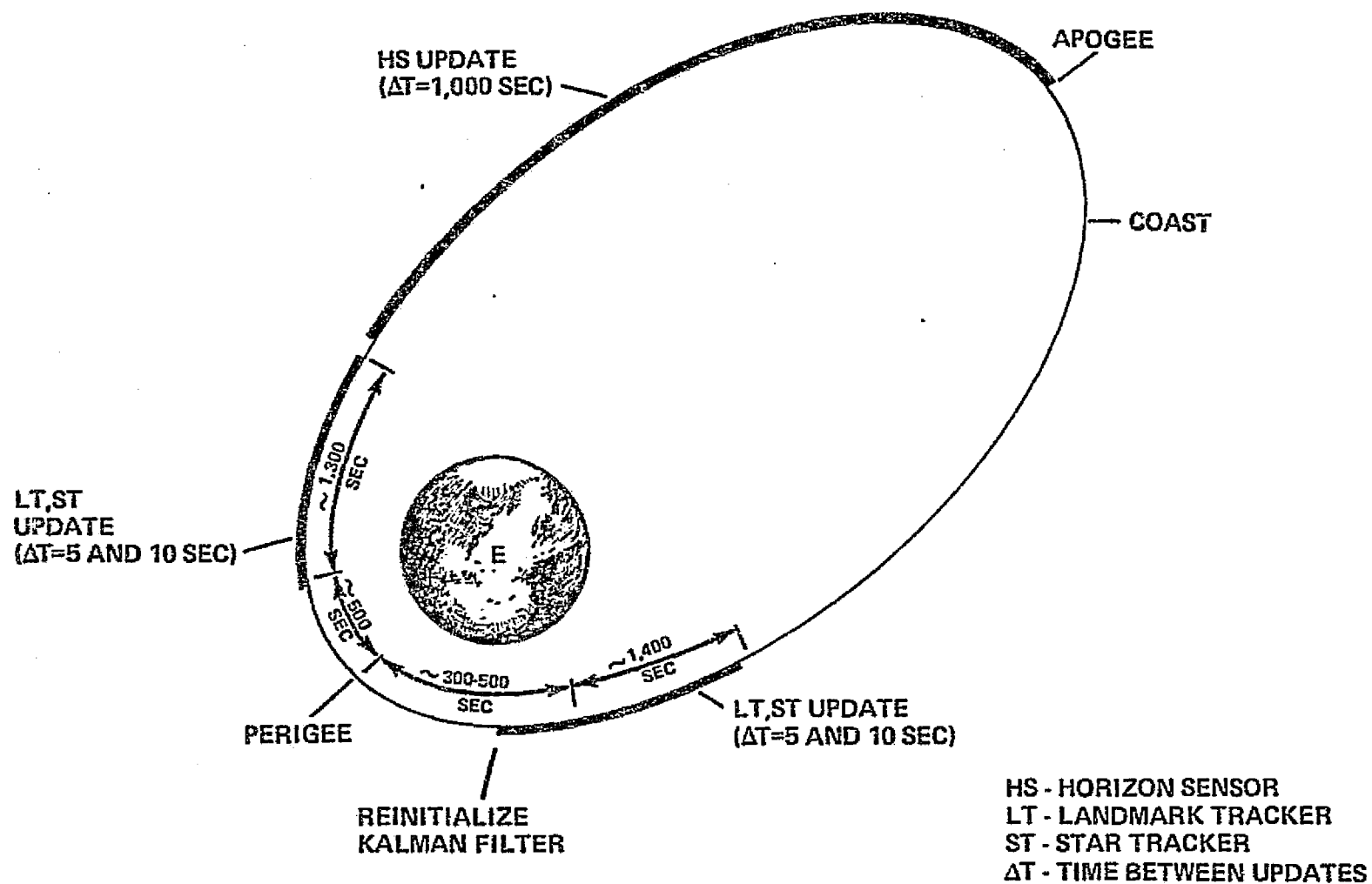


FIGURE 2.1.6.0-2. NAVIGATION UPDATE HISTORY

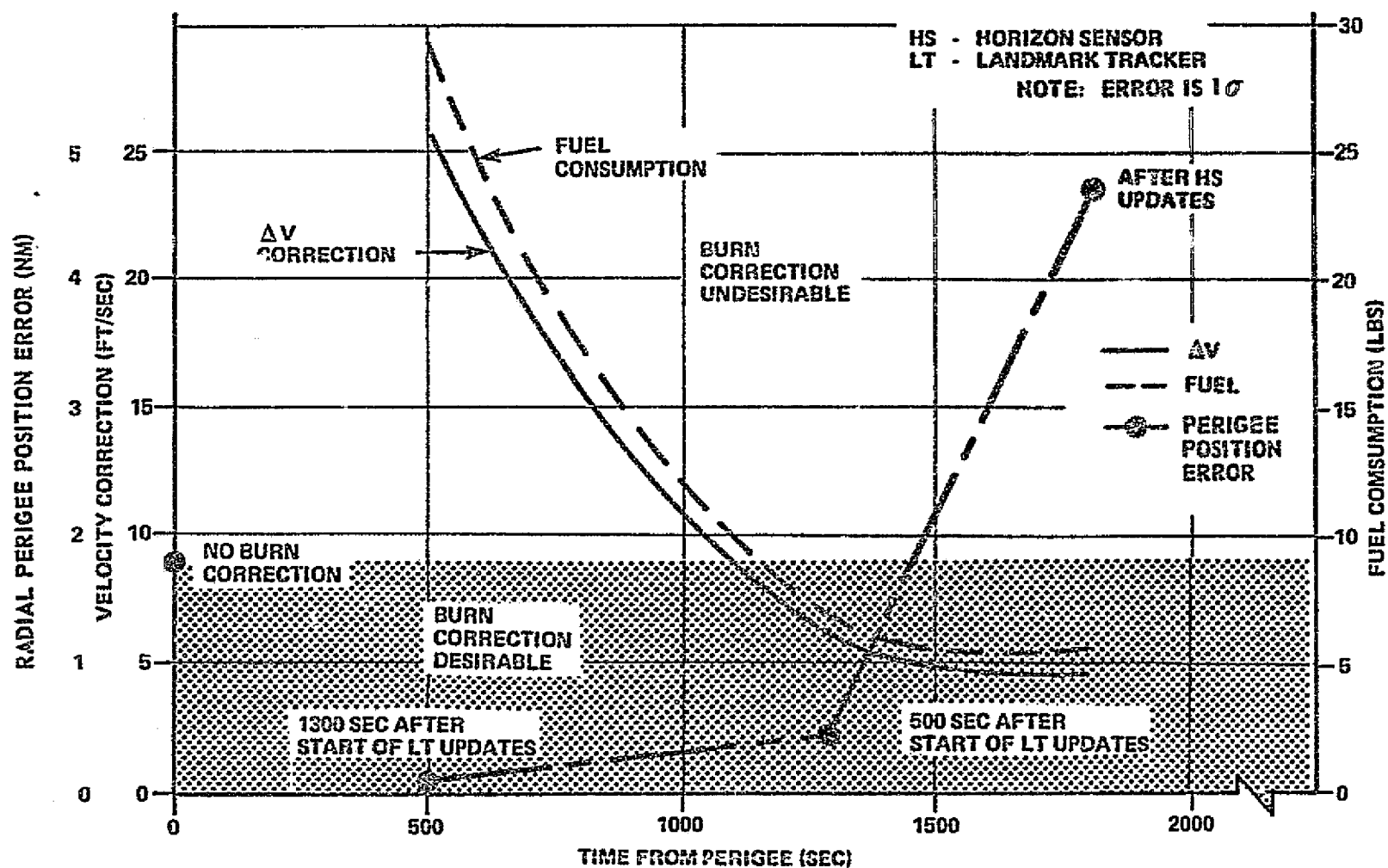


FIGURE 2.1.6.0-3: ORBITAL CORRECTION BURN, ΔV RCS FUEL CONSUMPTION, AND RADIAL PERIGEE POSITION ERROR

2.1.6 (Continued)

transistors in the electronics. Also, additional shielding, included as part of the component packaging, would decrease the effects of radiation.

The redundancy analysis indicated that additional components and hardware must be added to the basic astrionic system configuration as the mission time increases in order to maintain a 99% mission success probability.

In summary, power and redundancy provide the delta weight impacts required for aerobraking. The weight impacts of these items and the total weight deltas based on aerobraking mission time are summarized in Section 2.1.8, Figure 2.1.8.0-4.

2.1.6.1 Astrionics Conclusions

- o Autonomous navigation in synchronous orbit can limit navigation uncertainties to a RSS steady state accuracy of 5 n.m. (1σ) and 2 ft/sec. (1σ) using a horizon sensor (after 12 hours on orbit).
- o The perigee radial position uncertainties for the 5, 10 and 15 day missions are relatively insensitive to configuration. The perigee uncertainties for the two day mission are slightly higher for the basic (no flare) configuration.
- o The autonomous navigation configuration used for this study can limit radial perigee uncertainties to less than 0.35 n.m. (1σ) for initial passes and to the region of 0.05 n.m. (1σ) steady state.
- o Navigation updates after perigee and at higher altitudes are required to limit uncertainties during those periods and to prevent excessive perigee uncertainties on subsequent passes.
- o Minor midcourse corrections for navigation errors can reduce perigee position errors by an order of magnitude. These corrections should be based on the landmark tracker information.
- o Astrionics system weight increases as aerobraking mission duration increases. Therefore, minimum weight deltas are obtained by minimizing aerobraking mission time.
- o Additional reactant and tanks for electrical power (1-1/2 lbs/hr) and additional components to maintain acceptable astrionic system reliability are the prime contributors to weight increases to the astrionic system due to aerobraking.
- o The radiation impact increases as the aerobraking mission duration increases. Radiation impacts to electronics by the Van Allen radiation belt appear insignificant for missions of 10 days or less.

2.1.7 Materials

The aft heat shield and flare materials were selected to (1) withstand the maximum temperatures and pressure loads expected at a specific location on the vehicle and (2) have a minimum inert weight impact. The weights of the flares and aft shields shown in the succeeding Section 2.1.8 reflect the changes in materials selected as the environment varied. For the lower temperatures (500 to 1800°F) Titanium 6AL-4V, Inconel 718 and Rene' 41 were utilized. TD-nickel-chrome was used for the next higher temperature range (up to 2000°F). Temperatures (above 2000°F) as seen by the basic (no flare) configuration and by the short duration (5-10 pass) flared configurations' heat shields, require advanced state-of-the-art alloys such as Fansteels 85 and 60. For less than 5 passes, an ablative insulation over a titanium structure was used. The selected ablative was ESA-3560 IIA.

The Tug's sidewall insulation material is Johns Mansville microquartz. This insulation has a long life temperature capability to 2000°F (melting point 3000°F) and has a low density (3 pounds per cubic foot). The insulation thickness is varied as required to maintain the Tug's sidewall temperature at 400°F. To cover and protect this insulation material, a thin radiative sheet (0.002 inches) of L-605, a Haynes cobalt alloy (for higher sidewall temperatures) or titanium (for temperatures under 800°F) was used. The basic (no flare) or short 60° flare configurations' payload adapter also uses this same microquartz/titanium combination for thermal protection of the payload (300°F limit).

The payload/flare adapter is protected from the environment by the flare or by the payload insulation. Therefore, aluminum skin and structure is utilized for this adapter.

2.1.7.1 Material Conclusions

- o State-of-the-art radiative materials may be used for the long (~ 10 days) duration basic (no flare) configurations and for the medium (~ 3-4 days) duration flared Tug. Shorter mission durations will require advanced state-of-the-art radiative materials or the use of ablatives.
- o Ablatives are required for the one to four pass missions. They were not considered for longer multipass missions, (1) due to lack of data on the properties of the recycled ablative and (2) due to their high inert weight.
- o The aft heat shield will experience high temperatures which will cause unique problems in sealing and actuation.
- o Sidewall temperatures vary significantly down the length of the Tug. To minimize weight, a tapered insulation is desirable.

2.1.7.1 (Continued)

- o The temperatures experienced by the flares are such that metals are required except for long duration missions (above 10 days).

2.1.8 Weights

One of the key guidelines in the initial study activity was to maximize the payload capability by minimizing the weight penalty associated with performing the aerobraking operations. In the add-on study effort, mission duration was minimized and aerobraking kit weight was not considered the overriding guideline. For each of the selected configurations, the weights of the aerobraking components were determined as a function of number of passes. Figure 2.1.8.0-1 illustrates the weight of the radiative and ablative aft heat shield domes as functions of the number of passes for each of the configurations. The radiative dome materials were changed from tantalum to TD-nickel-chrome as the temperatures encountered decrease to 2000°F and lower. The impact of the atmospheric density on the weight of aerobraking components was computed for the basic (no flare) and 60° flare configurations. The atmospheric density had negligible effect in the maximum payload capability mission duration regions (25-35 passes).

For the two pass missions with the basic (no flare) and the 60° short flare Tugs, an ablative heat shield was required. The heat shield ablative was ESA-3560 IIA mounted atop a titanium support structure. Note: The use of ablatives resulted in high heat shield weights.

Similar type data was developed for the flare configurations and are shown in Figure 2.1.8.0-2. For each of the flare options, the flare weight was determined as a function of the number of passes. At approximately 30 passes, the material thickness reduces to where it will be necessary to maintain a minimum thickness for handling rather than that required for the pressure loads and thermal environments. The atmospheric density effects on inert weights are significant for low passes (5-10 passes), but are not significant in the maximum payload capability (25-35 pass) region.

The large nose flare is not shown in the figure as it is a unique concept which integrates the heat shield and flare into a composite structure. This concept employs a very large flare (72') diameter as compared to the other flares. The weight of this flare resulted in zero payload. (See Appendix F for Light Weight Large Flare Concept.)

The payload adapter weight is different for the baseline (non-aerobraked) Tug, the basic (no flare) aerobraked Tug and for the flared aerobraked Tug. The trajectory for the non-aerobraked Tug does not experience temperatures above 300°F and; therefore, requires only docking and holddown fixtures for the payload adapter components. The basic (no flare) and large nose flare Tugs' adapters weigh 350 pounds (exclusive of thermal protection materials). The payload adapter for the 30°, 45°, short 60° and 60° flare Tugs weigh 390 pounds (exclusive of thermal protection materials). This additional 40 pounds accounts for the supports for the flare actuation system.

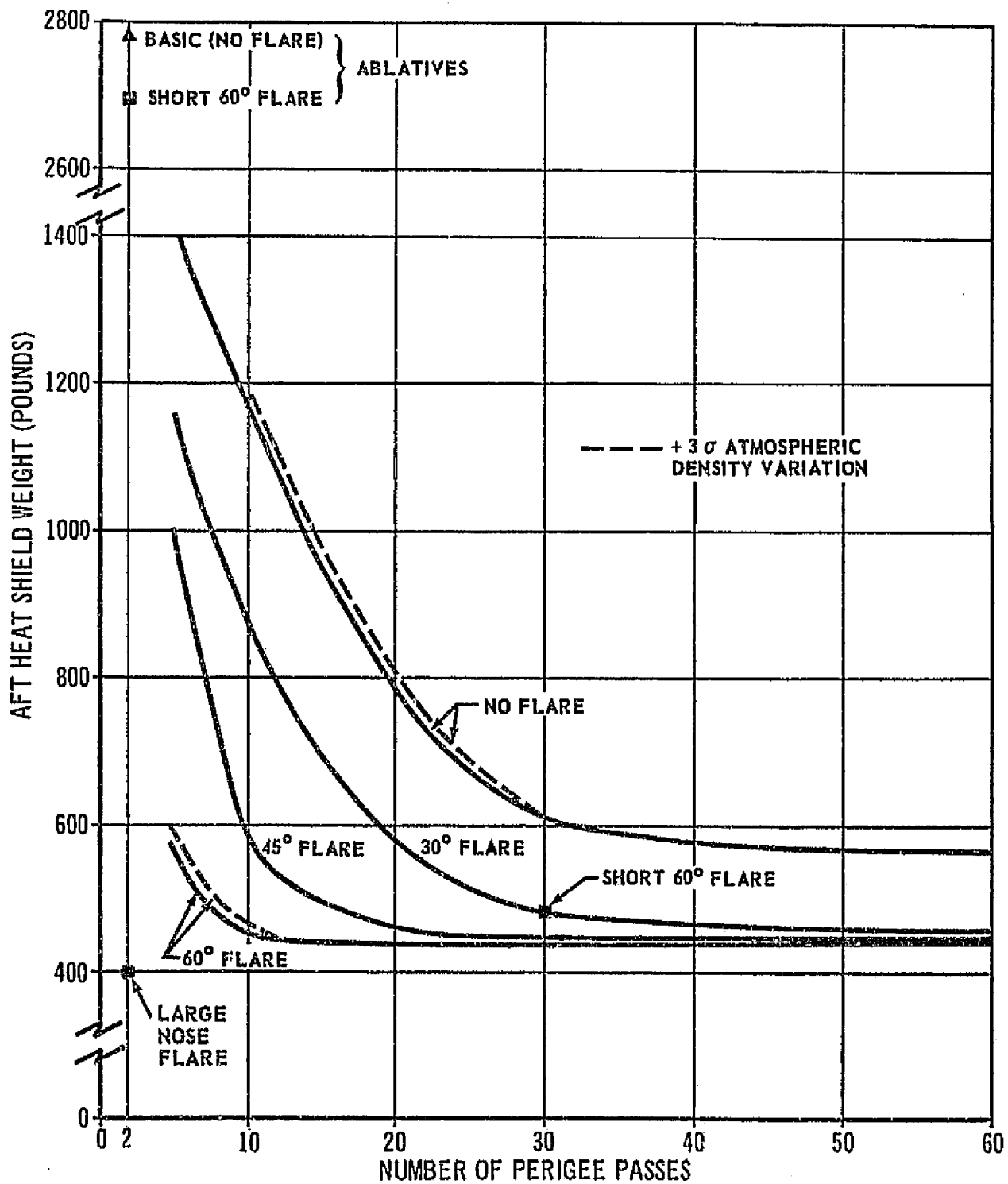


FIGURE 2.1.8.0-1: AFT HEAT SHIELD WEIGHT VS. NUMBER OF PASSES

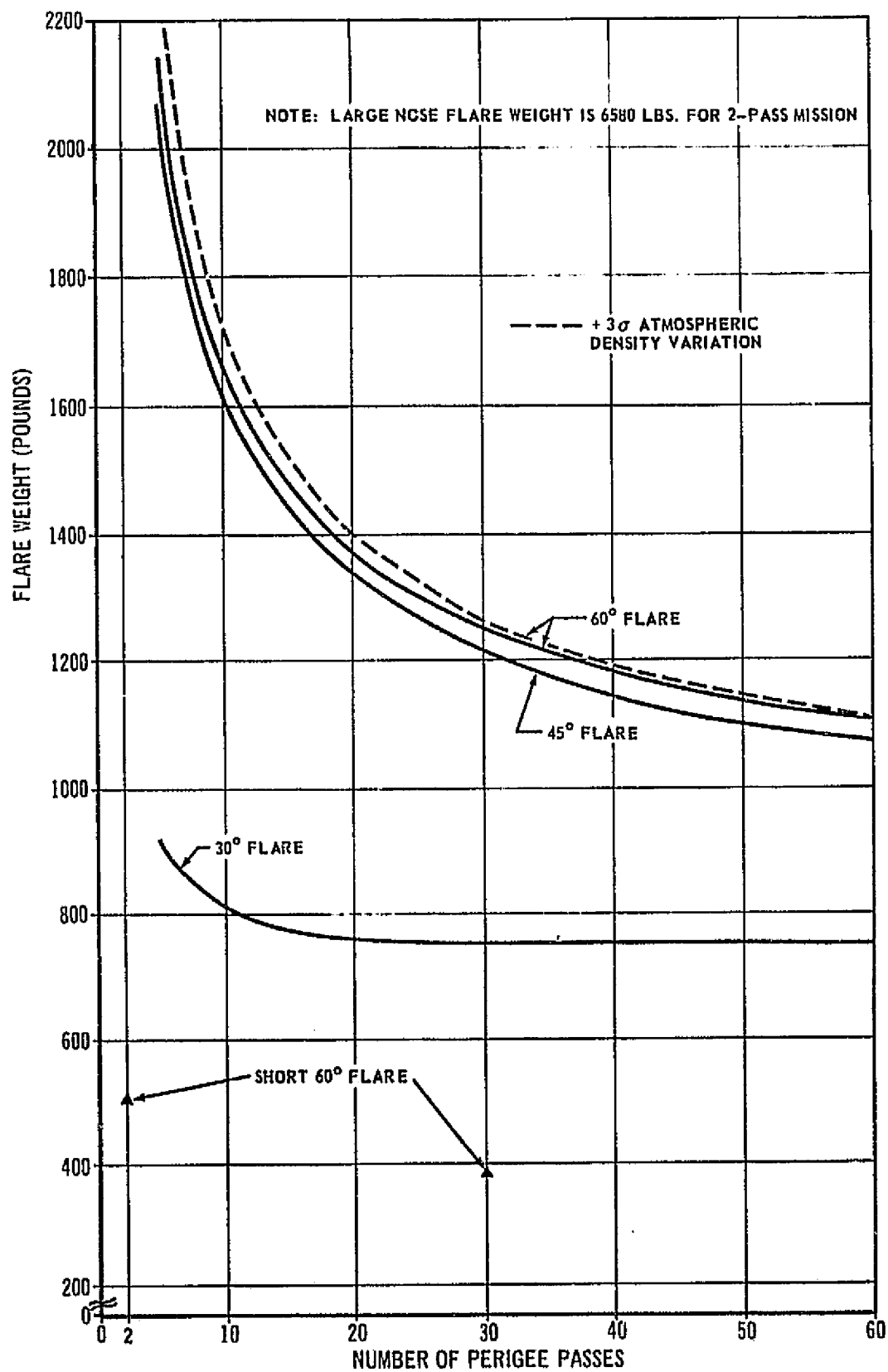


Figure 2.1.8.0-2: FLARE WEIGHT VS. NUMBER OF PASSES

2.1.8 (Continued)

The sidewall insulation weights are shown in Figure 2.1.8.0-3. The microquartz insulation thickness was varied depending on the thermal requirements to maintain a 400°F sidewall and a 300°F payload temperature on the aluminum below the insulation. The sidewall protection covers the cylindrical section of the propulsion module, the astronics module sidewall and, where applicable, the payload adapter. For both thermal and handling purposes, an outer foil is mounted over the insulation. For short duration missions where temperature along the Tug sidewall are high, L-605 was used. For the longer duration missions, the sidewall temperatures are lower and titanium may be used.

Figure 2.1.8.0-4 illustrates the astronics module weight change as a function of the number of passes. The changes to apply the aerobraking kit components did not influence the astronics weight. However, mission duration is significant and will effect the electrical power requirements and the redundancy requirements to maintain a 0.99 reliability.

The reaction control system propellant consumption generally increases with mission duration as shown in prior Figure 2.1.4.0-1. The basic (no flare) Tug and the short 60° flare Tug require significantly more fuel (to maintain aerodynamic stability) than the stable, 30°, 45°, 60° and large nose flare configurations. Atmospheric dispersions further increase the RCS fuel requirements.

Figure 2.1.8.0-5 illustrates the combined weight impact of all the aerobraking kit variables. The astronics and RCS fuel weights increase with mission duration while the heat shield, flare and thermal protection system decrease with mission duration. The minimum inert weight and hence the maximum payload is obtained when the mission duration is between 25 to 35 passes.

2.1.8.1 Weight Conclusions

- o The structural and thermal aerobraking kit weights decrease with increases in mission duration. Mission durations with approximately 25 to 35 atmospheric passages have the minimum aerobraked Tug gross weights (exclusive of payload).
- o Short duration missions have low payload capabilities due to large increase in aerobraking kit weights.
- o The use of radiative materials over ablative materials for the heat shield is desirable as lower weights are associated with radiative thermal systems.
- o The shorter duration missions (5-10 passes) have higher temperatures and air loads which significantly impact flare weights.
- o The weight of steep angle and long slant height flares decrease rapidly by increasing mission duration beyond 5 passes.

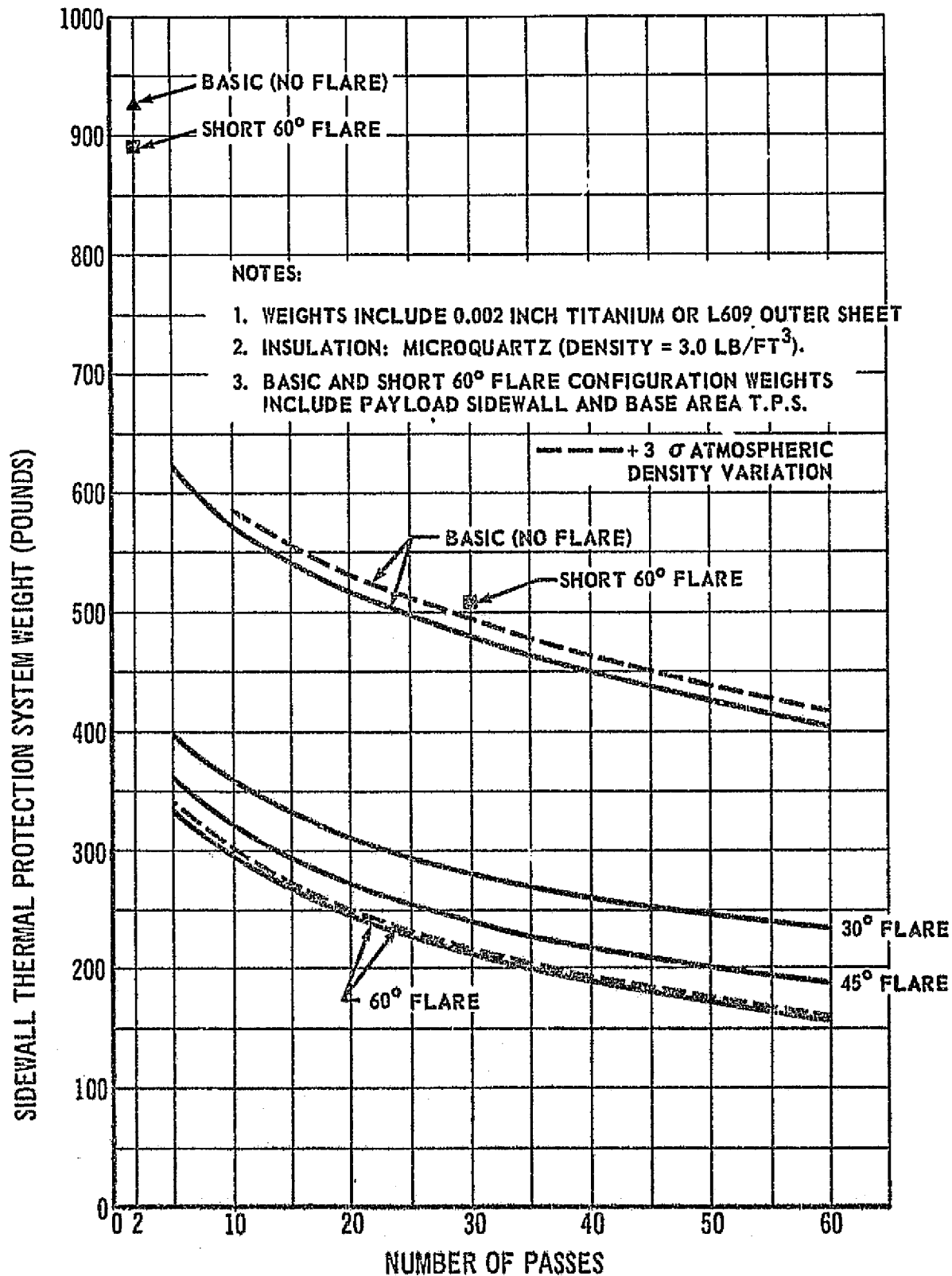


FIGURE 2.1.8.0-3: THERMAL PROTECTION SYSTEM WEIGHT VS. NUMBER OF PASSES

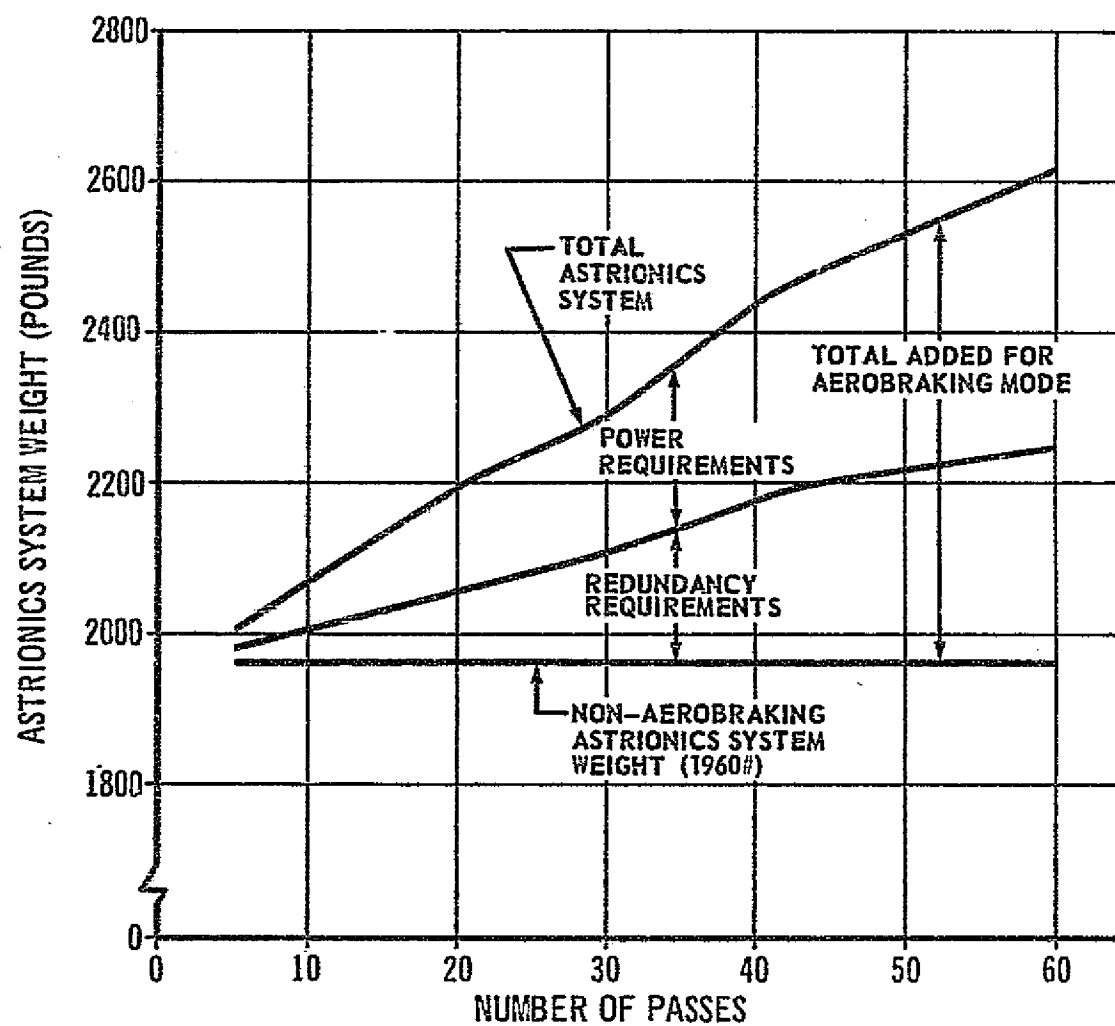


FIGURE 2.1.8.0-4: ASTRIONICS SYSTEM WEIGHT VS. NUMBER OF PASSES

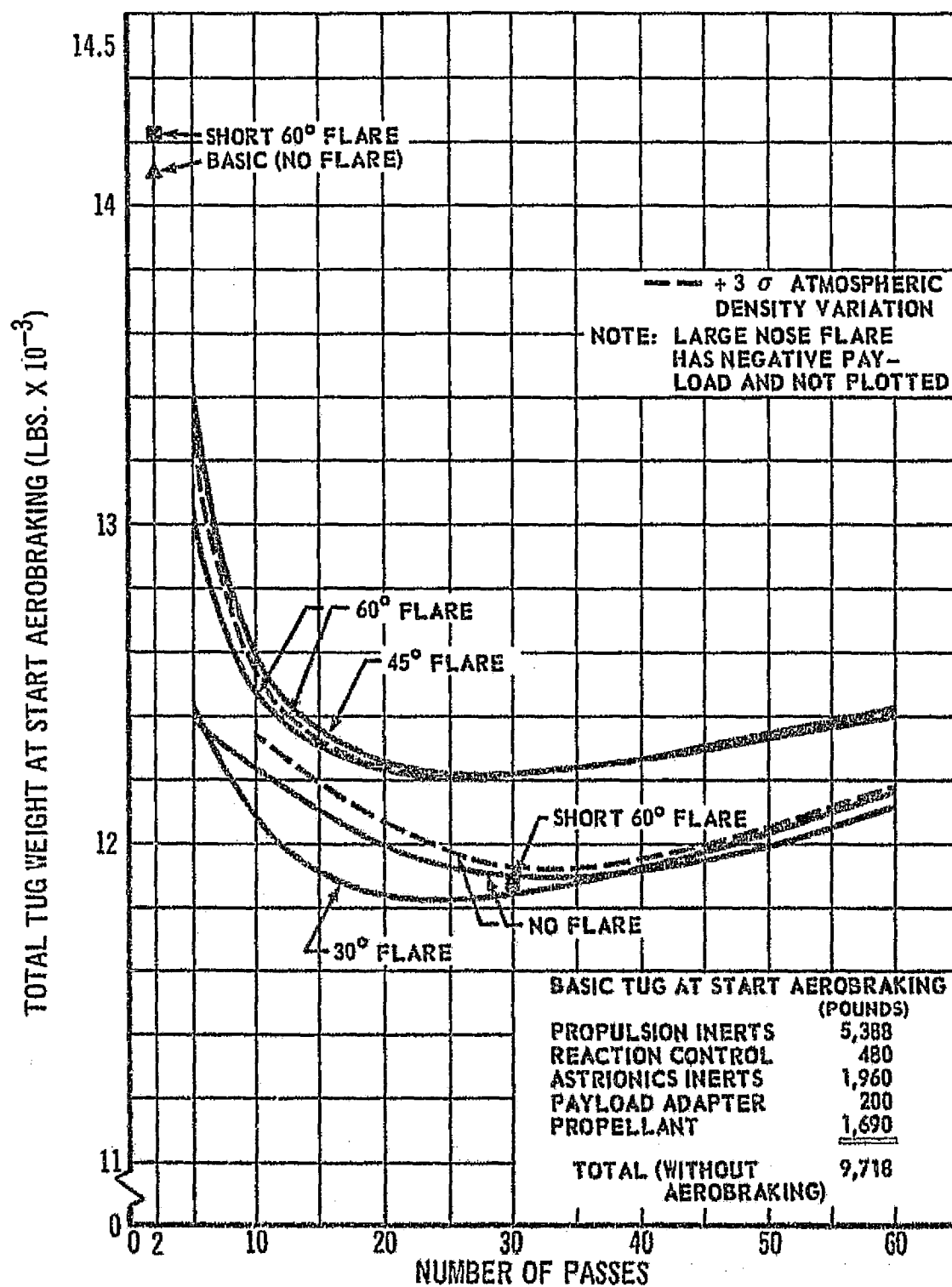


FIGURE 2.1.8.0-5: TOTAL TUG WEIGHT VS. NUMBER OF PASSES

2.1.8.1 (Continued)

- o Long duration mission flare thickness is dictated by handling and processing constraints rather than by loads or temperatures.
- o The constant High Density Atmosphere
 - Has insignificant impact on heat shield weights and on long duration mission flare weights
 - Has significant impact on short duration mission large flare weights (approximately 250 pounds for 5 pass 60° flare).

2.2 SUMMARY OF SENSITIVITY ANALYSIS RESULTS

Figure 2.2.0.0-1 shows the representative Shuttle payload capabilities used in this study. The Shuttle can place 65,000 pounds into 100 NM/28.5° circular orbit and approximately 60,000 pounds into 200 NM/28.5° orbit. Using the nominal operational mode shown in prior Figure 1.2.0.0-1 (100 NM \rightarrow geosynchronous \rightarrow 270 NM \rightarrow 100 NM), the gross weight of the Tug and its round trip payload is approximately 58,000 pounds. The paragraphs below identify the sensitivities to ideal conditions (Standard Atmosphere - no navigation error) and to realistic conditions (atmospheric perturbations and navigation errors).

2.2.1 Sensitivities Of Payloads And Temperatures For Tug Configurations For Standard Atmosphere

The geosynchronous round trip capability of the aerobraked Tug is sensitive to (1) the aerobraking kit weights and to (2) the delta velocities associated with the various operational modes, configurations and environments. The basic (no flare) configuration has a lesser aerobraking kit inert weight and a greater delta velocity requirement than do the flare configurations. When comparing the maximum round trip payloads among the no-flare and 30°, 45°, short 60° and 60° flared configurations, these two factors (weight and velocity) tend to equalize the capabilities of these two configuration types.

To more nearly optimize the Shuttle/Tug combination, a Tug departure and recovery altitude of 200 n.m. was selected. Using this operational mode, the gross weight of the Tug and payload is slightly less than 60,000 pounds and within the Shuttle's capability. This 200 n.m. mode substantially decreases the total Tug mission delta velocity budget since the requirement for the transfer to another orbit and subsequent circularization is deleted (i.e., 270 n.m. \rightarrow 100 n.m.). Approximately 1200 pounds of additional round trip payload capability is achieved by this partial optimization of the Shuttle/Tug combination.

Figure 2.2.1.0-1 shows the round trip payload capabilities of the six configurations as a function of the number of passes in a mission. The operational mode is the 200 NM Tug departure and recovery mode discussed above. The configurations maximize their payload capability-

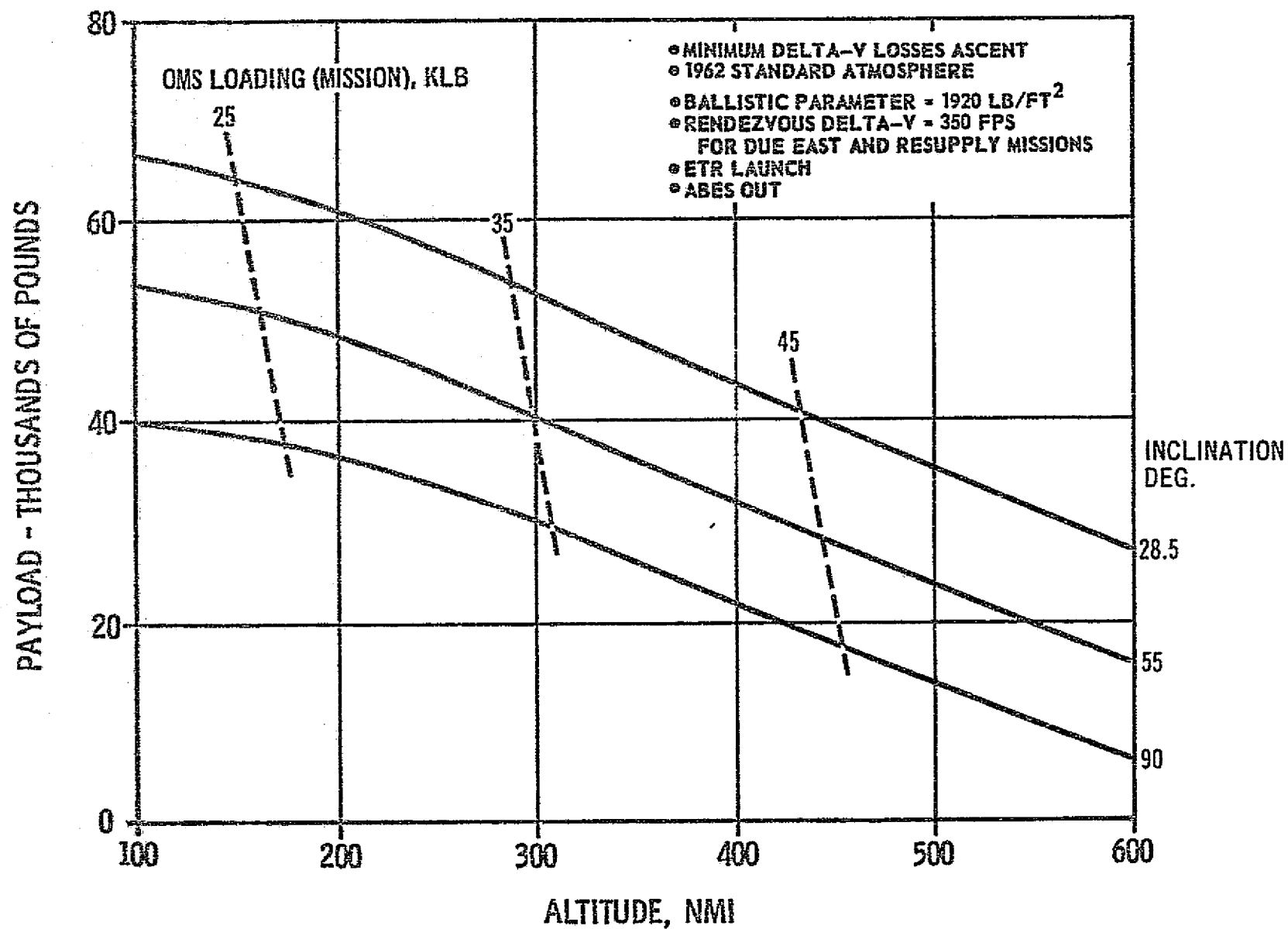


FIGURE 2.2.0.0-1: H-33 CONFIGURATION EXTERNAL H₂ TANK ORBITER
ALTERNATE MISSION CAPABILITY

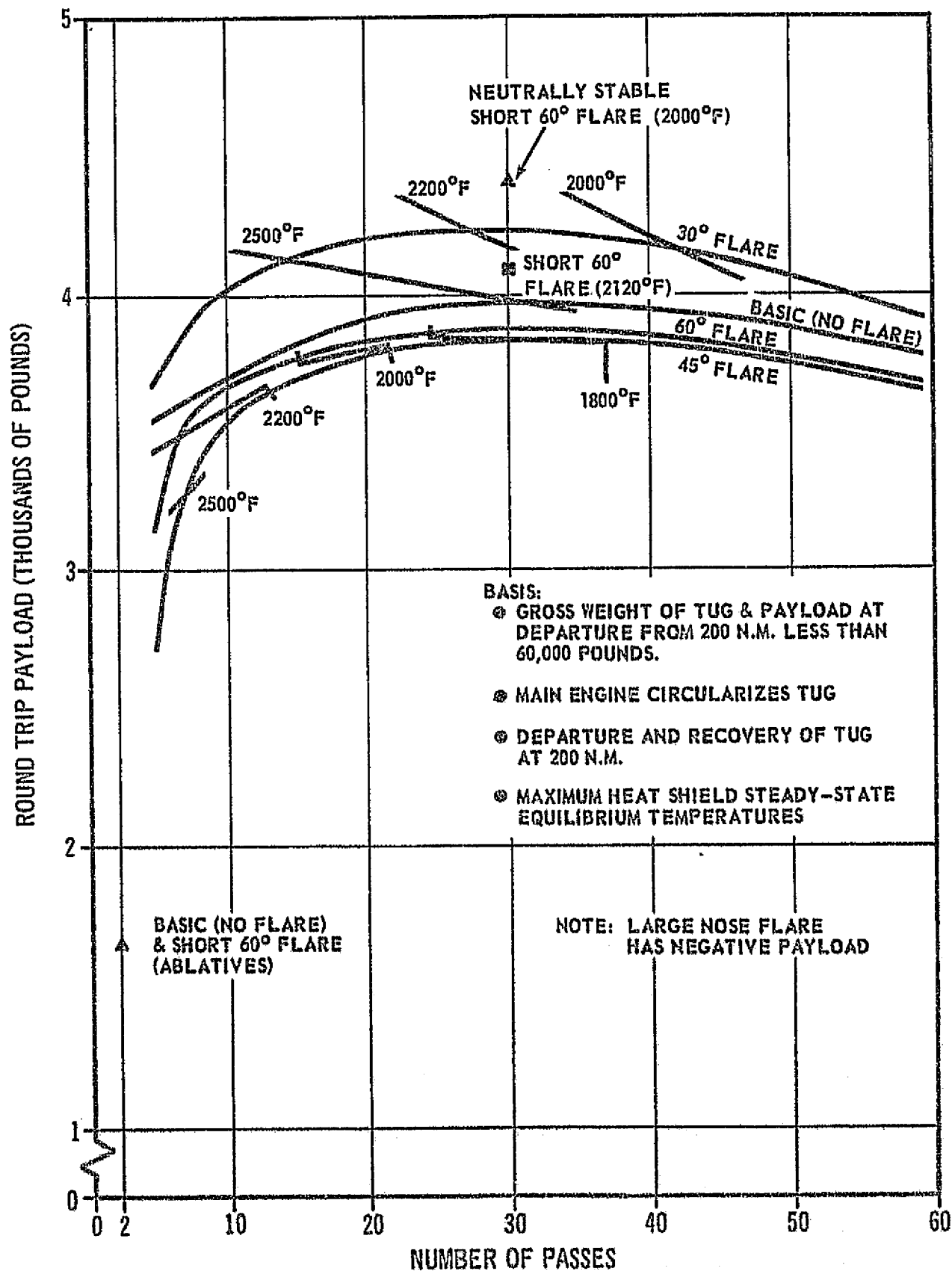


FIGURE 2.2.1.0-1: SYNCHRONOUS ROUND TRIP PAYLOAD VS. NUMBER OF PASSES (200 N.M. RECOVERY)

2.2.1 (Continued)

ties at approximately 30 passes and the payload capability is relatively insensitive over the mission duration range of 10-60 passes. The 30° flare configuration has the greatest round trip payload capability (4225 pounds) of the six configurations studied in depth. Also shown on the figure is an estimate of the 30 pass payload capability of a neutrally stable short 60° flare. Because the 30° flare is also neutrally stable, this data point indicates that near-neutral stability is a desirable attribute for an aerobraked Tug configuration.

The differences in payload capability for the flared configurations are severely impacted by the flare length which in turn directly impacts the flare weight. The neutrally stable 30° and short 60° flare configurations have relatively small and lightweight flares. Their delta velocity requirements are approximately the same as those of the heavier and more stable flared configurations. Shortening the 45° flare to achieve the same stability as the 30° flare should increase the payload capability of this shortened flare configuration to be comparable to the 30° flare. Further decreasing the flare length of the 45° and 60° flares to achieve a comparable ballistic coefficient to the 30° flare may result in decreased payloads. This is typified by the 30 pass short 60° flare shown on the figure. The increased RCS propellant consumption (stability) and the requirement to completely insulate the payload more than offset the decrease in flare weight.

Also shown on Figure 2.2.1.0-1 are the maximum steady state heat shield temperatures seen by the configurations having radiative aft heat shields. These steady state temperatures are based on thin wall analysis and do not include heat sink effects (see Thermal Analysis, Section 2.1.5 above). The 45°, 60° and neutrally stable short 60° flared configurations are not maximum payload limited by the use of TD-nickel-chrome (2000°F limit). The 30° flare configuration will only have a slight degradation in maximum payload capability (approx. 100 pounds) by the use of TD-nickel-chrome with a 2000°F limit.

2.2.2 Sensitivities of Payloads and Temperatures for Tug Configurations for Atmosphere Perturbations and Navigation Errors

The initial atmosphere perturbations data utilized in the study were based on a percentage range (approximately +50% constant High Density Atmosphere to -40% constant Low Density Atmosphere) from the 1962 Standard Atmosphere. The expected variations during the entire aerobraking mission duration or between individual passes were unknown.

Figure 2.2.2.0-1 shows the effects of the High Density Atmosphere on the payload capabilities of the basic (no flare) and 60° flare configurations. The maximum round trip payload capability of the basic (no flare) configuration (approx. 3600 pounds @ 30 passes) is reduced less than 10% from the Standard Atmosphere case (shown as dotted lines). The maximum round trip payload capability of the 60° flare configuration is reduced approximately 12%. Also shown on the figure

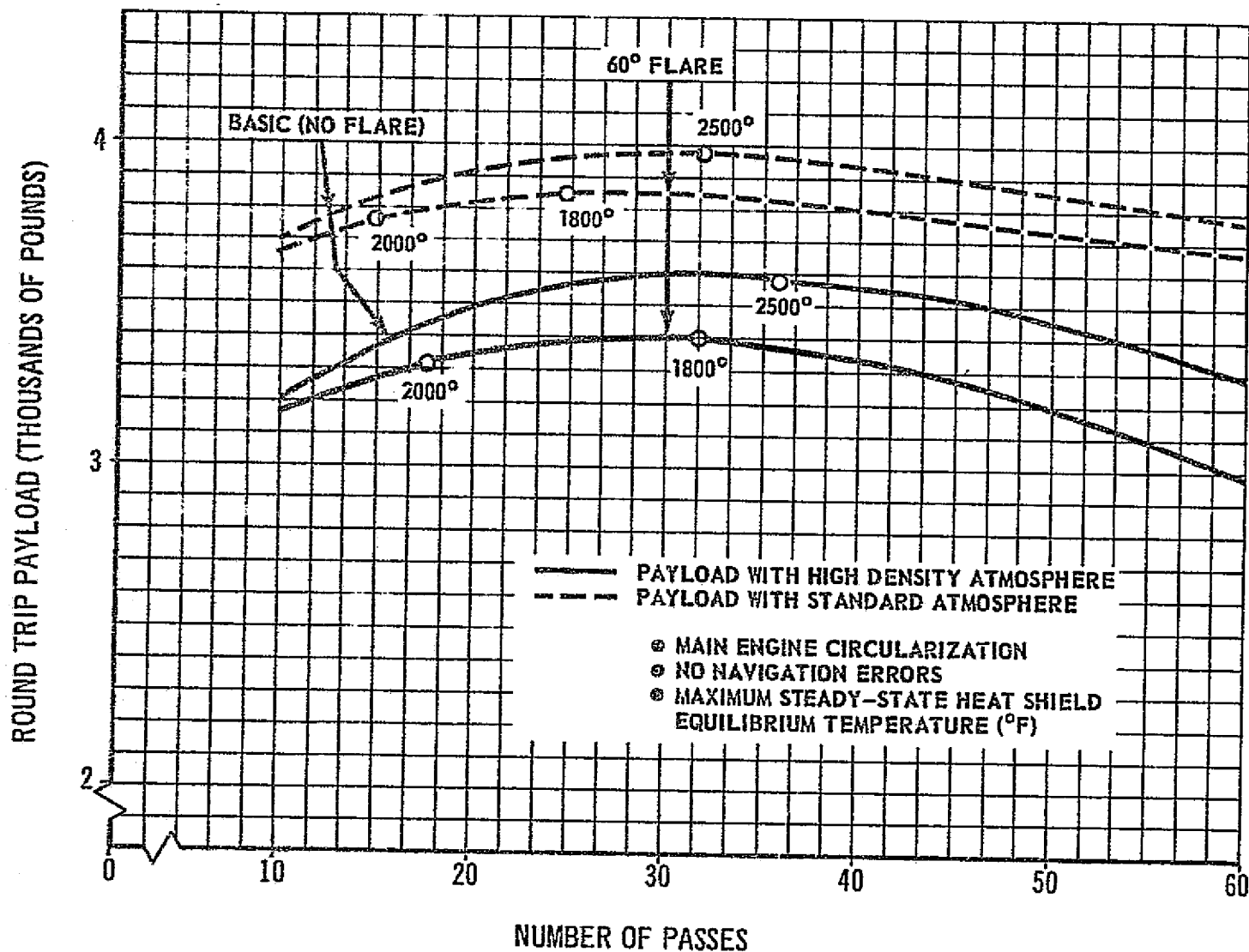


FIGURE 2.2.2.0-1: ROUND TRIP PAYLOAD VS. NUMBER OF PASSES
(DEPART AND RECOVER AT 200 N.M.)

2.2.2 (Continued)

are the maximum heat shield equilibrium temperatures (steady state). The effect of the High Density Atmosphere is to require four or five additional passes in a mission to maintain the equivalent Standard Atmosphere temperature.

Figure 2.2.2.0-2 shows the round trip payload sensitivities (10 pass mission) to atmospheric anomalies and navigational errors. Shown in the first two hatched columns of each configuration are the payloads and temperatures previously discussed (Figure 2.2.2.0-1). The third hatched column of each configuration shows the round trip payloads achievable under the combined effects of the High Density Atmosphere and the 3 sigma navigational errors (single correction burn at entry-after 1300 seconds of landmark tracking). Because the prior payload analyses have reserved 400 ft/second delta velocity for navigation error corrections, including the navigational errors has a minimum impact on the round trip payload. Even for the relatively short duration 10 pass mission, the 3000 pound payload capability is retained under these "worst" conditions depicted. The temperatures shown in Figure 2.2.2.0-2 are the heat shield nose stagnation temperatures. The expected increases are only 110°F for the 60° flare configuration and 160°F for the basic (no flare) configuration.

The atmospheric dispersion analysis conducted was based on a constant High Density and a constant Low Density Atmospheric model. This model results in a more severe environment than would be expected to be encountered. Therefore, the temperatures shown are higher than expected.

A Varying Atmosphere model was received at the time the add-on activity commenced. Due to the objectives and scope of the add-on activity, only two trajectories were flown using the Varying Atmosphere model. Because the Varying Atmosphere model is less severe, its effects on the payload capabilities are less than the High Density Atmosphere. For example, the ten pass basic (no flare) configuration required 180 ft/sec delta velocity to correct the trajectory for the High Density Atmosphere. The requirement decreased to 100 ft/sec for the Varying Atmosphere.

2.2.3 Conventional/Aerobraking Tug Performance Comparison

The groundrules used for the comparisons shown in this section were those established for the MSFC Point Design Tug Studies. They differ in some respects from those used in the Aerobraking Study. Therefore, no direct comparisons with other aerobraking results should be made without first rationalizing these differences.

Figure 2.2.3.0-1 shows the round trip payload capabilities of the conventional and aerobraked Tugs. The initial MSFC Point Design goal of 3000 pounds payload ($\lambda' = 0.895$, $I_{sp} = 470$ seconds, total usable propellant = 55,552 lbs) is shown at the top of the figure. If the

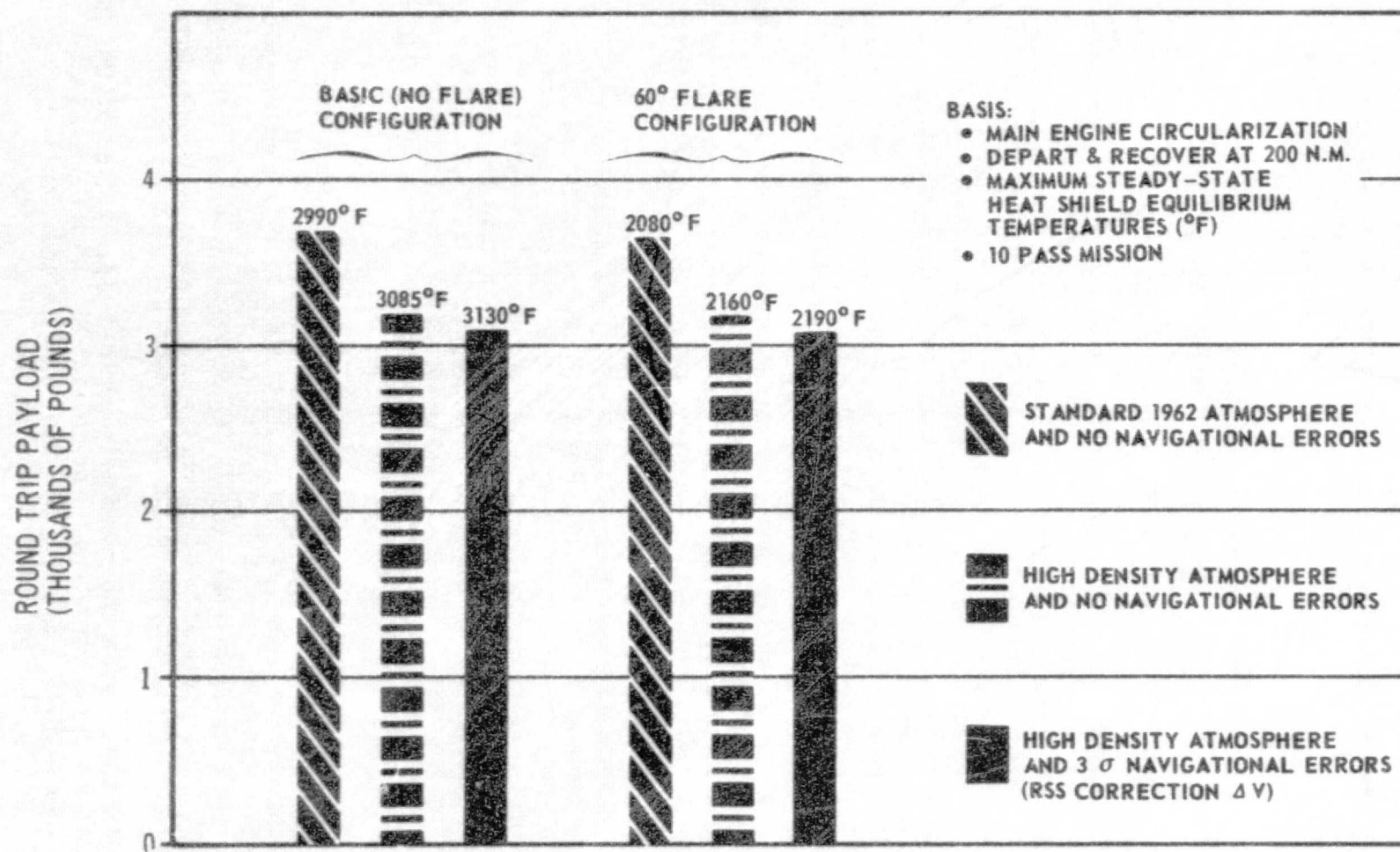


FIGURE 2.2.2.0-2: ATMOSPHERIC ANOMOLY AND NAVIGATION ERROR EFFECT ON ROUND TRIP PAYLOAD (10 PASS MISSION)

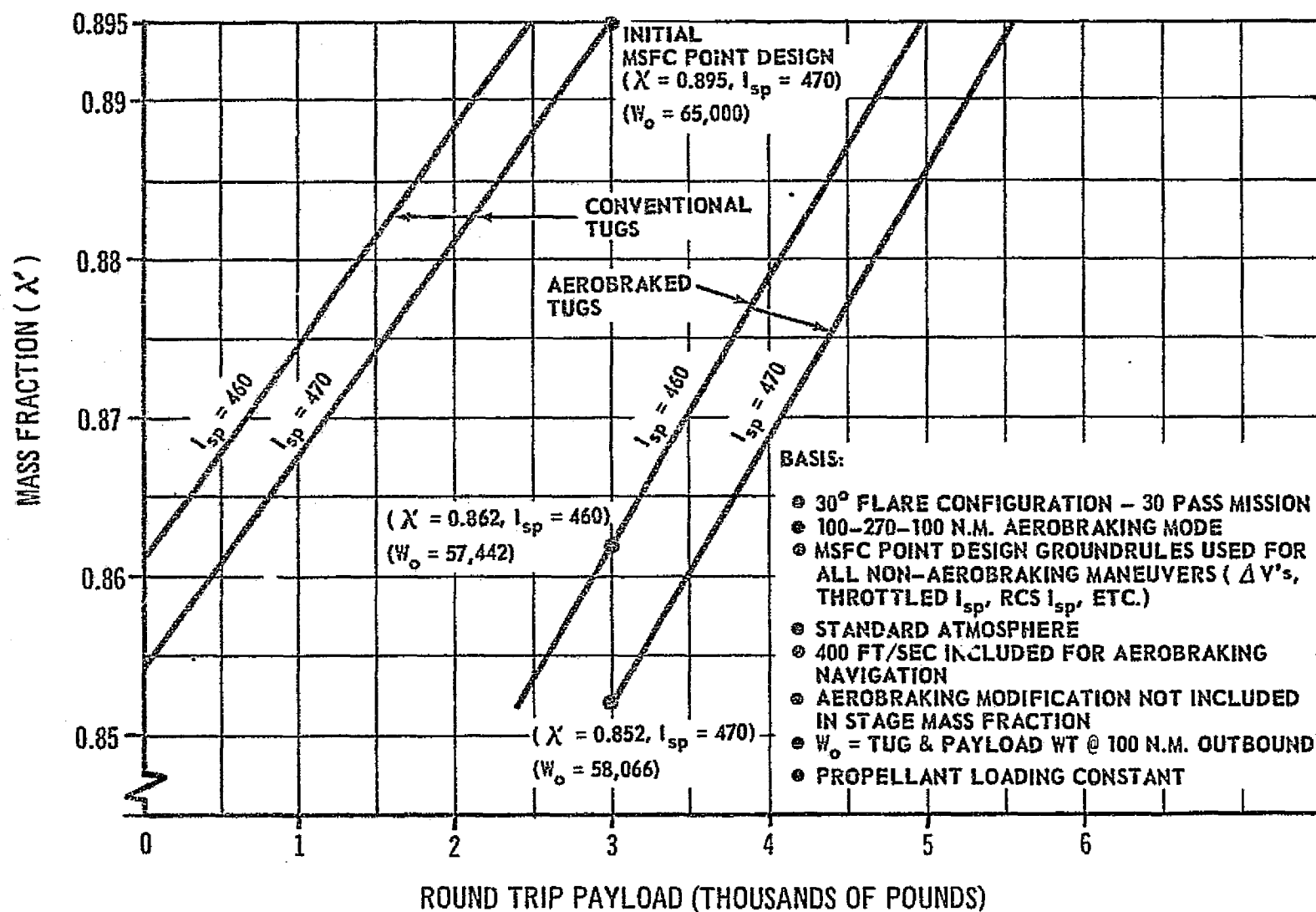


FIGURE 2.2.3.0-1: ROUND TRIP PAYLOAD CAPABILITIES OF CONVENTIONAL AND AEROBRAKED TUGS

2.2.3 (Continued)

main engine Isp were to be degraded to 460 seconds, approximately 500 pounds of payload capability would be lost. If the conventional stage mass fraction were degraded (while the propellant loading and Isp are held constant), the payload capability will be decreased as shown.

The conventional Tug used as a "Starting Point" for this aerobraking study has a mass fraction of 0.852 without the payload adapter (total usable propellant weight = 45,000 pounds). The 3000 pound round trip payload could be achieved by the aerobraked 30° flare configuration (30 pass mission) with the current stage mass fraction and with an uprated main engine having an Isp of 470 seconds. Using the current engine (Isp = 460 seconds), the stage would require a mass fraction of 0.862 to attain the 3000 pound payload capability. If the aerobraked Tug stage were designed similar to the Point Design and with a reasonable scaling factor to account for the differences in propellant loading, the aerobraked stage might have a mass fraction of 0.875. This would provide a round trip payload capability of approximately 4400 pounds.

In addition to the capability to use state-of-art technology (lower mass fractions and Ips), the aerobraked Tug with its 3000 pound payload has a lower gross weight in the Shuttle. If the Shuttle's payload were to be reduced by approximately 10 percent from its 65,000 pounds capability, the aerobraked Tug could more easily withstand the transition.

2.2.4 Sensitivity Conclusions

- o The Tug's propulsion module technology requirements are significantly reduced by aerobraking.
- o The single Shuttle/Tug launch per geosynchronous mission is possible for 95% of the missions using Tug aerobraking.
- o Round trip geosynchronous payloads of 3000-4000 pounds are achievable by a 45,000 pound propellant aerobraked Tug.
- o Placement and retrieval of geosynchronous payloads of 7000-9000 pounds are within the capability of the 45,000 pound propellant aerobraked Tug.
- o The operational mode used by the aerobraked Tug should utilize the Shuttle's capability to deliver and recover in orbits above the 100 NM earth orbit.
- o Near-neutral static stability will maximize payloads for flared configurations.

2.2.4 (Continued)

- o The round trip payload capability of the aerobraked Tug is relatively insensitive to mission times of 10-60 passes in a Standard Atmosphere. This payload sensitivity to mission duration is somewhat greater in the perturbed atmospheres.
- o The atmosphere variation and navigation error correction burns can be combined into one burn, thereby reducing the total delta velocity requirement.
- o The application of the aerobraking concept to the Space Tug will:
 - approximately double the round trip payload capability of the advanced technology Space Tug;
 - permit the use of a lower mass fraction (if advanced technology does not meet goal) and permits the use of a lower specific impulse (existing engines) to deliver the desired payload to the high energy orbits;
 - Still deliver the desired payload even if the Shuttle's cargo bay size decreases and a 10% loss in Shuttle payload capability occurs.

SECTION III GROUNDRULES, GUIDELINES AND ASSUMPTIONS

3.0 GENERAL

The Space Tug must interface with all of the elements in the Integrated Space Program. This includes: The Space Shuttle, Space Station, Nuclear Shuttle, other Space Tugs and variable size and weight payloads. These interfaces impose on the Tug (1) dimensional and weight constraints, (2) thermal and aerodynamic environmental constraints, (3) handling and transportation constraints, and (4) operational mode constraints. The impact of the major constraining factors were incorporated into this study. Additional analyses are required to fully assess all the influencing factors.

The guidelines and assumptions were grouped into three categories: Overall Space Tug, Propulsion Module, and Astrionics Module. Each of these categories are discussed in more detail in the following subparagraphs.

3.1 OVERALL SPACE TUG

- a. The study activity was directed to identify the maximum payload capability aerobraked Space Tug concept, i.e., the concept with the least aerobraking kit weight penalty.
- b. Minimum duration aerobraking re-entry missions (1 to 2 passes) were given limited study due to the thermal limits of the state-of-the-art radiative materials and reduced aerobraked Tug payload capability.
- c. The unmanned geosynchronous, round trip mission was used as the baseline aerobraking mission.
- d. The geosynchronous missions considered nominal geosynchronous on-orbit time (1/2 to two days) and aerobraking return times from one pass to 85 passes (1/4 to 15 days).
- e. The baseline (non-aerobraked Tug configuration) was scaled from the configuration developed in the Boeing Pre-Phase A Space Tug study and is compatible with a 65,000 pound Shuttle payload capability.
- f. The baseline Tug configuration used in this study was based on state-of-the-art technology. The latest proposed Tug modifications incorporating advanced engines and other Tug advanced technology were not assessed.
- g. The aerobraking kit modifications were designed to be removable and to be applied in kit form. The kit elements were to impose minimal penalty to the conventional Tug configuration.
- h. The kit elements were sized to fit within the Shuttle cargo bay constraints (15 foot diameter by 60 feet long).

3.1 (Continued)

- i. The Space Shuttle was assumed to deliver and retrieve the Space Tug at a 100 n.m. orbit. The impact of other altitudes was assessed.
- j. The payloads will be protected by the payload adapter. The maximum temperature the payload would experience was restricted to 300°F.
- k. The baseline return trajectory mode used was: (1) Deorbit from geosynchronous orbit; (2) use aerodynamic drag to decrease the apogee altitude on each pass; (3) circularize at 270 n.m. after aerobraking; (4) phase with the Shuttle; (5) deorbit to 100 n.m.; (6) circularize at 100 n.m.; and (7) rendezvous with the Shuttle.
- l. The Tug provided all rendezvous and docking delta velocity with the payloads.
- m. A spherical earth was assumed for trajectory analysis. The impact of solar, lunar and earth harmonics were assessed.
- n. The study investigated the effects of the zero and small angle of attack trajectories.
- o. Atmospheric effect above 600,000 feet were assumed negligible.
- p. A 1962 U. S. standard atmosphere was assumed. The impacts of high and low density atmospheric perturbations were assessed.
- q. No solar heating or hot gas radiation was assumed.

3.2 PROPULSION MODULE

- a. The propulsion module was scaled from the 39,800 pounds propellant loading of the Boeing Space Tug Pre-Phase A Study (prior Reference 1.1.0.0-1) to a 45,000 pound propellant loading. Affected propulsion module inerts were scaled upwards.
- b. The gaseous LOX/LH₂ reaction control system used for this study was not modified from the previous study.
- c. The upper temperature limit for state-of-the-art radiative materials was TD-nickel-chrome with 2000°F capability. Advanced materials were identified for thermal environments exceeding 2000°F.
- d. Selected materials used for the thermal protection system were identified by Boeing and NASA and were based on Shuttle era technology. No material trade studies were conducted.

3.3 ASTRIONICS MODULE

- a. The astrionics system proposed by IBM in "Preliminary Definition of an Astrionics System for Space Tug Mission Vehicle Payload", Final Report, (Reference 3.3.0.0-1) was used as the baseline from which aerobraking Space Tug astrionics requirements were defined.
- b. The technology used for the Space Tug astrionics systems was Shuttle era technology.
- c. The Space Tug was based and maintained on the ground.
- d. The Space Tug astrionic module was designed to minimize the need for ground support.
- e. The astrionic module design concept was modular and provided the capability of automatic operation.
- f. The astrionic module concept was designed to allow a remove and replace maintenance and reconfiguration concept in space and/or on the ground.
- g. The astrionic system was designed to be self-sustaining.
- h. The astrionics systems was designed for automatic rendezvous and docking operations.
- i. The 180 day quiescent mode impact was not considered as a part of this aerobraking study. The astrionics system was sized to accomplish the round trip synchronous aerobraking mission.

SECTION IV PERFORMANCE AND TRADE STUDIES

4.0 GENERAL

This section presents the results of the detailed studies of the aerobraking aerodynamics, configurations, trajectories, control, thermal, astrionics, materials and weights. Shown in parentheses on Figure 4.0.0.0-1 are the applicable subsections for each of the technical discipline results discussed in this section.

4.1 Aerodynamic Analysis

Aerodynamic data is a required input for the trajectory, loads and controls analysis for the space tug aerobraking study. However, in order to proceed with the aerodynamic data analysis, the flight regime characteristics and the configuration geometry had to be defined.

In order to identify the flight regimes of interest, parametric trajectory data were generated to define the relationship between the initial perigee altitude and the total time to decay to an orbit with an apogee of 270 n. mi., as a function of the configuration $W/C_D A$ (assumed constant for the parametric trajectory data). The results indicated that for decay times between $\approx .25$ and ≈ 20 days, perigee altitudes ranged between ≈ 220 K ft and 340 K ft and perigee velocities between ≈ 22 Kfps and ≈ 34 Kfps for a $W/C_D A$ range from 10 to 80 psf. Using these preliminary trajectory results, a 2:1 ellipsoid heat shield was selected from an aeroheating analysis and the "basic" tug configuration was defined as a 2:1 ellipsoid nose/cylinder configuration.

The aerodynamic analysis required for the aerobraking study is somewhat unique due to the flight regimes involved. The preliminary trajectory data indicates that the flow field encountered by the space tug vehicle will range from hypersonic, slightly rarefied (slip flow) to highly rarefied (free molecule flow). Thus, the primary objective of the aerodynamic analysis is to predict the aerodynamic characteristics (C_{D0} , C_{N0} , CP/D and C_p) of the space tug vehicle configuration(s) in the rarefied flow regimes encountered.

Both the Apollo type vehicle and Ballistic missile Reentry vehicles encounter these flight regimes during their reentry mission profile; however, both terminate their missions in the continuum flow regime. The problems of aerodynamic heating, airloads, and vehicle dynamics are so much more severe in the continuum regime than in the very brief duration, rarefied flow regimes, that the latter have received relatively little experimental attention to date, particularly for complex configurations. The lack of experimental data is compounded by the almost total lack of theoretical or analytical methods applicable to aerodynamic characteristic prediction in the slightly and moderately rarefied flow regimes.

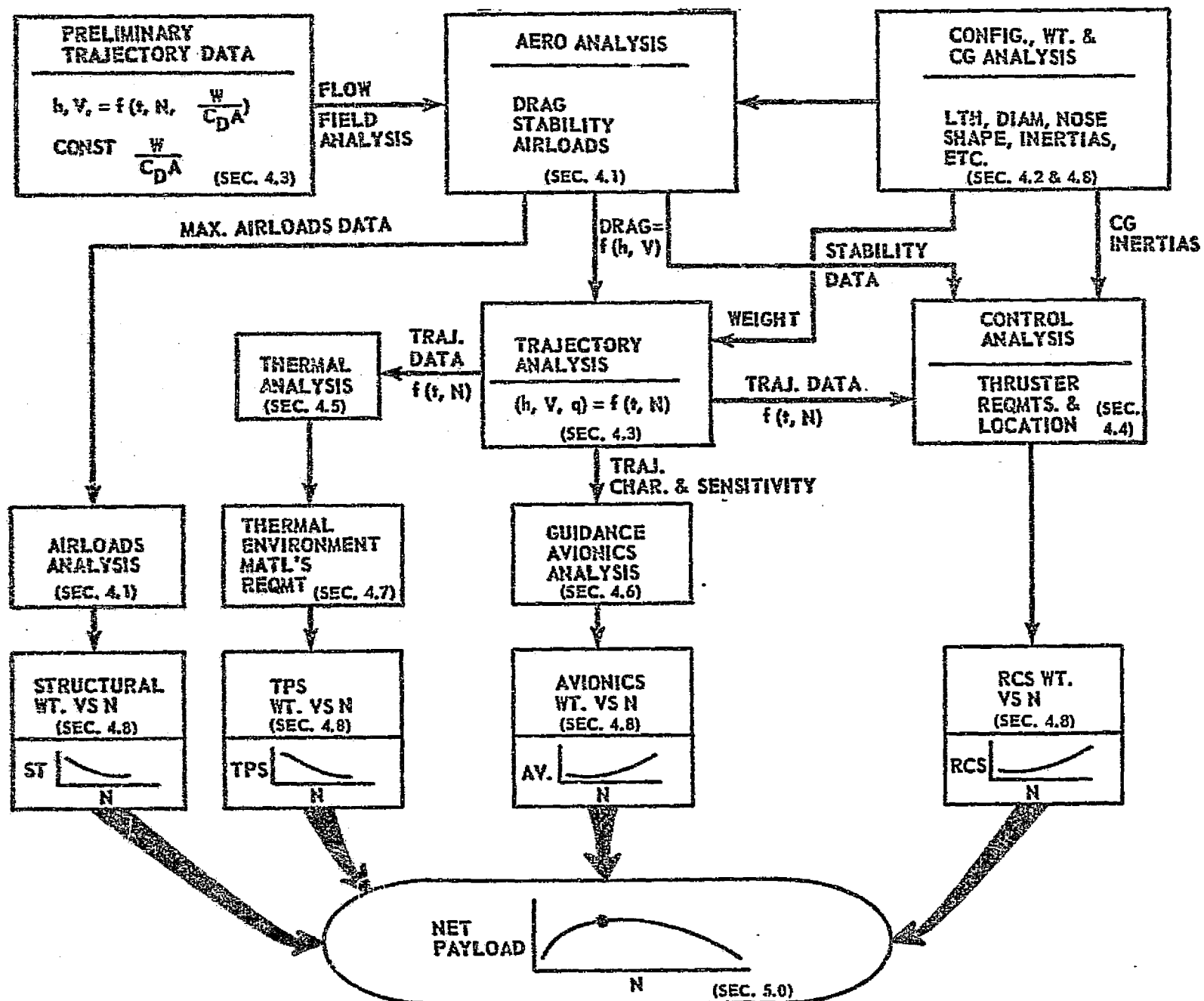


FIGURE 4.0.0.0-1: PERFORMANCE AND TRADE STUDY LOGIC

DS-17142

4.1 (Continued)

In the Free Molecule Flow (FMF) regime the problem of predicting aerodynamic characteristics is somewhat different in nature. A large amount of experimental work has been performed; however, it primarily deals with rather simple shapes such as spheres, flat plates, cylinders normal to the flow direction, etc. In addition, theoretical techniques and results are readily available for many complex as well as simple shapes. The main source of uncertainty in the FMF regime forces result from lack of knowledge of the incident molecule/surface interaction phenomena on which aerodynamic forces are primarily dependent. However, quantitative aerodynamic force coefficient values may be calculated once the molecule/surface interaction phenomena has been defined.

With the above in mind, the following approach was defined to predict the Space Tug aerodynamic characteristics. The best estimate of the vehicles aerodynamic characteristics would be calculated in the continuum and FMF regimes. Then, based on available wind tunnel data trends and empirical interpolation or "bridging" schemes, a "K" factor would be defined which would allow the aerodynamic coefficient at any altitude and velocity (h, V) to be expressed as a function of the continuum and FMF values. That is,

$$X(h, V) = X_{\text{CONT}} + K (X_{\text{FMF}} - X_{\text{CONT}})$$

where

X is the aerodynamic coefficient

X_{FMF} is the free molecule flow value

X_{CONT} is the continuum flow value

K is the "bridging" parameter = $f(h, V) = f(M_{\infty}, Re_{\infty})$

(The Bridging K factor will be discussed in more detail below. The choice of h & V for the independent variable results from trajectory analysis considerations. Presentation of the aerodynamic coefficients, specifically drag, as a function of $K_{N_{\infty}}$ or M_{∞} and Re_{∞} was unsuitable for the trajectory analysis.)

With this general "Bridging" K factor approach defined, the detailed aerodynamic analysis was performed.

The overall problem for the aerodynamics analysis may be divided into two portions: The "basic" or no flare Tug configuration; and the flared Tug configuration analyses. Since the aero data required for the basic Tug configuration is also required for the flared Tug configuration, the basic Tug analysis was considered first.

4.1.1 Basic Tug Aerodynamic Analysis

The basic Tug configuration is presented in Figure 4.1.1.0-1. Prior Figure 4.0.0.0-1 shows that the aerodynamic data required consist of drag data for trajectory analysis, static stability data for the controls analysis, and aerodynamic loading data for the structural analysis. (Dynamic stability data was not required, since the controls analysis did not encompass vehicle dynamics). Since the trajectory data was required for both the controls and aero heating analysis, the drag data was considered first.

4.1.1.1 Drag Data

The basic Tug drag characteristics result from pressure drag on the nose and skin friction drag on the nose and cylinder sidewalls. The variation of these two drag components in the slip and transition regimes are treated independently. That is, the bridging analysis, mentioned previously, is utilized for the nose pressure drag, while an alternate method is employed for the skin friction component.

The nose (pressure) drag component is assumed to have the form

$$C_D(h,V) = C_{D_{CONT}} + (C_{D_{FMF}} - C_{D_{CONT}}) K(h, V)$$

where $C_{D_{CONT}}$, $C_{D_{FMF}}$ and $K(h,V)$ must all be determined. The first requirement was to define the continuum and FMF "limiting" values.

The continuum drag characteristics for the ellipsoid nose were obtained from Reference 4.1.1.1-1. As expected, the wind tunnel data agreed well with the modified Newtonian theory value. In the Free Molecular Flow limit, the following assumptions were made:

- 1) Diffuse Molecular reflection
- 2) Complete thermal accommodation; $\alpha=1$, $T_w=T_r$
- 3) $T_w=T_\infty$ uniformly over the entire Tug surface in the altitude range of $\approx 550,000$ ft (\approx FMF limit)

These two assumptions eliminate the need to consider the majority of the interesting physical phenomena associated with free molecular flow. Justification of these assumptions are:

- A) Conservative drag estimate
- B) Simplicity of diffuse reflection aero analysis compatible with scope of aerobraking feasibility study
- C) Second order nature of the effects of T_r at large molecular speed ratios ($7 \leq S_\infty \leq 12.5$ for the current aerobraking study)

- ① 2:1 ELLIPSOID NOSE
- ② MAIN PROPULSION SYSTEM GIMBAL POINT
- ③ ASTRIONICS MODULE
- ④ PAYLOAD ADAPTER
- ⑤ PAYLOAD

DIAMETER = 14 FT.

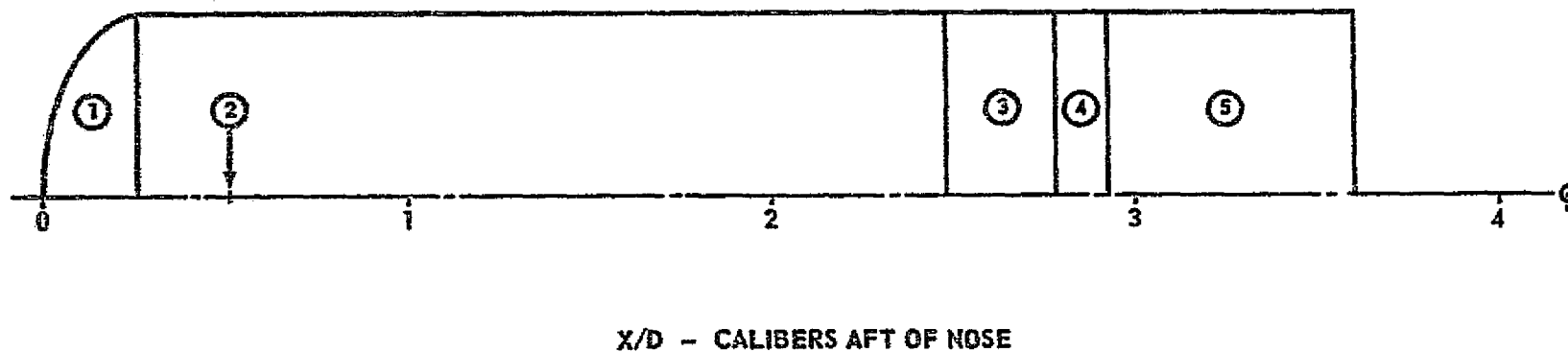


FIGURE 4.1.1.0-1. BASIC (NO FLARE) CONFIGURATION

DS-17142

4.1.1.1 (Continued)

The actual FMF drag characteristics for the ellipsoid nose were based on an interpolation of wind tunnel data and theory for spheres and flat plate as a function of the molecular speed ratio; S_{∞} .

In order to estimate the ellipsoid nose drag characteristics in the slip and transition flow regimes, a "bridging" analysis of sphere drag characteristics was utilized. Sphere (drag) data was chosen to define the bridging parameters due to the geometric similarity to the ellipsoid nose, and due to the large amount of experimental data available in the rarefield flow regimes. In addition to the experimental results, most investigators have attempted to "fit" the data with some empirical K factor analogous to the bridging parameter, K, employed herein. (Reference 4.1.1.1-2 presents some suggested "bridging" schemes, which were among those considered for this analysis). Most empirical approaches can be manipulated to the form equivalent to

$$C_D = C_{D\text{CONT}} + K (C_{D\text{FMF}} - C_{D\text{CONT}})$$

where K is a function of a variety of parameters such as, $(\rho_{\infty}, R_{\text{NOSE}})$, $(M_{\infty}, Re_{\infty})$, (Re_{∞}) , $(Re \text{ behind a normal shock}, ReS)$, $(\rho_{\infty}, \rho_s, \lambda_s, R_{\text{NOSE}})$, (wall to free stream enthalpy ratio), $(S_w, S_{\infty}, K_{N_{\infty}}, T_{\infty}, M_{\infty})$, plus a number of schemes which have experimentally defined "free constants".

The following approach was employed to select K for the ellipsoid nose drag bridging. The various empirical methods were converted to a common set of independent variables, altitude and velocity (h,V) and a "best estimate" K (h,V) determined. The best estimate K is based on Reference 4.1.1.1-1, ReS approach in the near continuum regime and a method suggested by Willis (Reference 4.1.1.1-1) in the near FMF regime. A smooth fairing was utilized between the two schemes.

As discussed in Reference 4.1.1.1-3 the small percentage of the blunt body experimental data which indicate an "overshoot" of the FMF boundary can be explained via either incomplete thermal accommodation in the near molecular flow regime, or a non diffuse surface reflection phenomena. Thus, with the assumption of complete thermal accommodation and diffuse reflection, the bridging parameter was limited to values from 0 to 1. Therefore, the slip and transition flow nose drag coefficient is bounded by the continuum and FMF values.

In addition, the best estimate of the K(h,V) was constrained to comply with the following continuum/slip and transition/FMF boundaries:

SLIP OCCURS @ $M_{\infty} / \sqrt{Re_{\infty}} \approx .01$ (References 4.1.1.1-4, -5 and -6)

FMF OCCURS @ $\lambda_{\infty} / D \approx 10$ (References 4.1.1.1-4, -5, -6 and -7)
 Note that for $T_w = T_r = T_{\infty}, \lambda_{\infty} \approx \lambda_w$

4.1.1.1 (Continued)

(The reference length, D , is the nose radius of curvature at the stagnation point, which for the 2:1 ellipsoid nose geometry equals the body diameter of 14 ft. Atmospheric properties which were not available from the 1962 U. S. Standard Atmosphere were obtained from the 1963 Patrick Air Force Base extension to the 1962 USSA.)

Applying the best estimate $K(h,V)$ resulting from the sphere analysis to the 2:1 ellipsoid nose (pressure) drag bridging, allows definition of the nose drag as a function of altitude and velocity. A best estimate $K(h,V)$ applied to the 2:1 ellipsoid nose is presented in Figure 4.1.1.1-1 along with a comparison of some alternate bridging approaches.

The skin friction variation between the continuum and free molecular flow regimes was not "bridged" by the nose drag K factor. Instead the following approach was used. The continuum limit was determined from Reference 4.1.1.1-8 and modified to account for compressibility effects (Reference 4.1.1.1-9), assuming the cylinder sidewall was equivalent to a flat plate. THE FMF limit was calculated (References 4.1.1.1-4 and -8) based on the previously stated assumptions. The slip flow effects were then estimated via the techniques of References 4.1.1.1-5, -10 and -11 and a "best estimate" relationship defined which was consistent with the continuum and FMF limits.

Combination of the skin friction drag characteristics with the bridged nose drag characteristics allows definition of the basic Tug drag coefficient as a function of altitude and velocity as presented in Figure 4.1.1.1-2. Figure 4.1.1.1-3 presents the "original" basic Tug drag coefficient based on a total length of 60 ft. The final Tug total length of 50.4' drag characteristics were used in a trajectory analysis and only a slight variation in trajectory parameters was found, due to the small change in the near continuum characteristics combined with the low perigee altitudes required for the high $W/C_D A$ basic Tug configuration.

4.1.1.2 Static Stability Data

The second set of aerodynamic data desired was the static stability characteristics, $C_{N\alpha}$ and CP/D as a function of altitude and velocity.

The $C_{N\alpha}$ and CP/D contribution of the ellipsoid nose in the continuum regime was based on the wind tunnel characteristics of Reference 4.1.1.1-1.

In the FMF regime, the nose component $C_{N\alpha}$ and CP/D were again estimated by an interpolation of flat plate and sphere theoretical and wind tunnel as a function of the molecular speed ratio, S_{∞} .

The embedded Newtonian theory (References 4.1.1.2-1 and -2) is utilized for the determination of the static stability contribution ($C_{N\alpha}$ and CP/D) of the cylinder in the continuum flow limit. The embedded Newtonian theory requires a knowledge of the bow shock structure due to the nose and the flow field properties "embedded" between the body and bow shock. The following method was employed to estimate the bow shock profile and the embedded flow field properties: The ellipsoid nose bow

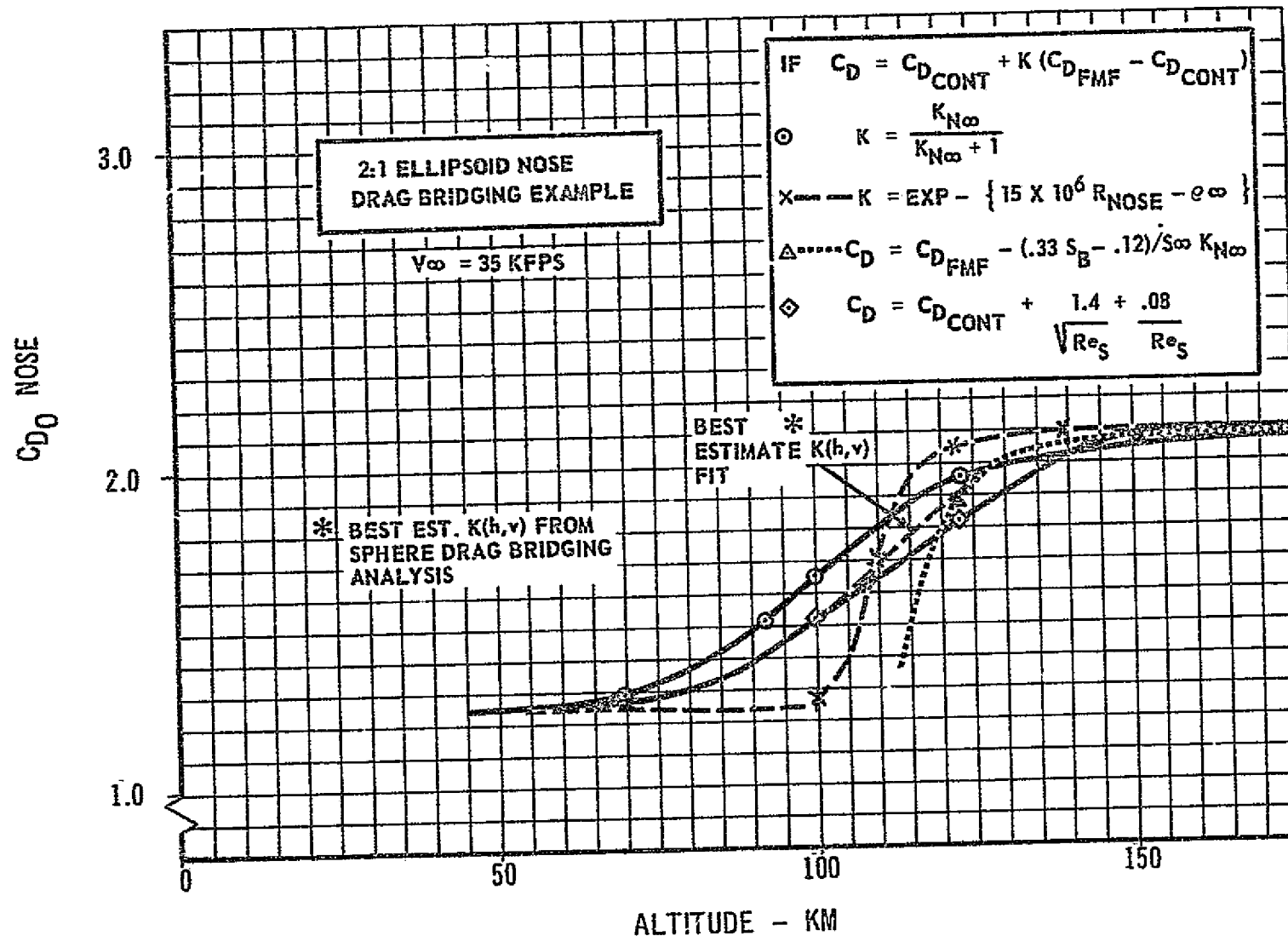


FIGURE 4.1.1.1-1. DRAG BRIDGING SCHEME ILLUSTRATION

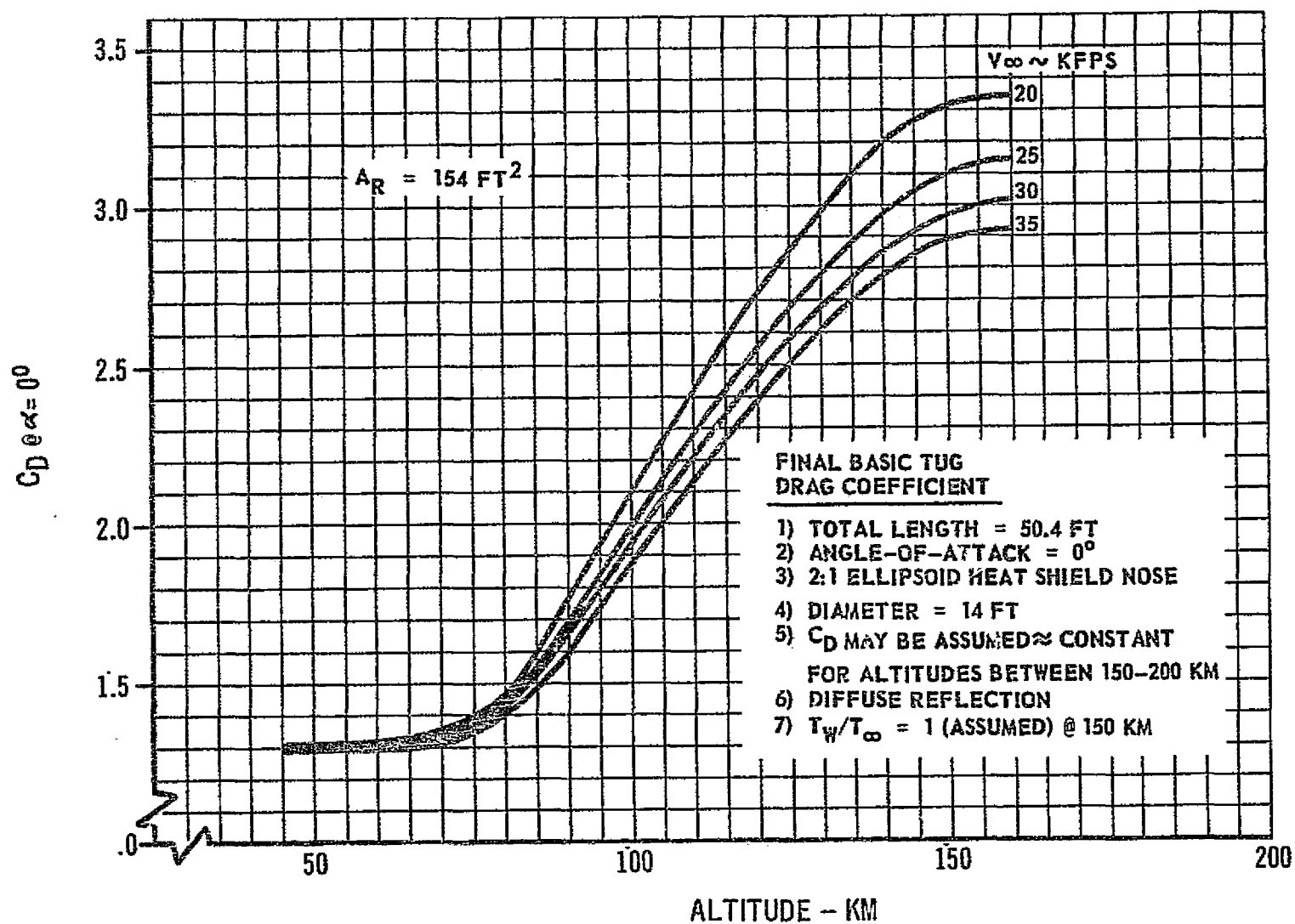


FIGURE 4.1.1.1-2. FINAL BASIC (NO FLARE) TUG DRAG CHARACTERISTICS

$0 = \infty @ C_D$

4-10

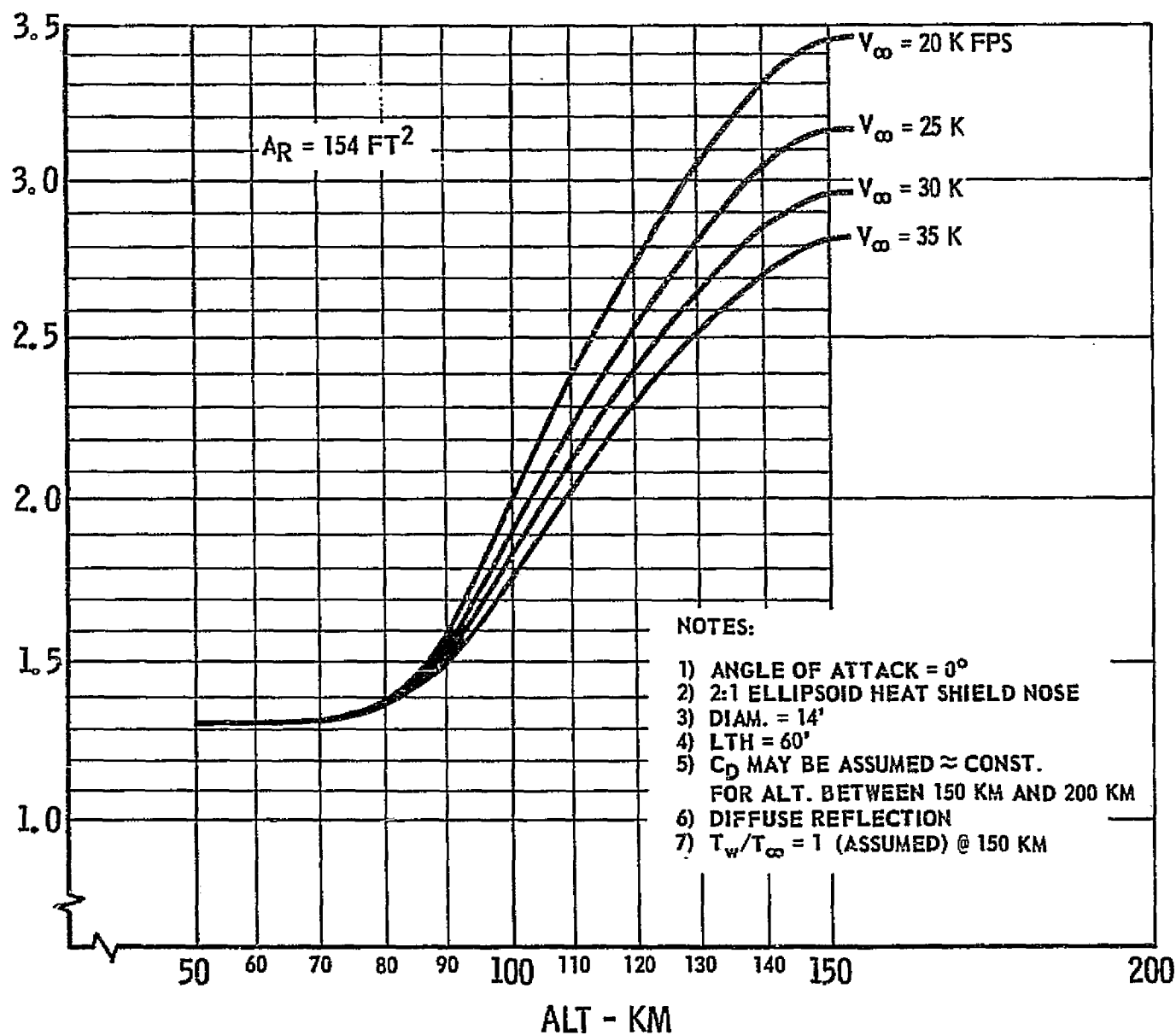


FIGURE 4.1.1.1-3: PRELIMINARY (NO FLARE) BASIC TUG DRAG CHARACTERISTICS

DS-17142

4.1.1.2 (Continued)

shock profile was estimated based on the data and method of References 4.1.1.2-1 and -3. The flow field characteristics (P_1/P_∞) and (q_1/q_∞) in the embedded flow field at a given X/D (cal. aft of the nose) and Y/D cal. normal to the Tug center-line axis) were assumed to be proportional to the characteristics of References 4.1.1.2-1 and -2 hemisphere-cylinder configuration when normalized with respect to Y/R_{SHOCK} .

Thus, the simple Newtonian cylinder normal force (with centrifugal correction) of Reference 4.1.1.2-4 was modified to account for the embedded flow field properties in order to estimate the distribution of $C_{N\alpha}$ along the cylinder sidewalls, $dC_{N\alpha}/d(X/D)$. Numerical integration of the distribution and its moment resulted in both the cylinder $C_{N\alpha}$ and CP/D in the continuum limit.

In the FMF limit, the cylinder $C_{N\alpha}$ and CP/D were determined via the method and tabulated data of References 4.1.1.1-7 and 4.1.1.2-5. Again, fully diffuse reflection at complete thermal accommodation is assumed, and $T_W = T_\infty$ is also assumed uniformly over the entire vehicle.

Combining the nose FMF contribution allows the total $C_{N\alpha}$ and CP/D to be calculated in the FMF limit as a function of S_∞ . With the continuum and free molecular flow limits defined, some method must again be determined to "bridge" the characteristics in the slip and transition regimes. As suggested in References 4.1.1.2-6 and -7 the same bridging relationship employed for the drag characteristics have been utilized to bridge the normal force coefficient and center of pressure between the continuum and FMF limits. As discussed previously, the non-existence of the phenomena of "overshoot" is also assumed to apply to $C_{N\alpha}$ and CP/D . The final basic Tug configuration $C_{N\alpha}$ and CP/D are presented in Figure 4.1.1.2-1 as a function of altitude and velocity. These data are required for the controls and RCS propellant requirements analysis.

4.1.1.3 Nose Pressure Distribution

The aerodynamic data requirements for the basic Tug will be completed with the definition of the nose pressure distribution and the corresponding maximum loading case. As stated in the discussion of the continuum nose drag, modified Newtonian theory agreed well with experiment. Thus the following approach was utilized for the nose pressure distribution. The local coefficient was assumed to have the form of $C_{P_{LOCAL}} = C_{P_{MAX}} \sin^2 \alpha_{LOCAL}$.

$C_{P_{MAX}}$ was based on a γ of 1.2 and the relationship, $C_{P_{MAX}} = \left(\frac{\gamma+3}{\gamma+1} \right) \left(1 - \frac{2}{\gamma+3} \left[\frac{1}{M_\infty} \right]^2 \right)$.

The nose geometry plus a 6° angle of attack was used to determine α_{LOCAL} . The effects of bow shock induced cylinder pressures were analyzed based on the data of Reference 4.1.1.3-1 (checked with References 4.1.1.3-2, -3 and -4), slightly modified for differences in the nose/cylinder geometry. The resulting pressure coefficient distribution on the nose and nose/cylinder region is presented in Figure 4.1.1.3-1. In order to determine the worst

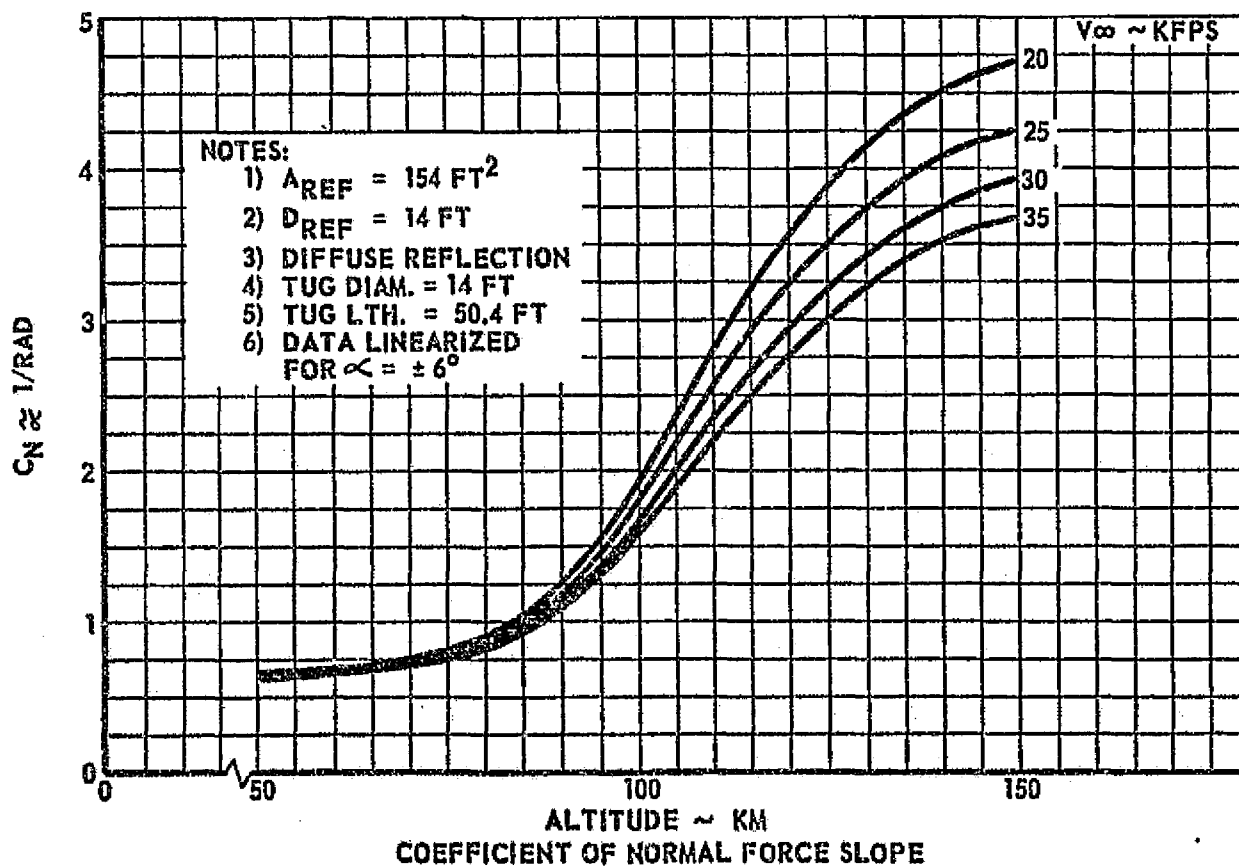
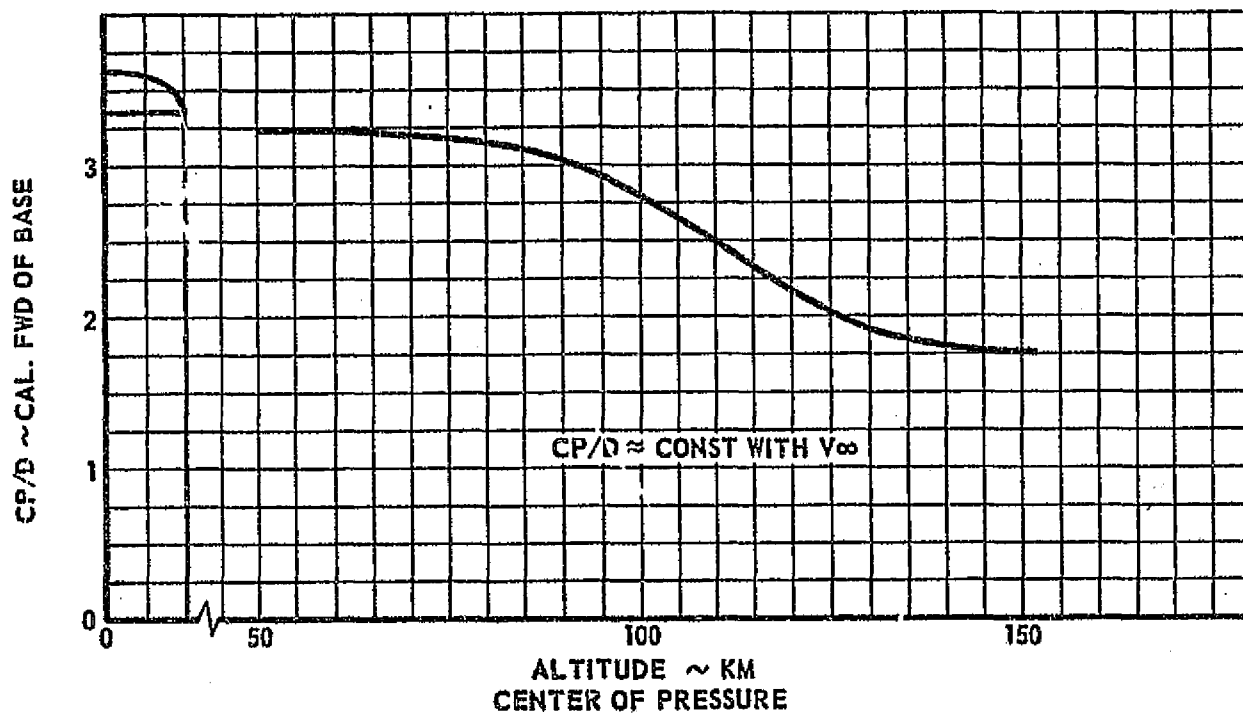


FIGURE 4.1.1.2-1. BASIC (NO FLARE) TUG STATIC STABILITY CHARACTERISTICS

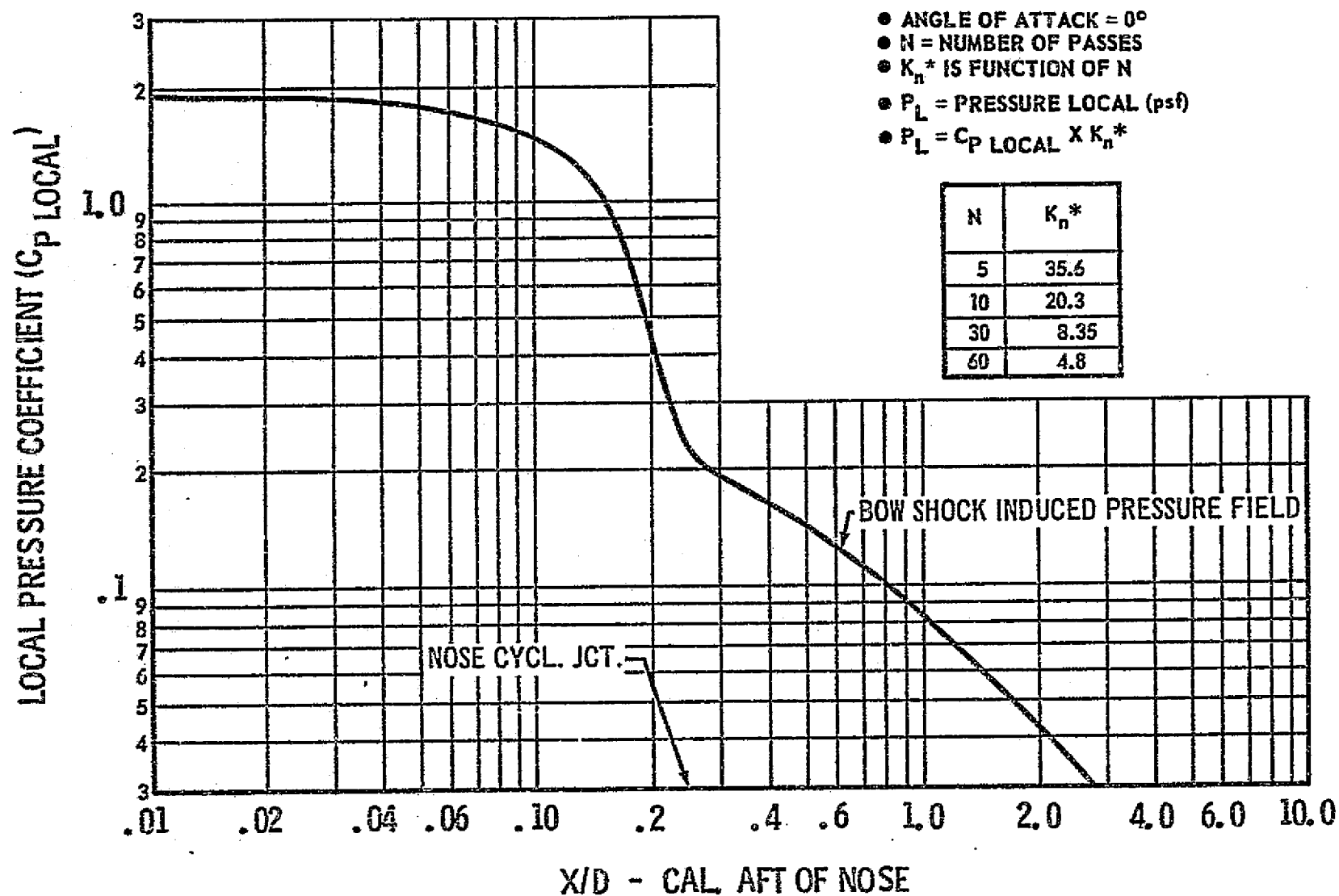


FIGURE 4.1.1.3-1: BASIC (NO FLARE) PRESSURE COEFFICIENT DISTRIBUTION

4.1.1.3 (Continued)

case airloads condition the following approach was employed. The trajectory characteristics (h, M) at MAX q on each pass were determined from the nominal trajectory data. From the bridging analysis, the maximum divergence of the aerodynamic coefficients from their continuum value was determined at the (h, M) of q_{MAX} and the product $K_{BRIDGE} \cdot q_{MAX}$ DEFINED. The maximum product was used to define a K^* which would allow direct conversion of $C_{P, LOCAL}$ to the local pressure P_l . (A small correction factor is added to account for the small ambient pressure). The conversion factor, K^* , is also presented in Figure 4.1.1.3-1 as a function of the number of passes required to achieve an apogee of 270 NM.

The coefficients of local pressure (C_p) and the K_p^* factors shown in Figure 4.1.1.3-1 were converted to a local pressure profile (in pounds per square inch) over the heat shield and cylindrical section of the basic configuration. Figure 4.1.1.3-2 illustrates the rapid decrease in local pressure from the nose to the base of the heat shield. This near-order of magnitude decrease is followed by a gradual decrease along the Tug's sidewall. For a nominal mission time of 30 passes (5 day) for the basic (no flare) Tug configuration, the local pressure is 0.12 psi at the heat shield nose; 0.013 at the heat shield/sidewall interface; 0.002 at the propulsion/astrionics module interface and 0.0017 at the astrionic/payload interface. These low pressure loads will not have a significant design impact on the configuration aft of the heat shield.

4.1.2 Flared Tug Configuration Analysis

The objective of the flared Tug aerodynamic analysis is somewhat broader than the basic Tug configuration analysis. Actually, the aerodynamics analysis had two specific requirements: First, the configurations had to be defined, and then, their aerodynamic characteristics had to be determined. The first objective was to define the configurations. Figure 4.1.2.0-1 presents simplified versions of the technical approach to sizing the flares.

4.1.2.1 Flow Field and Flare Sizing Analyses

A preliminary configuration analysis identified three preliminary flare configurations for consideration. The physical constraints placed on the configurations were:

1. Avionics visibility capability, and
2. Attachment at some main structure location

In addition to these constraints, the following criteria were defined for the flare selection: The "large" flare would be defined such that its W/C_{DA} would be approximately an order of magnitude less than the basic Tug, and, also, provide a large static stability margin (both calculated in the continuum flow regime for expediency).

4.1.2.1 (Continued)

The "small" flare would be defined such that it would be approximately neutrally stable in the continuum flow regime.

The criteria for the third or "intermediate" flare selection will be discussed later.

Having defined the flare selection criteria and constraints, the first requirement for the flare sizing study was to determine the flow characteristics in the continuum flow regime. As discussed above, the basic Tug nose bow shock profile was estimated via the methods of References 4.1.1.2-1 and -3, and is presented in Figure 4.1.2.1-1. The flow field characteristics, P_L/P_∞ , q_L/q_∞ , were estimated on the basis of the data in References 4.1.1.2-2 and -3, and are presented in Figure 4.1.2.1-2. For the current study, the following two groundrules were established which seemed justified on the basis of the reduced scope of the current feasibility study. First, flow separation effects would not be quantitatively analyzed. Although some degree of flow separation will undoubtedly exist above some limiting (small) flare angle, these effects are expected to decrease progressively in the slip flow regime. In addition, various geometric modifications might be employed to reduce flow separation and the associated problems (for example, a configuration similar to Reference 4.1.2.1-1).

The second groundrule was that boundary layer would be assumed "small enough", such that the flare characteristics in the presence of the boundary layer would not differ appreciably from the characteristics defined, assuming a boundary layer thickness of zero.

Both of these groundrules should be given extensive consideration in future aerobraking studies. While both appear incompatible with a rigorous analytical analysis, they should be appraised on the basis of the following considerations:

1. A detailed flow field analysis was beyond the scope of the aerodynamic study.
2. The expenditure of a large amount of time analyzing flow separation and boundary layer characteristics would not be warranted, if, by disregarding these effects, the flare concept still appears unfeasible due to either weight or thermal protection system requirements.
3. The optimum perigee altitude for the flared configurations may be sufficiently high that the continuum flow analysis may be inapplicable; i.e., slip flow effects may dominate the flow field and thus render a continuum regime flow separation analysis overly pessimistic.
4. The continuum flow characteristics are utilized primarily to establish the "lower bound" on the flared configuration aerodynamic characteristics.

4.1.2.1 (Continued)

Thus, with the flow field characteristics and above groundrules defined, consideration was directed to the parametric flare effectiveness analysis.

The concept of embedded Newtonian theory (References 4.1.1.2-1, -2 and -3), plus the analysis of Reference 4.1.2.1-2, are utilized for the parametric flare effectiveness analysis. The flare attach point was chosen as the payload adapter for the following reasons:

1. Minimize astronics module visibility problems (field of view = $90^\circ + (90^\circ - \delta_v)$).
2. Aft flare location will result in large flare stabilizing effect.
3. Payload adapter should qualify as a strong structural attachment point.
4. Location of flares at same body position will allow maximum extrapolation of flare length and semivertex angle results.

Figures 4.1.2.1-3 and 4.1.2.1-4 present the $\Delta C_d @ \alpha=0$ and ΔC_{M_α} due to the flare as a function of the flare semivertex angle and flare slant length. These data plus the following rationale allowed definition of the flare configurations.

4.1.2.2 Flare Selection Rationale

A 60° flare angle was selected for the large flare configuration. A steep flare angle is required in order to obtain the maximum ΔC_{d0} per-unit flare length and per unit flare surface area. One may be able to "live with" or "fix" the flow separation problems associated with a 60° flare, but possibly not a 90° flare. Thus, the limiting case of a forward facing flat plate ($90^\circ \delta_v$) was groundruled out.

A flare slant length of one caliber (14') was selected, in order to insure that the bow shock would not impinge on the flare at 6° angle of attack. As can be seen from Figure 4.1.2.1-4, the 1 caliber, 60° flare, produced a restoring moment of approximately seven times the basic Tuq nose/cylinder disturbing moment. (The effects of the flare shock/bow shock interaction have not been considered). Figure 4.1.2.2-1 presents the geometry of all flare configurations analyzed.

As previously stated, the selection criteria for the small flare was neutral stability in the continuum regime. From Figure 4.1.2.1-4 one can see that a neutrally stable configuration can be obtained (continuum flow, $M_\infty \approx 35$) with the 60° , 45° , 30° , or 15° configuration, if the flare lengths are .625, .65, .805 or 1.315 calibers, respectively.

Since it appeared that some configuration optimization study would be desirable near the studies conclusion, the decision was made to consider three different semivertex angle flares. Ideally then, the parametric

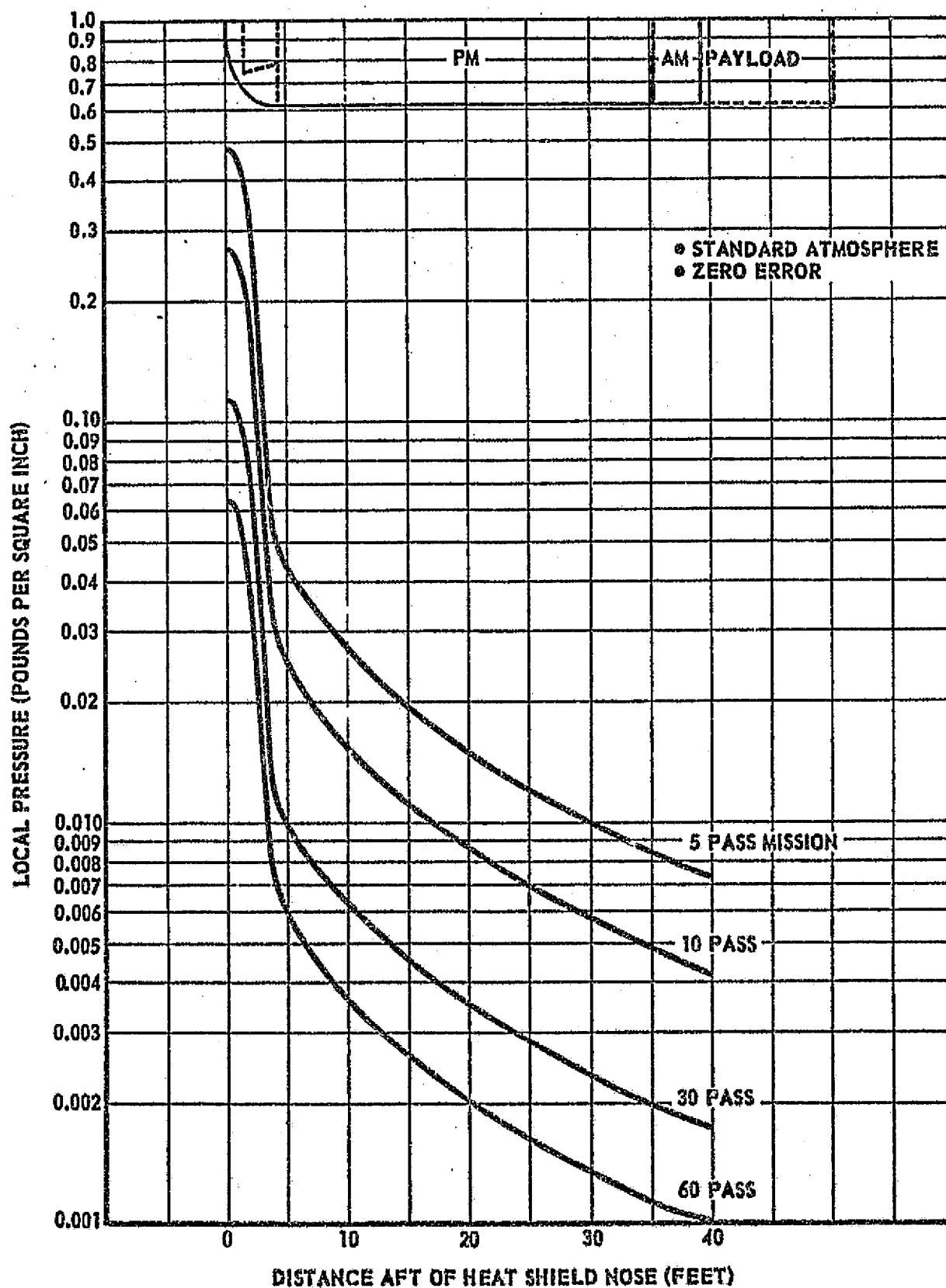


FIGURE 4.1.1.3-2: MAXIMUM LOCAL PRESSURE PROFILE
(BASIC - NO FLARE)

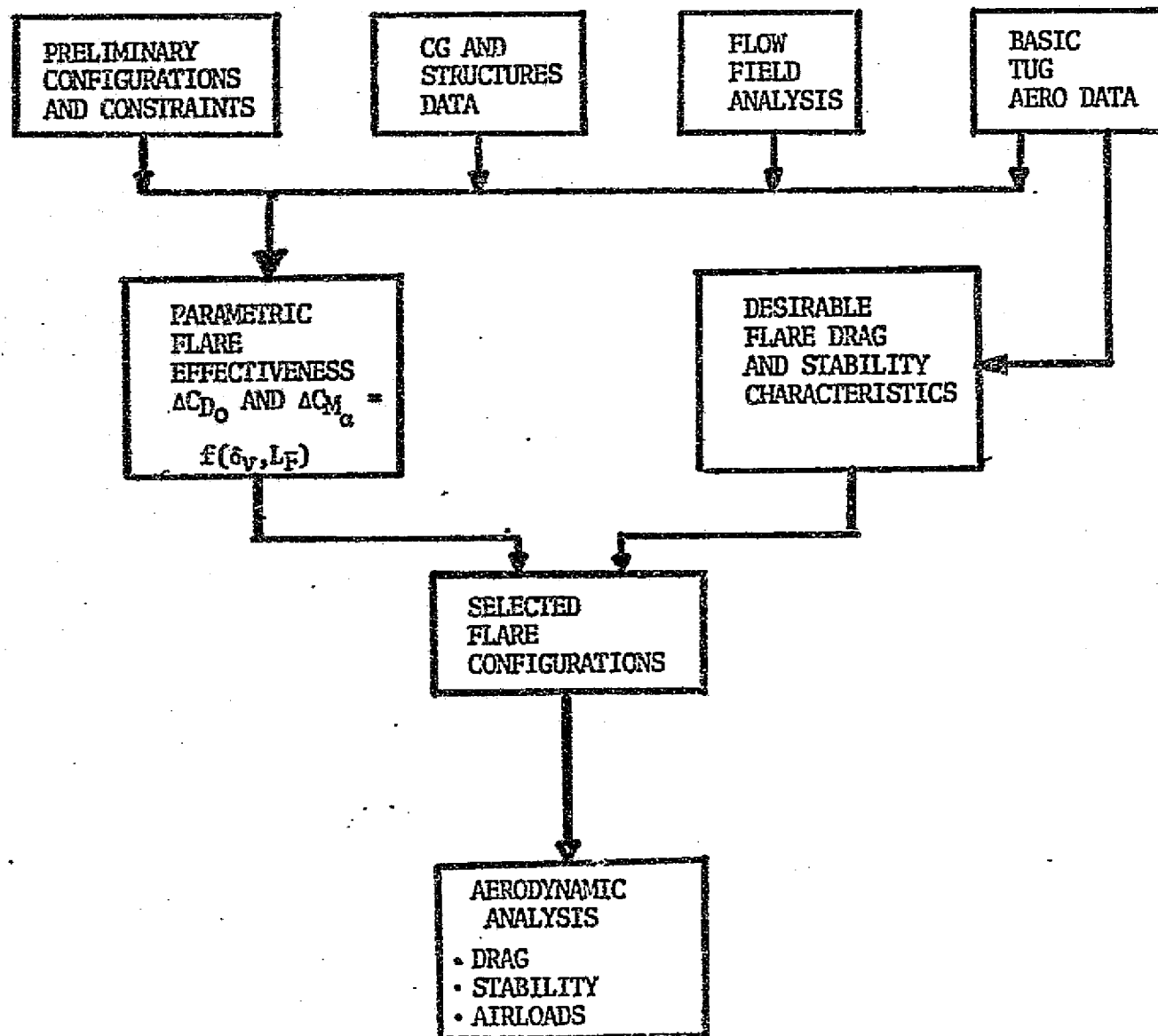


FIGURE 4.1.2.0-1 FLARE SIZING STUDY - SIMPLIFIED TECHNICAL APPROACH

DS-17142

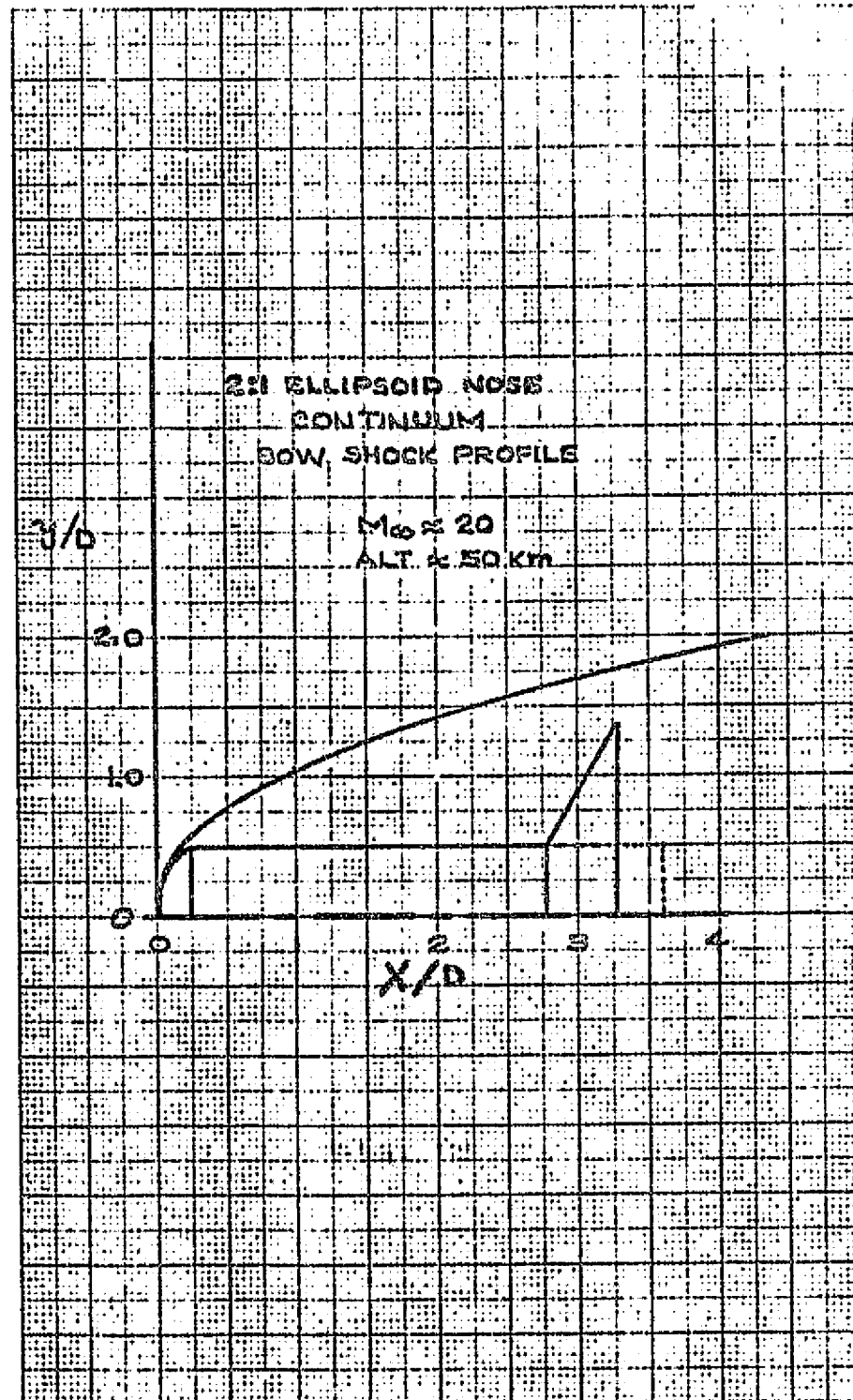


FIGURE 4.1.2.1-1 ELLIPSOID NOSE BOW SHOCK PROFILE

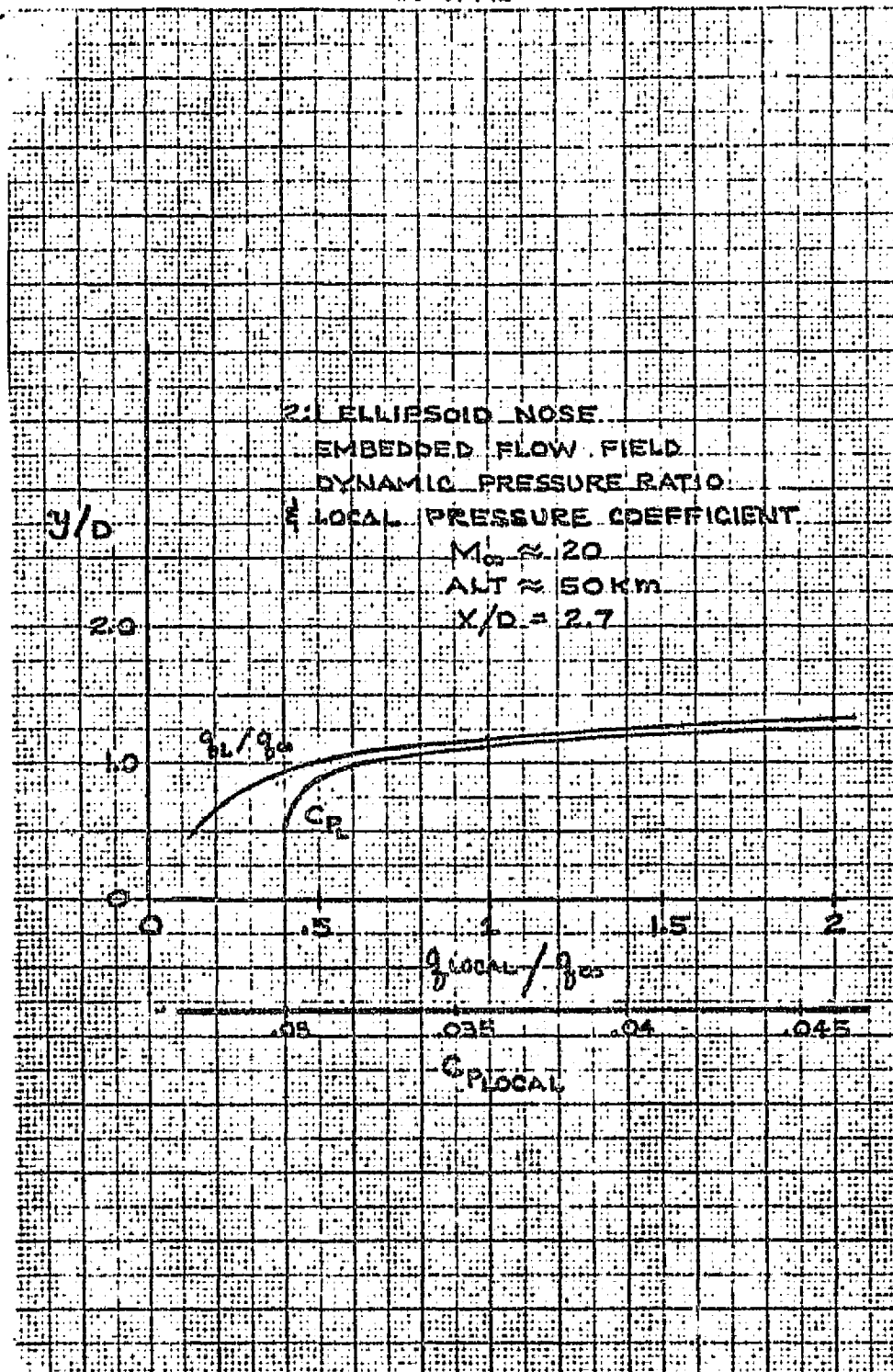


FIGURE 4.1.2.1-2 EMBEDDED FLOW FIELD CHARACTERISTICS

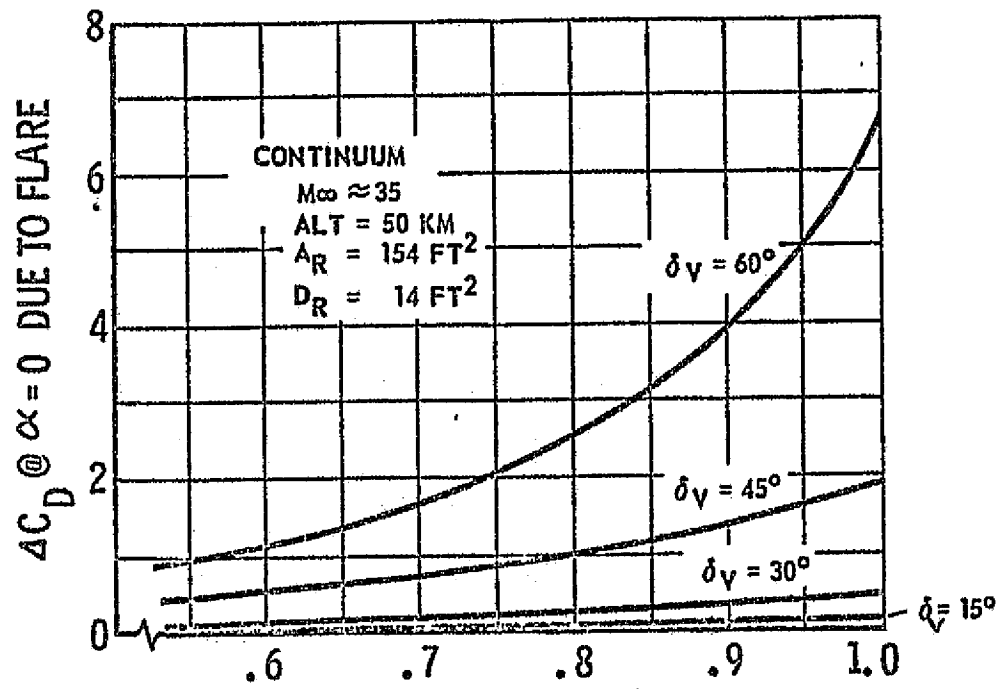


FIGURE 4.1.2.1-3: PARAMETRIC FLARE DRAG CHARACTERISTICS

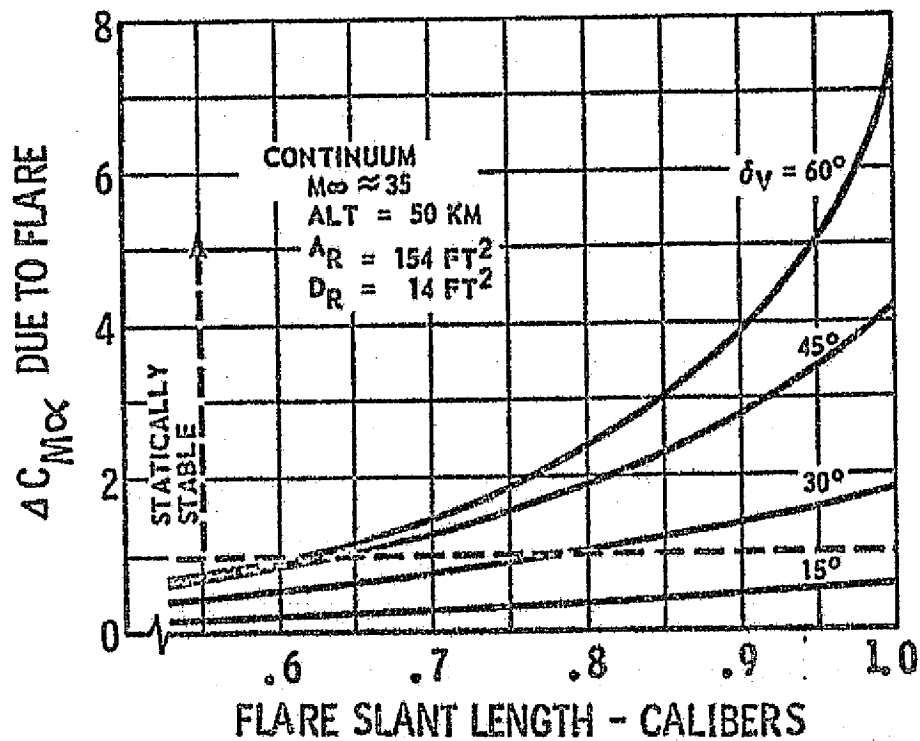


FIGURE 4.1.2.1-4: PARAMETRIC FLARE STATIC STABILITY CHARACTERISTICS

NOTES:

- ① 2:1 ELLIPSOID NOSE COMMON TO ALL CONFIGURATIONS
- ① MAIN PROPULSION GIMBAL POINT
- ② ASTRIONICS MODULE
- ③ PAYLOAD ADAPTER
- ④ PAYLOAD

TUG DIAM. = D_R = 14 FT.

CONFIG.	δ_v	SLANT LTH. - FT.
LARGE	60°	14.0
INTERM.	45°	14.7
SMALL	30°	11.25
OPT. #1	15°	17.4
OPT. #2	30°	18.4

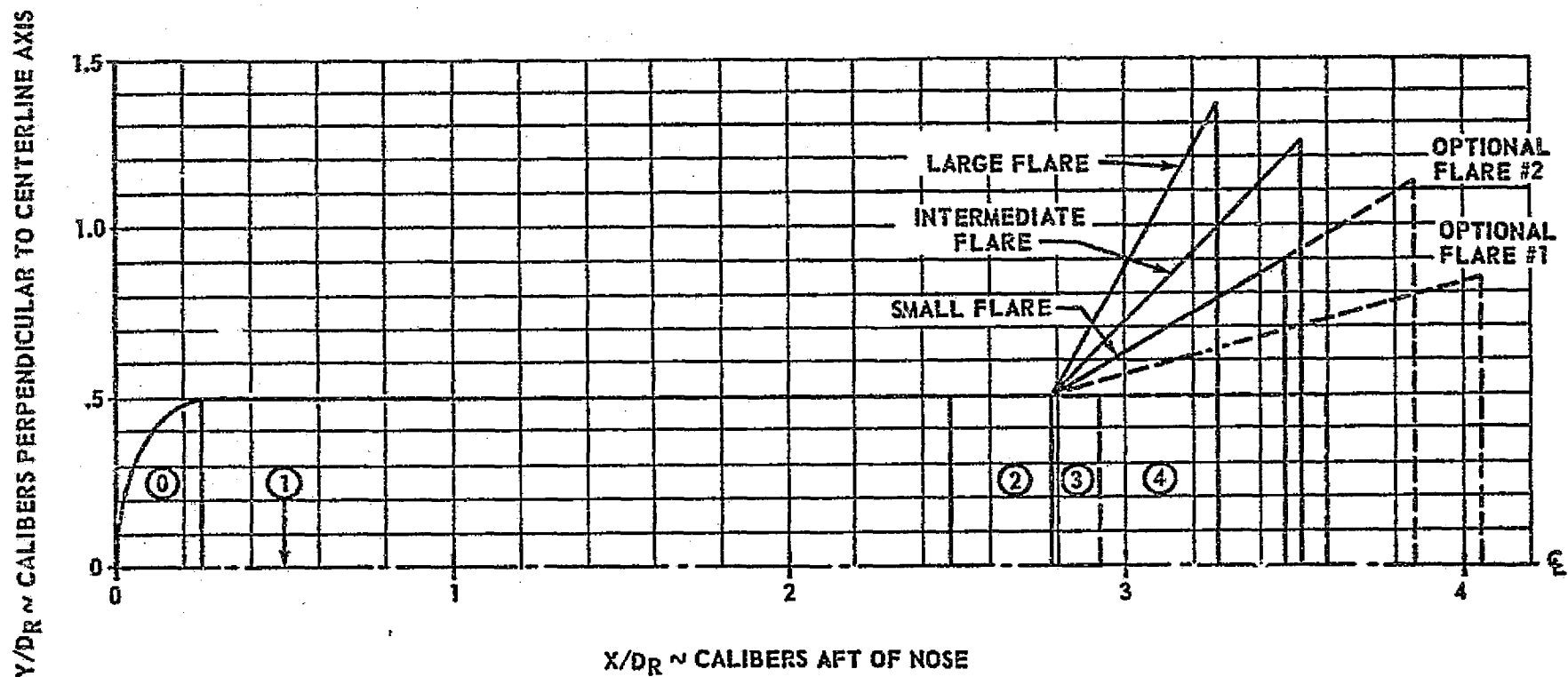


FIGURE 4.1.2.2-1. FLARED TUG CONFIGURATION(S) GEOMETRY

4.1.2.2 (Continued)

flare data, combined with the trajectory, aerodynamics, weights, and thermal analysis might allow at least a qualitative trade study to be performed which would include δ_v as a parameter. Thus, the 30° flare was chosen for the "small" flare configuration. Note that the flare slant length required for neutral stability is $\approx .805$ calibers.

Optional flare #1 is a 15° semivertex angle which also results in neutral stability. Its slant length is 1.315 calibers. The choice of the 30° δ_v for the "small" flare rather than the 15° δ_v is based on the following:

1. ΔC_{D0} 30° flare is approximately 2 times the ΔC_{D0} for the 15° flare in the continuum limit.
2. The total flare surface area is $\approx 63\%$ lower for the 30° flare. Thus, although the TPS weight per unit area will probably increase as δ_v increases (at a given flow field environment), the total TPS weight may be less due to the lower surface area.
3. The TPS required for the 15° flare may not differ appreciably from the basic Tug cylinder requirements, and, hence, given the 15° flare trajectory characteristics, the TPS required might be estimable without a rigorous aero heating analysis.

A complete set of aerodynamic data is included for the "small" 30° flare. The drag characteristics for the 15° flare have also been generated for the trajectory analysis in case this data is desired in the final configuration optimization studies. Both neutrally stable configurations are presented in Figure 4.1.2.2-1.

The remaining flare configuration, the "intermediate" flare, was selected primarily on the basis of the W/C_{DA} required for trajectory analysis.

Figure 4.1.2.2-2 indicates the nonlinear relationship between time to decay, N and W/C_{DA} . Figure 4.1.2.2-3 illustrates the C_D and W/C_{DA} range of the basic Tug, large and small flare configurations, and the W/C_{DA} and C_D of the "intermediate" flare required to investigate the nonlinear N vs. W/C_{DA} relationship. As discussed earlier, it was also desired to investigate flare semivertex angle effects with the three flare configurations.

Thus, the "intermediate" flare was defined as the following: 45° semivertex angle, flare slant length of 1.05 calibers. The continuum value of W/C_{DA} for the "intermediate" flare configuration is ≈ 30 psf.

Optional flare #2 was defined as a 30° semivertex angle flare with a 1.24 caliber slant height. This configuration is close to the W/C_{DA} of the 45° flare, and might allow flare length changes to be investigated (at least qualitatively) in the final configuration optimization studies.

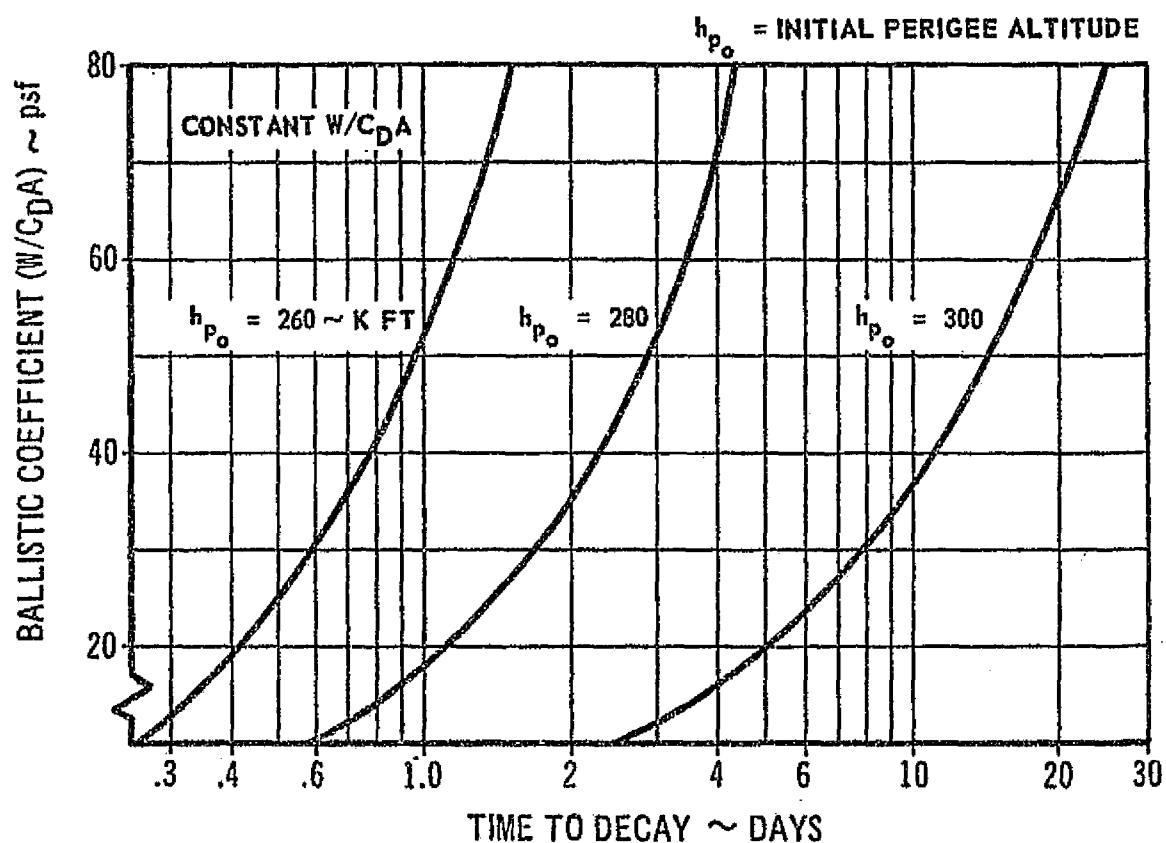


FIGURE 4.1.2.2-2. PRELIMINARY VARIATION OF TIME TO DECAY WITH RESPECT TO BALLISTIC COEFFICIENT (W/C_{DA})

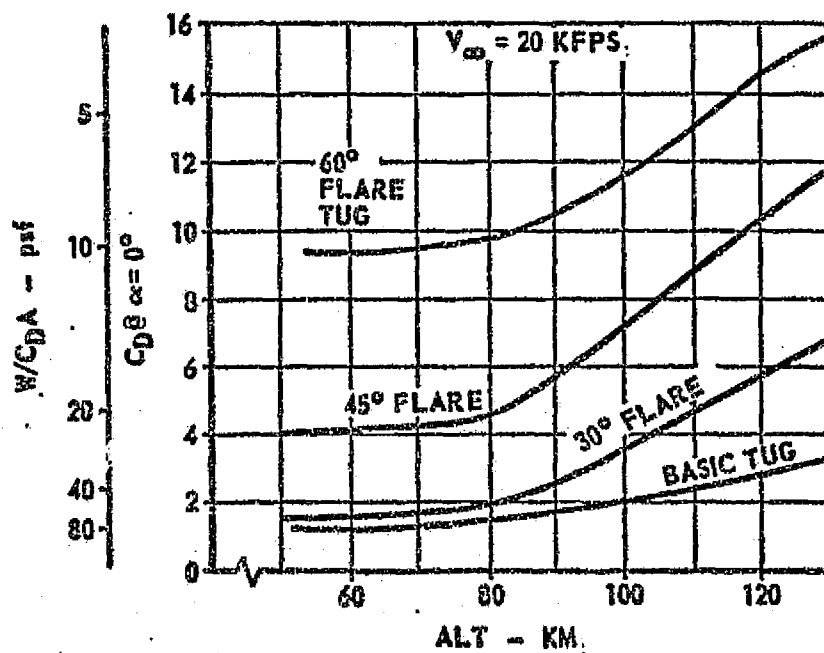


Figure 4.1.2.2-3: C_D AND W/C_{DA} RANGE FOR AEROBRAKED SPACE TUG CONFIGURATIONS

4.1.2.2 (Continued)

The "family" of flared Tug configurations is presented in Figure 4.1.2.2-1. The configurations have been selected in order to satisfy the following requirements and objectives:

Requirements:

- 1) Avionics visibility
- 2) Reasonable structural attachment point

Objectives:

- 1) Investigate an approximate order of magnitude variation in $8 \leq W/C_D A \leq 80$ psf.
- 2) Select configurations such that any non linearities in the time to decay vs. $W/C_D A$ will be analyzed.
- 3) Investigate a range of static stability from approximately neutral stability to large static stability.
- 4) Investigate flare semi-vertex angle, δ_v , effects.

Having defined the flare configurations, the task remained to estimate their aerodynamic characteristics, (C_{D0} , $C_{N\alpha}$, CP/D , and C_p) over the entire altitude and velocity flight regime of interest. As with the basic Tug configuration, the drag data was the first objective.

4.1.2.3 Flared Tug Drag Characteristics

Prediction of the flared Tug configuration drag characteristics requires combination of the basic Tug nose drag and skin friction drag characteristics with the flare pressure drag and skin friction characteristics. The skin friction drag component for the flared configurations was assumed to have the same altitude and velocity (M_∞ , Re_∞) variation as the basic Tug, based on the flared Tug wetted area. The ellipsoid nose pressure drag component was assumed unchanged due to the presence of the flare. (Note that this is equivalent to assuming that the characteristic dimension of the vehicle is the nose characteristic dimension (vehicle diameter), for the nose aerodynamic characteristics and flow regime analysis, even though the vehicle actually has a much larger maximum dimension, such as the flare diameter. While this assumption surely is invalid for very large flares or flares close to the nose, it appears reasonable for the configurations considered). Thus, having defined the nose and skin friction drag contributions throughout the flight regimes, the remaining task is to define the flare drag contribution.

The flare continuum drag contribution estimate is based on the embedded Newtonian theory (Reference 4.1.1.2-1, -2 and -3), plus the analytical approach of Reference 4.1.2.1-2. The FMF contribution is obtained via the method and data of References 4.1.1.1-7 and 4.1.1.2-5. The basic Tug bridging factor, $K(h, V)$, is correlated to a $K(M_\infty, Re_\infty)$, and re-defined for the flare characteristics using a reference length equal to

4.1.2.3 (Continued)

the flare base diameter. (With the assumption of nose drag independence with flare configuration, this is equivalent to saying that the nose will reach FMF at a lower altitude (smaller λ_∞) than the flare. While the $K(h,V)$ so defined for the flare characteristics bridging analysis is somewhat less justifiable than that for the nose bridging analysis, it is the only approach which appeared within the scope of the current feasibility study. Utilizing this $K(h,V)$ allowed definition of the flare component drag characteristics over the (h,V) range of interest. Combining these data with the ellipsoid nose data and the total vehicle wetted area skin friction contribution, allowed definition of the flare configuration drag characteristics.

Presented in Figures 4.1.2.3-1 and -2 are the drag characteristics for the flared Tug (large, intermediate, small, option #1 and optional #2) configurations. It is noteworthy to compare the variation of C_D of the five configurations in the continuum and FMF limits. In the continuum regime, the embedded flow field characteristics (primarily the reduced local dynamic pressure), dominate the flare drag effectiveness; however, in the FMF limit, the drag characteristics are more closely proportional to the flares maximum cross-sectional area.

Having completed the flare configuration drag analysis, attention was directed to the static stability characteristics.

4.1.2.4 Static Stability Analysis

The approach to the flared configuration static stability analysis parallels the approach to the drag analysis exactly. The contribution of the basic Tug nose/cylinder was modified for the shorter effective cylinder length and assumed independent of the flare configuration. The same (drag analysis) referenced data and bridging factor was utilized to determine the static stability contribution of the flare(s). Combination on the nose/cylinder $C_{N\alpha}$ and CP/D with the flare contribution results in the static stability characteristics of the flared Tug configurations. The large, medium and small flare configuration static stability data, $C_{N\alpha}$ and CP/D , are presented in Figures 4.1.2.4-1 and -2, respectively. (Recall that only drag data was to be defined for the optional flare configurations).

One rather interesting aspect of the static stability data is the variation of CP/D from the continuum limit to the FMF limit. In comparing the basic Tug CP/D variation, (Figure 4.1.1.2-1), with the flared configurations, the following items should be noted:

1. Each flare configuration is opposing the same basic Tug disturbing moment.
2. For the basic Tug, the CP/D (Figure 4.1.1.2-1) variation from continuum to FMF is primarily a "planform" effect, i.e., the CP moves from the nose region in the continuum regime towards the vehicle "area centroid" in the FMF regime.

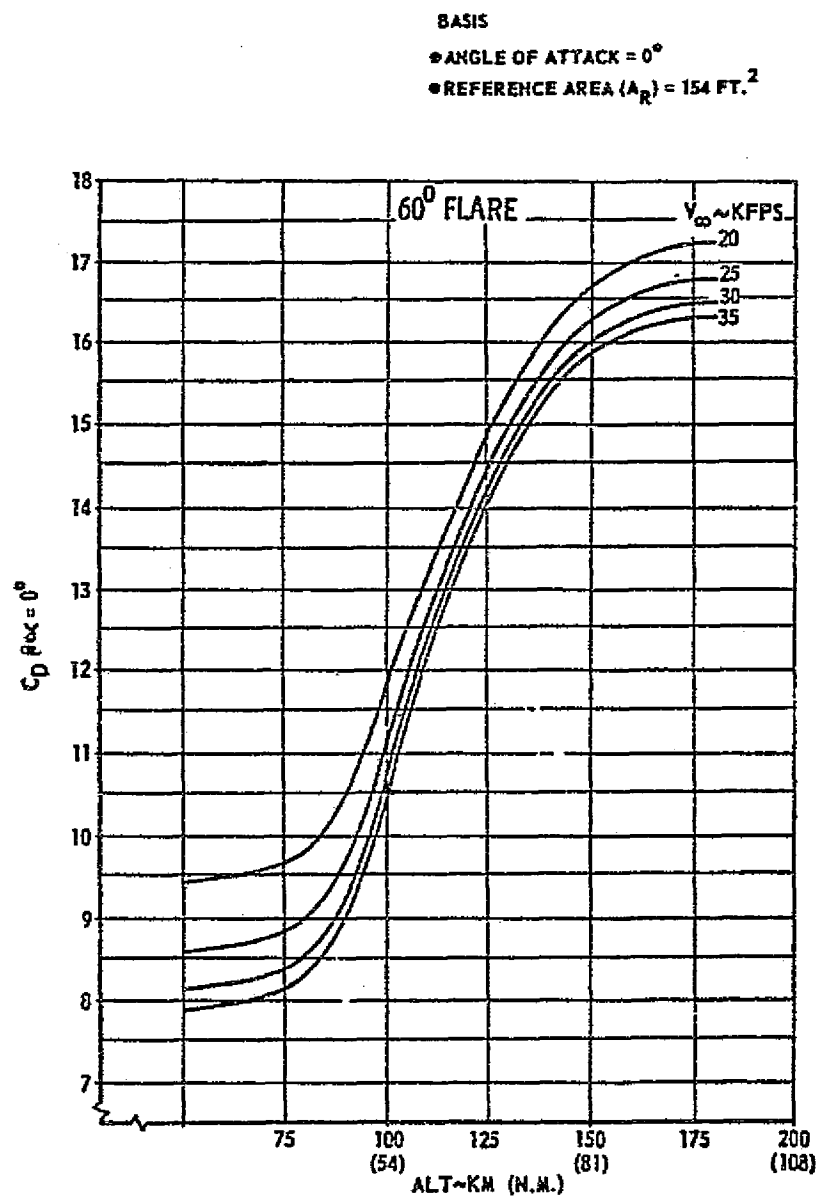
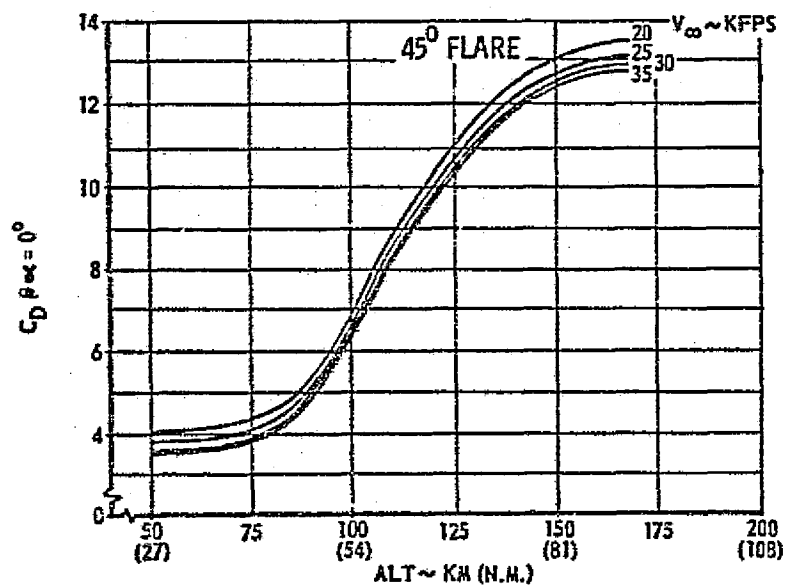
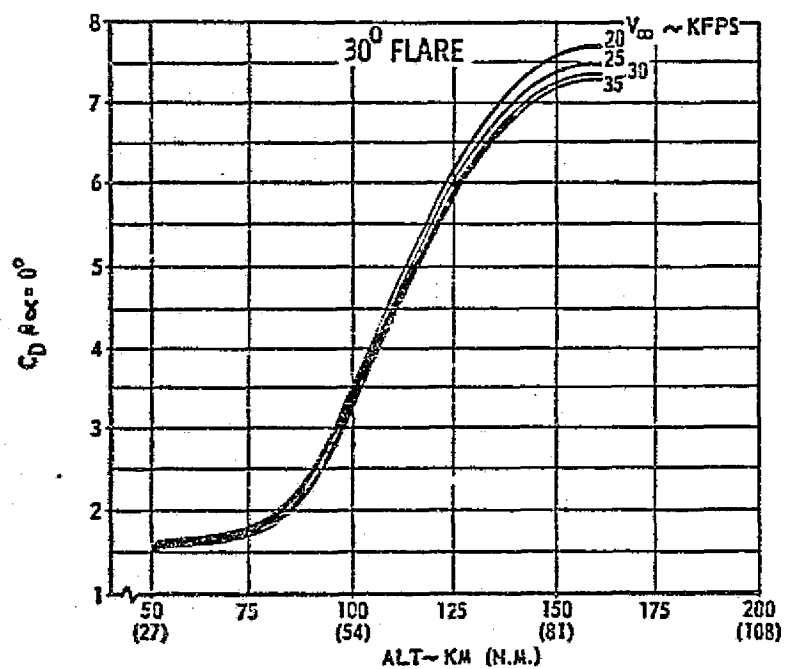


FIGURE 4.1.2.3-1: DRAG COEFFICIENTS FOR SELECTED FLARE CONFIGURATIONS

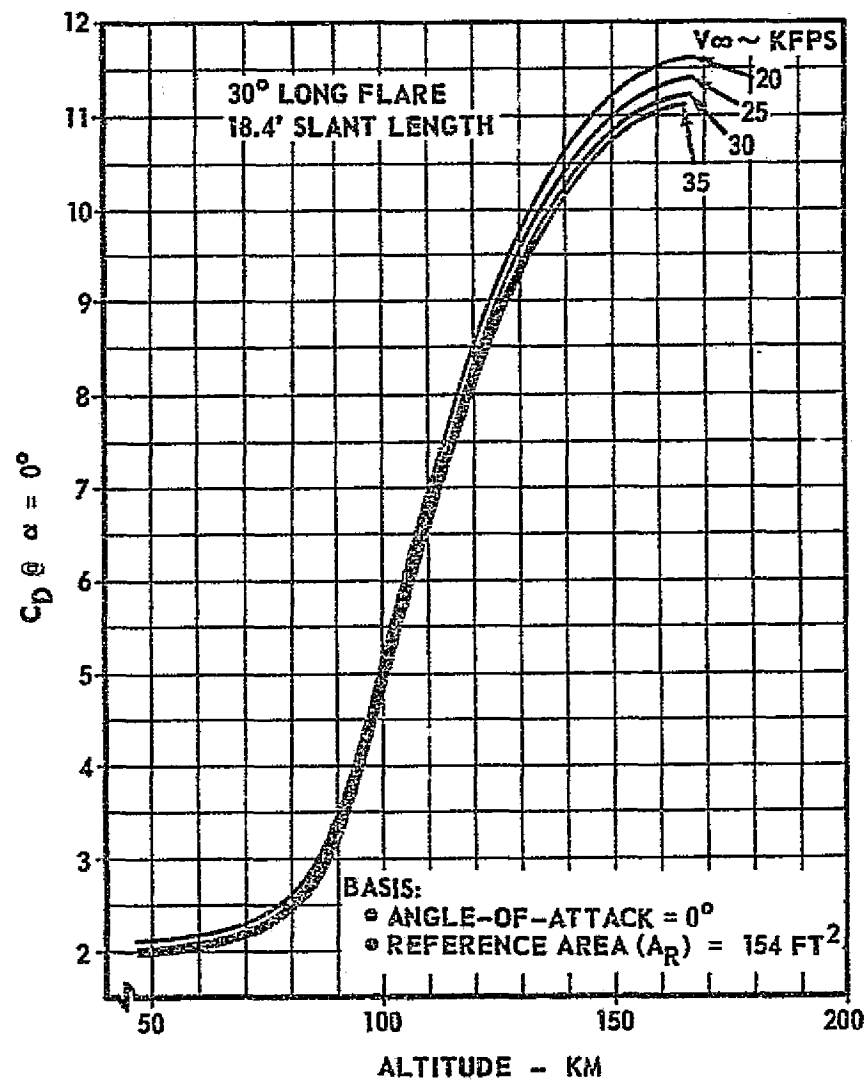
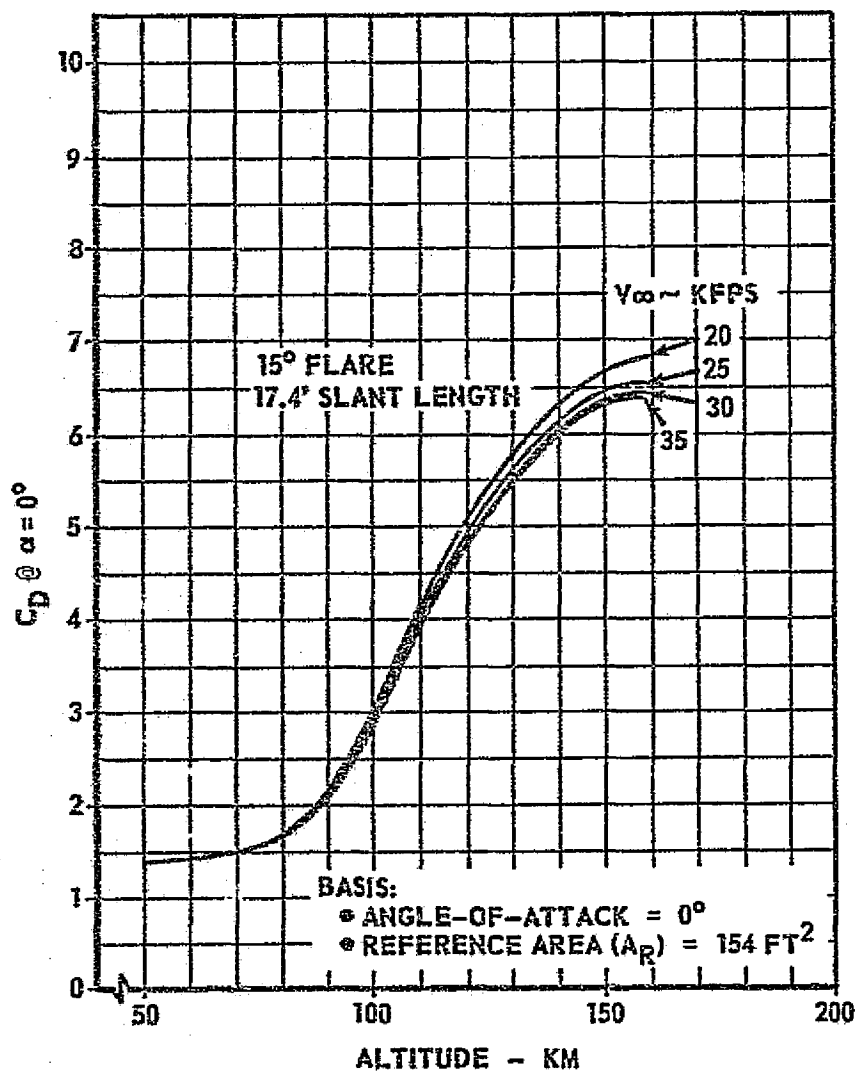


FIGURE 4.1.2.3-2. DRAG COEFFICIENTS FOR OPTIONAL FLARED CONFIGURATIONS

BASIS

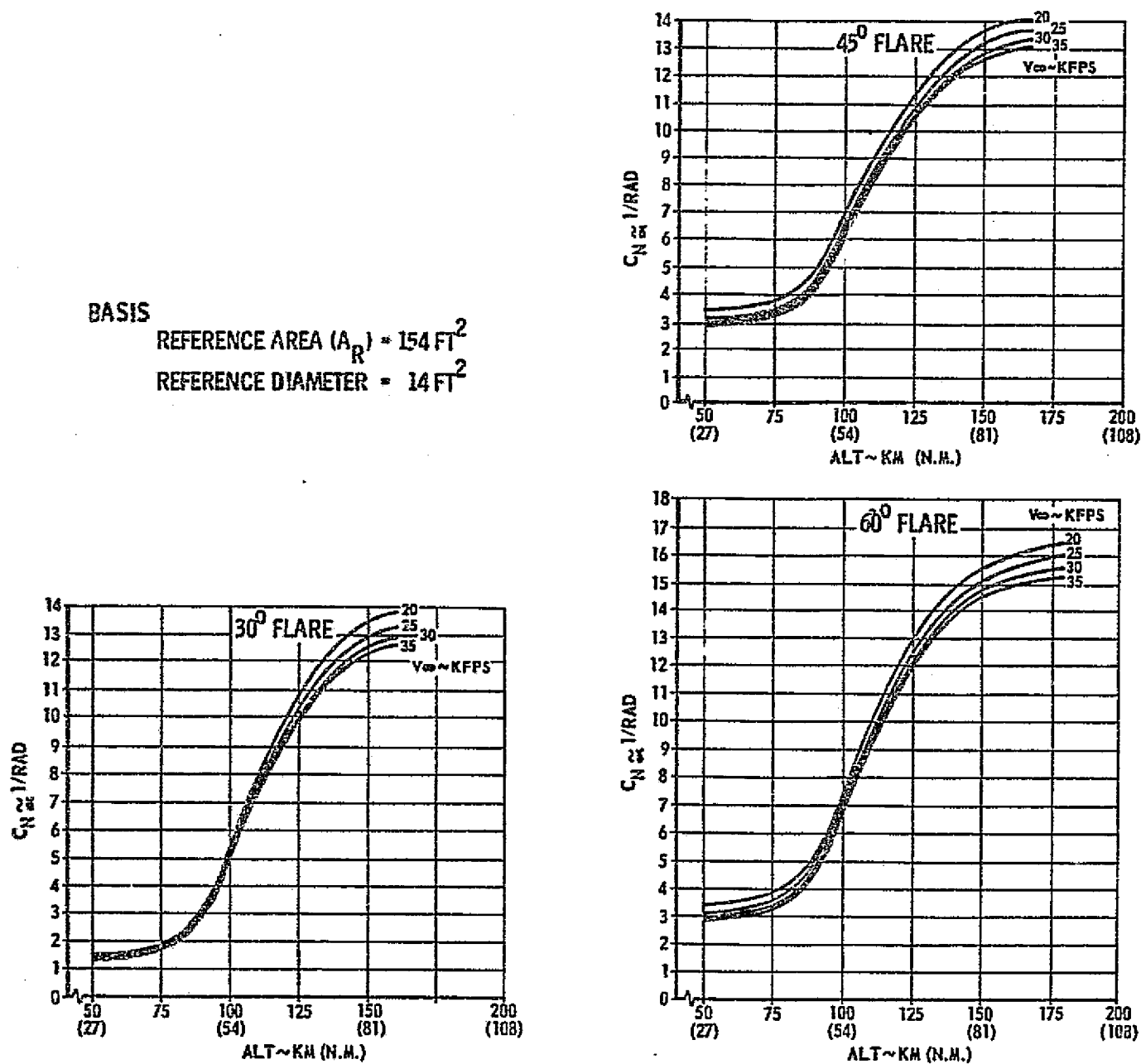
REFERENCE AREA (A_R) = 154 FT²REFERENCE DIAMETER = 14 FT²

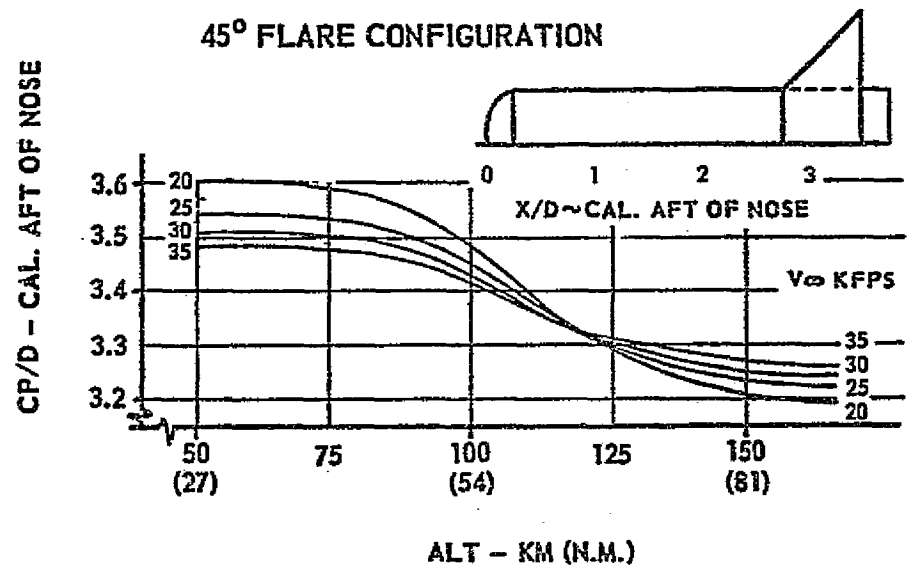
FIGURE 4.1.2.4-1: COEFFICIENT OF NORMAL FORCE SLOPE FOR FLARED CONFIGURATIONS

BASIS

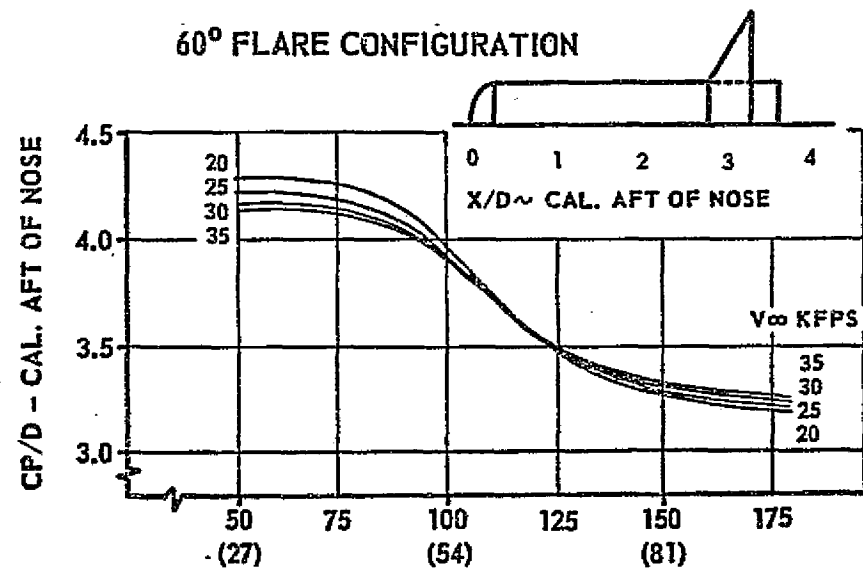
REFERENCE AREA (A_R) = 154 FT²

REFERENCE DIAMETER = 14 FT

45° FLARE CONFIGURATION



60° FLARE CONFIGURATION



30° FLARE CONFIGURATION

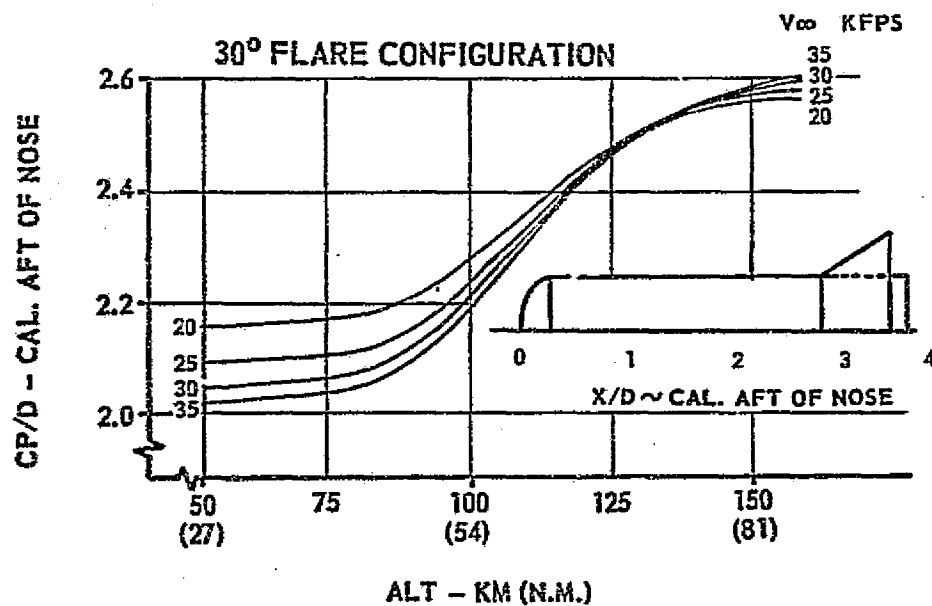


FIGURE 4.1.2.4-2: CENTER OF PRESSURE FOR FLARED CONFIGURATIONS

DS-17142

4.1.2.4 (Continued)

3. For a $30^\circ \delta_v$ flare, the CP of the flare is approximately at the base of the flare in both the continuum and FMF regime. Thus, the planform effect of the basic Tug nose cylinder dominates the CP variation with altitude, and the CP again moves from the nose aft.
4. For the 45° and $60^\circ \delta_v$ flares, the continuum flare CP is ≈ 1.0 and 4.0 calibers aft of the flare base, respectively, in the continuum limit. However, in the FMF limit, the CP of both flares moves forward to approximately the flare base. Thus, for the large and intermediate flare configurations (60° and 45°), the large negative flare C_{M_α} 's and associated forward CP shift from continuum to FMF dominate the total vehicle CP/D variation with altitude. Hence, CP moves forward, towards the nose, as the flow regime changes from continuum to FMF.

In determining the C_M and C_N of the flared configurations in the continuum limit, the effects of flow shielding on the "upper" side of the flare have not been included. The reason for this is that neglecting the shielding effects will result in a conservative estimate of the continuum stability at a considerable savings in time, due to the complexity involved in the shielding analysis.

With the completion of the flared configuration static stability, the only remaining aerodynamics analysis task was the definition of the nose and flare pressure coefficient distribution.

4.1.2.5 Pressure Coefficient Distribution Data

The nose and cylinder sidewall pressure coefficient distributions at zero angle of attack were determined in exactly the same manner as the basic Tug. The distributions for the flares are presented in Figure 4.1.2.5-1. The distributions are seen to differ only in the K^* factor (determined in the same manner as discussed in Section 4.1.1.3), supplied to convert C_p to local pressure in psf.

The flare pressure coefficient distributions, are based on a similar, maximum ($K_{BRIDGE} \cdot q_{max}$) product plus the local embedded flow field properties determined from the flow field analysis (P_l/P_∞ and q_l/q_∞). Both the uniform distribution at $\alpha = 0^\circ$ and the non-uniform distribution at $\alpha = 6^\circ$ were considered since it appeared conceivable that the worst possible load case might result from an asymmetrical flare load. Thus, flow shielding effects are considered in defining the flare pressure coefficient distribution.

Figure 4.1.2.5-2 presents the flare pressure coefficient distributions for the large, intermediate, and small flare configurations. Definition of the pressure coefficient distributions completes the aerodynamic data requirements for the Space Tug Aerobraking Study.

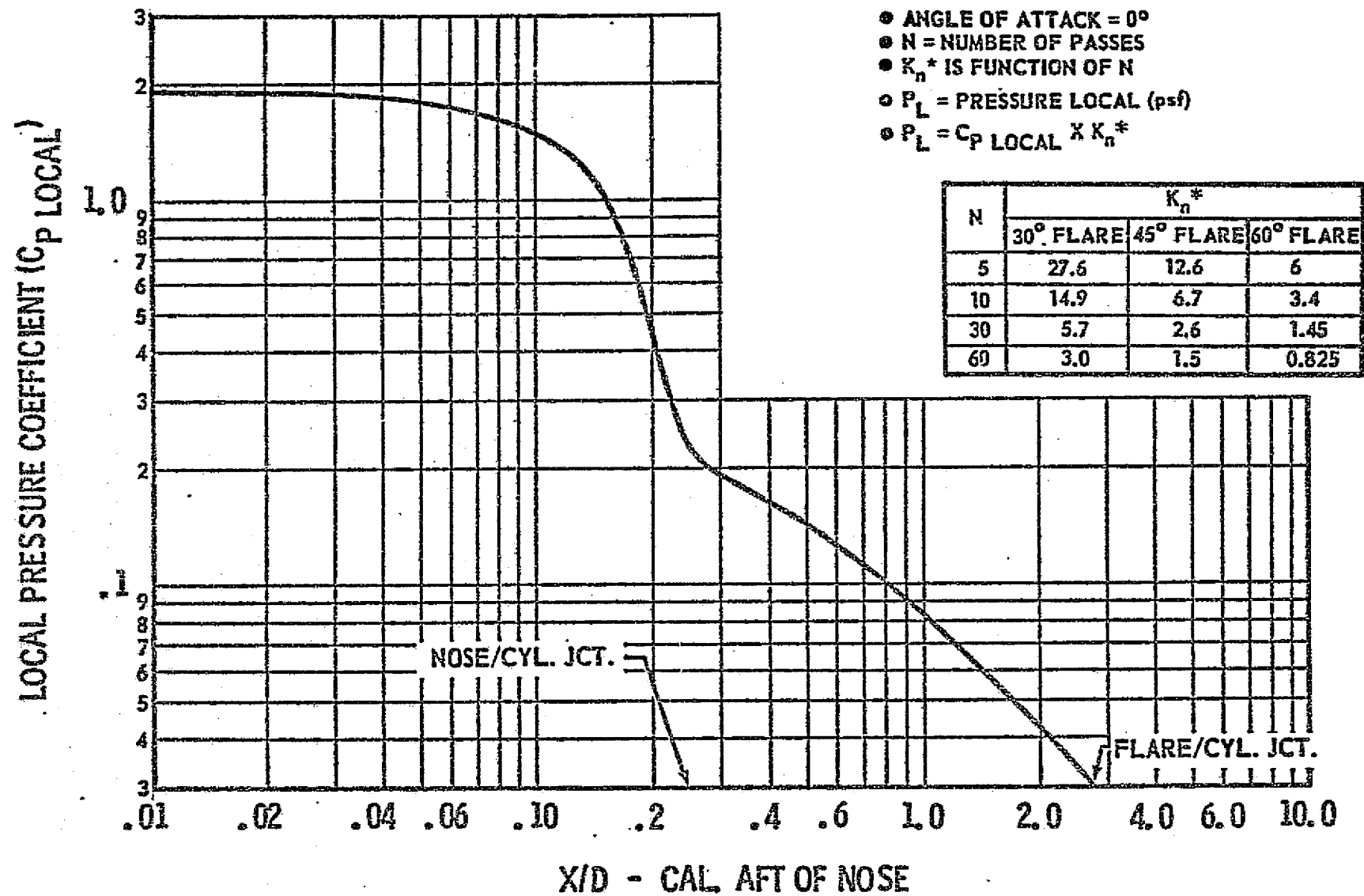
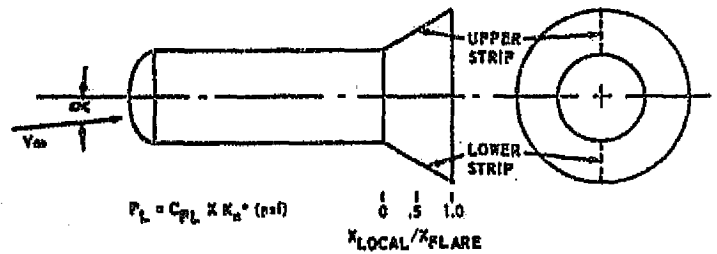
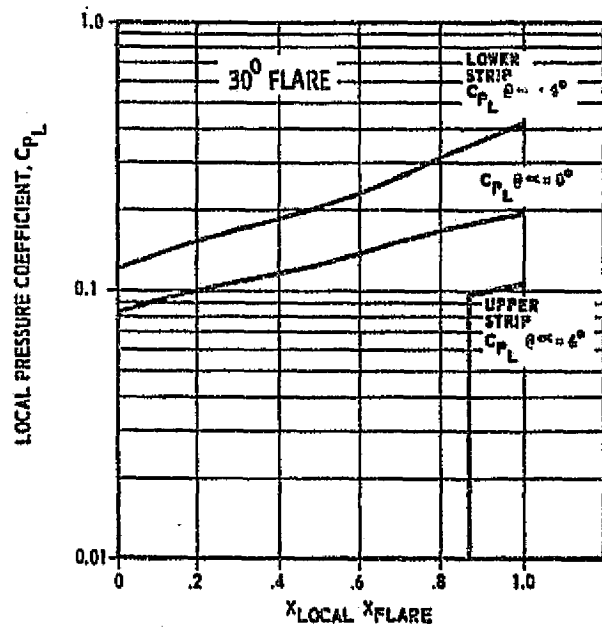


FIGURE 4.1.2.5-1: LOCAL PRESSURE COEFFICIENTS OVER HEAT SHIELD AND CYLINDER (FLARED CONFIGURATIONS)



NO. OF PASSES N	K_n^*		
	30° FLARE	45° FLARE	60° FLARE
5	25.2	10.35	5.2
10	14.0	5.65	2.9
30	5.4	2.16	1.22
60	2.9	1.22	0.68

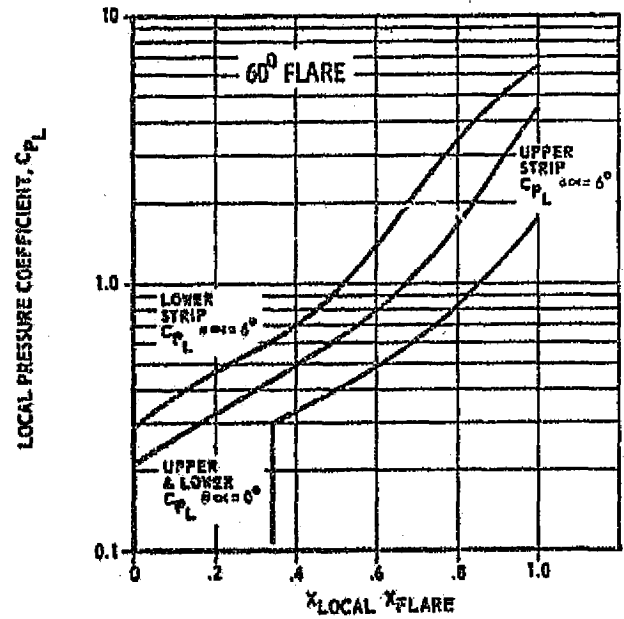
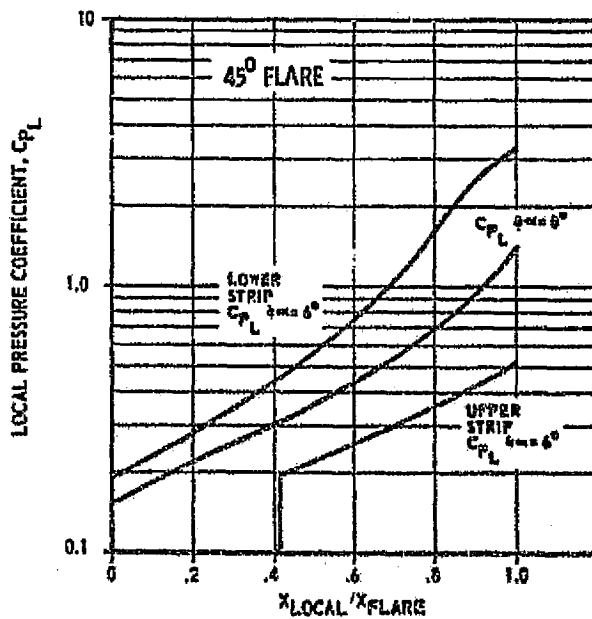


FIGURE 4.1.2.5-2: LOCAL PRESSURE COEFFICIENTS OVER FLARES

4.1.2.5 (Continued)

The local pressure (C_p) and the K_n^* factors given in the prior Figure 4.1.1.3-1 and in Figure 4.1.2.5-1 were converted as shown in Figure 4.1.2.5-3 to illustrate the pressure loads (in pounds per square inch) for the heat shields of the basic (no flare) and 30°, 45° and 60° flared Tug configurations. The maximum pressure occurs at the nose for each configuration and decreases from 0.47 psi for the basic (no flared) Tug to 0.08 psi for the 60° flared Tug. As the number of passes increases from 5 to 60, the pressure loads on the shield decrease by approximately an order of magnitude.

The local pressure coefficient (C_p) and the K_n^* values for the flares are shown in Figure 4.1.2.5-2. This data was converted to pressure loads (pounds per square inch) as shown in Figure 4.1.2.5-4. The data presented is the "worst case" pressure loads which would occur at the outer edge of the flare lower surface (assuming a zero or six degree angle of attack). The 45° and 60° flare configurations with a six degree angle of attack have approximately the same pressure loads. For a zero angle of attack the pressure loads on the 60° flare are approximately 1.6 times as great as that on the 45° flare. The shorter length and lesser angle 30° flare has a significant drop in pressure loads compared to either the 45° or 60° flare. The pressure loads on the outer edge of the flares represent the "worse" loads conditions on the flare; however, the loads are extremely low but do impact the design of the flare for the low pass missions (5-10 passes).

The above figures have identified the pressure levels at specific points (heat shield nose, flare outer edge) as a function of the number of passes. Figure 4.1.2.5-5 illustrates the local pressure loads along the entire length of the vehicle for the 30°, 45° and 60° flared configurations. The 30 pass mission and zero angle of attack was selected as representative of the mission variables. The local pressure has a rapid decrease over the edges of the heat shield ellipsoid. The 30° flare configuration has a higher pressure (0.75 psi) on the nose than on the outer flare edge (0.0076 psi). The 45° flare has a smaller pressure differential between the nose and outer flare edge (0.34 psi to 0.21 psi). The pattern is reversed for the 60° flare with the outer flare edge's pressure (0.38 psi) greater than that on the nose (0.019 psi). The increase in pressure along the slant height of the flares is more pronounced with the steeper angles. These flare pressure profiles impact the flare thickness and supporting structure which contributes to the heavier weights of the 60° and 45° flares versus the lighter weight of the 30° flare.

D5-17142

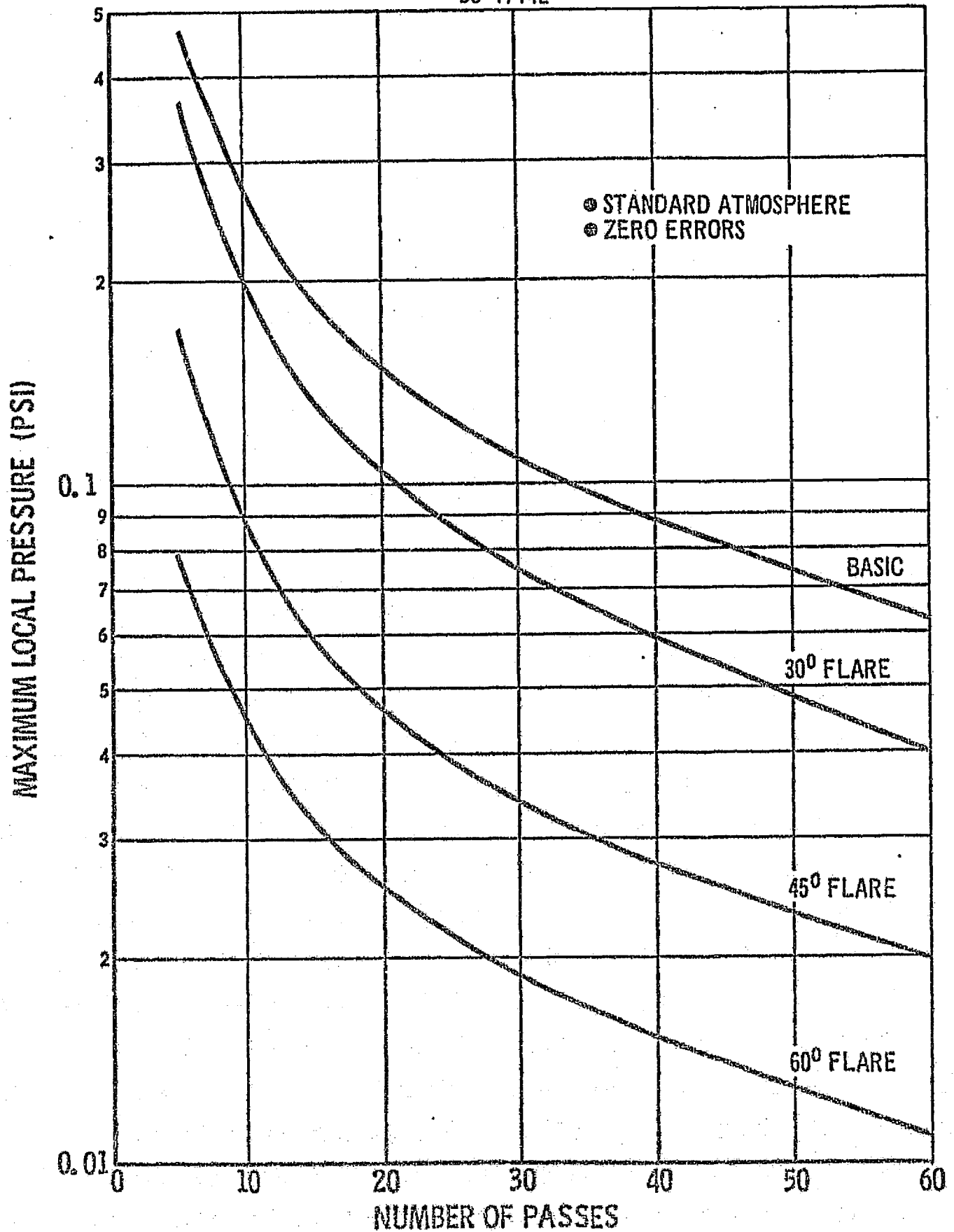


FIGURE 4.1.2.5-3: MAXIMUM LOCAL PRESSURE ON HEAT SHIELD NOSE

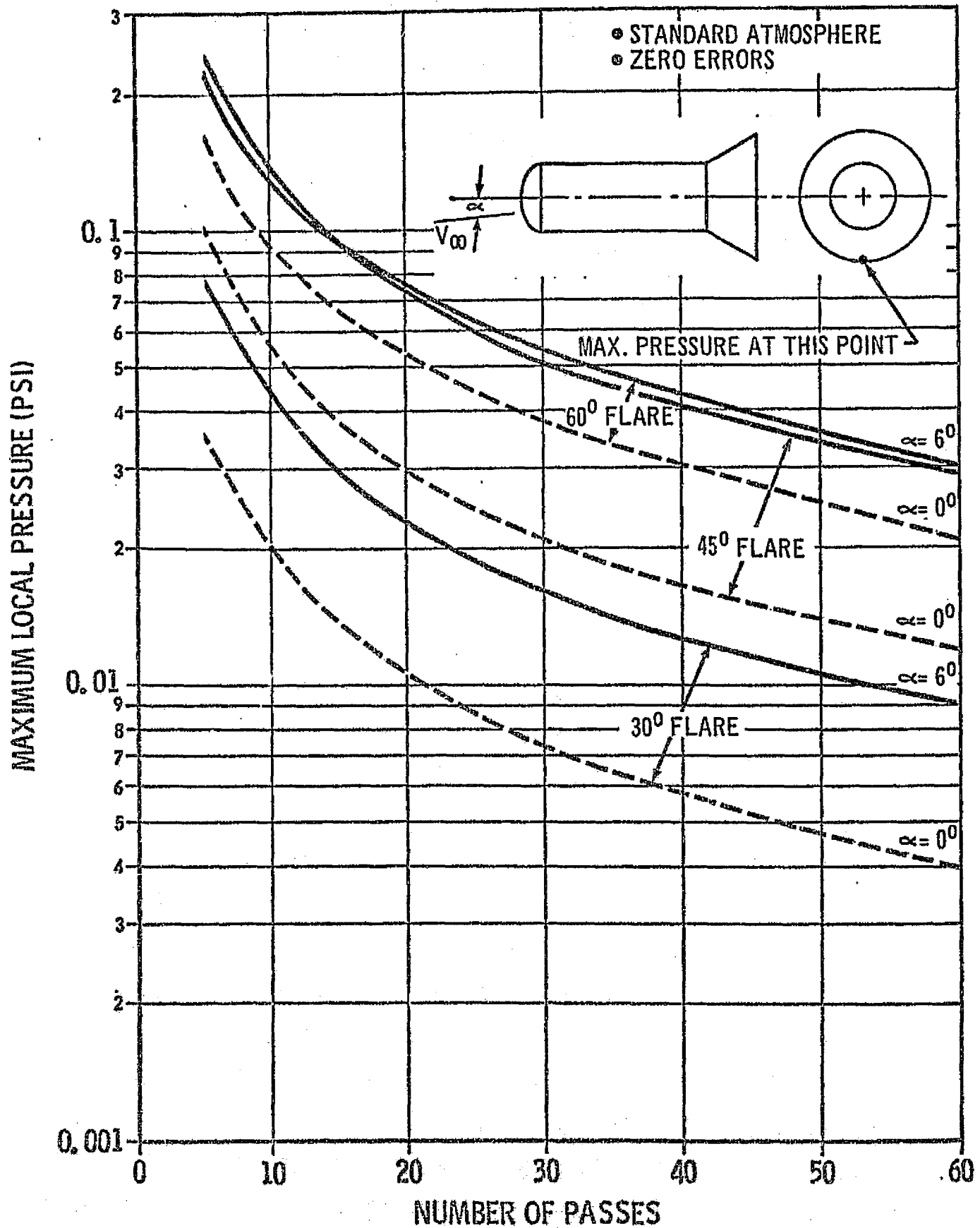


FIGURE 4.1.2.5-4: MAXIMUM LOCAL PRESSURE AT OUTER EDGE OF FLARE

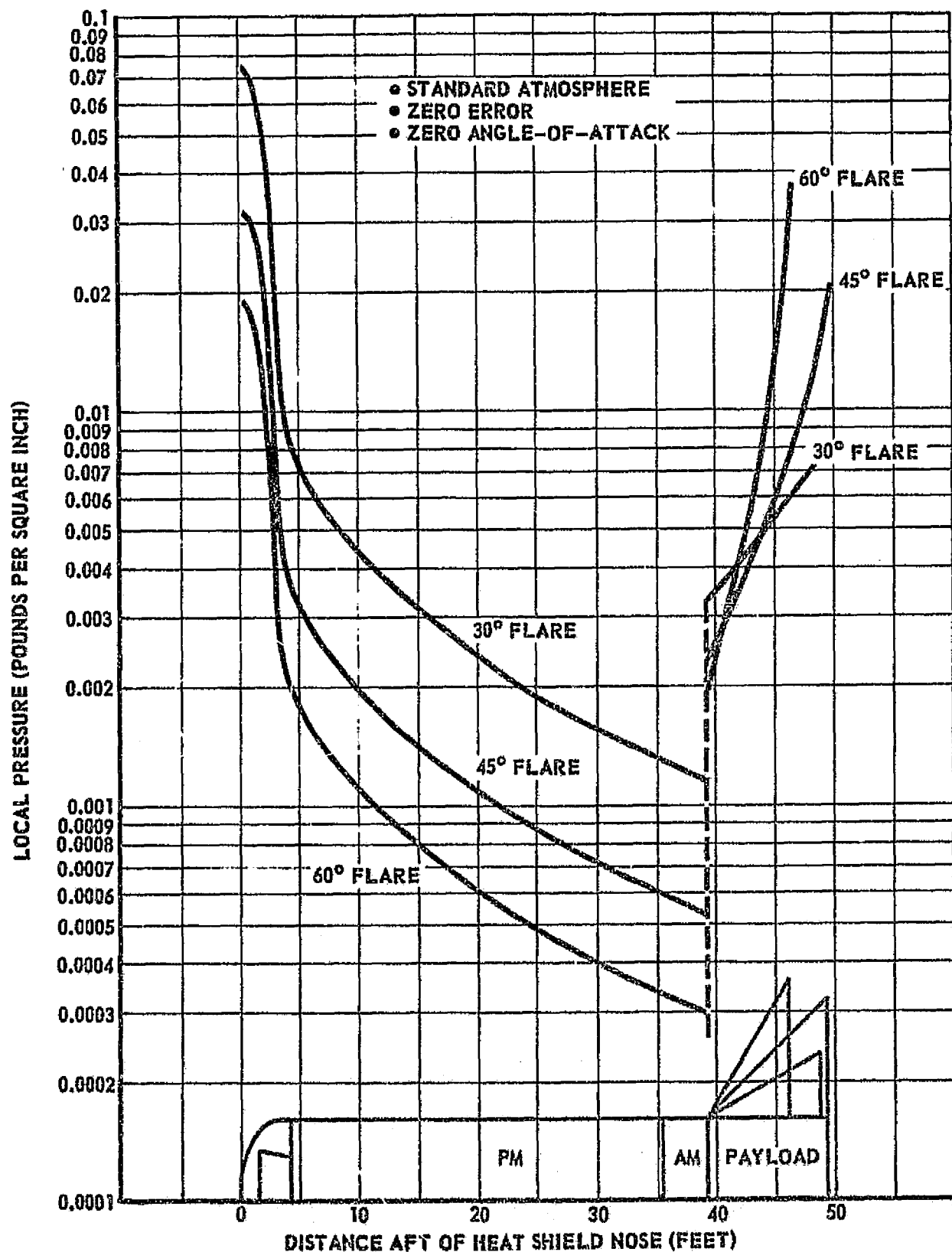


FIGURE 4.1.2.5-5: MAXIMUM LOCAL PRESSURE PROFILE
(30 PASS MISSION-FLARED CONFIGURATIONS)

4.2 AEROBRAKING CONFIGURATION CONCEPTS

This section describes the aerobraking Space Tug configuration concepts. These aerobraking concepts were bounded by the study groundrules to aerobraking kits which can be applied to the conventional Space Tug. The study duration (four months) coupled with the limited funding did not permit analyses of all of the feasible aerobraking kits nor did it permit an examination of all of the more practical modifications to the Space Tug to enhance its aerobraking capabilities. The study did, however, provide insight to aerobraking capabilities of the Space Tug and did identify the environmental criteria effecting material selection and design concepts. Aerobraking design concepts were investigated in sufficient depth to define some reasonable configuration concepts, their functional capabilities and their weights.

The key study groundrules which impacted the aerobraking kit design concepts are listed below. These were:

- a. The baseline (non-aerobraked Space Tug configuration) would be that developed in the Boeing Pre-Phase A Space Tug Study (prior Reference 1.1.0.0-1) and is compatible to the 65,000 pound Shuttle payload capability.
- b. The aerobraking kit modifications were designed to be removable and were designed to be applied in kit form.
- c. The kit elements imposed minimal weight or configuration penalty to the conventional Tug configuration.
- d. The kit elements were designed to fit within the Space Shuttle cargo bay constraints (15 foot diameter by 60 feet long).
- e. The payload thermal limit was 300°F. The aerobraking payload adapter kit was designed to this limit.
- f. The aerobraking kit elements were designed to be reusable, where practical.
- g. The weights of the aerobraking elements were minimized in order to maximize payload capabilities. The design concepts were, therefore, directed to use lightweight as the governing design criteria.
- h. The thermal protection systems applied to the Tug for the aerobraking usage would be shuttle era technology.
- i. The state-of-the-art for radiative thermal protection materials was assumed to be 2000°F capability with a TD-nickel-chrome alloy.
- j. The avionics systems applied for the aerobraking would be shuttle era technology.

4.2 (Continued)

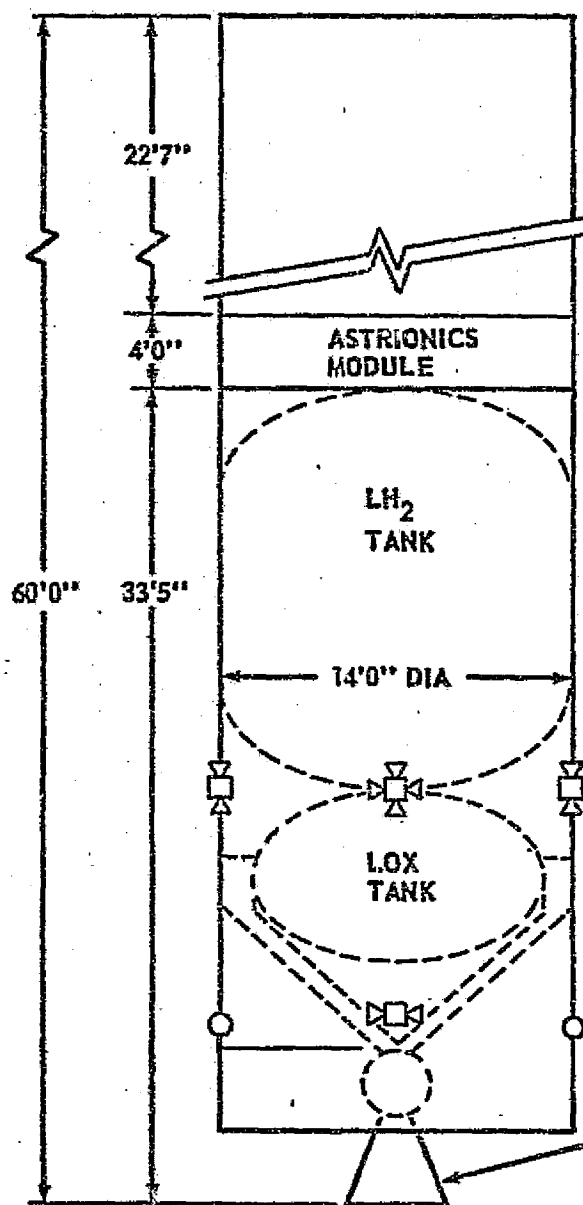
The subsequent paragraphs of this section identify the conventional trajectory Space Tug configuration used as a starting point for the study (Section 4.2.1), the aerobraking kit elements (Section 4.2.2) and then identifies the aerobraking kit design options and recommendations (Section 4.2.3).

4.2.1 Conventional Trajectory Space Tug Configuration

The study groundrules stipulated that the aerobraking kits would be applied to the conventional trajectory Space Tug configuration. Figure 4.2.1.0-1 illustrates the conventional Space Tug used as the baseline. The Tug consists of a propulsion module, an astronics module, payload adapter and the payload. The Boeing Space Tug design concept used a 14 foot diameter rather than the 15 foot Shuttle cargo bay diameter as a design limit. The one foot diameter difference was allowed to account for micrometeoroid shielding, reaction control system nozzle clearances and to allow for other proturbances the vehicle may require. The propulsion module stage length with the two position nozzle retracted (as during delivery to orbit by the Shuttle) is 33.4 feet. After removal from the Shuttle, the propulsion module with the nozzle extended is 38.25 feet. The stage has a LOX/LH₂ propulsion system with an uprated RL-10A-3-8 engine. The reaction control system consists of four sets of four thrusters located 90° apart at a vehicle station comparable to the bottom of the LH₂ tank. These thrusters are used for pitch and yaw maneuvers. The eight roll thrusters are located at a station comparable to the engine gimbal point and are spaced 90° apart. The astronics module is 14 feet diameter and four feet high. It is mounted atop the propulsion module and below the payload adapter. The combined length of the propulsion and astronics module is 37.5 feet. The remaining length (60 foot long Shuttle cargo bay minus 37.5 feet) is 22.5 feet which is available for housing the payload adapter and payload.

The propellant loading in the propulsion module is 45,000 pounds of LOX/LH₂. The propulsion module inerts weigh 5,868 pounds, giving a stage weight of 50,868 pounds and a stage mass fraction of 0.885. The astronics module weighs 2526 pounds (from IBM's previous Space Tug Study - prior Reference 3.3.0.0-1). This module used state-of-the-art technology and was updated in this study to reflect Shuttle era technology. The advanced technology reduced the astronics module weight to 1960 pounds. The mass fraction of the overall Space Tug with the old astronics module and the new astronics module are 0.840 and 0.849, respectively.

To provide the docking and holddown capability of the payload to the Space Tug, a payload adapter will be required. This adapter was designed to be a separate, removable kit. The weight of the adapter is 200 pounds. The payload adapter, when used with a flared configuration aerobraking Tug, is used as a multipurpose structure: (1) To mount the aerobraking flare to the Tug; (2) to provide housing for the flare actuation system; and (3) to provide a thermal protection housing for the payload. Because this adapter is a special fixture required for



WEIGHT ESTIMATE (LBS)

● PROPULSION MODULE

● PROPELLANT

● INERTS

● ENGINE

● PROP/MECH

● THERMO/MICRO

● STRUCTURE

● CONT. & RESID.

● ASTRIONICS MODULE

● ELECTRICAL

● AVIONICS

● STRUCTURE

● THERMAL

● PAYLOAD ADAPTER

TOTAL SPACE TUG WEIGHT
MASS FRACTIONRL-10A-3-8 ENGINE
(NOZZLE RETRACTED)PRE-PHASE A
SPACE TUGSPACE TUG
WITH
UPRATED
ASTRIONICS

50,868

50,868

45,000

5,868

639

801

573

2912

943

2,526

1,960

841

625

400

660

200

200

53,594

53,028

0.840

0.849

FIGURE 4.2.1.0-1: CONVENTIONAL SPACE TUG CONFIGURATION

4.2.1 (Continued)

aerobraking, it was considered an aerobraking kit element.

The conventional Space Tug configuration was based on the previously conducted Boeing Pre-Phase A Space Tug Study and on the IBM Astrionics Module Study. Both of these studies based their design concepts on Saturn era (pre-1970) technology, i.e., state-of-the-art technology per the prior study groundrules. In this study, the astrionics module was updated to reflect the Shuttle era (1972-1974) technology. The propulsion module was not updated as the current studies are in the process of updating the Tug technology. It is expected that the propulsion module inert weights will be significantly reduced by new high performance engine systems, new propulsion/mechanical systems, integrated astrionics and integrated structures. The engine system for the advanced Tug will be specifically designed for earth orbital operations and will have lower thrust levels and higher specific impulses (470 seconds).

These changes may increase the overall Space Tug mass fraction to 0.860 or 0.870. The lower inert weights coupled with the improved specific impulse will increase the payload capability of the aerobraked Space Tug well beyond the payload capabilities shown in the summary and the sensitivities sections of this report.

4.2.2 Aerobraking Kit Elements

The selection of aerobraking kit elements are dependent on the re-entry mode used. The Tug could perform the aerobraking re-entry with tumbling or in a controlled planform mode. A tumbling mode was rejected due to its impact on the guidance and navigation systems and upon the need to protect larger Tug surface areas from the thermal environments. In the controlled planform mode, the Tug may be flown payload end first, sideways or aft end (propulsion module) first.

The highest temperatures are encountered on the forward end of the vehicle. The payload has the lowest temperature capability (300°F) of any element of the vehicle. The propulsion module first re-entry would have the engine system exposed to the higher thermal environments. The engine systems can withstand greater temperatures and have some thermal protection already supplied with the conventional Tug concept. Therefore, the payload end first trajectory would require more thermal protection than the aft end first trajectory. Further, the provision for payload thermal protection would have to be of variable length due to the differences in length of the potential payloads.

A sideways controlled mode would require the use of the reaction control system continuously to provide static stability. The variable payload sizes would change the vehicle configurations from mission to mission and would require a mission by mission correction analyses prior to launch. The sideways entry also has high sidewall temperatures as this would be the forward end of the vehicle. Continual rotation would be required to evenly disperse the heat.

4.2.2 (Continued)

Therefore, the aft end first mode of controlled entry appears to offer the greatest advantage. With this mode, the aft surface presents the smallest area to the high temperatures, is partially protected from the aerobraking thermal environment by the conventional thermal protection, and thus may be protected with the least thermal weight penalties of any of the re-entry modes.

In the initial studies of the aft end re-entry, some thought was given to re-entry without the use of an aft heat shield. An examination of the temperatures the engine components could withstand indicated that large quantities of thermal protection would be required to protect these components during aerobraking. Further, the complexities of the aerodynamics associated with a protruding nozzle would necessitate that wind tunnel type testing be performed to provide realistic aerodynamics input data for the control, airloads and trajectory analyses. These problems indicated that it would be desirable to provide some aerodynamic and thermal protection type aft heat shield to protect the engine system on each of the four selected aerobraking configurations investigated.

For the basic (no flare) configuration, the payload adapter identified in the previous Pre-Phase A Space Tug Study could be used. However, an extension would be required to totally house the payload in order to protect it from the thermal environment. For the configurations employing a flare, a payload adapter with additional capabilities for mounting the flare and housing the actuation system is required.

The flared configurations require some aerobraking kit element which will increase the cross sectional area and thus increase the drag. For three of the four selected configurations, different angle flares of different lengths were investigated.

The control requirements for the aerobraking Tug can be accomplished with the conventional Tug's reaction control system with no additional thruster and/or support bottles, accumulators, etc. However, the amount of reaction control system fuel required will vary from configuration to configuration depending on the stability of the configuration, the number of passes required and the corrective maneuvers required.

The Tug sidewalls (both the propulsion and astronics modules) will require some additional thermal protection as a result of aerobraking re-entry. This can be accomplished with removable sidewall insulation.

The astronics systems for the aerobraking trajectory mode will require some additional guidance and navigation sensor systems, increased electrical power capability, and redundant systems for maintenance of reliability during long duration missions. The astronics module systems will be discussed in Section 4.6, except for the sidewall thermal protection for the astronics module which is discussed herein.

4.2.2 (Continued)

Therefore, the aerobraking kit elements consist of:

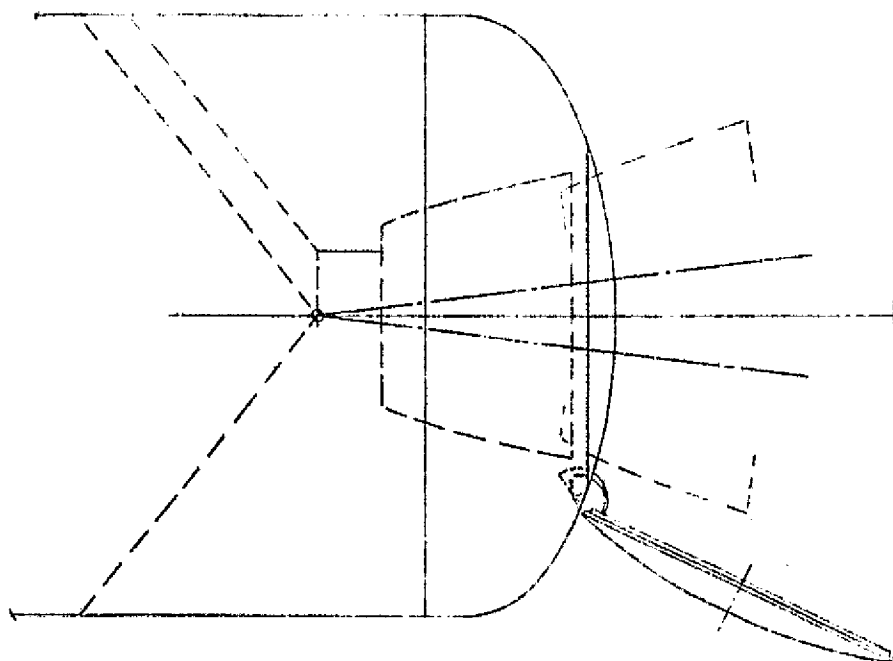
- a. Aft heat shield (Paragraph 4.2.2.1)
- b. Sidewall insulation (Paragraph 4.2.2.2)
- c. Reaction control systems (Section 4.4)
- d. Astrionics systems (Section 4.6)
- e. Flares (Paragraph 4.2.2.3)
- f. Payload adapters (Paragraph 4.2.2.4)

4.2.2.1 Aft Heat Shield

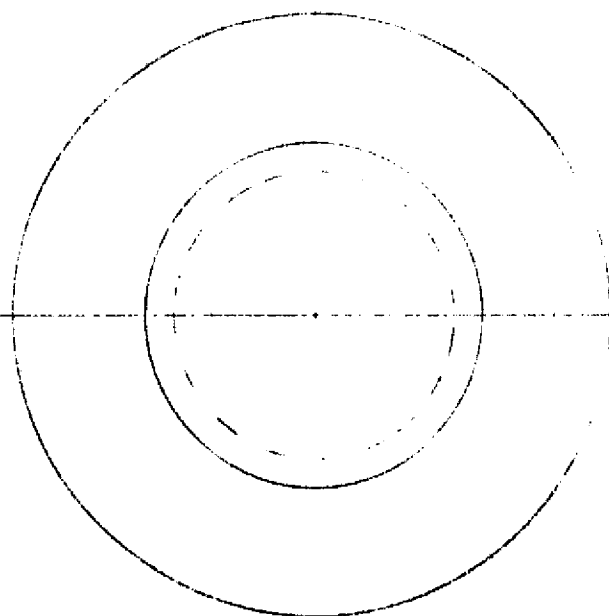
The aft heat shield is required to protect the engine nozzle and engine systems from aerodynamic heating and pressure loads during atmospheric braking. This aft protection system must be removable so that during the normal Tug operations, the main engine system may be operated. When the Tug is loaded into the Shuttle payload bay, the aft heat shield is positioned over the engine in the same position as during aerobraking operations. After the Tug has been delivered to orbit, the heat shield is retracted or removed.

A large number of heat shield concepts were investigated. The use of ablatives was not considered due to the lack of data on the recycle capabilities of ablatives. Therefore, by study groundrules, only radiative type materials were considered for use as a heat shield. All were feasible and differed only in the weight penalty associated with the heat shield. The metals used in these radiative shields were dependent upon the maximum temperatures encountered. Rene 41 and TD-nickel-chrome were used for the configurations and mission durations having the lower temperatures (2000°F or below). The Fansteels were used for the configurations and mission durations experiencing the high temperatures (above 2000°F).

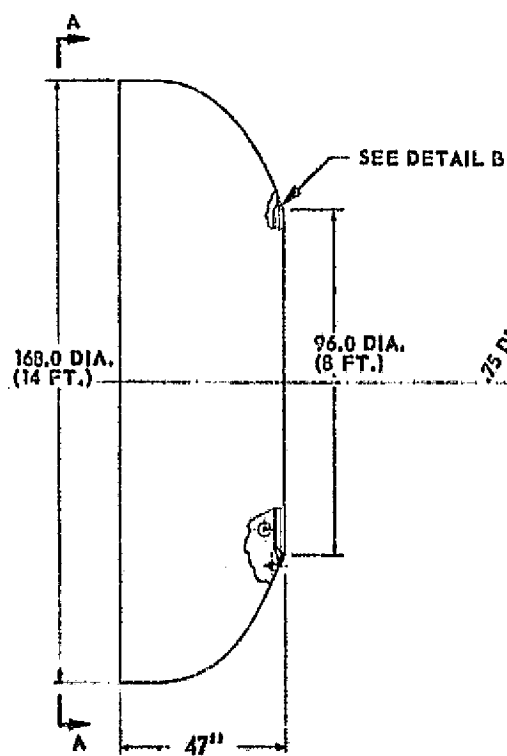
The selected heat shield used in the performance analyses was the lightest weight system. Figure 4.2.2.1-1 illustrates this system. It consists of a fixed dome section and a removable cap. The fixed dome is mounted to the aft skirt of the propulsion module. The dome section has a one foot cylindrical segment (to provide for engine clearance) starting at the aft skirt joint. The forward end of the fixed dome portion of the heat shield is a 2:1 elliptical contoured dome with a center port opening eight feet in diameter. This opening allows for the engine nozzle extension and movable gimbal motion during normal Tug operations. The lip on the fixed dome port has several 90° turns on its sealing surface to match that on the movable cap.



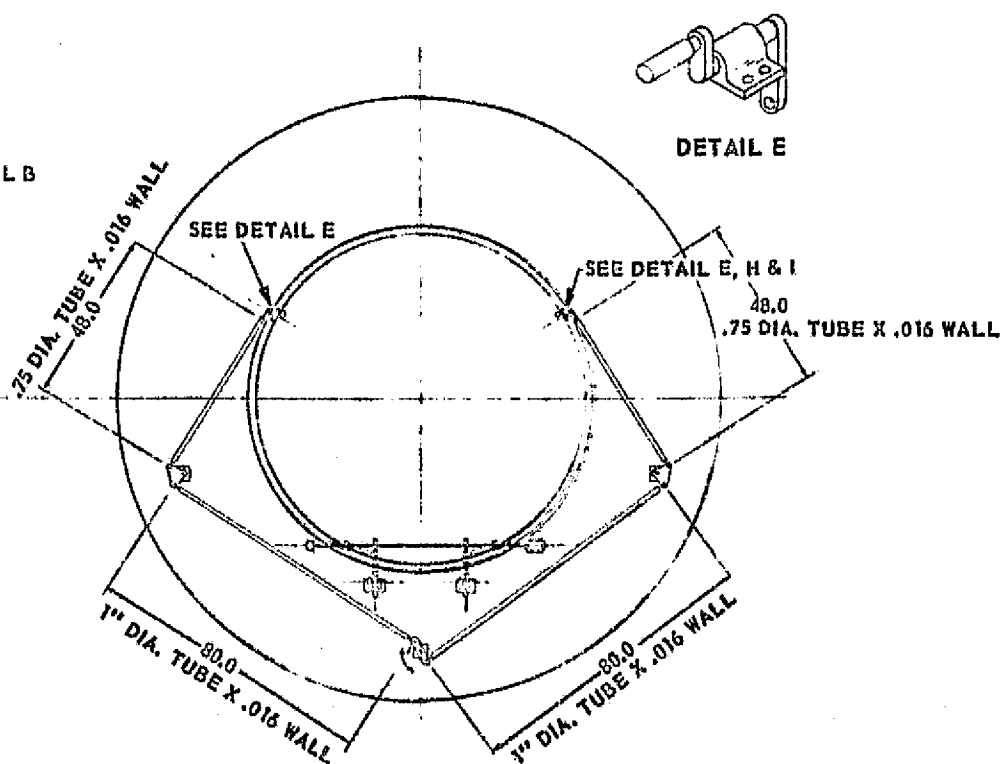
SPACE TUG WITH AFT HEAT SHIELD CAP IN OPEN POSITION



TOP VIEW - CAP CLOSED



SIDE VIEW - FIXED DOME



VIEW A-A

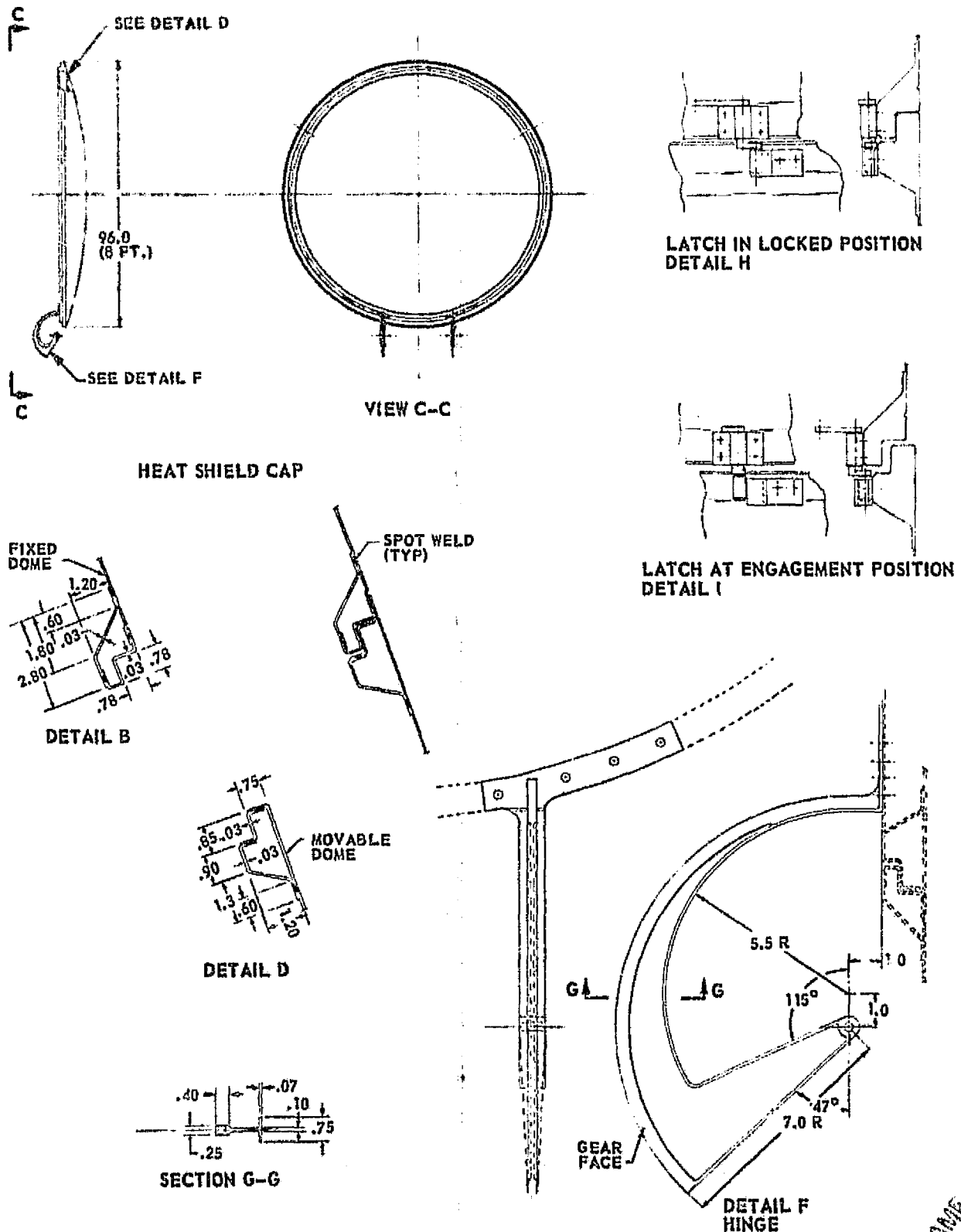


FIGURE 4.2.2.1-1: AFT HEAT SHIELD

4.2.2.1 (Continued)

View A-A of Figure 4.2.2.1-1 illustrates the latching mechanism. The four tie rods are interconnected so that a rotational motion at the key pivot point moves the connecting rods which in turn move the latch into the desired locked or unlocked position at two points. The details on the figure illustrate this mechanism in the locked and unlocked position.

The movable cap is eight feet in diameter and is tied to the fixed dome at two hinged points approximately two feet apart. The hinges allow the cap to be rotated approximately 145° outward. The hinges are geared to two matching gears connected by a drive shaft and driven by an electric motor.

Figure 4.2.2.1-2 illustrates an alternative aft heat shield concept. This concept has an internal cap which is rotated out of position during normal engine operations. The cap is first retracted several inches to lower it below the fixed portion of the dome. Then a gear mechanism located on the fixed dome section of the heat shield rotates it 90° . A motor located on the cap extends or retracts eight movable arms which actuate the latching mechanism. This system is the second lightest heat shield concept investigated.

Figure 4.2.2.1-3 illustrates the internally actuated, clam shell concept. This concept has a fixed dome heat shield section to the required eight foot port opening. The port opening is covered by a two piece clam shell during aerobraking. To operate the shell, an electric motor drives a gear/pinion mechanism to elevate the clam shell upward. After the shell has cleared the fixed dome portion of the aft heat shield sufficiently, each side of the clam shell is rotated outward approximately 145° . Retraction operations are performed in the reverse order, i.e., first the shells are rotated inward, then they are lowered into the port opening.

Figure 4.2.2.1-4 illustrates the single actuation point, total ellipsoidal dome retraction concept. This concept does not use a two piece heat shield (fixed dome and movable cap) but rather retracts/emplaces the total ellipsoidal portion of the heat shield. When in place on the aft end of the vehicle, the aft heat shield is held in place by four latches spaced 90° around the vehicle. Heat blocks are provided between the aft skirt and cylindrical portions to prevent heat transfer to the Tug. Along channels located on either side of the Tug, the heat shield actuation system pivot points would be extended aft approximately six feet. This would elevate the heat shield away from the vehicle and will permit clearance between the shield and nozzle when the shield is rotated to the retracted position. This longitudinal movement could be made by a small cable/winch/electric motor or by a worm gear/rod system. Upon reaching the aft stop, a microswitch would activate an electric motor/gear chain to rotate the pivot point, its attached rods, and the entire ellipsoidal dome. Another microswitch device would be provided to stop the rotation upon touching the Tug's exterior wall. If desired, the pivot point could be drawn forward to its original emplaced position, clearing the heat shield from the aft end completely. The main engine nozzle can

D5-17142

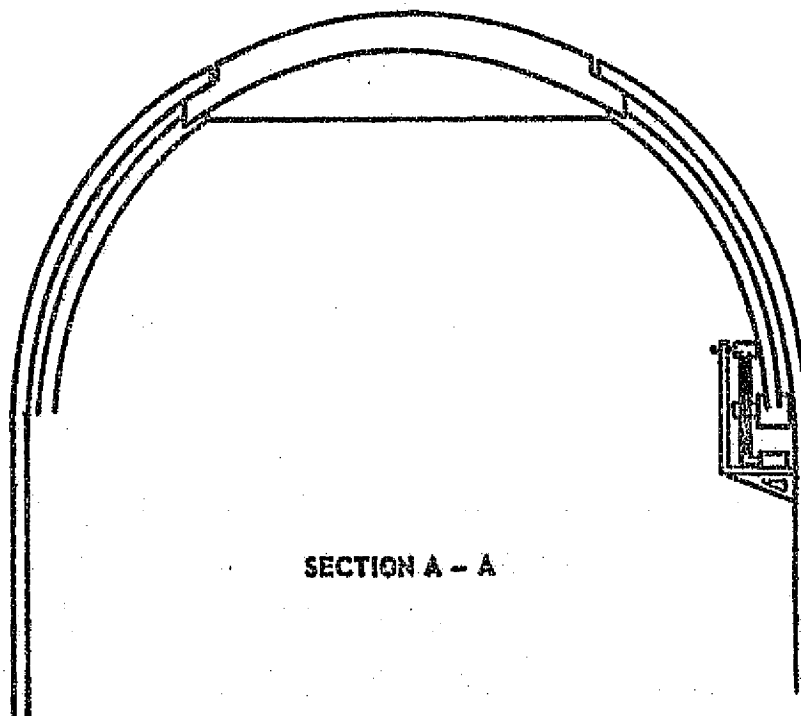
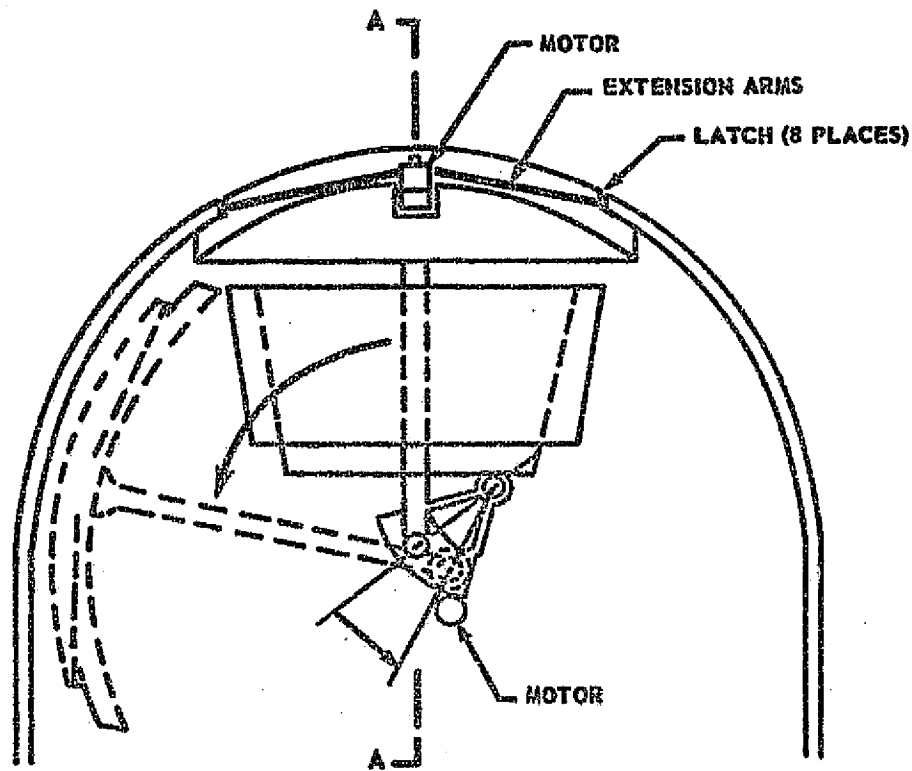
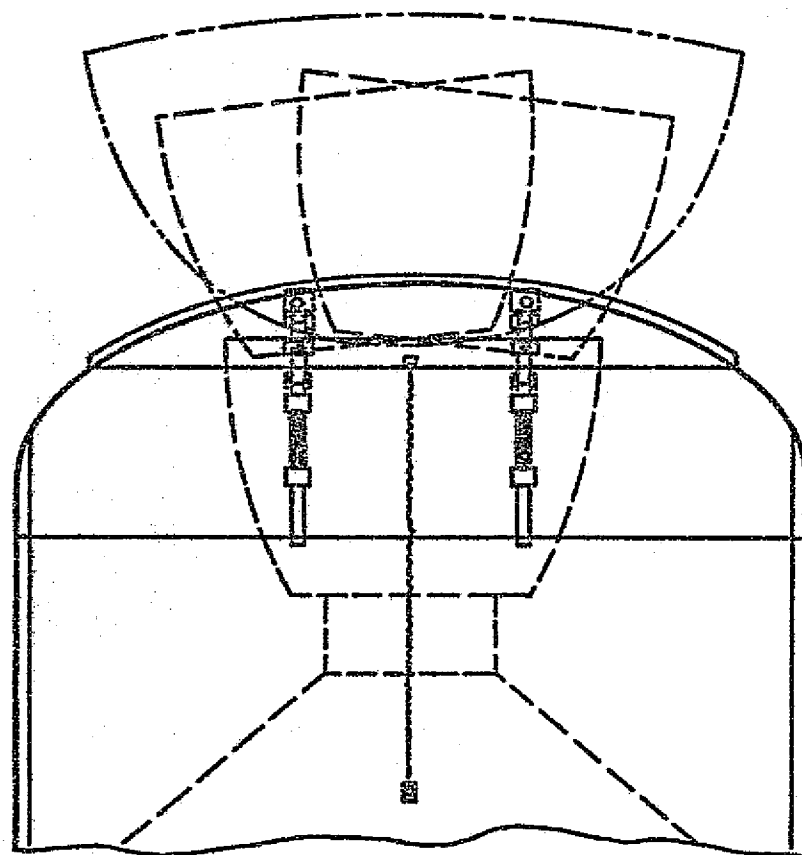
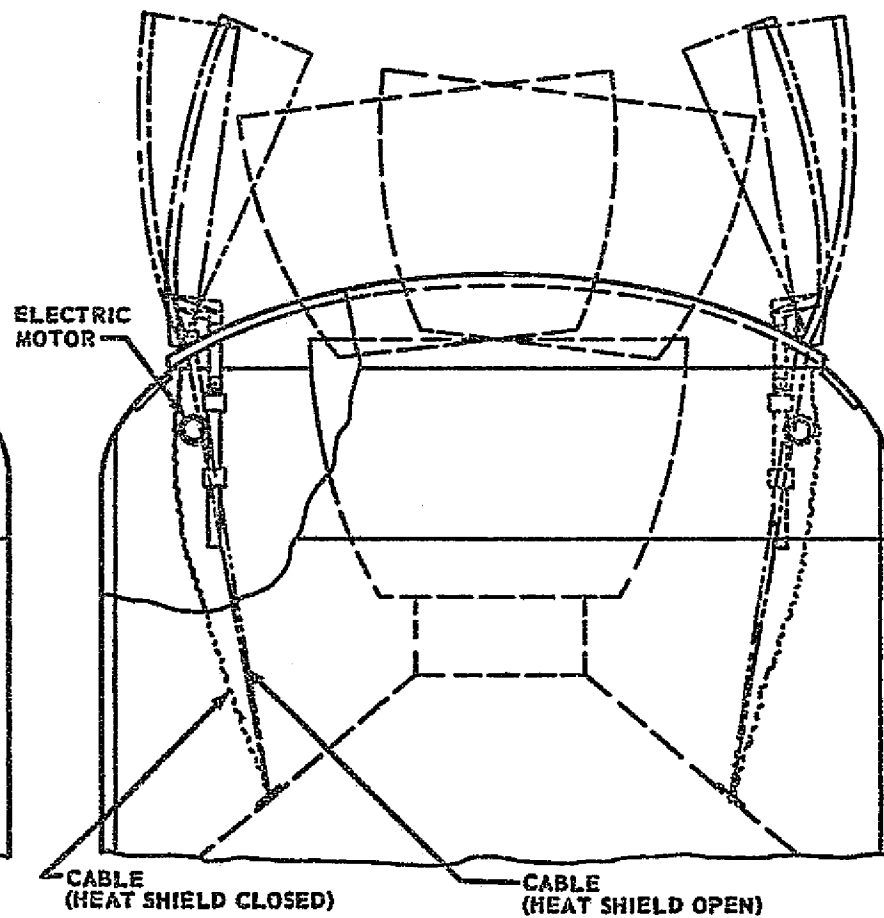


FIGURE 4.2.2.1-2. INTERNAL CAP HEAT SHIELD CONCEPT



FRONT VIEW OF CLAM SHELL



SIDE VIEW OF CLAM SHELL

FIGURE 4.2.2.1-3. CLAM SHELL AFT HEAT SHIELD CONCEPT

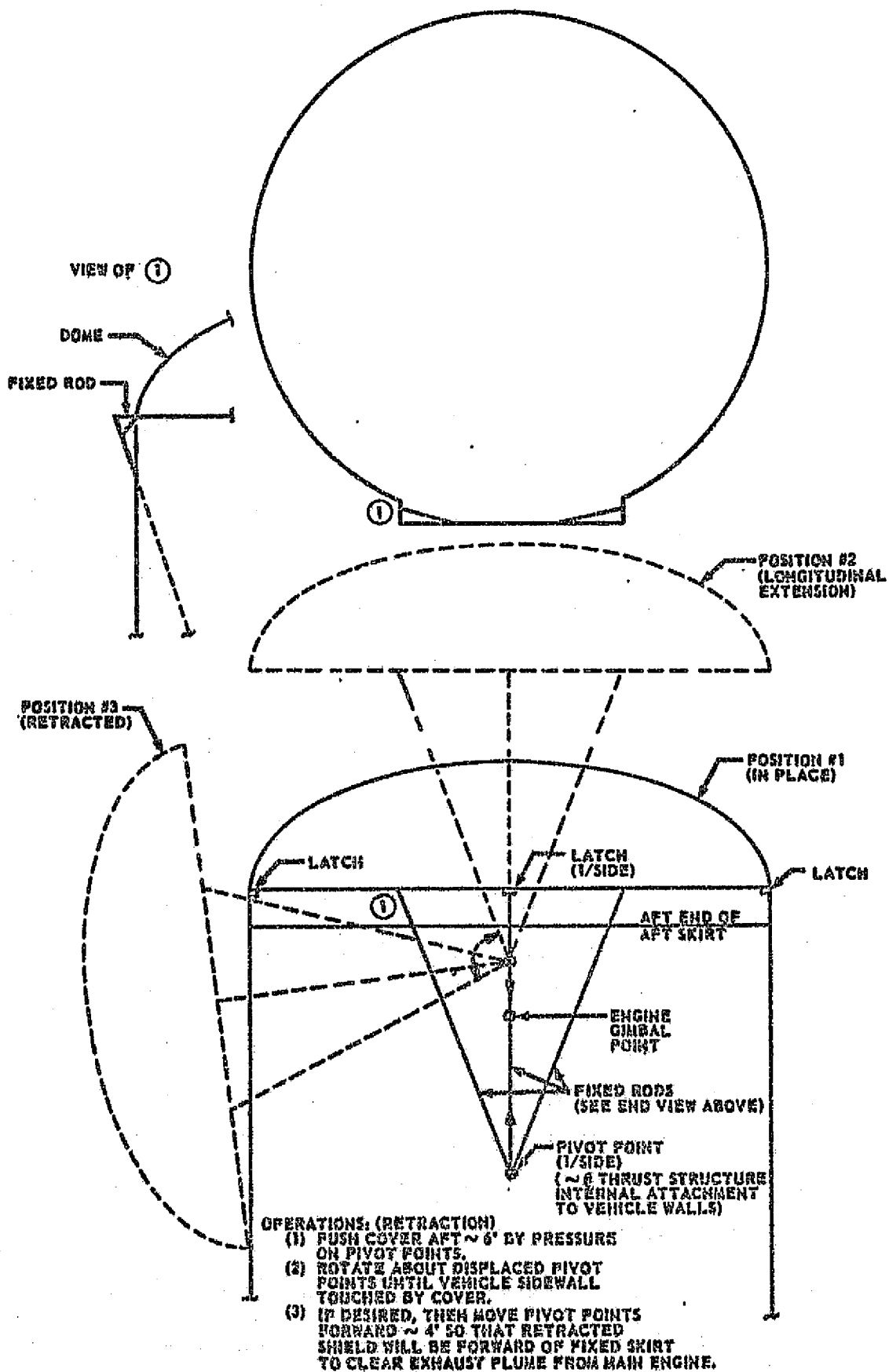


FIGURE 4.2.2.1-4: SINGLE PIVOT POINT-TOTAL ELLIPTICAL DOME RETRACTION CONCEPT

4.2.2.1 (Continued)

then be extended and the engine operated in a normal manner. Although the vehicle CG will be asymmetrical, main engine gimbaling and RCS trim could compensate.

After deorbit burn and prior to the first perigee pass, the heat shield will be elevated, rotated 90°, lowered, emplaced and latched. The method is an exact reversal of the steps used to retract.

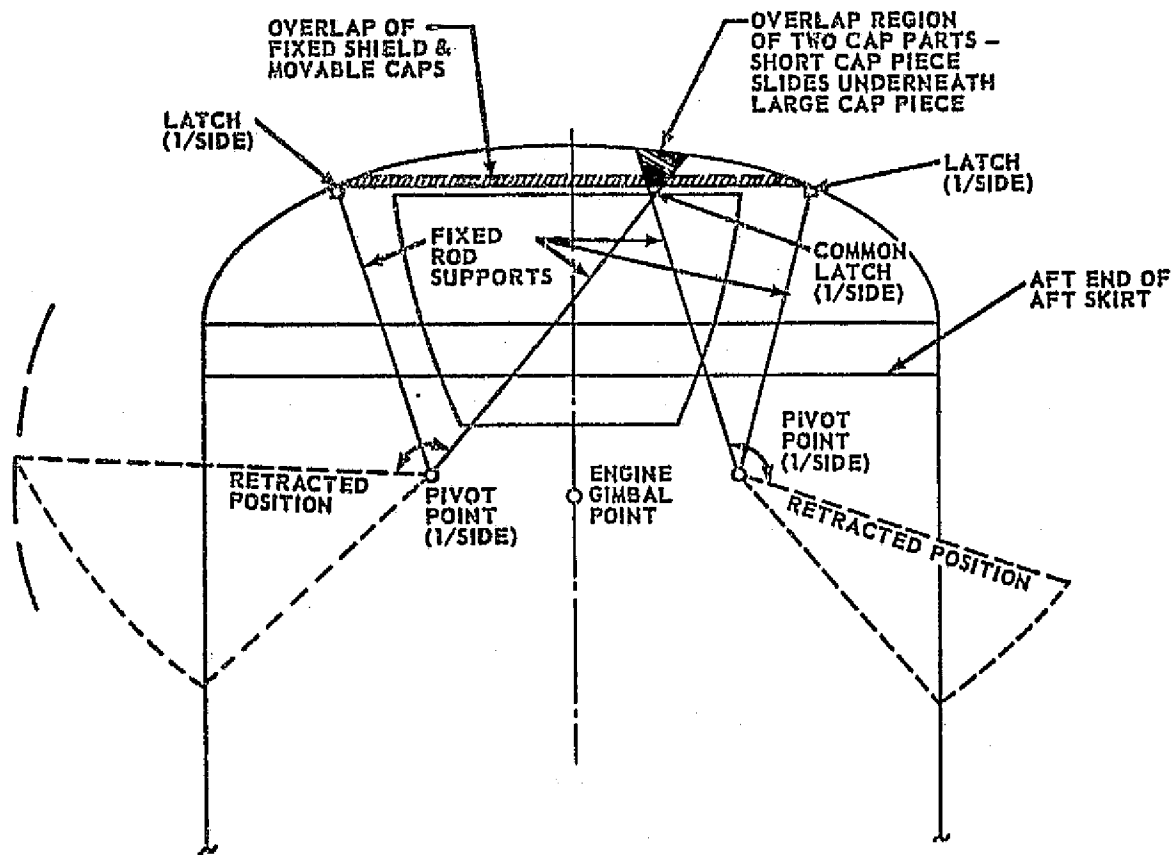
Although it is possible that the shield could be retracted after aerobraking, it is not likely because of damage to the external structure and possible fusion of the ellipsoidal heat shield to the cylinder. Therefore, a jettison backup device must be provided to separate the shield from the Tug either at the aft skirt or at the cylinder joints.

Figure 4.2.2.1-5 illustrates the double actuation pivot point, clam shell concept. This concept used the movable cap which is divided into two nonsymmetric sections. An offset cap joint was used so that the maximum stagnation temperature would not occur at the joint. The pivot points for the two parts are likewise nonsymmetrical with respect to vehicle location. A fixed dome portion of the heat shield extends from the Tug aft skirt to the heat shield port opening.

The operational sequence and requirements are similar to that of previous concept. However, this concept has a less complex actuation system. Only rotation of the cap sections about the two pivot points is required to emplace/retract the cap. The clam shell has the advantage of a more symmetrical CG location during normal (non-aerobraked) flight thus requiring less main engine gimbal or RCS attitude control impulse.

Figure 4.2.2.1-6 illustrates the single actuation pivot point, one piece cap concept. As with the previous concept, this concept uses the movable cap principle. The operational sequence and requirements are basically similar to the single point total elliptical dome retraction concept substituting the word "cap" for "ellipsoid" in the above description. Compared to the double pivot point clam shell concept, this concept has a more complex actuation system, better cap properties (one-piece), and a greater unsymmetrical CG location during normal flight.

Figure 4.2.2.1-7 illustrates the single actuation pivot point, clam shell concept. This concept could achieve the clam shell opening through the use of a single pivot point. It is considered to be the least attractive alternate concept investigated. The actuation system complexity is increased by requiring both translation and rotation. The rotation requires either a double-shafted motor (shafts rotating in opposite directions) or a clutch arrangement to turn one section in one direction followed by an opposite gearing to turn the other section. This complexity, coupled with the basic disadvantages of splitting the cap, negated the possibility of selecting this concept for the baseline.



FIXED ROD CONFIGURATION:
(TYPICAL 8 PLACES)

FIGURE 4.2.2.1-5: DOUBLE PIVOT POINT-CLAM SHELL CONCEPT

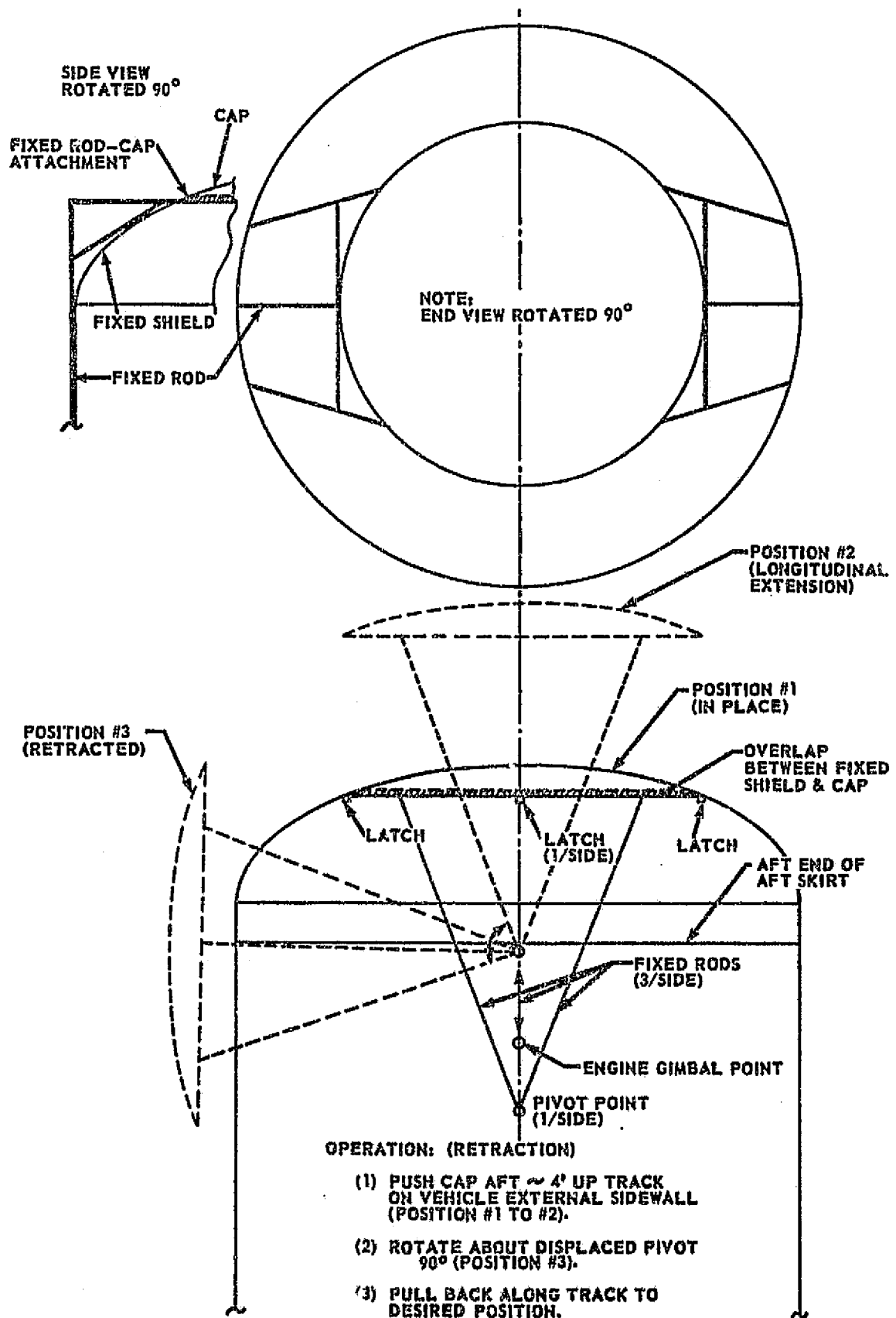
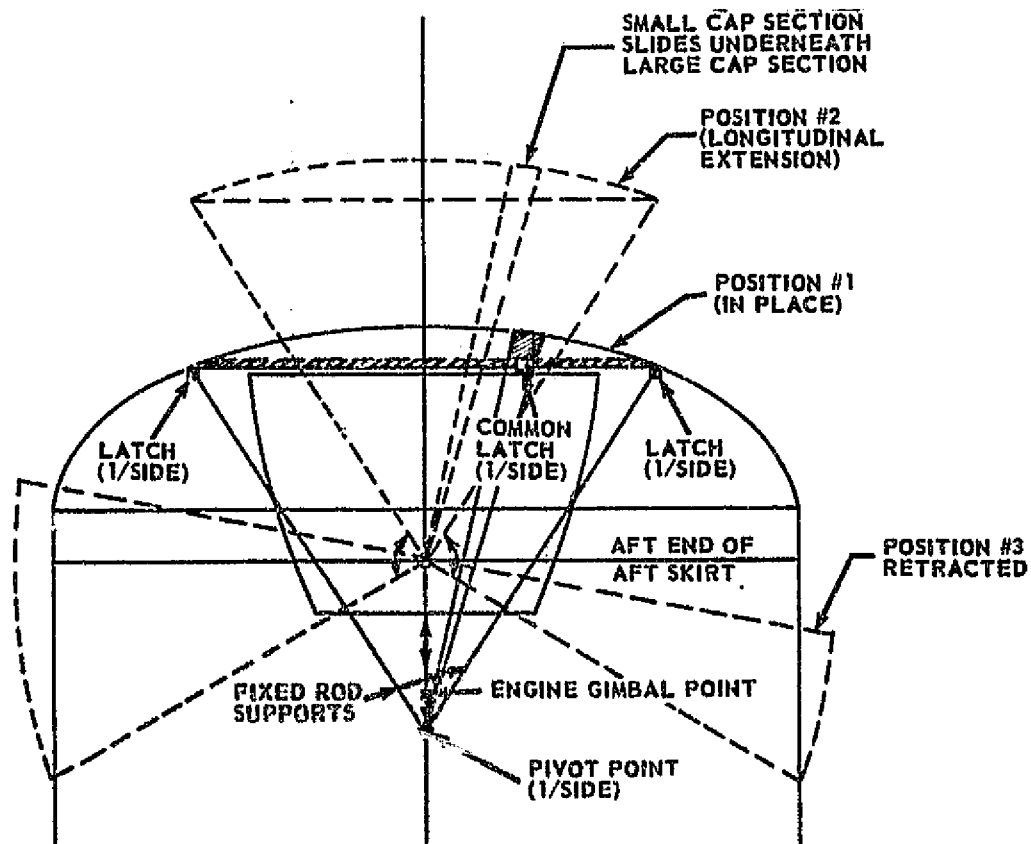


FIGURE 4.2.2.1-6: SINGLE PIVOT POINT - ONE PIECE CAP CONCEPT



OPERATIONAL CONCEPT:

POSITION #1: IN PLACE LATCHED TO FIXED PORTION OF HEAT SHIELD.

POSITION #2: PIVOT POINTS SLIDE AFT 3.2' TO AFT END OF AFT HEAT SHIELD - LIFTING TOTAL CAP 3.2'.

POSITION #3: CAP SEGMENTS SEPARATE AND ROTATE ABOUT PIVOT POINTS TO VEHICLE SIDEWALLS.

FIXED ROD CONFIGURATION:

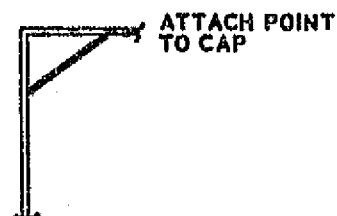


FIGURE 4.2.2.1-7: SINGLE PIVOT POINT-CLAM SHELL CONCEPT

4.2.2.1 (Continued)

In addition to the aft heat shield concepts, a forward heat shield mounted over the payload was investigated. Figure 4.2.2.1-8 shows the payload heat shield operational concept which is identical to that used for the propulsion module total dome heat shield retraction system (Figure 4.2.2.1-4). The pivot points for the shield are extended outward along a channel on the Space Tug side wall, then the whole shield is rotated clearing the payload. Disadvantages of this concept (and for most concepts employing heat shields over the payload) are associated with the variable payload lengths. Shown in the figure is the forward end of a "typical" payload but these payload lengths may be considerably shorter or longer. This variable payload length could be compensated for by several methods: (1) The three rods supporting the shield on each side could be telescoping; (2) the pivot point locations could be made more flexible; (3) tailored shields for payload length could be made; (4) the shield could be made to fit the longest payload and allow a gap for the remainder; or (5) combinations of the above. No analysis has been made comparing these methods.

A six inch overhang is provided for payload airstream protection. This fully utilizes the Shuttle's cargo bay diameter constraint. If further overhang is required, the ends could be folded along the Tug sidewall. This latter concept is not shown and would be expected to increase inert weight. A 14 foot diameter ring with cross members will provide the structural strength and adequate attachment points for the fixed and telescoping rods.

4.2.2.2 Sidewall Thermal Protection System

The conventional Space Tug load carrying sidewall is designed to withstand temperatures to 300°F. A 400°F limit is used for the micrometeoroid shield as the shield does not serve as a load carrying structure. Therefore, thermal protection will be required for Space Tug vehicle sidewalls when the Tug is operating in an aerobraking mode. The temperatures on the sidewalls will vary due to (1) distance aft of the re-entry heat shield, (2) the aerobraking configuration, and (3) mission duration. These factors coupled with the desirability for a removable thermal protection system and a minimum Tug weight penalty identified the major criteria for selecting the sidewall protection system. In addition to protecting the sidewall of the propulsion module, the sidewalls of the avionics module and the payload adapter (basic no flare configuration only) must be insulated.

The basic (no flare) Tug sidewall temperatures (from the heat shield to the payload) will vary from 1100°F to 1600°F (one day mission) down to 700°F to 1000°F (10 day missions). The flared configurations will not experience temperatures as severe. The temperatures will vary from 800°F to 1050°F (one day mission) down to 450°F to 600°F (10 day mission). Figure 4.7.2.0-1 in Section 4.7 tabulates the expected sidewall temperature.

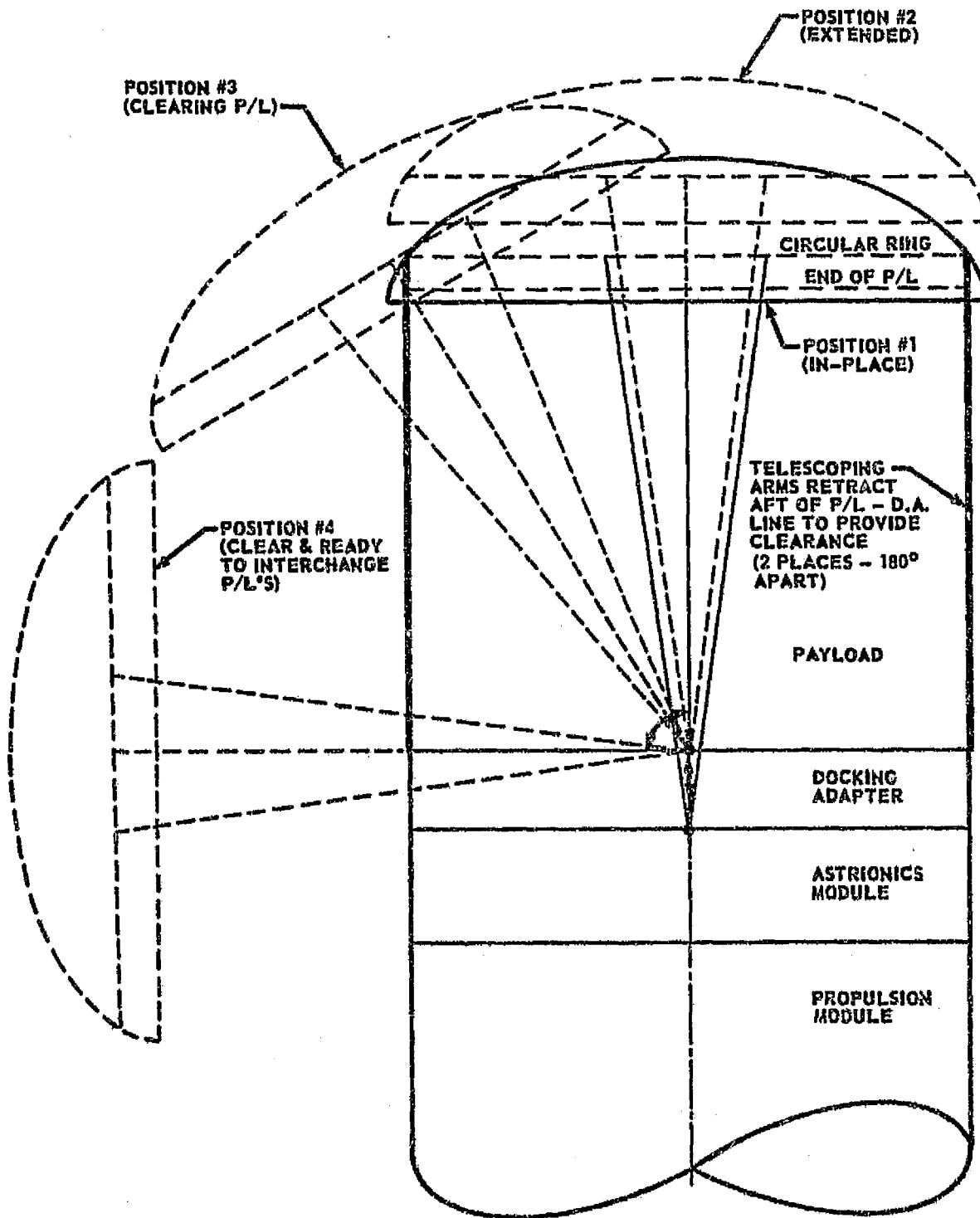


FIGURE 4.2.2.1-8. PAYLOAD END HEAT SHIELD CONCEPT

4.2.2.2 (Continued)

The material selected for the insulation must have a wide range of temperature capability and be light weight. John Mansville microquartz, a fibrous material, was selected. It has a low density of three pounds per cubic foot and a long life temperature capability of 2000°F. Its thermal conductivity varies from 0.36 at 3600°F to 0.91 BTU/hr/ft²/in./°F at 1000°F. This material can be cut to the desired shape and tapered down from the greater thicknesses required at the heat shield/sidewall to the lesser thickness required at the end of the payload sidewall. It can be mounted and bonded atop the aluminum micrometeoroid shield of the propulsion module, over the louver doors of the astronics module and atop the aluminum skin of the payload adapter. To prevent damage to the microquartz during handling and transportation, a thin foil (0.002 inch) of titanium or inconel may be used. Figure 4.2.2.2-1 illustrates the sidewall insulation for the 30 pass (5 day) mission using the 60° flared aerobraking Space Tug concept.

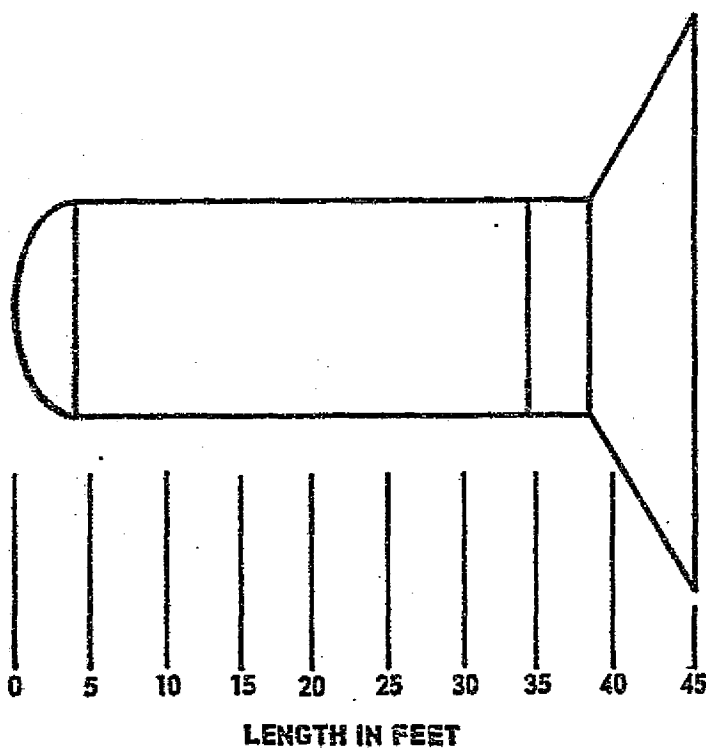
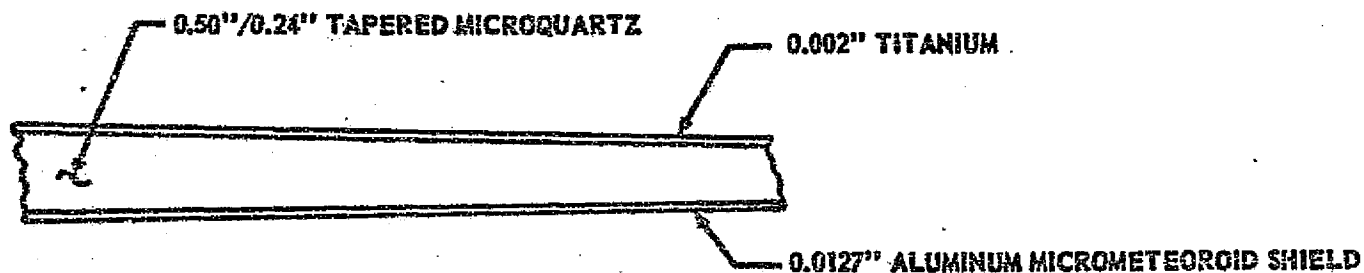
4.2.2.3 Aerodynamic Flare

The basic (no flare) Tug configuration experiences severe thermal environments due to its low drag/high ballistic coefficient. One method of increasing the drag and thereby reducing the ballistic coefficient is through the use of an aerodynamic flare. Several design concepts were investigated ranging from silicon rubber inflated bags for low temperature environment flares to all metallic flares for high temperature environments.

The selected flare concept is a metallic flare as shown for the 60° flare in Figure 4.2.2.3-1. The same concept is applicable to the 30 and 45° flares and is the lightest weight concept investigated. Because the flares will encounter temperatures ranging from approximately 1300°F (30° flare, 5 pass mission) down to 540°F (60° flare, 60 pass mission), an Inconel 718 was used for the flare skin.

The baseline aerodynamic flare concept is built from 72 panels. The panels are designed so that when they are retracted, they will not exceed the 15 foot diameter Shuttle bay limit. These are 36 intermediate panels and 18 (each) inner and outer panels. The intermediate panels do not extend to the Space Tug outer skin and thus reduce the overlapping of panels which will reduce the overall flare weight.

The flare actuation sequence is as follows. The aerodynamic flare is in place and in the retracted position when delivered to orbit by the Shuttle. After the Tug has accomplished its mission and has deorbited for the aerobraking return, the flare is extended. First the electric motor releases the 36 cables connected to the 36 struts. The cable connects to the two segment struts at the strut mid-point. The flare is connected to the Tug wall by spring hinges. Similarly the strut is connected to the Tug by spring hinges. Releasing the cables allow these spring hinges to elevate the flare and to extend the strut segments. The strut will extend until the lower strut segment and the upper strut segment are in line and then the two sections lock in place. When



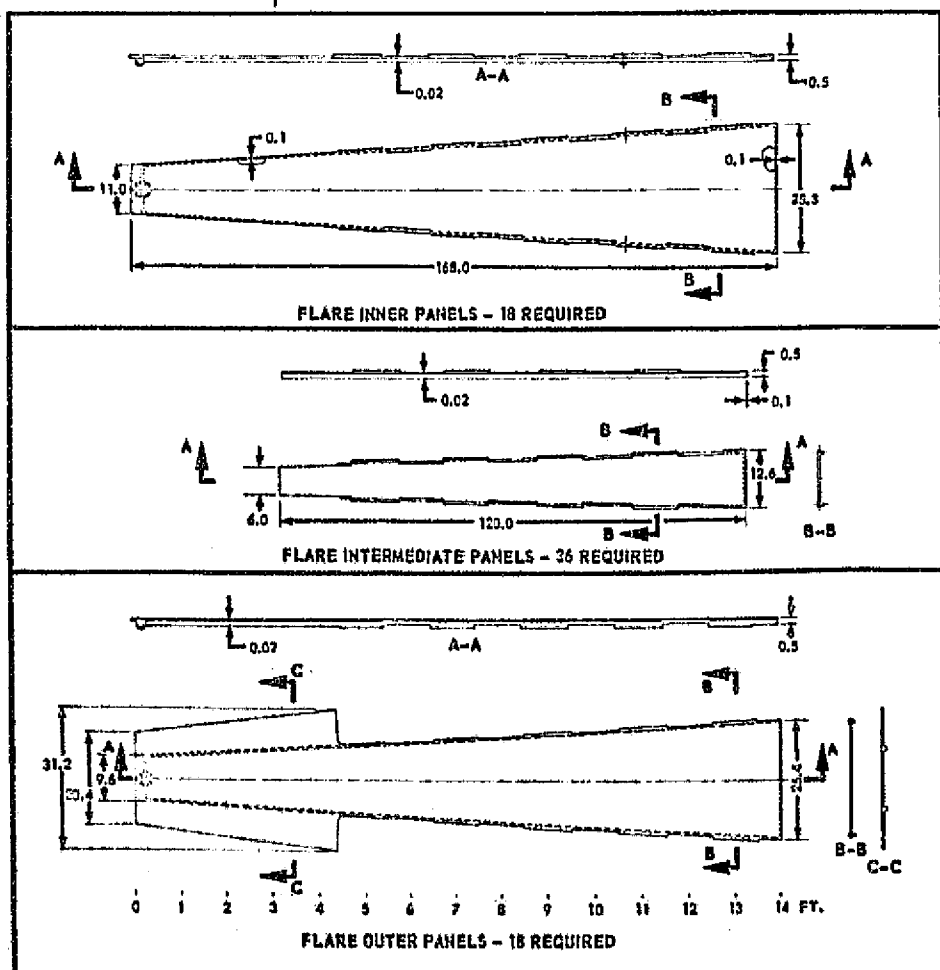
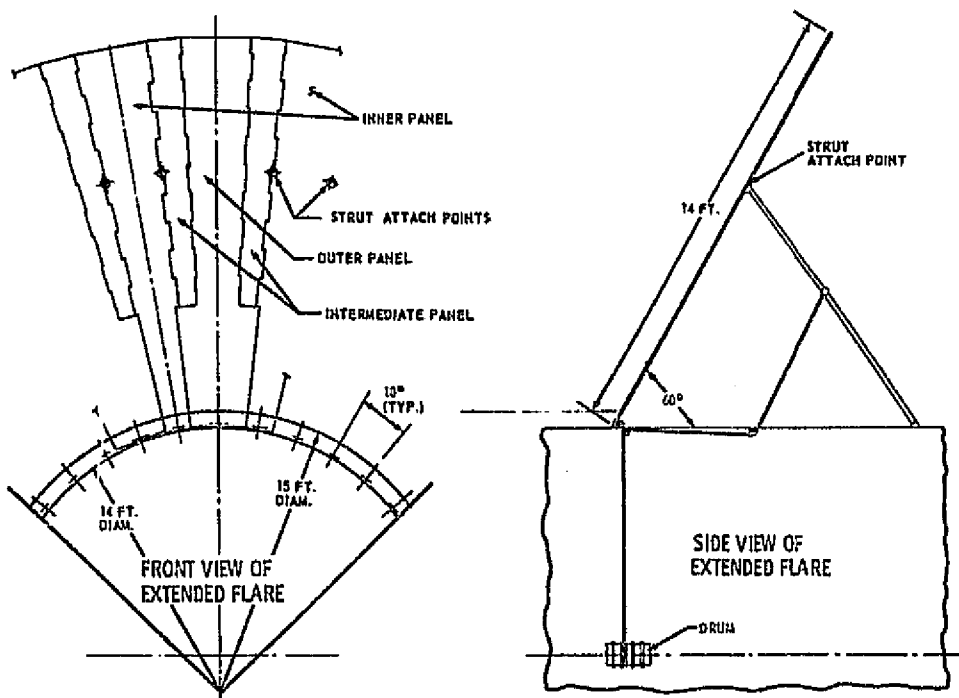
SIDEWALL INSULATION REQUIREMENTS								
LENGTH (FEET)	5	10	15	20	25	30	35	40
THICK- NESS (INCHES)	0.5	0.46	0.42	0.39	0.35	0.32	0.28	0.24

INSULATION - MICROQUARTZ (3#/FT³)

OUTER SKIN - TITANIUM OR INCONEL
CONSTANT THICKNESS
0.002 INCH

FIGURE 4.2.2.2-1. SIDEWALL INSULATION - 60 DEGREE FLARE SPACE TUG
CONFIGURATION - 30 PASS (5 DAY MISSION)

DS-17142



05-17142

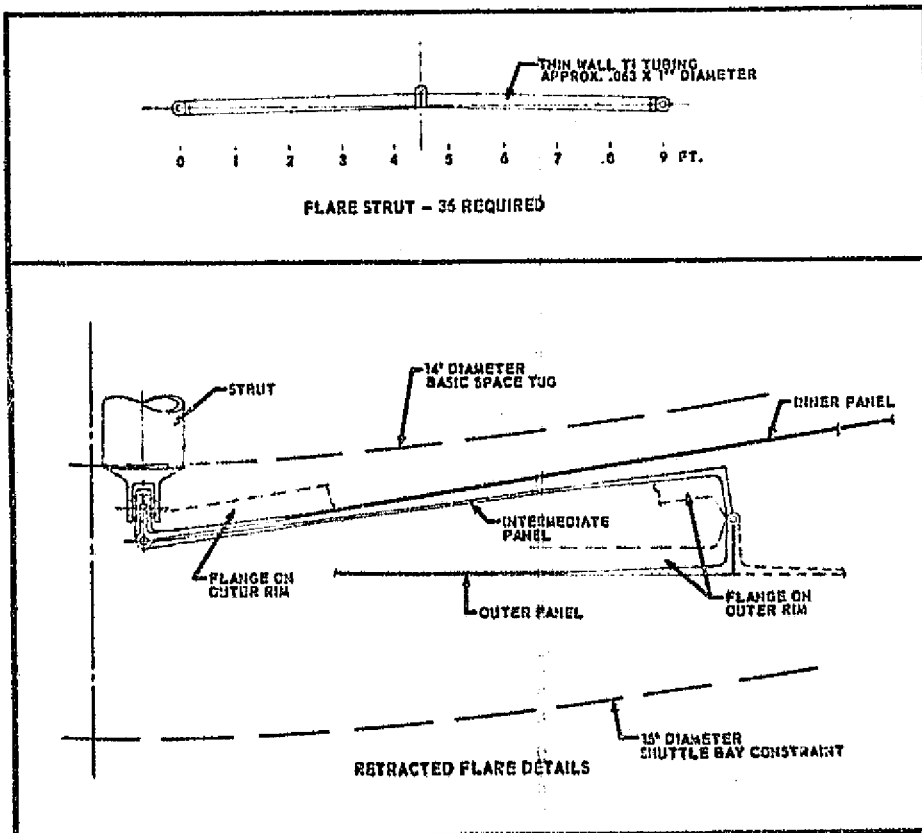
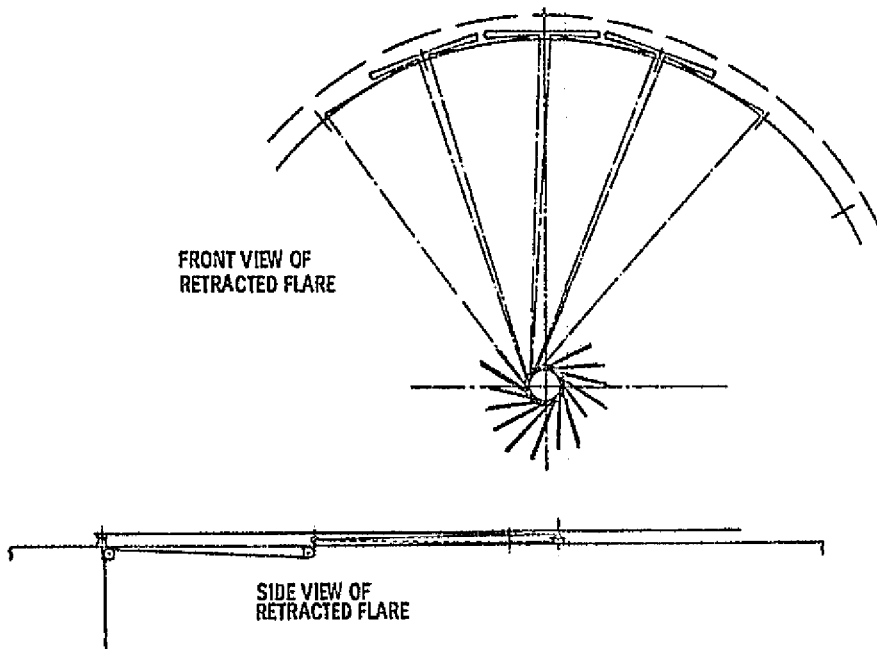


FIGURE 4.2.2.3-1. BASELINE FLARE CONCEPT

4-59

4-60

FOLDOUT FRAME
2

4.2.2.3 (Continued)

aerobraking is complete, the flare is retracted by actuation of the electric motor which rewinds the 36 cables on the cable drum. The retracting cables collapse the strut segments which draws the flare and the struts inward toward the Tug sidewall. The panels are folded so that the 18 outer panels formed the collapsed outer flare surface. The 18 inner panels are against the Tug sidewalls. The 36 intermediate panels are folded between the inner and outer panels. When folded, the flare increases the Tug diameter to 14'6", still within the Shuttle cargo bay limit.

The 72 panels are connected by piano hinges in an inner panel, intermediate panel, outer panel, intermediate panel-back-to-inner panel pattern as shown in Figure 4.2.2.3-1. The inner and outer panels are 0.02 inches thick and are reinforced by ribs 0.50 inches thick extending the entire slant height length and along both of the piano hinge joints. The outer edge is similarly ribbed. The intermediate panels are also 0.02 inches thick and have 0.50 inch thick ribs along each side and on the outer edge.

The skin thicknesses shown on the figure are based on the "worst case" thickness requirements. For the 60 pass, 10 day mission, a thickness of only 0.006 inches would be required. As a practical fabrication thickness, an 0.010 inch thickness was considered the minimum handling and processing thickness.

To provide bending support for the extended panels, 36 support struts, evenly spaced at 10° increments are used. The struts are tubular titanium 1-1/4 inch diameter and 1/32 inch wall thickness. The struts vary in diameter from 1 to 1-3/4 inches and from 0.030 to 0.0625 inches in wall thickness. The struts are composed of two equal sections per strut. The cables join the strut at the joint between the sections. The cables then are wound around pulleys located approximately 56 inches down the payload adapter (aft of the astronics module). The cables then follow the payload adapter wall until another set of pulleys located at the hinge points redirect the cables inward toward the cable drum located in the forward section of the payload adapter.

Several alternative flare concepts were investigated. Figure 4.2.2.3-2 illustrates another metallic panel concept (upper portion of figure) and an inflatable bag concept (lower portion of figure). The metallic concept uses 10 sets of panels located 36° apart. Each set consists of an inner panel and two outer panels. Each of the outer panels divide into two sub-panels. Upon actuation the outmost sub-panels slide outward until the subsections extended to the ends of the middle panels. Then the middle panels separate until the sub-panels reach the ends of the inner panel. Retraction will be performed in the reverse order.

The ten sets of panels are elevated by 10 spring leafs located at the Tug sidewall/flare joint. Twenty support struts, spring actuated, provide flare rigidity. Each strut consists of a two piece support section

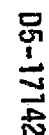


FIGURE 4.2.2.3-2. ALTERNATE FLARE CONCEPT

4.2.2.3 (Continued)

which locks the flare in the extended position. Retraction is accomplished by retracting the 20 cables joining the mid-points of the support legs. This concept was not used because the overlapping panels were heavy and friction may prevent the panels from sliding properly.

The inflated bag concept (shown in the lower portion of the figure) uses a Kapton or silicon rubber bag to elevate the flare. The bag may be used for long duration missions where the temperature on the flare would not exceed approximately 700°F. A metal panel with insulation on the surface facing the bag may be used to cover the bag for high temperature use. Helium is recommended for use to inflate the bags as helium bottles were already proposed to pressurize the oxygen tank of the Tug. By partial inflation, a variable angle flare could be obtained for changing the drag and ballistic coefficient. This would permit variable mission durations and/or corrections to the trajectory through modifying the flare angle. This concept is practical. However, there are complex design problems associated with this concept which could not be investigated and therefore it was not selected as the baseline flare concept.

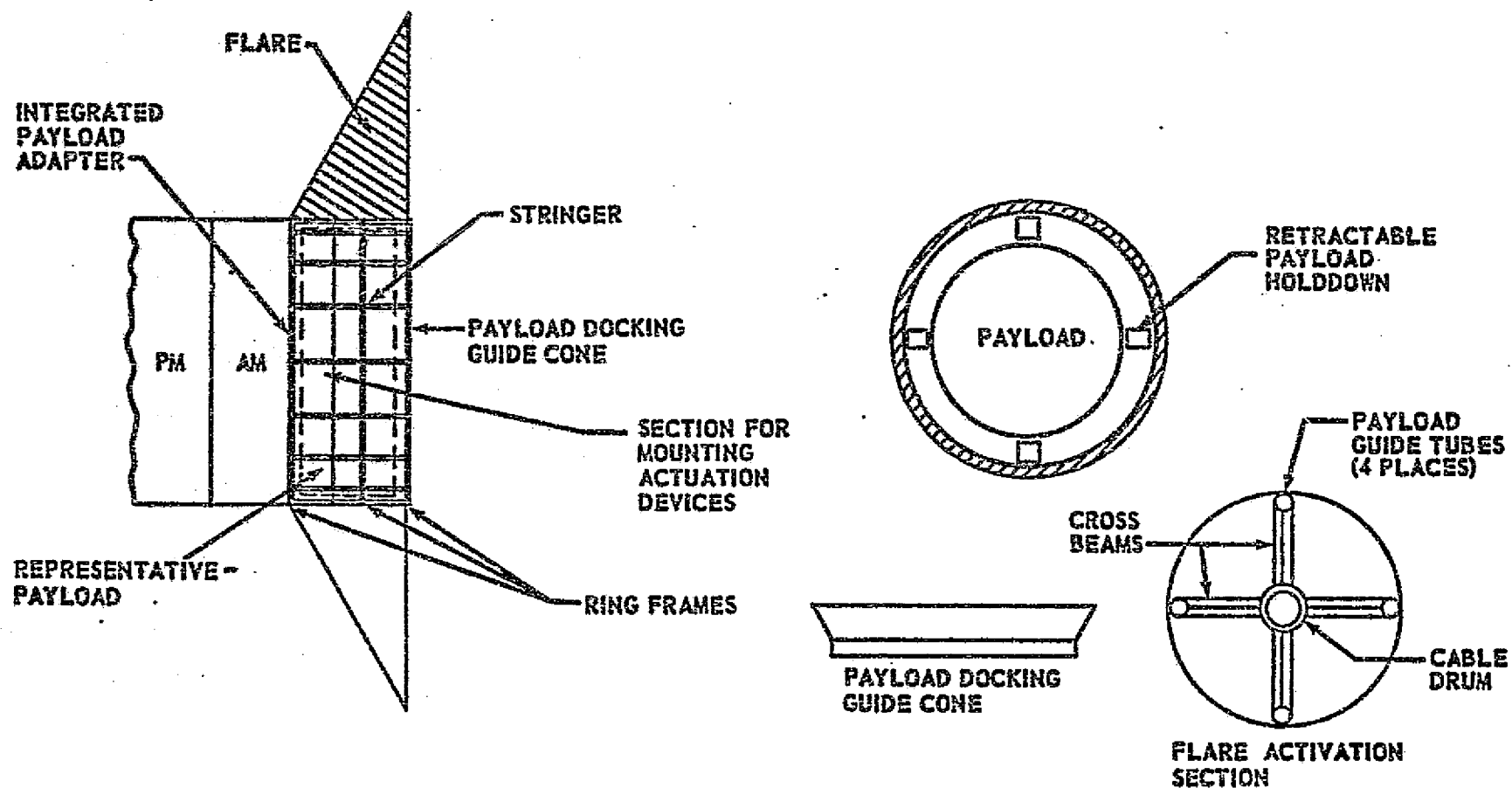
The concepts studied for the flare configuration were limited by study duration and by funding limitations. There are other flare concepts, other drag devices, other locations and other actuation methods which may perform equally as well as the baseline flare concept. These options should be studied in future aerobraking studies.

4.2.2.4 Payload Adapter

The payload adapter for the basic (no flare) configuration is mounted atop the astronics module and serves only to hold down the payload and protect it from the thermal environments. The payload adapter for the flare configuration aerobraking Space Tug has the additional functions of serving as the flare mounting fixture and the housing structure for the flare actuation mechanism. Figure 4.2.2.4-1 illustrates the payload adapter for the flared configurations:

The payload adapter would be the same diameter (14 feet) as the propulsion and astronics modules. The length would be approximately 10 feet long. The structure is an aluminum stiffened skin structure. The stiffener consists of 36 stringers which also serve as the mounting structure for the 36 flare support struts. Three ring frames are employed. The forward ring frame is used to bolt the payload adapter to the astronics module. The intermediate ring flare is welded to the 36 stringers at the point where the flare support struts are mounted (flared configurations only). The aft ring frame is used to support the payload guide structure.

For the flared configurations only, the forward ring frame also is used to mount the flare spring hinge and to mount 36 pulleys used to control the cables during flare actuation. This area is also reinforced by cross beams which are used to mount the electric motor and the cable



DS-17142

FIGURE 4.2.2.4-1: PAYLOAD ADAPTER CONCEPT FOR FLARED AEROBRAKING TUG CONCEPTS

4.2.2.4 (Continued)

drum. The flare actuation system is housed within the first six inches of length.

At the aft end of the payload adapter is a payload guide cone. This is a conical frustum 14 feet diameter at the entrance, six inches long and 13 feet at the base. Another cylindrical extension six inches long, 13 feet in diameter completes the guide cone structure. This device is used to assist the payload docking operations by overcoming possible misalignment between the payload and Tug. Four guide tubes (90° apart) extending the length of the payload adapter also help to align the payload.

The payload is held in position by the payload holddown fixtures. These fixtures are located at four places, 90° apart, five feet from the front of the payload adapter. These devices would be solenoid actuated.

The skin surface of the payload adapter is a thin aluminum sheet. For the basic (no flare) configuration, microquartz insulation with an outer titanium foil cover provides thermal protection to 300°F for the payload. For the flared configurations the temperatures will not be as severe. No additional protection other than the aluminum skin is expected to be required except for short duration missions. For these missions, some protective insulation (microquartz with the titanium foil) may be required.

The base area of the payload adapter for the no flare aerobraking Tug configuration will require a protective cover. The cover may be opened and closed with an electric motor/gear mechanism or by a spring loaded cable mechanism. The cover would be microquartz insulation between an aluminum inner cover and a titanium outer cover. This cover may also be required for the short mission duration flared Tug configurations.

The weight of the payload adapter for the basic (no flare) configuration is 400 pounds (including end cover). This is higher than the 390 pounds required for the flared configuration. The difference between the no flare and flare Tug payload adapter weights is the requirement for the crossbeams - 40 pounds added weight - for mounting the actuation mechanisms for the flared configurations and the deletion of the end cover (flared configuration only) - 50 pounds. This integrated payload adapter/flare mounting fixture/flare actuation device housing fixture is one of several concepts investigated. No significant weight difference among the various concepts investigated were observed. This one was selected as the baseline payload adapter configuration.

4.2.3 Configuration Design Options and Recommendations

The aerobraking kit elements consist of the aft heat shield, sidewall insulation, modified astrionics, flares and payload adapters. Each of these kit elements may have alternatives which will reduce weight, complexity, or may modify operational methods or increase versatility.

4.2.3 (Continued)

This study could only examine several representative, practical, low weight systems. The kit alternatives should be investigated in more depth.

For example, the aft heat shield could be replaced by an ablative shield, by exhaust gas cooling techniques, or by a forward aerodynamic flare. Different nose shapes could be used in lieu of the 2:1 ellipsoidal shape including hemispherical and blunted conical frustrum shapes.

The sidewall insulation may be replaced with ablatives, foam insulation, or insulations used in conjunction with the micrometeoroid shielding. Methods of providing heat blocks, accounting for heat leaks, pumping of insulation and insulation shielding techniques require investigation.

The astronics module is covered with the same sidewall insulation as the propulsion module so the above comments apply to it also. The astronics guidance and navigation systems are discussed in Section 4.6. Methods of reducing weight of the electrical systems, determining the reliability and accuracy of existing and new sensor systems require investigation.

The flare concept is only one of many practical concepts. For larger flares, the weights would become prohibitive using this concept. Low weight alternatives require investigation including open flare structure near to the Tug's sidewall, split flares, inflatable bag flares, lift to drag flares, and steeper angle or flat plate flares.

The payload adapter is normally not considered a part of the aerobraking kit. However, for the flared configurations its multipurpose made it a trade variable. Only limited design activity was undertaken to provide some understanding of the weight penalty, payload environmental considerations on the aerobraking mode and upon aerobraking kit design. More detailed analysis of the payload/Space Tug interfaces is required.

In summary, the configuration options considered for the aerobraking kit elements were practical. Low design risk kit elements were selected to operate with the existing Boeing Pre-Phase A Space Tug Concept. The payload capability obtainable with the aerobraking kit elements were identified. The major considerations were directed toward low weight as the aerobraking kit weight is traded pound for pound with round trip payload. Designs were prepared only to the degree necessary to determine inert weights. Follow-on activities should consider the design of aerobraking kits that are reusable and can be refurbished. The design impact of aerobraking on the Shuttle/Tug interfaces such as handling and transporting and environmental constraints of Shuttle/Tug/payload are secondary considerations but should be evaluated in future studies. The design of the conventional Tug should be investigated to determine what design modifications should be considered to provide the best compromise Tug design applicable to both aerobraking and non-aerobraking applications.

4.3 TRAJECTORY ANALYSIS

The baseline mission selected for analysis in this study was the geosynchronous round-trip payload mission, since this mission imposed the most stringent performance requirements on conventional tug systems. In this mission profile the tug is deployed by the shuttle in 100 NM, 28° inclination orbit. The tug transfers the payload via Hohmann transfer to equatorial synchronous orbit with the 28° plane change being made at apogee. In synchronous orbit the payload is exchanged for an equal weight return payload. At the proper time the tug and payload are placed on the aerobraking return ellipse by applying the deorbit and 28° plane change ΔV . During the aerobraking return the apogee of the ellipse is reduced to 270 NM by drag dissipation of the orbital kinetic energy on one or more passes through the upper atmosphere. The orbit is circularized at 270 NM for phasing with the shuttle at 100 NM and at the proper time a final Hohmann transfer is made to 100 NM for rendezvous with the shuttle.

Initial trajectory analysis consisted of generating preliminary trajectories with constant ballistic coefficients ($W/C_D A$) and estimated drag coefficients (C_D) to establish the flight regime for the aerodynamic analysis. The drag coefficient was varied parametrically to vary the ballistic coefficient from 10 PSF to 80 PSF, the expected range for the tug. These trajectories established the altitude and velocity range that the expected configurations would traverse. Final trajectory analysis consisted of generating trajectories using the refined aerodynamic data. These trajectories were then used for thermal, astronautics, control, and loads analyses to determine subsystem weight penalties associated with the aerobraking concept.

4.3.1 Analytical Model

Space Tug trajectories involve flight through two different mediums; an atmosphere and a vacuum. As a result, it is expedient to simulate each type of flight differently to reduce computer time and maintain integration accuracy. The following technique was used to generate trajectory data for this study.

- o Flight through the sensible atmosphere was simulated by numerically integrating the equations of motion in rectangular coordinates.
- o Vacuum flight was simulated by conic segments where the orbital elements are determined based on Kepler's laws.
- o The total flight path was constructed by patching together the conic trajectory and the integrated trajectory as illustrated in Figure 4.3.1.0-1.

D5-17142

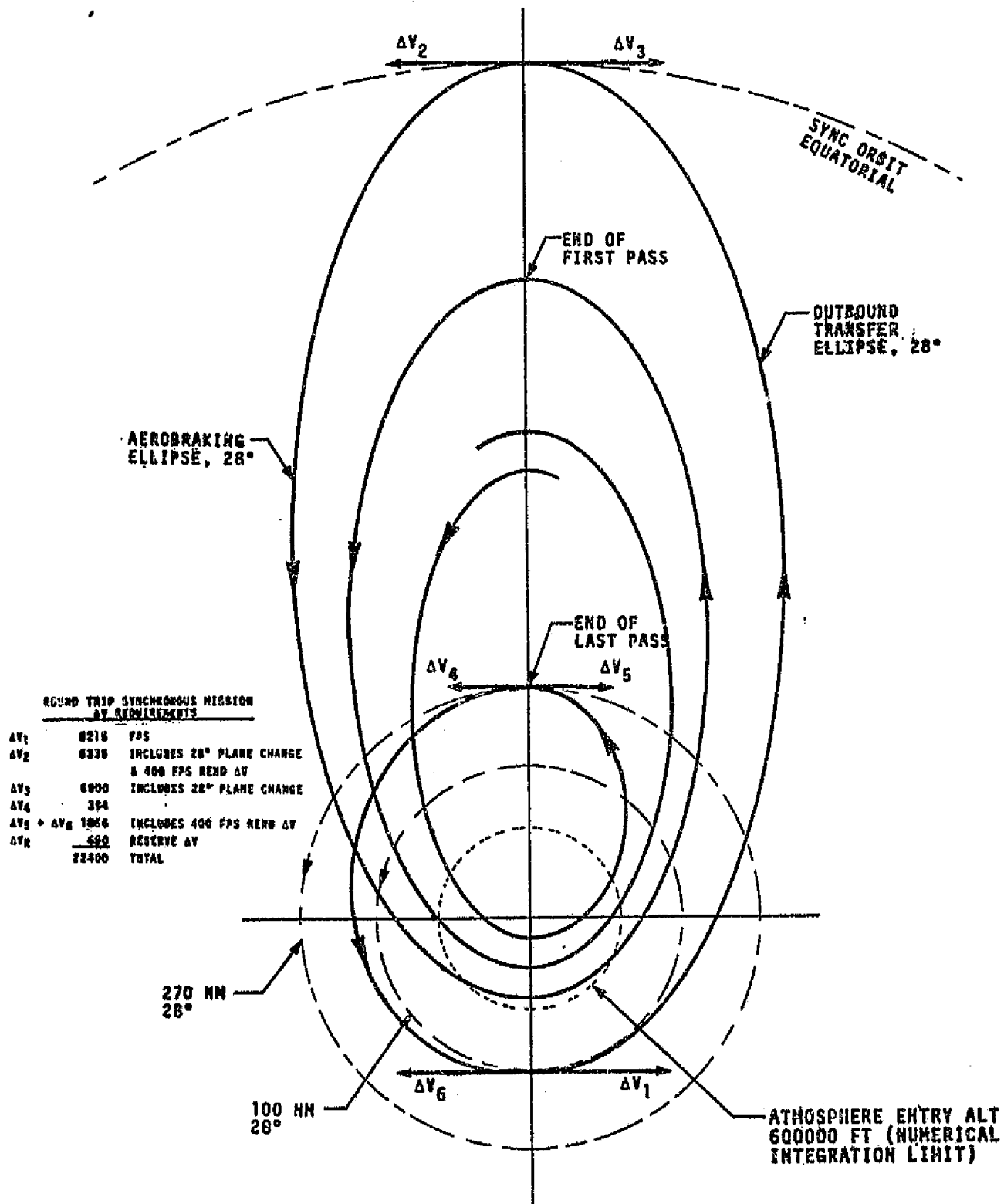


FIGURE 4.3.1.0-1 MISSION PROFILE

4.3.1.1 Assumptions and Groundrules

The earth model, tug configuration constants and assumptions pertinent to the mission profile shown in Figure 4.3.1.0-1 are given below (References 4.3.1.1-1, -2, and -3).

Mission and Trajectory Assumptions and Constants

1. Initial Orbit = 100 NM circular
2. Synchronous orbit altitude = 117440496 ft
(19316 NM)
3. Intermediate orbit at conclusion of aerobraking = 270 NM circular
4. Final orbit = 100 NM circular
5. Mission total ΔV = 22400 fps
 - a. ΔV to synchronous orbit = 14550 fps
(includes 400 fps rendezvous)
 - b. ΔV to start aerobrake descent = 6000 fps
(descent trajectory assumed to have a 250 KFT perigee)
 - c. ΔV at end of aerobraking = 1850 fps
(includes 400 fps rendezvous and 400 fps reserve)
6. The vacuum perigee at atmosphere entry on a pass is the vacuum perigee that results from the decaying orbit of the previous pass, i.e., the orbit is allowed to decay naturally. No corrections are made in perigee altitude. (This applies only to the nominal atmosphere trajectories.)

Tug Constants

1. Total initial weight of tug as deployed by shuttle = 57740 lbs
2. Total propellant weight = 45000 lbs
3. Entry weight at start aerobrake = 14430 lbs
(Based on using the 45000 lbs of propellant to perform the ΔV of 22400 fps)
4. Main engine specific impulse, I_{sp} = 460 sec
5. Tug reference area, A = 154 ft²
6. Lift-to-drag ratio, L/D = 0
(zero angle of attack)

4.3.1.1 (Continued)

Earth Model Constants and Assumptions

1. Spherical, rotating earth and atmosphere
2. Limit of sensible atmosphere = 600,000 ft altitude
3. Nominal atmosphere = 1962 U. S. Standard
4. Equatorial radius = 20925722 ft
5. Gravity constant = $14.076539 \times 10^{15} \text{ ft}^3/\text{sec}^2$
6. Earth rotation rate = $.729211585 \times 10^{-4} \text{ rad/sec}$

4.3.2 Preliminary Trajectory Analysis

The preliminary trajectory analysis using constant ballistic coefficients ($W/C_D A$) produced the data shown in Figure 4.3.2.0-1. This data was generated to establish the basic relationships between $W/C_D A$, mission time, and initial perigee altitude.

These data identify the reasonable tug configuration requirements and associated altitude and velocity ranges necessary to develop preliminary aerobraking design concepts and determine associated aerodynamic characteristics.

4.3.3 Final Trajectory Analysis

Aerodynamic analyses (Section 4.1) identified the following tug configurations for detailed evaluation in this study.

1. Basic Tug (no flare)
2. 30° Flare (short flare)
3. 45° Flare (Intermediate Flare)
4. 60° Flare (Large Flare)

The vacuum perigee altitude of the initial descent trajectory from synchronous orbit was varied to change the total number of passes (and therefore return time) required for apogee decay to 270 NM. (This perigee is the equivalent Kepler orbit perigee of the first atmospheric pass; it is not the actual low point of the trajectory in the atmosphere.) Results for the four selected tug aerobraking configurations are presented in Figure 4.3.3.0-1. Data for an optional configuration (a long 30° flare) is also shown. The initial vacuum perigee was varied for each configuration for entry pass numbers between one (.24 days) and 60 (11 days). The relationship between number

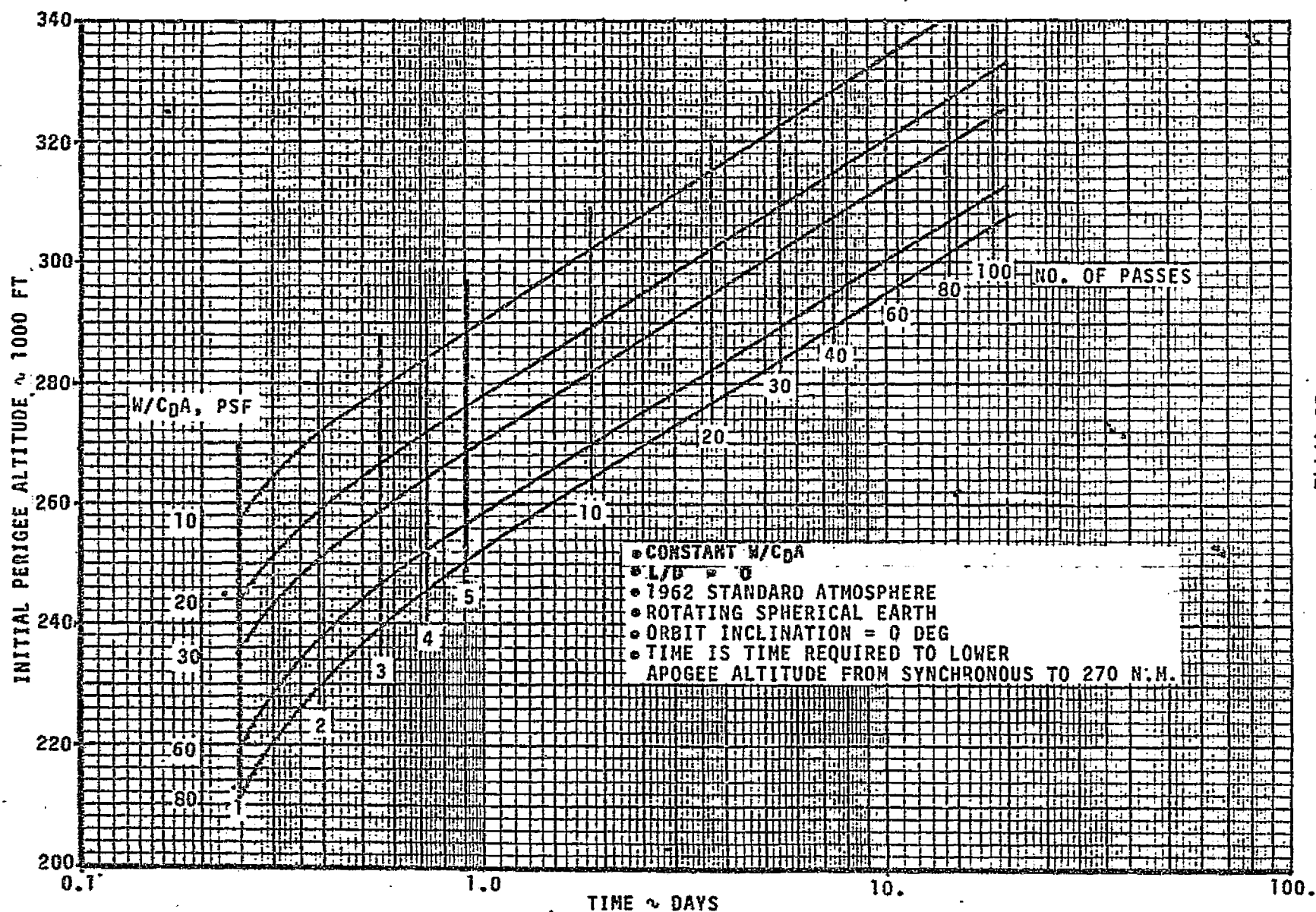
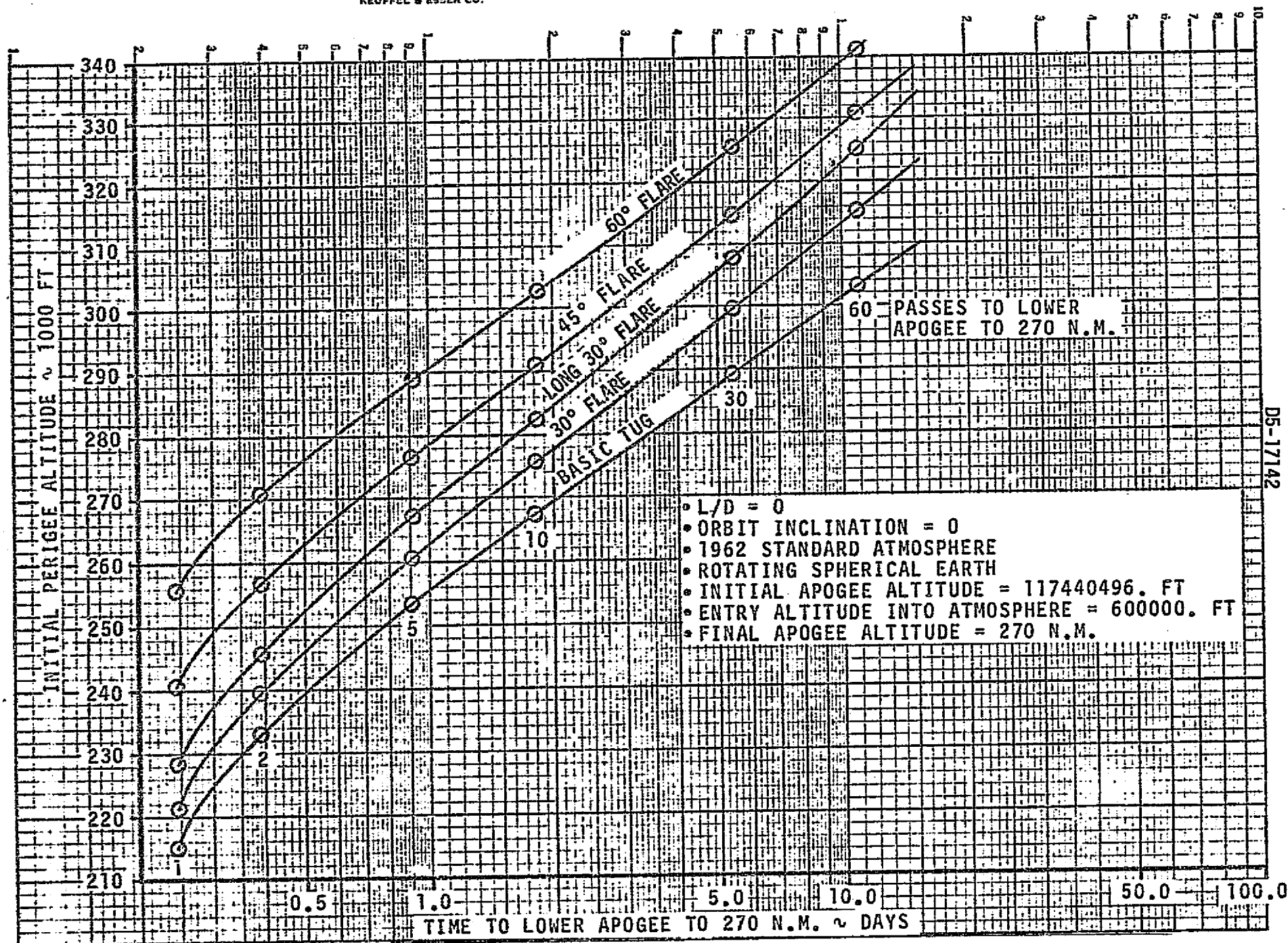


FIGURE 4.3.2.0-1 SPACE TUG AEROBRAKING RETURN FROM SYNCHRONOUS ORBIT - PRELIMINARY TRAJECTORY DATA



DS-17142

FIGURE 4.3.3.0-1 SPACE TUG AEROBRAKING RETURN FROM SYNCHRONOUS ORBIT - INITIAL PERIGEE ALTITUDE

4.3.3 (Continued)

of passes and return time proved to be nearly linear and independent of the Tug configuration. This relationship is shown in Figure 4.3.3.0-2.

The apogee altitude decay is shown as a function of pass number for the basic Tug and the 60° flare configurations in Figures 4.3.3.0-3 and 4.3.3.0-4. The apogee shown is the apogee that occurs at the end of each individual pass. Only these two configurations are shown, since they represent the limiting extremes in $W/C_D A$. It should be noted that there is no appreciable difference in the apogee decay of these two configurations. The other configurations have similar apogee decay history.

The vacuum perigee altitude at the end of each individual pass is presented in Figures 4.3.3.0-5 and 4.3.3.0-6 for the basic Tug and the 60° flare configurations. This perigee is the equivalent vacuum perigee at atmospheric exit for the pass, and it is the vacuum perigee of the orbit at atmosphere entry on the descent leg of the next pass. These curves are presented for the two extreme Tug configurations.

The maximum dynamic pressure as a function of pass number is presented in Figures 4.3.3.0-7 through 4.3.3.0-9 for all of the Tug configurations analyzed. It should be noted that the highest Q_{MAX} occurs on the last pass for all configurations. This is caused by the sharp drop in perigee altitude during the last few trajectory passes, as illustrated in Figures 4.3.3.0-5 and -6.

Figures 4.3.3.0-10 and -11 show the maximum inertial velocity attained on each pass as a function of the number of passes in the mission. The inertial velocities are relatively insensitive to the configurations as shown in the figures and as tabulated below. On the longer missions (30 and 60 passes), the decrease in maximum velocity per pass is nearly linear for the majority of the mission. The latter part of the mission has an increasingly larger drop in maximum velocity. The shorter missions (5 and 10 pass) have nearly linear decreases. The first pass has a maximum velocity of approximately 34,000 ft/sec for all mission times shown with the last pass minimums of approximately 26,700 to 28,800 ft/sec for both the basic (no flare) and the 60° flare configurations. The maximum inertial velocities shown do not occur at perigee because of the braking effects of the atmosphere. Rather, these values occur from a few seconds to approximately two minutes prior to perigee dependent on the number of mission passes and the individual pass number. For comparison,

A-74

TIME TO LOWER APOGEE TO 270 NM - DAYS

12
10
8
6
4
2
0

0 10 20 30 40 50 60

NO. OF PASSES TO LOWER APOGEE

INITIAL APOGEE ALT = SYNC. ALT
FINAL APOGEE ALT = 270 NM

NOTE: APPLICABLE TO ALL TUG
AEROBRAKING CONFIGURATIONS

FIGURE 4.3.3.0-2 TUG AEROBRAKING RETURN TIME FROM SYNCHRONOUS ORBIT

D5-17142

4-75

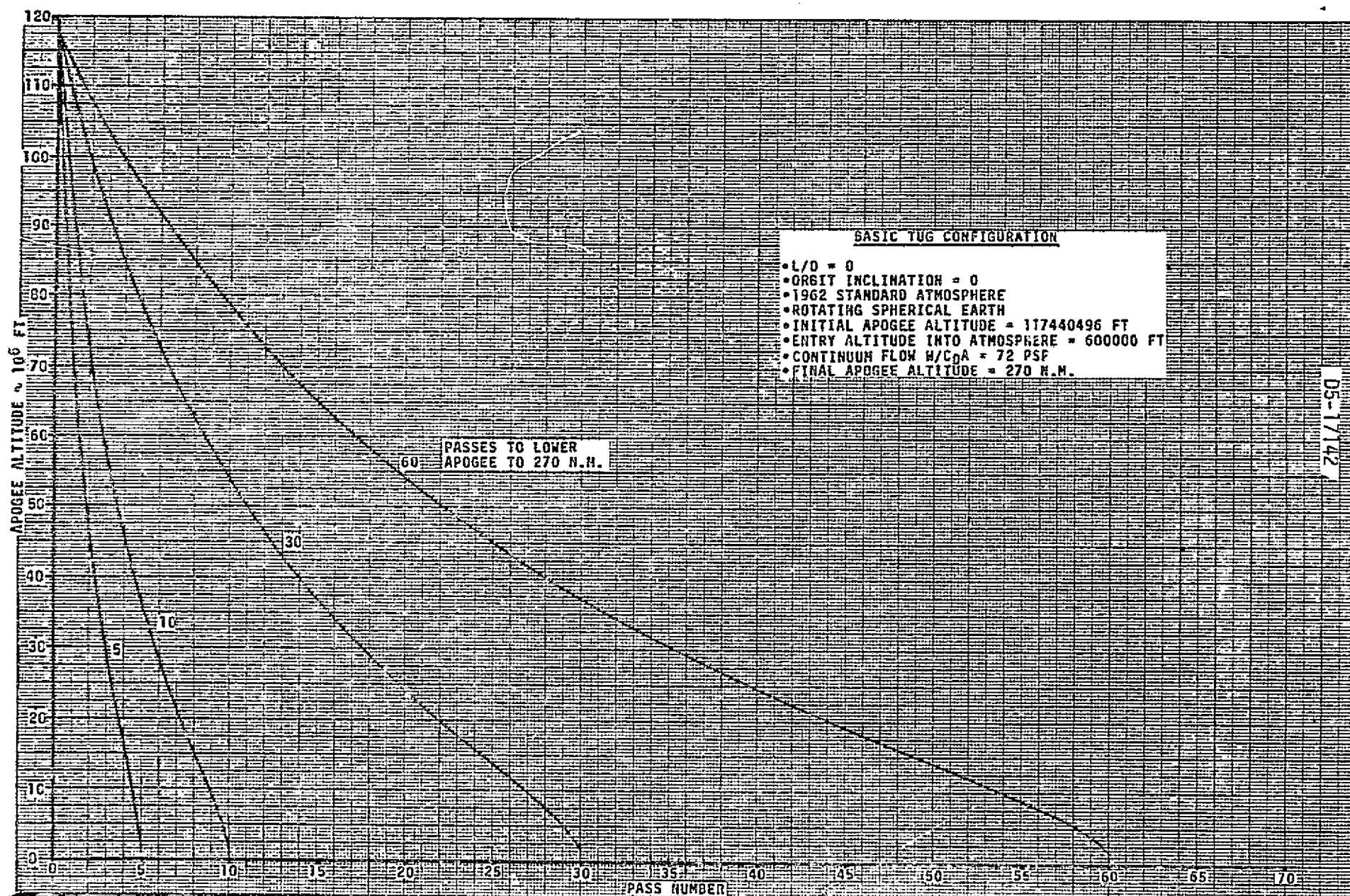


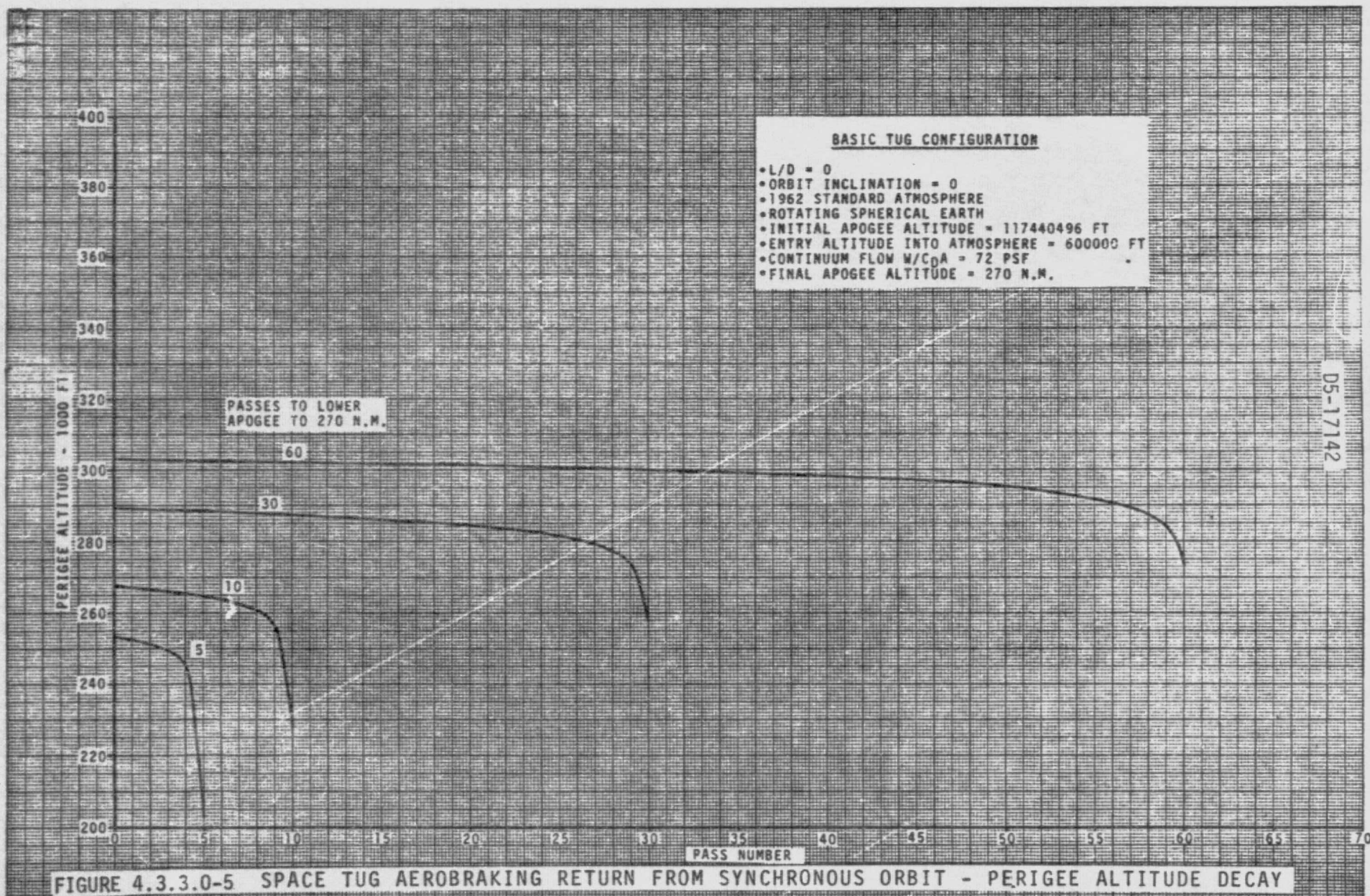
FIGURE 4.3.3.0-3 SPACE TUG AEROBRAKING RETURN FROM SYNCHRONOUS ORBIT - APOGEE ALTITUDE DECAY

```

LARGE FLARE CONFIGURATION
* L/D = 0
* ORBIT INCLINATION = 0
* 1962 STANDARD ATMOSPHERE
* ROTATING SPHERICAL EARTH
* INITIAL APOGEE ALTITUDE = 117440496. FT
* ENTRY ALTITUDE INTO ATMOSPHERE = 600000. FT
* CONTINUUM FLOW W/COR = 9.94+11.90
* FINAL APOGEE ALTITUDE = 1640551.185 FT

```

FIGURE 4.3.3.0-4 SPACE TUG AEROBRAKING RETURN FROM SYNCHRONOUS ORBIT - APOGEE ALTITUDE DECAY





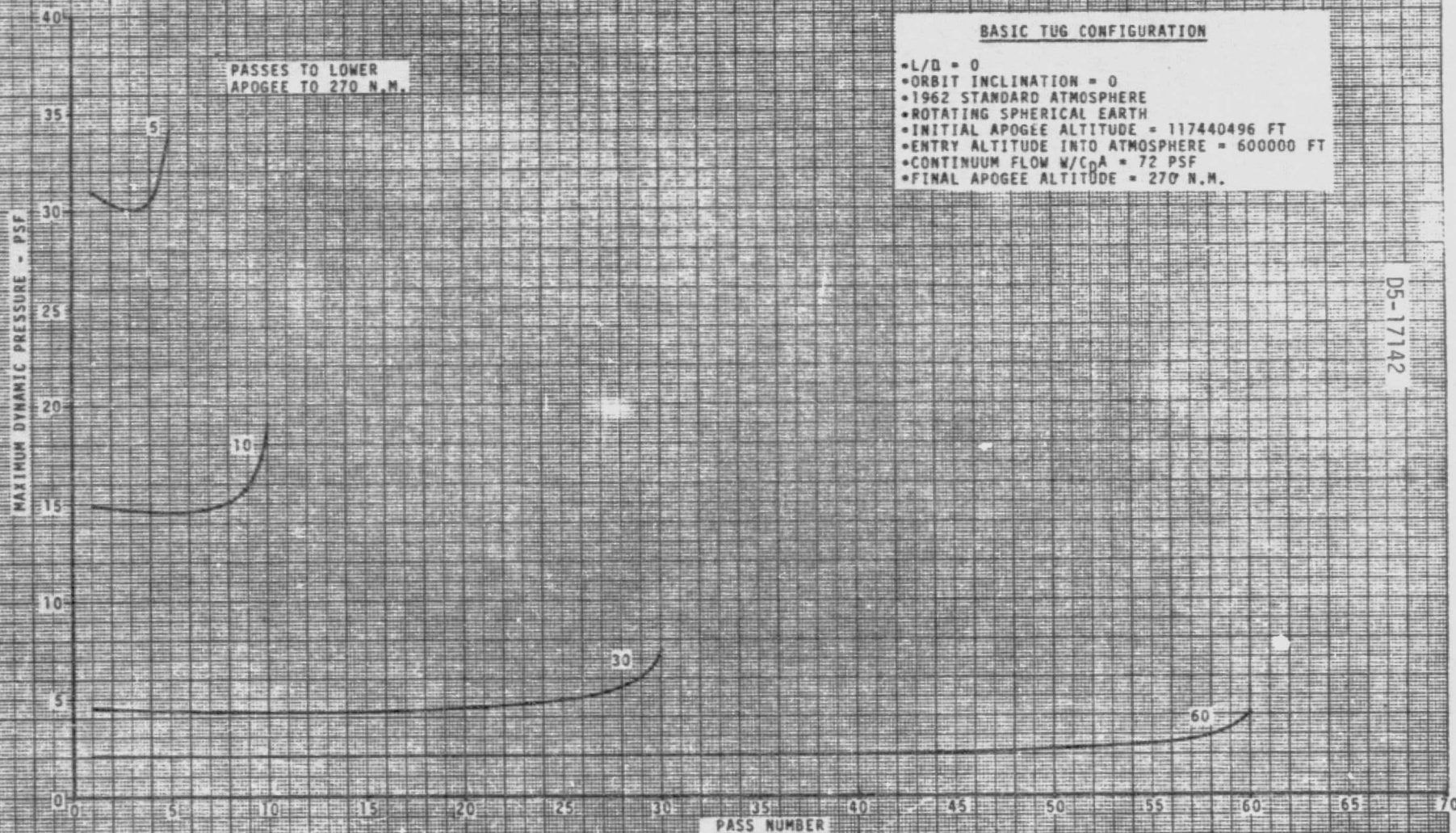
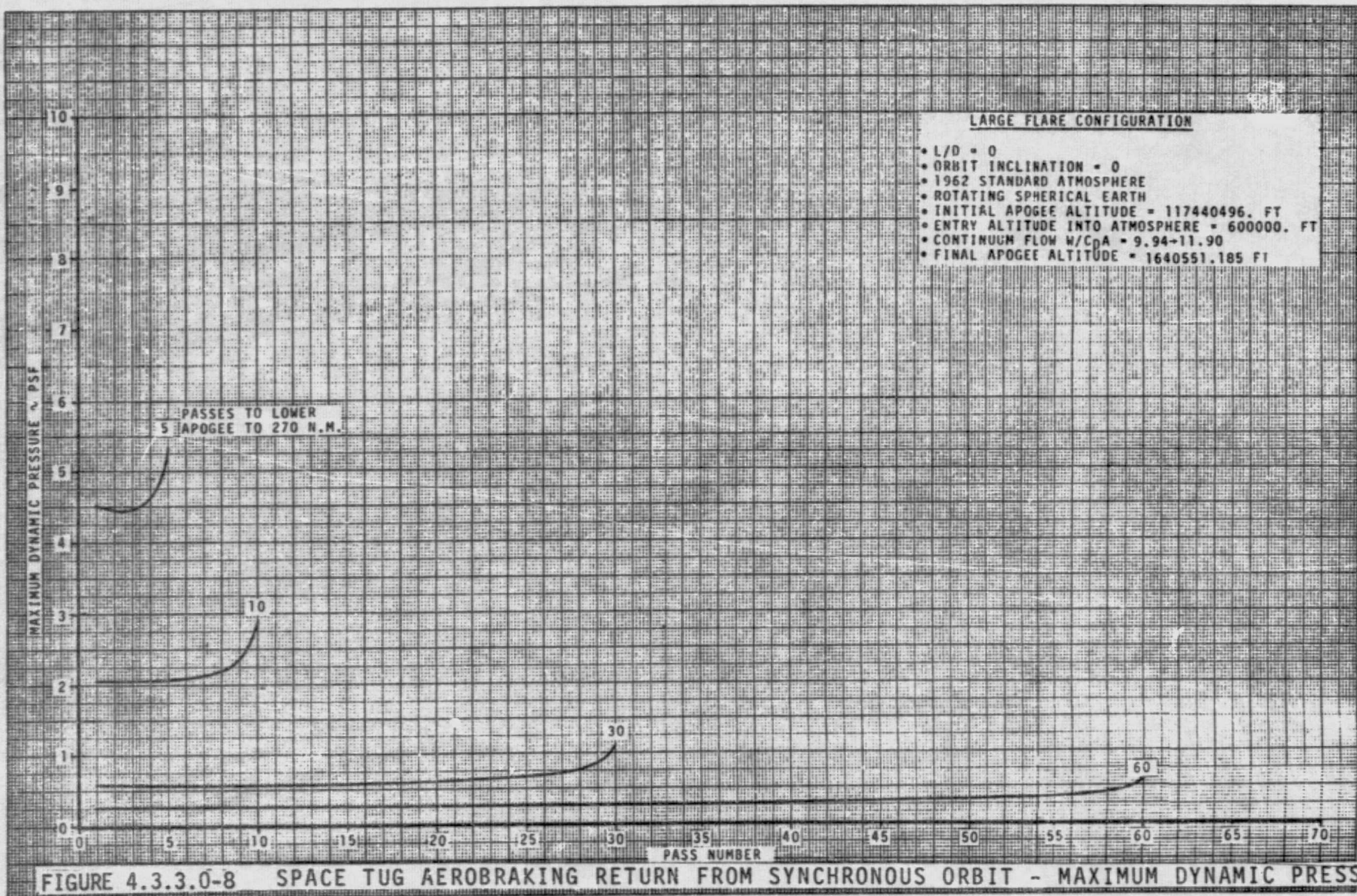


FIGURE 4.3.3.0-7 SPACE TUG AEROBRAKING RETURN FROM SYNCHRONOUS ORBIT - MAXIMUM DYNAMIC PRESSURE

4-80

10.5 IN TO THE CENTER
47 IN IN
M-2
10.5 IN TO THE CENTER
47 IN IN
M-2

D5-17142

- L/D = 0
- ORBIT INCLINATION = 0
- 1962 STANDARD ATMOSPHERE
- ROTATING SPHERICAL EARTH
- INITIAL APOGEE ALTITUDE = 117440496. FT
- ENTRY ALTITUDE INTO ATMOSPHERE = 600000. FT
- FINAL APOGEE ALTITUDE = 270 N.M.

30° FLARE
OPTIONAL LONG 30° FLARE
45° FLARE

PASSES TO LOWER
APOGEE TO 270 N.M.

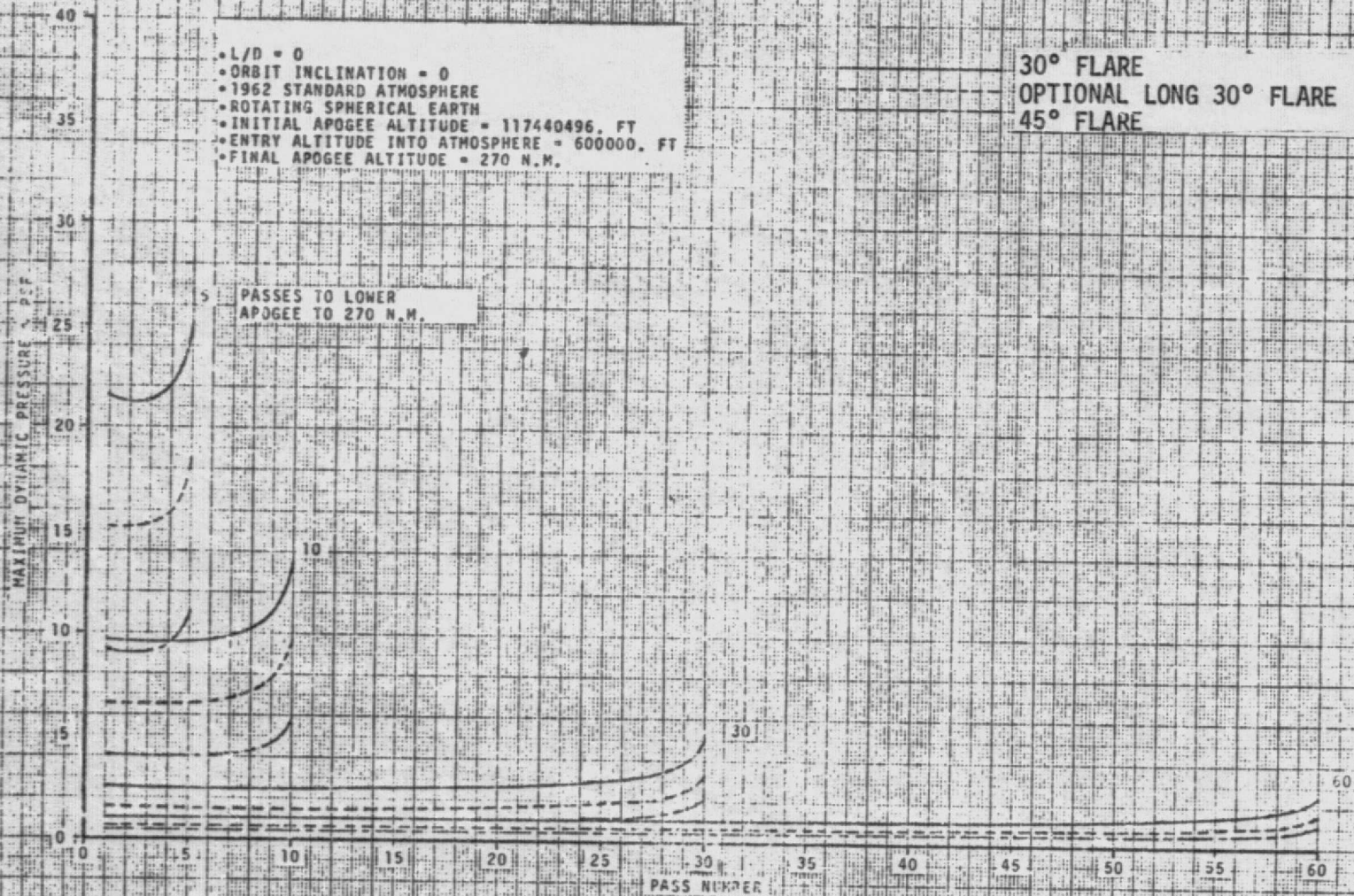


FIGURE 4.3.3.0-9 SPACE TUG AEROBRAKING RETURN FROM SYNCHRONOUS ORBIT - MAXIMUM DYNAMIC PRESSURE

D5-17142

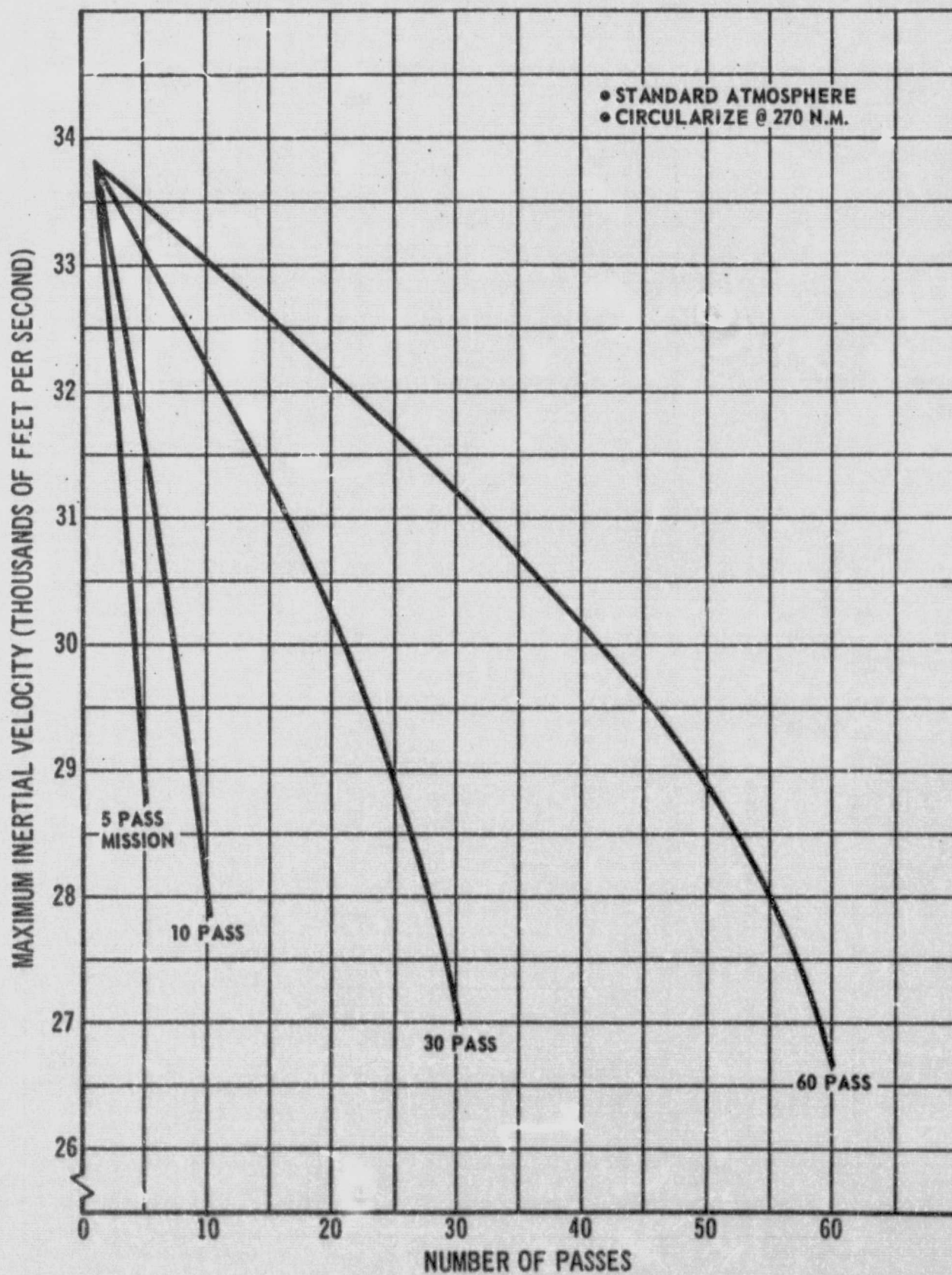


FIGURE 4.3.3.0-10. MAXIMUM INERTIAL VELOCITY PER PASS
BASIC TUG (NO FLARE) CONFIGURATION

D5-17142

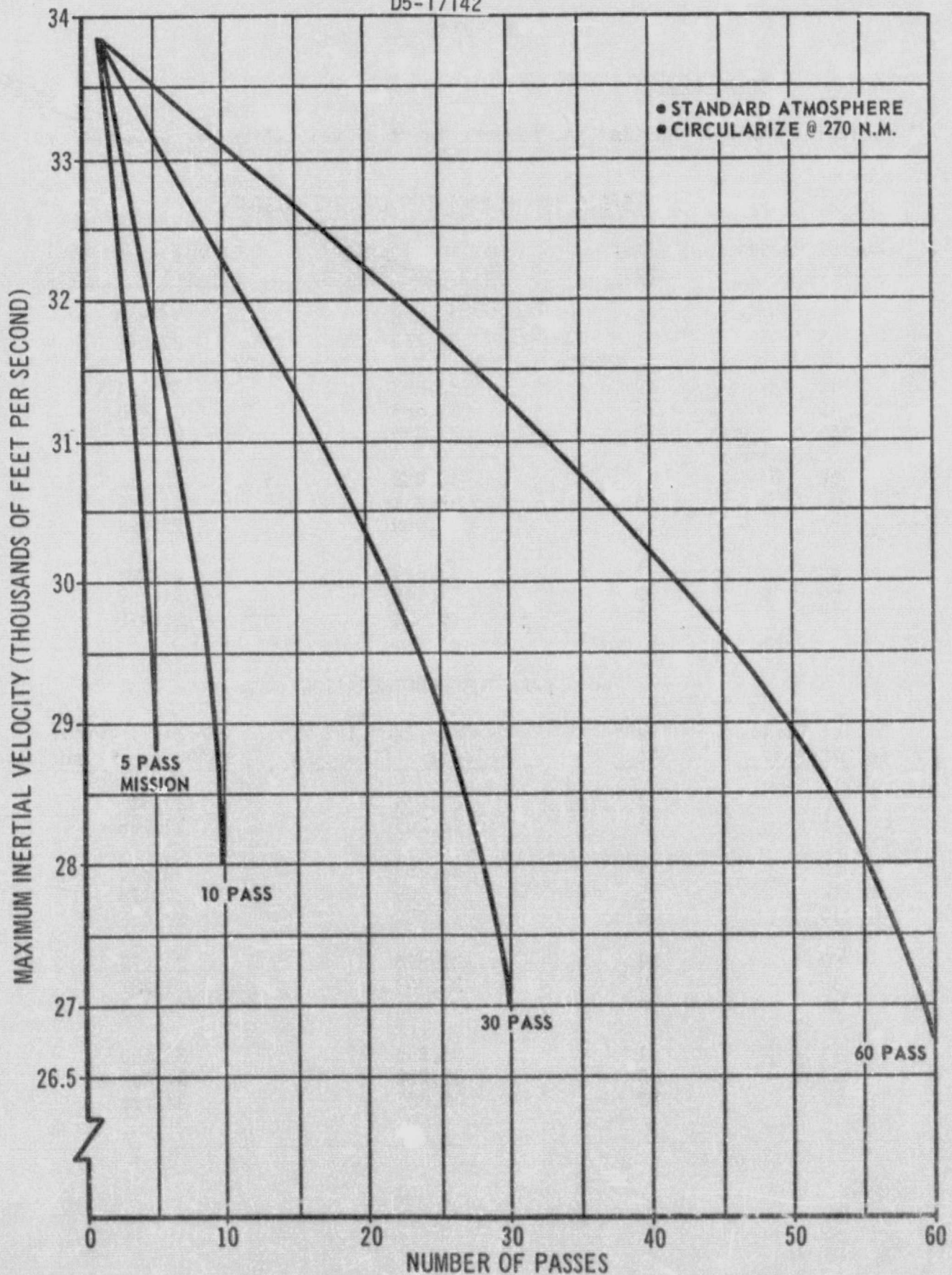


FIGURE 4.3.3.0-11. MAXIMUM INERTIAL VELOCITY PER PASS
60° FLARE TUG CONFIGURATION

4.3.3 (Continued)

selected maximum inertial and perigee inertial velocities are shown below:

BASIC (NO FLARE) TUG CONFIGURATION

<u>No. of Passes in Mission</u>	<u>Pass No.</u>	<u>Maximum Inertial Velocity (ft/sec)</u>	<u>Perigee Inertial Velocity (ft/sec)</u>
5	1	33,895	33,409
5	5	28,768	27,650
10	1	33,892	33,704
10	5	31,683	31,415
10	10	27,849	27,165
30	1	33,889	33,831
30	15	31,331	31,259
30	30	26,989	26,651
60	1	33,885	33,869
60	30	31,249	31,227
60	60	26,669	26,470

60° FLARE TUG CONFIGURATION

<u>No. of Passes in Mission</u>	<u>Pass No.</u>	<u>Maximum Inertial Velocity (ft/sec)</u>	<u>Perigee Inertial Velocity (ft/sec)</u>
5	1	33,854	33,381
5	5	28,824	27,738
10	1	33,857	33,672
10	5	31,709	31,478
10	10	27,888	27,178
30	1	33,854	33,814
30	15	31,343	31,282
30	30	27,000	26,653
60	1	33,850	33,833
60	30	31,258	31,232
60	60	26,667	26,452

4.3.3 (Continued)

Figure 4.3.3.0-12 illustrates the relationship of time spent in a free space environment (above 600,000 feet altitude) to the time spent in the atmosphere (below 600,000 feet) for the basic (no flare) configuration. The upper portion of the figure represents the time per pass (orbit) when the Tug is above 600,000 feet. Subsequent to the initial 18,700 second coast period from geosynchronous orbit to the first pass re-entry and its atmospheric passage, the 30 pass mission Tug will be in a free space environment for approximately 34,000 seconds (9.44 hours) prior to its second pass re-entry. The succeeding free space environment times decrease as the number of passes increases. Between the 29th and 30th passes, the Tug's time above 600,000 feet is decreased to 5156 seconds (1.43 hours). These long duration free space environment times can be regarded as vehicle "cool-down" periods as contrasted to the short duration "heating" periods below 600,000 feet.

The bottom portion of Figure 4.3.3.0-12 represents the time per pass spent below 600,000 feet. Using the same example as above, the 30 pass mission Tug is below 600,000 feet for 337 seconds on the first pass. This time increases as shown until the longest time (1194 seconds) per pass is reached on the 30th (final) pass. For all of the missions examined, the total time spent below 600,000 feet is less than 4% of the total aerobraking mission time.

The velocities shown in Figure 4.3.3.0-10 indicated acceleration experienced with atmospheric passage which displaced the maximum velocity from the normal conical perigee for the basic (no flare) configuration. This is reflected in the differences in times down to and up from perigee. Representative times for different passes of different mission durations are listed below.

BASIC (NO FLARE) CONFIGURATION

No. of Passes in Mission	Pass No.	Total Time Spent Below 600,000 ft (sec)	Time from 600,000 ft to Perigee (sec)	Time from Perigee to 600,000 Feet (sec)
5	1	363	176	187
5	5	1,017	320	697
10	1	348	168	180
10	5	422	208	214
10	10	1,110	374	736
30	1	337	168	169
30	15	414	206	208
30	30	1,194	480	714
60	1	325	160	165
60	30	407	200	207
60	60	1,333	544	789

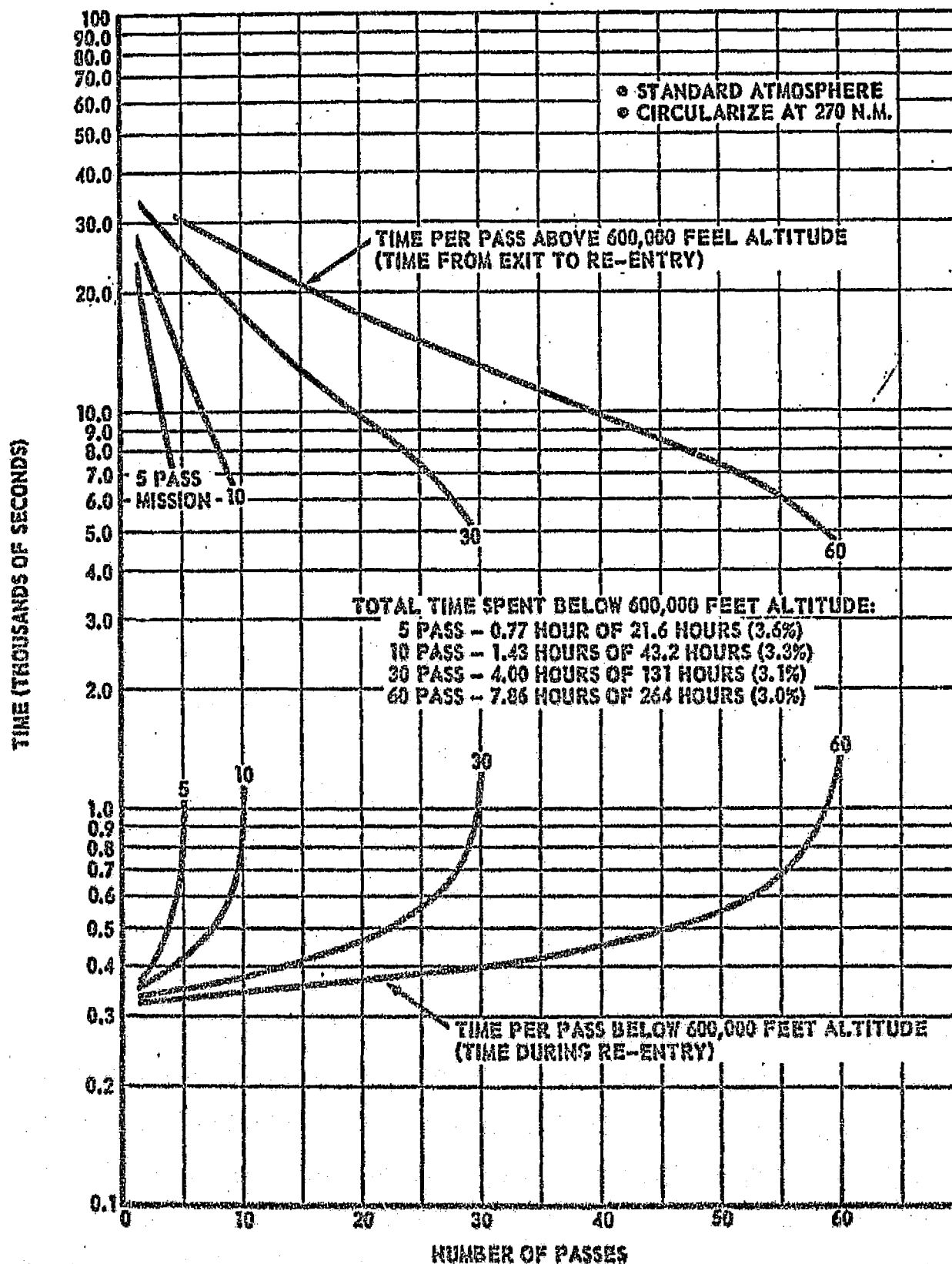


FIGURE 4.3.3.0-12: COMPARISON OF FREE SPACE AND RE-ENTRY TIMES
(BASIC-NO FLARE CONFIGURATION)

4.3.3 (Continued)

The column "Time from 600,000 Feet to Perigee" is significant in that this value is one factor in the minimum allowable time for a final mid-course correction burn prior to re-entry. As such, it impacts the navigation and accuracy analysis and the RCS requirements.

Similarly, Figure 4.3.3.0-13 illustrates the same data for the 60° flared configuration. The shape of the curves is similar to that presented for the basic (no flare) configuration. Because of the higher perigees flown with the flares, slightly less of the total mission time is spent below 600,000 feet. Representative time divisions between "600,000 Feet to Perigee" and "Perigee to 600,000 Feet" are shown below.

60° FLARED CONFIGURATION

No. of Passes in Mission	Pass No.	Total Time Spent Below 600,000 Ft (sec)	Time from 600,000 Feet to Perigee (sec)	Time from Perigee to 600,000 Feet (sec)
5	1	344	168	176
5	5	956	296	660
10	1	330	160	170
10	5	397	192	205
10	10	1,041	352	689
30	1	313	152	161
30	15	389	192	197
30	30	1,174	448	726
60	1	304	150	154
60	30	379	187	192
60	60	1,252	512	740

4.3.4 Dispersed Atmosphere Effects

The effect of atmospheric dispersion on the aerobraking trajectory of the basic Tug and large flare (60°) configurations are presented in this section. In addition, two candidate schemes for controlling the trajectories once a dispersion has been encountered are presented.

The dispersed atmosphere models (Reference 4.3.4.0-1) used are given in Figures 4.3.4.0-1 and -2. The more dense atmosphere used was the summer, high solar activity model of Figure 4.3.4.0-1 (+ density). The less dense atmosphere used was the winter, low solar activity model of Figure 4.3.4.0-2 (- density). These dispersed atmosphere density versus altitude functions were assumed to be invariant with time during the period of an entry trajectory.

D5-17142

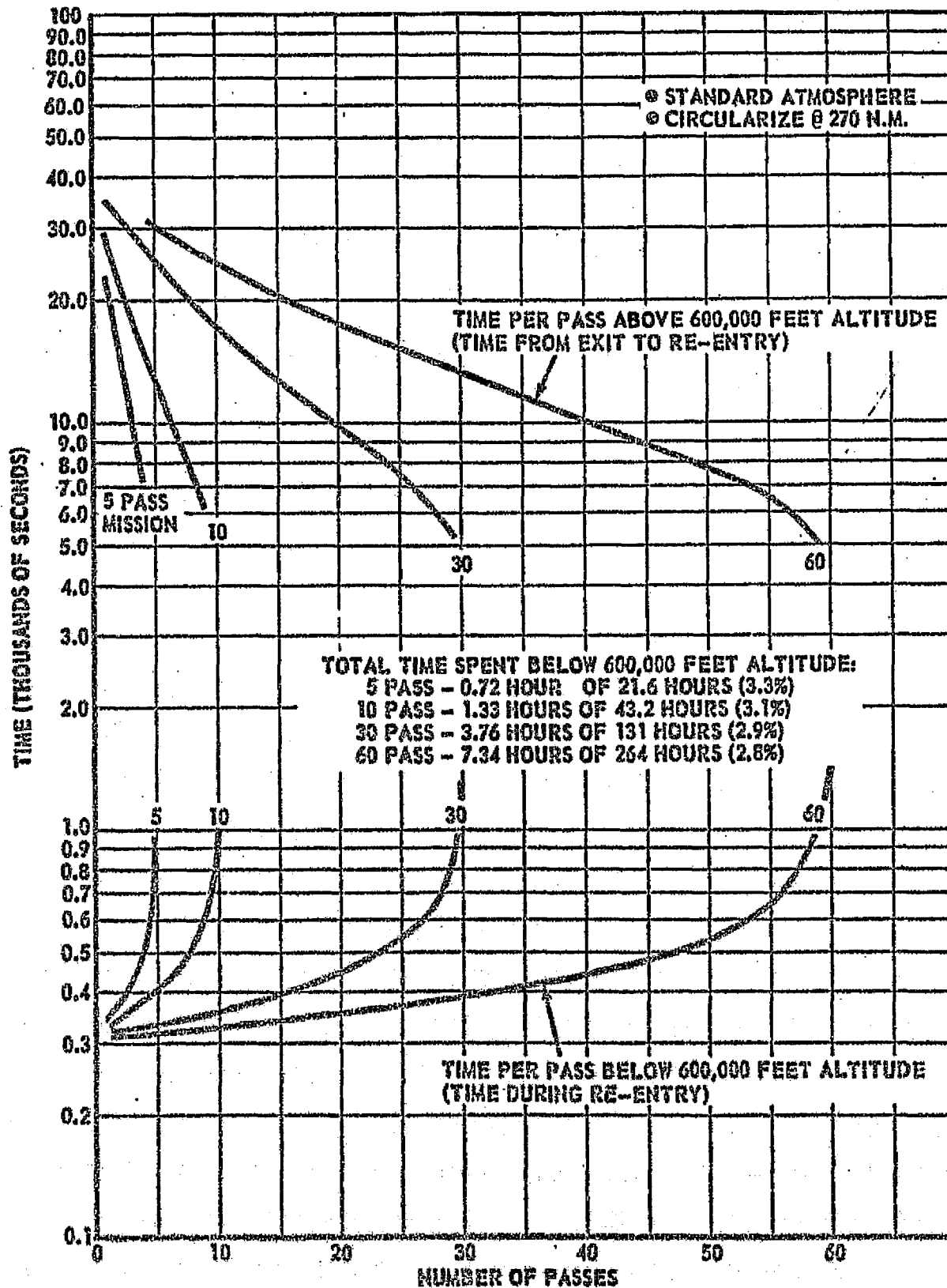
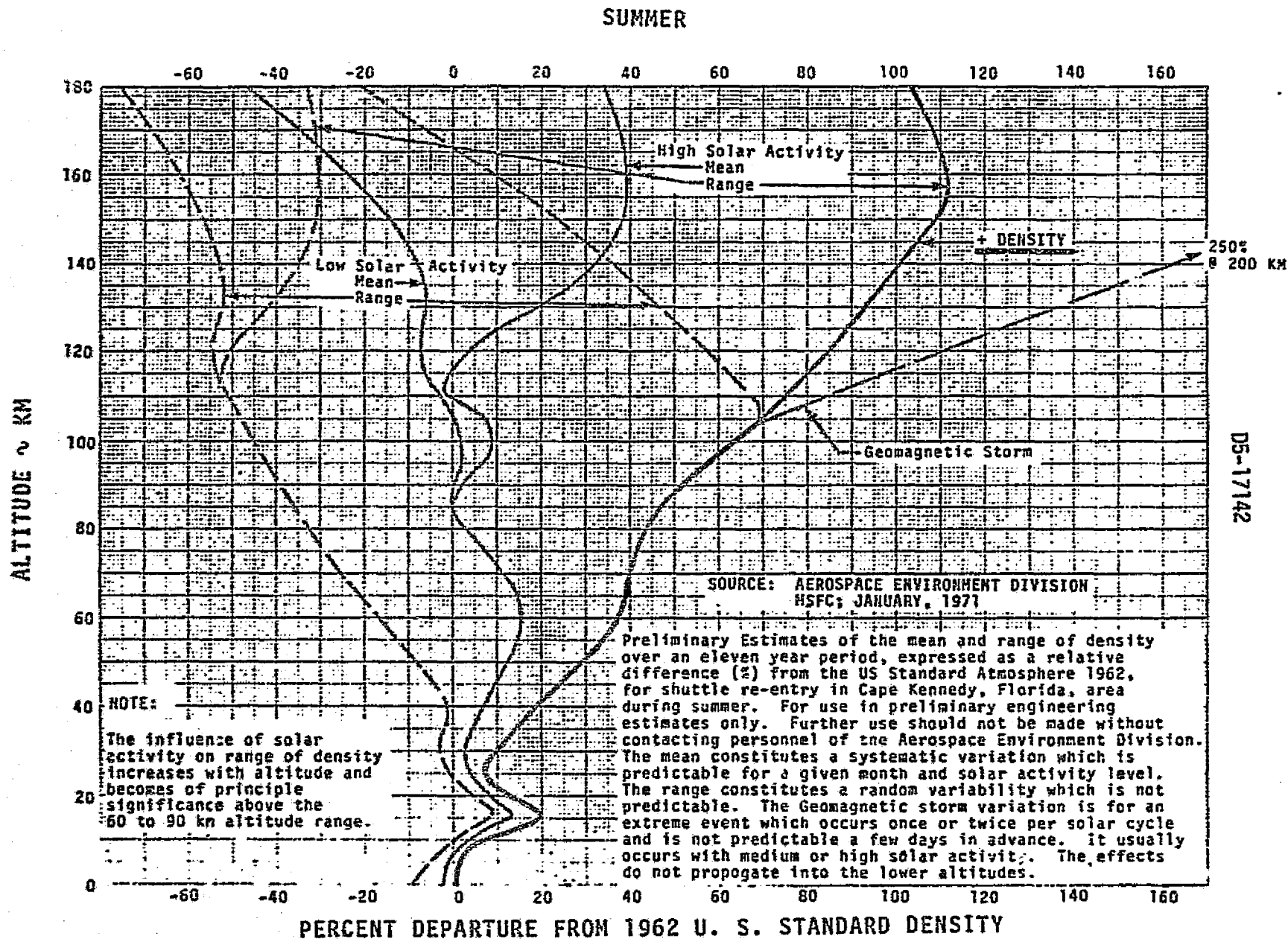
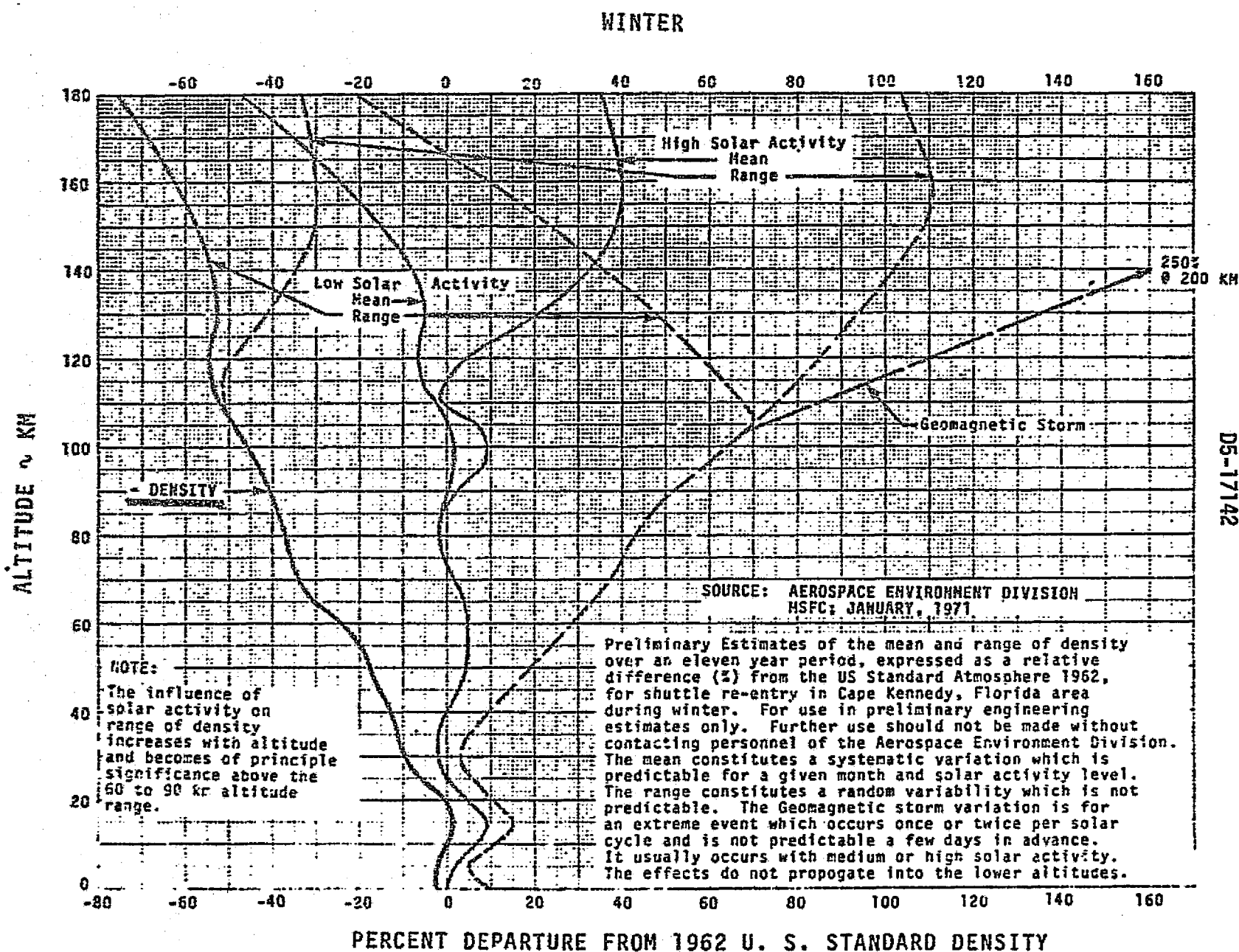


FIGURE 4.3.3.0-13: COMPARISON OF FREE SPACE AND RE-ENTRY TIMES (60° FLARE)



**FIGURE 4.3.4.0-1 SPACE TUG AEROBRAKING RETURN FROM SYNCHRONOUS ORBIT - SUMMER
ATMOSPHERIC DENSITY DISPERSIONS**



**FIGURE 4.3.4.0-2. SPACE TUG AEROBRAKING RETURN FROM SYNCHRONOUS ORBIT - WINTER
ATMOSPHERIC DENSITY DISPERSIONS**

4.3.4 (Continued)

Figure 4.3.4.0-3 presents the initial perigee altitude required for decay to a 270 NM orbit for the 1962 standard atmosphere and the dispersed atmospheres. The solid curves of Figure 4.3.4.0-3 are a result of re-isolation of the initial perigee altitude required to force the trajectory to end up at 270 NM in the presence of the dispersed atmosphere. The data illustrates the range of entry time due to atmospheric dispersions if the vehicle flies an uncorrected trajectory. For example, the flight time of the basic Tug nominal 30 pass trajectory varies from 3.6 days (19 passes) for the more dense atmosphere to 9.6 days (53 passes) for the less dense atmosphere. This large range in entry time implies the need for a trajectory correction technique that will significantly reduce this range.

4.3.4.1 Trajectory Correction Techniques

The following analysis pertains to a more dense atmosphere. The same logic will apply in the reverse direction to a less dense atmosphere.

When descent begins, the density of the atmosphere that is to be encountered is not known, therefore, descent will be made on a trajectory that is targeted to the initial perigee altitude dictated by the nominal atmosphere. If the atmosphere is more dense than that expected, the trajectory apogee will be too low on this pass and all succeeding passes. The result is that the Tug will reach the target altitude much too soon. This means that adjustments must be made in the trajectory in order to reach 270 NM in the required number of passes. To control the trajectory, a target parameter that specifies the correct trajectory must be known or calculable. For the aerobraking trajectories, the apogee decay is practically invariant with respect to $W/C_D A$ and/or density for a fixed entry pass number. As a result, this parameter is chosen as the target parameter.

In addition to apogee altitude itself, the rate of apogee decay must be controlled. This decay rate is dependent entirely (for spherical earth) on the amount of aerodynamic drag per pass. Since the ballistic coefficient ($W/C_D A$) function is invariant for a given Tug configuration, the only control over drag is the depth to which the vehicle penetrates the atmosphere. This depth is controlled by varying the vacuum perigee altitude at atmosphere entry. For each atmospheric model there exists a unique vacuum perigee pass history that will have both the proper apogee altitude and apogee decay rate. Currently, the necessary perigee pass history is not calculable in advance. Thus, a scheme for controlling apogee altitude will also consist of a search for the correct perigee.

Adjustments in the trajectory may be made by applying an impulse either near atmosphere exit or at the uncorrected apogee. The first method (impulse at exit) forces the ascent trajectory through the target apogee. Thus, the increase in the drag losses of the previous pass would be taken out by use of a propulsive ΔV . The second method (impulse at apogee) increases the perigee of the descent trajectory of the next pass so that less drag would be encountered on that pass. This causes the apogee to decay less, and after a number of passes are corrected in this manner, the apogee decay approaches the target apogee. Thus, the increase in

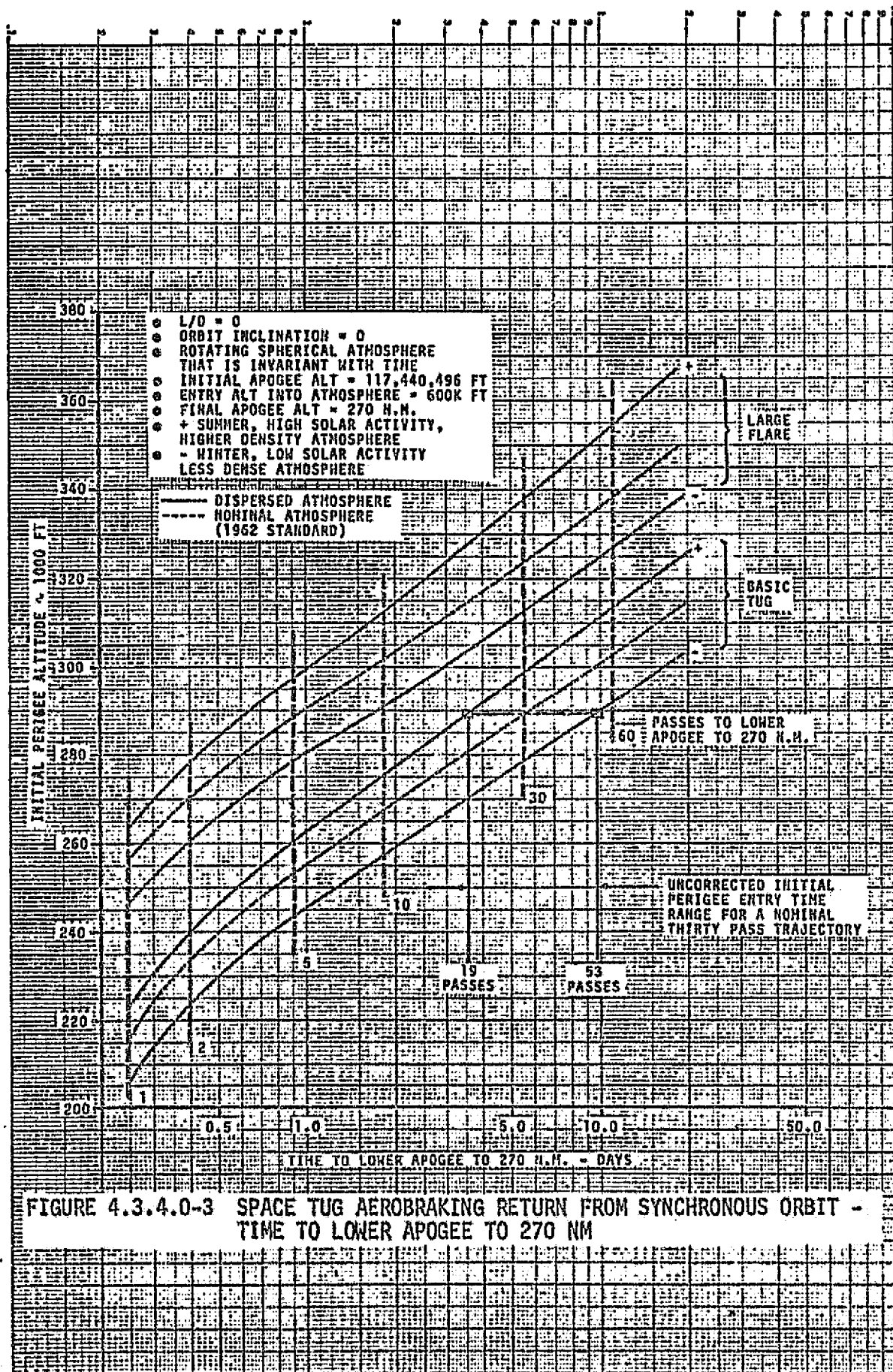


FIGURE 4.3.4.0-3 SPACE TUG AEROBRAKING RETURN FROM SYNCHRONOUS ORBIT - TIME TO LOWER APOGEE TO 270 NM

4.3.4.1 (Continued)

drag losses of the previous pass are taken out by having less drag on succeeding passes.

1. Impulse At Exit

The propulsive ΔV for the impulse at exit is applied at atmosphere exit (600,000 feet) and co-linear with the exit velocity. The ΔV magnitude is determined by computing the velocity required at that point to cause the vehicle to be on an ascent trajectory with the target apogee. The resultant trajectory also has a higher perigee. This perigee value is not necessarily the perigee altitude required for the dispersed density, but the perigee does change in the correct direction.

An example of this method is presented in Figures 4.3.4.1-1, -2, and -3 where the trajectory correction ΔV , perigee altitude, and apogee altitude are shown for the basic Tug, nominal 30 pass trajectory. (The total ΔV shown in Figure 4.3.4.1-1 is the accumulated trajectory correction ΔV and does not include correcting the final pass to 270 NM). Figure 4.3.4.1-2 shows the perigee altitude required for decay to a 270 NM orbit in the presence of the dispersed atmosphere (the solid line). In the real case, this perigee history is not known in advance. Thus, an impulse is applied on each pass to correct the apogee (Figure 4.3.4.1-3) until the resultant perigees (circled points) converge to the desired value.

2. Impulse At Apogee

An example of impulse at apogee is illustrated in Figures 4.3.4.1-4, -5 and -6. At the end of the first pass the apogee is too low. This means that the perigee must be raised to reduce the rate of apogee decay. The amount the perigee must be raised is not known in advance. Thus, the perigee must be incremented in upward steps (circled points on Figure 4.3.4.1-5) by applying an impulse at apogee until the target apogee has been approached (at Pass #7 on Figure 4.3.4.1-6). At this point, enough information has been gained to indicate the perigee (solid line, Figure 4.3.4.1-5) required for this atmosphere model. By averaging the perigee magnitudes over the passes now completed, a perigee guess may be obtained that lies very close to the desired perigee. The next pass then uses this averaged value of perigee. Since the perigee and apogee values on this pass are not exactly those desired, the next pass will be in error, but not nearly so much as initially. From this point, the perigee is again incremented until the target apogee curve is crossed. The perigee is again set to the average value of the series of steps made since the last average was determined. This procedure is repeated up until two passes from the nominal final pass number. The cutoff is made at this point because the perigee curve becomes very nonlinear and an average value of perigee would be very much in error. (The total ΔV shown in Figure 4.3.4.1-4 is the trajectory correction ΔV and does not include correcting the final pass to 270 NM).

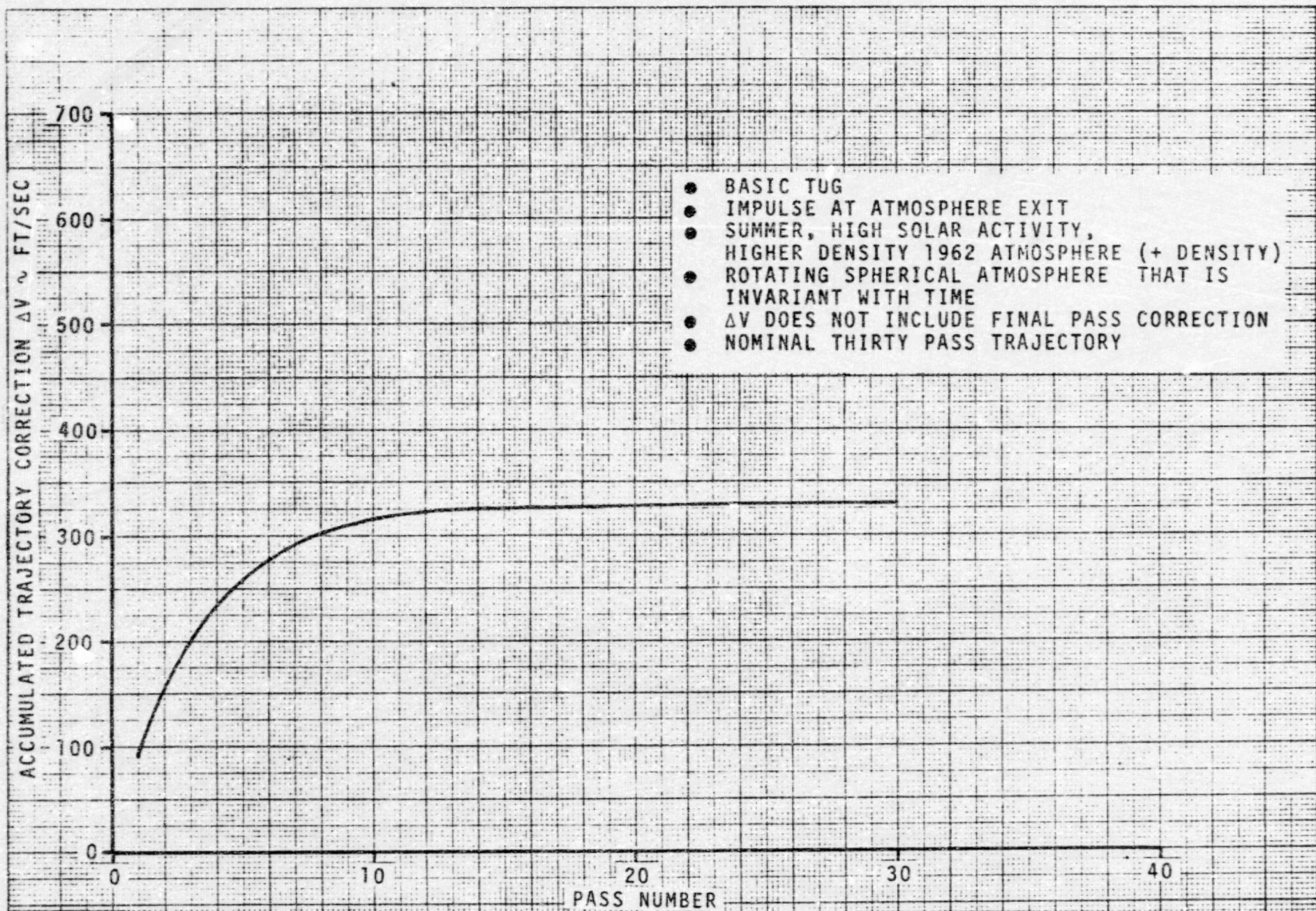
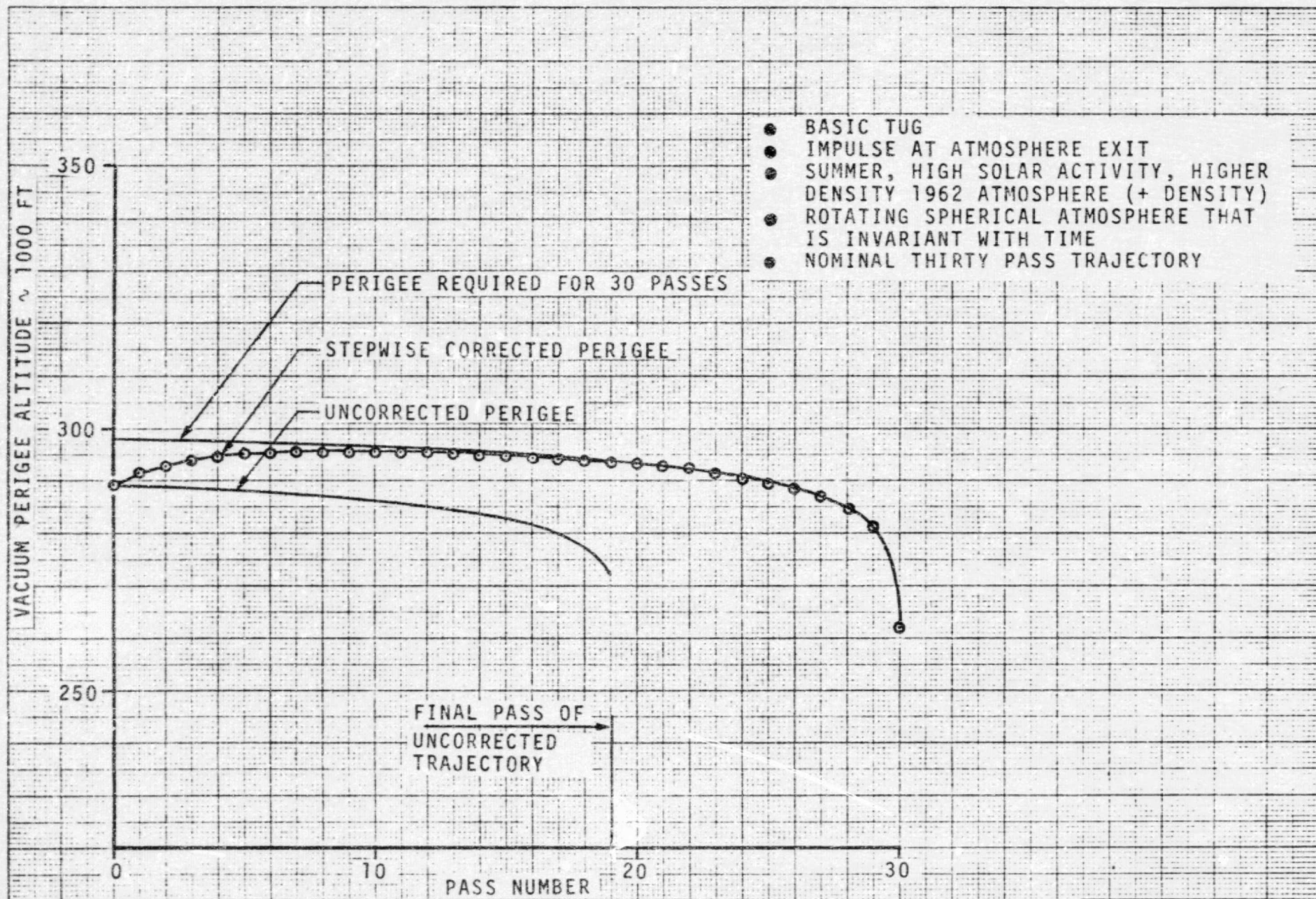


FIGURE 4.3.4.1-1 SPACE TUG AEROBRAKING RETURN FROM SYNCHRONOUS ORBIT - ACCUMULATED TRAJECTORY CORRECTION ΔV FOR IMPULSE AT ATMOSPHERE EXIT

4-94

05-17142



05-17142

FIGURE 4.3.4.1-2 SPACE TUG AEROBRAKING RETURN FROM SYNCHRONOUS ORBIT - VACUUM PERIGEE ALTITUDE AT ATMOSPHERE EXIT

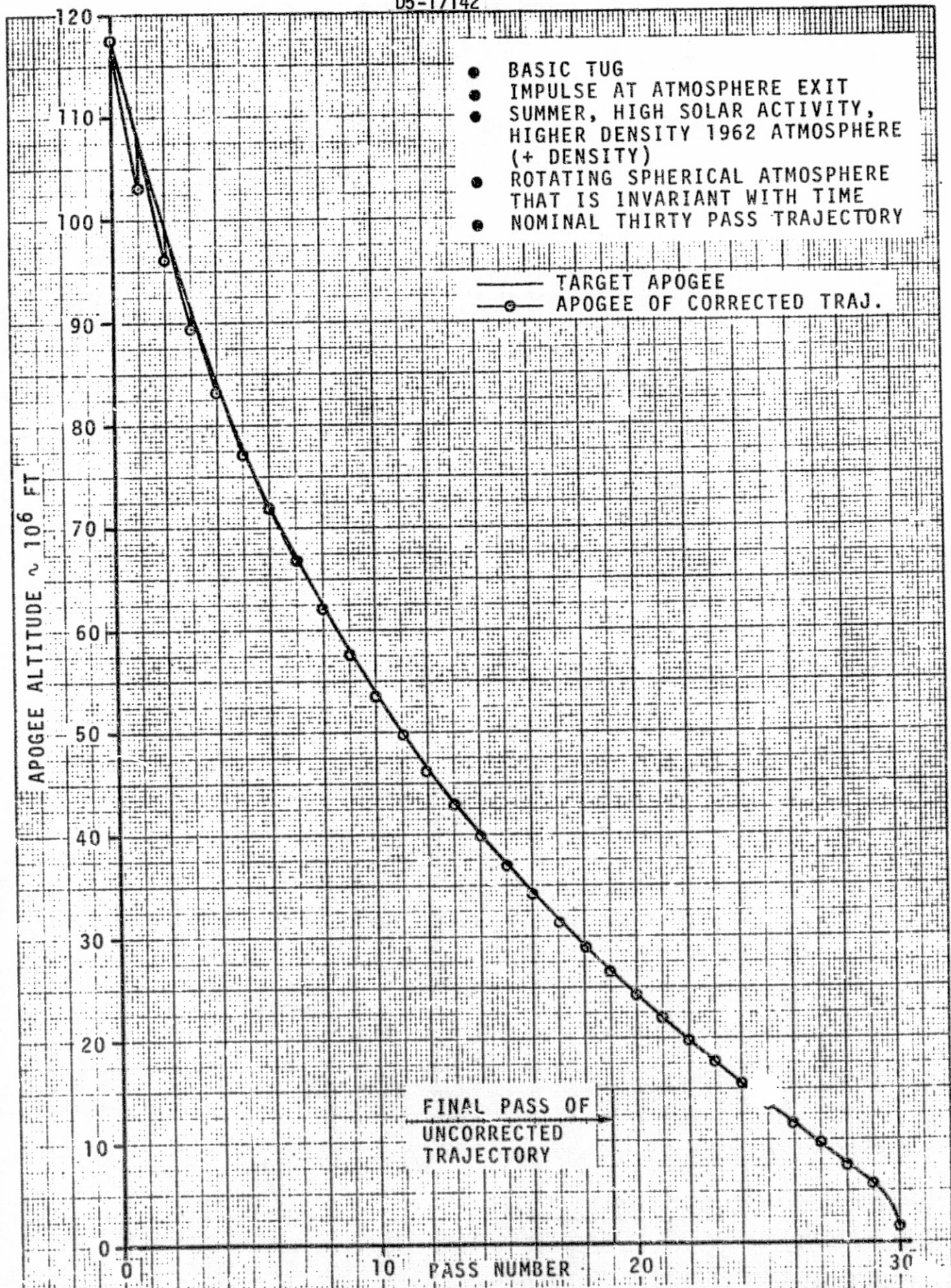


FIGURE 4.3.4.1-3 SPACE TUG AEROBRAKING RETURN FROM SYNCHRONOUS ORBIT - APOGEE ALTITUDE AT END OF PASS

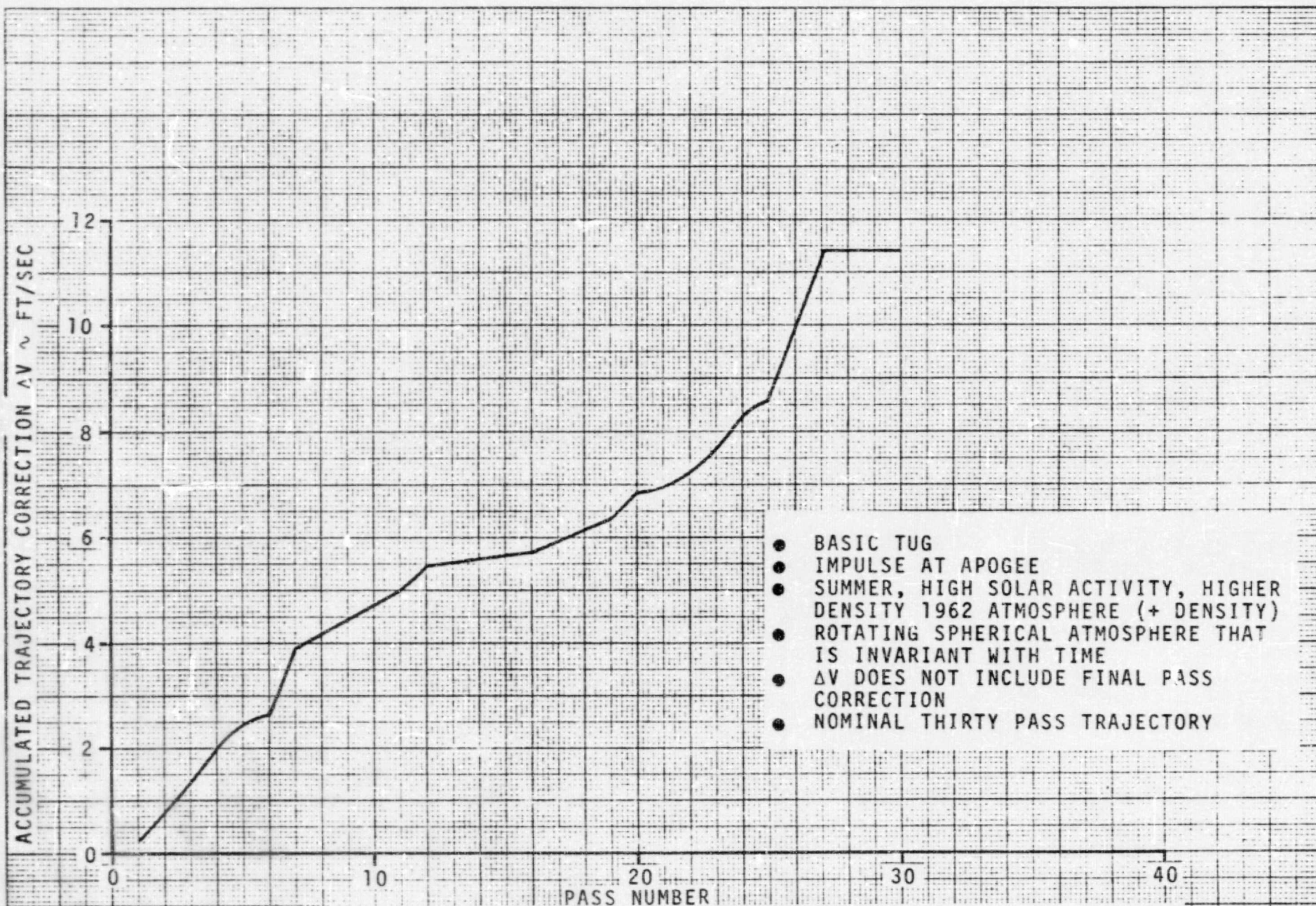
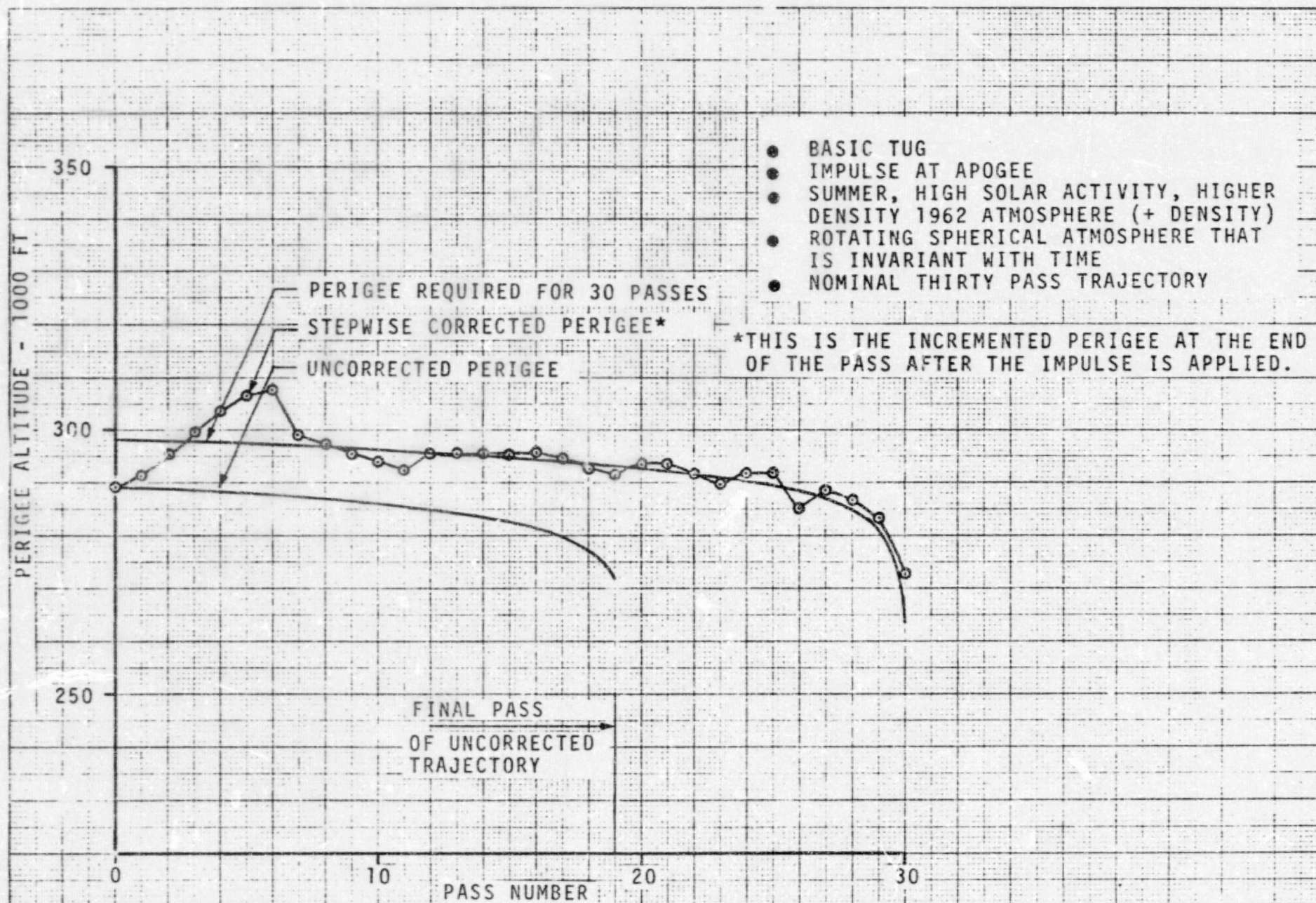


FIGURE 4.3.4.1-4 SPACE TUG AEROBRACING RETURN FROM SYNCHRONOUS ORBIT - ACCUMULATED TRAJECTORY CORRECTION ΔV FOR IMPULSE AT APOGEE

05-17142



05-17142

FIGURE 4.3.4.1-5. SPACE TUG AEROBRAKING RETURN FROM SYNCHRONOUS ORBIT - VACUUM PERIGEE ALTITUDE AT ATMOSPHERE EXIT

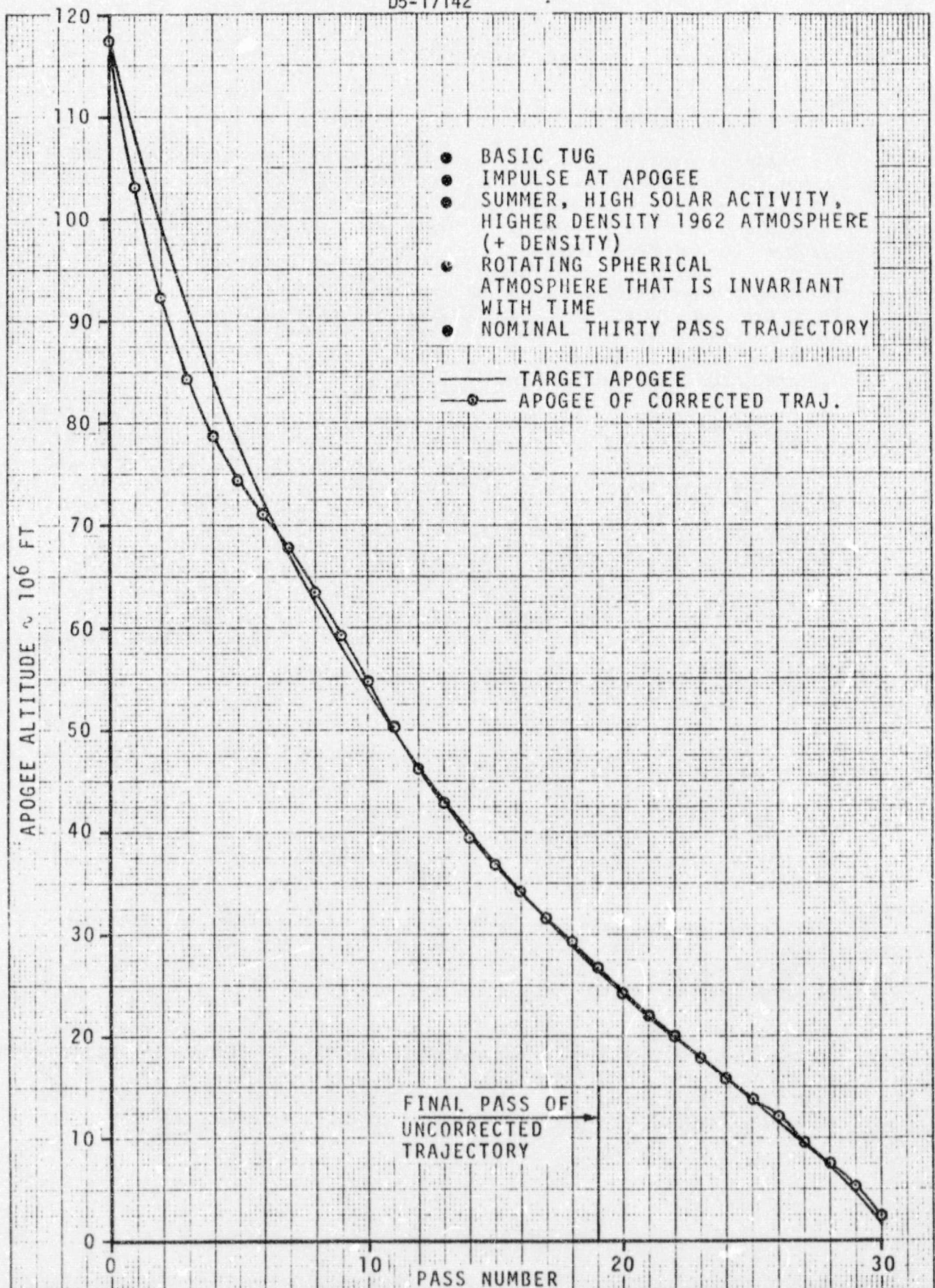


FIGURE 4.3.4.1-6. SPACE TUG AEROBRACING RETURN FROM SYNCHRONOUS ORBIT
- APOGEE ALTITUDE AT END OF PASS

4.3.4.1 (Continued)

The trajectory correction ΔV 's for impulse at exit run higher than 300 ft/sec for both the basic Tug and large flare configurations. Resulting final pass errors in apogee altitude are within 200K ft for the basic Tug and within 1M ft for the large flare Tug. The trajectories have no error in the number of passes.

The trajectory correction ΔV 's for impulse at apogee are less than 20 ft/sec, but the errors in the final apogee altitude and pass number are more significant. This is illustrated in Figures 4.3.4.1-7 and -8 where the errors in apogee altitude and pass number are given for basic Tug and large flare respectively.

The ΔV 's mentioned in the above two paragraphs are the ΔV 's for trajectory correction before reaching the final pass. They do not include the ΔV 's to correct the final apogee altitude error. The total increase in the ΔV requirements due to atmospheric uncertainties are given in Figures 4.3.4.1-9 and -10. These ΔV 's are the total increase in the ΔV 's (trajectory and final pass correction) required to end up at 270 NM over that required for the unperturbed trajectories. Either of the two targeting schemes can control Tug aerobraking trajectories in the presence of large, unpredictable atmospheric density dispersions. The impulse at exit scheme will require 300 to 800 ft/sec correction ΔV . Improvements in this scheme to effect better convergence on final apogee altitude will not reduce the ΔV requirements significantly because of the inherently large impulses necessary at atmospheric exit to make minor trajectory changes. Except for the 10 pass trajectory, ΔV requirements of the impulse at apogee scheme are generally comparable to or less than impulse at exit requirements. Impulse at apogee scheme ΔV requirements are mostly ΔV necessary to correct the final apogee altitude error, hence improvements in this scheme to obtain better convergence on the desired final apogee altitude will significantly reduce these ΔV requirements. Thus the 400 fps ΔV reserved for trajectory correction in the original mission ΔV requirement, will be sufficient assuming further development of impulse at apogee targeting.

The maximum dynamic pressure in the presence of the dispersed atmosphere is compared in Figures 4.3.4.1-11 through -16 for the impulse at exit target scheme and in Figures 4.3.4.1-17 through 4.3.4.1-22 for the impulse at apogee target scheme.

The loads (Section 4.1) and thermal (Section 4.5) analysis was performed on the first pass of the 10, 30 and 60 pass dispersed atmosphere trajectories of the basic and large flare tugs (the first pass events are identical for both targeting schemes). A controls analysis (Section 4.4) was performed using the trajectories of the impulse at apogee targeting scheme.

D5-17142

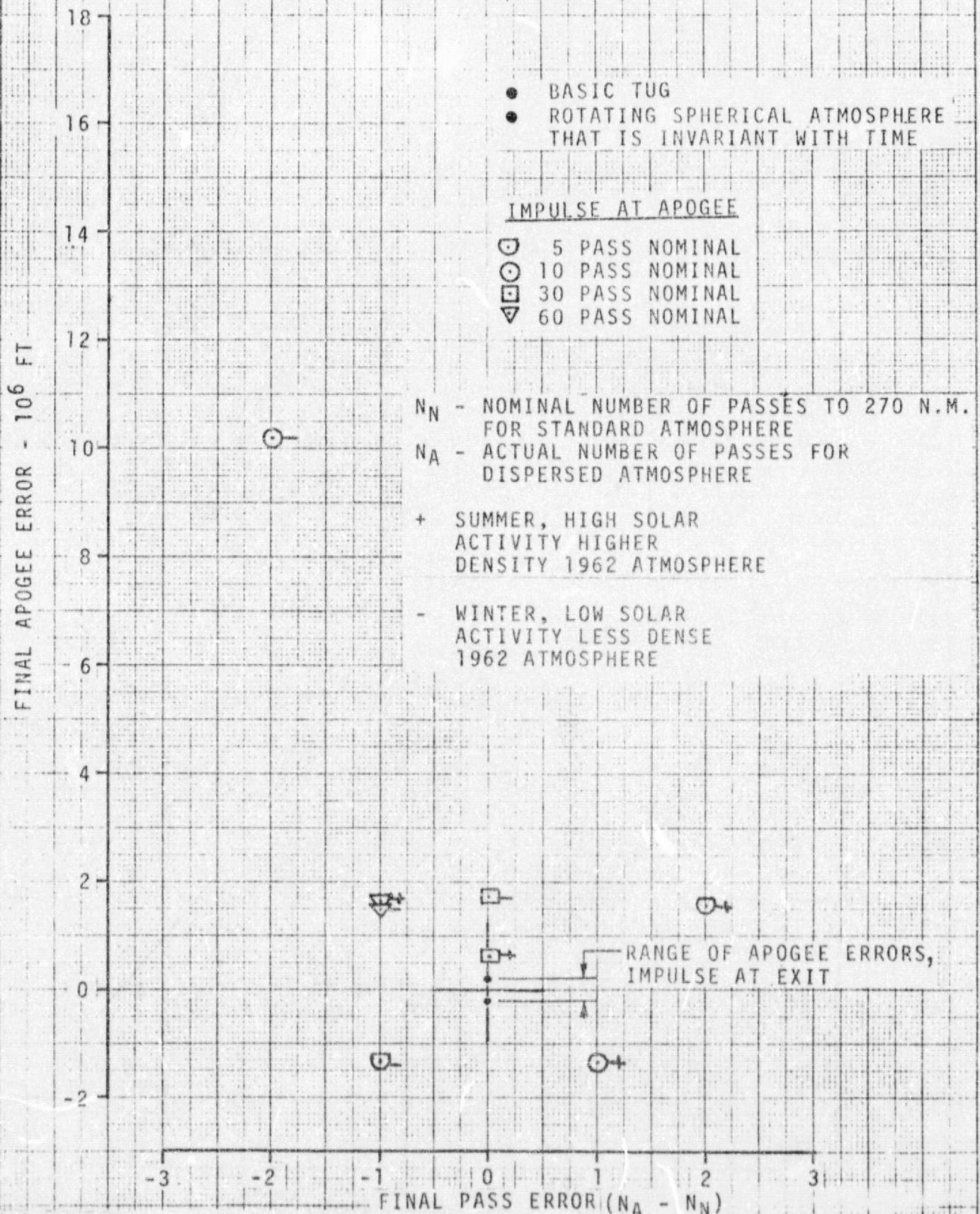


FIGURE 4.3.4.1-7 SPACE TUG AEROBRAKING RETURN FROM SYNCHRONOUS ORBIT
- FINAL PASS AND APOGEE ERROR FOR IMPULSE AT APOGEE

D5-17142

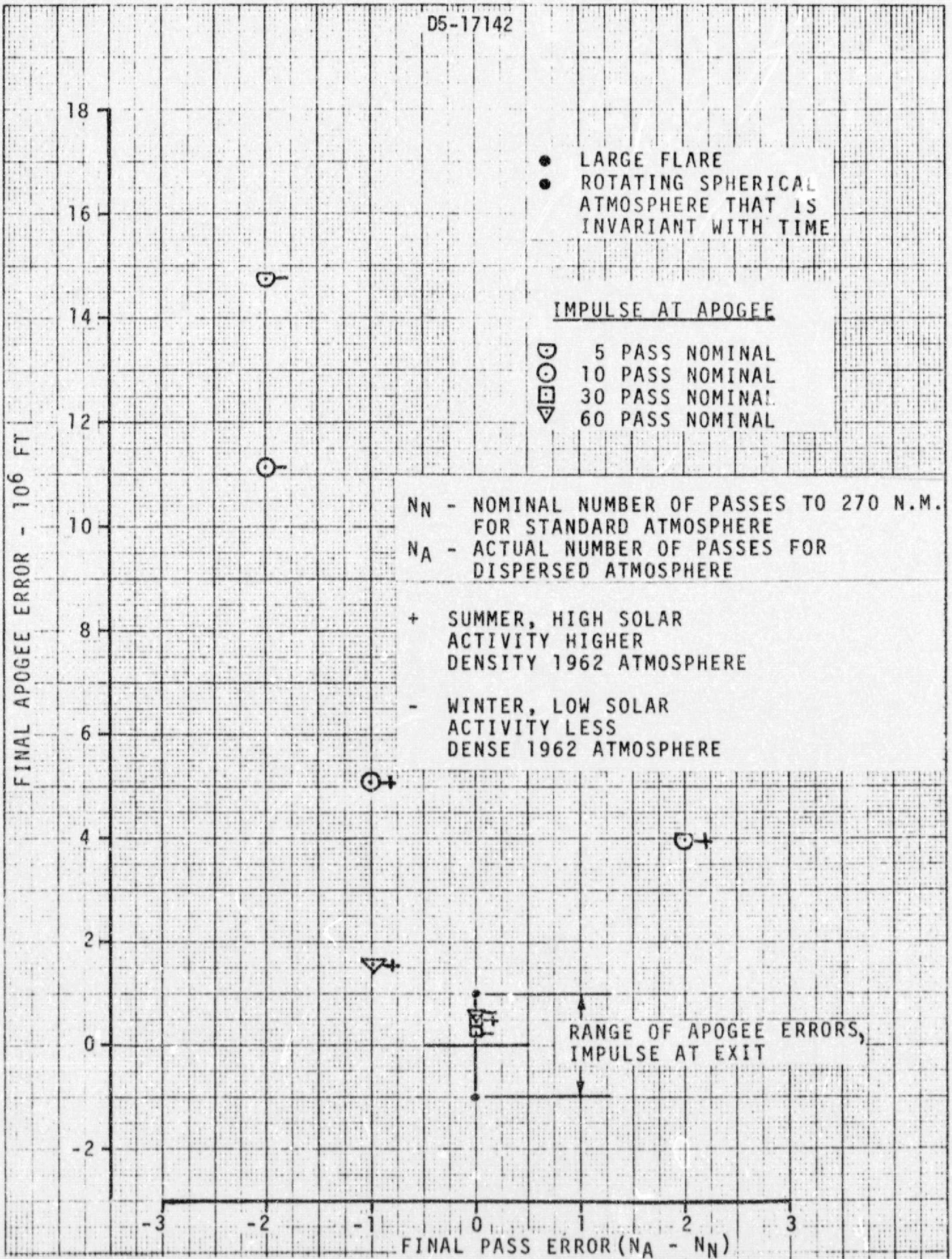


FIGURE 4.3.4.1-8. SPACE TUG AEROBRAKING RETURN FROM SYNCHRONOUS ORBIT
 [Legend symbols] - FINAL PASS AND APOGEE ERROR FOR IMPULSE AT APOGEE

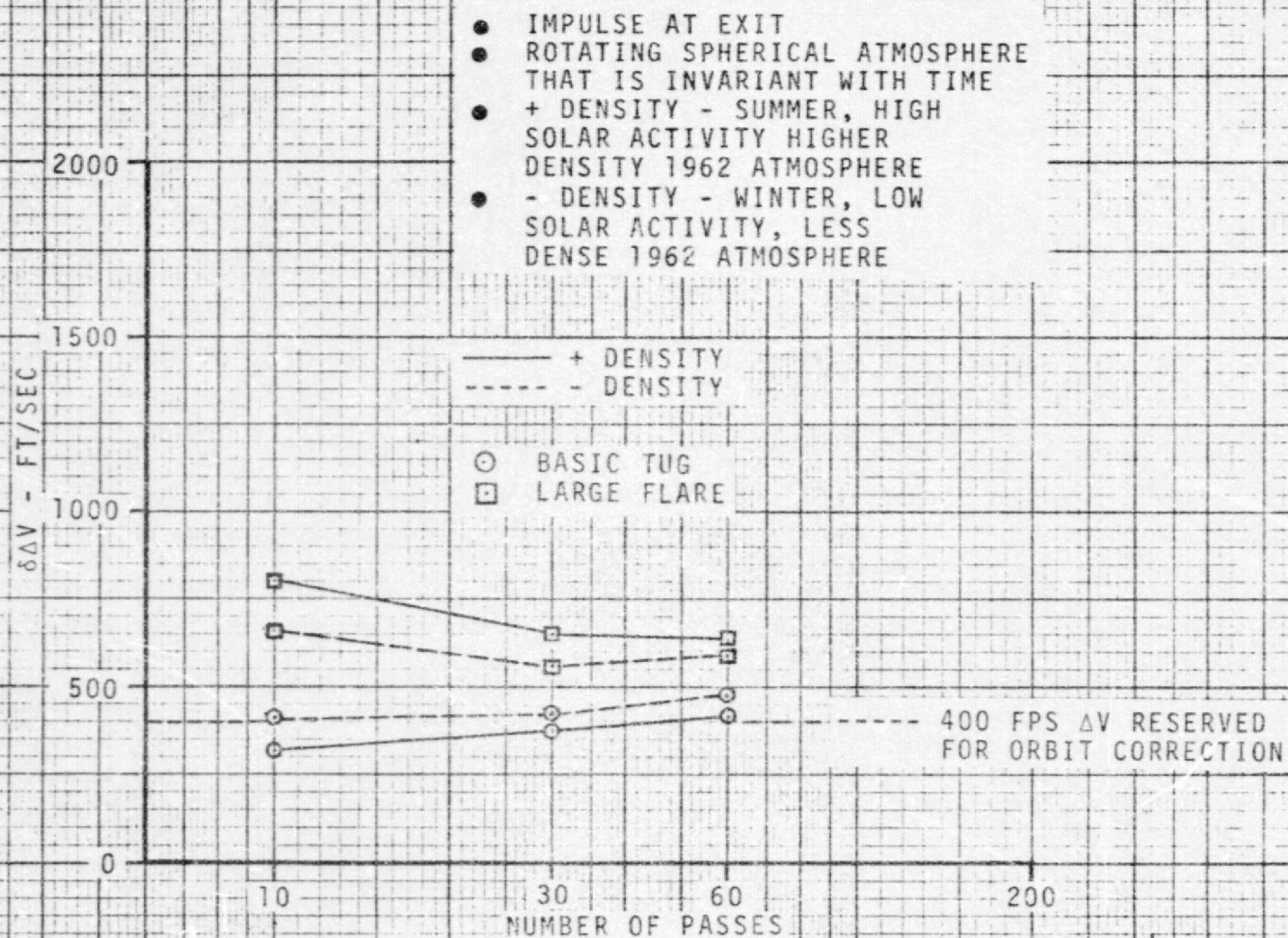


FIGURE 4.3.4.1-9 SPACE TUG AEROBRAKING RETURN FROM SYNCHRONOUS ORBIT - INCREASE IN ΔV TO GO TO 270 N.M. FOR IMPULSE AT EXIT

D5-17142

4-103

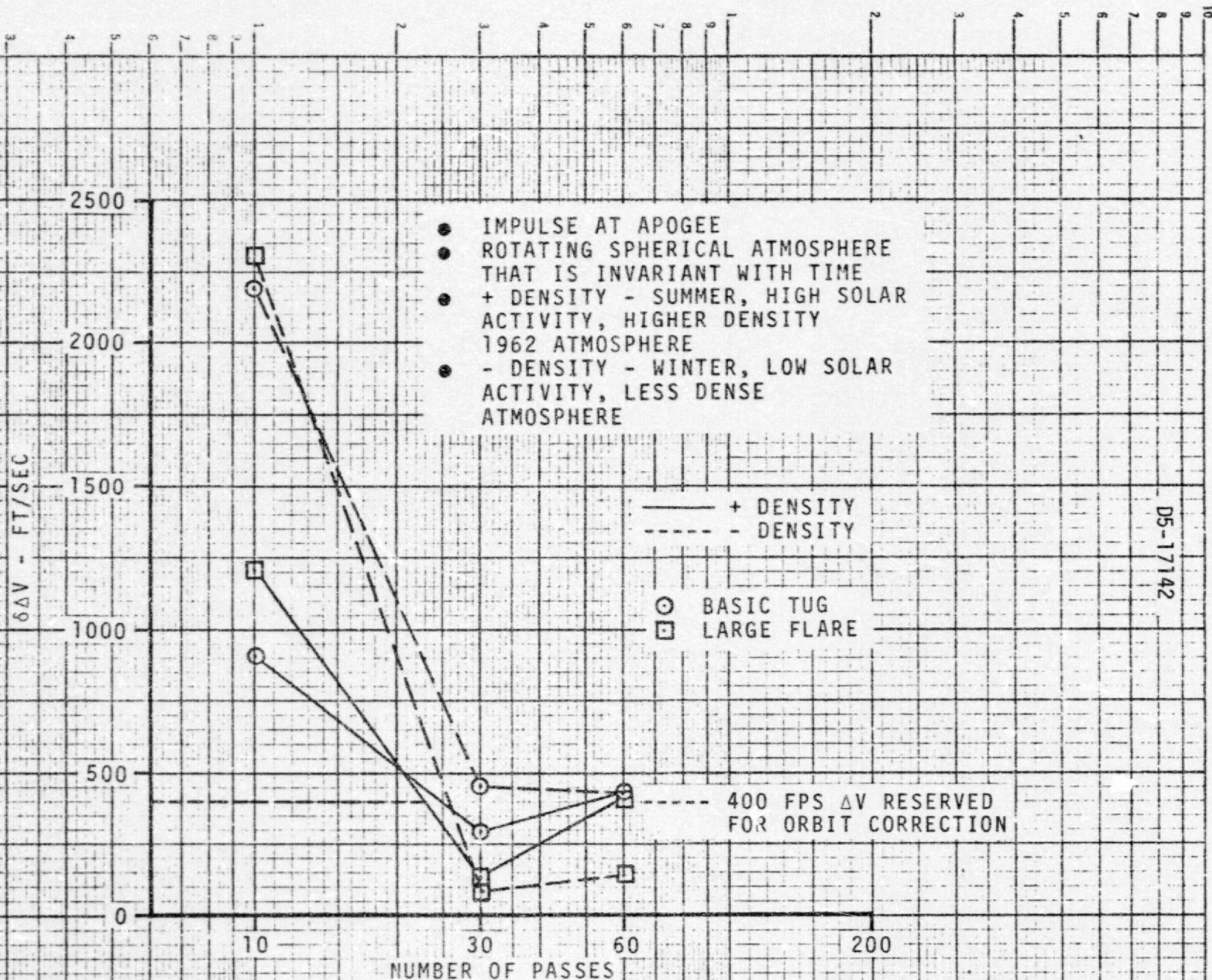
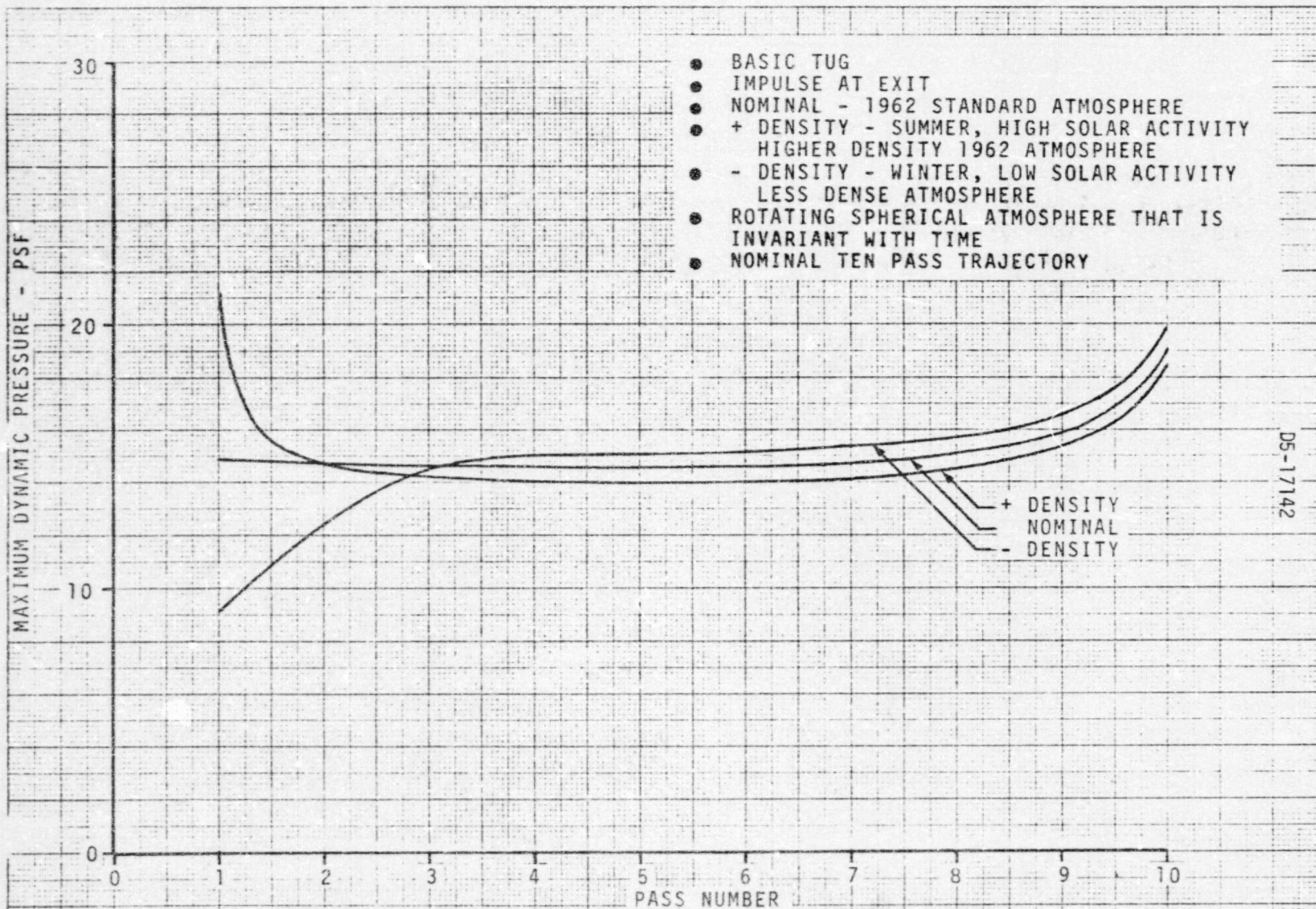


FIGURE 4.3.4.1-10 SPACE TUG AEROBRAKING RETURN FROM SYNCHRONOUS ORBIT - INCREASE IN ΔV TO GO TO 270 N.M. FOR IMPULSE AT APOGEE

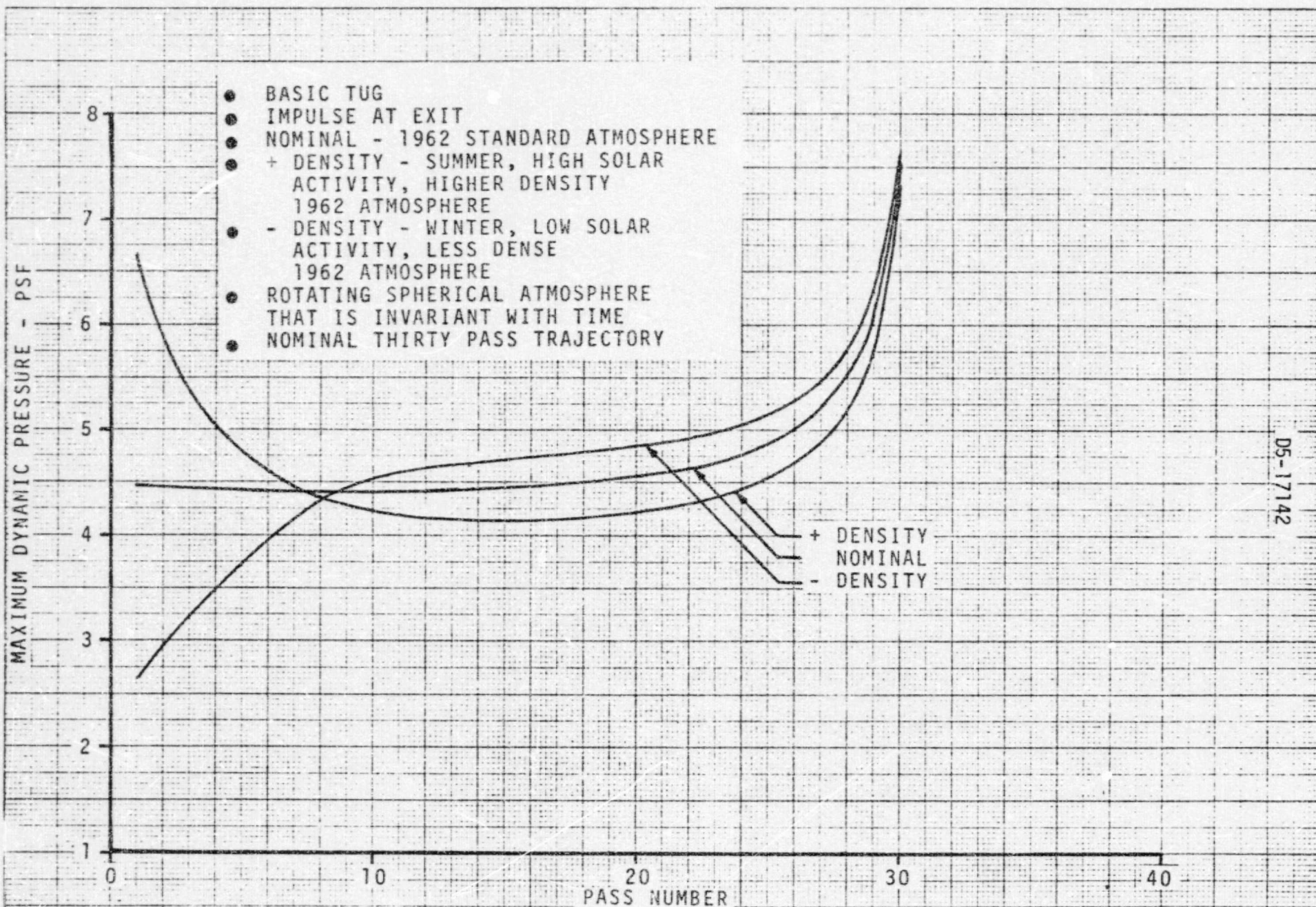
D5-17142

4-104



DS-17142

FIGURE 4.3.4.1-11 SPACE TUG AEROBRAKING RETURN FROM SYNCHRONOUS ORBIT - MAXIMUM DYNAMIC PRESSURE FOR BASIC TUG IMPULSE AT EXIT



DS-17142

FIGURE 4.3.4.1-12 SPACE TUG AEROBRAKING RETURN FROM SYNCHRONOUS ORBIT - MAXIMUM DYNAMIC PRESSURE FOR BASIC TUG IMPULSE AT EXIT

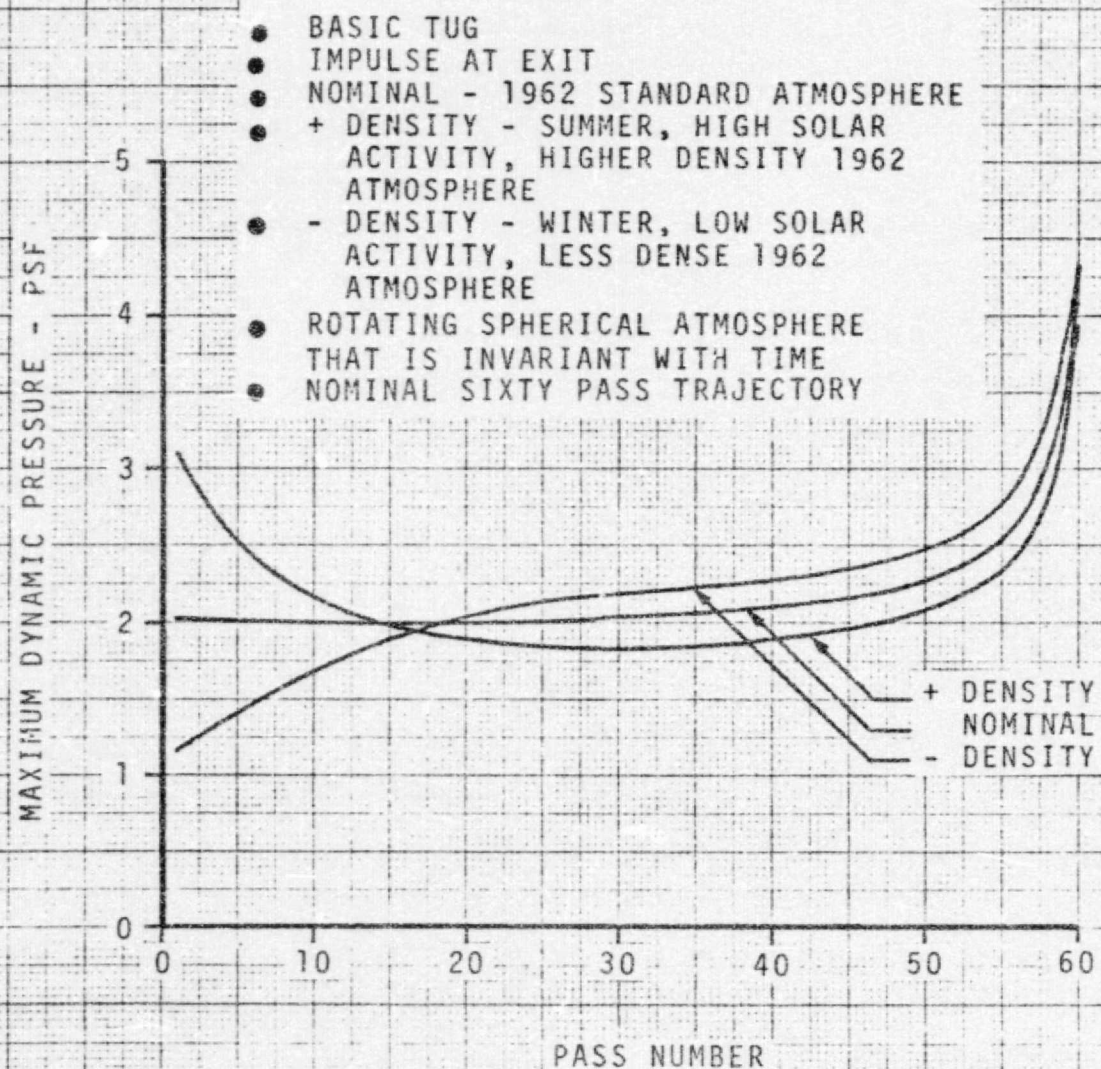
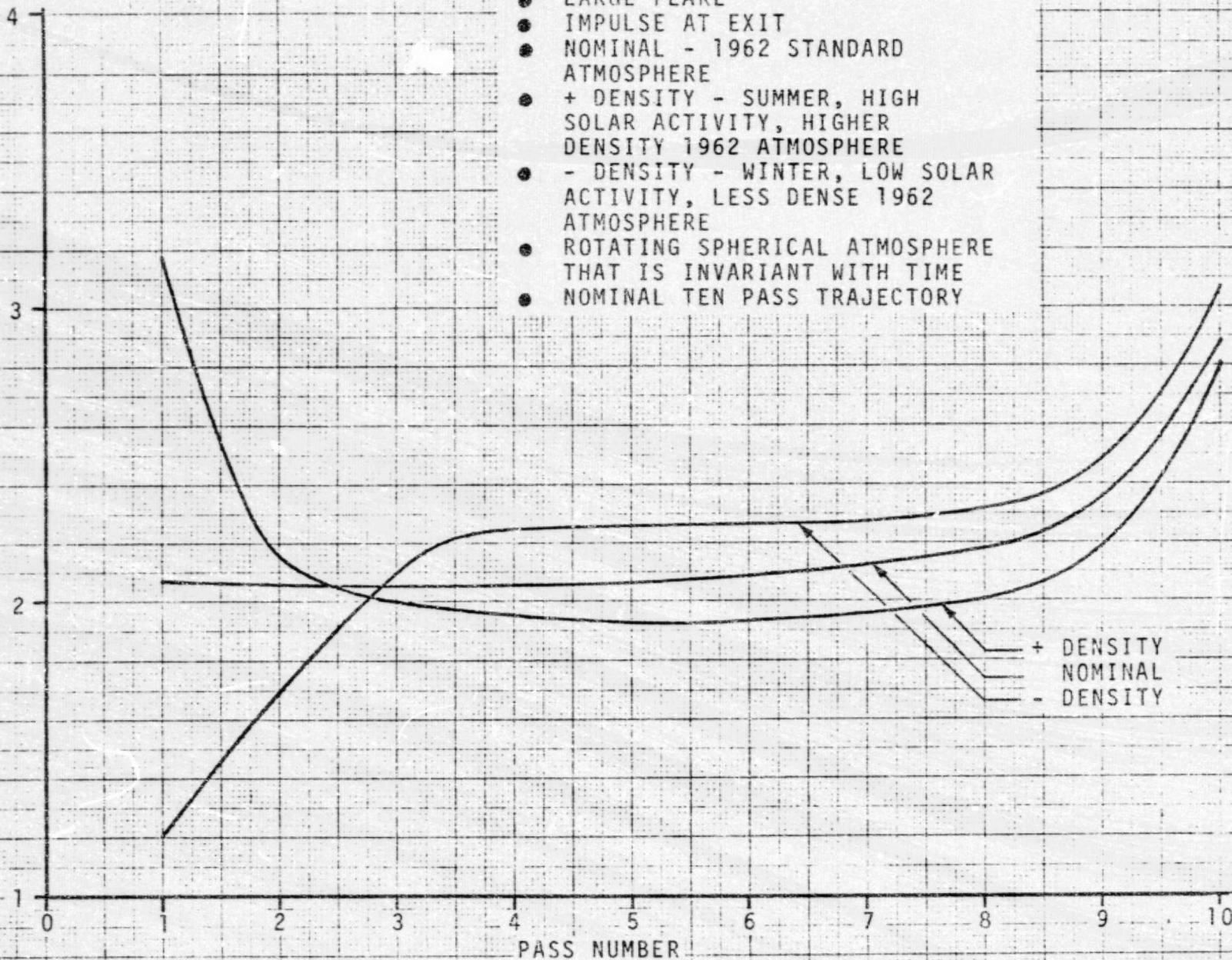


FIGURE 4.3.4.1-13 SPACE TUG AEROBRAKING RETURN FROM SYNCHRONOUS ORBIT - MAXIMUM DYNAMIC PRESSURE FOR BASIC TUG IMPULSE AT EXIT

MAXIMUM DYNAMIC PRESSURE ~ PSF

- LARGE FLARE
- IMPULSE AT EXIT
- NOMINAL - 1962 STANDARD ATMOSPHERE
- + DENSITY - SUMMER, HIGH SOLAR ACTIVITY, HIGHER DENSITY 1962 ATMOSPHERE
- - DENSITY - WINTER, LOW SOLAR ACTIVITY, LESS DENSE 1962 ATMOSPHERE
- ROTATING SPHERICAL ATMOSPHERE THAT IS INVARIANT WITH TIME
- NOMINAL TEN PASS TRAJECTORY



DS-17142

FIGURE 4.3.4.1-14 SPACE TUG AEROBRAKING RETURN FROM SYNCHRONOUS ORBIT -
MAXIMUM DYNAMIC PRESSURE FOR LARGE FLARE TUG IMPULSE AT EXIT

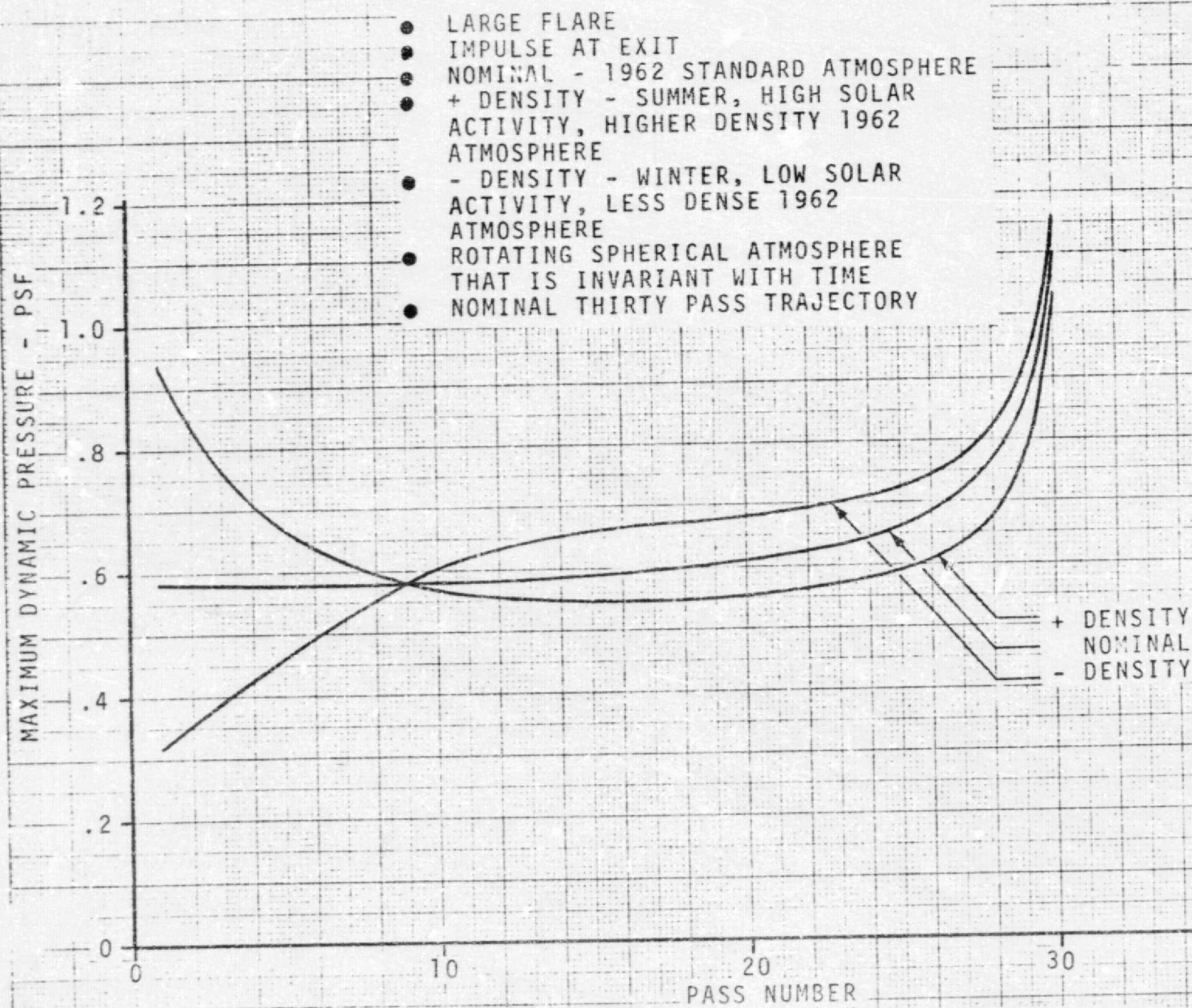


FIGURE 4.3.4.1-15 SPACE TUG AEROBRAKING RETURN FROM SYNCHRONOUS ORBIT - MAXIMUM DYNAMIC PRESSURE FOR LARGE FLARE TUG IMPULSE AT EXIT

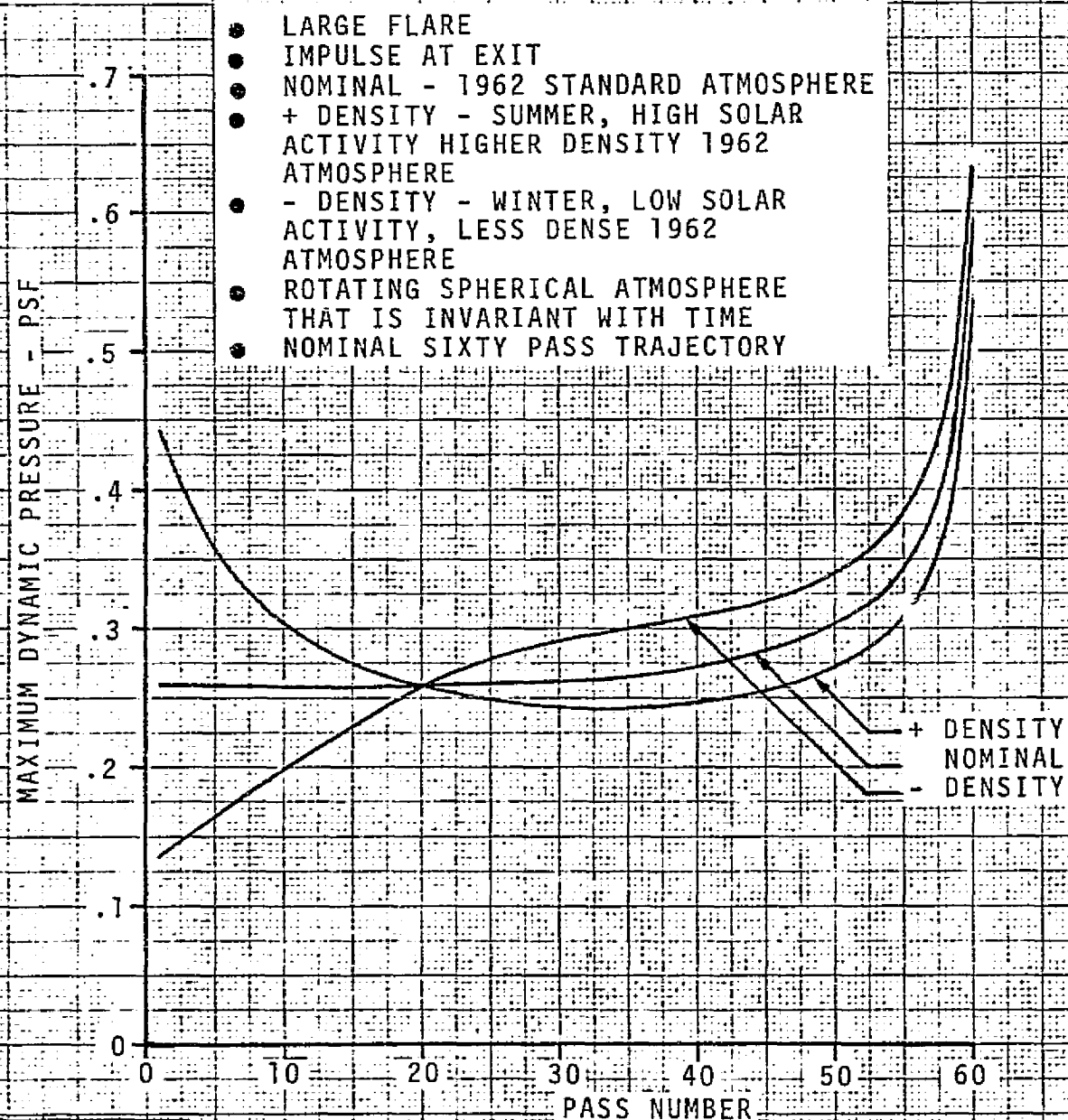


FIGURE 4.3.4.1-16. SPACE TUG AEROBRAKING RETURN FROM SYNCHRONOUS ORBIT - MAXIMUM DYNAMIC PRESSURE FOR LARGE FLARE TUG IMPULSE AT EXIT

4-111

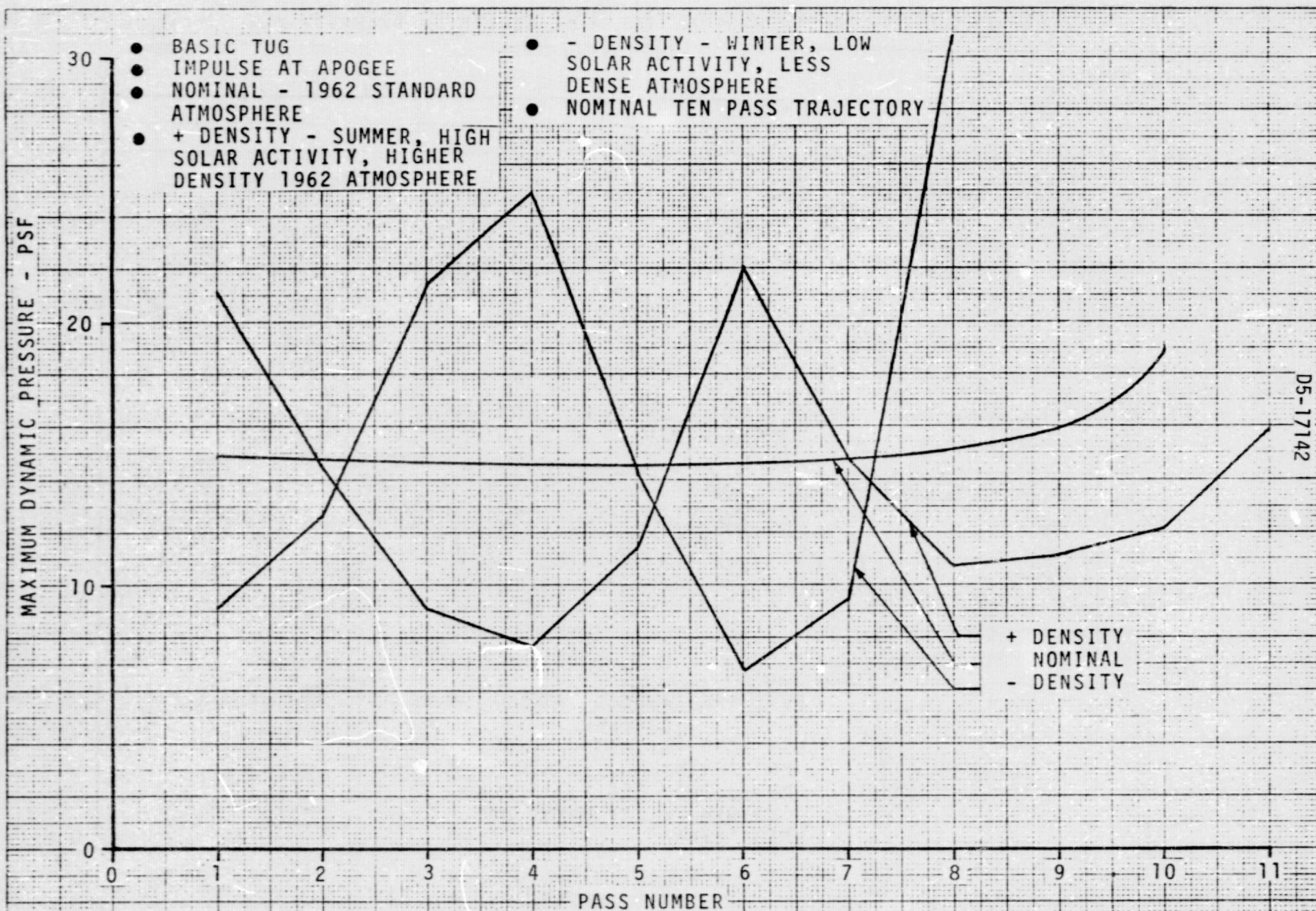


FIGURE 4.3.4.1-17. SPACE TUG AEROBRAKING RETURN FROM SYNCHRONOUS ORBIT - MAXIMUM DYNAMIC PRESSURE FOR BASIC TUG IMPULSE AT APOGEE

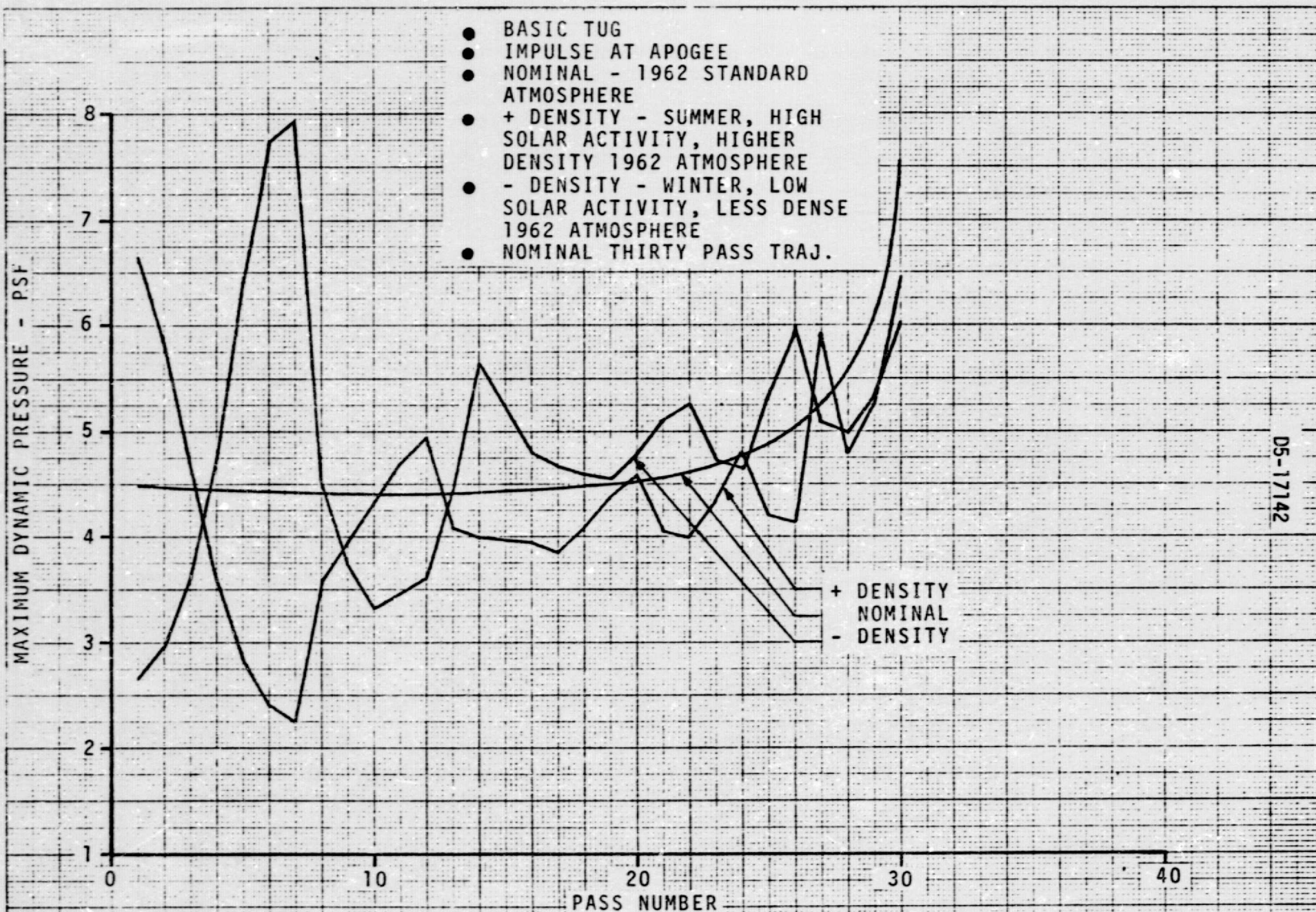


FIGURE 4.3.4.1-18 SPACE TUG AEROBRAKING RETURN FROM SYNCHRONOUS ORBIT - MAXIMUM DYNAMIC PRESSURE FOR BASIC TUG IMPULSE AT APOGEE

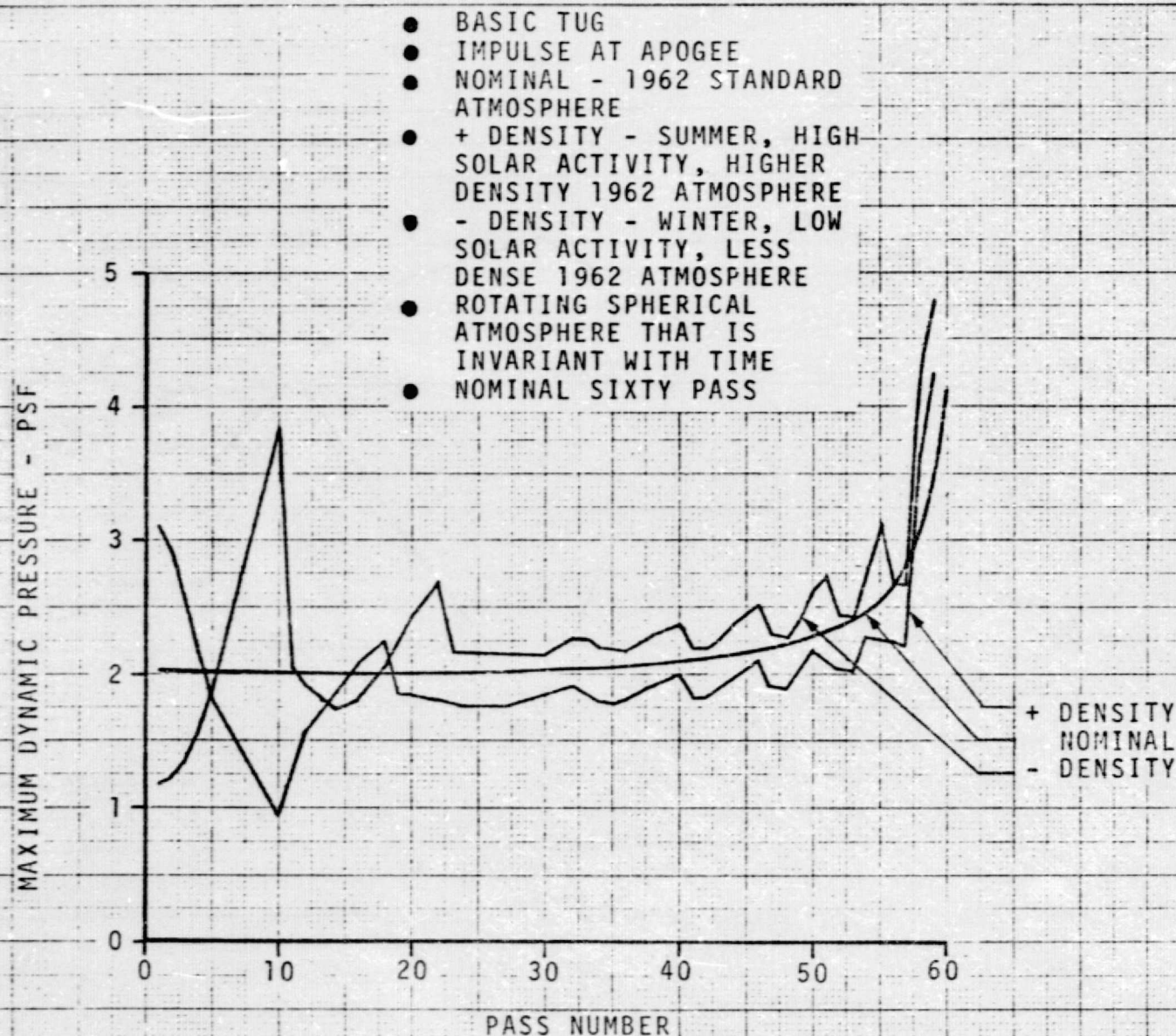


FIGURE 4.3.4.1-19 SPACE TUG AEROBRAKING RETURN FROM SYNCHRONOUS ORBIT -
 MAXIMUM DYNAMIC PRESSURE FOR BASIC TUG IMPULSE AT APOGEE

DS-17142

4-113

- LARGE FLARE
- IMPULSE AT APOGEE
- NOMINAL - 1962 STANDARD ATMOSPHERE
- + DENSITY - SUMMER, HIGH SOLAR ACTIVITY, HIGHER DENSITY 1962 ATMOSPHERE
- - DENSITY - WINTER, LOW SOLAR ACTIVITY, LESS DENSE 1962 ATMOSPHERE
- NOMINAL TEN PASS

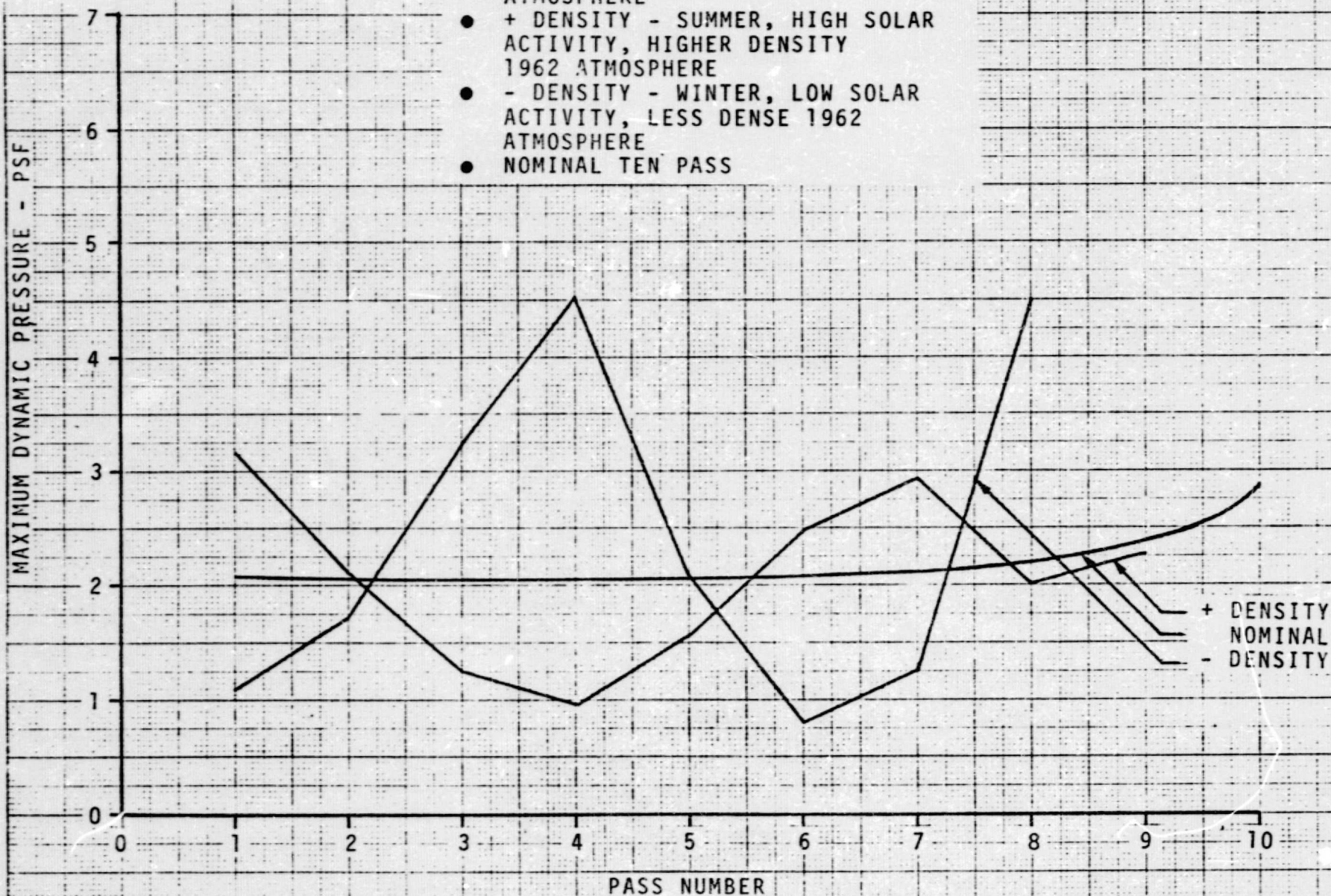
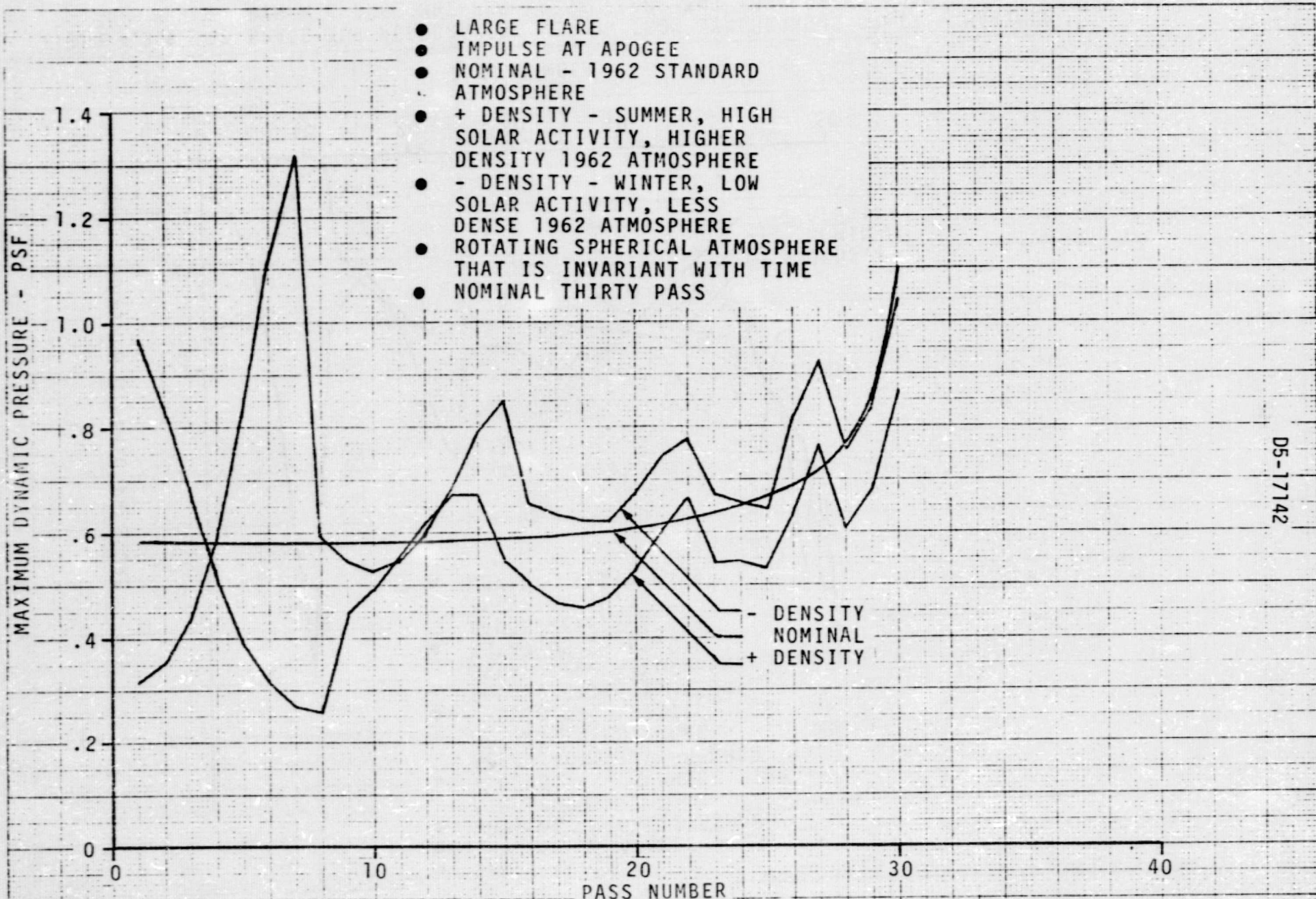


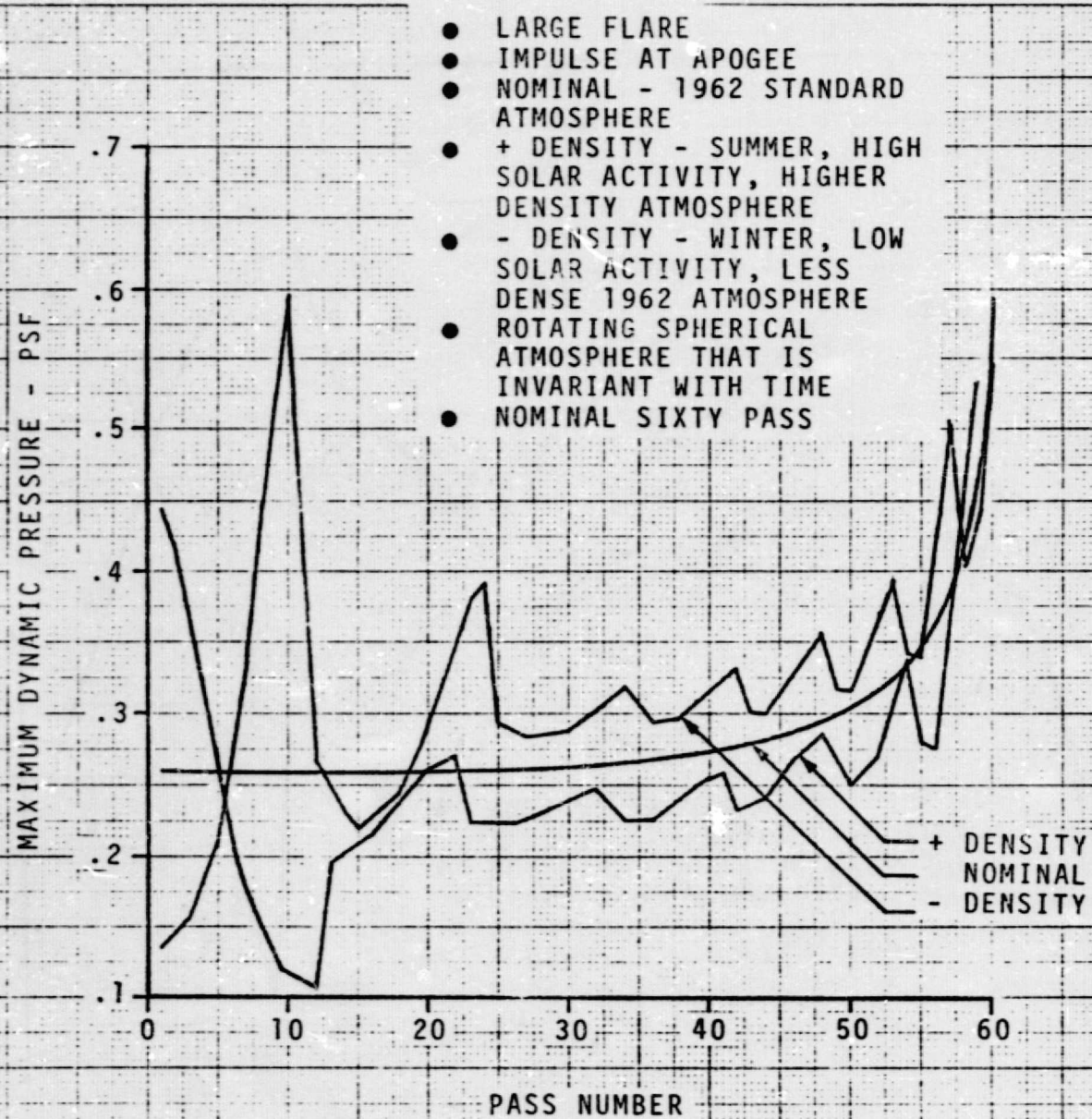
FIGURE 4.3.4.1-20 SPACE TUG AEROBRAKING RETURN FROM SYNCHRONOUS ORBIT - MAXIMUM DYNAMIC PRESSURE FOR LARGE FLARE IMPULSE AT APOGEE

4-115



DS-17142

FIGURE 4.3.4.1-21 SPACE TUG AEROBRAKING RETURN FROM SYNCHRONOUS ORBIT - MAXIMUM DYNAMIC PRESSURE FOR LARGE FLARE IMPULSE AT APOGEE



05-17142

FIGURE 4.3.4.1-22 SPACE TUG AEROBRACING RETURN FROM SYNCHRONOUS ORBIT - MAXIMUM DYNAMIC PRESSURE FOR LARGE FLARE TUG IMPULSE AT APOGEE

4.3.4.2 Dispersed Atmosphere Effects on Inertial Velocity

Prior Figure 4.3.4.1-3 illustrated the mission duration range that could result from atmospheric dispersions. The high density atmosphere can significantly shorten the mission duration. Similarly, the low density atmosphere can significantly increase the mission duration. The mission duration is a direct function of the velocity (kinetic energy) decrease on each pass. This subsection discusses the impact of atmospheric perturbations on the first pass inertial velocities. The first pass inertial velocity is independent of the targeting techniques discussed in Subsection 4.3.4.1 above and is a determining factor for the maximum equilibrium temperatures experienced (Section 4.5).

As discussed in Subsection 4.3.3 above, the orbit's maximum inertial velocity is attained at some time prior to perigee because of the atmospheric braking. Figure 4.3.4.2-1 shows the trends of the elapsed time between the orbit's maximum inertial velocity point and the perigee for the first pass of the mission. The greater velocity (kinetic energy) loss per pass for the shorter duration missions is reflected in the relatively long elapsed time periods for the 5 and 10 pass missions. The longer duration missions, because of the higher perigee altitudes and less velocity loss per pass, have shorter elapsed times. The elapsed time is significantly lower for the low density atmosphere because of the smaller decelerations experienced.

Figure 4.3.4.2-2 shows the sensitivity of the basic (no flare) configuration's first pass inertial velocities to atmospheric effects. The first pass maximum inertial velocity is nearly insensitive to mission duration and/or atmosphere. This relatively constant velocity is the result of the nearly identical elliptical free space trajectories flown from geosynchronous orbit to the first atmospheric entry. The first pass perigee inertial velocity is sensitive to the atmospheric state. For a 5 pass mission, the perturbed atmosphere changes the first pass perigee velocity by 200 ft/sec from that of the standard atmosphere. This first pass perigee velocity change is less for longer duration missions. The impact of these relatively small perigee velocity changes is reflected in significantly longer or shorter mission durations as seen in prior Figure 4.3.4.1-3.

Figure 4.3.4.2-3 shows similar data for the 60° flare configuration. This configuration has the same trends noted in Figure 4.3.4.2-2 for the no flare configuration.

The difference between the first pass maximum and perigee velocities shown in Figures 4.3.4.2-2 and -3 is only an indicator of the velocity loss during the pass. There will be some losses prior to attaining the maximum inertial velocity. Between perigee and exit at 600,000 feet altitude, another major velocity loss occurs. Also, in a free space environment, the perigee inertial velocity is the maximum inertial velocity along the trajectory and would be somewhat greater than that shown as the maximum in either figure. This additional factor represents another velocity loss not shown in the figures.

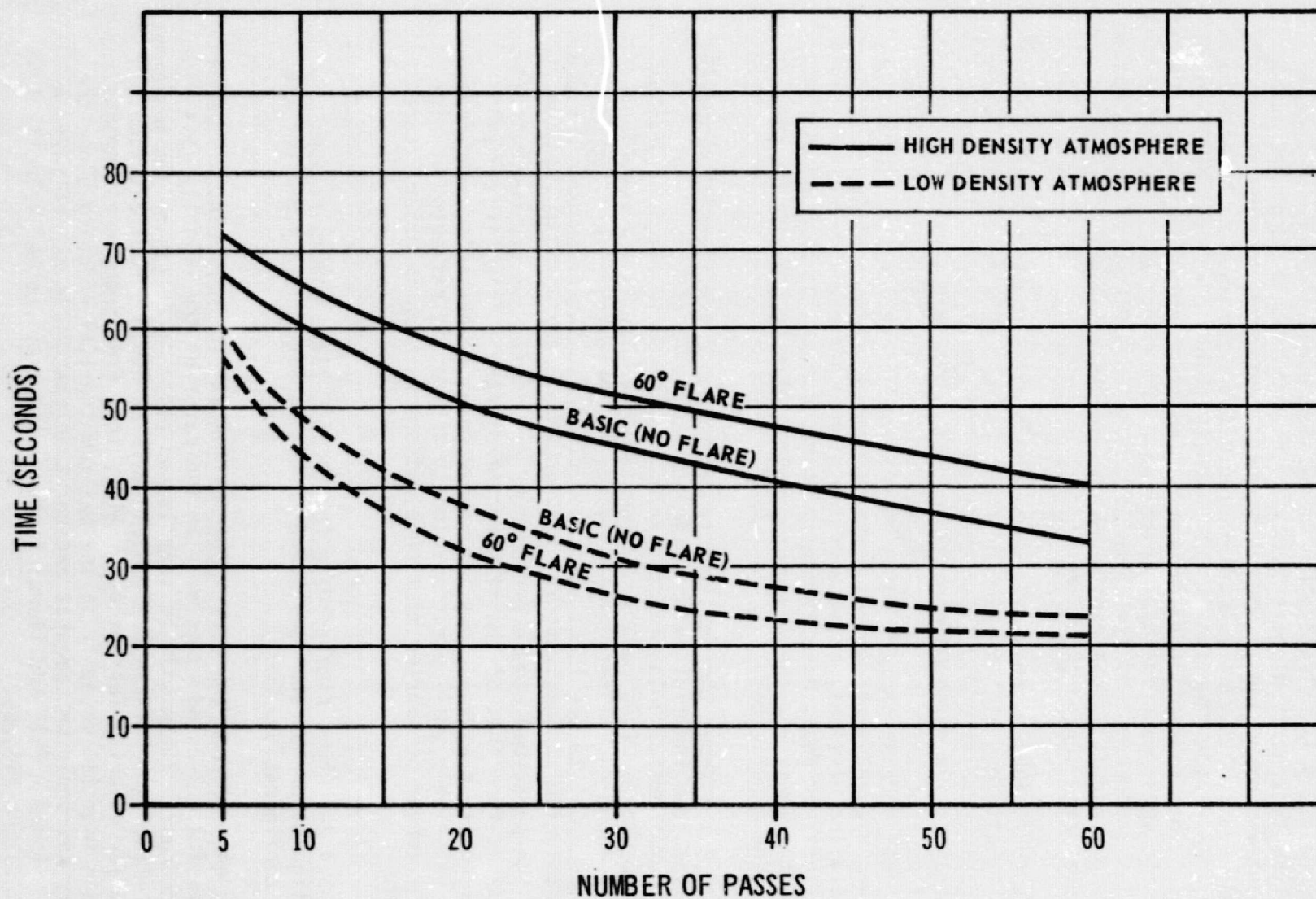


FIGURE 4.3.4.2-1. ELAPSED TIME TREND FROM MAXIMUM INERTIAL VELOCITY TO PERIGEE (FIRST PASS)

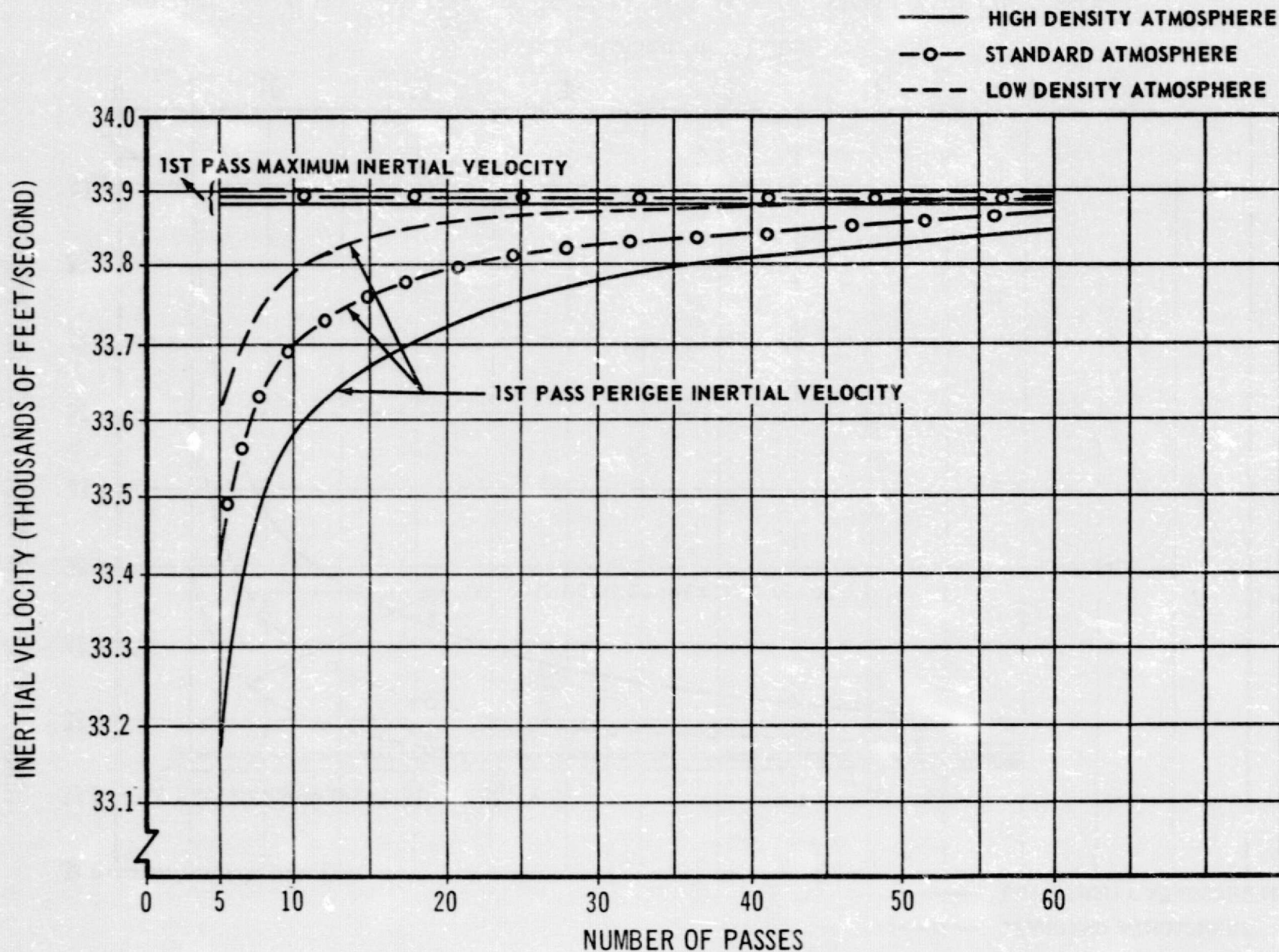


FIGURE 4.3.4.2-2. SENSITIVITY OF FIRST PASS INERTIAL VELOCITY TO ATMOSPHERE
BASIC TUG (NO FLARE) CONFIGURATION

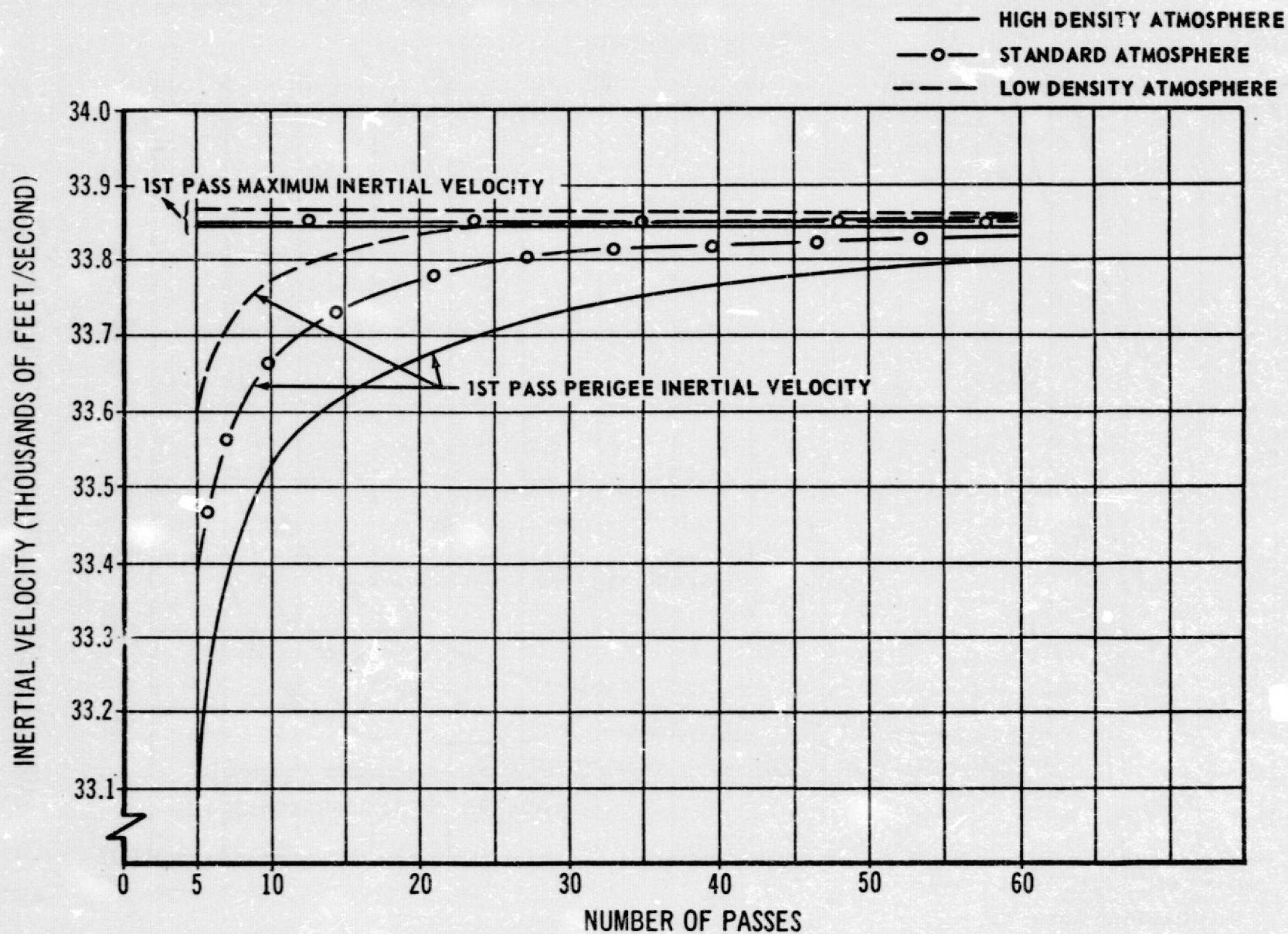


FIGURE 4.3.4.2-3. SENSITIVITY OF FIRST PASS INERTIAL VELOCITY TO ATMOSPHERE
(60° FLARE CONFIGURATION)

4.3.5 Lunar, Solar, and Earth Harmonics Perturbations

Because of the large amount of computer time necessary to simulate the effects on the trajectories of earth gravity harmonics and Lunar and Solar Perturbations, these effects are not included in the trajectory data presented in previous sections. However, to assess the impact of these perturbations on the study results, some trajectories were simulated including these perturbations. The most pronounced effect of the perturbation is a reduction in the semi-major axis of the orbit so that by the time the Tug reaches the entry altitude of 600,000 feet the perigee altitude is less than what it would have been in the absence of the perturbing accelerations. This is illustrated in Figure 4.3.5.0-1 where the behavior of perigee altitude with true anomaly in the presence of gravity perturbations is compared with the non-perturbed behavior. In the absence of gravity perturbations the perigee altitude is constant until the atmosphere is encountered at a true anomaly of about -15° . Drag perturbations then decrease perigee altitude slightly and there is no further effect on perigee altitude for the remainder of the orbit. Gravity perturbations cause perigee altitude to decrease on the descending part of the orbit until at perigee the perigee altitude is almost 10,000 feet lower than the non-perturbed perigee. The cumulative result of this effect on the first and succeeding passes is that the nominal 10 pass trajectory re-enters and impacts the earth on the sixth pass. This means that the initial perigee altitude (as calculated at apogee and ignoring the non-spherical gravity perturbations) required to produce apogee decay to 270 NM in a given number of passes must be greater than that shown in the previous data (Figure 4.3.3.0-1). This effect is shown in Figure 4.3.5.0-2 for five, ten, and thirty pass basic Tug trajectories.

Obviously then, gravity perturbations must be considered in the targeting scheme analysis. It is felt, however, that the principal of the targeting schemes discussed in Section 4.3.4 can still be used in the presence of gravity perturbations with the major effect being modification of the targeting parameters, apogee altitude and decay rate, to include the perturbation effects.

Impact of gravity perturbations on heating and loads environment encountered during the time in the atmosphere can be assessed by comparing the altitude time histories of the perturbed and spherical earth trajectories. This comparison is made in Figure 4.3.5.0-3 for the portion of the trajectory below 600,000 feet on the first pass of a 10 pass trajectory. Similarity of the curves indicates that heating, loads, and control data presented in the following sections will not be changed significantly by perturbation effects on the trajectory.

Other perturbation effects on the orbital parameters, while not significant from a performance standpoint, will be operationally important. For example, the line of nodes will regress about 8° for the thirty pass trajectory while the argument of perigee advances 9° and the orbit plane inclination decreases half a degree. These perturbations must therefore be considered for proper timing and phasing of the mission.

BASIC TUG

- ORBIT INCLINATION = 28°
- 1962 STANDARD ATMOSPHERE
- ENTRY ALTITUDE - 600,000 FT
- $J_2 = 1082.7 \times 10^{-6}$
- $J_3 = -2.56 \times 10^{-6}$
- $J_4 = -1.58 \times 10^{-6}$
- DATE: 1 JULY, 1976

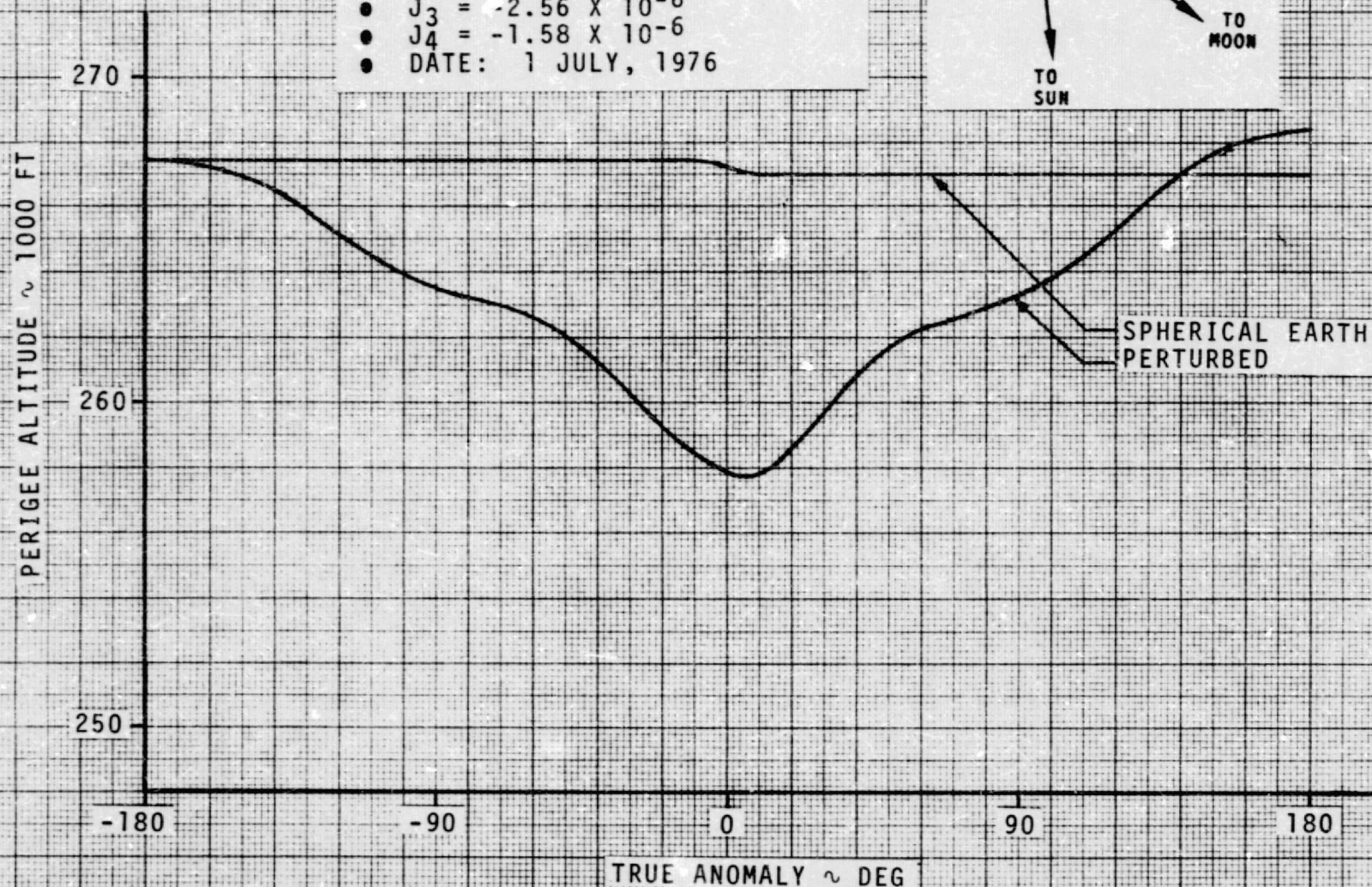
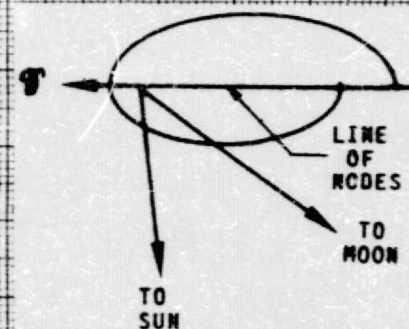


FIGURE 4.3.5.0-1 SPACE TUG AEROBRAKING RETURN FROM SYNCHRONOUS ORBIT -
VACUUM PERIGEE HISTORY OF THE FIRST PASS OF A TEN PASS TRAJECTORY

05-17142

4-122

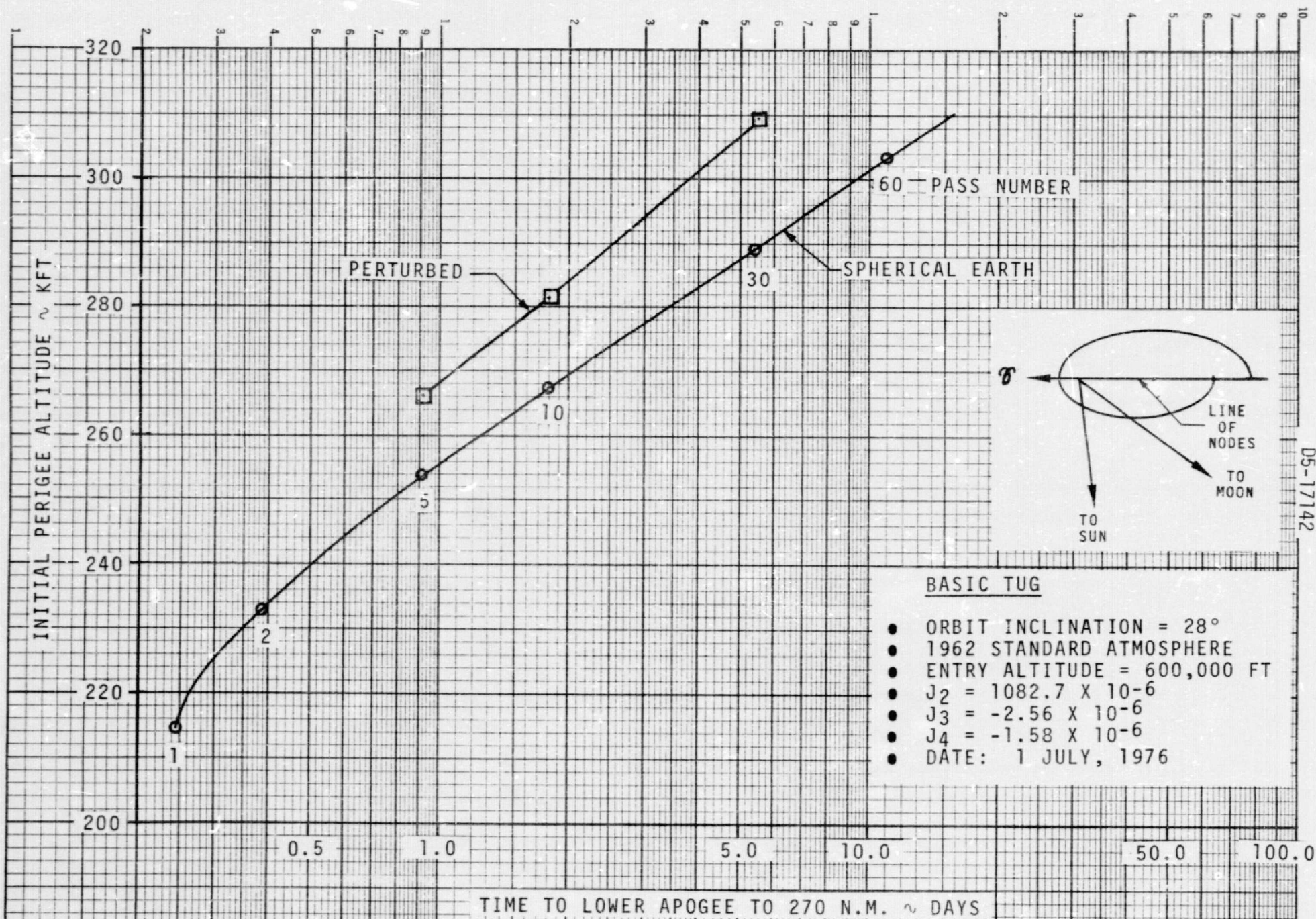


FIGURE 4.3.5.0-2 SPACE TUG AEROBRAKING RETURN FROM SYNCHRONOUS ORBIT - TIME TO LOWER APOGEE TO 270 N.M.

BASIC TUG

- ORBIT INCLINATION = 28°
- 1962 STANDARD ATMOSPHERE
- ENTRY ALTITUDE = 600,000 FT
- $J_2 = 1082.7 \times 10^{-6}$
- $J_3 = -2.56 \times 10^{-6}$
- $J_4 = -1.58 \times 10^{-6}$
- DATE: 1 JULY, 1976

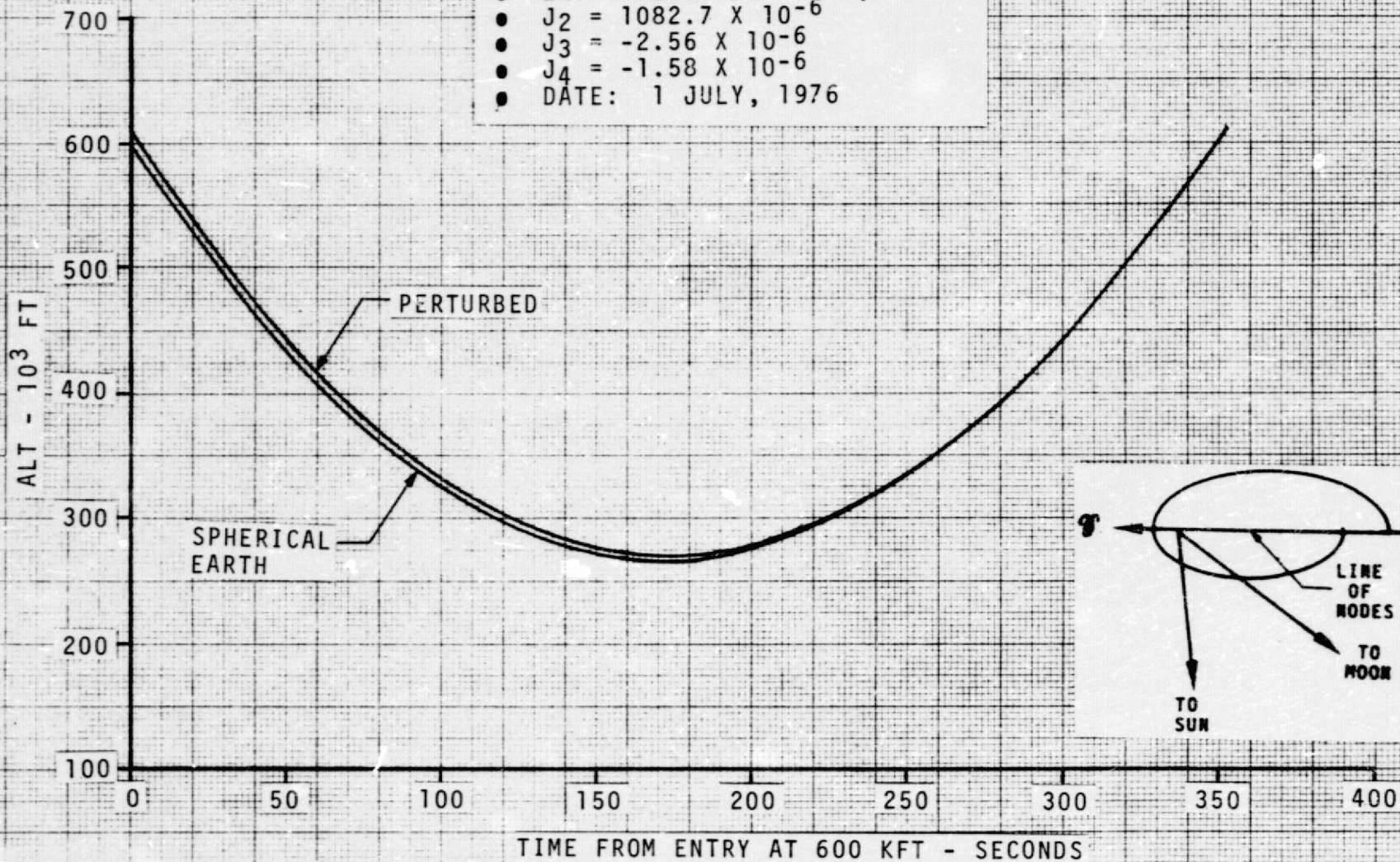


FIGURE 4.3.5.0-3 SPACE TUG AEROBRAKING RETURN FROM SYNCHRONOUS ORBIT - ALTITUDE TIME HISTORY OF THE FIRST PASS OF A TEN PASS TRAJECTORY

4.4 CONTROL ANALYSIS

Attitude control in pitch, yaw, and roll is accomplished with the RCS system both outside and within the atmosphere. The RCS system also performs trajectory corrections, vehicle maneuvers, and docking. This analysis gives propellant consumption needed for the RCS system to maintain attitude control. Trade studies on critical parameters are also given.

4.4.1 Control Methods

The total RCS propellant consumption required for attitude control is calculated by summing the consumption due to each mode of operation. The modes of operation are:

1. Attitude control by limit-cycling between system firing limits (deadband) in pitch, yaw, and roll.
2. Aero-moment control within the atmosphere for the unstable basic Tug.
3. Aero-moment control within the atmosphere for the stable flared tugs.
4. Directional control, keeping the tug aligned along the velocity vector throughout the period of orbit change.

The fuel consumption calculations are as follows:

1. Consumption due to limit-cycling is given by the following equation:

$$\text{PROPELLANT WEIGHT} = \frac{57.3 T_T \ell N^2 F^2 T^2}{4 I D I_{SP}}$$

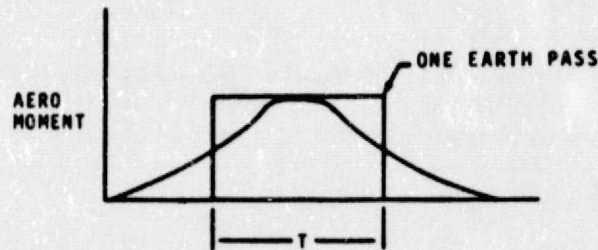
where:

T_T	=	total time of entry
ℓ	=	radius of vehicle
N	=	number of thrusters
F	=	thrust of one engine
T	=	minimum firing time
I	=	vehicle inertia
I_{SP}	=	specific impulse
D	=	system deadband in degrees

2. Consumption due to an unstable aero-moment:

The aero-moment is calculated by approximating Q and time of aero influence as follows:

4.4.1 (Continued)



Aero-moment at 1° angle of attack: $AM = C_N QA (X_{CP} - X_{CG}) (1/57.3)$

where: A = vehicle crosssectional area
 Q = dynamic pressure
 X_{CP} = center of pressure
 X_{CG} = center of gravity
 $C_{N\alpha}$ = coefficient of aerodynamic normal force

CONTROL MOMENT (CM) = $N\delta F$

2. To determine the burn time necessary to control the tug during maximum aero-moment, assume worse-case aero influence as shown in Figure 4.4.1.0-1

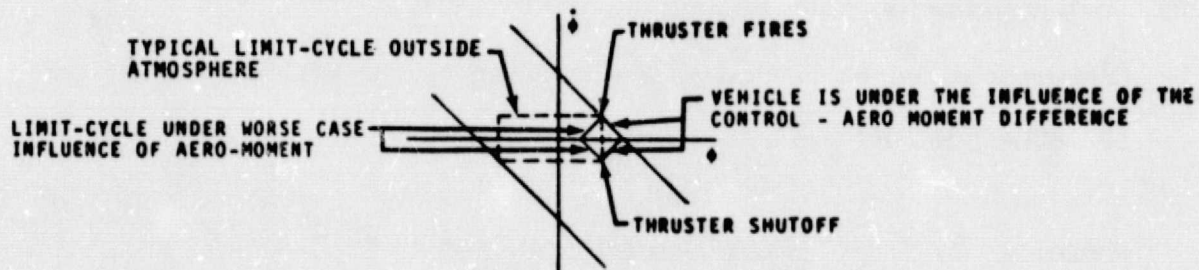


Figure 4.4.1.0-1 RCS System Limit-Cycle Under Worse Case Influence of Aero-Moment

From Figure 4.4.1.0-1, after thruster burn ends, the only moment acting on vehicle is the aero-moment. To reignite thrusters, δ must become equal the negative of the value at thruster shutoff.

Ratio of thruster burn time (T_{BT}) to cycle-time (T_{cycle}).

$$\frac{T_{BT}}{T_{CYCLE}} = \frac{AM}{CM} = \frac{\text{average aero-moment for all passes}}{\text{control moment of RCS}}$$

Engine burn time due to aero-moment = [time under aero-moment influence for all passes] $\left[\frac{T_{BT}}{T_{CYCLE}} \right]$

4.4.1 (Continued)

$$\text{Total propellant} = \frac{[\text{engine burn time due to aero-moment}] \quad [\text{NF}]}{\overline{I_{SP}}}$$

3. Consumption due to a stable aero-moment:

As the space tug enters the atmosphere, the aero-moment increases causing the tug oscillations to converge and increase in frequency as shown in Figure 4.4.1.0-2. After passing max q, the Tug oscillations diverge. The minimum ϕ for the tug oscillations at max q depends on the aero-moment and on the deadband when the tug enters the atmosphere, or the initial conditions at start of the damping influence (increasing aero-moment). From Figure 4.4.1.0-2, ϕ decreases to $\pm .25$ degree at max q. For a 5 degree deadband, ϕ decreases to approximately ± 1.0 degree. A configuration less stable than the 60 degree flare tug will give a larger value of ϕ_{MINIMUM} .

The amount of the deadband in or outside the atmosphere depends on guidance requirements. However, if small oscillations are desired at max q a small deadband such as 1.0° , 0.5° , 0.3° , etc., could be set by the RCS system prior to entering the atmosphere.

4. Consumption required for directional control

The tug must rotate 360° for each earth pass to maintain an alignment with the velocity vector. A conservative propellant consumption of 0.3 lbs/pass is used for this operation. This will give a rotation rate of 0.5 degrees/second, which is an order of magnitude greater than the maximum rate for the 60th pass of a 60 pass trajectory.

4.4.2 Atmospheric Effects on Controls

There are two types of attitude control within the atmosphere for the different tug configurations:

1. For the aerodynamically unstable basic tug, the RCS system must control the aero-moment causing greater fuel consumption than for a stable tug. The fuel consumption is dependent on the system deadband, since the aero-moment increases as the angle-of-attack increases. The analysis uses a $\pm 1.0^\circ$ deadband. Effects of using a 0.5° deadband are shown in Figure 4.4.2.0-1.
2. For the aerodynamically stable flared tugs, the aero-moment will cause the tug pitch/yaw attitude deadbands to converge. This reduces RCS fuel consumption by up to 550 pounds from the basic tug configuration.

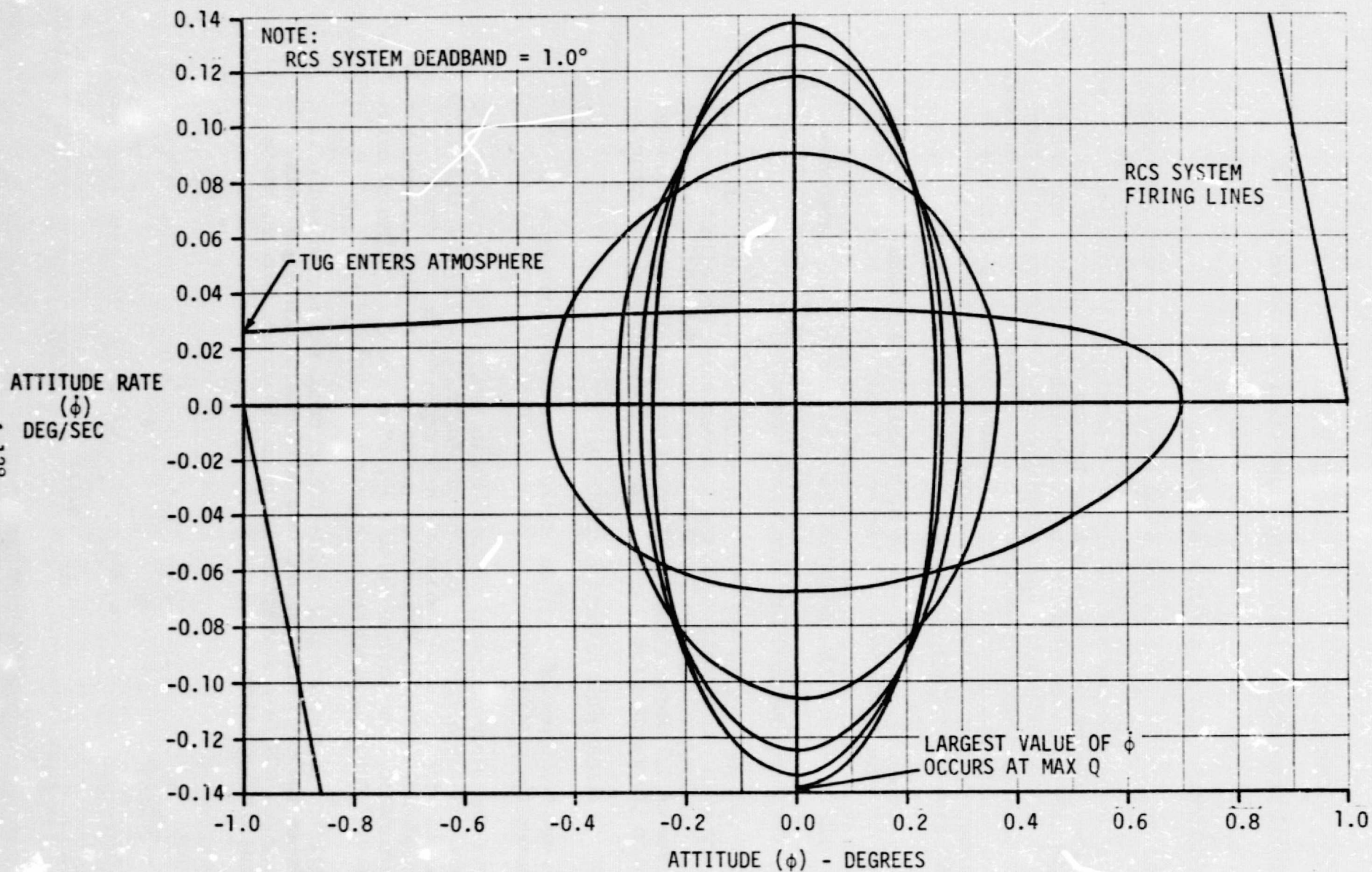


FIGURE 4.4.1.0-2 PHASE PLANE TRAJECTORY SHOWING TUG OSCILLATIONS FROM TIME TUG ENTERS ATMOSPHERE UNTIL IT PASSES MAX Q

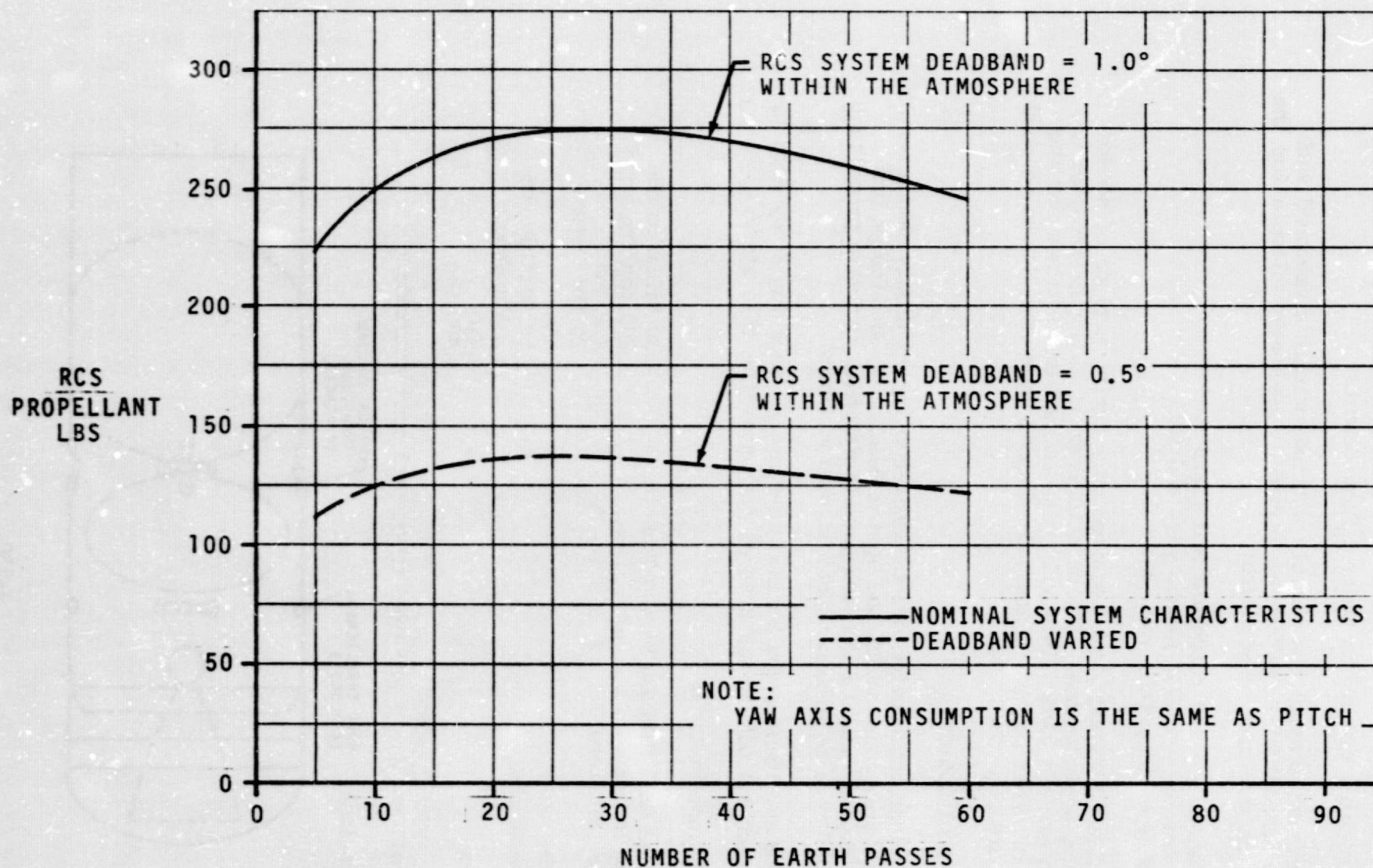


FIGURE 4.4.2.0-1 PITCH AXIS PROPELLANT CONSUMPTION DUE TO THE AERO MOMENT FOR THE BASIC TUG

4.4.3 Astrionics Effects on Control Requirements

The RCS system must control the vehicle attitude within a deadband such that guidance sensors will operate accurately. Deadbands suitable for the operation of the guidance sensors are:

1. Horizon sensor - $\pm 10^\circ$ pitch/yaw and ± 2.5 roll
2. Landmark tracker - $\pm 3.75^\circ$ pitch, yaw, and roll
3. Star Tracker - $\pm 5^\circ$ pitch, yaw, and roll

These, or smaller deadbands, are required only during periods of sensor operation. The analysis uses $\pm 5^\circ$ for pitch/yaw outside the atmosphere, where the sensors are used. This will give conservative values for the total change of orbit period, since a deadband larger than 5° can be used when sensors are not operating.

4.4.4 Control Options

The RCS propellant consumption due to limit-cycling is highly sensitive to minimum thruster pulse width and system deadband. An attempt has been made to choose values for these parameters which minimize propellant consumption and remains within practical design limits.

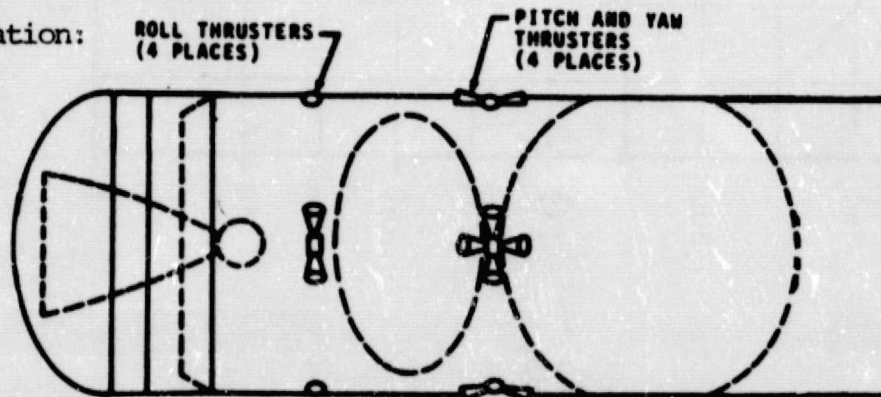
The RCS system as given in the Boeing Pre-Phase A Space Tug Study Report, (prior Reference 1.1.0.0-1) was used as the basis for this study.

RCS System Characteristics:

Pitch, Yaw, and Roll Minimum Firing Time	30 Milliseconds
Pitch and Yaw Thrust	200 Lbs/Engine
Pitch and Yaw Thrusters	4/Plane
Roll Thrust	20 Lbs/Engine
Roll Thrusters	8*
Pitch and Yaw Deadband	5° Outside the Atmosphere
Roll Deadband	2.5°
ISP	400 Sec

*Only four roll thrusters are used to control roll attitude.

RCS Configuration:



4.4.5 Results

Consumption values for the different modes of RCS operation, except for the rotational mode (0.3 lbs/pass), are given in Figures 4.4.2.0-1 and 4.4.5.0-1 through 4.4.5.0-3 for the basic and 60° flare Tugs. For pitch and yaw limit-cycle control only one set of curves are given for the basic and 60° flare Tugs. This is due to the vehicles having little difference in pitch and yaw moments of inertia and consequently little difference in consumption. Variations account for different values of system deadband and minimum pulse width. Propellant consumption values for the different Tug configurations are shown below. (Note that these requirements do not include that required for navigational error or atmospheric dispersions effects.)

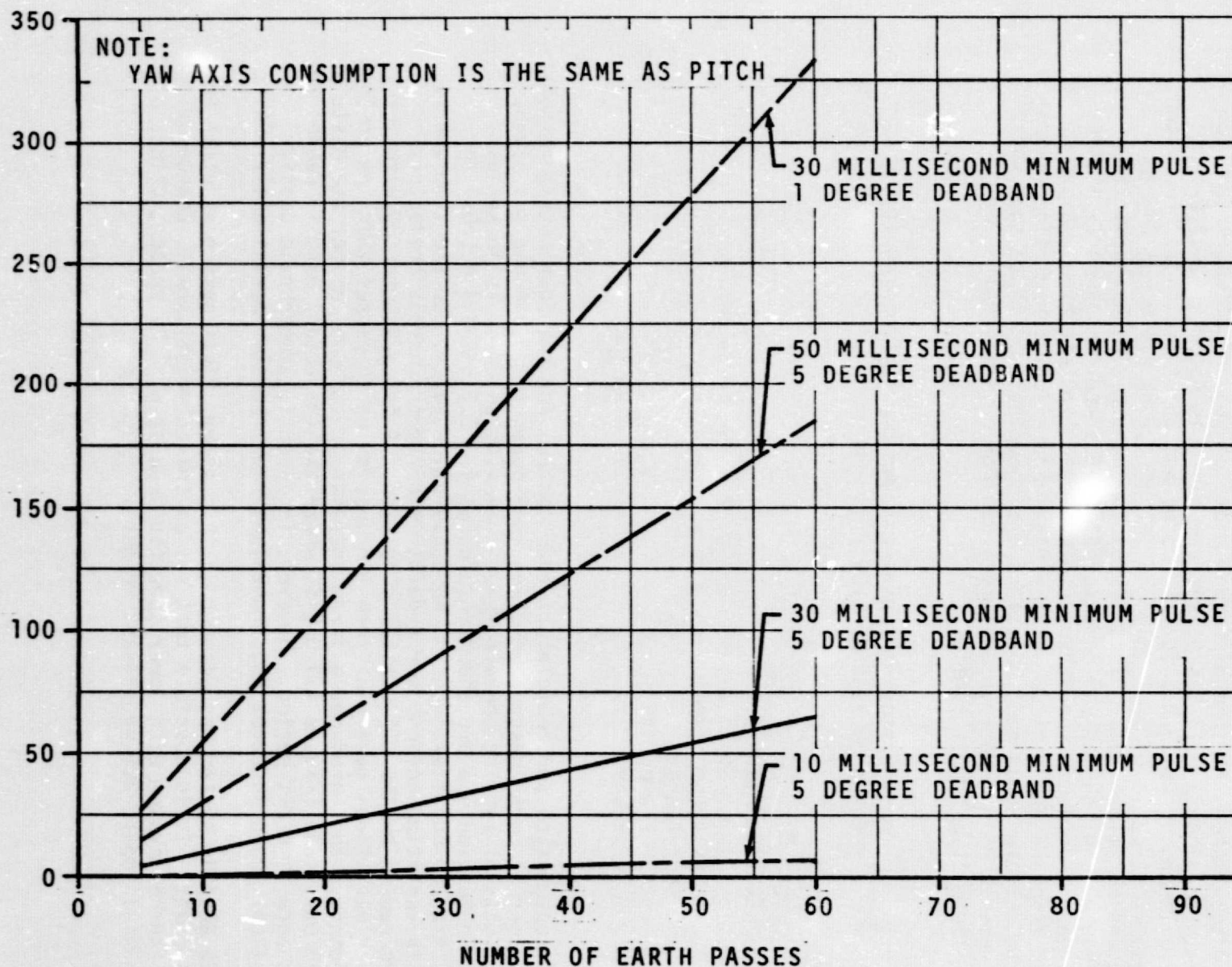
CONSUMPTION DIFFERENCES AMONG THE TUG CONFIGURATIONS
FOR A 30 PASS MISSION

TUG CONFIGURATION	CONSUMPTION (LBS)
Basic (no flare)	620.0
60° Flare	76.0
45° Flare	80.0
30° Flare	82.0

Total consumption for vehicle attitude control for the four configurations vs. number of earth passes are given in Figures 4.4.5.0-4 and 4.4.5.0-5. The effects of varying the atmospheric density based on trajectories given in Section 4.3 are shown in Figures 4.4.5.0-6 and 4.4.5.0-7 for the basic and 60° flare Tugs. The consumption values for the atmospheric density variation account for a delta velocity to correct trajectory errors caused by the off-nominal condition. A few trajectories with the density variations gave a different number of earth passes than the nominal trajectory. This produced a large increase in consumption for the basic Tug 10 pass case (Figure 4.4.5.0-5) where the trajectory gave 11 passes for the change of orbit period. However, in general, atmospheric density variations could increase RCS propellant requirements approximately 10%.

An RCS GO_2/GH_2 system was assumed in this study. This system is still in development. It is possible that system characteristics will change or that another system with lower specific impulse will be chosen, either of which will impact RCS propellant weights.

RCS
PROPELLANT
LBS



05-17142

FIGURE 4.4.5.0-1 PITCH AXIS PROPELLANT CONSUMPTION DUE TO LIMIT CYCLING FOR THE BASIC AND 60° FLARE TUGS.

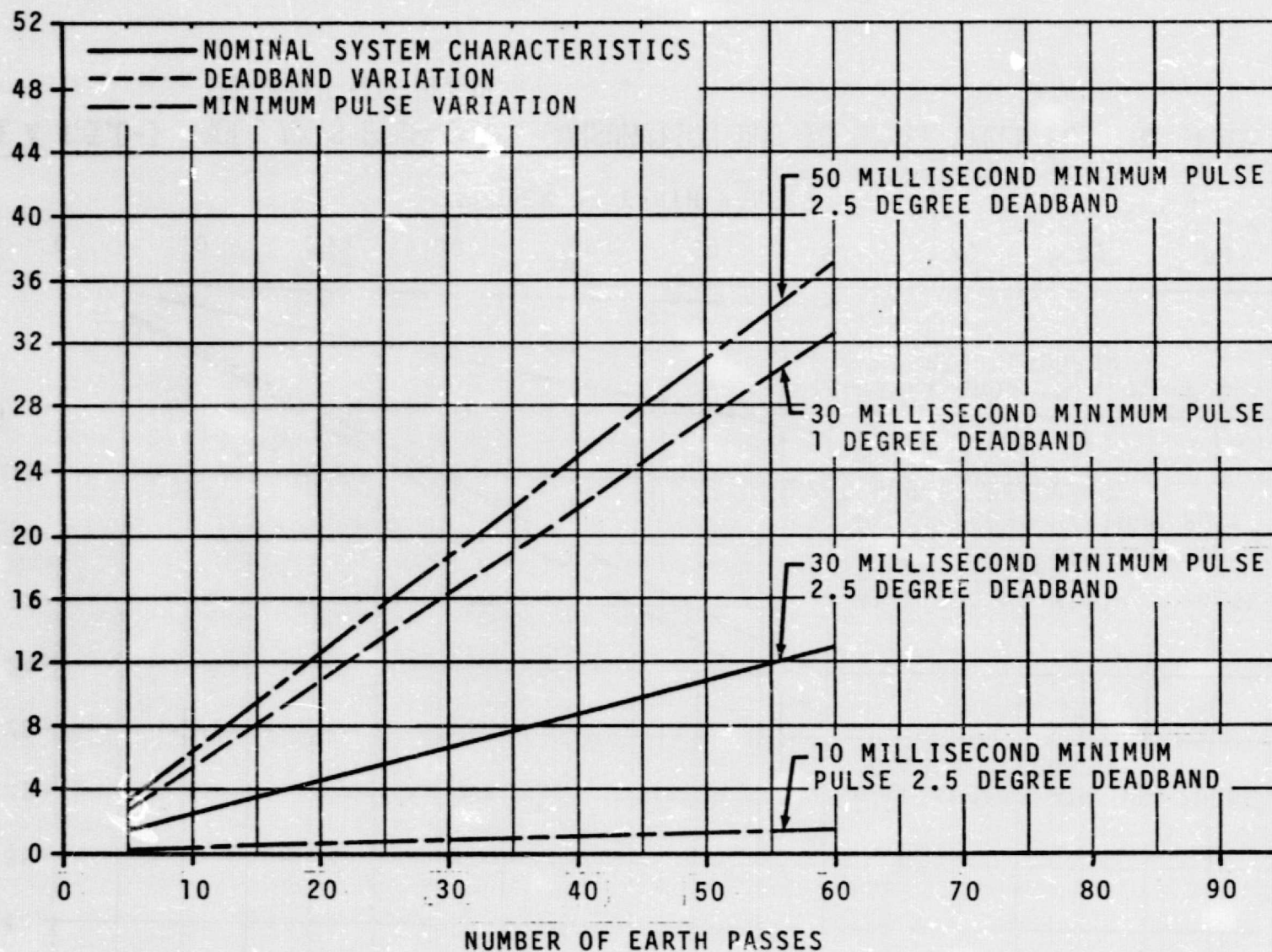
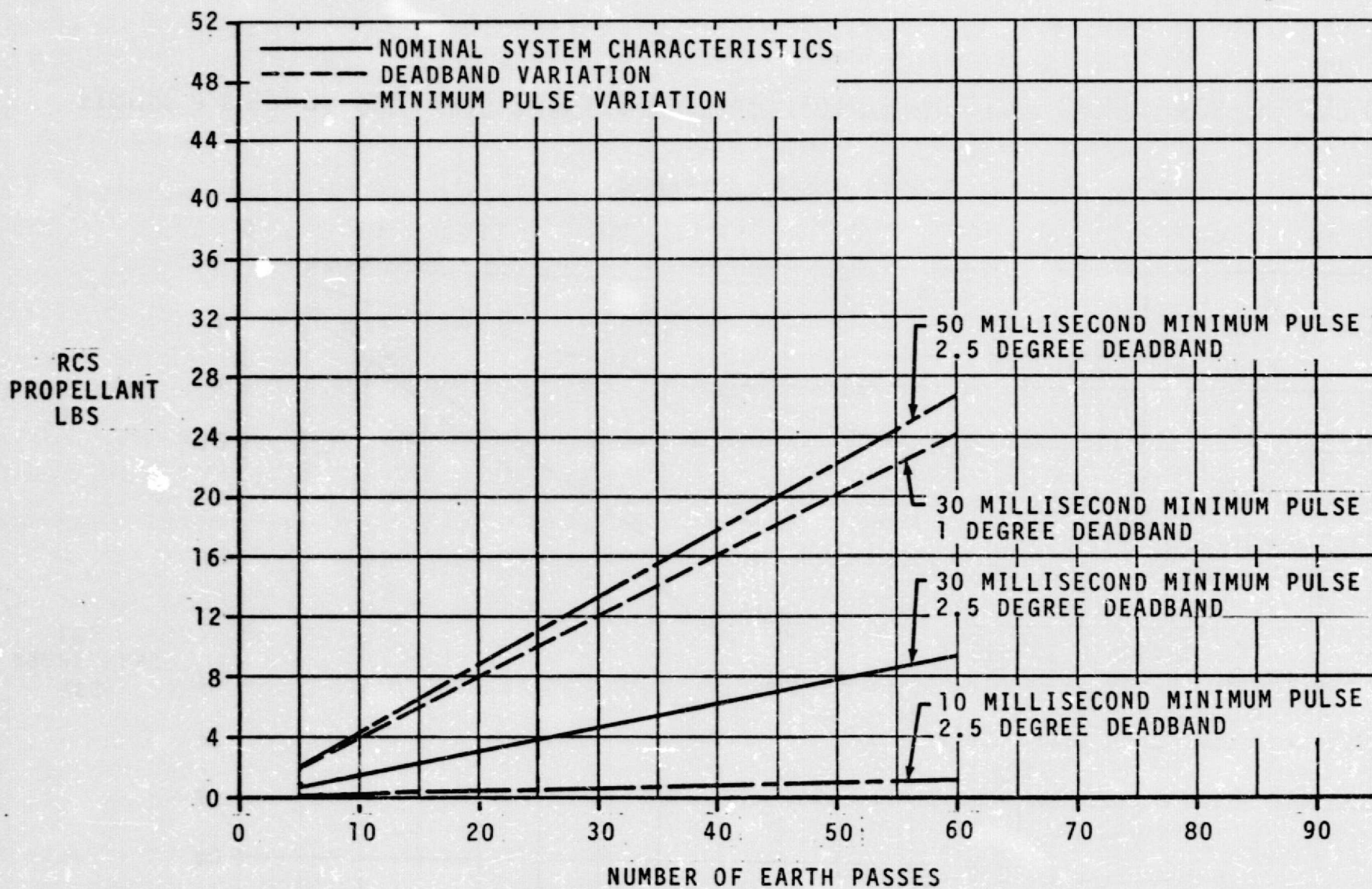


FIGURE 4.4.5.0-2 ROLL AXIS PROPELLANT CONSUMPTION DUE TO LIMIT CYCLING FOR THE BASIC TUG



05-17142

FIGURE 4.4.5.0-3 ROLL AXIS PROPELLANT CONSUMPTION DUE TO LIMIT CYCLE FOR THE SPACE TUG WITH 60° FLARE

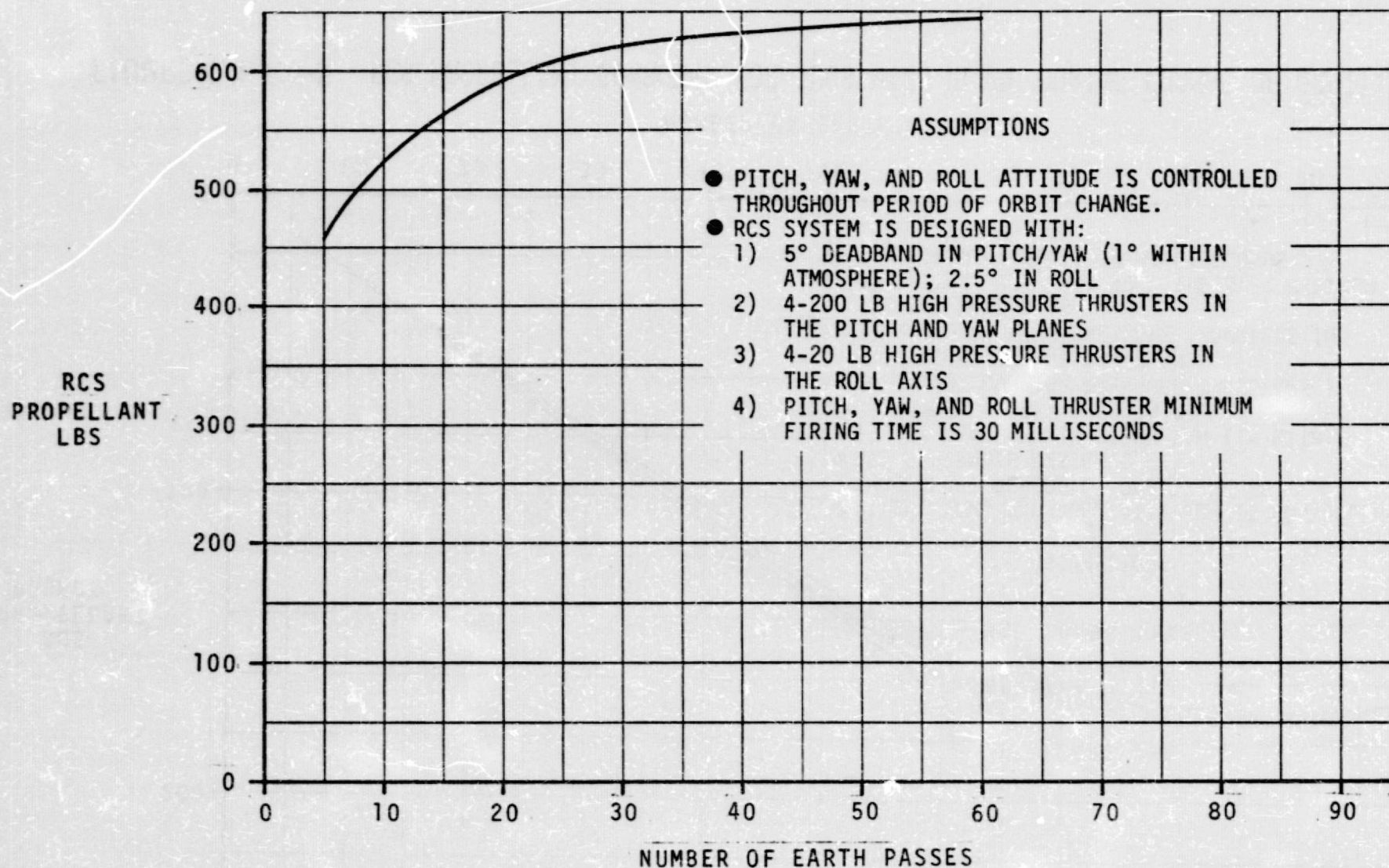


FIGURE 4.4.5.0-4 RCS PROPELLANT CONSUMED FOR THE BASIC TUG DURING CHANGE OF ORBIT PERIOD

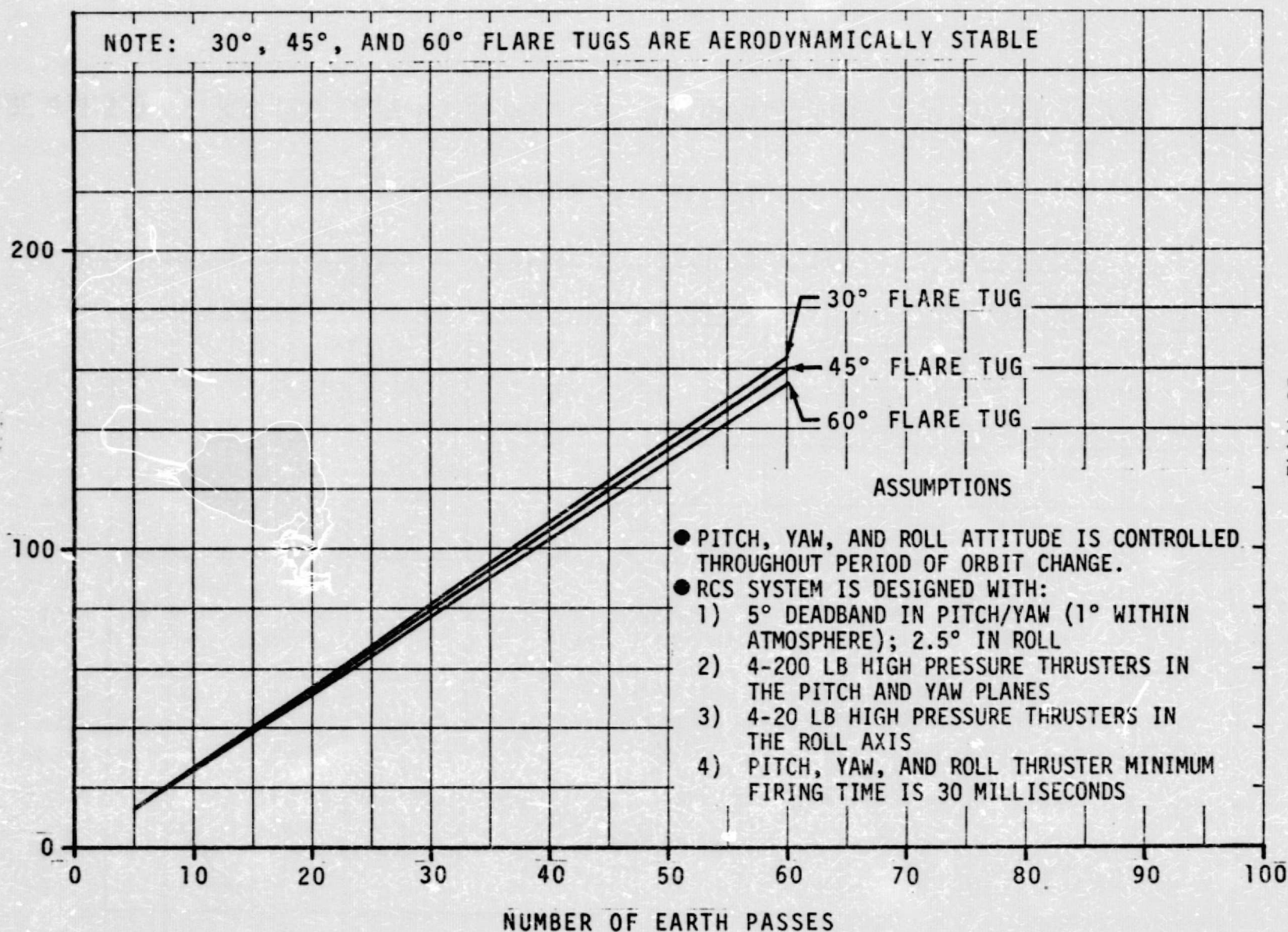
RCS
PROPELLANT
POUNDS

FIGURE 4.4.5.0-5 RCS PROPELLANT CONSUMED FOR TUGS WITH FLARE DURING CHANGE OF ORBIT PERIOD

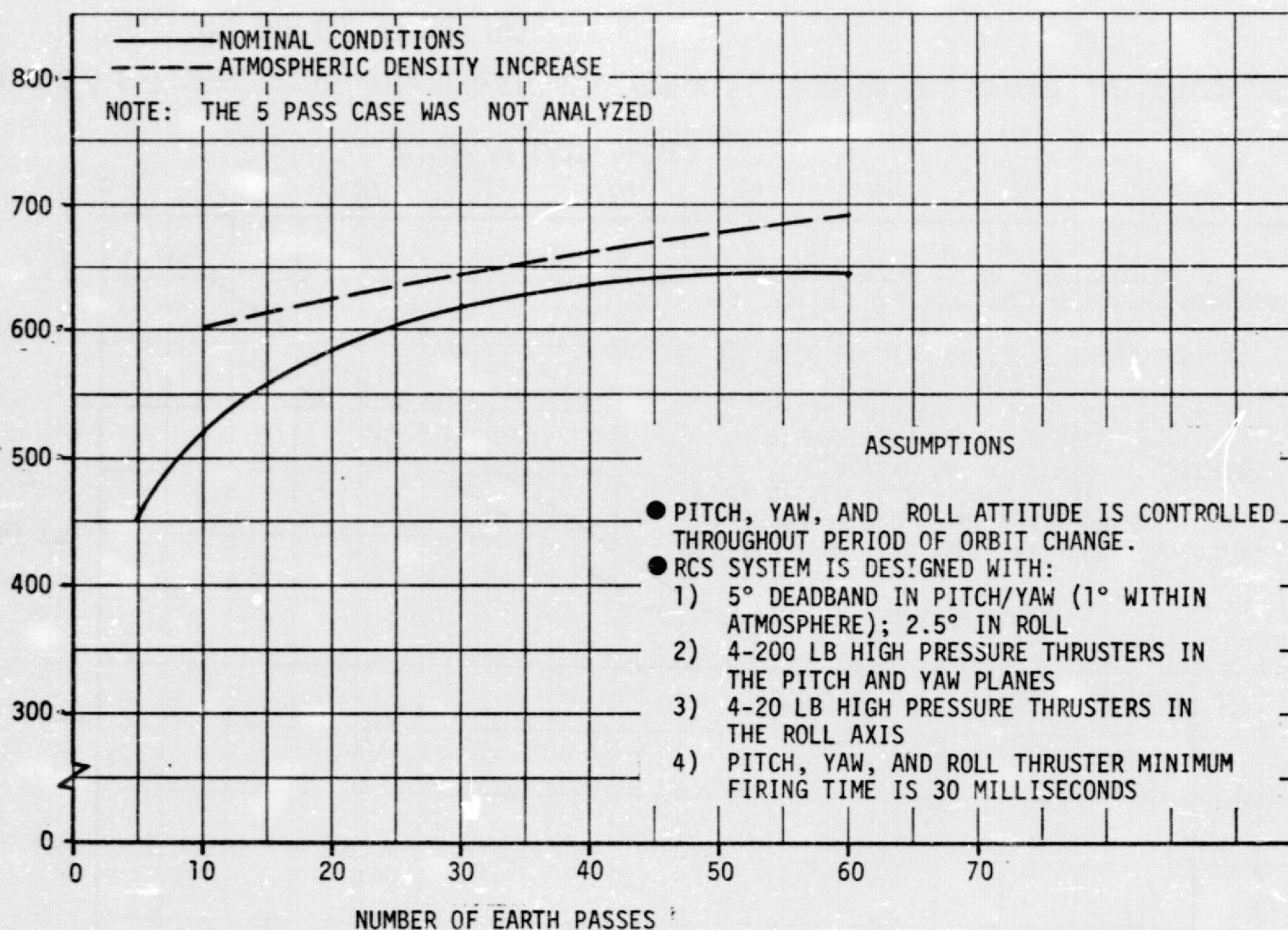


FIGURE 4.4.5.0-6 EFFECTS OF ATMOSPHERIC DENSITY VARIATION ON RCS PROPELLANT CONSUMPTION FOR THE BASIC TUG

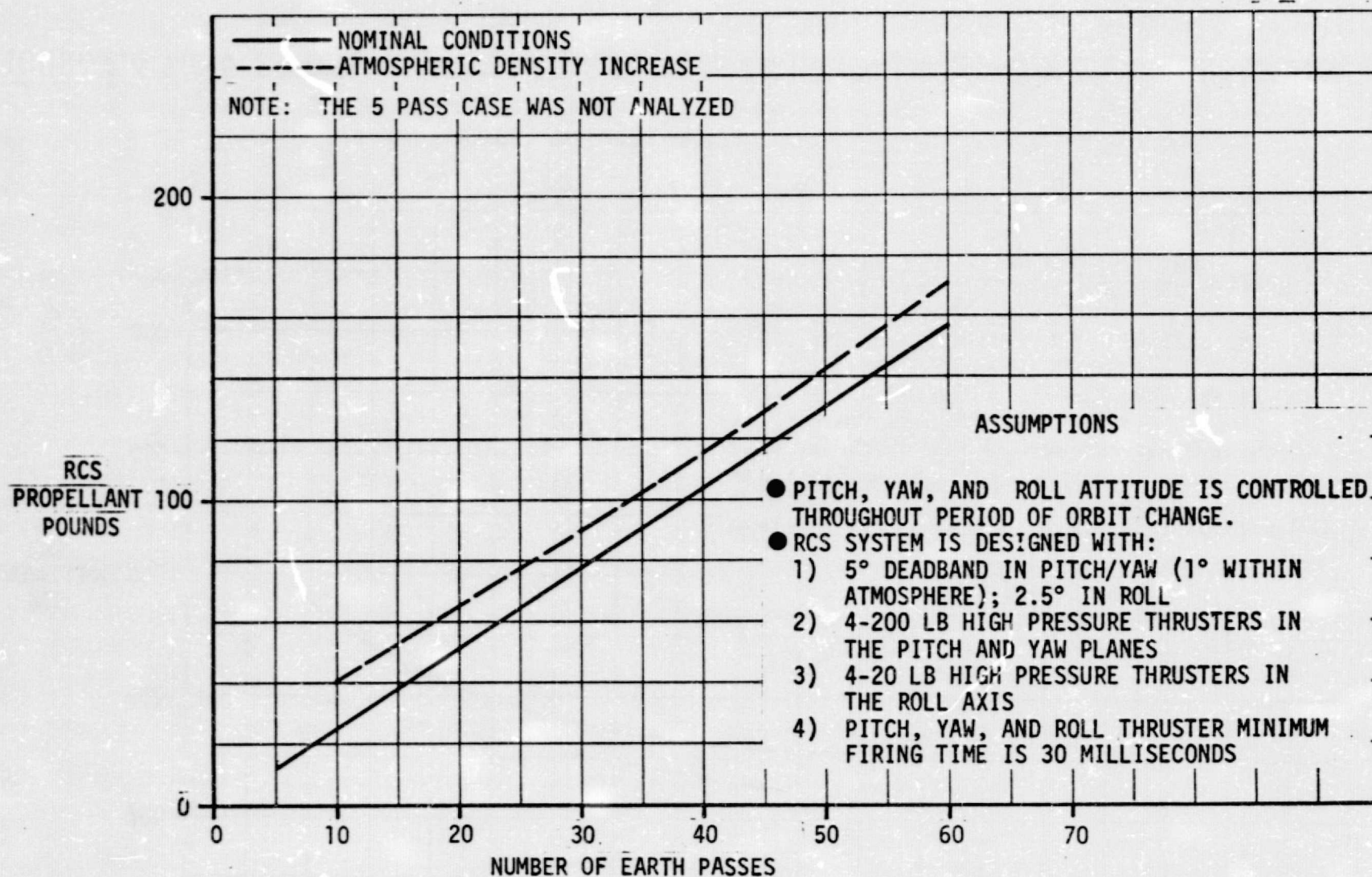


FIGURE 4.4.5.0-7 EFFECTS OF ATMOSPHERIC DENSITY VARIATION ON RCS PROPELLANT CONSUMPTION FOR THE 60° FLARE TUG

4.5 THERMAL ANALYSIS

A detailed thermal analysis of the Space Tug configuration during the aerobraking mode should encompass all areas which affect thermal design. The limitations imposed by the period of performance allowed for this study, however, made it necessary to restrict the thermal analysis to the determination of heating rates, equilibrium temperatures and insulation requirements, with only a cursory analysis of heat-leak, boiloff and payload base area thermal environment.

4.5.1 Analytical Methods

Convective heating rates were calculated with the Boeing Convective Heating and Ablation Computer Program (CHAP). The 1962 U.S. Standard Atmosphere is an integral part of CHAP and was used in the analysis for all calculations based on a nominal atmosphere. Convective heating rates based on the atmospheric density (+) variation are consistent with the density variations used to calculate trajectory dispersions in Section 4.3.

Equilibrium temperatures based on convective heating rates for both nominal and a $+3\sigma$ density atmosphere were determined from the relation,

$$T_{eq}' = (q/\sigma\epsilon)^{0.25}$$

where, T_{eq} = equilibrium temperature
 q = heating rate
 σ = Stefan-Boltzmann constant
 ϵ = surface emissivity

An analysis of flow conditions at the base of the Space Tug payload section for the basic (no-flare) configuration was conducted to determine heating rates and equilibrium temperatures at the payload base area. The analysis utilized test data from References 4.5.1.0-1 and -2 for separated flow behind a base. In order for the flow along a streamline within the mixing layer to be able to overcome the pressure rise through the reattachment zone and pass downstream, its total pressure must be greater than the terminal static pressure at the end of the reattachment zone. If the total pressure is lower than the terminal static pressure, the flow is reversed and flows back toward the base. For analytical purposes the maximum base temperatures were assumed to occur at the point of impingement of the reversed flow. Empirical relations from Reference 4.5.1.0-2 for flow in a separated region were used to determine heating rates. Equilibrium temperatures were determined from relations given above.

4.5.1 (Continued)

Thermal analysis of the Tug sidewall thermal protection system (TPS) was accomplished with a one-dimensional heat conduction analysis utilizing finite difference techniques to determine thermal gradients in the sidewall insulation blanket.

4.5.1.1 Assumptions

In order to provide a thermal analysis of the four Space Tug aerobraking configurations within the time allocated for this study, certain assumptions were necessary. These assumptions are given below:

1. Zero angle of attack during each perigee pass through the atmosphere.
2. Equilibrium temperatures based on a surface emissivity of 0.90.
3. Heating rates based on a constant wall temperature of 80°F.
4. Micrometeoroid shield temperature should not exceed 400°F.
5. Space Tug thermal protection system will be a re-radiation system. Ablative materials will not be considered.

4.5.2 Heating Rates

Convective heating rates based on aerobraking trajectories of 5, 10, 30 and 60 perigee passes were determined for the Space Tug basic configuration (no flare) and the 30°, 45° and 60° flare configurations. Maximum heating rates as a function of the number of perigee passes are presented in Figures 4.5.2.0-1 through 4.5.2.0-4 for the four configurations. A comparison of heating rates for the four configurations is shown in Figure 4.5.2.0-5. A typical heating rate distribution as a function of perigee pass time for the 1.8 day (10 pass) aerobraking trajectory is shown in Figures 4.5.2.0-6 through 4.5.2.0-9 for the four configurations.

The effect of atmospheric density variations on the convective heating rates is shown in Figure 4.5.2.0-10. The atmospheric density variations used in the determination of the heating rates are discussed in Section 4.3.

4.5.3 Equilibrium Temperatures

Maximum equilibrium temperatures for the Space Tug basic configuration and the 30°, 45° and 60° flare configurations are presented in Figures 4.5.3.0-1 through 4.5.3.0-4, respectively. A comparison of equilibrium temperatures for the four configurations is presented in Figure 4.5.3.0-5.

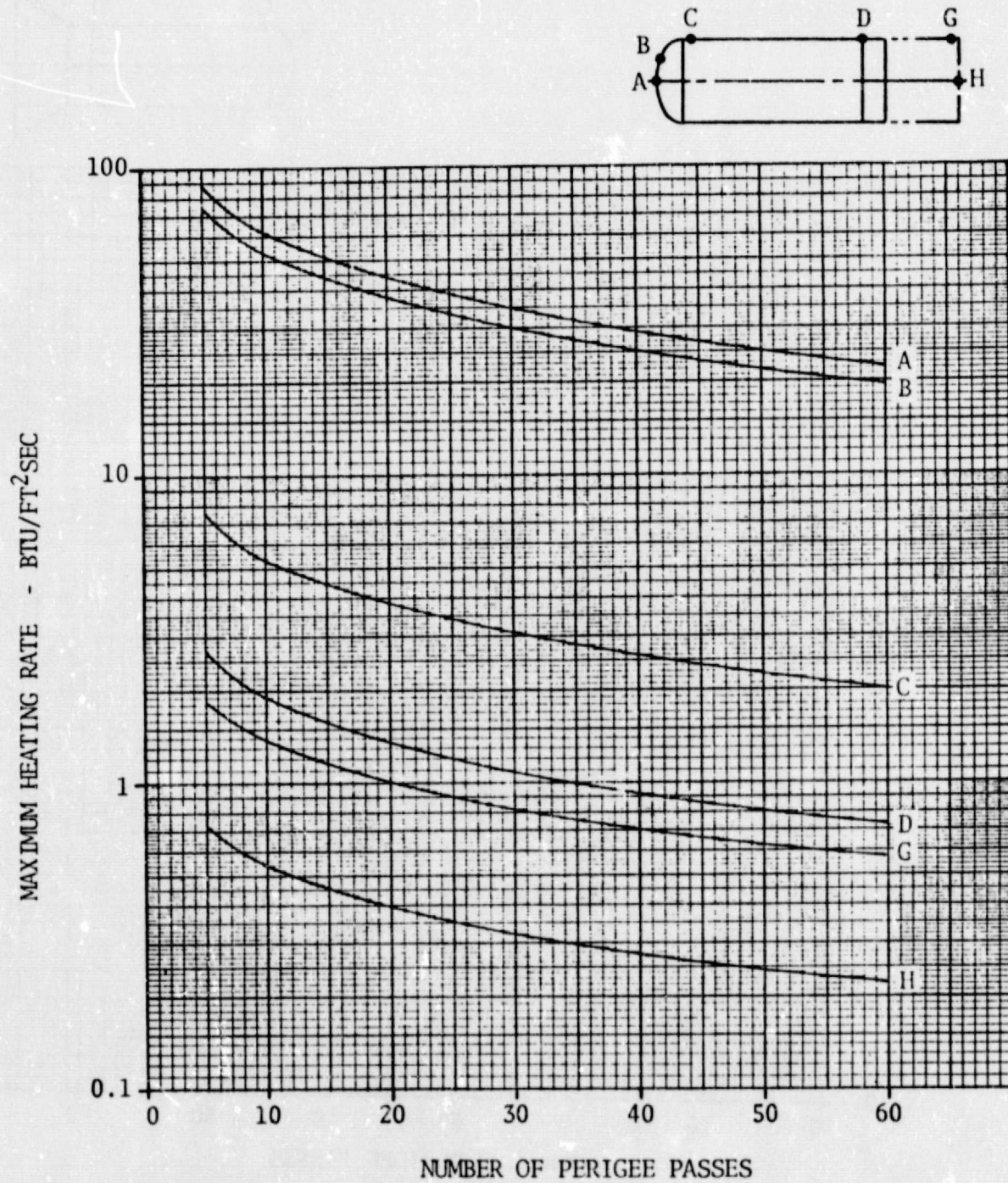


FIGURE 4.5.2.0-1 MAXIMUM HEATING RATES - BASIC CONFIGURATION

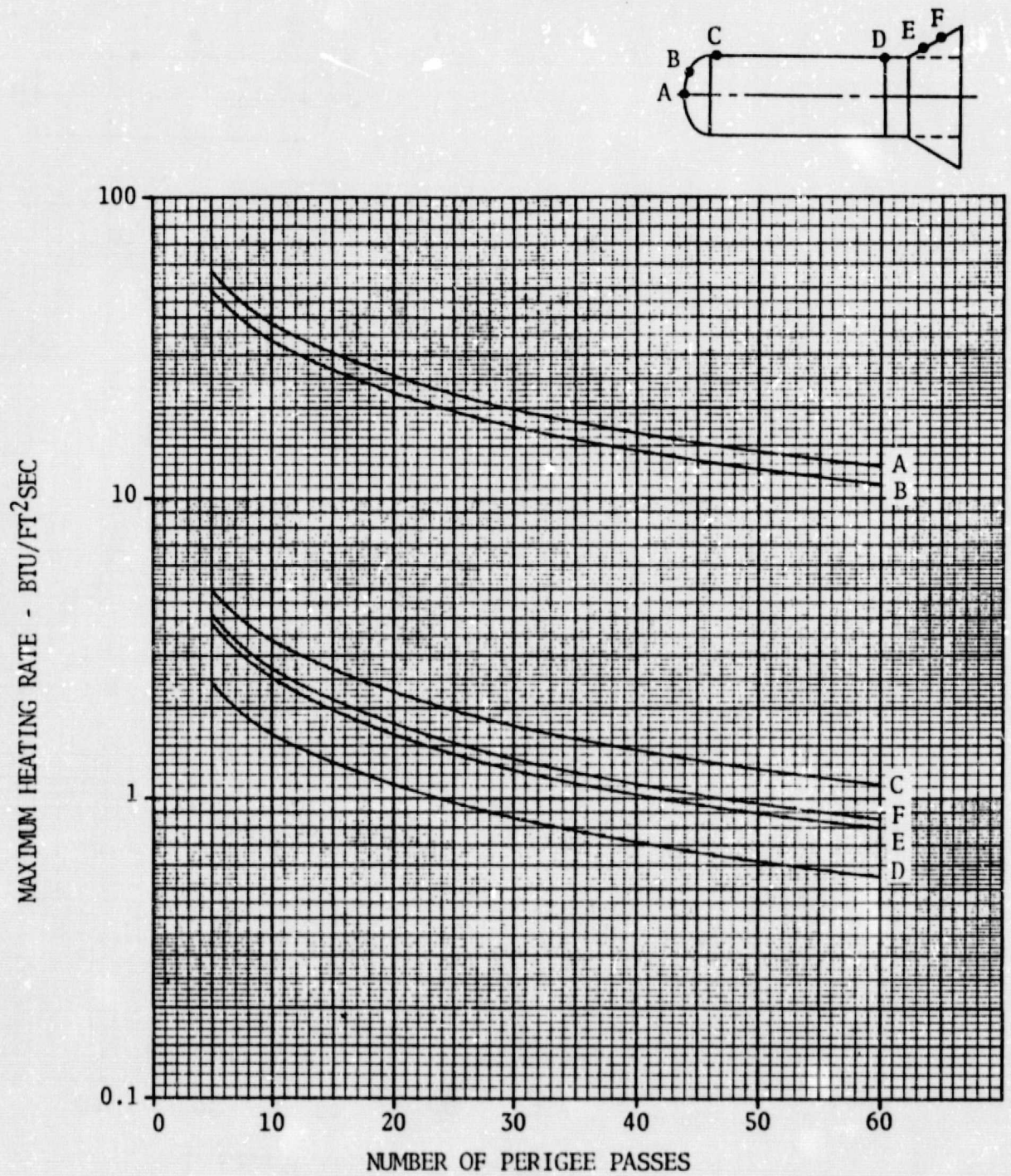


FIGURE 4.5.2.0-2 MAXIMUM HEATING RATES - 30° FLARE CONFIGURATION

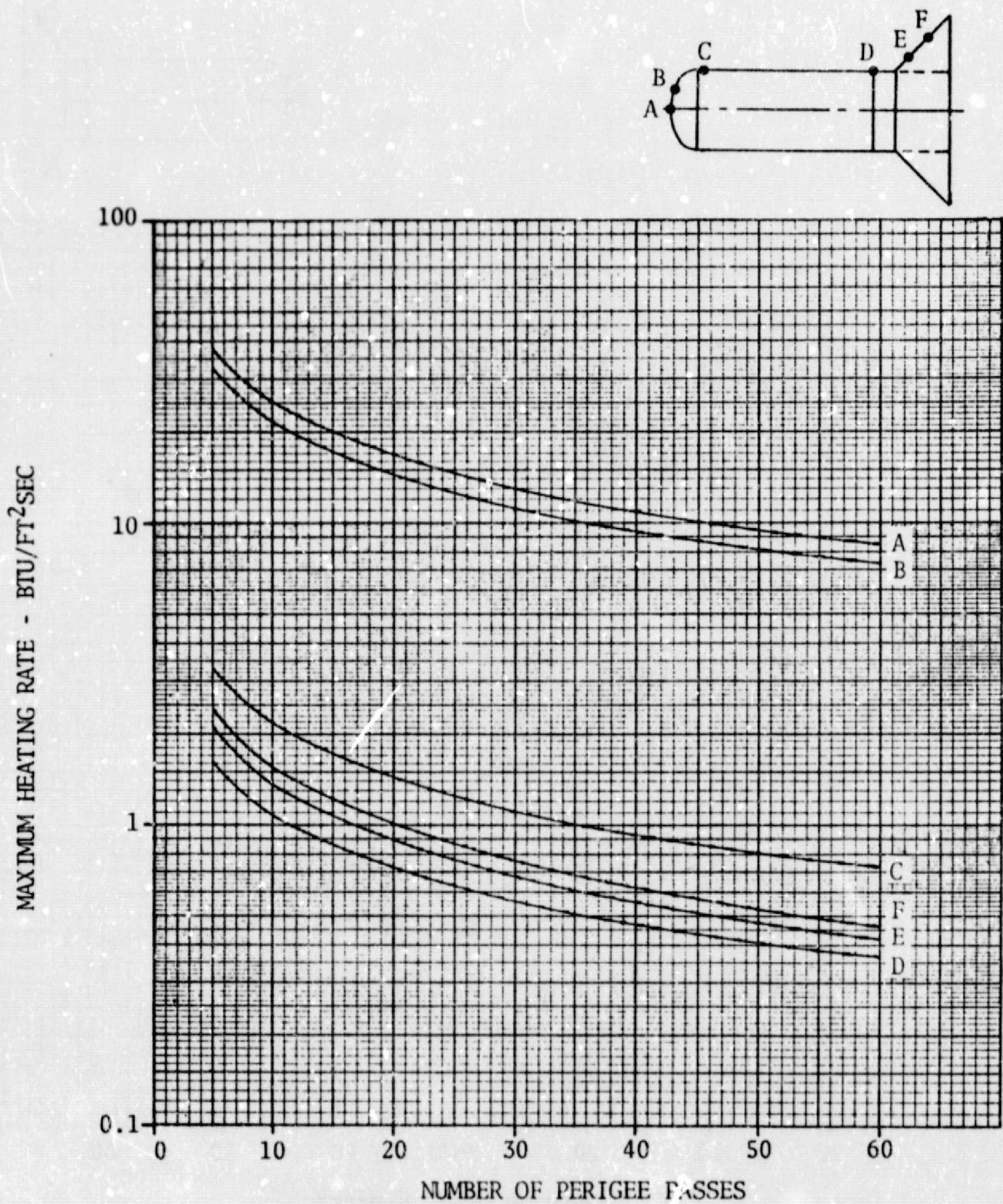


FIGURE 4.5.2.0-3 MAXIMUM HEATING RATES - 45° FLARE CONFIGURATION

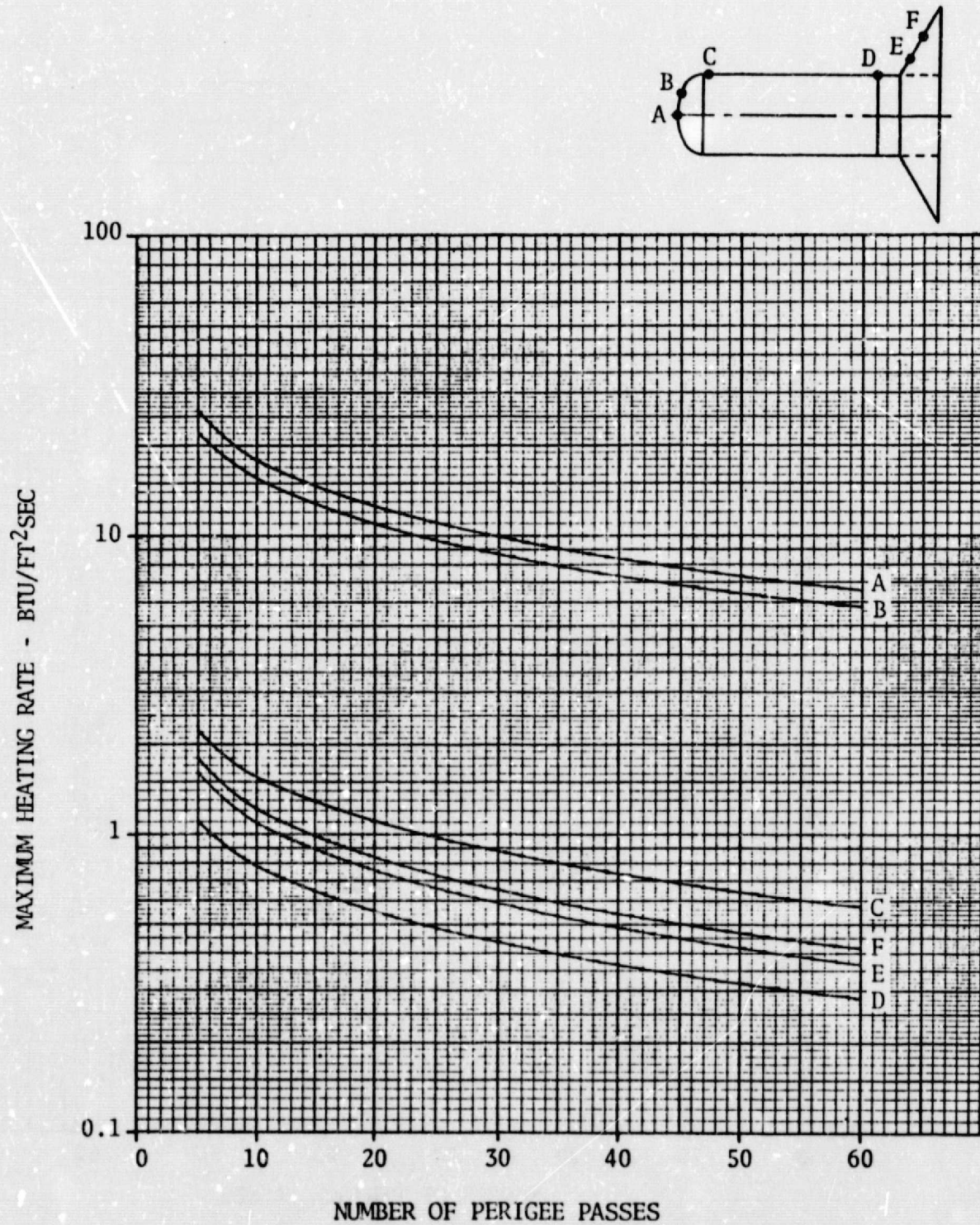


FIGURE 4.5.2.0-4 MAXIMUM HEATING RATES - 60° FLARE CONFIGURATION

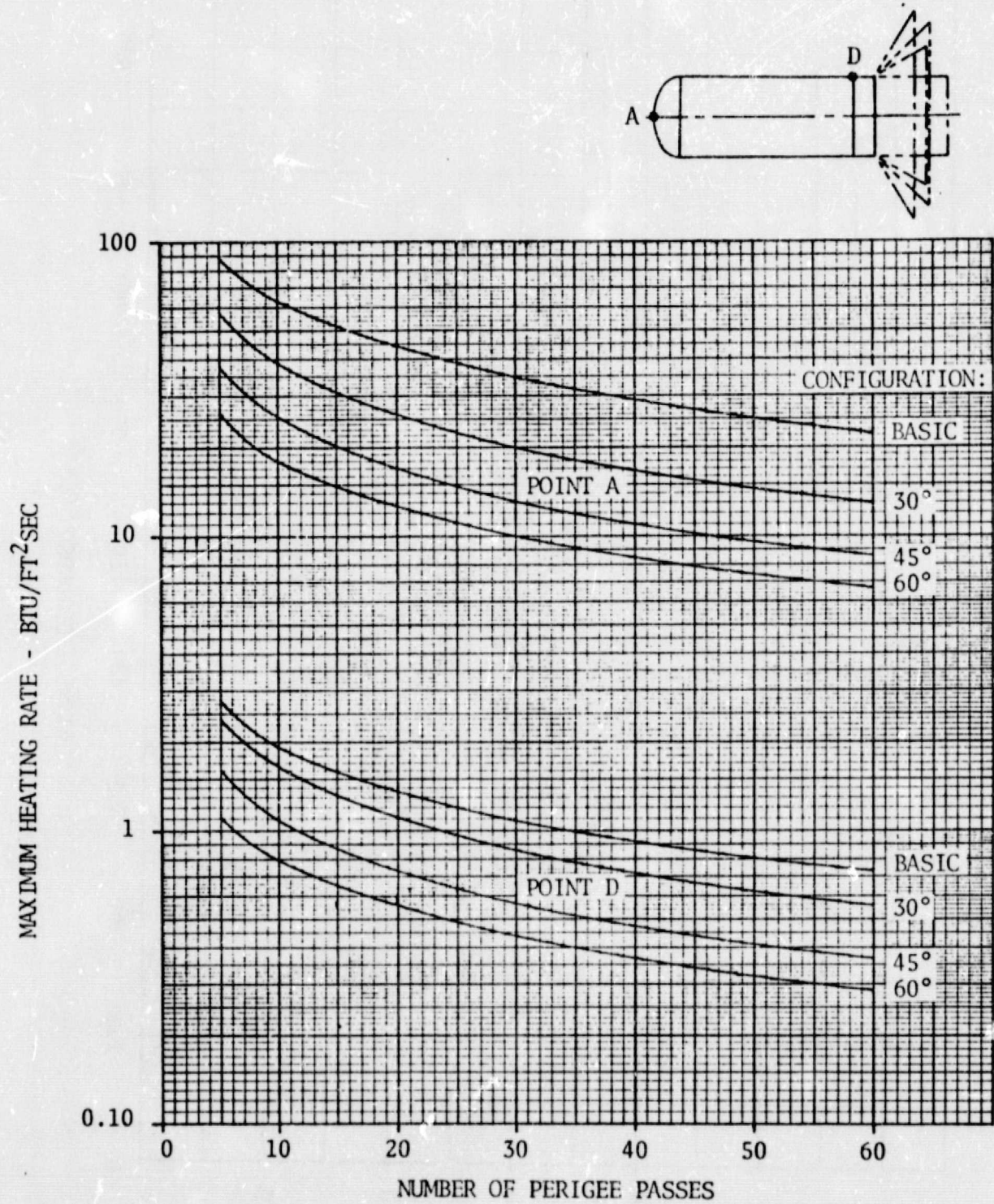


FIGURE 4.5.2.0-5 . COMPARISON OF MAXIMUM HEATING RATES

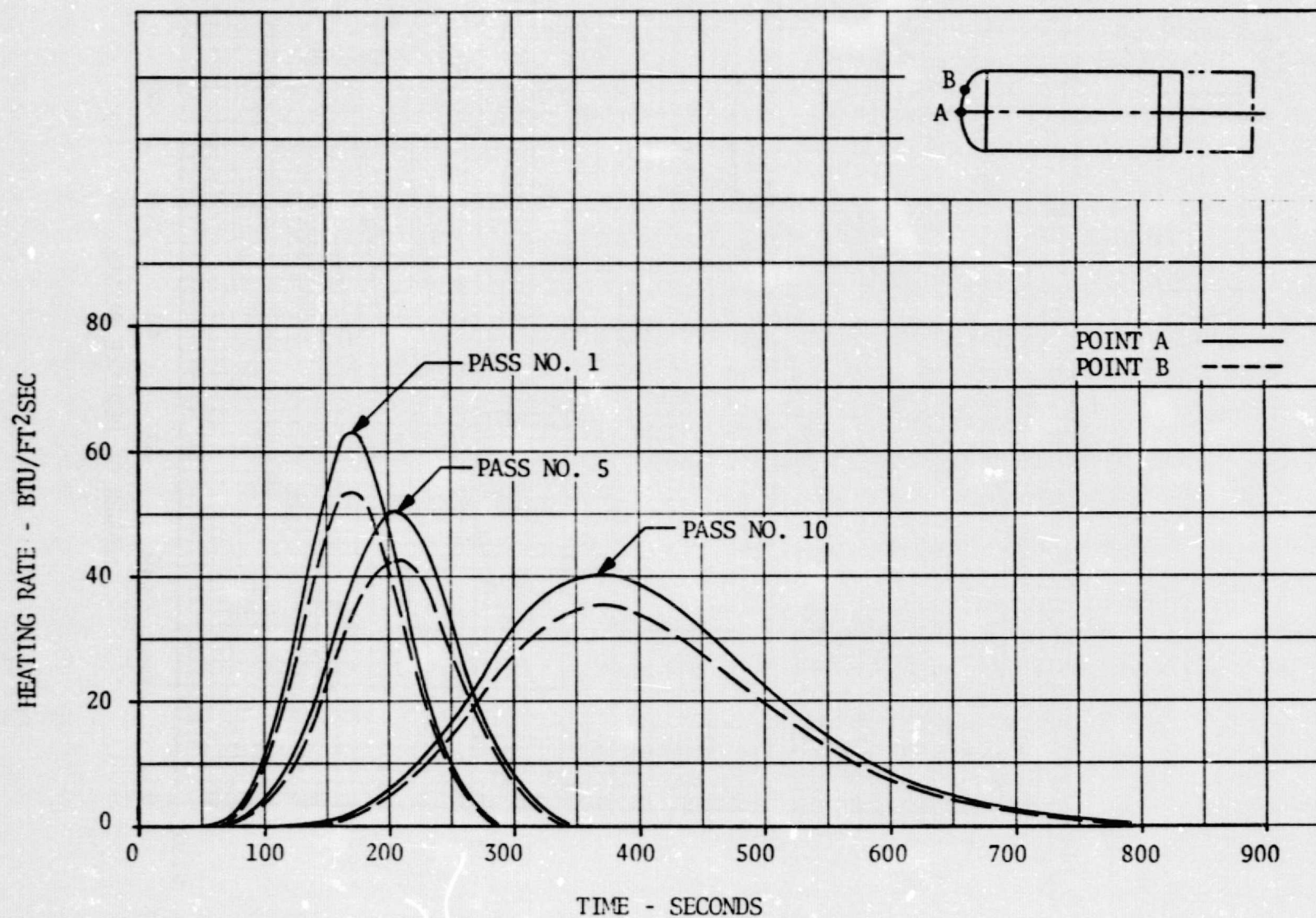


FIGURE 4.5.2.0-6 HEATING RATE DISTRIBUTION - 10-PASS BASIC CONFIGURATION

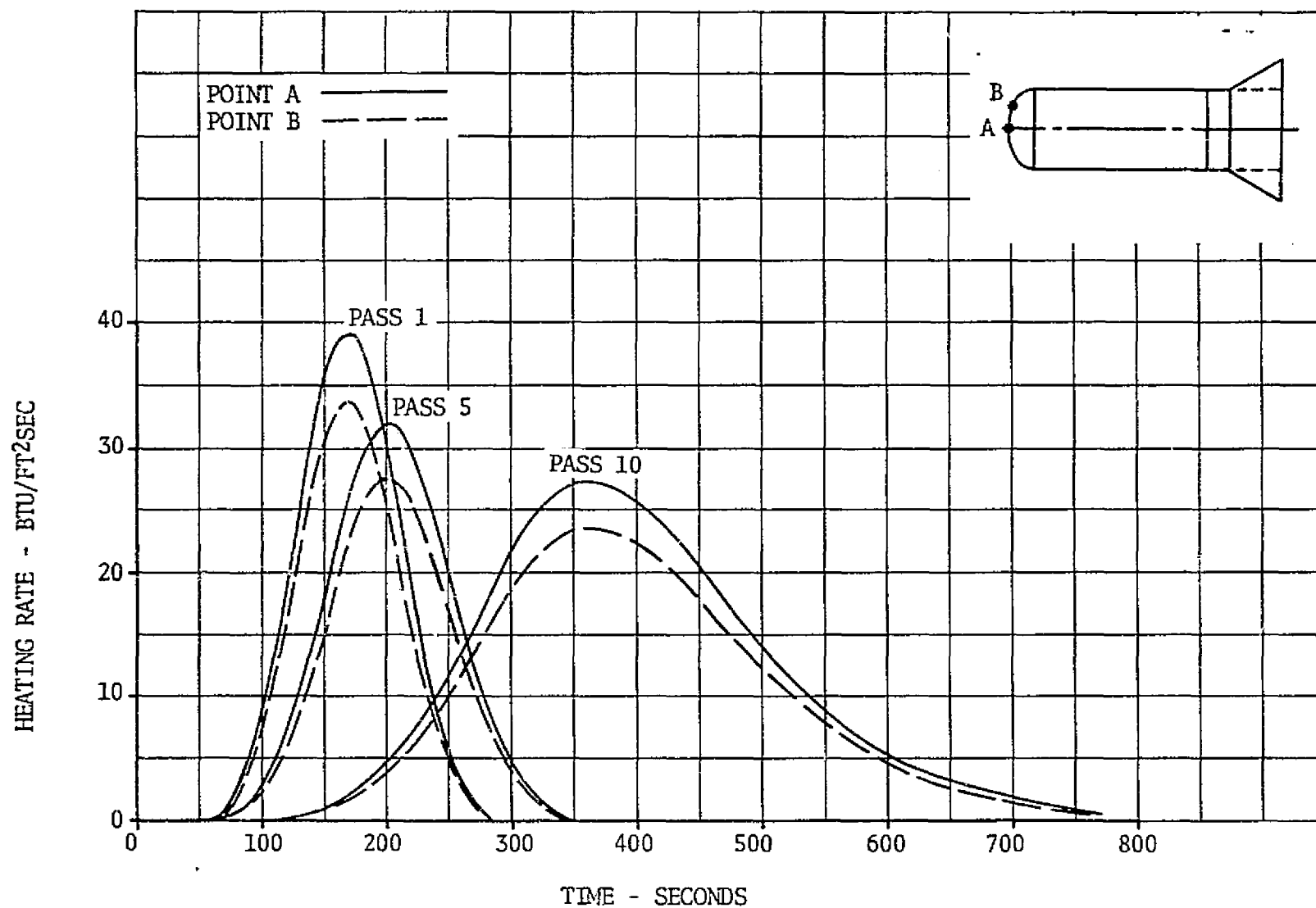


FIGURE 4.5.2.0-7 HEATING RATE DISTRIBUTION - 10-PASS 30° FLARE CONFIGURATION

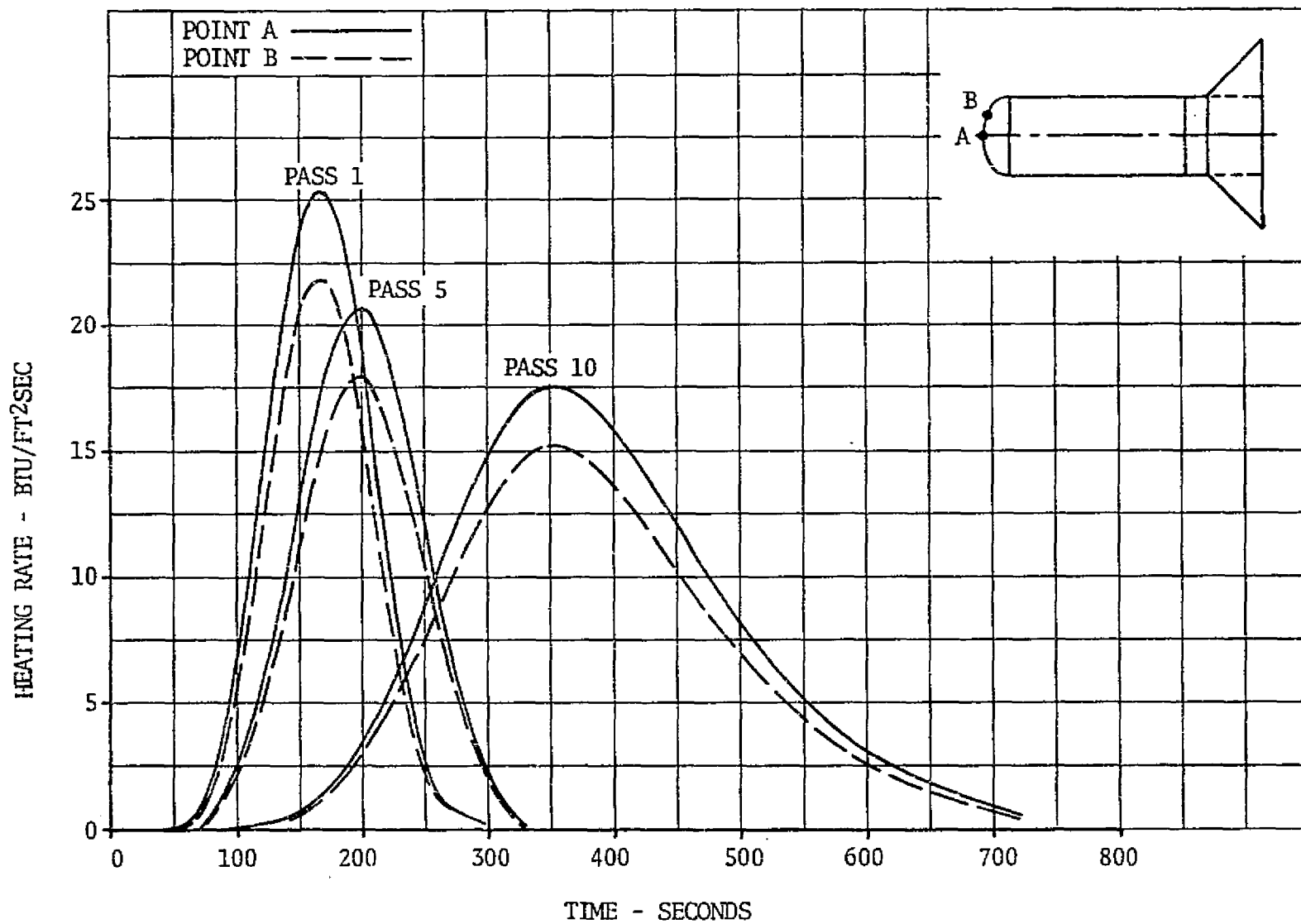


FIGURE 4.5.2.0-8 HEATING RATE DISTRIBUTION - 10-PASS 45° FLARE CONFIGURATION

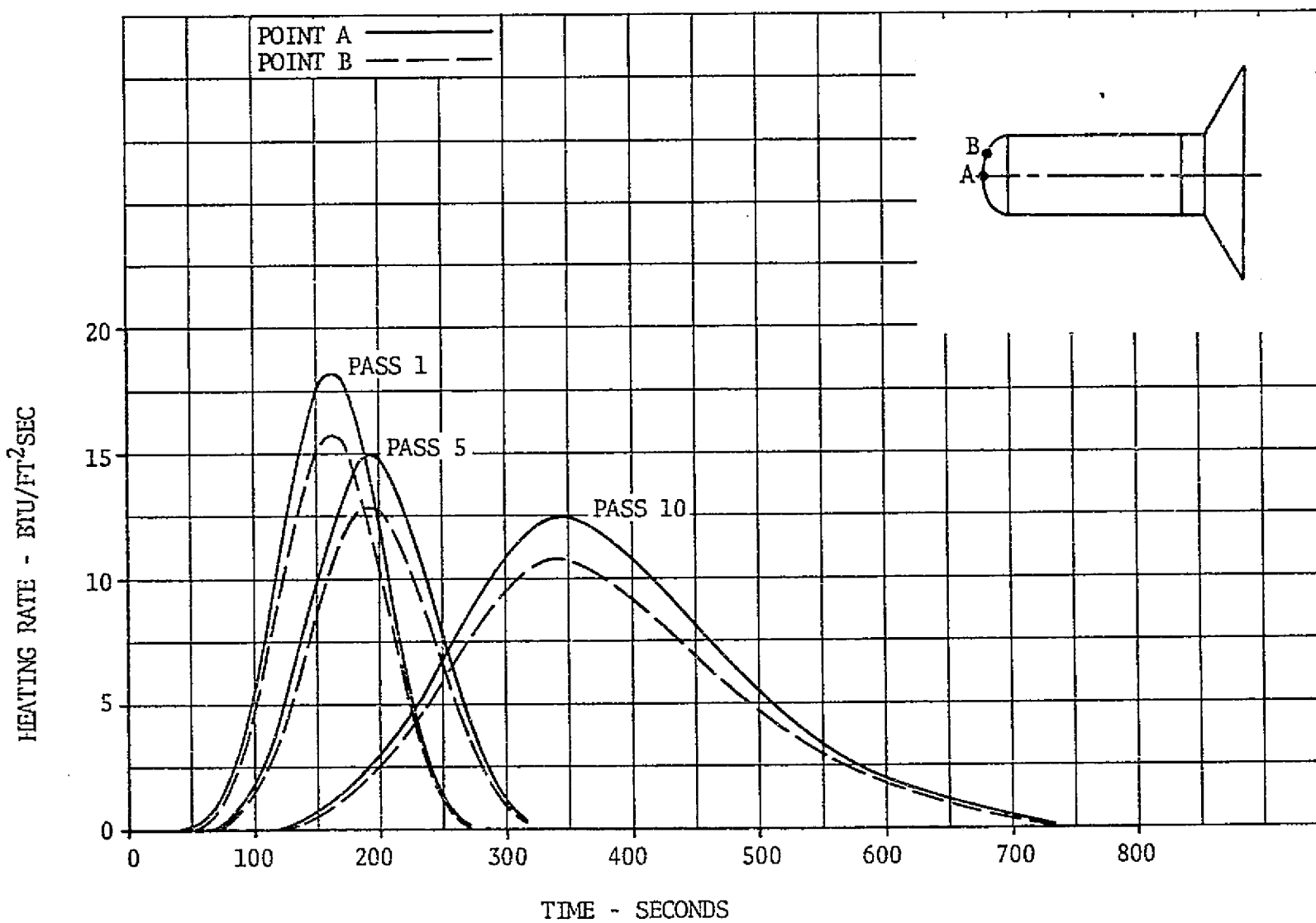


FIGURE 4.5.2.0-9 HEATING RATE DISTRIBUTION - 10-PASS 60° FLARE CONFIGURATION

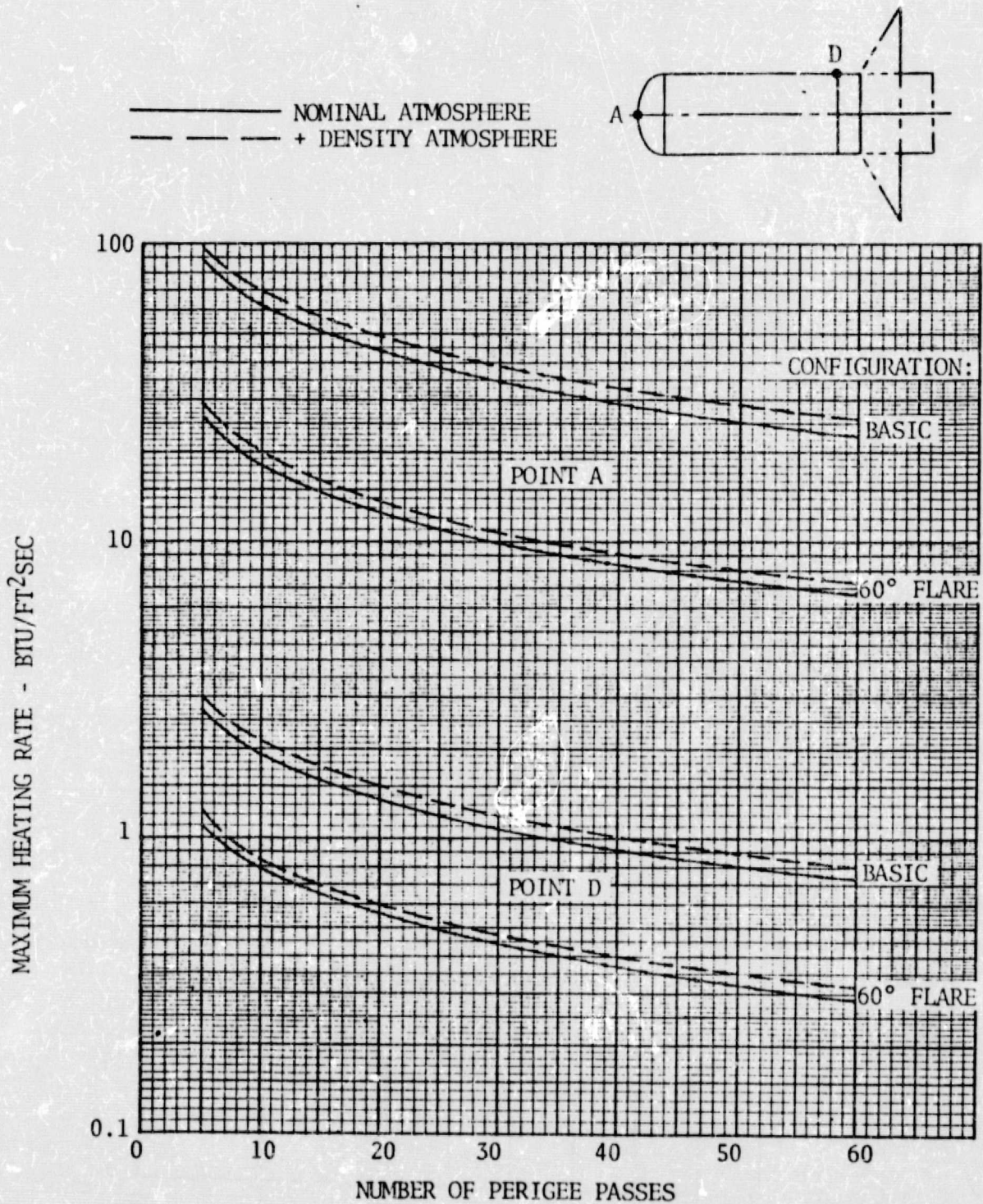


FIGURE 4.5.2.0-10 MAXIMUM HEATING RATES FOR BASIC AND 60° FLARE CONFIGURATIONS - NOMINAL AND (+) DENSITY ATMOSPHERE

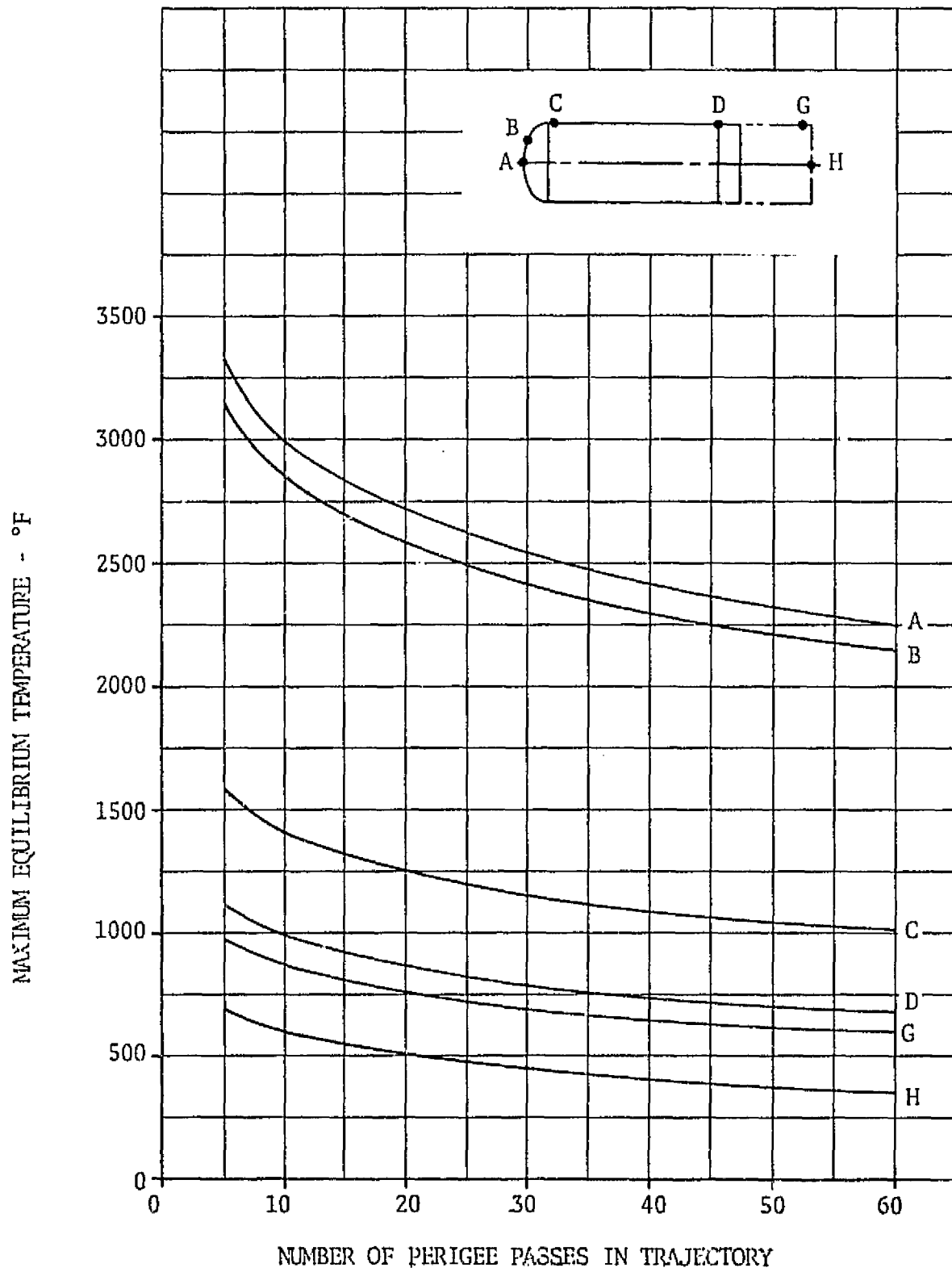


FIGURE 4.5.3.0-1 MAXIMUM EQUILIBRIUM TEMPERATURES - BASIC CONFIGURATION

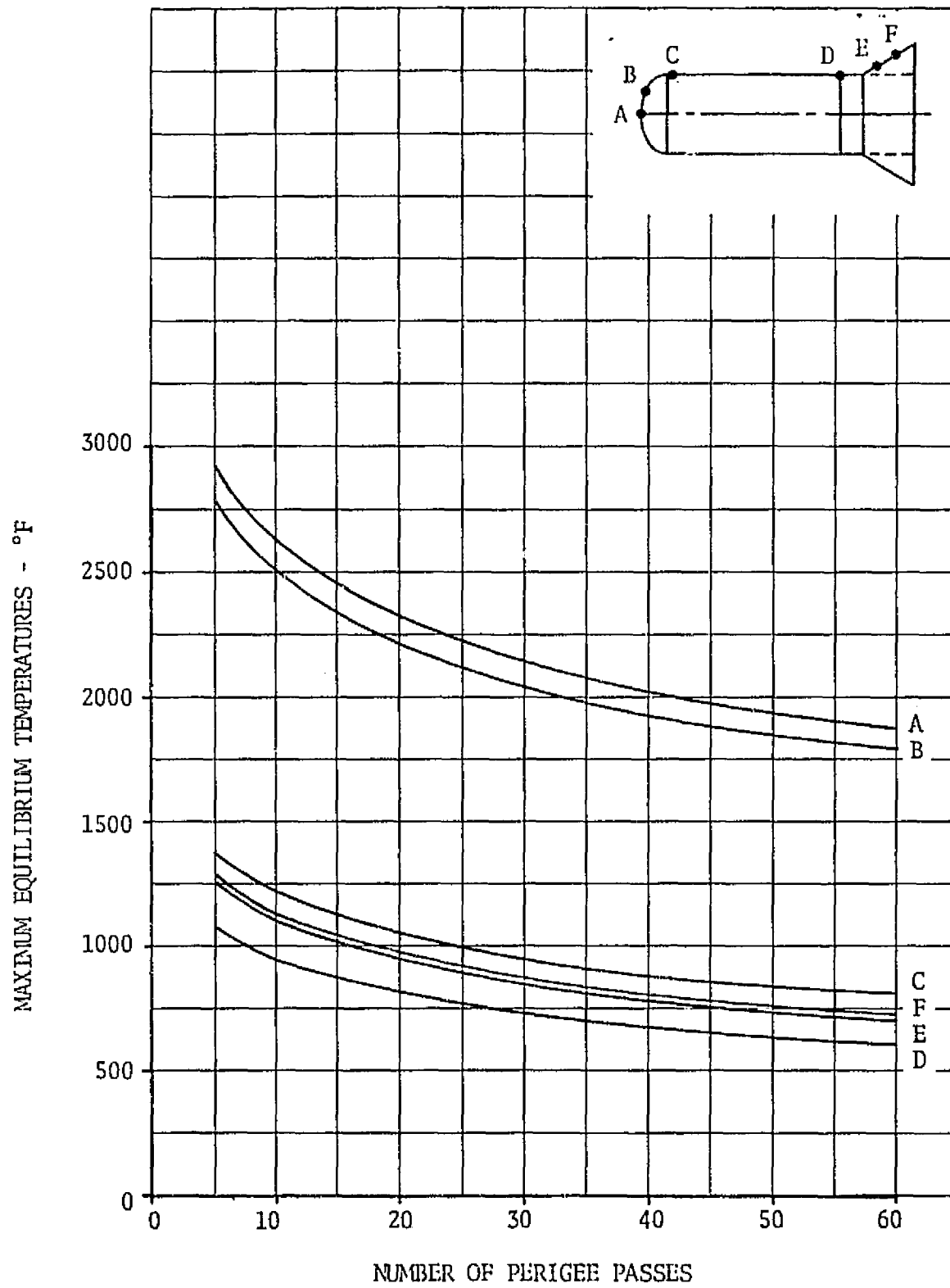


FIGURE 4.5.3.0-2 MAXIMUM EQUILIBRIUM TEMPERATURES - 30° FLARE CONFIGURATION

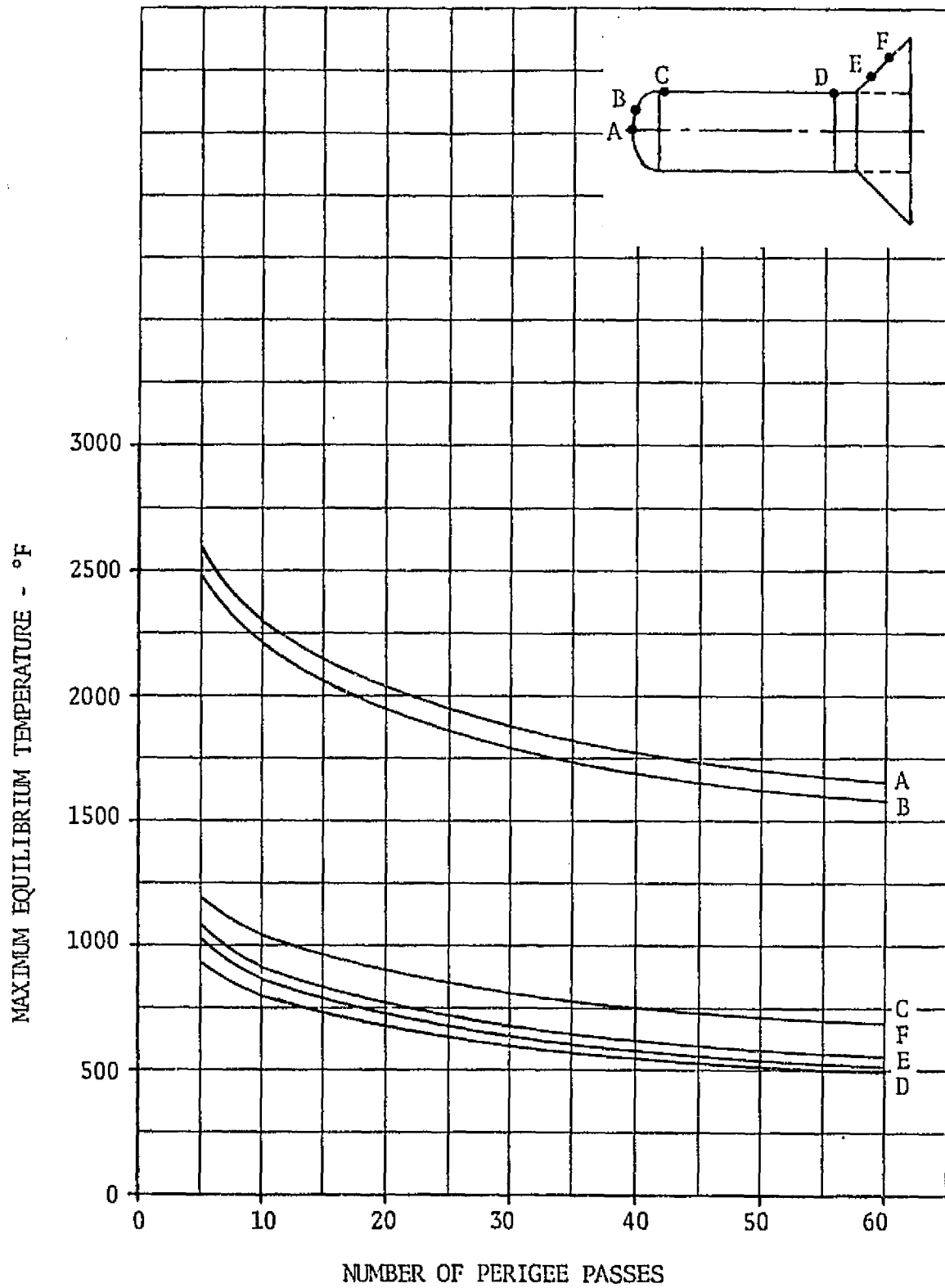


FIGURE 4.5.3.0-3 MAXIMUM EQUILIBRIUM TEMPERATURES - 45° FLARE CONFIGURATION

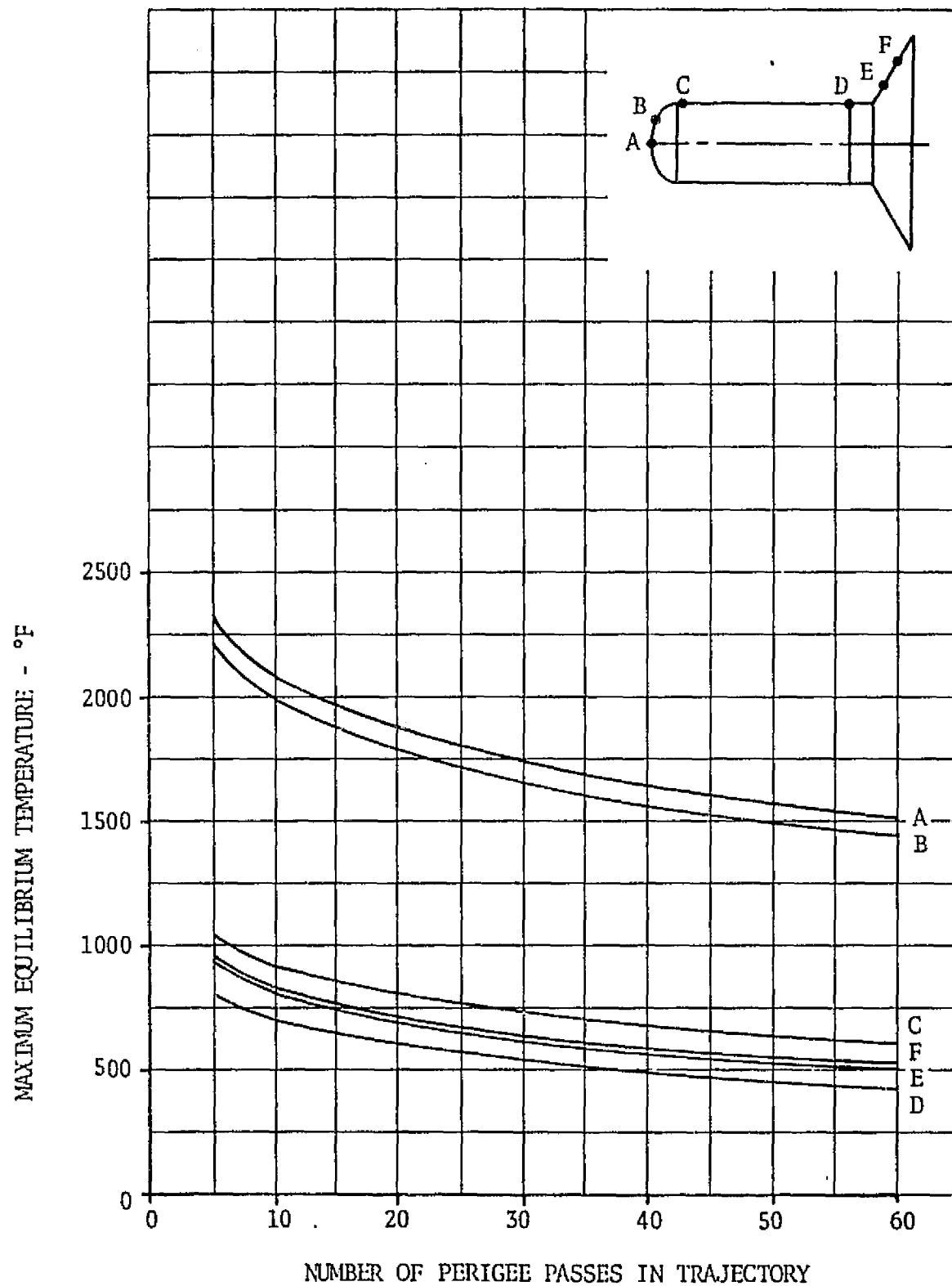
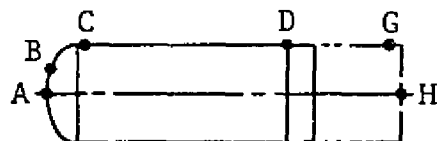
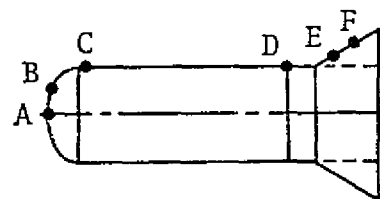


FIGURE 4.5.3.0-4 MAXIMUM EQUILIBRIUM TEMPERATURES - 60° FLARE CONFIGURATION



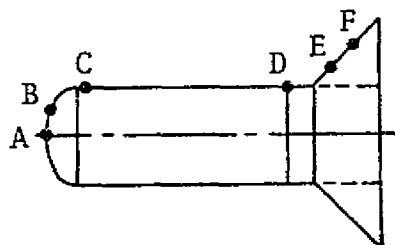
SPACE TUG BASIC CONFIGURATION

TRAJECTORY	MAXIMUM EQUILIBRIUM TEMPERATURES (°F)					
	A	B	C	D	G	H
5 PASS	3320	3175	1585	1120	975	682
10 PASS	2990	2860	1410	987	875	591
30 PASS	2540	2420	1166	797	720	451
60 PASS	2240	2140	1005	676	615	364



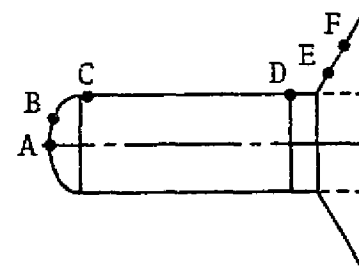
SPACE TUG 30° FLARE CONFIGURATION

TRAJECTORY	MAXIMUM EQUILIBRIUM TEMPERATURES (°F)					
	A	B	C	D	E	F
5 PASS	2940	2800	1382	1082	1272	1293
10 PASS	2630	2520	1215	943	1104	1124
30 PASS	2160	2060	957	733	850	869
60 PASS	1880	1790	809	605	706	729



SPACE TUG 45° FLARE CONFIGURATION

TRAJECTORY	MAXIMUM EQUILIBRIUM TEMPERATURES (°F)					
	A	B	C	D	E	F
5 PASS	2590	2480	1195	927	1037	1085
10 PASS	2300	2205	1040	800	874	919
30 PASS	1886	1798	812	608	635	680
60 PASS	1660	1580	691	507	513	558



SPACE TUG 60° FLARE CONFIGURATION

TRAJECTORY	MAXIMUM EQUILIBRIUM TEMPERATURES (°F)					
	A	B	C	D	E	F
5 PASS	2325	2220	1048	806	943	970
10 PASS	2080	1990	917	697	804	829
30 PASS	1740	1660	733	540	621	648
60 PASS	1512	1467	609	439	503	538

FIGURE 4.5.3.0-5 COMPARISON OF MAXIMUM EQUILIBRIUM TEMPERATURES

Equilibrium temperatures based on atmospheric density variations are presented in Figure 4.5.3.0-6 and compared with nominal atmospheric density based equilibrium temperatures.

4.5.4 Thermal Protection System Requirements

The thermal protection system (TPS) proposed for the Space Tug aerobraking configurations is a re-radiation system utilizing a passive approach to thermal control. Temperatures behind the re-radiation shield are controlled by layers of insulation either directly attached to the re-radiation shield or remote, such as local insulation of temperature critical components or structure.

4.5.4.1 Heat Shield Dome

The Space Tug heat shield dome is a re-radiative structure capable of performing within the thermal environment imposed on it during the aerobraking mode. Materials considered for various temperature ranges are discussed in Section 4.7. The dome is designed as a hot structure and must be thermally isolated at all support and contact points. Temperature critical components and structure behind the dome will be subjected to radiation from the backside of the dome, consequently local thermal protection in the form of foil-backed microquartz insulation should be provided in this area.

4.5.4.2 Flare Structure

The flare configurations are designed to allow re-radiation thermal control during the aerobraking mode. There is no requirement for insulation on the back surface of the flare structure. All supporting structure and attach points are assumed to be thermally isolated.

4.5.4.3 Sidewall Area

The Space Tug sidewall area, Astrionics Module and payload section (basic no-flare configuration only) will require insulation in order to prevent the micrometeoroid shield from exceeding 400°F. A passive system utilizing a 0.002 inch Titanium outer skin with a layer of microquartz insulation attached was analyzed for thermal adequacy. A sketch showing a cross-section of the Tug sidewall is shown in Figure 4.5.4.3-1. The basic configuration (no flare) will require insulation along the Tug sidewall, Astrionics Module, payload sidewall and payload base area. The flare configurations will require insulation along the Tug sidewall and Astrionics Module only. The payload section is assumed to be thermally shielded by the flare structure. Minimum insulation thicknesses for the basic configuration and the 30°, 45° and 60° flare configurations are presented in Figures 4.5.4.3-2 through 4.5.4.3-5, respectively.

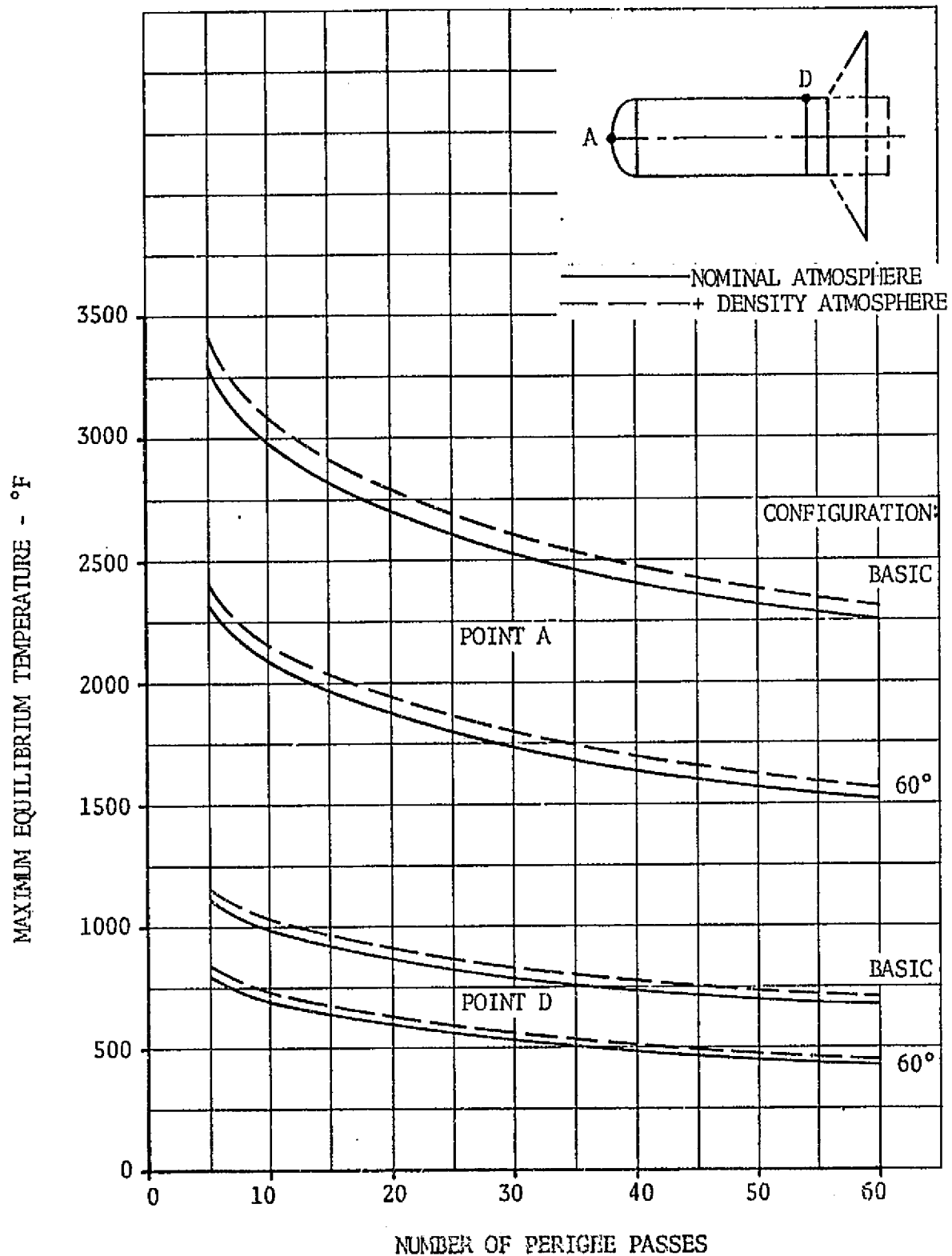


FIGURE 4.5.3.0-6 MAXIMUM EQUILIBRIUM TEMPERATURES FOR BASIC AND 60° FLARE CONFIGURATIONS - NOMINAL AND (+) DENSITY ATMOSPHERE

D5-17142

- NOTES: 1. ALL DIMENSIONS ARE INCHES
2. CROSS-SECTION IS TYPICAL
FOR LH₂ TANK WALL

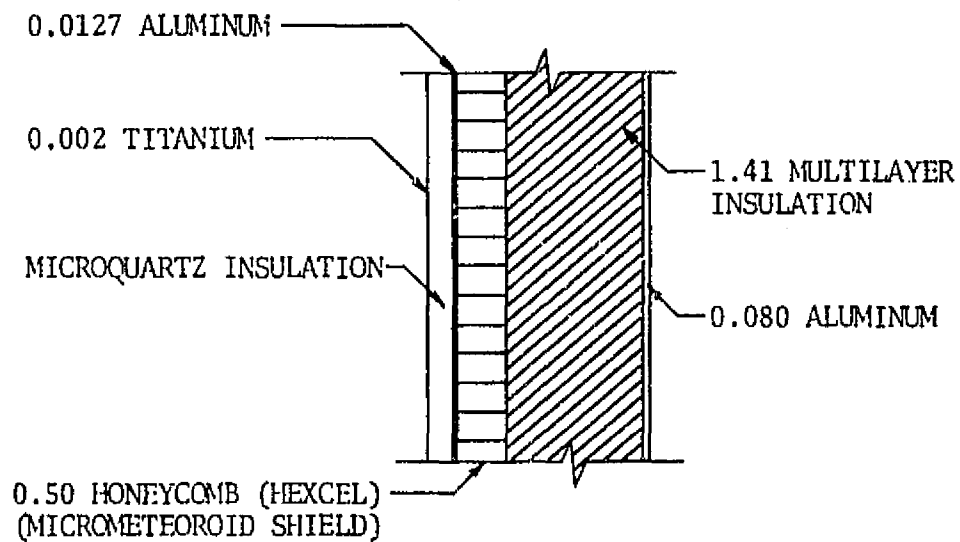


FIGURE 4.5.4.3-1 SPACE TUG SIDEWALL CROSS-SECTION

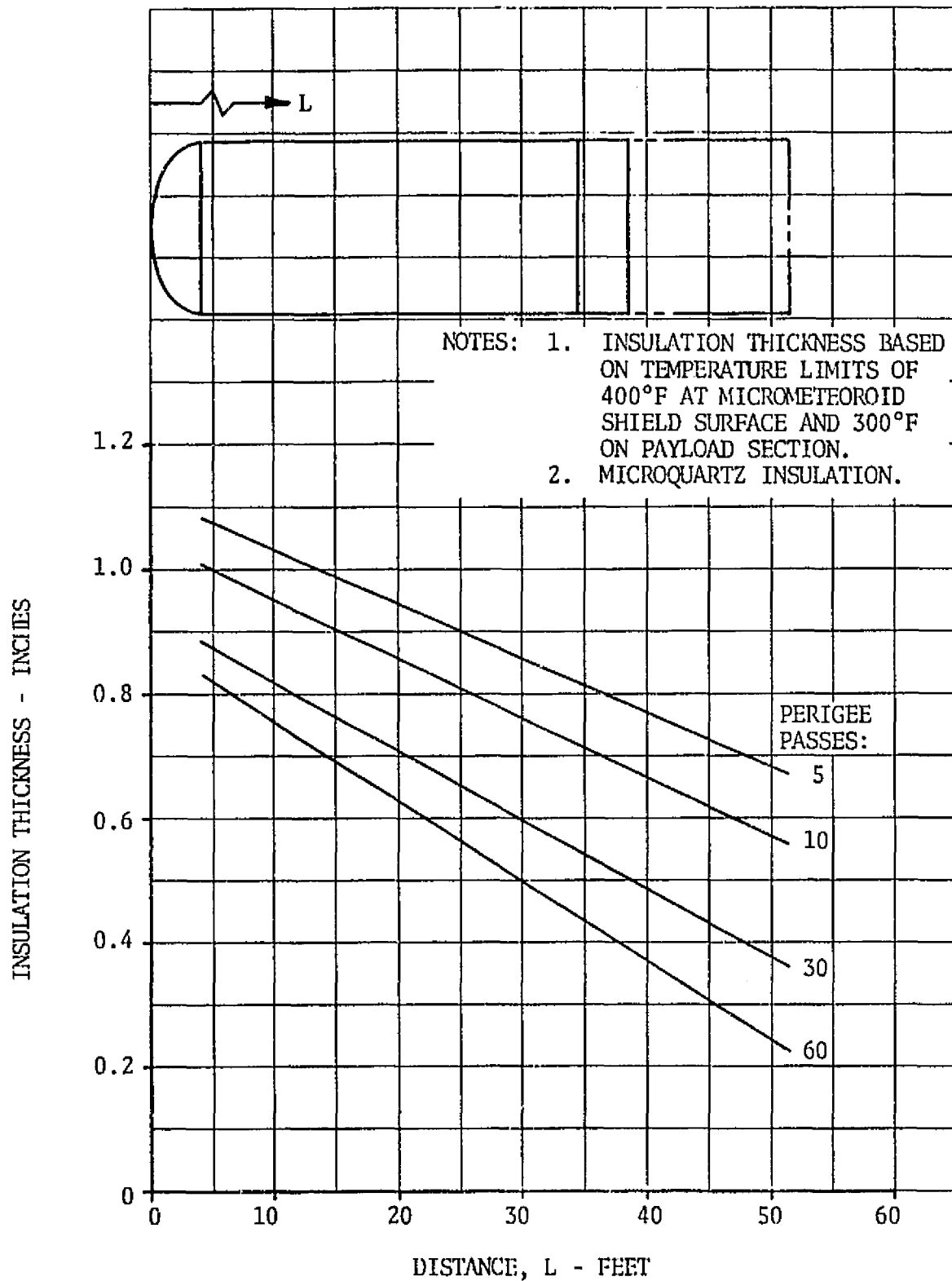


FIGURE 4.5.4.3-2. SPACE TUG SIDEWALL INSULATION THICKNESS - BASIC CONFIGURATION

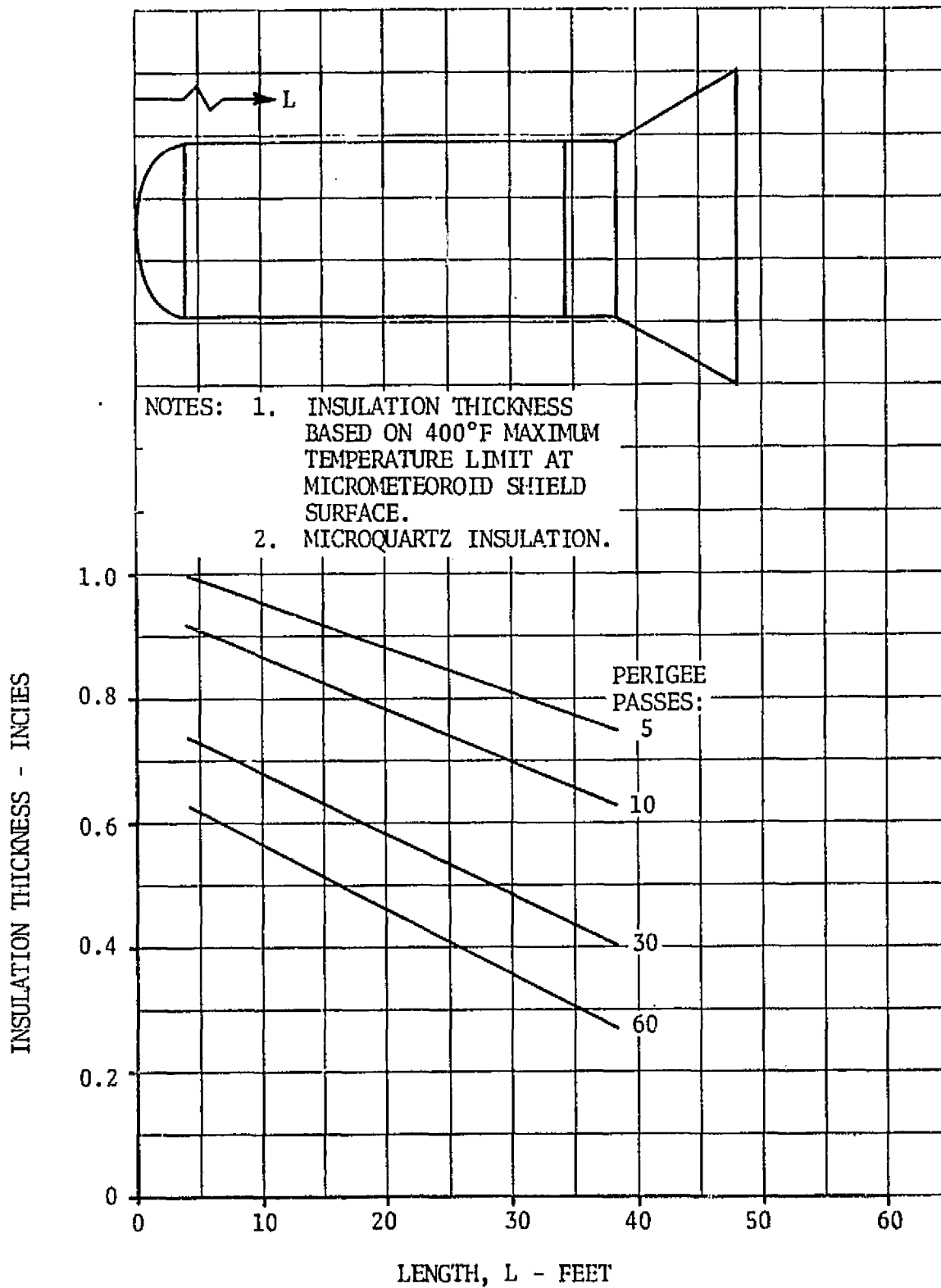


FIGURE 4.5.4.3-3 SPACE TUG SIDEWALL INSULATION THICKNESS - 30° FLARE CONFIGURATION

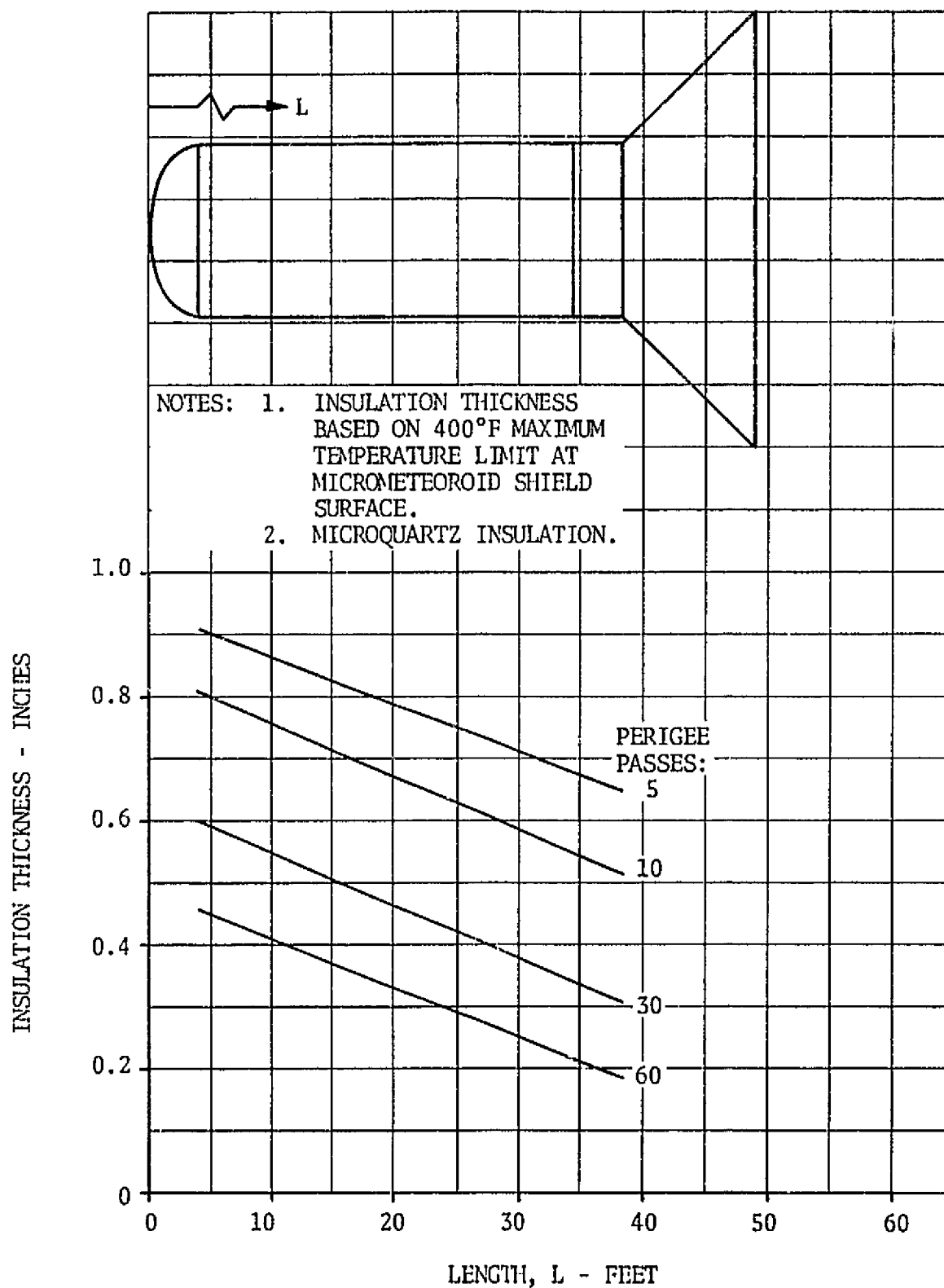


FIGURE 4.5.4.3-4 SPACE TUG SIDEWALL INSULATION THICKNESS - 45° FLARE CONFIGURATION

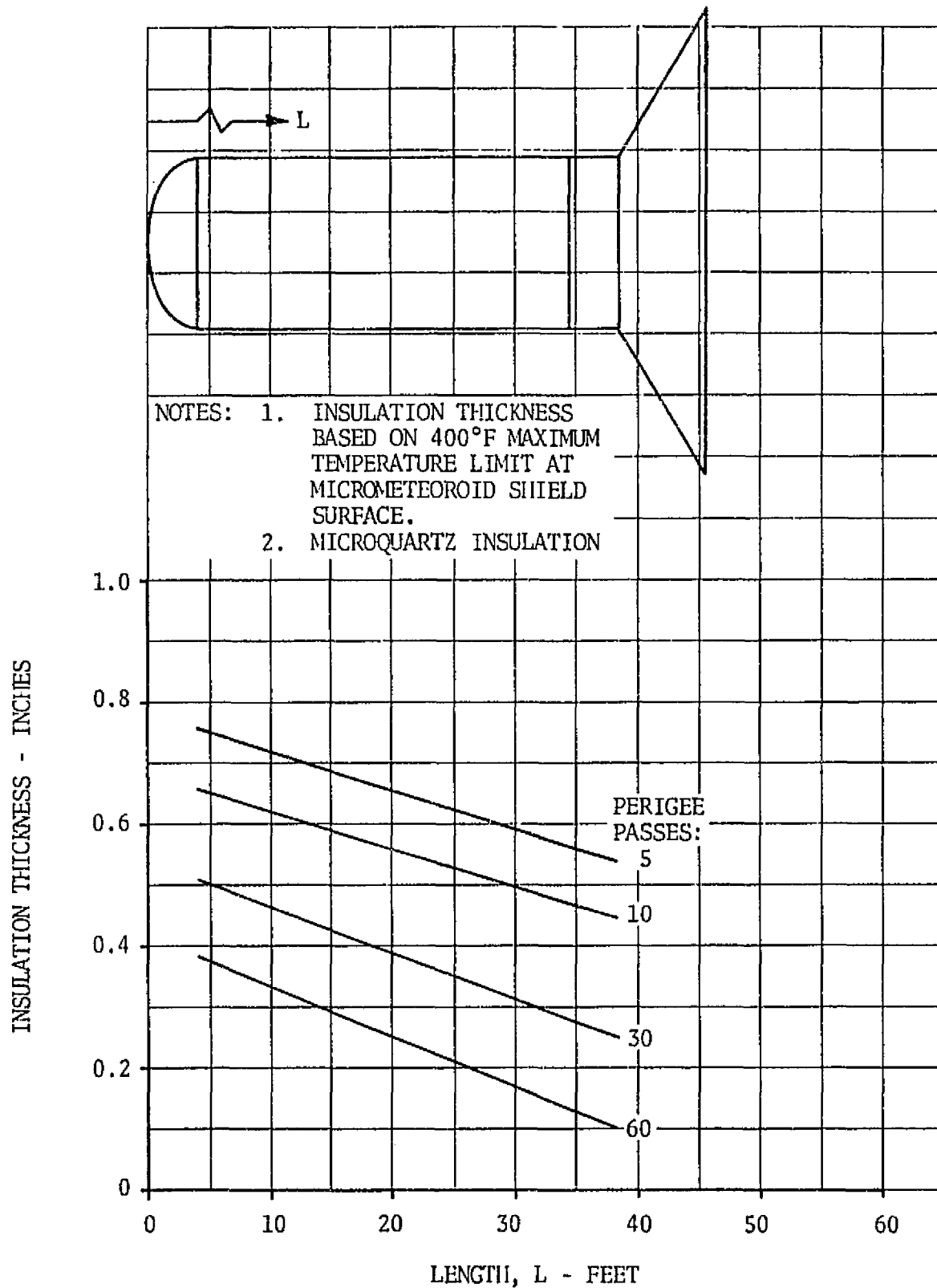


FIGURE 4.5.4.3-5 SPACE TUG SIDEWALL INSULATION THICKNESS - 60° FLARE CONFIGURATION

4.5.4.4 Thermal Protection System Weights

Thermal protection system (TPS) weights for the basic configuration and the 30°, 45° and 60° flare configurations (Tug sidewall, Astrionics Module and payload section only) are presented in Figure 4.5.4.4-1. These weights are based on the minimum insulation thickness defined in Section 4.5.4.3 and include the weight of the 0.002 inch titanium outer skin. The effect of increased heating due to atmospheric density variations on the TPS weights is also shown in Figure 4.5.4.4-1. The dome heat shield (including local insulation requirements) and flare re-radiation shield weights are presented in Section 4.8.

The thermal analysis presented and discussed herein is considered adequate for the Space Tug aerobraking feasibility study. There are areas, however, that should be investigated in more detail in order to better define thermal performance of the aerobraking configurations. One of these areas is the thermal protection system. A detailed analysis of the thermal protection system should be performed in order to optimize system performance and weight, including evaluation of alternate system concepts. In conjunction with a more detailed thermal protection system analysis, heat-leak analyses are needed in order to define internal structural temperatures and propellant boiloff.

4.6 ASTRIONICS ANALYSIS

The Space Tug Aerobraking Astrionics System Study was performed by the International Business Machines Corporation (IBM), Electronic Systems Center, under contract to The Boeing Company, and for the Marshall Space Flight Center, NASA Contract NAS8-27501.

This astrionics system study is an extension of a previous Space Tug analysis performed jointly by the IBM and The Boeing Company. The astrionics study results were separately reported in "Astrionic System Optimization and Modular Astrionics for NASA Missions after 1974 - Preliminary Definition of Astrionic System for Space Tug Mission Vehicle Payload (MVP)", (prior Reference 3.3.0.0-1).

4.6.1 Introduction

The objective of the astrionic system analysis task of the study was to investigate the navigation techniques and accuracies, system redundancy, power-weight-impacts, radiation impacts and resultant physical characteristics of the astrionic system areas where new technology is required and areas where follow-on study effort is desirable were identified.

The approach to this study effort is given in Figure 4.6.1.0-1. Boeing data and the study groundrules were inputs to the study. The baseline astrionic configuration from IBM Document Number 69-K44-0006H was refined to provide the baseline configuration. Navigation analysis was performed for the 2, 5, 10 and 15 days missions to determine sensors for aerobraking and the magnitudes of navigation uncertainties (i.e., statistical standard deviations expected) for the various sensor combinations. A redundancy/reliability analysis was performed to determine baseline (60-hour, defined

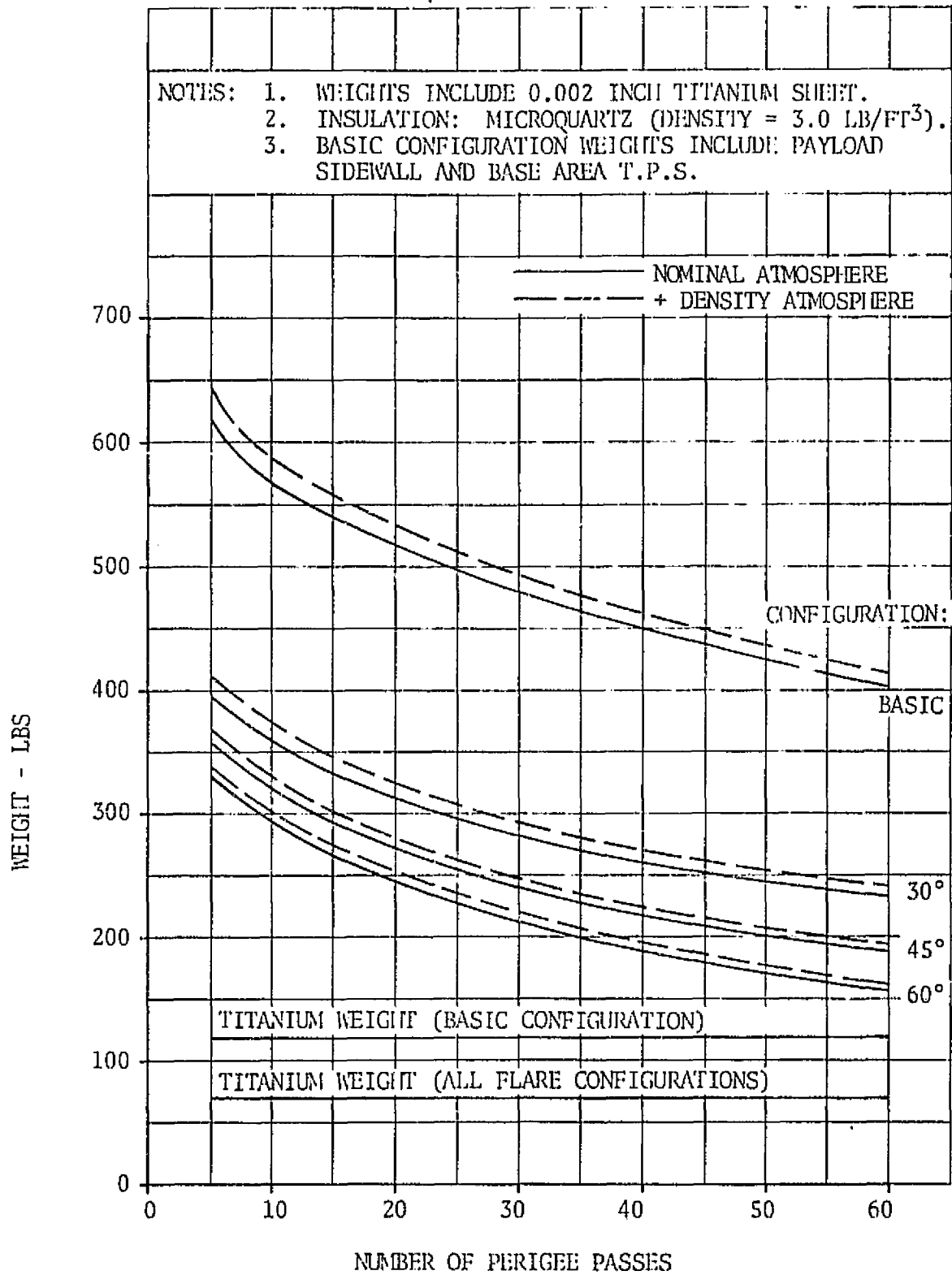
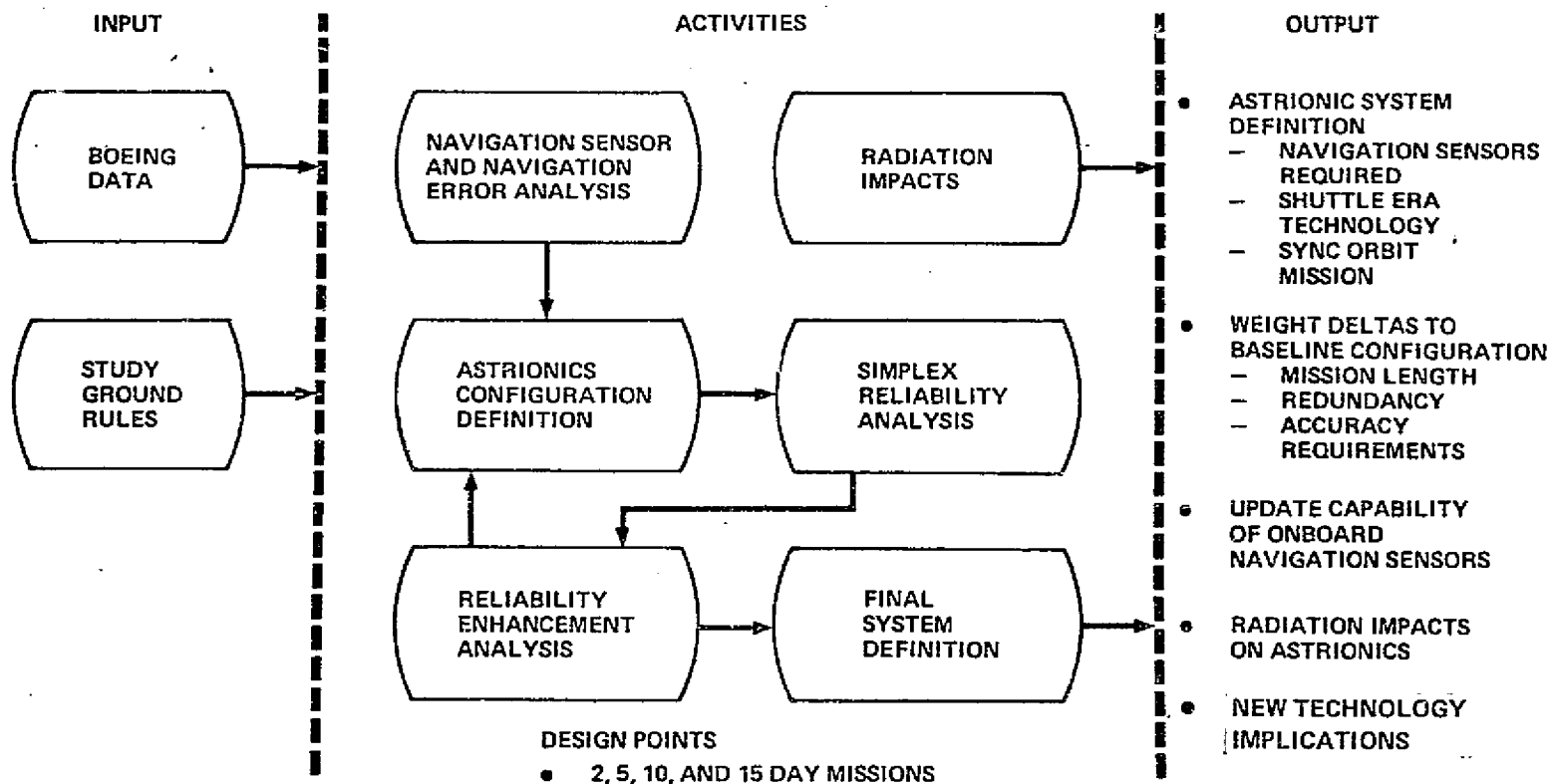


FIGURE 4.5.4.4-1 SPACE TUG SIDEWALL THERMAL PROTECTION SYSTEM WEIGHTS



DS-17142

FIGURE 4.6.1.0-1 ASTRIONIC STUDY APPROACH

4.6.1 (Continued)

in prior Reference 3.3.0.0-1) astrionic module weights and weight increases (deltas) to this baseline for a final system definition. A radiation impact study was performed to determine if repeated passes through the Van Allen radiation belt would present problems. Study outputs are as indicated on Figure 4.6.1.0-1.

Section 4.6.2 of this report defines the study groundrules and guidelines and Section 4.6.3 gives a summary of the study results and conclusions. Sections 4.6.4 through 4.6.8 present the detailed analyses performed for the navigation, configuration, redundancy, power and radiation areas during this study. Sections 4.6.9 and 4.6.10 summarize the recommended future study effort to enhance the present study. Appendices B, C and D are included for related study data.

4.6.2 Astrionic System Study Groundrules and Guidelines

The following groundrules and guidelines were used for this study:

- o The Space Shuttle will be used to deliver and retrieve the Space Tug from low earth orbit.
- o The basic Tug configuration will have minimal changes to apply aerobraking components.
- o The geosynchronous payload round trip mission was used as the baseline mission to conduct the aerobraking analysis.
- o The aerobraking mode examined in this study was limited to unmanned missions.
- o The astrionics system proposed by IBM in "Preliminary Definition of an Astrionics System for Space Tug Mission Vehicle Payload", Final Report, was used as the initial baseline from which aerobraking astrionics requirements will be defined.
- o The technology used for the Tug astrionic system was Shuttle era technology.
- o The Tug was based and maintained on the ground for this aerobraking study.
- o The Space Tug astrionic module was designed to minimize the need for ground support during the active mission.
- o The astrionic module was of modular design to provide the capability of automatic operation.
- o The astrionic system was designed to be self-sustaining.
- o The astrionic system was designed to use Shuttle related components where possible.
- o The astrionic system was designed to be capable of automatic rendezvous and docking operations.
- o The 180-day quiescent mode impact was not considered as a part of this aerobraking study.

4.6.3 Astrionic System Analysis Summary and Observations

The major items for consideration in the astrionic system analysis were the weight delta penalties associated with aerobraking and the analysis of navigation uncertainties. A summary of the results is included in this section. The detailed results for the astrionic system study are presented in the following sections and in the appendices.

4.6.3.1 Astrionic System Aerobraking Weight Deltas

To provide a basis for the weight delta analysis, the basic Tag configuration (see prior Reference 3.3.0.0-1) was updated and weight penalties associated with long-duration space-based modes were deleted. The resulting astrionic system configuration for a basic 60-hour mission with aerobraking weighed approximately 1960 pounds. Four areas were evaluated for weight delta impacts: Power; redundancy; radiation; and navigation sensors.

The power analysis showed that for a 1 kw nominal astrionic system power load, with power generated by fuel cells, approximately 1.5 pounds of H_2/O_2 and tanks are required for each hour of aerobraking mission time required.

The navigation sensor analysis indicated that the same complement of equipment is required for all mission durations and that no equipment other than redundant components is added or deleted as the mission time increases. Therefore, no weight delta is imposed by navigation.

The radiation impact analysis also indicated that no weight deltas are added due to increased aerobraking mission time.

The redundancy analysis indicated that additional components and hardware must be added to the basic astrionic system configuration as the mission time increases to maintain a 99% mission success probability.

In summary, power and redundancy provide the delta weight impacts required for aerobraking. The weight impacts of these items and the total weight deltas based on aerobraking mission time are summarized in Figure 4.6.3.1-1.

4.6.3.2 Navigation Analysis

The navigation analysis was performed to determine the navigation sensors required for the aerobraking mission and to define the navigation accuracies obtained with these sensor combinations. The IMU, star tracker, landmark tracker, horizon sensor and laser radar were selected as the required navigation sensors. It was determined that the same complement of hardware was required for all aerobraking mission durations, and that only redundant hardware would be added to achieve reliability.

An IMU is required to provide an inertial reference. Because of platform drift over extended periods of time, a star tracker is required for attitude update and, in addition enhances the accuracy of navigation updates.

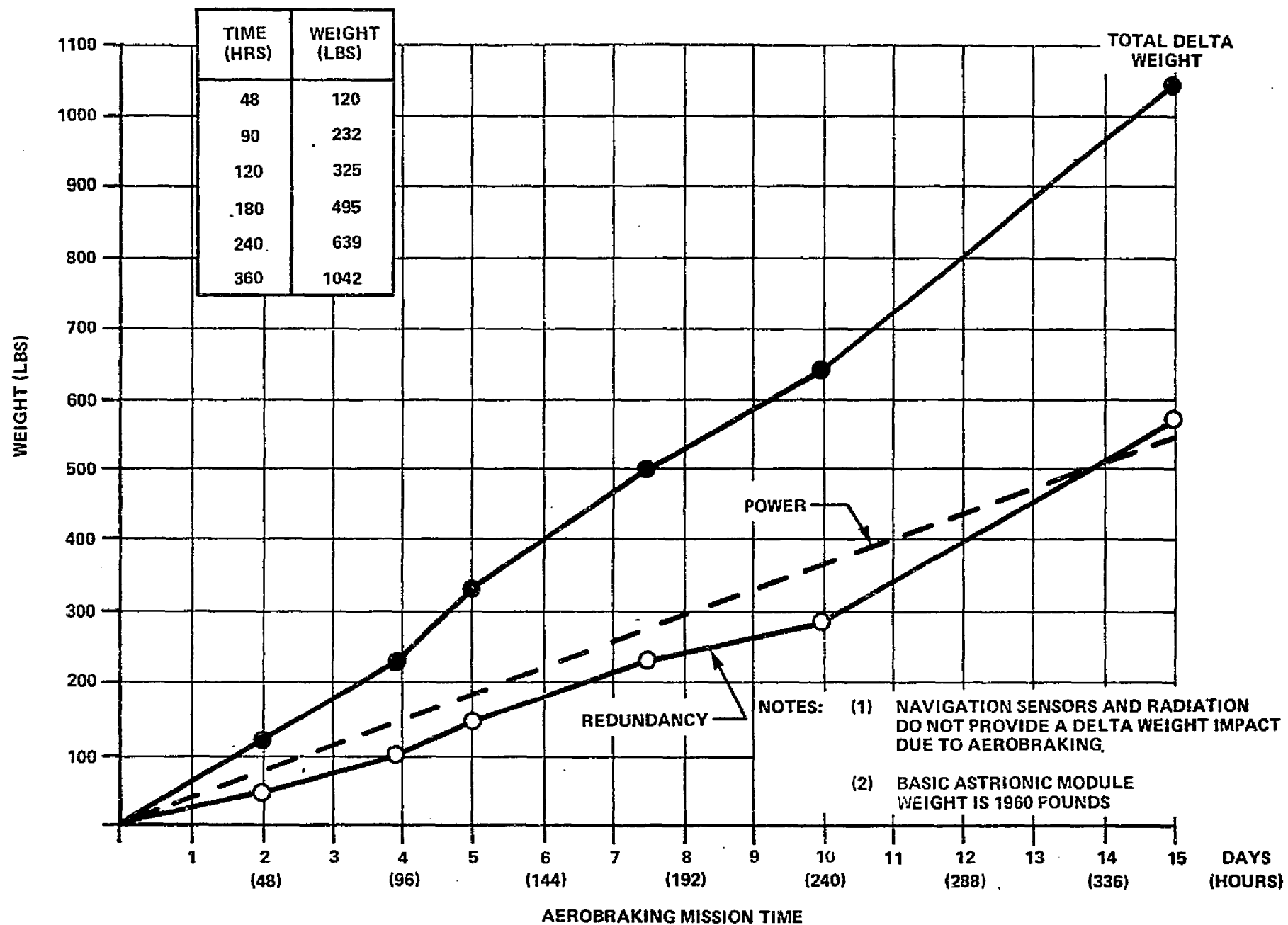


FIGURE 4.6.3.1-1. ASTRIONIC SYSTEM AEROBRAKING WEIGHT DELTA SUMMARY

4.6.3.2 (Continued)

The landmark tracker is required for precision navigation updates and, since the effective range of the landmark tracker is limited to low altitudes, a horizon sensor is required for navigation updates at high altitudes. The laser radar is required for automatic rendezvous and docking but was not considered in the navigation analysis.

The results of the navigation analysis indicated that the navigation perigee uncertainties were rather insensitive to configurations (basic or flared Tug). A summary of the perigee uncertainties for the basic configuration is shown in Figure 4.6.3.2-1. This figure shows that the maximum 1σ uncertainty (first pass of mission) expected for the 2 to 15 day missions (10 to 85 passes) are less than .35 NM and the steady state values are in the order of 0.05 NM. It should also be noted that the navigation perigee uncertainties are generally smaller for the longer duration mission because of the decreased atmospheric perturbations.

4.6.3.3 Radiation Impacts Analysis

The impacts of repeated passes through the Van Allen radiation belt for the aerobraking mission do not appear significant at this time. Assuming a vehicle skin thickness of approximately .090 inches of aluminum, no problems appear for times up to 10 days. The 15 day analysis indicates that care must be taken in the selection of silicon transistors in the electronics. Also, additional shielding, included as part of the component packaging, would decrease the effects of radiation.

4.6.3.4 Observations and Conclusions

The following salient observations were made during the study. It should be noted that these observations are for the astrionic system only.

- o Additional reactant and tanks for power and additional components to maintain acceptable astrionic system reliability are the prime contributors to weight increases to the astrionic system due to aerobraking.
- o Astrionic system weight increases as aerobraking mission duration increases. Therefore, minimum weight deltas are obtained by minimizing aerobraking mission time.
- o Long duration space basing of the Space Tug astrionic system produces significant weight penalties for the astrionic module because of additional thermal conditioning, shielding and power requirements.
- o The autonomous navigation configuration used for this study can limit radial perigee uncertainties to less than 0.35 NM (1σ) for initial passes and to the region of 0.05 NM (1σ) steady state.
- o Uncertainties are generally greater for the initial perigee passes of shorter duration missions because of increased atmospheric density and more sensitivity to orbital parameters.

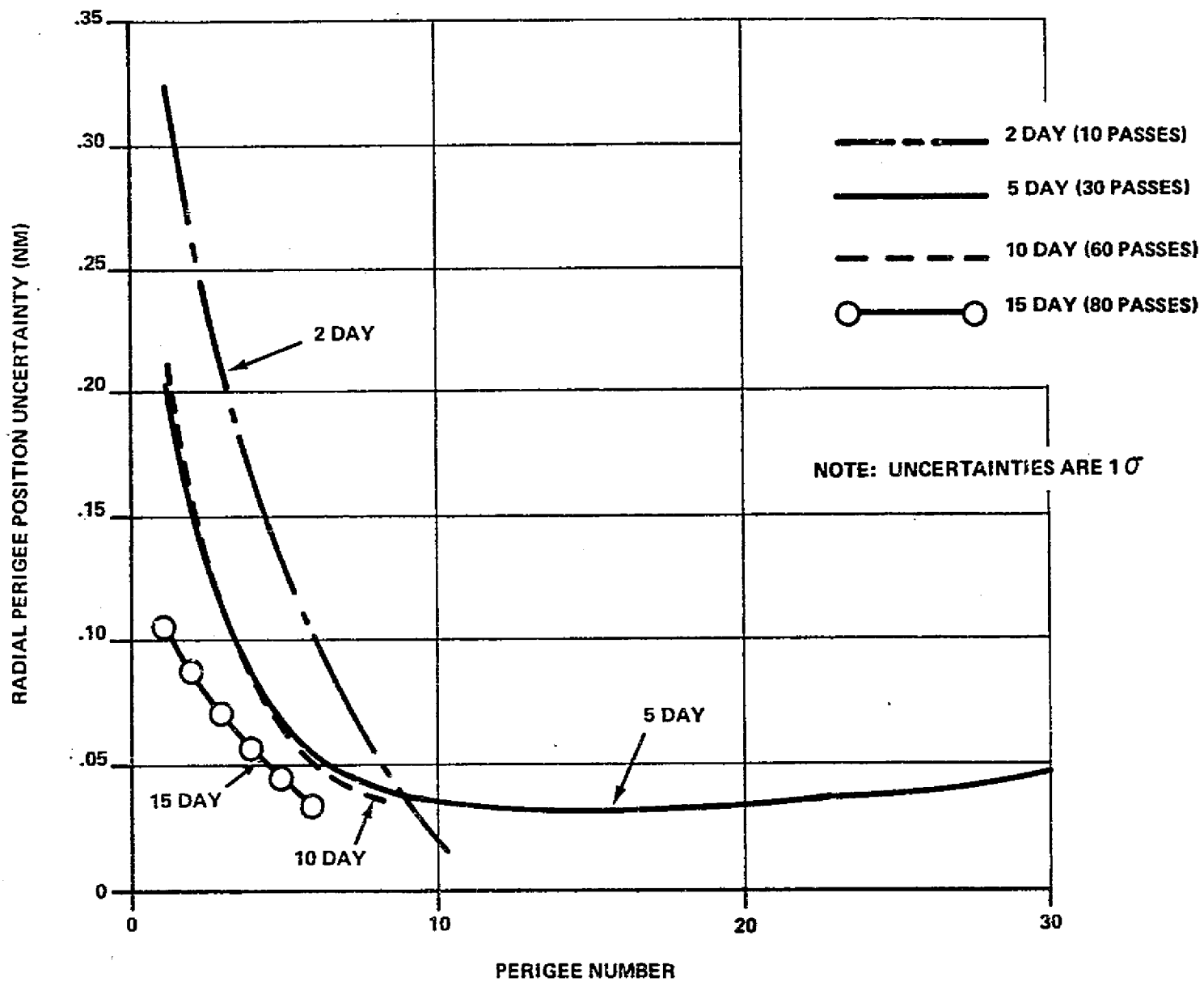


FIGURE 4.6.3.2-1. PERIGEE NAVIGATION POSITION UNCERTAINTY SUMMARY

4.6.3.4 (Continued)

- o In general, better navigation accuracy is obtained for longer duration missions on comparable perigee passes.
- o Autonomous navigation in synchronous orbit can limit navigation uncertainties to a RSS steady state accuracy of 5 NM (1σ) and 2 ft/sec (1σ) using a horizon sensor.
- o The perigee radial position uncertainties for the 5, 10 and 15 day missions for both the non-flared and flared Tug configurations are essentially the same. The perigee uncertainties for the 2 day mission are slightly higher for the non-flared Tug configuration.
- o Navigation updates after perigee and at higher altitudes are required to limit uncertainties during those periods and to prevent excessive perigee uncertainties on subsequent passes.
- o Radiation impacts to electronics by the Van Allen radiation belt appear insignificant. The impact increases as the aerobraking mission duration increases.

4.6.4 Navigation Accuracy Analysis

4.6.4.1 Introduction

This section describes the selection of navigation sensors required, the navigation accuracy attainable, trajectory correction burn impacts, and sensitivities associated with navigation imposed by the aerobraking maneuver. Navigation sensor selection was based on the following criteria:

- o Navigation sensor availability within the Shuttle era.
- o Consideration of navigation sensor accuracy.
- o Minimizing vehicle delta velocity correction requirements to reduce RCS fuel consumption.

The navigation scheme selected for the Space Tug employs a Kalman filter (see Appendix B for brief description of Kalman filtering) to process recursively navigation sensor measurement data to obtain an optimal estimate of the vehicle "state". Selected combinations of navigation components including Inertial Measuring Unit (IMU), star-tracker, horizon sensor, sun sensor, and landmark tracker were considered as candidates for the Tug mission.

Data inputs to the study were:

- o Preliminary trajectory data on the aerobraking maneuver from The Boeing Company.
- o Vehicle configuration parameters from The Boeing Company.
- o 1962 Standard Atmosphere Density Model.
- o Navigation sensor definition by IBM.
- o Preliminary estimates of the mean and range of density of the earth's atmosphere over an 11-year period (obtained from The Boeing Company).

4.6.4.1 (Continued)

The navigation analysis assumed that the perigee was allowed to decay at the expected rate, with a constant perigee not maintained. Navigation uncertainties were calculated for these orbits and the uncertainties shown in this section are all 1σ . No correction burns were factored into the navigation analyses except those discussed in Section 4.6.4.6.

4.6.4.2 Navigation Sensors

The hardware elements that were considered as candidates for the Space Tug aerobraking navigation subsystem are as follows, with detailed descriptions given in Appendix D.

- o IMU - Typified by Kearfott KT-70

The IMU consists of two two-degree-of-freedom gyros for attitude reference and three orthogonal accelerometers for velocity increment measurement.

- o Star Tracker - Typified by ITT AEROBEE 150A

The Star Tracker is a strapped down optical sensor using electronic gimbaling to determine star positions within an eight-degree field-of-view (FOV).

- o Sun Sensor - Typified by Ball Brothers Design

The sun sensor is a strapped down optical sensor that determines the location of the sun vector relative to vehicle axes.

- o Landmark Tracker - Typified by the Westinghouse Design

This optical sensor measures tracking angles to earth features such as islands and lakes.

- o Horizon Scanner - Typified by the Lockheed Edge Tracker
(under development)

This horizon sensor is an infrared radiometer that scans the earth's horizon to determine the vehicle's local vertical.

A summary of the preceding navigation sensor accuracy characteristics is shown in Figure 4.6.4.2-1.

It should be noted that a ground network was not considered for this study due to the desirability of having autonomous navigation. However, previous study experience indicates that if a ground network, such as MSFN, were available, its update capability would be comparable to that described for the landmark tracker/star tracker autonomous sensor combination.

IMU (KEARFOTT KT-70)

- o 0.02 DEG/HR DRIFT
- o .003% SCALE FACTOR

LANDMARK TRACKER (WESTINGHOUSE)

- o 100 ARC SEC ANGULAR MEASUREMENT UNCERTAINTY

HORIZON SENSOR (LOCKHEED)

- o 216 ARC SEC HORIZON AND ATTITUDE UNCERTAINTY

STAR TRACKER (ITT)

- o 36 ARC SEC ALIGNMENT

SUN SENSOR (BALL BROTHERS)

- o 120 ARC SEC ANGULAR MEASUREMENT UNCERTAINTY

Figure 4.6.4.2-1. Typical Navigation Sensor Characteristics

4.6.4.3 Analytical Tools

The following computer programs were used throughout the analysis:

- o Autonomous Navigation Simulation (ANS)

The Autonomous Navigation Simulation Program simulates autonomous navigation along a Keplerian orbit as performed by a Kalman filter using data from selected combinations of horizon sensor, star tracker, landmark tracking telescope, radar altimeter and range finder (laser). A detailed description of this program is contained in Appendix C.

- o Inertial Platform Error Program (IPEP)

The Inertial Platform Error Program utilizes the normalized integral technique developed by George R. Pitman, Jr. (author of INERTIAL GUIDANCE) to propagate platform hardware errors during the powered phases of flight.

- o Tug Integration Program

This program is a six-dimensional orbital simulator that generates accurate orbital trajectories. The simulation is in single precision and utilizes a Runge Cutta 6th order integration routine, a PRA 63 or 1962 standard reference atmospheric model and a gravitational potential model of an oblate spheroid. The program calculates and prints the orbital trajectory parameters. A detailed description of this program is contained in Appendix C.

4.6.4.4 Synchronous Orbit Navigation Uncertainty Analysis

Previous studies performed by IBM (Astrionic System Study for Saturn S-II Expendable Second Stage - see Reference 4.6.4.4-1) analyzed the navigation accuracy attainable using various navigation sensor configurations during a 100 NM parking orbit.

The navigation position and velocity uncertainties for the 100 NM parking orbit are as follows:

<u>Position</u>	<u>Navigation Uncertainties (1σ)</u>
Radial (R)	320 ft
Tangential (T)	370 ft
Normal (N)	360 ft
<u>Velocity</u>	
Radial (R)	0.53 ft/sec
Tangential (T)	0.37 ft/sec
Normal (N)	0.42 ft/sec

4.6.4.4 (Continued)

The 100 NM parking orbit uncertainties and the errors generated during the burn to synchronous altitude were propagated to synchronous orbit altitude. These uncertainties were combined with the final orbit insertion uncertainties to obtain a Root-Sum-Square (RSS) uncertainty for synchronous orbit insertion. These uncertainties are as follows:

<u>Position</u>	<u>Navigation Uncertainties (1σ)</u>
Radial (R)	54,000 ft
Tangential (T)	52,000 ft
Normal (N)	3,300 ft
<u>Velocity</u>	
Radial (R)	7.2 ft/sec
Tangential (T)	2.0 ft/sec
Normal (N)	1.0 ft/sec

These values were used as the initial uncertainties for synchronous orbit coast. Accuracies for a spectrum of typical sensors were input to the ANS program and a navigation uncertainty analysis performed. The results are shown in Figure 4.6.4.4-1. These results indicate that for the accuracies derived from the horizon sensor/star tracker combination ("worst case" accuracy), an RSS position accuracy of about 5 NM (1σ) and 2 ft/sec (1σ) can be achieved after 12 hours in orbit.

4.6.4.5 Aerobraking Descent Orbit Navigation Accuracy Analysis

This section analyzes the navigation accuracies attainable using the previously described navigation sensors during the aerobraking descent orbit mission phase. Two Space Tug vehicle configurations supplied by The Boeing Company (no flare and 60° flare configurations) and four different mission durations (2, 5, 10 and 15 days) were used to parametrically analyze the aerobraking navigation problem. In addition, a brief discussion of a one pass deorbit mission is included.

The aerobraking mission phase begins at the initiation of the synchronous orbit deboost burn. The delta velocity required to target for a perigee of approximately 50 NM and perform a plane change of 28° is approximately 6000 ft/sec. The IPEP program was used to determine the navigation uncertainties that accumulated during the deboost burn. These uncertainties were then RSS'ed with the navigation uncertainties obtained from the Synchronous Orbit navigation uncertainty analysis (Section 4.6.4.4). The

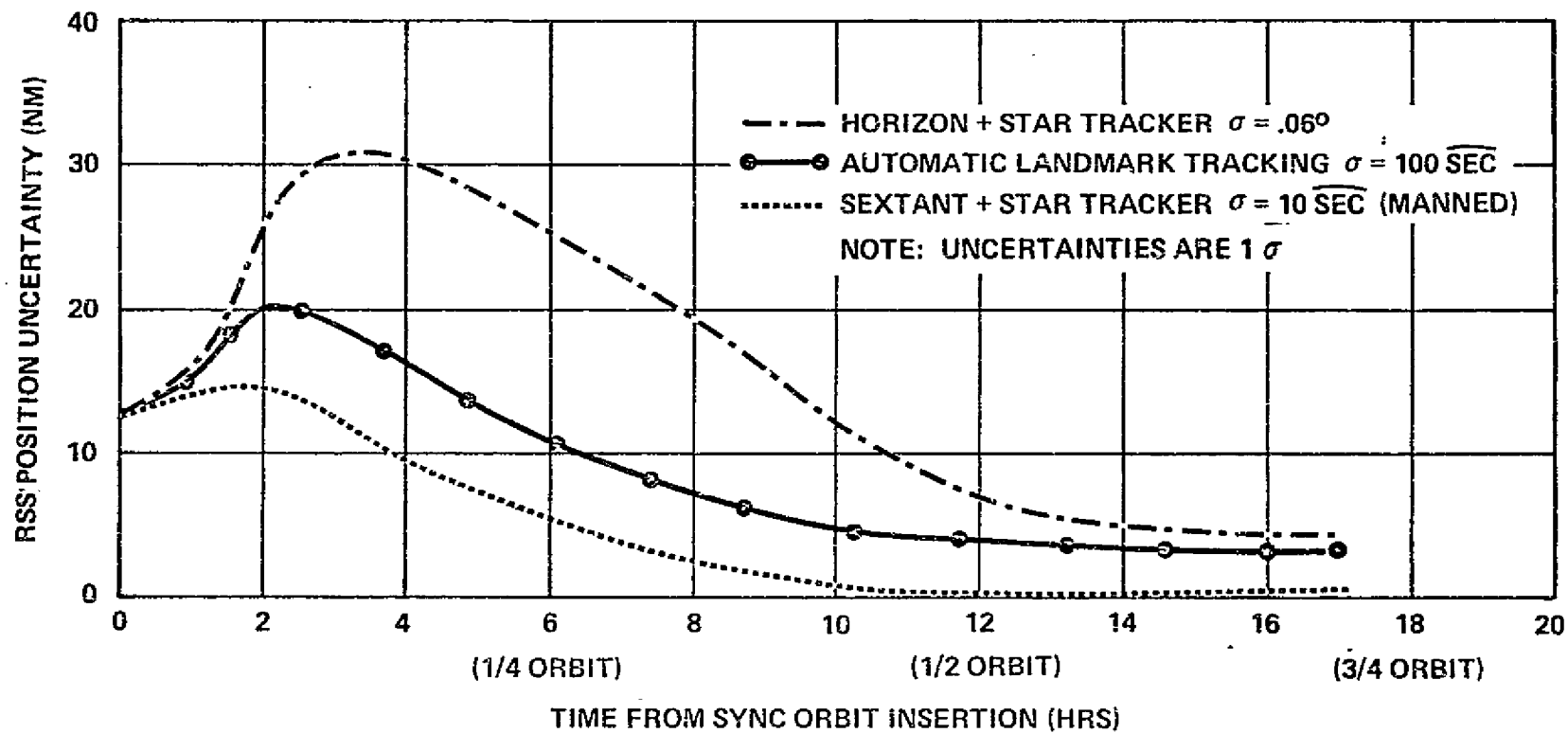


FIGURE 4.6.4.4-1 SYNC ORBIT ANALYSIS

4.6.4.5 (Continued)

resultant uncertainties at the end of the deboost burn were:

<u>Position</u>	<u>Navigation Errors (1σ)</u>
R	20,000 ft
T	20,000 ft
N	3,300 ft
<u>Velocity</u>	
R	3.3 ft/sec
T	.66 ft/sec
N	1.0 ft/sec

These RSS uncertainties were used as the initial navigation uncertainties for the onboard navigation program following the synchronous deboost burn.

A typical aerobraking mission navigation sensor observation schedule to provide a base for the navigation analysis was required and it was determined using the following criteria:

- o Observations would be made before and after perigee to refine the old trajectory for possible midcourse correction burns and define the new trajectory after passing through the atmosphere.
- o Observations would not be taken while passing through the atmosphere.
- o Time was allotted to perform delta velocity correction burns and attitude maneuvers prior to atmospheric entry.
- o The duration of the navigation sightings was limited to the navigation instrument operational range.
- o Low deadband and prolonged attitude stabilization requirements should be minimized.

If a sun sensor were used, the attainment of the attitude requirements for "fine" sensing of the sun vector would require prohibitive amounts of RCS fuel. In addition, the sun could be occulted by the earth or moon thus preventing its use as a navigation sensor. This is particularly true in the vicinity of the earth where the sightings are designed to occur. Because of these considerations and the update criteria, the sun sensor was eliminated from consideration as a candidate navigation sensor.

4.6.4.5 (Continued)

Investigation of the navigation accuracy attainable using only a horizon sensor for navigation updates resulted in navigation uncertainties of ± 9 NM on the first pass through perigee. Such inaccuracies at perigee were unacceptable for thermal reasons. Therefore, the horizon sensor was eliminated as the prime navigation update sensor. However, it was later found to be required to limit uncertainties near apogee and was added to the navigation subsystem.

Thus, the landmark tracker was determined to be the best available sensor for obtaining navigation updates. However, the operational range of the landmark tracker is limited to the order of 4,000 NM. An update profile was selected to assure acceptable operation of the landmark tracker and to provide time for midcourse corrections or any required maneuver after the completion of navigation updating. The landmark tracker observations began approximately 1800 seconds prior to perigee (to assure tracker's maximum range limit not exceeded) and were stopped approximately 500 seconds prior to perigee (to allow time for RCS midcourse corrections prior to encountering the sensible atmosphere).

An analysis of the two-day (ten-orbit) aerobraking mission was performed using the previously described observation schedule for the landmark tracker. This analysis revealed that both the apogee and perigee uncertainties grew unbounded until the navigation uncertainties during the third perigee were larger than typical trajectory errors which would cause the vehicle to re-enter. Therefore these uncertainties were unacceptable. Investigation revealed that the Kalman filter had to be reinitialized after exiting from the earth's atmosphere on each pass because the vehicle has then attained a new orbit. Since the Kalman filter maintains knowledge of the past orbit, this knowledge prevents proper convergence of the filter and the filter must be reinitialized each orbit after leaving the atmosphere.

After incorporating filter reinitialization on each pass, further analysis revealed that navigation uncertainties grew prohibitively during the interval when no landmark tracker measurements were made. To limit the growth of navigation uncertainties during this interval, landmark tracker observations were added from approximately 300 seconds after perigee to approximately 1700 seconds after perigee. In addition, horizon sensor measurements were included in the filter computations from apogee until the reception of landmark tracking measurements at approximately 1800 seconds prior to perigee. The final navigation sensor measurement update history developed from the previous analysis is shown in Figure 4.6.4.5-1.

Basic (No Flare) Tug Navigation Analysis

The initial navigation analysis was performed for the basic (no flare) Boeing Tug configuration. Analyses were performed for the 2, 5, 10 and 15 day mission durations. Results for the 11 day (60 passes) mission were considered typical of the results for all mission durations considered and are shown in detail to indicate the type of analysis performed during this study. All cases considered are summarized in this section.

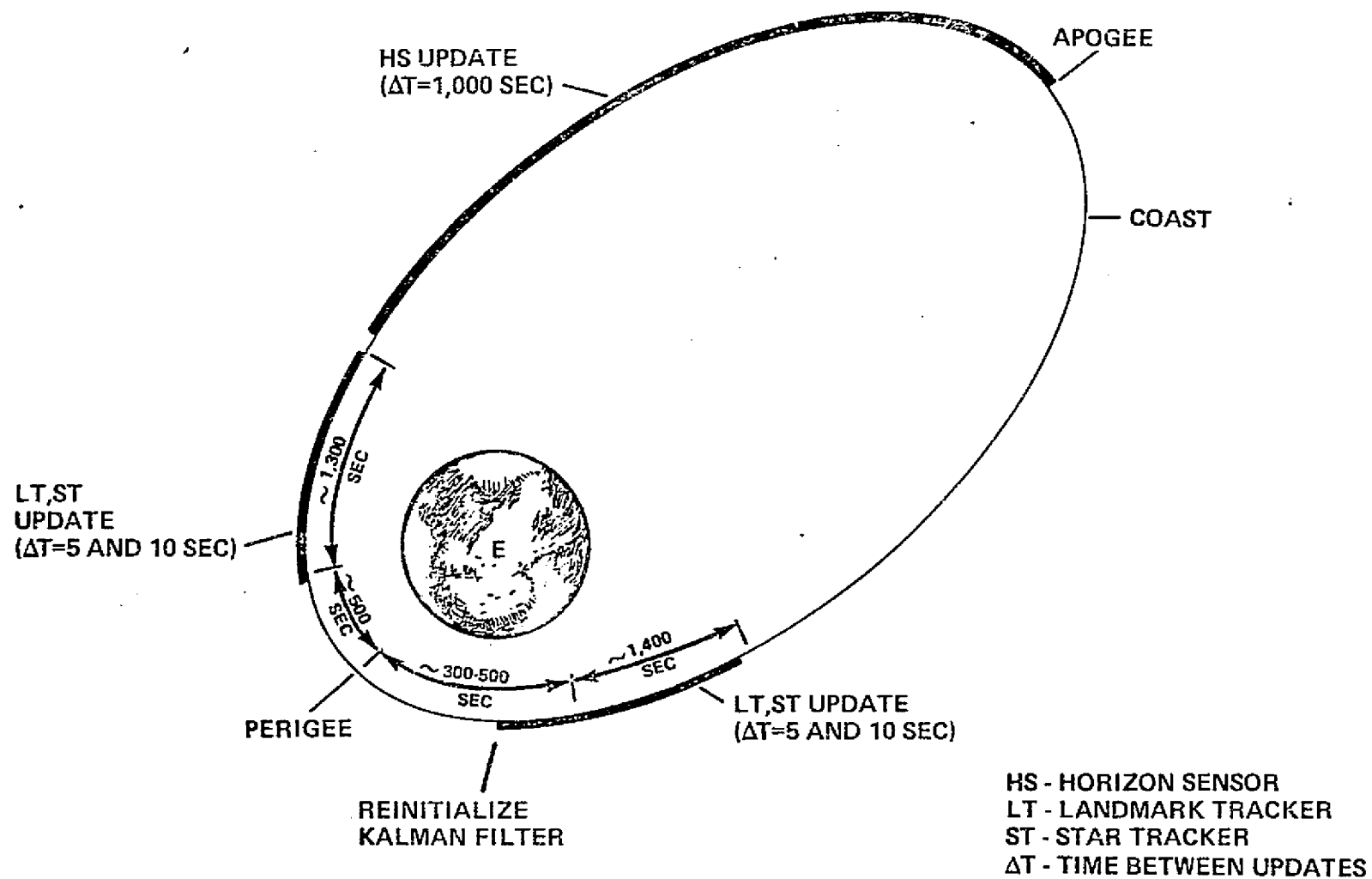


FIGURE 4.6.4.5-1 NAVIGATION UPDATE HISTORY

4.6.4.5 (Continued)

Using the previously defined navigation update history, the results of navigation analysis for the first five orbits of the 11 day (60 passes) mission are presented in Figure 4.6.4.5-2. The figure depicts the RSS position uncertainty as a function of time from deboost initiation.

As the figure shows, uncertainties build up prior to apogee, or until the horizon sensor can begin converging the uncertainties, after which the horizon sensor updates then reduce the uncertainties to the region of 5 NM as the vehicle approaches perigee. The landmark tracker then quickly reduces the uncertainties and limits them prior to and following perigee. After the range of the landmark tracker is exceeded, the uncertainties grow until the process described above is repeated.

A plot of the RSS position uncertainty at perigee for the 11 day (60 pass) mission navigation accuracy analysis using the basic Tug is shown in Figure 4.6.4.5-3. The RSS position at perigee on the first pass is 0.24 NM decreasing to less than 0.075 NM (1σ) steady state.

The basic Tug aerobraking navigation analysis was expanded to include the 2, 5, 10 and 15 day mission.

Figure 4.6.4.5-4 provides a comparison of the RSS apogee position uncertainties achieved for all the reference missions. The major conclusions that can be derived from observations of the data presented on the graph are:

- o The second apogee navigation uncertainty is the largest for most missions.
- o After the second apogee, the apogee navigation uncertainties decrease rather rapidly to a fairly constant value.
- o Initial apogee uncertainties reduce as the mission duration increases.
- o The final apogee uncertainties for all missions are less than 1 NM.

Figure 4.6.4.5-5 provides a comparison of the perigee radial position uncertainties achieved for all the basic Tug reference missions. The major observations derived from the figure are:

- o The perigee uncertainties of the 2 day mission are consistently higher than those for the longer duration mission because of increased atmospheric drag at lower altitudes.
- o The 5, 10 and 15 day perigee position uncertainties are essentially those achieved by the landmark tracker because of reduced atmospheric drag orbital perturbation at higher altitudes. Because of this, the difference in perigee position

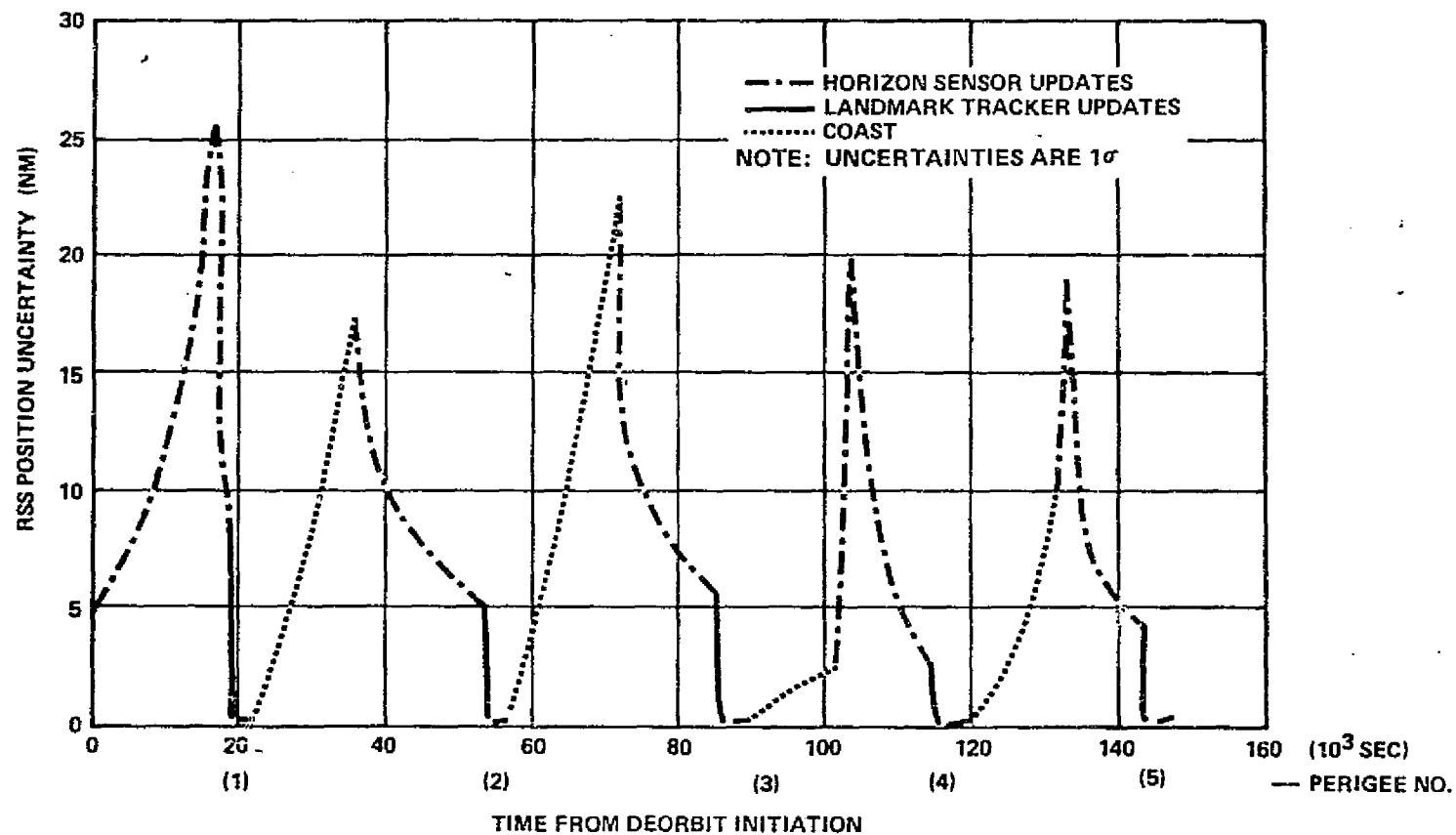


FIGURE 4.6.4.5-2 NAVIGATION POSITION UNCERTAINTIES (10 DAY - 60 PASS)

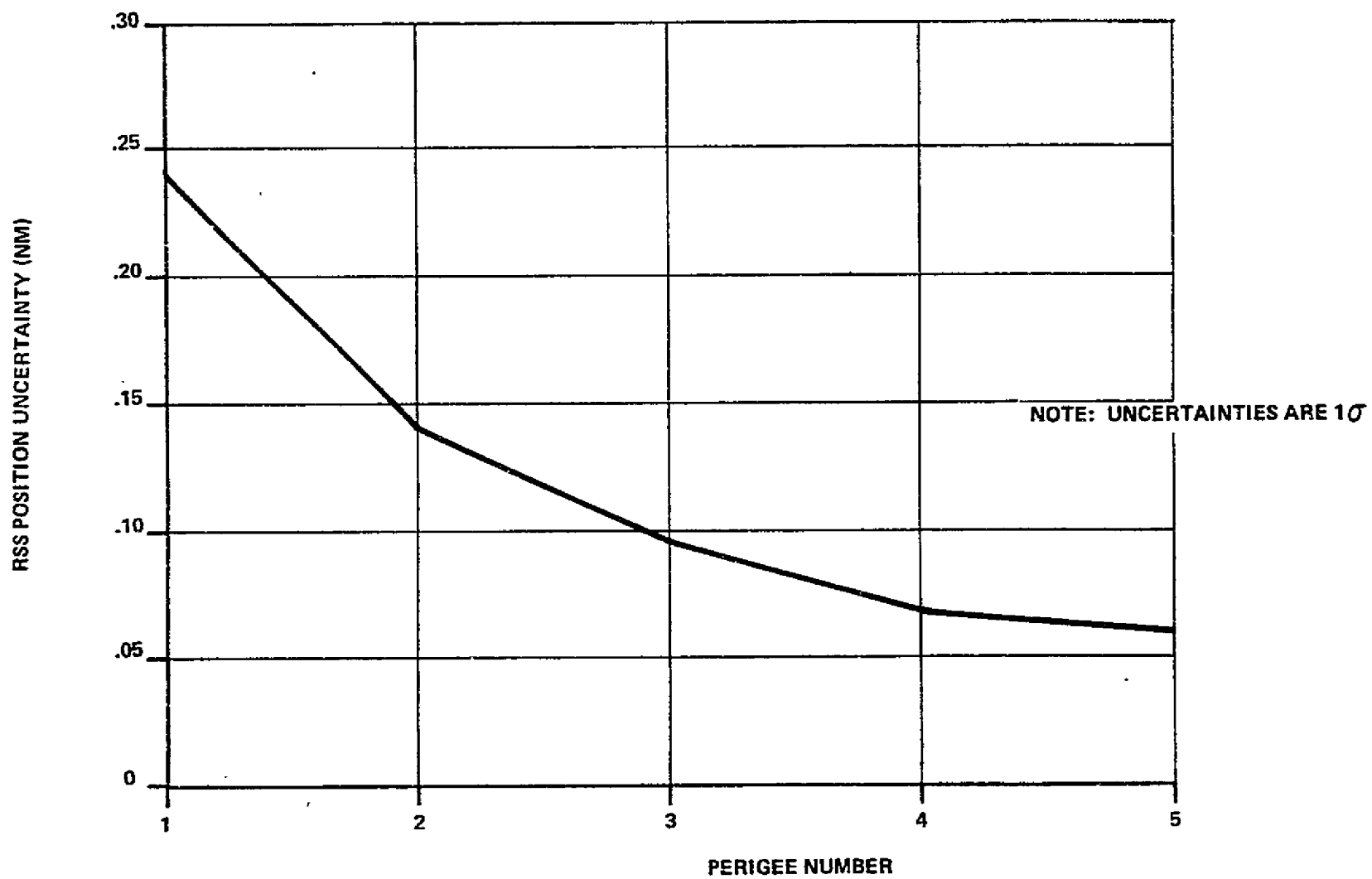


FIGURE 4.6.4.5-3. RSS PERIGEE POSITION UNCERTAINTY (BASIC TUG CONFIGURATION-60 PASS)

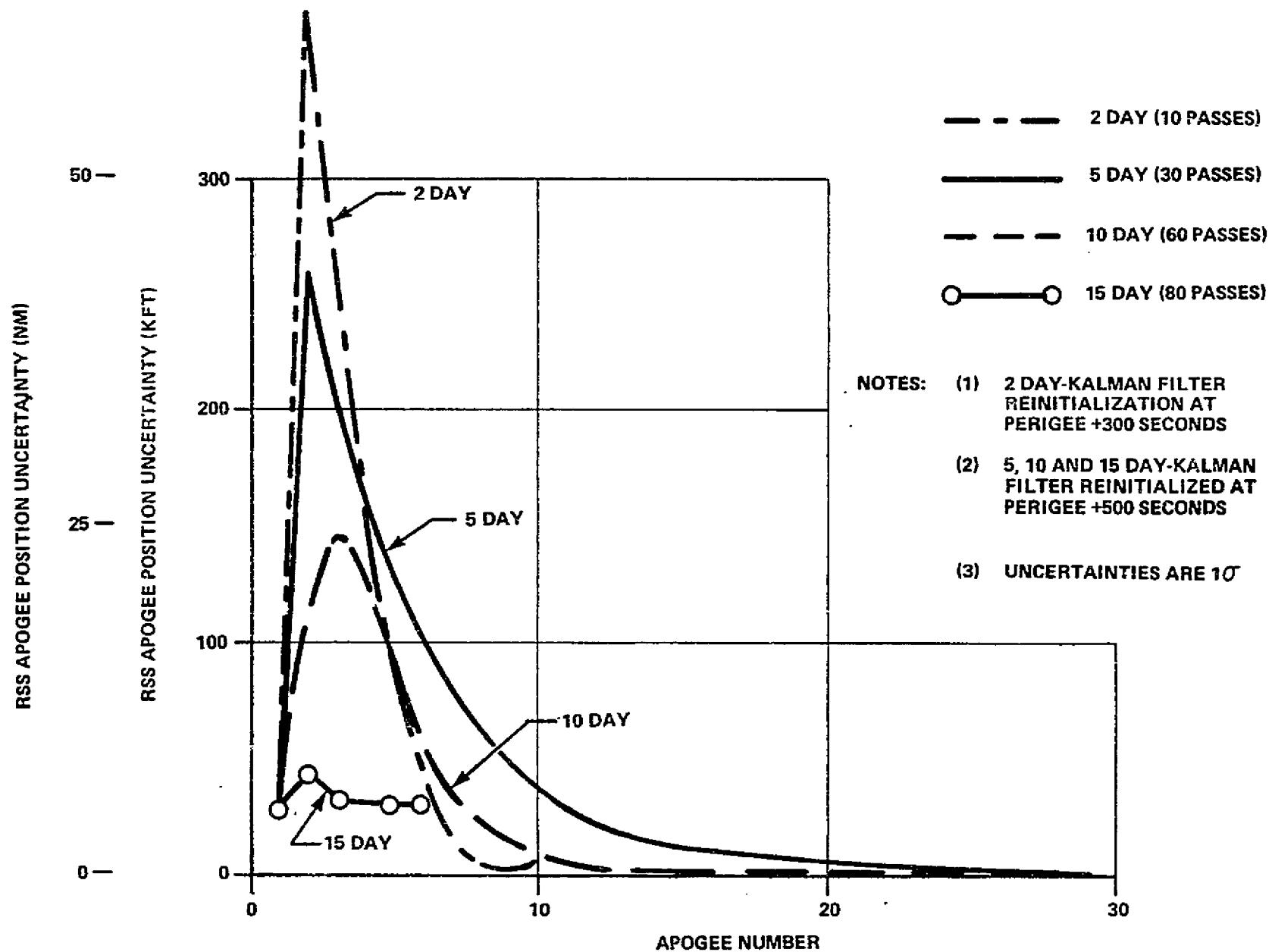


FIGURE 4.6.4.5-4. RSS APOGEE POSITION UNCERTAINTIES (BASIC TUG CONFIGURATION)

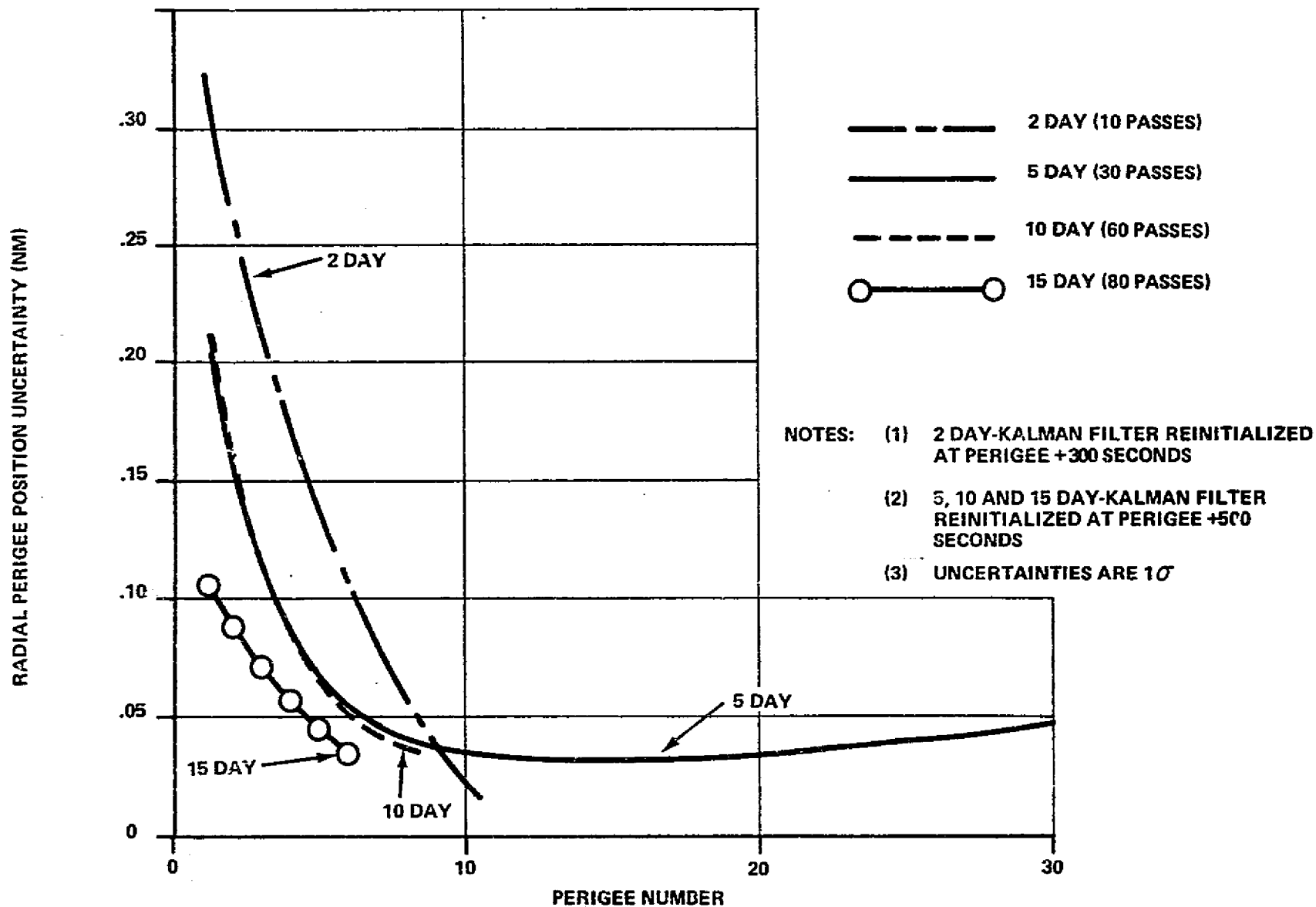


FIGURE 4.6.4.5-5. RADIAL PERIGEE POSITION UNCERTAINTIES (BASIC TUG CONFIGURATION)

4.6.4.5 (Continued)

uncertainties is negligible after approximately 10 passes regardless of mission duration.

- o The perigee uncertainties for the longer duration missions appear to stabilize around 0.04 NM after about 10 orbits.
- o During the final passes of the longer missions when the vehicle is in the atmosphere longer, the perigee uncertainties increase slightly.

In summary, the apogee and perigee uncertainties are greater during the first few passes and reduce to a minimum at approximately 10 orbits. The magnitudes of the final apogee uncertainties are small, permitting precise navigation at the time of orbit circularization.

Flared Tug Configuration Navigation Analysis

The initial conditions, mission timelines and navigation sensor configurations of the 60° flare Tug configuration analysis are identical to those used for the basic Tug (no flare) configuration navigation analysis, thus allowing the same rate of decay at higher altitudes.

The flared Tug aerobraking navigation analysis results are depicted in Figures 4.6.4.5-6 and 4.6.4.5-7. The major observations derived from the figures are:

- o The apogee and perigee uncertainties of the 2 day mission are significantly lower for the flared configuration than for the basic (no flare) Tug configuration due to the decreased atmospheric density and orbital state vector sensitivities at higher altitudes.
- o The perigee errors for both the basic and flared Tug configurations for the longer duration missions are essentially the same.
- o The apogee errors for the longer duration missions for the flared configuration decay slower.

One Pass (1/4 Day) Mission Aerobraking Impacts

The 1/4 day (1 orbit) mission was not considered in the basic navigation analysis. However, a "quick look" assessment was made to determine some of the impacts expected if a one orbit aerobraking deboost mission were considered. Using the previously discussed navigation update history and navigation sensors, the navigation accuracy achieved for the one pass mission is shown in Figure 4.6.4.5-8.

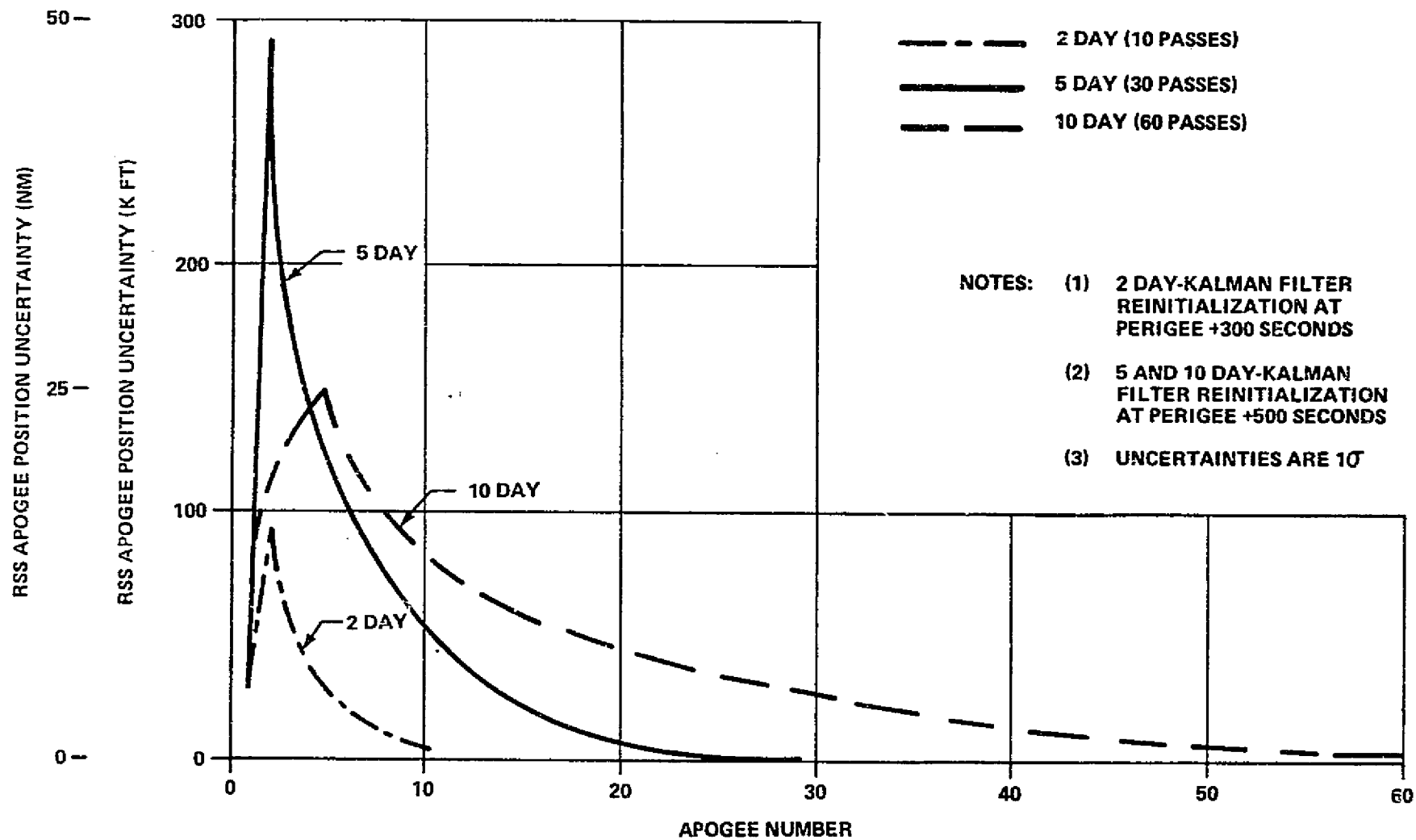


FIGURE 4.6.4.5-6. RSS APOGEE POSITION UNCERTAINTIES (FLARED TUG CONFIGURATION).

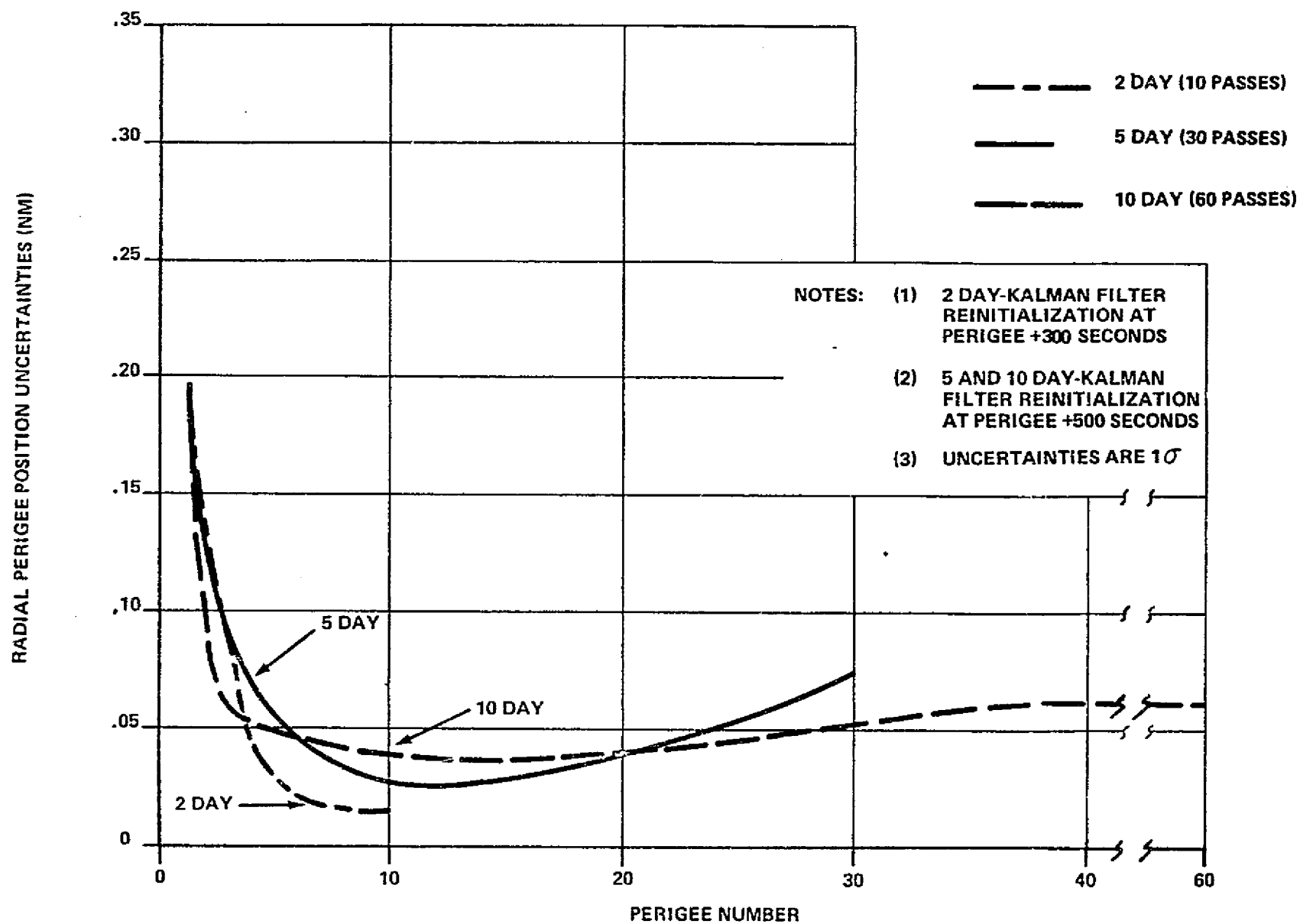


FIGURE 4.6.4.5-7. RADIAL PERIGEE POSITION UNCERTAINTIES (FLARED TUG CONFIGURATION)

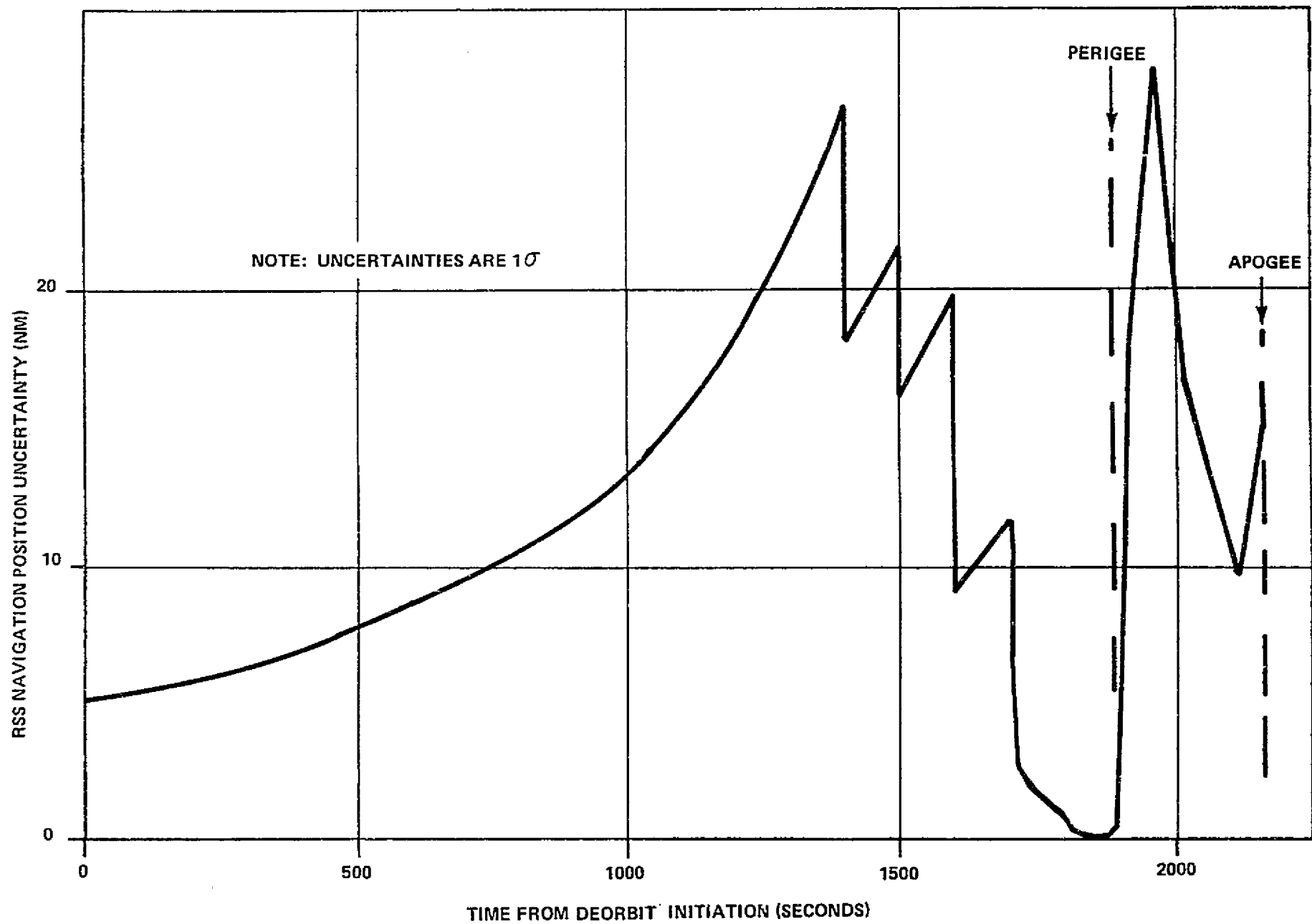


FIGURE 4.6.4.5-8. ONE PASS NAVIGATION POSITION UNCERTAINTIES

4.6.4.5 (Continued)

The navigation accuracies from deorbit initiation to the end of landmark tracking are similar to those of the other missions (2, 5, 10 and 15 days) during the first pass. The radial position error of .35 NM is near that achieved at the first pass perigee of the 2 day (10 passes) mission. However, the growth of navigation uncertainties is very great after perigee. As a result, at filter reinitialization, the navigation uncertainty is approximately 18 NM which is too large for the Kalman filter to handle using landmark tracker updates (see Reference 4.6.4.5-1). Therefore little improvement in the estimate of the orbit is achieved. After landmark tracking, the uncertainties again grow to a value of 15 NM at apogee (270 NM). Had horizon sensor updates been used instead of the landmark tracker after perigee, a navigation accuracy of about 5 NM could have been achieved at apogee. This is because the horizon sensor has a greater region of filter convergence than the landmark tracker. Therefore, if a one pass mission is contemplated, horizon updates should be used soon after perigee to limit the navigation uncertainties to 5 NM at apogee.

Another problem associated with the one pass mission is that the sensitivity of deboost velocity error to final second pass apogee altitude (Figure 4.6.4.5-9) is very large (approximately 10,000 NM/ft/sec). As the figure shows, small plus or minus ft/sec variations cause large variations in the apogee obtained following the initial perigee. In addition, a one pass mission requires a lower initial perigee altitude than the longer duration missions. Therefore, without any midcourse corrections, the chances of re-entering at the first perigee are great. Any midcourse corrections would require a high degree of accuracy to obtain the desired perigee. Figure 4.6.4.5-9 indicates that a .25 ft/sec error in deboost velocity could result in the vehicle re-entering on the first pass. Even the deboost velocity tailoff uncertainty (.5 ft/sec) is greater than deboost velocity error necessary to re-enter on the first pass.

The results of a preliminary study for the one pass mission indicate:

- o Accurate midcourse corrections are required prior to the first perigee. Even with these corrections, large apogee uncertainties are expected.
- o The large orbital sensitivities and large expected error imply that obtaining an apogee of 270 NM following the first perigee will be difficult. Therefore, delta velocity requirements to obtain a 270 NM circular orbit can be expected to be larger than those required for a longer duration mission in order to overcome these expected errors.

If the one pass mission is selected for further study, additional effort should be expended in the following areas to aid in the determination of

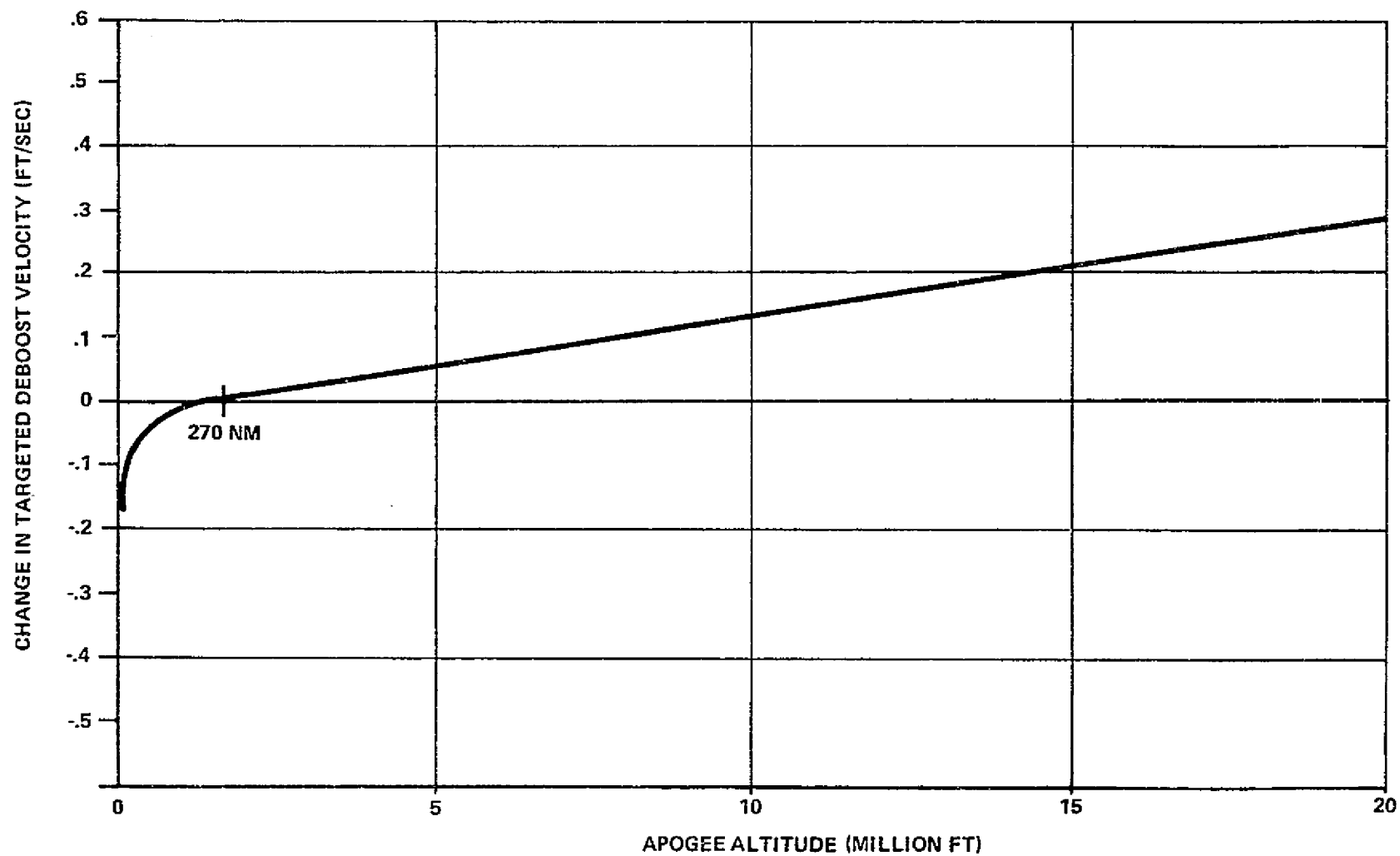


FIGURE 4.6.4.5-9. ONE PASS MISSION APOGEE ALTITUDE AS A FUNCTION OF DELTA DEBOOST VELOCITY (BASIC TUG CONFIGURATION)

4.6.4.5 (Continued)

feasibility of the one pass approach.

- o Navigation accuracy and associated midcourse correction capability to accurately hit initial target perigee.
- o Problems associated with uncertainties in obtaining a 270 NM apogee at the end of the first pass and solutions to the identified problem areas.

4.6.4.6 Trajectory Correction Burn Uncertainty Analysis

Guidance, navigation, atmospheric and burn errors cause the actual orbit of the aerobraking mission to deviate from the desired orbit. Thus, it is necessary to provide propulsive correction impulses to force the vehicle back to the desired profile. This can be achieved by two means:

- o Apply an impulse to place the vehicle in the original trajectory.
- o Apply an impulse to achieve a new orbit decay profile that achieves the desired end conditions, i.e., perigee altitude.

This section discusses the navigation uncertainties (1) for selected times during navigation updating, (2) for the error magnitudes expected using a ballistic trajectory, and (3) for the velocity increments necessary to correct for errors encountered. The above data is discussed for the first orbit, with selected discussions of the second orbit case. The analysis of the first two orbits represents the "worst case" situation because the greatest uncertainties in the atmosphere and navigation occur during these orbits. Both the knowledge of the actually achieved orbits and the knowledge of the earth's atmosphere improve with successive orbits.

Initial Deboost Trajectory Burn Analysis (5 Day - 30 Orbit Mission)

The major trajectory dispersion parameters of the initial deboost orbit are:

- o The deboost velocity increment uncertainty at synchronous orbit.
- o The initial state vector uncertainty in synchronous orbit just prior to the deboost burn.
- o The Kalman filter determined state vector uncertainties at the instant of application of the velocity correction burns.
- o The velocity correction burn guidance and navigation uncertainties.

A deboost burn navigation and guidance analysis was performed for a 5 day

4.6.4.6 (Continued)

(30 orbit) mission as follows:

- o The initial state uncertainties prior to the deboost burn were determined in the synchronous orbit navigation analysis previously discussed.
- o The deorbit burn uncertainties were computed using a desired burn profile as input to the IPEP program.

The results of this analysis are presented in Figure 4.6.4.6-1. The total navigation uncertainties in position and velocity due to the deboost burn are shown in the figure. These uncertainties when propagated to perigee will result in a perigee radial position uncertainty (1σ) of approximately 10,340 ft (1.72 NM).

For analysis purposes, it was assumed that a trajectory correction would be desired prior to the first perigee. Therefore, the velocity correction burn delta velocity and associated fuel consumption were computed at different portions of the deboost trajectory. Specifically, computations were made:

- o at the conclusion of horizon sensor updates
- o 500 seconds after initiation of the landmark tracker observations
- o after termination of the landmark tracker observations

The results of this analysis are presented in Figure 4.6.4.6-2. Shown on the same figure are the radial position uncertainties at perigee that result from (1) no delta velocity burn correction, and (2) delta velocity burn corrections applied to the previously specified times. Both sets of data were derived from the initial deboost uncertainties (see Figure 4.6.4.6-1), the navigation uncertainties determined during the descent, and the burn uncertainties.

Salient features of Figure 4.6.4.6-2 are:

- o It is not advantageous to provide a corrective burn prior to the use of the landmark tracker sensor.
- o Fuel consumption can be minimized if the corrective burn is performed as soon as the navigation data indicates an acceptable perigee can be obtained.

Second Orbit Burn Correction Analysis (5 day - 30 Orbit Mission)

The major trajectory dispersion parameters of the second orbit are:

- o The statistical uncertainties of the initial perigee pass.

PARAMETER	NAVIGATION POSITION UNCERTAINTY (feet)	NAVIGATION VELOCITY UNCERTAINTY (feet/sec)	RADIAL POSITION AT PERIGEE UNCERTAINTY (feet)
State Uncertainties			
R	20,000		6594.3
T	20,000		109.5
N	3,300		---
R		3.3	60.7
T		0.66	6225
N		1.0	
Inertial Navigation Uncertainties			
R	93		30
T	10		---
N	93		---
R		1.38	254
T		0.16	1510
N		1.38	---
Tailoff Uncertainty		0.5	4720
RSS	28,476.4	4.05	10,339.2

NOTE: Uncertainties are 1σ .

Figure 4.6.4.6-1. Deboost Burn Uncertainty Analysis

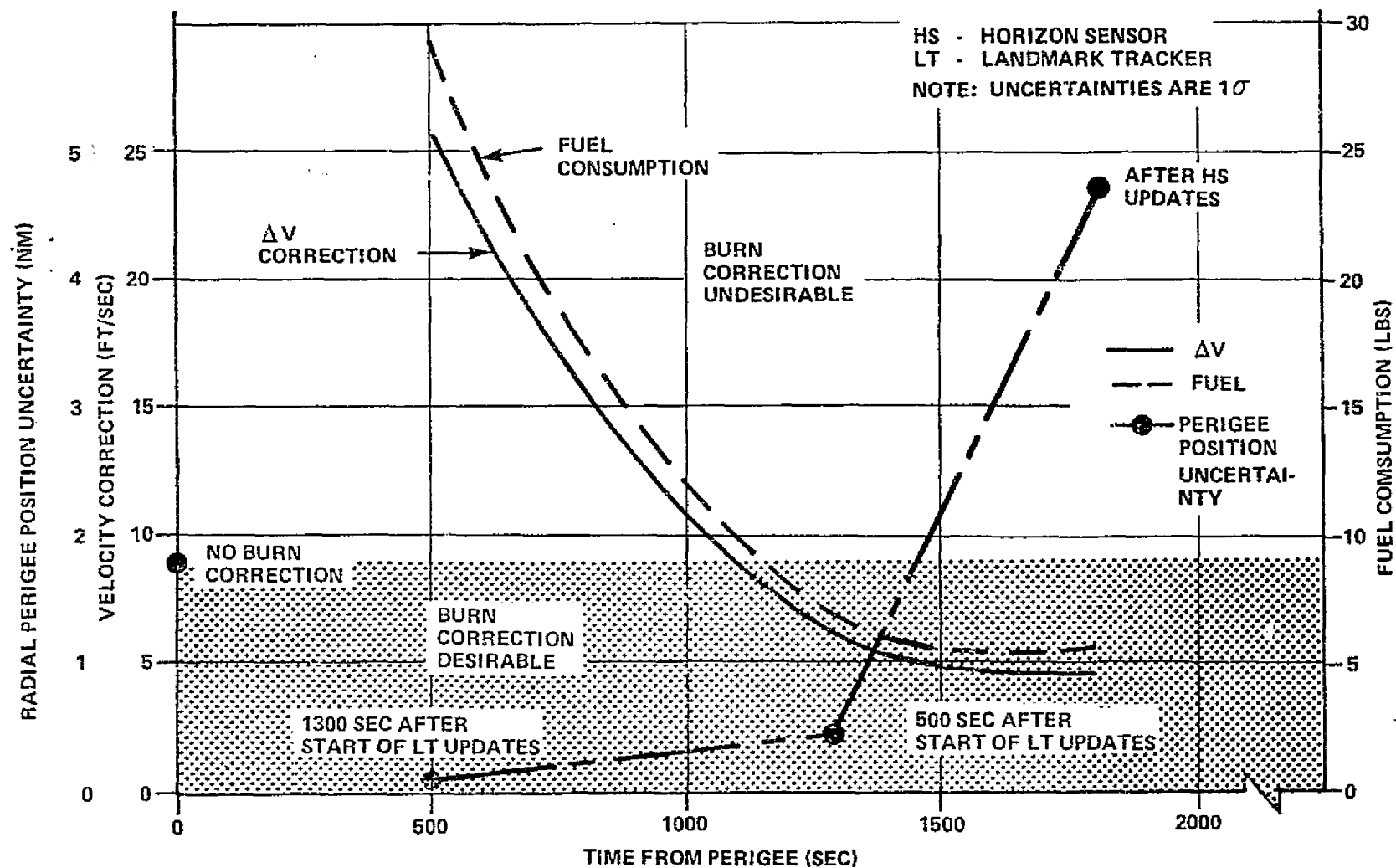


FIGURE 4.6.4.6-2. ORBITAL CORRECTION BURN, ΔV RCS FUEL CONSUMPTION, AND RADIAL PERIGEE POSITION UNCERTAINTY

4.6.4.6 (Continued)

- o The atmospheric uncertainties of the first pass through the atmosphere (as supplied by TBC).
- o The navigation uncertainties during the newly achieved orbit.
- o The trajectory correction burn uncertainties prior to the second perigee pass.

A ballistic trajectory propagation of first pass perigee uncertainties (atmospheric and state vector) was performed. Because of the relative magnitude of the propagated trajectory perturbations and the desirability of performing corrective burns at apogee, the second pass perigee uncertainties were computed as a function of the timing of a corrective burn. Selected times for corrective burns and resultant perigee uncertainties are plotted on Figure 4.5.4.6-3. The problem of performing a corrective burn prior to the second perigee is comparable to those for the initial deboost phase previously discussed.

4.6.4.7 Aerobraking Navigation Uncertainty Analysis Sensitivities

The aerobraking navigation subsystem, analyzed in previous sections utilized an observation schedule with specific navigation update rates, observation sample intervals, and observation sample initialization times. This section analyzes the navigation uncertainty sensitivities to changes in these parameters, specifically the parameters addressed are:

- o Variation of navigation update rates during landmark tracking.
- o Variation of Kalman filter reinitialization times after perigee.

Variation of Navigation Update Rates during Landmark Tracking

The landmark tracker navigation update rate during the landmark tracking interval prior to the first perigee was 5 and 10 seconds between samples. Samples close to perigee were taken every 5 seconds and were increased to 10 seconds between samples at higher altitudes. Other cases considered were 10 and 25 seconds between samples and 25 and 100 seconds between samples. The results of this analysis are shown in Figure 4.6.4.7-1. The figure indicates that the navigation uncertainty at the conclusion of landmark tracking is insensitive to navigation update rate during the landmark tracking interval prior to perigee.

The landmark tracker navigation update rate during landmark tracking after Kalman filter reinitialization subsequent to perigee was varied in the same manner. The results of this analysis are shown Figure 4.6.4.7-2. This figure indicates a distinct sensitivity to variations in navigation update rate during this landmark tracking interval. The effects of this sensitivity is illustrated in Figure 4.6.4.7-3 where the second orbit apogee and perigee are greatly affected. The figure indicates that a navigation update rate of 25 and 100 seconds between samples

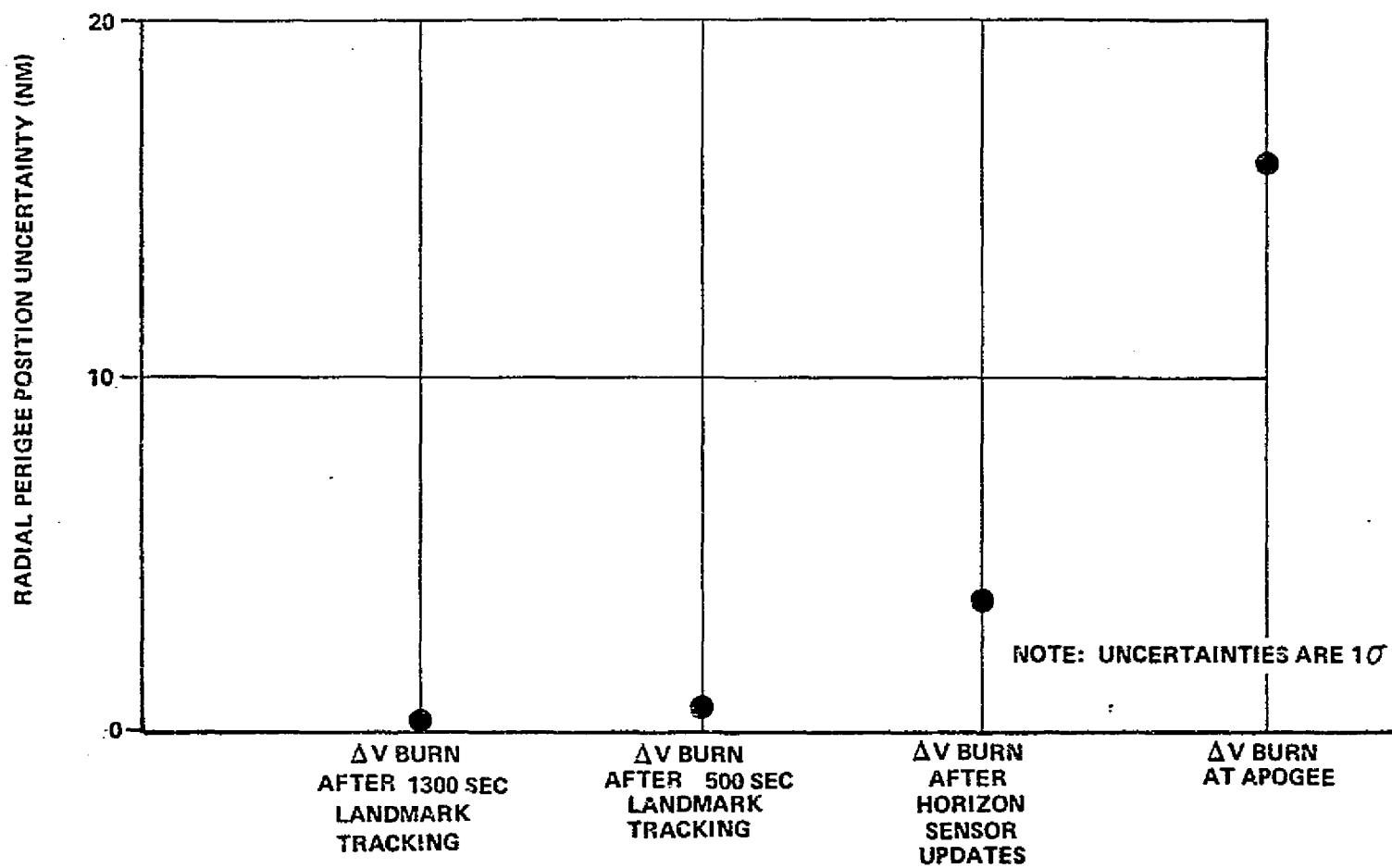


FIGURE 4.6.4.6-3. RADIAL POSITION UNCERTAINTY AS A FUNCTION OF CORRECTIVE BURN TIMING

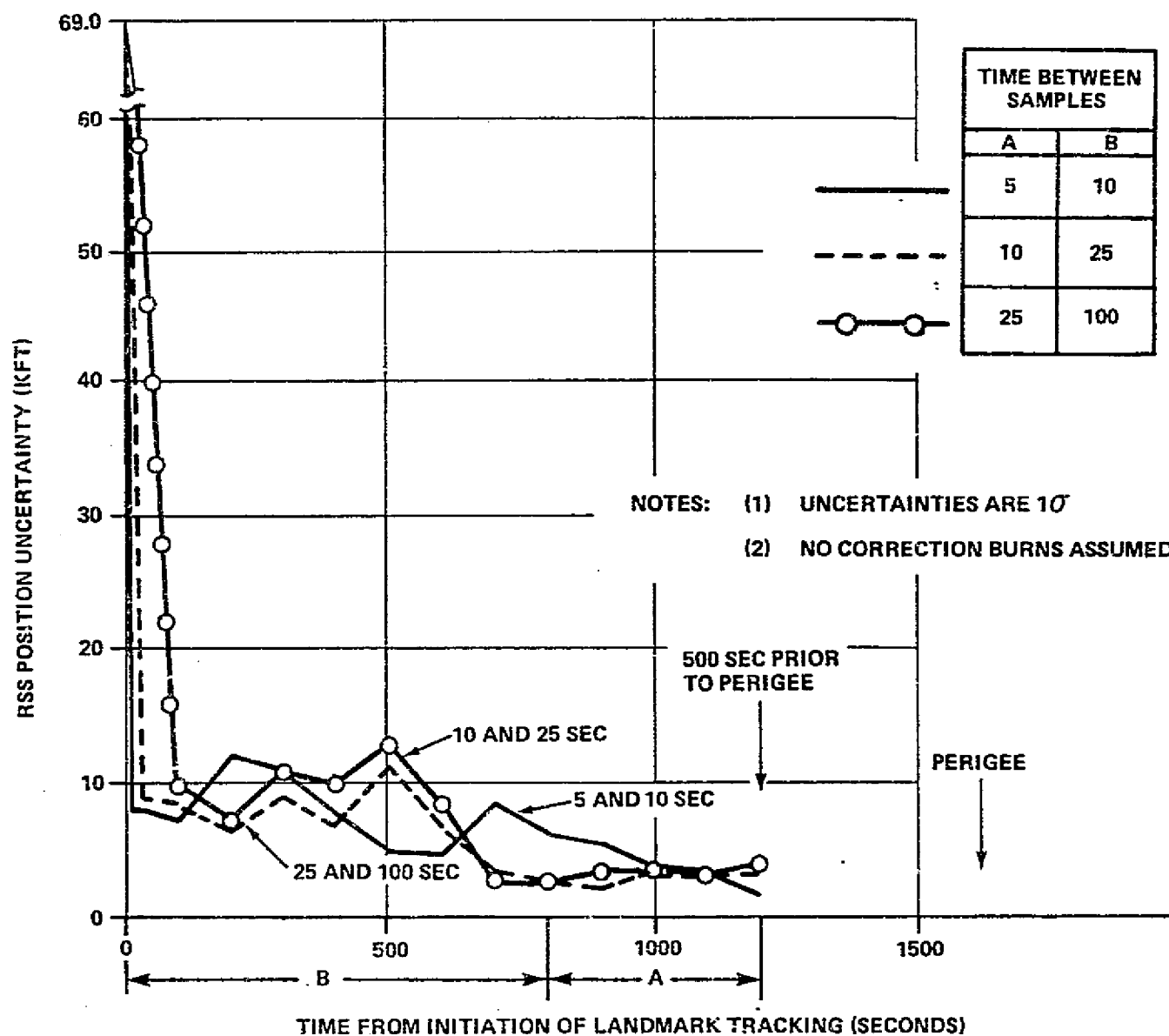


FIGURE 4.6.4.7-1. EFFECTS ON NAVIGATION DUE TO VARIATION OF NAVIGATION UPDATE RATE DURING LANDMARK TRACKING PRIOR TO PERIGEE

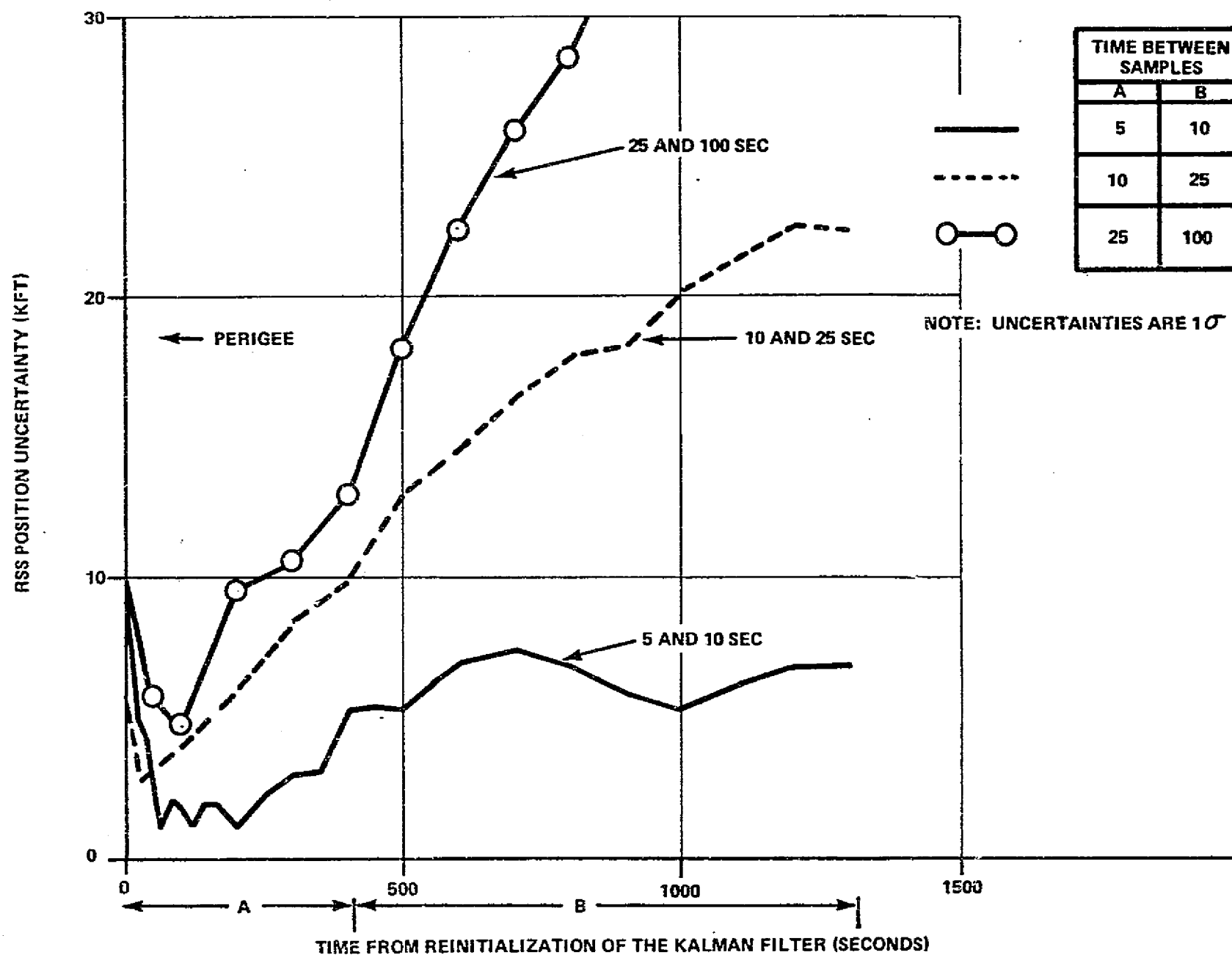


FIGURE 4.6.4.7-2. EFFECTS OF NAVIGATION DUE TO VARIATION OF NAVIGATION UPDATE RATE DURING LANDMARK TRACKING AFTER PERIGEE

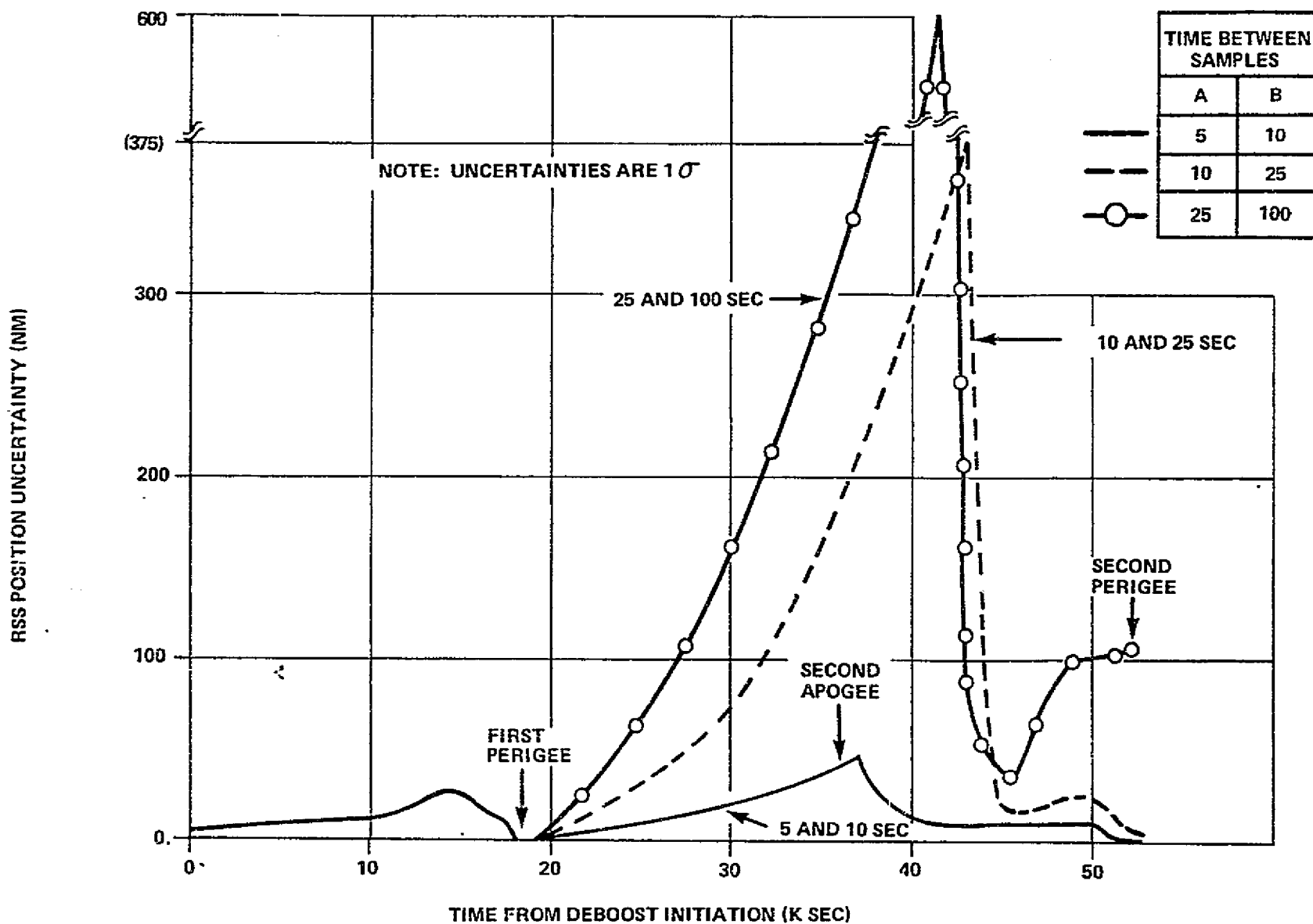


FIGURE 4.6.4.7-3. RSS NAVIGATION POSITION FOR VARIOUS NAVIGATION UPDATE SAMPLE RATES

4.6.4.7 (Continued)

produces large second perigee errors. The 10 and 25 second interval navigation update rate also produces significantly higher apogee uncertainties than for the 5 and 10 second update interval. Therefore, the 5 and 10 second interval sample rate is recommended during the landmark tracking after perigee.

Variation of Reinitialization Times for the Kalman Filter after Perigee

The Kalman filter reinitialization time after perigee was varied between 300 and 600 seconds for both the 2 day (10 pass) and 11 day (60 pass) missions. The results of this analysis are presented in Figure 4.6.4.7-4. The major observations derived from the figure are:

- o The 2 day reinitialization time is very critical and should not occur more than 500 seconds after perigee. Best results are achieved if the filter is reinitialized as soon as possible after leaving the atmosphere following perigee.
- o The filter reinitialization time for the 11 day (60 pass) mission indicates the lack of any sensitivity. Because of this, the longer duration missions can be reinitialized at a later time without effecting the apogee uncertainty.

Oblateness Sensitivities

The earth's oblateness has a significant effect on orbital characteristics and must be taken into account when targeting for a perigee which will achieve the desired mission duration. Although the orbital perturbations due to oblateness are large, they are considerably more predictable than those due to the atmosphere. Therefore, the uncertainties of long duration prediction of oblateness may result in trajectory perturbations that may require burn correction. These uncertainties are expected to be small in magnitude.

4.6.5 Astrionic System Configuration

The previous Tug astrionics study (see prior Reference 3.3.0.0-1) performed by IBM used shuttle-era technology and components for the Space Tug astrionic system. Since that study, some of the shuttle concepts have changed. Therefore, to present an up-to-date system, selected Space Tug astrionic components were replaced with comparable shuttle-era components. In addition, the previous effort included a spectrum of missions and an all-purpose Tug concept. For this study, the astrionic system was updated to reflect the requirements imposed by a synchronous orbit mission only and the deletion of excess weight penalties due to extended periods in space, such as the 180-day quiescent mode. The resulting configuration and its associated component weights and characteristics for the non-aerobraking synchronous orbit mission (60-hour length) was used as a baseline for this study.

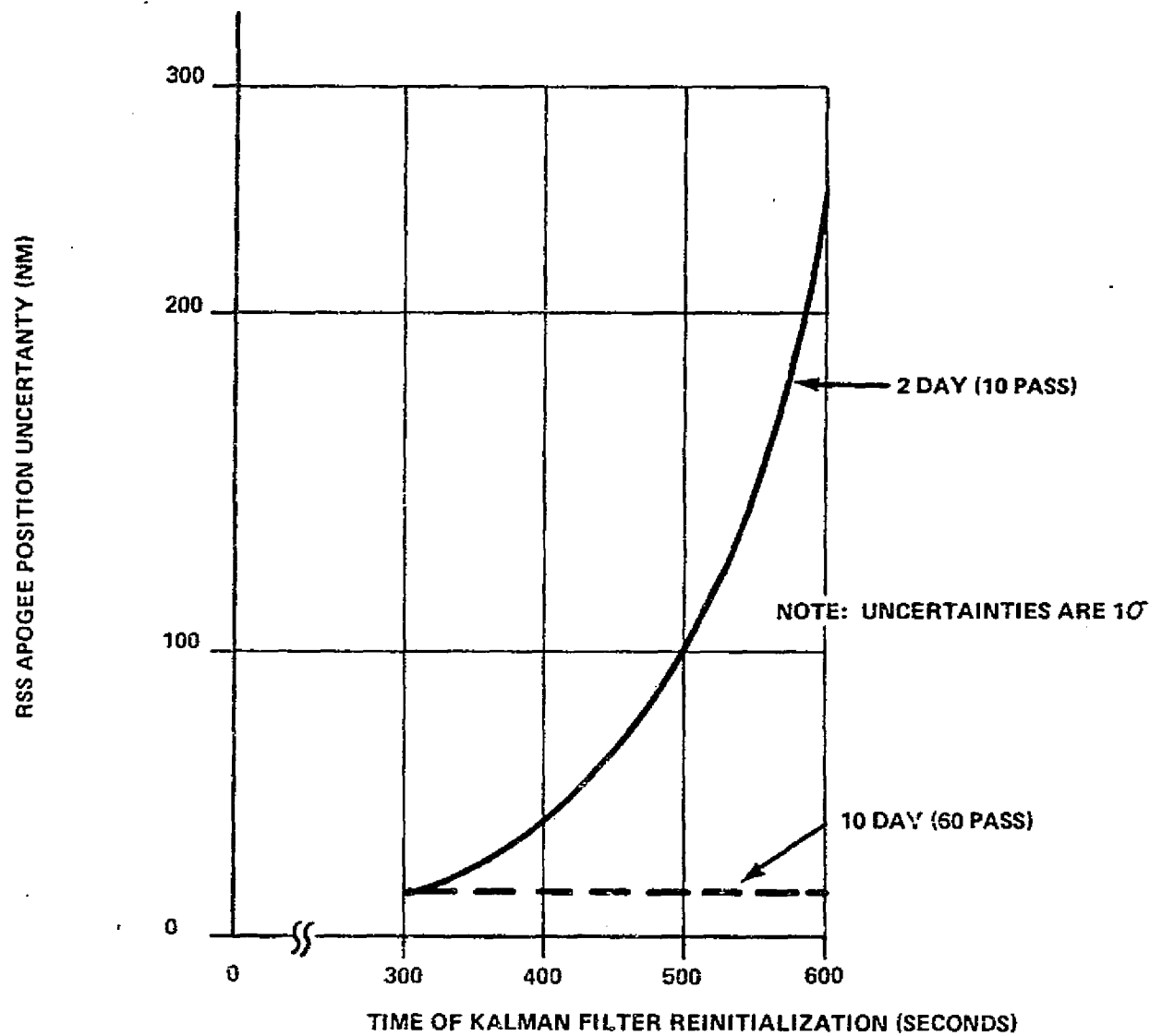


FIGURE 4.6.4.7-4. SECOND APOGEE RSS POSITION UNCERTAINTY VS. TIME OF REINITIALIZATION OF KALMAN FILTER

4.6.5.1 Astrionic System Configuration Description

The updated Space Tug astrionic system configuration is shown in Figure 4.6.5.1-1. A centralized computer (CPU/10) concept with a data bus for data transmission is used as the baseline. A core main storage (40K of 32 bit words) and a magnetic tape mass storage supplement the computer. Acquisition, Control and Test (ACT) units provide a standardized interface between the data bus and the other subsystem components.

The navigation sensors are as shown, with inertial reference provided by the IMU, automated rendezvous and docking capability provided by the laser radar, attitude update capability provided basically by the star tracker, and navigation update capability provided by the horizon sensor and landmark tracker.

The onboard sequencing and monitoring function and interface with engine controls are also provided by the ACT units. ACT/Select Buffer provides the capability of extracting selected data from the data bus and is used in conjunction with the communication and external vehicle interfaces.

Power is provided to the astrionic system by 1 Kw fuel cells with thermal control provided by a combination active/passive system using coolant, cold plate/radiators/louvers combinations. The astrionic components are housed in an astrionic module.

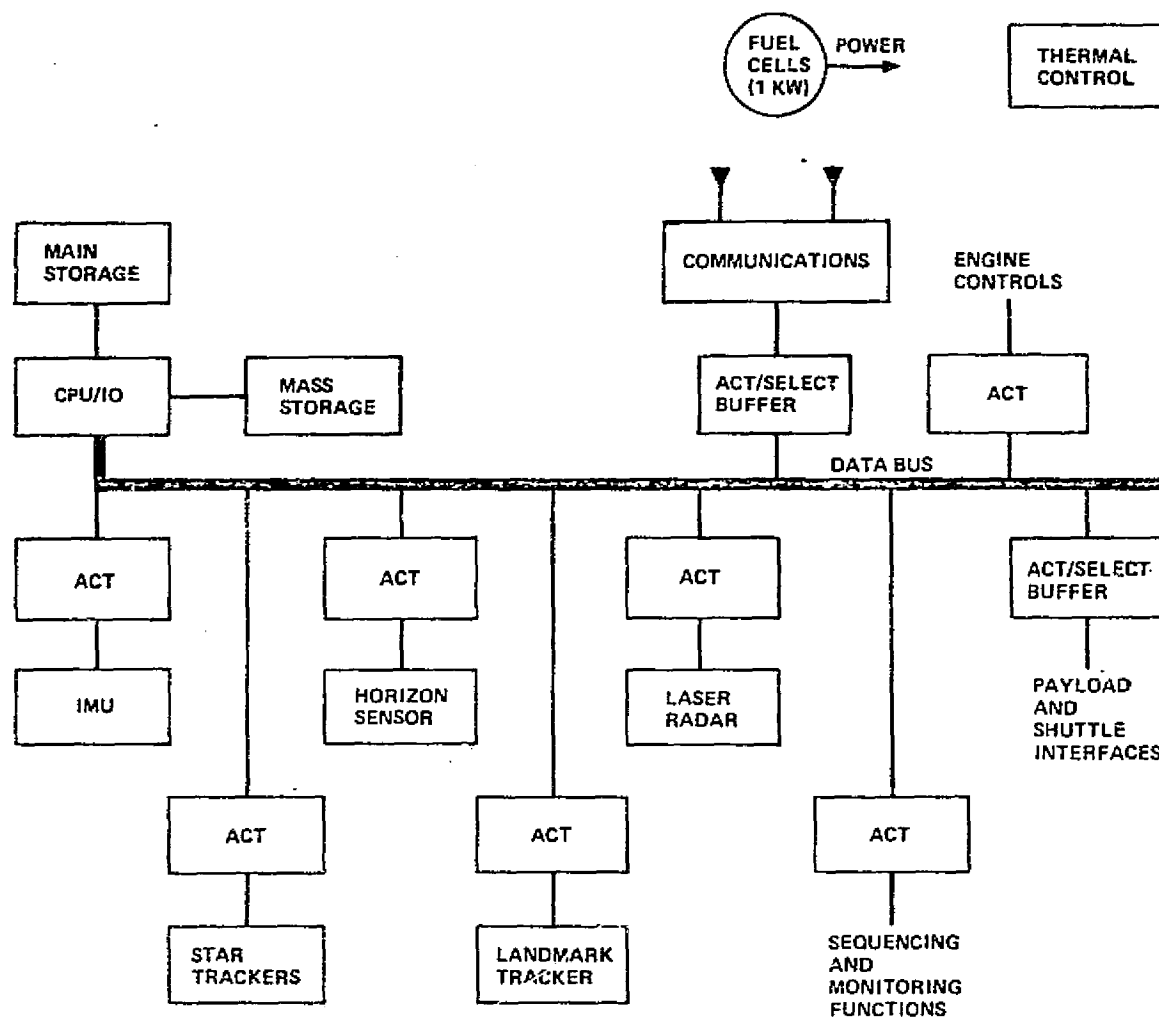
It should be noted that the philosophy for design of the astrionic system is based on using the shuttle components, if possible and as applicable, to provide commonality between space vehicle astrionics and to minimize development cost and associated hardware cost for other components used on the Tug. Selection of other components, such as 1 Kw fuel cells instead of 6 - 7 Kw fuel cells used on the shuttle, is based on meeting the astrionic system requirements with shuttle-era technology.

4.6.5.2 Weight and Power Summary

The weight and power summaries for unit components and for redundant basic astrionic system based on the redundancy study (detailed in Section 4.6.6) is shown in Figure 4.6.5.2-1. The subsystem weight and power summaries and astrionic module weight and power totals are summarized in Figure 4.6.5.2-2.

4.6.6 Redundancy Analysis

A redundancy analysis was performed to determine the redundancy required for the nominal 60-hour Space Tug synchronous mission and to determine the weight deltas to perform for additional periods of up to 15 days. The astrionics configuration was described in the preceding section. This section explains the redundancy analysis performed for this study.



NOTES:

- REDUNDANCY NOT SHOWN
- ACT = ACQUISITION CONTROL AND TEST UNIT
- CPU/IO = CENTRAL PROCESSOR UNIT/INPUT-OUTPUT UNIT
- IMU = INERTIAL MEASUREMENT UNIT

FIGURE 4.6.5.1-1 TUG ASTRIONIC SYSTEM CONFIGURATION

COMPONENT	UNIT		REDUNDANT CONFIGURATION		
	Power (watts)	Weight (lbs)	Quantity P B	Total Power (watts)	Total Weight (lbs)
DATA MANAGEMENT					
CPU/IO	136	34	1 1	136	68
Main Storage (8K BOM)	43/56(1)	28.7	5 1	227	142
ACT	1.5	4	40	60	160
ACT/Select Buffer	75	13	3	150 (2)	39
Magnetic Tape	15	10	1 1	15	20
Data Bus	--	7.5	2 1	--	22.5
Total				588	452
NAVIGATION					
IMU	120	47	1 1	120	94
Landmark Tracker	40	30	1	40	30
Horizon Sensor	10	10	1	10	10
Star Tracker	21	18	1	21	18
Laser Radar	30	28	1 1	30	56
Total				221	208
POWER					
Fuel Cell	--	79	1 1	--	158
O ₂ /H ₂	--	--	1	--	90
H ₂ /O ₂ Tanks	--	--	1	--	10
DC Regulator	--	5	2	--	39
Power Distributor	--	39	1	--	52
Aux. Pwr. Distributor	--	13	4	--	16
Junction Box	--	2	8	--	20
Mounting Hardware	--	--	-	--	130
Wires & Cables	--	--	-	--	0
Total				0	515
COMMUNICATIONS					
USB Equipment	23	32	1	23	32
USB Antenna	--	2.5	2	--	5
USB Dir. Antenna	10	30	1	10	30
Command Decoder	12	21	1 1	12	42
Antenna Selector	5	1	1	5	1
Signal Processor	13	15	1	13	15
TV Camera & Control	9	7	1	9	7
Total				72	132

NOTES: (1) 43 watts standby/56 watts active
 (2) Assumes 2 of 3 active
 P - Primary; B - Backup

Figure 4.6.5.2-1. Nominal Mission Weight and Power (Sheet 1 of 2)

COMPONENT	UNIT		REDUNDANT CONFIGURATION		
	Power (watts)	Weight (lbs)	Quantity P B	Total Power (watts)	Total Weight (lbs)
THERMAL CONDITIONING					
Coolant Pump	150	25	1	150	25
Service Heat Exchanger	--	10	1	--	10
Coolant Accumulator	--	30	1	--	30
Coldplate/Radiator	--	12.5	8	--	100
Louver	--	11	8	--	88
Coolant Fluid	--	--	-	--	20
Misc. Plumbing	-- --	-		--	30
Totals				150	303
STRUCTURES					
Structures Total					300
INSTRUMENTATION					
Instrumentation Total					50

Figure 4.6.5.2-1. Nominal Mission Weight and Power (Sheet 2 of 2)

c4

<u>ASTRIONIC SUBSYSTEM</u>	<u>TOTAL POWER* (watts)</u>	<u>TOTAL WEIGHT (lbs)</u>
DATA MANAGEMENT	588	452
NAVIGATION	228	208
ELECTRICAL POWER	---	515
COMMUNICATIONS	72	132
THERMAL CONDITIONING	150	303
INSTRUMENTATION	TBD	50
STRUCTURES	<u>---</u>	<u>300</u>
TOTALS	1031	1960

*Nominal active units

Figure 4.6.5.2-2. Weight and Power Summary

4.6.6.1 Redundancy Study Assumptions

Several assumptions were made for this study. These assumptions along with explanations, as applicable, are as follows:

- o Equipment on/off failure rate ratio was assumed to be 3:1, i.e., equipment was 3 times as likely to fail when operating as when it was powered off.
- o The goal was to achieve a mission success probability equal to or greater than 99% for all mission times considered. As mission time increased, system modifications to improve reliability were made to maintain the 99% success criteria.
- o Only components deemed mission critical were considered in the redundancy analysis. The components considered and their associated typical failure rates are given in Figure 4.6.6.1-1.
- o The component unit weights considered for this study are assumed to include Built-In-Test-Equipment (BITE), self-test hardware, or software test capability to obtain 95% coverage (which is the probability of successful fault detection, isolation, and switching) without adding additional hardware.

4.6.6.2 Analytic Programs

The reliability calculations for this study were performed on an APL/360 time-sharing terminal system. The use of such a system enables an interactive design process in that the engineer can quickly model the system and ascertain its expected performance. The system parameters can be easily modified and the improvement (or degradation) in performance ascertained. The design process is continued until an acceptable system configuration is attained.

The basic important input parameters are component failure rates, coverage and on/off failure rate ratios. Using the above input data, the program calculates component reliability, expected component failure numbers, mission success probability, the mission losses due to equipment failure and to uncoverage and the weights of the configured redundant systems.

4.6.6.3 Reliability Enhancement/Coverage

In applying redundancy to a simplex system, several means of enhancing reliability are prominent. Redundant simplex components may be added and/or equipment coverage (the capability to detect, isolate and switch failed component), may be increased. The former adds weight as simplex units are added, while the latter case adds weight in the form of fault recognition reconfiguration and recovery hardware to aid in coverage.

It is significant to note that adding spares alone can go only so far in enhancing reliability. When spared components are increased above some

<u>COMPONENT</u>	<u>FAILURE RATE</u> <u>(Per 10⁶ Hours)</u>
CPU/IO	50
Main Store (8K BOM)	50
Magnetic Tape	77
IMU	200
Landmark Tracker	25
Horizon Sensor	8
Star Tracker	38.5
Laser Radar*	300
Fuel Cell	71
Coolant Pump	19.4
USBE	1.3
USBE Antenna	0.09
Command Decoder	40
Antenna Selector	0.18
Signal Processor	1.3

*Required for rendezvous and docking at synchronous orbit only.

Figure 4.6.6.1-1. Failure Rates of Critical Components

4.6.6.3 (Continued)

level, additional spares will not significantly aid reliability unless failures in the original spares can be detected, isolated and switched. This explains the importance of increasing component coverage as well as the need to add spares.

For this study, a 95% baseline coverage is assumed for all components. With this assumption, greater reliability enhancement is obtained by initially adding spares. After some redundant units have been added, coverage becomes the dominant factor in reliability enhancement, and becomes more and more prominent as the mission time increases. The redundancy study results reflect the addition of both spares and coverage to the Tug astrionic system.

For the reliability calculations previously described, a coverage weight model, based on previous study experience which indicated that the BITE approximately doubled the weight of a MARCS computer when circuits were added to obtain coverage of 99.5%, was used to obtain the weight deltas for increasing the coverage above 95%. It was further assumed that the unit weight of the components listed in Section 4.6.5 included 70% for simplex hardware weight and 30% for BITE weight to obtain 95% coverage.

4.6.6.4 Nominal Mission Without Aerobraking

The initial redundancy study effort was to enhance the reliability of the simplex system configuration described in the preceding section. Using a mission time of 60 hours, redundant components were added until the 99% mission success goal was attained. The results of this analysis, showing the redundant system with its associated weights, was shown in previous Figures 4.6.5.2-1 and -2.

4.6.6.5 Aerobraking Redundancy Impacts

Using the reliability enhanced configuration developed for the basic 60 hour mission time and also using the assumptions previously detailed, delta weights were developed for maintaining the 99% mission success probability as the aerobraking maneuver increased the mission time by up to 15 days. Weight analyses were made for delta mission times (above the 60 hour basic mission) of 48, 90, 120, 180, 240 and 360 hours. The resulting weight deltas due to aerobraking are summarized in Figure 4.6.6.5-1. The results show that the weight deltas for the 4 - 8 day aerobraking mission range from 100 to 240 pounds while increases of greater than 500 pounds are expected for the 15 day aerobraking mission.

4.6.6.6 Redundancy Analysis Observations

The redundancy weights increase as a function of mission time and minimum weight deltas would be obtained by minimizing aerobraking mission time.

Another observation which is significant is the sensitivity of sparing and coverage to mission time. Equal reliability enhancement occurs

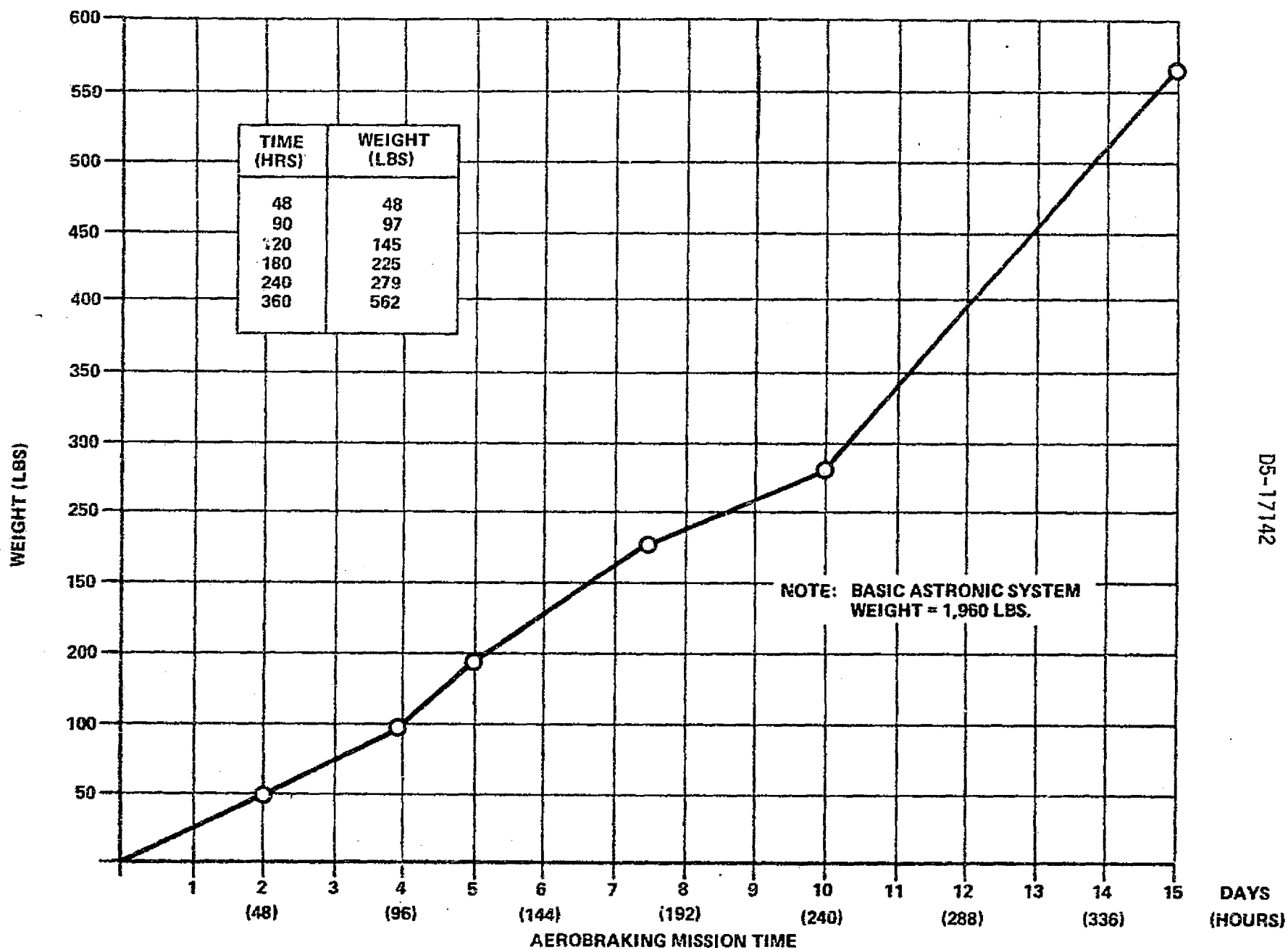


FIGURE 4.6.6.5-1. AEROBRAKING REDUNDANCY WEIGHT IMPACTS

4.6.6.6 (Continued)

whether spares are added or coverage is increased in the 4- to 6-day region. Below 4 days, adding spares supplies the greatest enhancement, while above 6 days, increasing coverage is the pacing factor. Since the implementation of fault detection, isolation and switching is not a trivial problem, increasing aerobraking time above 6-8 days is a risk in the area of redundancy implementation. Therefore, aerobraking mission time below 6-8 days incurs less redundancy implementation risk.

4.6.7 Power Weight Impacts

The Space Tug power subsystem is included in the astrionic module for this study. As aerobraking mission time increases, the onboard total power consumption increases and there is an associated weight delta.

4.6.7.1 Space Tug Power Requirements

To determine the weight deltas for power, the astrionic module power requirements, based on this study and the previous studies, were calculated to be an average of approximately 1 Kw. This assumes that the astrionic module is powered continuously, and the observations from this study proved that is a realistic assumption. The selected 1 Kw fuel cell can handle these loads with inherent fuel cell capability for handling larger peak loads. If the fuel cells were also used for both propulsion module and astrionic module power loads (500 w and 1 Kw, respectively), then a redundant fuel cell operating during peak power periods could easily handle the expected power requirements.

4.6.7.2 Aerobraking Weight Deltas

The H₂ and O₂ reactant weights and the tanks (required to store the reactants) weights were calculated to obtain the weight delta required for power during aerobraking. The H₂/O₂ consumption is approximately 0.83 lbs/Kwh, while the tanks are approximately 0.4 lbs/lb reactant. The weight for 1 Kwh of power would then be

$$\begin{aligned} &= 0.83 \text{ lb/Kwh} \times 1 \text{ Kwh} + 0.4 \text{ lb/lb reactant} \times 0.83 \text{ lb reactant} \\ &= 0.83 \text{ lb} + .332 \text{ lb} = 1.162 \text{ lb/Kwh} \end{aligned}$$

Assuming an approximately 30% contingency for boiloff, peak loading, unexpected power loads, and/or increased mission time, the weight per Kwh would be approximately 1.5 pounds.

The weight increase for H₂/O₂ and tanks is a linear function. Since the average power load is 1 Kw/hr and the weight is 1.5 lbs/Kwh, then the weight increase is approximately 1.5 pounds for each additional hour used for aerobraking. For example, a 200 hour aerobraking mission would require approximately 300 pounds of weight for power. The power weight deltas versus aerobraking mission time are shown in Figure 4.6.7.2-1.

4.6.8 Astrionic System Radiation Impacts

This section summarizes the results of a study of natural radiation belt effects on the electronics of Space Tug systems for the 2, 5 and 10 day

4-212

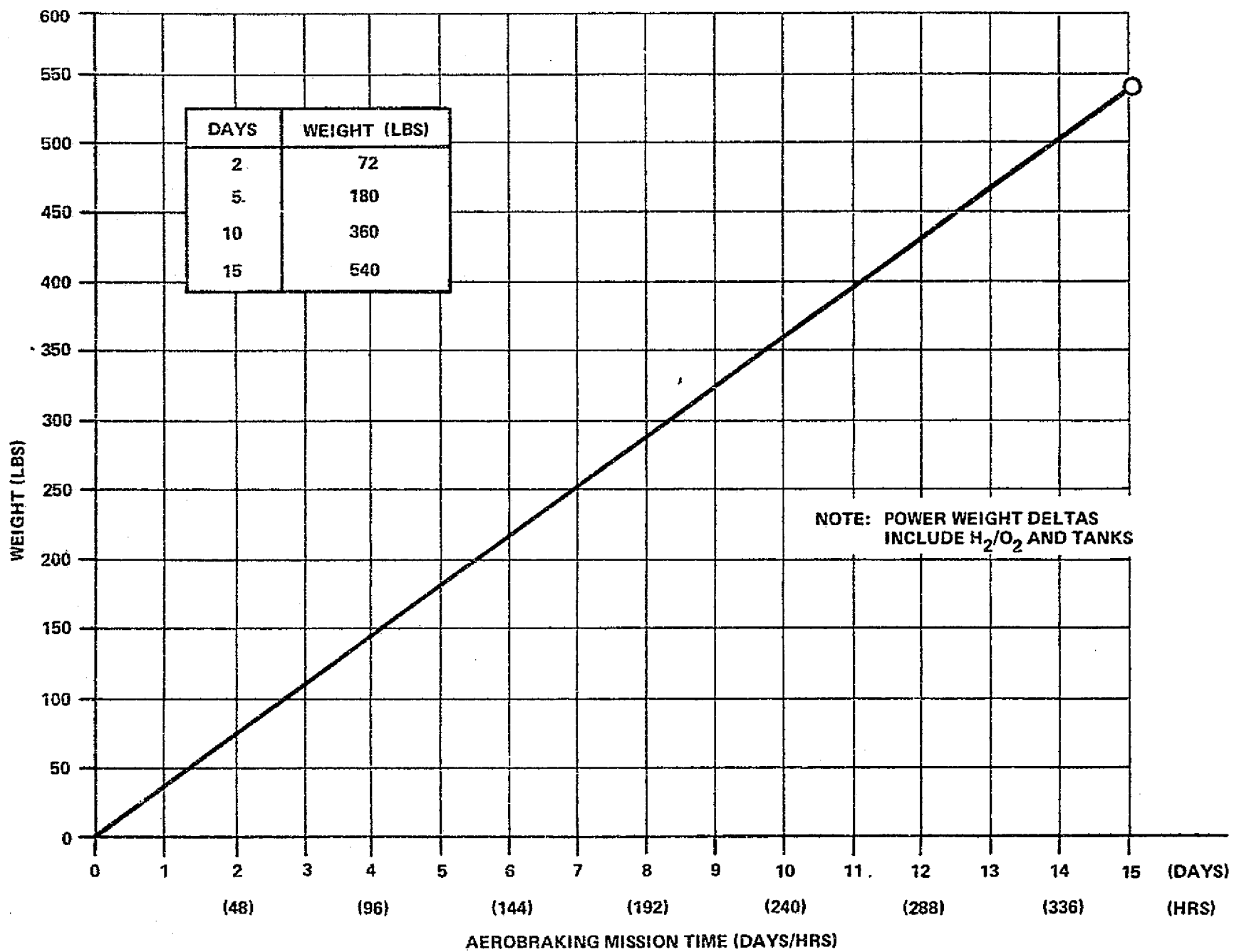


FIGURE 4.6.7.2-1. AEROBRAKING POWER WEIGHT DELTAS

D5-17142

4.6.8 (Continued)

aerodynamic aerobraking profiles.

A qualitative explanation of the external fluence (particles/cm²) calculation is presented first, followed by the internal dose analysis. Finally, the ramifications of the internal dose to electronic devices are considered.

4.6.8.1 External Radiation Environments

Each aerobraking mission consists of a series of elliptical orbits (approximately 30° inclination) with monotonically decreasing eccentricities starting with maximum apogee at synchronous orbit altitude. The natural radiation belts are distributed in an approximately toroidal shape around the earth between 70° north and south latitudes and radially between about 160 NM to 6,500 NM for the protons. The omnidirectional fluxes (particles/cm² sec) vary strongly with altitude, orbital inclination, particle energy and weakly with time.

The method by which the cumulative particle fluences were estimated for each orbit was to derive an expression for the length of the radial vector extending from the center of the earth to the orbit periphery and to divide the ellipse into equal areas.

From the trapped radiation models by Dr. Vette (References 4.6.8.1-1 and -2) the flux was obtained at apogee, perigee and radius for each orbit. The mean flux between each of these orbital points was determined. Given the period of each orbit and employing the Areal velocity law of orbital mechanics, (this is, equal areas swept out in equal times), the period was divided by 4 and multiplied by each mean flux value to obtain the particle fluence encountered in the traversal of each segment of the orbital path defined by apogee, perigee and radius. These partial fluences were summed over each orbit and again over all the orbits for a particular mission length. These particle fluences are shown in Figure 4.6.8.1-1 under the headings electrons/cm² and protons/cm². This approximate technique tends to give an over-estimate of the fluence.

4.6.8.2 Internal Radiation Environments

Charged particulate radiation damage in electronic devices is manifested in two general modes, ionization and atomic displacement. The former is characterized by rads (Si), which is the amount of radiation energy absorbed relative to silicon, and the latter by equivalent fission neutron fluence (neutrons/cm²).

The dose in the electronic devices is dependent on the intensity and spectral distribution of the radiation penetrating through component packaging and vehicle shielding. These in turn are dependent on the fluences and spectra incident on the vehicle. A further complication is the altitude dependence of the electron and proton energy spectra. Because of the large variation in altitude, nominal spectra were used to estimate

Missions	IONIZING DOSE AND EQUIVALENT FISSION NEUTRON FLUENCE						
	ELECTRONS			PROTONS			TOTAL DOSE*
	EXTERNAL DOSE	INTERNAL DOSES		EXTERNAL DOSE	INTERNAL DOSES		INTERNAL
	Electrons/cm ²	Rads (Si)	Neutrons/cm ²	Protons/cm ²	Rads (Si)	Neutrons/cm ²	Rads (Si)
Case 1 10 Orbits 2 Days	2.1×10^{11}	103	7.4×10^6	3.1×10^9	< 310	10^{10}	< 413
Case 2 30 Orbits 5 Days	3.8×10^{11}	190	1.4×10^7	4.6×10^9	< 460	2×10^{10}	< 650
Case 3 60 Orbits 10 Days	8.4×10^{11}	418	3.3×10^7	9.4×10^9	< 940	3×10^{10}	< 1350

*Sum of electron and proton ionizing dose behind 0.63 g/cm² aluminum.

Figure 4.6.8.1-1. Summary of External and Internal Van Allen Radiation Environments For Three Proposed Mission Profiles

4.6.8.2 (Continued)

internal doses. The typical shielding configuration used is shown in Figure 4.6.8.2-1.

Internal Electron Dose

The internal electron and associated Bremsstrahlung dose/unit incident electron fluence was obtained as a function of aluminum shielding thickness by computer transport calculations (Reference 4.6.8.2-1). This function is illustrated in Figure 4.6.8.2-2. It is apparent that for the assumed shielding thickness, the electron dose dominates the Bremsstrahlung contribution. This function can be used, for example, to compute the internal electron dose for case 1 (2 days) behind 0.63 gm/cm^2 by taking the product of the ordinate value for that thickness (5×10^{-10}) and the incident electron fluence (2.1×10^{11}) to obtain 103 rads (Si). It is also evident that a slight change in shielding thickness will drastically change the internal dose from Van Allen electrons for shielding thicknesses less than 2 gm/cm^2 .

The equivalent fission neutron fluence for the incident electron spectrum was obtained by a conversion of the electron spectrum to an equivalent 1 Mev electron fluence and the results are shown in Figure 4.6.8.1-1. An appropriate 1.0 Mev electron to fission neutron conversion permits integration over shielding thickness to give equivalent fission neutron fluence behind 0.63 gm/cm^2 of aluminum.

Internal Proton Dose

The natural proton belt spectrum varies so strongly with altitude that the choice of a dose/unit incident fluence factor is probably best chosen as the maximum value at cutoff energy due to shielding. For 0.63 gm/cm^2 , the proton cutoff energy is approximately 20 Mev. That is, only protons of energy $E > 20 \text{ Mev}$ will penetrate the electronics. The maximum fluence to dose conversion factor at this energy is about 10^{-7} rads (Si) - $\text{CM}^2/\text{proton}$ at the cutoff. This results in an over-estimate of the internal dose by X2 to X3 at high altitudes and under-estimate by the same amount at lower altitudes. This factor was used to convert the proton fluences to internal dose in Rads (Si) to obtain the values given in Figure 4.6.8.1-1.

Relative to fission neutrons, the protons cause considerably more atomic displacement damage than electrons. The values of equivalent neutron fluence for the protons are indicated as "worst case" or upper bounds because they are based on a solar flare proton spectrum which is somewhat lower energy than the Van Allen proton spectrum.

4.6.8.3 Electronic Device Effects

At the internal doses indicated in Rads (Si) in Figure 4.6.8.1-1 there will be no significant effects on electronic devices in the Space Tug astrionics. However, it can be inferred from the progression of doses

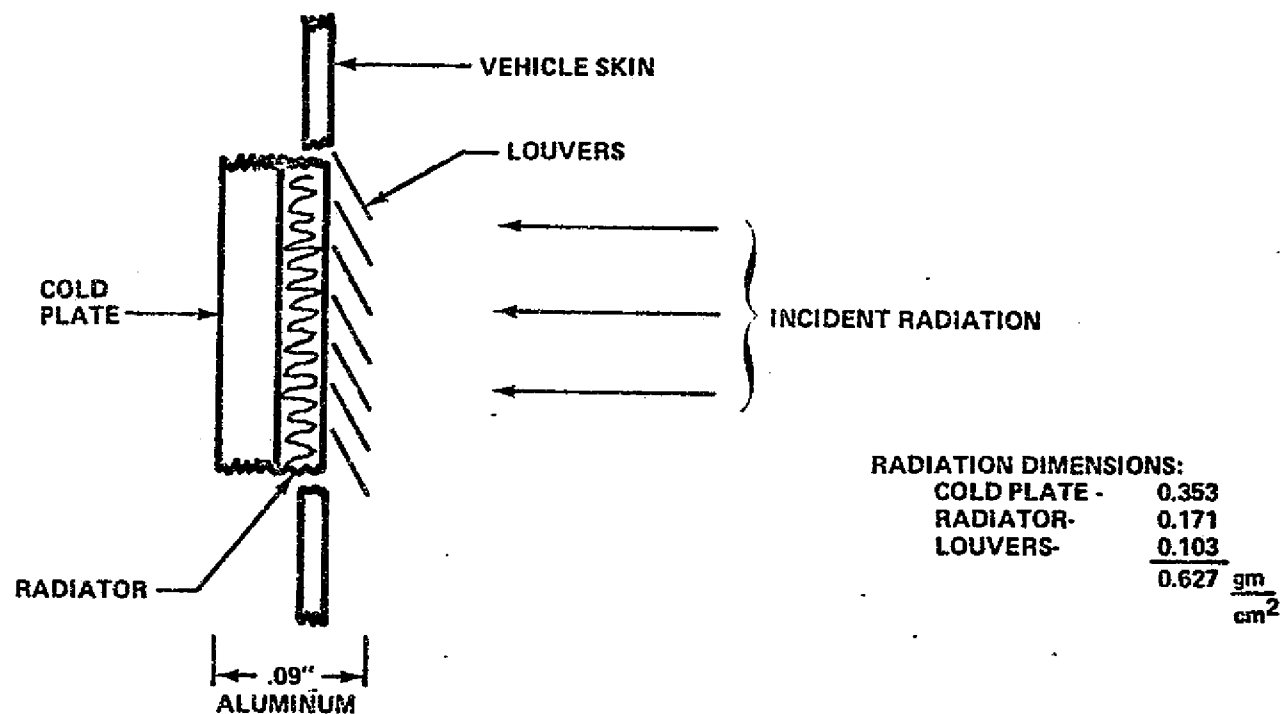


FIGURE 4.6.8.2-1 PRESCRIBED SHIELDING CONFIGURATION

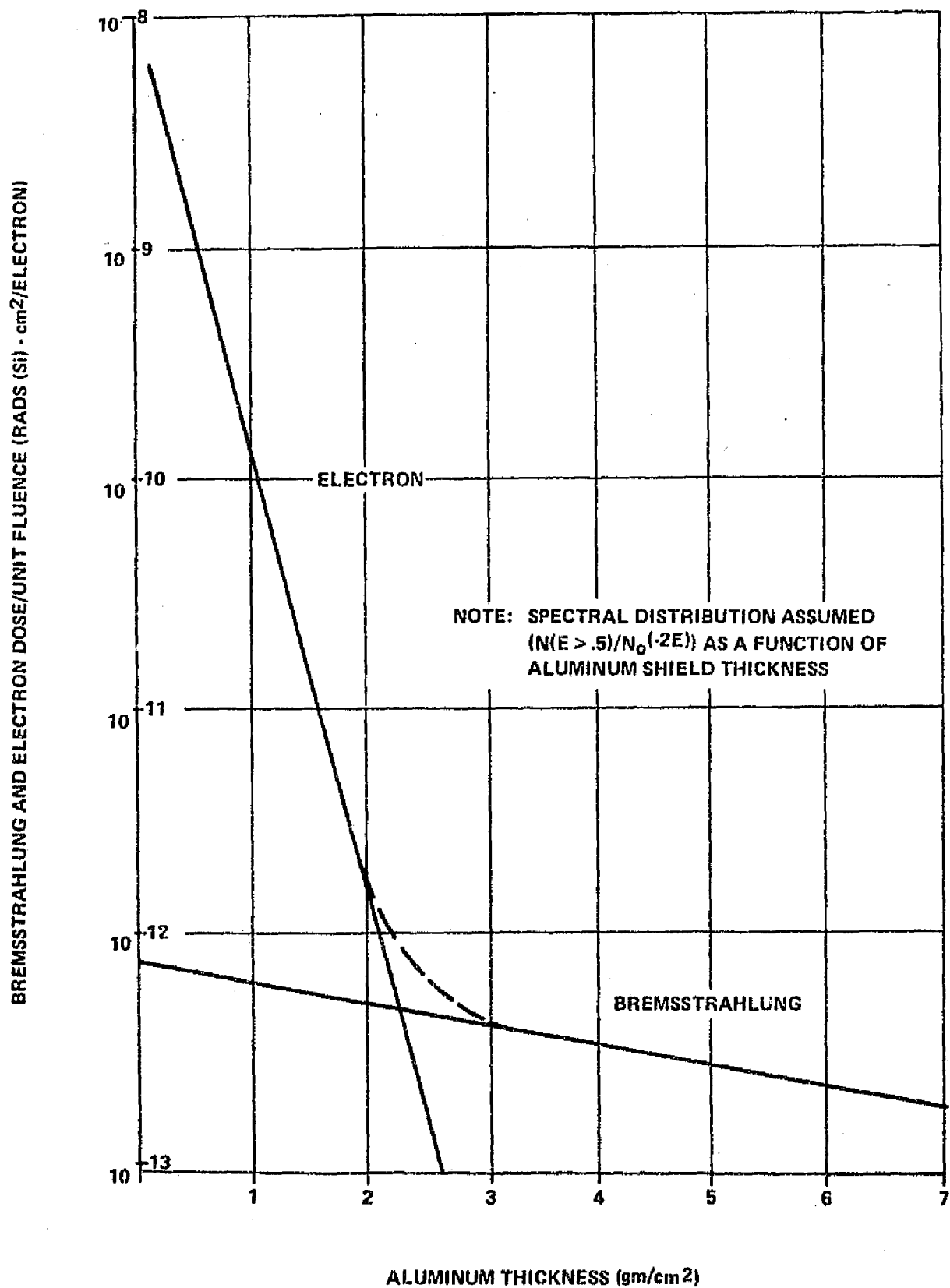


FIGURE 4.6.8.2-2. ELECTRON AND BREMSSTRAHLUNG DOSE/UNIT FLUENCE FOR A VAN ALLEN ELECTRON FLUENCE

4.6.8.3 (Continued)

for the three aerobraking cases that the dose for an aerobraking mission time of 15 days (80 orbits) will be well over 1300 Rads (Si). At doses approaching 10^4 Rads (Si), MOSFET devices begin to suffer a shift in threshold voltage. Consequently, there is some question regarding the use of these devices should the 15 day mission time be selected.

The displacement damage effects of the electrons are negligible. However, the displacement damage effects of the protons for the 10 day mission will begin to cause significant gain degradation in silicon transistors with an alpha cutoff frequency of less than 10 MHz, operating at nominal current levels and having an end-of-life Beta greater than 100.

In general, no significant radiation impacts are expected for the aerobraking mission times studied. Some electronic components, however, are very sensitive to radiation and the observations related to these components and for the radiation impacts study are included in this section.

4.6.8.4 Observations

If a 15 day mission is selected, it may be necessary to characterize the radiation response of MOS devices for a comparison of radiation induced threshold voltage shift to circuit tolerances. Should the 2 to 10 day mission times be chosen, there is no problem in this regard.

If silicon transistors with alpha cutoff frequency less than 10 MHz and end-of-life Beta greater than 100 are proposed for astronics design it may then be necessary to find substitute transistors for all aerobraking missions, depending on the circuit tolerance for forward current transfer ratio decrease. The latter is not normally a difficult problem at the radiation levels of interest.

It should be noted that device packaging was not included in the shielding configuration. This results in a radiation overestimate for some devices with relatively heavy packaging such as power devices. For others, such as flatpacks with 10 mil aluminum covers, there is no appreciable overestimate of the dose. Consequently, very slight quantities of localized shielding should attenuate the electron and proton fluences to quite tolerable levels of MOSFETs and power transistors when device packaging is considered.

Because of the technique used in determining their values, the radiation doses established in this study are slightly overestimated. Greater accuracy can be attained with computer codes (Reference 4.6.8.4-1) specifically designed to calculate fluxes for this type of mission profile. Such calculations should be performed prior to making any firm decisions regarding the use of additional shielding or generating design groundrules for circuit design.

4.6.9 New Technology Implications

Throughout performance of the Tug aerobraking study, functional requirements of the astronics were compared to conventional implementations and evaluations made to determine the need for development of new technologies. This section describes the specific items identified which would provide a significant contribution to the realization of an aerobraking mode Tug.

4.6.9.1 Redundancy Implementation

As discussed in Section 4.6.6 (Redundancy Analysis), the successful completion of the Tug aerobraking mission depends on an operational astronics system which in turn depends on "coverage" (failure identification) to "key-in" redundancy components at the proper time. Current technology depends heavily on BITE (Built-In-Test-Equipment), off-line dynamic response testing, voting or comparison or reasonableness testing to identify failed components. These methods have had limited success with electromechanical sensors and hence necessitates the development of a new component evaluation technology.

The basic conventional evaluation limitations can be overcome by using a random or pseudo-random noise input and correlation techniques. The advantages of using correlation identification techniques are:

- o The system may be checked out "on-line".
- o Test signals can be kept small and will not interfere with normal operation.
- o Results can be obtained in the presence of random noise and parameter drifts.
- o The technique can be easily applied to existing hardware. Correlation is inherently a simple digital process.

The objective of such a new technology study would be to define the suitability and application of "on-line" system evaluation by digital methods.

4.6.9.2 Navigation Sensor Integration

The navigation analysis performed in this study utilized an optimal filter (Kalman) implemented on a general purpose floating point computer (IBM 360/75). In a space application the sensor integration routines must be programmed in a limited memory machine in fixed point arithmetic. A new technology task is recommended to define a sub-optimal filter routine in 16 bit fixed point arithmetic to provide integration of the landmark, horizon and star sensors and IMU.

4.6.9.3 Navigation and Guidance Analyses

The study effort to date has evaluated navigation uncertainties and preliminary evaluated burn corrections with associated navigation updates. To enhance this effort, a study should be made of the vehicle attitude control, retargeting and predictive problems associated with orbit disturbances that result from uncertainties in atmospheric drag, navigation sensor inaccuracies and vehicle dynamics. The study would involve development of a guidance law to (1) predict future orbital variations based on past inputs (accelerations, state vectors), (2) compute new orbital perigees to achieve mission objectives, and (3) control vehicle forces during atmospheric braking to achieve the desired end conditions. The guidance law would then be tested using available simulations to verify its operation under a variety of disturbances.

4.6.10 Follow-On Study Effort

The Space Tug Aerobraking study performed to date was an overview of selected astrionic system areas and parameters to aid in the determination of feasibility of the aerobraking concept to the Space Tug synchronous mission. During the course of the study, areas requiring study and/or further study have been identified. The following gives brief recommendations of follow-on study efforts for aerobraking (and in some cases better Tug definition) to aid in evaluation of parameters.

4.6.10.1 Astrionic System Configuration Analysis

The analysis performed for the present study was an updating of the initial Space Tug astrionic system design using the latest Shuttle concepts and components as applicable to streamline the Tug to perform only the synchronous mission instead of the broad spectrum originally studied.

Present Shuttle emphasis appears to be in the area of cost without weight being a pacing item. For the Space Tug, weight and cost would be pacing items. Therefore, additional effort should be expended to integrate Shuttle astrionic system concepts and components into the Tug while maintaining minimum weight where possible. Although this is not an aerobraking analysis per se, it is important to provide a well-defined baseline system configuration as a basis for future aerobraking study effort.

4.6.10.2 Redundancy Analysis

The redundancy effort to date has defined the typical redundancy weight deltas to be expected for aerobraking mission. In the vein of Section 4.6.10.1, additional effort should be expended to provide a more detailed redundancy analysis using the updated astrionic system components, and to look individually at each component to determine methods of reliability and coverage enhancement. In addition, the risks associated with redundancy management for long duration missions should be addressed.

4.6.10.3 Navigation Timeline Analysis

The navigation analysis to date selected a typical navigation update timeline which provided satisfactory update accuracy. However, more analysis is required to perform a detailed operations analysis, using attitude constraints, sensor acquisition and reacquisition constraints, loss of navigation update, burn perturbations, length and frequency of updates, etc., to investigate the limitations of autonomous navigation during aerobraking.

4.6.10.4 Advanced Sensor Systems

This study would look at existing and potential autonomous navigation sensors to investigate improvement of autonomous space navigation by using new technology sensors and/or concepts. The critical post-perigee sighting should be given priority treatment and include investigation of the state-of-the-art in interferometer or other all-weather landmark tracker technology. A second part of the study would include an analysis of navigation sensor hardware to determine means of enhancing reliability and to determine operating modes and limitations of the hardware.

4.6.10.5 Updating Capability versus Control Requirements

This study effort would be an expansion of the effort included in the navigation analysis. The effort would perform detailed trades to determine the updating capability of onboard navigation components versus the required control penalties. This would include attitude control deadbands and requirements during sensor observations as well as the accuracy versus RCS penalties to perform navigation update burns for various times during the aerobraking orbit prior to perigee.

4.6.10.6 Radiation Analysis

The radiation analysis for this study was a cursory evaluation to identify any significant astrionic system impacts due to repeated passes through the Van Allen radiation belt. Additional study effort would include a more accurate determination of the elliptical orbit profiles using the BOFES (Burrell Orbital Flux and Spectra) code. The impacts of both single aerobraking missions and repeated aerobraking missions for a ground based Tug would be evaluated. Sensitivities of various components for various shielding and radiation doses would be addressed.

4.6.10.7 Astrionic System New Technology Component Analysis

Weight is the pacing item for the Space Tug. The astrionic system weight can be reduced if new technology components (in lieu of an off-the-shelf Shuttle components) are considered. However, development costs and certain development risks would be associated with the new technology components. A study effort to evaluate the relative merits of using new technology components in the astrionic system of the Tug, giving the advantages and disadvantages of weight and cost trades is recommended. This would include a survey of potential new technology components (such as

4.6.10.7 (Continued)

LSI computers) and the relative development progress of each.

4.7 AEROBRAKING KIT MATERIALS SELECTION

The materials selection portion of this study was limited to identifying suitable materials to be used for the aerobraking kit components without a detailed material analysis and selection. The location of the aerobraking kit components on the Space Tug resulted in a wide range of potential temperatures on the components. Selection of materials was further complicated by the parametric nature of the study. The shorter the aerobraking mission time, the more severe the thermal environment the aerobraking kits would encounter.

The materials portion of the study used the aerobraking kit designs (Section 4.2) and the thermal data (Section 4.5) as input data for the selection of materials. Material selection criteria was established and the materials were then selected for each of the aerobraking kit components. For the same component, different materials were recommended for use dependent on the thermal environment imposed by the mission duration.

4.7.1 Materials Groundrules and Criteria

The study was not able to investigate the materials requirements to the depth necessary to fully understand the materials/structure/performance interfaces. The study groundrules recognized this situation and limited the scope of the materials investigation. More detailed studies are required in advanced technology and follow-on Space Tug activities. The key material study groundrules are as follows:

- a. The Boeing Pre-Phase A Space Tug configuration (prior Reference 1.1.0.0-1) scaled upward for increased propellant capability was selected as the baseline Space Tug. Modifications were restricted to changes to apply the aerobraking kit to conventional Tug configuration.
- b. The materials technology was restricted to state-of-the-art thermal materials.
- c. The TD-nickel-chrome with 2000°F capability was used as an upper radiative thermal protection system material limit. Materials such as tantalum and columbium were considered advanced state-of-the-art.
- d. The use of ablative materials were restricted to single pass applications. The recycling capability was considered advanced technology.
- e. The maximum allowable temperature the payload may experience was limited to 300°F.

4.7.1 (Continued)

The materials selection criteria was identified for the aerobraking kit components in terms of the type of thermal protection system it would provide, i.e., radiative or insulative. Key selection criteria are shown in Figure 4.7.1.0-1. All of the criteria shown is self-explanatory except for oxidation resistance, bonding characteristics, form and purging. Oxidation resistance refers to the ability of the material to withstand the environments without an additional protective coating which would require replacement after each mission. Bonding refers to methods of applying insulation to structure (e.g., welding, brazing, adhesives, etc.). Form refers to the ability to obtain the materials in bars, sheets, rods, plate, etc. Purging refers to the ability of the insulation type materials to be purged of entrapped, heated gases with a cooling gas or by drawing a vacuum. Other less critical selection criteria are shown on the materials properties sheets (Figure 4.7.3.0-1).

4.7.2 Thermal Environments of Aerobraking Kit Elements

The aerobraking kit elements consist of (1) an aft heat shield, (2) sidewall insulation over the propulsion module, astronics module and payload adapter (where required), (3) a flare, and (4) a payload adapter. (Astronics aerobraking kit elements are identified in Section 4.6.)

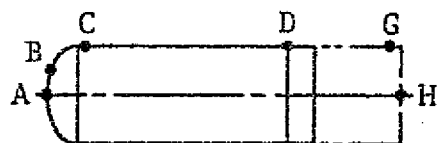
The study investigated four different mission durations. These were a one, two, five and 11 day missions. Four aerobraking configuration concepts were studied. These concepts included a no flare configuration and three different flared configurations. Figure 4.7.2.0-1 tabulates the thermal data for the four configurations.

Although shorter mission durations than the one day (5 pass) were not fully investigated, the short duration missions were given a preliminary thermal investigation. The temperatures that would be encountered on the aft heat shield for the basic (no flare) configuration are approximately 3600°F to 4000°F for one to two pass missions (References 4.7.2.0-1 and -2). For the configurations with flares, the temperatures encountered for one to two pass missions would vary from approximately 3300°F to 3700°F. For these temperatures, either ablatives or some of the advanced state-of-the-art tantalum and columbium alloys (e.g., Fansteel 60) would be required for the aft heat shield.

Short mission durations (less than one day) will cause the sidewall temperatures to be considerably higher than those shown in Figure 4.7.2.0-1. These high sidewall temperatures would require a more complex design with both radiative and insulation materials combined to offset the temperatures. The temperatures on the flares would also increase and may require the relatively heavy TD-nickel-chrome to withstand the thermal environment. The payload adapter could be fabricated from aluminum for the flared configurations but would require some insulation to protect the sidewalls and a cover to protect the aft end of the payload (300°F payload temperature limit). For the basic (no flare) configuration, the payload adapter is not shielded by a flare and would encounter more severe

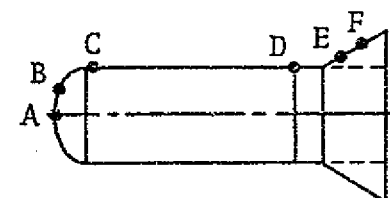
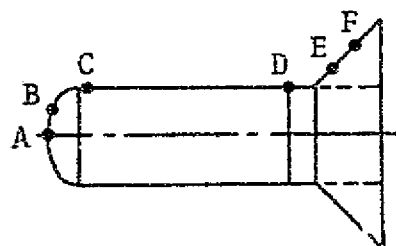
CRITERIA	DOMES & FLARE (RADIATION)	SIDEWALL (INSULATION)
DENSITY	LOW WEIGHT	LOW WEIGHT
THERMAL CAPABILITY	HIGH TEMP.	HIGH DECOMP. TEMP.
THERMAL CONDUCTIVITY	----	LOW
EMISSION	HIGH	----
TENSILE STRENGTH	HIGH AT ELEV. TEMP.	----
WELDABILITY	STRENGTH & EASE	----
MACHINEABILITY	GOOD PROPERTIES	----
OXIDATION RESISTANCE	NO SPECIAL TREAT.	----
BONDING CHARACTERISTICS	----	EASE
FORM	----	VARIOUS
PURGING	----	GOOD
COST	NOT IDENTIFIED IN THIS STUDY SHUTTLE ERA (1973 - 74)	
AVAILABILITY		

FIGURE 4.7.1.0-1: MATERIALS SELECTION CRITERIA



SPACE TUG BASIC CONFIGURATION

TRAJECTORY	MAXIMUM EQUILIBRIUM TEMPERATURES (°F)					
	A	B	C	D	G	H
5 PASS	3320	3175	1585	1120	975	682
10 PASS	2990	2860	1410	987	875	591
30 PASS	2540	2420	1166	797	720	451
60 PASS	2240	2140	1005	676	615	364



SPACE TUG 30° FLARE CONFIGURATION

TRAJECTORY	MAXIMUM EQUILIBRIUM TEMPERATURES (°F)					
	A	B	C	D	E	F
5 PASS	2940	2800	1382	1082	1272	1293
10 PASS	2630	2520	1215	943	1104	1124
30 PASS	2160	2060	957	733	850	869
60 PASS	1880	1790	809	605	706	729

SPACE TUG 45° FLARE CONFIGURATION

TRAJECTORY	MAXIMUM EQUILIBRIUM TEMPERATURES (°F)					
	A	B	C	D	E	F
5 PASS	2590	2480	1195	927	1037	1085
10 PASS	2300	2205	1040	800	874	919
30 PASS	1886	1798	812	608	635	680
60 PASS	1660	1580	691	507	513	558

SPACE TUG 60° FLARE CONFIGURATION

TRAJECTORY	MAXIMUM EQUILIBRIUM TEMPERATURES (°F)					
	A	B	C	D	E	F
5 PASS	2325	2220	1048	806	943	970
10 PASS	2080	1990	917	697	804	829
30 PASS	1740	1660	733	540	621	648
60 PASS	1512	1467	609	439	503	538

FIGURE 4.7.2.0-1 COMPARISON OF MAXIMUM EQUILIBRIUM TEMPERATURES

4.7.2 (Continued)

temperatures. This payload adapter would require an inconel housing with additional insulation on the sidewall and on the payload aft end cover.

In addition to the four selected configurations, the basic (no flare) configuration with no aft heat shield was assessed. The aft heat shield must protect the engine systems from the re-entry aerobraking temperatures. The RL-10A-3-8 engine used in the Space Tug for this study has many limited temperature capability components. This constraint was one reason the unshielded aerobraking Tug was not considered practical. For example, some elements only have 160°F temperature capability. These elements would have to be insulated even when protected by the heat shield. The temperature capabilities of these systems are shown in Figure 4.7.2.0-2.

These temperature limits coupled with the complex aerodynamic flow fields of an unshielded nozzle and the aerothermodynamics of the exposed engine during aerobraking eliminated the unshielded aerobraking Tug configuration from further consideration.

The payload may only experience a temperature limit of 300°F. The temperatures encountered at the payload base for the basic (no flare) configuration are as follows:

<u>Trajectory</u>	<u>Equilibrium Temperature (°F)</u>
5-Pass	682
10-Pass	591
30-Pass	451
60-Pass	364

Therefore, for the basic (no flare) aerobraking Tug configuration, the thermal protection system must completely encase the payload. The flared configuration's payload adapter temperatures were not defined due to the complexity of the thermal analyses required to determine the temperatures on the payload adapter under the flare and the payload adapter base. However, the design of the payload adapter does include a reflective painted surface to reduce heat input to the payload. The temperatures at the payload adapter base are expected to be below 300°F for the mission durations which optimize payloads (30 pass - 5 day missions). For shorter duration missions, a protective cover would be required.

4.7.3 Materials Selection

The materials which were investigated are shown in Figure 4.7.3.0-1 and 4.7.3.0-2. The effect of temperature on the strength to density properties are shown in Figure 4.7.3.0-3. Based on the criteria shown in 4.7.1 and the thermal environments shown in 4.7.2, the following materials were selected for each of the aerobraking kit elements.

<u>Component</u>	<u>Limiting Item</u>	<u>Material</u>	<u>Max. Allow. Temp.</u>
Thrust Chamber	Tube Braze	PWA 85	1900°R
Thrust Control Valve	Thin Wall Housing	AMS 4130	760°R
Lox Flow Control Valve	Thin Wall Housing	AMS 4130	760°R
Turbopump Assembly	Thin Wall Housing	AMS 4130	760°R
Fuel Injector Manifold	Angle Gasket	Teflon	860°R
Ignition Exciter Unit	Electrical Insulation		620°R
Pressure Switch	Elec. Insulation		620°R
Gimbal Assembly	Conical Mount Housing	AMS 4139	760°R

* Reference 4.7.2.0-3

Figure 4.7.2.0-2 RL-10A-3-8 ENGINE MAXIMUM ALLOWABLE TEMPERATURE LIMITS FOR NON-OPERATING ENGINE

REFRACTORY ALLOYS

ALLOY	DENSITY LBS/IN ³	TENSILE (F _T) @ 70°F KPS	TENSILE (F _T) @ 70° (2%) KPS	TENSILE (F _T) EL. TEMP. KPS	TEN. MOD. (E _T) @ 70° X 10 ⁶	TEN. MOD. (E _T) EL. TEMP. X 10 ⁶	COMP. YLD. (F _C) @ 70° - KPS	COMP. YLD. (F _C) EL. TEMP. KPS	COMP. MOD. (E _C) @ 70° X 10 ⁶	EL. TEMP. % CHANGE (F _W , E _T)	RUPTURE STR @ 1800° KPS	RUPTURE STR @ 2000° KPS	RUPTURE STR MAX. TEMP KPS	CREEP IN/IN/HR X 10 ⁻³	CO. EXPANSION IN/IN X 10 ⁻⁶	THERM. COND. BTU _h /in ² /in/°F	EMISSIVITY	SPECIFIC HEAT BTU/LB.	MELTING POINT
<u>Tantalum</u> TA-222	.605	110	105 24.1 @ 3000°	24.9 @ 3000°	28.30						28. @ 2400° 100 Hrs.	4.9 @ 3000° 100 Hrs.					.43	.036	
<u>Tantalum</u> TA-111	.604	135	130 14.1 @ 3000°	16.3 @ 3000°	28.30							24. @ 2400° 10 Hrs.			4.2 @ 80° 3000°			.036	5400°
<u>Tantalum</u> TA-10W	.607	165	165	20 @ 3000°	28 - 30	15.0 @ 3000°					45. @ 2000° 20 Hrs.	23 @ 2400° 16 Hrs.	8.6 @ 3000° 10 Hrs.		3.5 @ 500° - 2400°	313 mean		.036	5516°
<u>Columbium</u> D 43	.326	95	75. 24. @2400°	27. @ 2400°							26. @ 2000° 100 Hrs.	6.5 @ 2400° 100 Hrs.			12. @ 2400°				4695°
<u>Columbium</u> (Fansteel) SF-85 (TDC 823)	.393	119	109 14.3 @ 2600°	14.7 @ 2600°	20.	12. @ 3000°					26. 10 Hrs.	11.8 @ 2400° 10 Hrs.	22.5 @2400°		5.18 @ 2700°	290.3			4695°
<u>Columbium</u> CB-752	.326	89.6	71.3 18.2 @ 2400°	25 @ 2400°	15.0	14.5 @ 700°					18. 100 Hrs.	8. @ 2400° 100 Hrs.			4.5 @ 68° - 2200°	300 @ 500° - 2400°			
<u>Columbium</u> (Web-Chang) WC-3015	.365	142	128	114. @ 1400°								20. @ 2400° 100 Hrs.							
<u>Molybdenum</u> TZC	.363	120	95	60. @ 2400°	40.0	10. @ 2500°					54.5 100 Hrs.	21. @ 2400° 100 Hrs.			2.7 @ 70°		.95	.065	4730°
<u>Molybdenum</u> TZM	.367	110	90	53.5 @ 2400°	40.0	10. @ 2500°					52.8 100 Hrs.	14. @ 2400° 100 Hrs.			2.7 @ 70°	933 @ 70° 233 @ 2500°	.95	.065	4730°
<u>Tungsten</u> W-25Re	.710			11.3 @ 4000°								5.8 @ 3000°							
<u>Nickel</u> TD-NiCr	.306			12.5 @ 2200°		12. @ 1800°						5.6			6.8 @ 1800°	193. @ 2000°			2550°

FIGURE 4.7.3.0-1 MATERIAL PROPERTIES

REFRACTORY ALLOYS

ALLOY	DENSITY LBS/IN ³	TENSILE (F _u) @ 70°F KPS	TENSILE (F _{ty}) @ 70° (F _{ty}) KPS	TENSILE (F _{tu}) EL. TEMP. KPS	TEN. MOD. (E _t) @ 70° X 10 ⁶	TEN. MOD. (E _t) EL. TEMP. X 10 ⁶	COMP. Y'LD. (F _{cy}) @ 70° - KPS	COMP. Y'LD. (F _{cy}) EL. TEMP. KPS	COMP. MOD. (E _c) @ 70° X 10 ⁶	EL. TEMP. % CHANGE (F _{tu} , E _t)	RUPTURE STR @ 1800° KPS	RUPTURE STR @ 1800° KPS	RUPTURE STR MAX. TEMP KPS	CREEP IN/IN/HR X 10 ⁻³	CO. EXPANSION IN/IN X 10 ⁻⁴	THERM. COND. BTUe/in ² /in ² /in/F°	EMISSIVITY	SPECIFIC HEAT BTU/LB.	MELTING POINT
Nickel Hastelloy R-235	.296	150	55. 12. in 2000°	31. in 1800°	30.	18 in 1800°	55.		29.		15 in 1500° 24 Hrs.	7.6 100 Hrs.			7.7 in 70° - 200°	62. in 70° 180. in 1700°	.88 in 2000° (oxide)	.1096	2300°
Nickel Inconel X750	.298	175	119 12.9 in 1700°	21.8 in 1700°	30. - 21.	18.5 in 1500°	121 (24)	98. in 1200°	31.		75. in 1600° 1000 Hrs.				7. in 70° 9.8 in 1800°	83. in 70° 164. in 1600°	.925 in 2000° (oxide)	.103 in 70° 171 in 1600°	2540°
Titanium 6AL-4V	.160	175.	163. 100. in 800°	130 in 800°	16.5		150.		17.		72 in 850°				5.6 in 70° - 1000°	66. in 70° - 800°	.52 in 800°	1.4 in 70° - 800°	3020°

FIGURE 4.7.3.0-1 Continued

05-17142

METALS - UNALLOYED

COMMON OR TRADE NAME	CHEMICAL SYMBOL	DENSITY LB./CU. FT. (GMS/CC.)	MELTING PT. OR DECOMP. TEMP.	MAX. LONG TIME TEMP. °F	MAX. SHORT TIME TEMP. °F	CONDUCTIVITY BTU/HR/FT/IN. ²	SPECIFIC HEAT BTU/LB. °F	DIFFUSIVITY FT. ² /HR X 10 ⁻⁶	EMISSIVITY	EXPANSION RATE IN./IN./°F X 10 ⁻⁶	TENS. STR. 70° X 10 ³ PSI	TENS. STR. EL. TEMP. X 10 ³ PSI	MODULUS X 10 ⁶ PSI	MOD. RCTURE PSI
<u>BERYLLIUM</u>	Be	113.4 (.0668)	2441°			1560. at 70° 516. at 1800°	.45 at 70° .84 at 1800°			10.37 at 70° 1832°	60. - 90.	20-22 at 1470°	40. - 44. at 70°	
<u>BORON</u>	B	144.8	3902°				.25 at 70°		.72 at 1 at	4.58 at 70°-1832°				
<u>CHROMIUM</u>	Cr	447. (.206)	3434°			463.2 at 70°	10 at 70° .27 at 3000°		.075 at 500° .45 at 1700°	6.84 at 70° 3272°	12.	26 at 1500°	36	
<u>COBALT</u>	Co	355.6 (.322)	2714°			478.6 at 70°	.10 at 70° .21 at 2000°			10.258 at 70°-1832°			30	
<u>HAFFNIUM</u>	Hf	417.2 (.473)	3992°		2000°	154 at 70° - 200°	.0351 at 70° - 200°			3.31 at 70° - 1832°	65.	34 at 700°	20. at 70°	
<u>GOLD</u>	AU	1204.9 (.698)	1.945°			2155.4 at 0° - 200°F	.0312			9.42 at 70° - 1832°	18,000 - 32,000		11.6	
<u>IRIDIUM</u>	Ir	1398.4 (.813)	4442°			406 at 70°	.0207 at 70°		.30 at 70°	5.07 at 70° 3632°	90	48 at 1830°	76	
<u>IRON</u>	Fe	490.7 (.2845)	2795°			580 at 70°	106 at 60° - 155 at 1700°		.4 at 70° (Bright)	8.89 at 70° -2534°	35 - 40		28.5	
<u>NICKEL</u>	Ni	555.6 (.322)	2650°		1472° Oxidi- zes Rapid- ly	570 at 70°	1125 at 200° 13 at 1100°		.355 at 70° (Bright)	9.50 at 70° 1832°	46,000		30. at 70°	

FIGURE 4.7.3.0-1 Continued

METALS - UNALLOYED

COMMON OR TRADE NAME	CHEMICAL COMPOSITION	DENSITY LB./CU. FT. (GMS/CC)	MELTING PT. OR DECOMP. TEMP.	MAX. LONG TIME TEMP. °F	MAX. SHORT TIME TEMP. °F	CONDUCTIVITY BTU'S IN. FT. IN. °F	SPECIFIC HEAT BTU'S/LB. °F	DIFFUSIVITY FT ² /HR X 10 ⁻⁶	EMISSIVITY	EXPANSION RATE (IN./IN. °F X 10 ⁻⁶)	TENS. STR. 70°F X 10 ³ PSI	TENS. STR. EL. TEMP. X 10 ³ PSI	MODULUS X 10 ⁶ PSI	MOD. RUPTURE PSI	
<u>PLATINUM</u>	Pt	1339.1 (.773)	3226°	2552 in Air		490 70° - 200°	.0314		.65	6.50 70° - 3210°	20. - 24.		21.3 70°		
<u>RHENIUM</u>	Rh	1306.3 (.756)	5738°		1112° forms volatile oxide	493.2 70°			.42 70° - 3662°	4.05 70° - 3632°	367.	25. 3000° F	66.7 70°		
<u>RHODIUM</u>	Rh	780.4 (.447)	3570°		2012° Oxide De-comp.	609.2 70°	.059 32° F		.24 70°	6.75 70° - 2732°	138. - 300.		42.5 70°		
<u>SILICON</u>	Si	149.8 (.084)	2538°		2012° Oxidizes	580.2 70°	.162 70°		.28 70° - 2400°	1.295 70° - 2552°			16.3 70°	9046	
<u>TANTALUM</u>	Ta	1036. (.600)	5432°		932° Reacts with O ₂	247.13 70°	.036 70° - 3600°	.222 70° - 2372° .247 70° - 3092°	.40 (Bright) .78 (Oxide)	4.45 70° - 4532°	75. - 180.	15.20 1832° F	27. 70° 22. 1832°		
<u>TITANIUM</u>	Ti	291. (.163)	3272°		1022° Imbrittled	108.3 70°	.138 70° - 932°		.30 70° - 1316°	5.2 70° - 1825°	34.	12 70° 1000° F	16 70°		
<u>TUNGSTEN</u>	W	1205 (.697)	6152°		1112° Oxidizes	470 70° - 3632°	.032 70°	.639 70°	.279 70° - 2192° .311 70° - 2600°	3.26 70° - 4532°	430. (.28 dia. Wire)	20. 70° 3600° F	59. 70° 50. 2192°		
<u>ZIRCONIUM</u>	Zr	398.3 (.230)	3320°			146.3 70°	.0659 70°		.46	3.57 70° - 2732°	62		13.7 70°		

Figure 4.7.3.0-1 Continued

D5-17142

4-231

METALS - UNALLOYED

COMMON OR TRADE NAME	CHEMICAL COMPOSITION	DENSITY LB/CU. FT. (LBS/IN. ³)	MELTING PT. OR DECOMP. TEMP.	MAX. LONG TIME TEMP. °F	MAX. SHORT TIME TEMP. °F	CONDUCTIVITY BTU'S HR FT. ² /IN. ² °F	SPECIFIC HEAT BTU'S LB/°F	DIFFUSIVITY FT. ² /HR X 10 ⁻⁶	EMISSIVITY %	EXPANSION RATE IN/IN/°F X 10 ⁻⁶	TENS. STR. 10 ³ PSI	TENS. STR. EL. TEMP. X 10 ³ °F	MODULUS X 10 ⁶ PSI	MOD. RUPTURE PSI	
<u>Niobium-Columbium</u>	Nb Cb	524.4 (.310)	4380°		750° oxidizes rapidly	340 @ 70° 1100°	.065 @ 70°		.76 @ 2500° .42 @ 3500°	5.02 @ 70° -3632°	40 - 85	13 - 17 @ 1932°	15. @ 77° 13. @ 1600°		
<u>Molybdenum</u>	Mo	637.6 (.369)	4760°		932° oxidizes rapidly	960. @ 70° 480. @ 3800°	.66 @ 70°		.04 @ 70° .15 @ 2500°	3.62 @ 70° -2732°	120-200	20 - 30 @ 1832°	46. @ 70° 39. @ 1832°		

FIGURE 4.7.3.0-1 Continued

05-17142

4-232

CARBON AND GRAPHITE MATERIALS

COMMON OR TRADE NAME	CHEMICAL COMPOSITION	FORM	DENSITY LB/CU. FT (LBS./IN. ³)	MELTING PT. OR DECOMP. TEMP.	MAX. LONG TIME TEMP. °F	MAX. SHORT TIME TEMP. °F	CONDUCTIVITY BTU _s /HR/FT ² /IN/°F	SPECIFIC HEAT BTU _s /LB/°F	DIFFUSIVITY BTU _s /FT ² /SEC X 10 ⁻⁶	EMISSIVITY	EXPANSION RATE IN/IN/°F X 10 ⁻⁶	COMP. STR. 70°F X 10 ³	COMP. STR. EL. TEMP. X 10 ³	MODULUS X 10 ⁶	MOD. RUPTURE	
Carbon	C	Block	140.5 (.0913)	6740°	Oxidi- zes Above 500°			.165		.99	3 - 24. @ 70° - 200°					
Carbon Plate H-205 Great Lakes Carbon	C	Plate Sheet	109.2 (.063)	6600°	"		960			.95	250.	58. @ av. 1300°		3.20 (Comp. HG)		
Pyrolytic Graphite Pyrogenics	C	Plate Sheet	124.8 (.0744)	6600°	"		13 WG 2580 AG	.45		.5 WG @ 1800 .42 WG @ 2600°	1.1 - 2.2	15. WG 60. AG				
Carbon Foam RC-45 Airco Speer	C	Foam Block	3.74 (.0022)	6600°	"		0.4 AV.	.4		.95		.33				
Graphite Foam RG-45 Airco Speer	C	Foam Block	4.99 (.0029)	6600°	"		.417 @ 400° -1600°	.32 AV @ 70° - 3000°		.95		.045				
Graphite Foam RG-45T Airco Speer	C	Foam Block	9.98 (0058)	6600°	"		0.4 AV.	"		.95		.44				
Graphoil (Pyrolytic G.) Nat'l Carbon	C	Flex Sheet	60 (.035)	6600°	"		15.6WG 300 AG @ 2000°				15. WG. -0.2 AG @ 70°-2000°	10.		.2		
Carbon Felt VDG National Carbon	C	Fib. Mat'l	5.2 (0031)	6600°	"		.25 @ 100° 4.5 @ 3500°	.17 @ 70° - 4@ 2500°		.99		10% Def. @ 7 PSI				
Graphite Felt Nat'l. Carbon	C	Fib. Mat'l	5.3 (.0031)	6600°	"		1.2 @ 100° 2.0 @ 3500°	.17 @ 70° .4 @ 2500°		.99		10% Def. @ .35				

FIGURE 4.7.3.0-1 Continued

FIBROUS CERAMIC INSULATION

COMMON OR TRADE NAME AND MANUFACTURER	CHEMICAL COMPOSITION	FORM	DENSITY LB. CU. FT. (0.015 ³)	MELTING PT. OR DECOMP. TEMP.	MAX. LONG TIME TEMP. °F	CONDUCTIVITY BTU'S IN/FT ² IN °F	SPECIFIC HEAT BTU'S LB. °F	EMISSIVITY	COMP. DEFLECTION 70°F. - 1	MOD. RUPTURE PSI. °F	SHRINKAGE % °F	WEIGHT LOSS AT TEMPERATURE °F	
JM Microquartz Johns Manville	SiO ₂ 98.5%	Fib. Matl.	3.0 (.00173)	3100°	2000°	.30 300 91 1000°	2.4-200° 28-2600°	1-2700°			4.5-1500° 7-2000°	5.5-1500° 7.0-2750°	
JM Microquartz Johns Manville	SiO ₂ 98.5%	Fib. Matl.	6.0 (.0034)	3100°	2000°	.30 300 68 1000°	2.4-200° 28-2600°	1-2700°			4.5-1500° 7-2000°	5.5-1500° 7.0-2750°	
JM Dynaquartz Johns Manville	SiO ₂ 98.5%	Fib. Matl.	4.5	3100°	2750° ??	.53 600 1.53 2100°	229-400° 292-1800°	4-2700°	2.4 1.5lbs. 8.7 4.5lbs.	19.0	1.0% 2750°	5.5-1500° 7.0-2750°	
JM Dynaquartz Johns Manville	SiO ₂ 98.5%	Fib. Matl.	6.2	3100°	2750° ??	.53 600 1.40 2100°	229-400° 292-1800°	4-2700°	2.4-3lbs. 8.7 9.6lbs.	35.0	1.0% 2750°		
JM Dynaquartz Johns Manville	SiO ₂ 98.5%	Fib. Matl.	8	3100°	2750° ??	.52 600 1.28 2100°	229-400° 292-1800°	4-2700°	2.4 4.5lbs. 8.7 9.6lbs.	58.0	1.0% 2750°		
JM Thermoflex RF-400 Johns Manville	Al ₂ O ₃ SiO ₂	Fib. Matl.	4	3200°	2300°	.31 200° 3.88 2000°	25 Av						
JM Thermoflex RF-600 Johns Manville	Al ₂ O ₃ SiO ₂	Fib. Matl.	6	3200°	2300°	.29 200° 2.31 2000°	25 Av						
JM Thermoflex RF-400 Johns Manville	Al ₂ O ₃ SiO ₂	Fib. Matl.	8	3200°	2300°	.28 200° 2.31 2000°	25 Av						

FIGURE 4.7.3.0-1 Continued

FIBROUS CERAMIC INSULATION

COMMON OR TRADE NAME AND MANUFACTURER	CHEMICAL COMPOSITION	FORM	DENSITY LB/CU. FT. (LB/IN ³)	MELTING PT. OR DECOMP. TEMP.	MAX. LONG TIME TEMP. °F	CONDUCTIVITY BTU _s /HR/FT ² /IN/°F	SPECIFIC HEAT BTU _s /LB/°F	EMISSIVITY	COMP./DEFLECTION 70°F - %	MOD. RUPTURE PSI @ °F	SHRINKAGE % 1000	% WEIGHT LOSS AT TEMPERATURE °F	
JM Dyna-Flex DF-300 Johns Manville	AL ₂ O ₃ SiO ₂ Cr ₂ O ₃	Fib. Matl.	1	3000°	2700°	.31 @ 200° 1.09 @ 2000°					3.5% @ 2600° 6.4% @ 2700°		
JM Dyna-Flex DF-600 John Manville	AL ₂ O ₃ SiO ₂ Cr ₂ O ₃	Fib. Matl.	8	3000°	2700°	.28 @ 200° 1.32 @ 2000°					3.5% @ 2600° 6.7% @ 2700°		
JM Dyna-Flex DF Johns Manville	AL ₂ O ₃ SiO ₂ Cr ₂ O ₃	Fib. Matl.	12	3000°	2700°	.27 @ 200° 1.53 @ 2000°					3.5% @ 2600° 6.7% @ 2700°		
MIN-K 200° (10 Lb.) Johns Manville	SiO ₂ MgFe Flex.	Fib. Matl.	10.0 (.0057H)		1800°	.32 @ 600° .67 @ 1200°	0.23 @ 400° 0.27 @ 1600°				1.0%		
MIN-K 2000 (20 Lb.) Johns Manville	SiO ₂ MgFe SiO ₃	Fib. Mat'l.	20.0 (.0115H)		1800°	.27 @ 800° .46 @ 1600°	0.23 @ 400° 0.27 @ 1600°		2.0% @ 33 PSI 6.0% @ 350 PSI				
Refrasil A-100 HITCO	SiO ₂ 97%	Fib. Matl. Blank	6 Lb. (.0035)		2000°	.96 @ 1600°	.20 @ 180° .29 @ 2540°				5.7% @ 2000° Max.		
TMS 0414 HITCO	AL ₂ O ₃ SiO ₂	Fib. Matl. Blank	6 Lb. (.0035)	3200°	2300°	1.61 @ 1600°	.255 @ 1800°						

FIGURE 4.7.3.0-1 Continued

FIBROUS CERAMIC INSULATION

COMMON OR TRADE NAME AND MANUFACTURER	CHEMICAL COMPOSITION	FOAM	DENSITY LB./CU. FT. (LB./IN. ³)	MELTING PT. OR DECOMP. TEMP.	MAX. LONG TIME TEMP. °F	CONDUCTIVITY BTU _s HR/FT ² IN./°F	SPECIFIC HEAT BTU _s /LB/°F	EMISSIVITY	COMP. / DEFLECTION 70°F - °F	MOD. RUPTURE PSI @ °F	SHRINKAGE %
<u>PV Superemp Block</u> Eagle Picher Ind	SiO ₂ Al ₂ O ₃ CaO	Fib. Matl. Board	17 Lb. (.0092)	3200°	1900°	.25 ft 200° .69 ft 1000°	0.25 AV.	.90	10° ft 166 PSI	40.	2.2 ft 1800°
<u>Ceramic Block</u> Eagle Picher Ind.	SiO ₂ Al ₂ O ₃	Fib. Matl. Board	15 Lb (.0086)	3200°	2300°	.39 ft 400° 1.01 ft 1600°	0.263 ft 2200°	.18	5° ft 243 PSI	55.	1.25 ft 2300°
<u>Fiberfrax 970</u> Carborundum	Al ₂ O ₃ SiO ₂	Fib. Felt Paper	12 Lb. (.007)	3200°	2300°	.37 ft 400° 1.55 ft 2200°	.25 AV.				
<u>Fiberfrax Block F-13</u> Carborundum	Al ₂ O ₃ SiO ₂	Fib. Block	16 Lb. (.0093)	3200°	2300°	.46 ft 400° 1.7 ft 1800°	.25 AV.			.130	2.5 ft 1800° 5.4 ft 2300°
<u>Barakald Paper</u> Norton Refractories	Al ₂ O ₃ SiO ₂ M ₂ O	Fib. Paper	12 Lbs (.007)	3090°	2300°	.35 ft 400° 1.4 ft 2000°	.255 ft 1800°				
<u>Barakald Blanket</u> Norton Refractories	Al ₂ O ₃ SiO ₂ TiO ₂ Fe ₂ O ₃	Fib. Matl.	4 Lbs. (.0023)	3200°	2300°	.36 ft 400° 2.2 ft 1800°	.255 ft 1800°				
<u>Zirconia Felt ZYF - 100</u> Union Carbide	ZrO ₂ HfO ₂ Y ₂ O ₃	Fib. Matl.	14 (.0081)	4700°	4500°	.35 ft 70° 2.1 ft 3000°	.14 ft 70° 1600°	.4 ft 70° 1500°			1.4 ft 2000° 2800°

FIGURE 4.7.3.0-1 Continued

CERAMIC - CERMET MATERIALS

COMMON OR TRADE NAME	CHEMICAL COMPOSITION	FORM	DENSITY LB/CU. FT. (LBS/IN ³)	MELTING PT. OR DECOMP. TEMP.	MAX. LONG TIME TEMP. °F	MAX. SHORT TIME TEMP. °F	CONDUCTIVITY BTU _s /HR/FT ² /IN/°F	SPECIFIC HEAT BTU _s /LB/°F	DIFFUSIVITY FT ² /SEC x 10 ⁻⁶	EMISSIVITY	EXPANSION RATE IN/IN/°F x 10 ⁻⁶	COMP. STR. 70°F x 10 ³	COMP. STR. EL. TEMP. x 10 ³	MODULUS x 10 ⁶	MOD. RUPTURE	
<u>Alumina</u> Aluminum Oxide Cast-Pressed-Fused AL-52.5% O ₂ - 47.1%	Al ₂ O ₃ (99.8%)	Dense Solid	247.5 (.141)	3060°	2700° 3000°	3100°	240. ft 70° 50. ft 2000°	.18 ft 70° .28 ft 2000°	.06 ft 2700°	.4 ft 2700°	4.4 ft 70° - 1650°	140. - 380. -	50. ft 3000°	52.4 ft 70° 25.6 ft 2700°	1800-3000 (75-85% Dense)	
<u>Alumina, Porous</u> 47% Density	Al ₂ O ₃	Brick	120 (.070)	3660°	2700° 2900°	3000°	6. ft 2400°	.18 ft 70° .28 ft 2000°		.4 ft 2700°				10. ft 2400°	1000 - 1600 psi (50% Dense)	
<u>Alumina Foam Brick</u> 15.2% Density	Al ₂ O ₃	Brick	37. (.021)	3660°	2700° 2900°	3000°	3. ft 1700°	.18 ft 70° .28 ft 2000°		.4 ft 2700°		11.7		1.0		
<u>Aluminum Silicate</u> (Sillimanite System) Al ₂ O ₃ - 63%, SiO ₂ - 37%	Al ₂ O ₃ SiO ₂	Block Brick Cast	202 (.117)	2950°	2550°	2730°	12.3 ft 200° 8.8 ft 2732°	.25 ft 1100°		.6 ft 1800° 2600°	3.12 ft 77° - 2730°	75 (87% Dense)		21. ft 70°		
<u>Aluminum Silicate</u> Mullite System 3 Al ₂ O ₃ - 71.8%, 2 SiO ₂ 28%	3 Al ₂ O ₃ 2 SiO ₂	Block Brick Cast	173.5 (.099)	3326°	2830°	3090°	42. ft 70° 27.6 ft 2000°	.25 ft 1100°			3.35 ft 70° - 2500°	100 - 150.		20.5 ft 70°	1000 - 3500 PSI (75 - 85% Dense)	
<u>Magnesium Aluminate</u> (Spinel System) Al ₂ O ₃ - 71.8%, 2 MgO - 28%	Al ₂ O ₃ 2MgO	Fused Block	220 (.124)	3875°		3452°	102 ft 200° 36. ft 2000°	.29 ft 70° - 2000°			5.0 ft 70° - 2600°	270.	8.5 ft 3000°	34.5 ft 70° 20.1 ft 2400°		
<u>Alum. - Lithium - Silicate</u> Pyroceram - CER-VIT C-100 Al ₂ O ₃ - 24%, Li ₂ CO ₃ - 17.7%, SiO ₂ 54%	Al ₂ O ₃ Li ₂ CO ₃ SiO ₂	Fused Shapes	156 (.0903)	2552°	1400°	1650°	9.6 ft 1500°	.196			.0 ft 70° - 1000°			13.3 ft 650° - 1000°	13,000	

FIGURE 4.7.3.0-1 Continued

CERAMIC - CERNET MATERIALS (CONTINUED)

COMMON OR TRADE NAME	CHEMICAL COMPOSITION	FORM	DENSITY LB/CU. FT. (LBS. IN ³)	MELTING PT. OR DECOMP. TEMP.	MAX. LONG TIME TEMP. °F	MAX. SHORT TIME TEMP. °F	CONDUCTIVITY BTU _s /IN/FT ² /IN/°F	SPECIFIC HEAT BTU/LB/°F	DIFFUSIVITY FT ² /SEC X 10 ⁻⁶	EMISSIVITY	EXPANSION RATE IN/IN/°F X 10 ⁻⁶	COMP. STR. 70°F X 10 ³	COMP. STR. EL. TEMP. X 10 ³	MODULUS X 10 ⁶	MOD. RUPTURE	
<u>Beryllium Carbide</u>	Be ₂ C		152.3 (.088)	3810°	1800°	2100°	9.0 @ 70° 15.6 @ 70° 1600° 2300°	.34 @ 70° .85 @ 2300°			5.8 @ 70° 1472°	105.	30. @ 2000°	45.6 @ 70°	16,000	
<u>Beryllium Oxide</u> <u>Berlox - Beryllia</u>	BeO 99.96%	Cast Press Fused	188. (.109)	4638°	2732°	3360°	1680. @ 70° 120. @ 2000° 113. @ 3000°	.378 @ 500° .53 @ 3000°		.64 @ 1600° .92 @ 3500°	9.54 @ 70° 2550°	200.	7. @ 3000°	45. @ 70° 20. @ 1300°		
<u>Beryllium Oxide</u> <u>Foam - 22% Dense</u>	BeO 99.5%	Block	41.4 (.024)	4658°	2732°	3360°	20. @ 70° 2. @ 1800°	.370 @ 50° .55 @ 3000°		.36 @ 1832° .50 @ 3270°	~ 1.5					
<u>Beryllium Aluminate</u>	BeO Al ₂ O ₃		235 (.136)	3420°			.2 @ 70° .35 @ 2000°				4.8 @ 70° 1830°					
<u>Boron Carbide</u> B = 78%, C = 20%	B ₄ C	Fused	156. (.090)	4440°	1000°	Oxidi- zes @ 1850°	180. @ 70° 95. @ 1800°	.217 @ 70° .51 @ 2000°		.76 @ 1650°	3.16 @ 70° 1470°	414.		66. @ 70°		
<u>Boron Nitride</u>	BN	Cast	137 (.079)	5430°		1300°	220 @ 70° 140 @ 2000°	.2 @ 70° .3 @ 3000°		.7 @ 1000° 3000°	3.38 @ 77° 2460°	34. - 45.	6. @ 1900°	12.4 @ 70° 1.6 @ 1800°		
<u>Calcium Oxide</u>	CaO	Fused	209 (.121)	4675°	2500°	4350°	52. @ 70° 48. @ 2000°	.18 @ 70° .22 @ 2000°			7.0 @ 70° 1000°					
<u>Calcium Silicate</u> 2 CaO - 64.5%, SiO ₂ - 34.9%	2CaO SiO ₂	Slip Cast	205. (.118)	3865°				.178 @ 70°			4.83 @ 70° 200° - 2200°	70				

FIGURE 4.7.3.0-1 Continued

CERAMIC - CERMET MATERIALS (CONTINUED)

COMMON OR TRADE NAME	CHEMICAL COMPOSITION	FORM	DENSITY LB/CU. FT. (G/CM ³)	MELTING PT. OR DECOMP. TEMP.	MAX. LONG TIME TEMP. °F	MAX. SHORT TIME TEMP. °F	CONDUCTIVITY BTU/HR FT ² IN/°F	SPECIFIC HEAT BTU/LB. °F	DIFFUSIVITY FT ² /SEC X 10 ⁻⁶	EMISSIVITY	EXPANSION RATE IN/IN °F X 10 ⁻⁶	COMP. STR. 70°F X 10 ³	COMP. STR., EL. TEMP. X 10 ³	MODULUS X 10 ⁶	MOD. RUPTURE	
<u>Magnesium Silicate</u> <u>Steatite</u>	MgO - SiO ₂	Cast Fused Block	171 (.099)	2830°	1832°	1990°	17.5 @ 70° 6.4 @ 1500°	.201 @ 70° .32 @ 2000°			6.02 @ 70° 2732°	80.		15		
<u>Magnesium Silicate</u> <u>Forsterite</u> 2MgO-59% SiO ₂ - 42%	2MgO SiO ₂	Cast Fused Block	201 (.116)	3416°	1800°	2000°	36.6 @ 200° 14.6 @ 1472°	.201 @ 70°			6.1 @ 70° 2600°	85		21 @ 70°	700-1300 psi (70 - 80% dense)	
<u>Mag. - Alum. Silicate</u> <u>Cordierite</u>	2MgO 2 Al ₂ O ₃ 5 SiO ₂	Cast Fused Block	156.6 (.0903)	2686°	2050°	2500°	22.2 @ 70° 8.8 @ 1500°				3.6 @ 70° 1650°	70		8.8 @ 70°		
<u>Magnesium Oxide</u> <u>Magnesia - Periclase</u>	MgO	Cast Fused Block	223. (.129)	5156°	2912°	3300°	240. @ 70° 48. @ 3000°	.283 @ 70° 3000°		.49 @ 900° .22 @ 2550°	6.45 @ 70° 1000° 9.5 @ 1800° -4000°	10 - 100	15 @ 3000°	22. - 40. @ 70° 4. @ 2300°		
<u>Silicon Dioxide</u> <u>Silica - Quartz - Vycor</u>	SiO ₂	Cast Fused	157. (.0903)	3100°	1500°	2000°	4.2 @ 70° 15.1 @ 2000°	15 @ 70° 32 @ 2000°			.5 @ 32° 1830°	20 - 25		11. @ 70° 2600°		
<u>Silicon Carbide</u>	SiC	Cast Fused	201. (.116)	4262	2500°	2900	111.3 @ 1100° 2732°	26 @ 1000° .35 @ 2822°		.79 @ 1400° .77 @ 2800°	2.6 @ 70° 3000°	82. - 120.		60. @ 70° 51. @ 2100°	2000 - 4000 psi (75 - 80% Dense)	
<u>Tantalum Beryllide</u>	Ta Be ₁₂		261. (.151)	3360°	2200°	2800° -3000°	180 -200. @ 500° 2800°	27 @ 700° 2800°			9.25 @ 70° 2750°			33. @ 70° 2500°		

FIGURE 4.7.3.0-1 Continued

CERAMIC - CERMET MATERIALS (CONTINUED)

COMMON OR TRADE NAME	CHEMICAL COMPOSITION	FORM	DENSITY LB./CU. FT. (G/CM ³)	MELTING PT. OR DECOMP. TEMP.	MAX. LONG TIME TEMP. °F	MAX. SHORT TIME TEMP. °F	CONDUCTIVITY BTU-IN/FT ² -IN ² -°F	SPECIFIC HEAT BTU/LB-°F	DIFFUSIVITY FT ² /SEC X 10 ⁻⁶	EMISSIVITY	EXPANSION RATE IN/IN-°F X 10 ⁻⁶	COMP. STR. 70°F X 10 ³	COMP. STR. FL. TEMP. X 10 ³	MODULUS X 10 ⁶	MOD. RUPTURE	
<u>Tantalum Monocarbide</u> Ta - 93.7%, C - 6.2%	TaC	Press. Sint.	8.72 (5.04)	7016°		1400° burns (1472°)	155.2	3.7 @ 70° 4000°		.36 @2912° 48 @ 4800°	4.21 @ 70°-3600°			52.7 @ 70°		
<u>Tantalum Diboride</u> Ta - 89.2%	TaB ₂		7.86.6 (4.55)	5600°	2000°		75.5 @ 70° 210.1 @ 3000°	.04 @ 70°			4.76 @ 70° - 2730°			36.		
<u>Thorium Dioxide</u>	ThO ₂	Press. Sint.	574.5 72° Dense	5830°	4530°	4892	72. @ 70° 18. @ 2000°	.055 @ 70° 075 @ 3800°		.77 @ 70° 62 @ 1500°	5.35 @ 70° - 2600°	214	1.4 @ 2730°	21 @ 70° 12.8 @ 2300°		
<u>Titanium Dioxide</u> <u>Anatase Rutile Titania</u>	TiO ₂	Cast Press.	266. (1.54)	3340°	1470° (oxidizes)		46 @ 20° 23.2 @ 2100°	16 @ 70° .208 @ 1900°		19 @ 900° 27 @ 1500°	4.9 @ 80° - 2730°			41 @ 70°		
<u>Titanium Monocarbide</u>	TiC	Cast Press. Sint.	307.5 (1.78)	5750°	1000°	2000° oxidizes	240. @ 800° 318. @ 4000°	.12 @ 70° 24 @ 4000°	8.61	.75 @ 1000° - 3000°	4.5 @ 70° - 4000°	200 - 400.		65 @ 70°		
<u>Titanium Nitride</u>	TiN	Cast Press. Sint.	338.5 (1.96)	5340°	1000°	1100° oxidizes	203. @ 70° 58 @ 3000°	.14 @ 70° .21 @ 2800°			5.0 @ 70° - 2600°	141		36.3		
<u>Titanium Diboride</u> Ti - 84.8%	TiB ₂	Cast Press. Sint.	282. (1.63)	5200°		2000° oxidizes	204. @ 70° 480. @ 3000°	.18 @ 80° - 1700°			4.8 @ 70° - 4000°	47. -97.		60. @ 70°/45. @3800°	19,000	
<u>Zirconium Dioxide</u> <u>Zirconia</u>	ZrO ₂	Cast Press. Sint.	350. (2.02)	4890°	2012°	3000°	12. @ 70° 6.4 @ 2190°	.105 @ 70° .16 @ 2000°		.65 @ 932° 34 @ 2552°	6.12 @ 70° 2700°	150	2.8 @ 2732°	25. @ 70° 12.5 @ 2700°	5000 - 12,000	
<u>Zirconium - Silicate</u> <u>Zircon</u> Zr - 49%, O ₂ - 34%, Si - 16%	ZrO ₂ SiO ₂	Slip Cast Fused	293 (1.70)	4550°	2000°		36. @ 70° - 2250°	.16 @ 70° - 2500°		.45 @ 1000° - 1800°	3.1 @ 70° - 2200°	100	6.0 @ 2732°	15. - 20. @ 70°		
<u>Zirconium Carbide</u> Zr - 86.2%	ZrC	Press. Sint.	410 (2.24)	6385°	1700°	2000° oxidizes	240. @ 1000° - 3000°	.08 @ 70° .124 @ 2000°	1.117 @ 3000°		3.7 @ 70° - 1500°	238		50. - 57. @ 70°		
<u>Zirconium Nitride</u> Zr - 81.8%	ZrN		442 (2.56)	5395°		2000° oxidizes	97. @ 70° 39. @ 2000°	.9 @ 70° .13 @ 2600°			3.58 @ 70° 1200°	70 - 100				

FIGURE 4.7.3.0-1 Continued

MATERIAL	NOMINAL COMPOSITION %	OXIDATION RESISTANCE °F	MELTING RANGE °F	COST \$/SQ FT .020 IN THICK	DENSITY LBS/IN ³	SERVICE TEMP. 800°F TO 1800°F				WELDABILITY	MACHINEABILITY	AVAILABILITY FORM & STATUS
						THERMAL EXPANSION IN/IN X 10 ⁻⁶	TENSILE KSI	YIELD KSI	ELONGATION %			
Inconel 718	Ni 50-55 Cr 17-21 Cb+Ta 4.75-5.5 Mo 2.8-3.3 Co 1.0 Max. Ti .65 - 1.15 Fe Bal	1800	2200- 2450	4.03	0.296	70°F - 5.9 200°F 7.2 500°F 7.9 1000°F 8.2 1500°F 9.3 2000°F 10.0	Room - 195 1200°F -160 1400°F -98 1600°F -49 1800°F -15 2000°F -8	Room - 160 1200°F -140 1400°F -91 1600°F -48 1800°F -15 2000°F -8	Room - 15 1200°F -15 1400°F 8 1600°F 88 1800°F 170 2000°F 125	Very Good Weld and annealed with no spontaneous hardening unless cooled slowly	Poor	Sheet Strip Plate Bar State-of-art
Inconel X750	Ni+Co 70.0 Min Fe 5.0-9.0 Cr 14.0-17.0 Ti 2.25-2.75 Cb+Ta 0.70-1.2	-	2350- 2600	2.46	.298	70°F - 5.7 200°F 7.0 500°F 7.4 1000°F 8.1 1500°F 9.1	Room - 175 1200°F -128 1400°F -98 1600°F 53 1800°F 9	Room - 125 1200°F 104 1400°F 78 1600°F 40 1800°F 5	Room - 20 1200°F 10 1400°F 5 1600°F 12 1800°F 89	Satisfactory	Poor	Tube Sheet Rod Bar, etc. State-of-art
Bene 41	Cr 19.0 Ni 53 Co 11 Mo 10 Ti 3.2 Al 1.60 Fe 2.0	-	2250- 2500	9.14	.296	70°F - 200°F 6.6 400°F 6.8 1000°F 7.5 1600°F 8.7	Room - 175 1200°F 164 1400°F 140 1600°F 88 1800°F 40	Room - 130 1200°F 130 1400°F 121 1600°F 84 1800°F 25	Room - 10 1200°F 8 1400°F 5 1600°F 5 1800°F 20	Good Like other High alum. & high titanium alloys	Poor Machine in aged condition with Tungsten carbide tools Soft & gummy	Sheet Plate Foil Bar Forging Billets Like Austenetic S. S. in anneal condition State-of-art
TD Nickel	ThO ₂ 2 Ni Bal	2000	2650	-	0.322	SERVICE TEMP. 1800°F TO 2200°F				Poor Brazing recommended 80% parent material strength	Poor Soft & gummy	Slabs Billets Rods Plates Sheets Tube Hollows Foil Wire tubing State-of-art
						Mean 70-1000°F 8.5	70°F - 65 1800°F 18 2000°F 14 2400°F 9	70°F 45 1800°F 17 2000°F 12 2400°F 7	70°F 15 1800°F 7 2000°F 7 2400°F 5			
TD Nickel Chromium	Cr 20 ThO ₂ 2 Ni Bal	2400	2600	110.00	.306	Mean 70-1800°F 8.8	Room 125 1200°F 65 1500°F 35 2000°F 16	Room 80 1200°F 54 1500°F 30 2000°F 15	Room 18 1200°F 8 1500°F 7 2000°F 3	Poor Brazing recommended 50-70% parent material strength	Poor Soft & gummy	Sheet Rod State-of-art

FIGURE 4.7.3.0-2: RADIATIVE MATERIAL PROPERTIES

SERVICE TEMP. 2200°F TO 2500°F																						
MATERIAL	NOMINAL COMPOSITION	OXIDATION RESISTANCE °F	MELTING RANGE °F	RAW MATERIALS COST \$/LB	DENSITY LBS/IN ³	THERMAL EXPANSION IN/IN X 10 ⁻⁶	TENSILE KSI	YIELD KSI	ELONGATION %	WELDABILITY	MACHINEABILITY	AVAILABILITY FORM & STATE										
Columbium C-129	Cb 80 Ta 9-11 W 9-11	-	4710	95.60	0.347	-	Room 85	Room 65	Room 25	Acceptable Electron Beam or TIG	Good	Threading and tapping are often difficult to accomplish										
							2000°F 39	2000°F 29	2000°F 40													
							2400°F 25	2400°F 22	2400°F 3													
							2700°F -	2700°F -	2700°F -													
							3000°F 11	3000°F 10	3000°F 65													
							3500°F 5	3500°F 4	3500°F 60													
NOTE: Columbium alloys exhibit a ductile brittle transition at subzero temperatures																						
Columbium C-103	Hf 10 Ti 1.8 Zr 0.5 Cb Bal	-	4400		0.320	Mean 32-212°F App. 0.60	Room 61	Room 43	Room 25	Acceptable TIG or Electron Beam	Good	High ductility causes problems with drilling and tapping										
							2000°F 27	2000°F 20	2000°F 45													
							2400°F 13	2400°F 11	2400°F 70													
							2700°F 9.5	2700°F 9	2700°F 70													
							3000°F 5	3000°F 4	3000°F 70													
Fansteel 85	Ta 26-29 W 10-12 Zr 0.6-1.1 Cb Bal	-	4695	-	0.383	-	Stress Relieved Sheet	Stress Relieved Sheet	Stress Relieved Sheet	Good TIG or Electron Beam	Fair	Tendency to tear and gall										
							-320°F 170	-320°F 135	-320°F 17													
							RT 92	RT 78	RT 18													
							2000°F 45	2000°F 42	2000°F 22													
							2400°F 22	2400°F 21	2400°F 61													
							2600°F 16	2600°F 14	2600°F 80													
							Recrystallized -320°F 150	Recrystallized -320°F 130	Recrystallized -320°F 16													
							RT 82	RT 60	RT 23													
							2000°F 35	2000°F 22	2000°F 40													
							2400°F 21	2400°F 19	2400°F 58													
							2600°F 18	2600°F 15	2600°F 30													
							SERVICE TEMP. 2500-3500°F															
							Tantalum Fansteel 60	W 8.5 - 11.0 Ta Bal	4500				5495	95.33	0.608	Mean 32-213°F 3.6	RT 80	RT 65	RT 25	Feasible GTA Welded Electron Beam Resistance Welding	Good	High ductility low hardness is chief cause of machining problems Threading and tapping are often difficult
2000°F -	2000°F -	2000°F -																				
2400°F 22	2400°F 17	2400°F 49																				
2700°F -	2700°F -	2700°F -																				
3000°F 14	3000°F 11	3000°F 50																				
3500°F 9.6	3500°F 8.4	3500°F 50																				

FIGURE 4.7.3.0-2: RADIATIVE MATERIAL PROPERTIES (Continued)

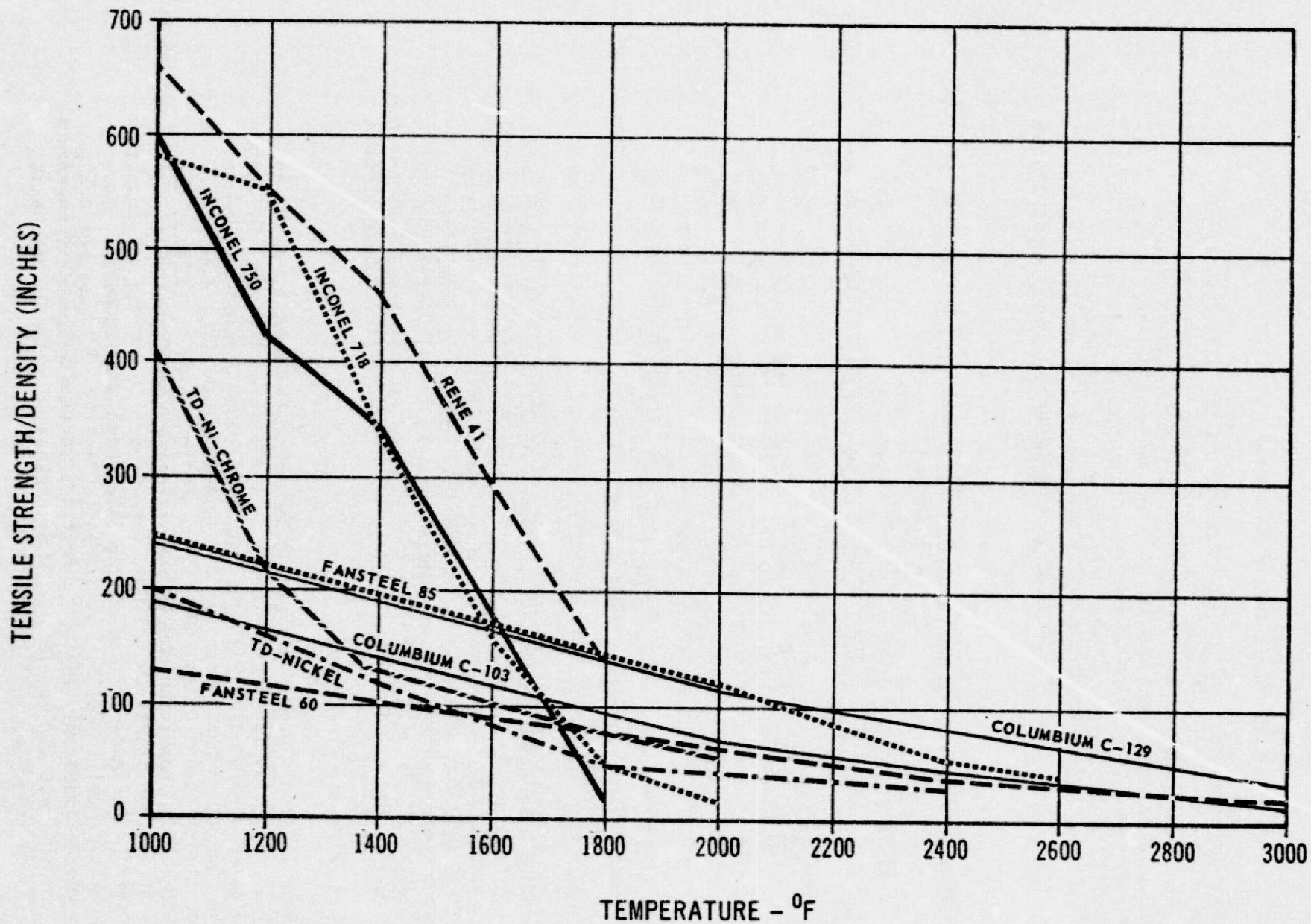


FIGURE 4.7.3.0-3. STRENGTH TO DENSITY PROPERTIES OF HIGH TEMPERATURE STRUCTURAL MATERIALS

4.7.3.1 Aft Heat Shield Materials Selection

The study groundrules limited the state-of-the-art radiative thermal protection material to 2000°F with TD-nickel-chrome. Therefore, the materials shown for temperatures above 2000°F represent areas where material technology would be required. The density of the high temperature materials are two to three times that of the lower temperature materials. Therefore, a different material was selected for the eight-foot movable cap in some instances than was used for the fixed portion of the aft heat shield to reduce the overall heat shield weight. The materials used are as listed below.

<u>CAP SECTION OF HEAT SHIELD</u>					<u>FIXED SECTION OF HEAT SHIELD</u>			
<u>No. of Passes</u>	<u>Basic Tug</u>	<u>30° Flare</u>	<u>45° Flare</u>	<u>60° Flare</u>	<u>Basic Tug</u>	<u>30° Flare</u>	<u>45° Flare</u>	<u>60° Flare</u>
1-4	A	A	A	A	A	A	A	FS60
5	FS60	FS60	FS60	FS85	FS60	FS60	FS60	FS85
10	FS60	FS60	FS85	TDNC	FS60	FS60	FS85	TDNC
30	FS85	TDNC	TDNC	R41	FS85	TDNC	TDNC	R41
60	FS85	TDNC	R41	R41	FS85	TDNC	R41	R41

LEGEND:

A = Ablatives
 FS60 = Fansteel 60
 FS85 = Fansteel 85

TDNC = TD-nickel-chrome
 R41 = Rene' 41

The latching mechanism for the heat shield will use the same materials as were proposed for the cap. Heat flow back to the Tug propulsion module aft skirt is reduced by heat blocks. The engine is located well aft (five to seven feet) of the heat shield. The limited temperature capability components are protected from the radiative heat transfer from the dome by (1) the retracted portion of the two position nozzle, and (2) by reflective metallic foil mounted atop the insulated limited temperature components.

4.7.3.2 Sidewall Insulation

The sidewall temperatures are shown in the prior Figure 4.7.2.0-1. The highest temperatures range from 1585°F at the aft skirt of the no flared configuration down to 1120°F at the astrionic module/propulsion module interface for the 5 pass mission. The lowest temperatures range from 609°F at the aft skirt of the 60° flared configuration to 430°F at the astrionic module/propulsion module interface for the 60 pass mission. For all of the configuration options, John Mansville microquartz insulation was selected. The material has a long life temperature capability to 2000°F (melting point 3000°F) and has a low density (3 pounds per cubic feet). The thickness was varied so that the maximum allowable temperatures on the sidewall was 400°F. The maximum thickness for the 5 pass basic

4.7.3.2 (Continued)

Tug at the aft skirt (1585°F) was 1.08 inches and at the propulsion/astrionics module joint was 0.78 inches thick. The maximum thickness for the 60 pass, 60° flare at the aft skirt (609°F) was 0.82 inches and at the propulsion/astrionic module joint was 0.38 inches thick.

To protect the microquartz from damage due to handling, transportation, vibration, etc., the microquartz will be covered by a thin outer skin of titanium (.002 inch). For temperatures too high for the titanium skin, an Inconel 718 foil (.002 inch thick) may be used.

4.7.3.3 Flare Materials Selection

The selection of the material for the flare was based on the high strength to density properties of Inconel 718 over other materials in the 1000°F range. The temperatures on the panels near the outer edge of the flares are as shown below:

<u>No. of Passes</u>	<u>30° Flare</u>	<u>45° Flare</u>	<u>60° Flare</u>
5	1260	1075	970
10	1175	900	829
30	850	670	648
60	700	550	538

The use of other materials were investigated but were not subjected to a weights analyses. Titanium has a lower density than Inconel 718 and may be a reasonable flare material for mission with durations greater than the 5 day (30 pass) mission. For longer duration missions or for large flares, it may be possible to use a metalized Kapton polyimide film bag material (short duration capabilities up to 800°F) as an inflatable flare.

In addition to the panels which constitute a major portion of the flare weight, there are support struts, piano hinges, cables, and spring hinges.

The 36 support struts will not see significant temperatures as they will be shielded by the flare panels. Titanium tubular rods may be used for all the flared concepts. If necessary, insulation may be wrapped around the rods for the high temperatures encountered with short duration missions. These remaining items constitute a small portion of the total flare weight. These items may be fabricated from any material compatible with the inconel panels and titanium struts and capable of withstanding the temperatures encountered.

4.7.3.4 Payload Adapter Material Selection

The allowable temperature limit of the payload (300°F) necessitates a payload adapter that serves both as a docking device and as a payload heat shield for the basic (no flare) configuration. For the flared configurations, the payload adapter performs the additional functions of flare mounting fixture and flare actuation mechanism housing. The payload adapter will consist of (1) skin and stringers, ring flames, cross beams, guide

4.7.3.4 (Continued)

tubes and guide cones. These will be fabricated from aluminum. The temperature will have to be controlled so that only 300°F will be encountered. For the basic (no flare) Tug, a microquartz insulation with a titanium outer cover will be used. For the flared configurations, no additional protection is required beyond the aluminum skin as the flare shields the payload adapter for the medium and long duration missions. The very short duration flared Tug missions may require the same microquartz insulation/titanium cover as was used with the basic (no flare) Tug.

4.7.4 Options and Recommendations

The materials selected for the aerobraking kit were based on a specific aerobraking concept and selected kit designs. Other methods of aerobraking (forward flare, active cooling with exhaust gases, larger flares, etc.) will significantly impact materials selection. As weight of payload is directly impacted by the aerobraking kit weights, low weight is a key factor in selection of materials.

4.8 WEIGHTS AND MASS PROPERTIES

Weight penalties associated with implementation of an aerobraking return mode of operation are presented in this section. These weights are given as a function of the number of perigee passes for each of the aerobraking kit elements. Figure 4.8.6.0-1 is a summary of the aerobraking weight penalties and resulting payload for each Tug configuration. Mass properties used in the controls and aerodynamic analyses are presented in Section 4.8.1.

4.8.1 Mass Properties Summary

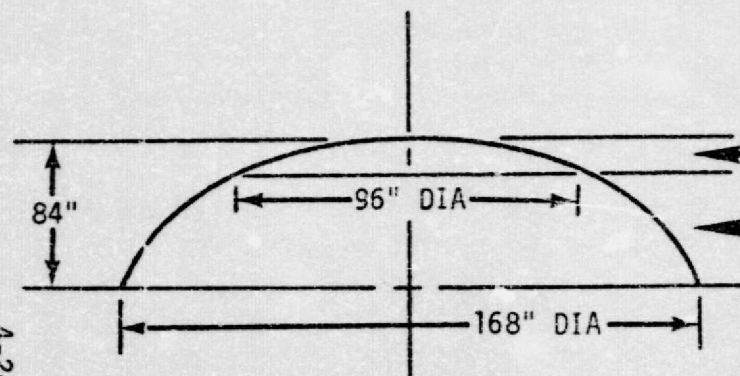
Mass properties for the four Space Tug configurations are presented in Figure 4.8.1.0-1. The mass properties, which include the weight, centers of gravity, and mass moments of inertia, were calculated for the conditions existing at the start of aerobraking.

4.8.2 Structural Weights

Structural weight penalties resulting from the modification of the basic nonaerobraking Space Tug are presented in Figures 4.8.2.0-1 through 4.8.2.0-6. Figures 4.8.2.0-2 and 4.8.2.0-3 present the weights for an aerodynamic shield (aft heat shield) and a flared aerobrake (flared skirt), respectively, as a function of the number of passes. The flared skirt was sized for repose angles of 30, 45, and 60 degrees. The aft heat shield was sized for the aerodynamic effects resulting from these flare angles in addition to a "no flare" configuration. Figure 4.8.2.0-4 presents the weights for a combination payload adapter/flared skirt support structure. Figure 4.8.2.0-6 presents the total structural weight penalties as a function of the number of passes.

	<u>NO FLARE</u>	<u>30° FLARE</u>	<u>45° FLARE</u>	<u>60° FLARE</u>
WEIGHT AT START OF AEROBRAKING (POUNDS)	14,430	14,430	14,430	14,430
CENTER OF GRAVITY \bar{X} (INCHES)	243.3	234.0	234.2	230.7
CENTER OF GRAVITY \bar{Y} (INCHES)	0	0	0	0
CENTER OF GRAVITY \bar{Z} (INCHES)	0	0	0	0
ROLL MOMENT OF INERTIA (SL.-FT. ²)	10,388	12,443	17,021	21,268
PITCH MOMENT OF INERTIA (SL.-FT. ²)	101,686	94,748	97,078	94,604
YAW MOMENT OF INERTIA (SL.-FT. ²)	101,686	94,748	97,078	94,604

FIGURE 4.8.1.0-1 SPACE TUG MASS PROPERTIES



	5 PASSES		10 PASSES		30 PASSES		60 PASSES	
	MATL.	\bar{t} (IN.)	MATL.	\bar{t} (IN.)	MATL.	\bar{t} (IN.)	MATL.	\bar{t} (IN.)
NO FLARE	④	.137	④	.091	③	.047	③	.030
30° FLARE	④	.091	④	.066	②	.041	②	.030
45° FLARE	④	.058	③	.038	②	.030	①	.030
60° FLARE	③	.037	②	.032	①	.030	①	.030
NO FLARE	④	.030	④	.030	③	.030	③	.030
30° FLARE	④	.030	④	.030	②	.030	②	.030
45° FLARE	④	.030	③	.030	②	.030	①	.030
60° FLARE	③	.030	②	.030	①	.030	①	.030

- ① RENE 41
- ② TD NICKEL CHROME
- ③ FANSTEEL 85
- ④ TANTALUM FANSTEEL 60

- MINIMUM MATERIAL THICKNESS = 0.030 (IN.)
- \bar{t} = EQUIVALENT MONOQUE THICKNESS

FIGURE 4.8.2.0-1 AFT HEAT SHIELD MATERIALS SUMMARY

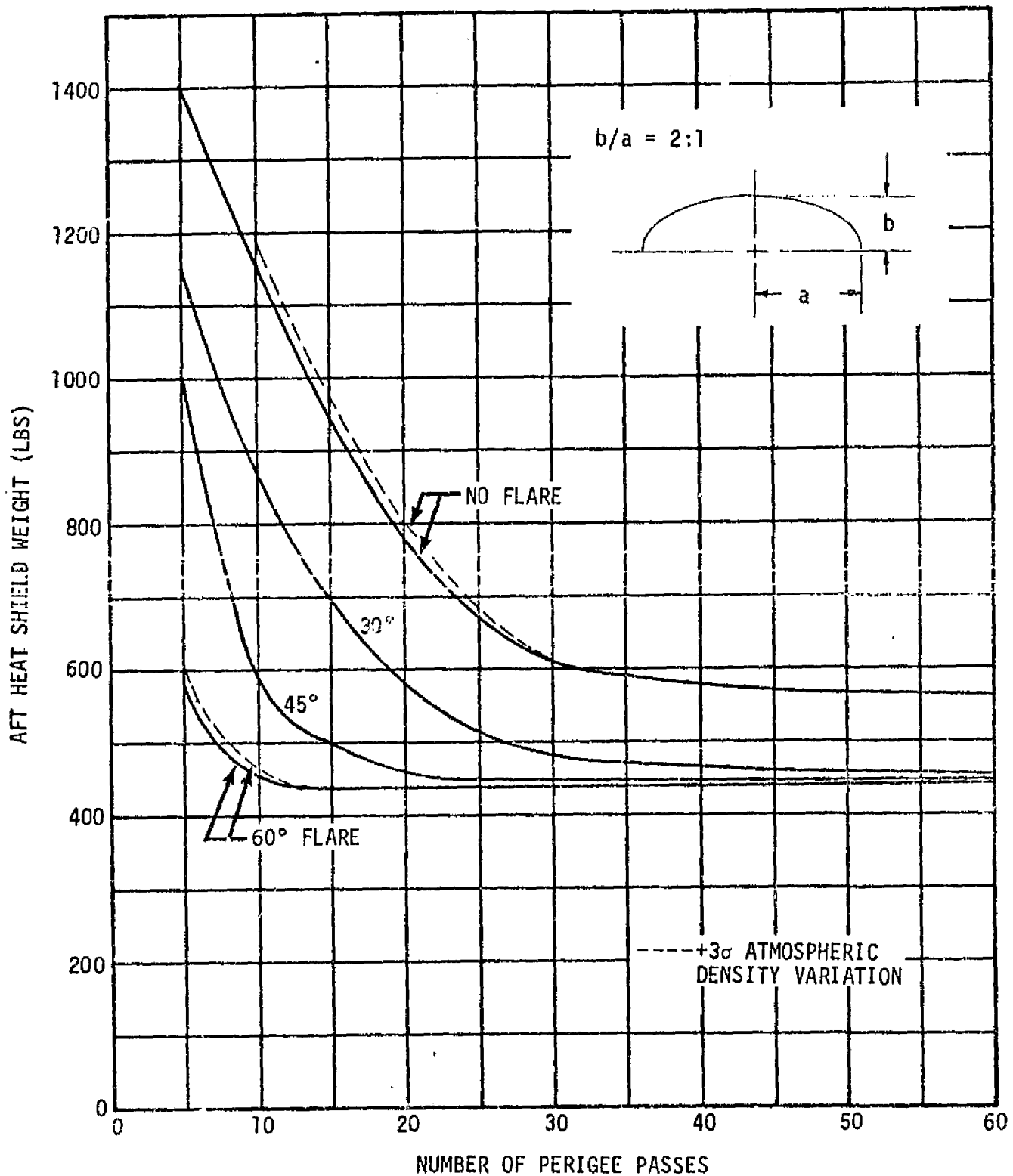


FIGURE 4.8.2.0-2 AFT HEAT SHIELD WEIGHT VS NUMBER OF PASSES

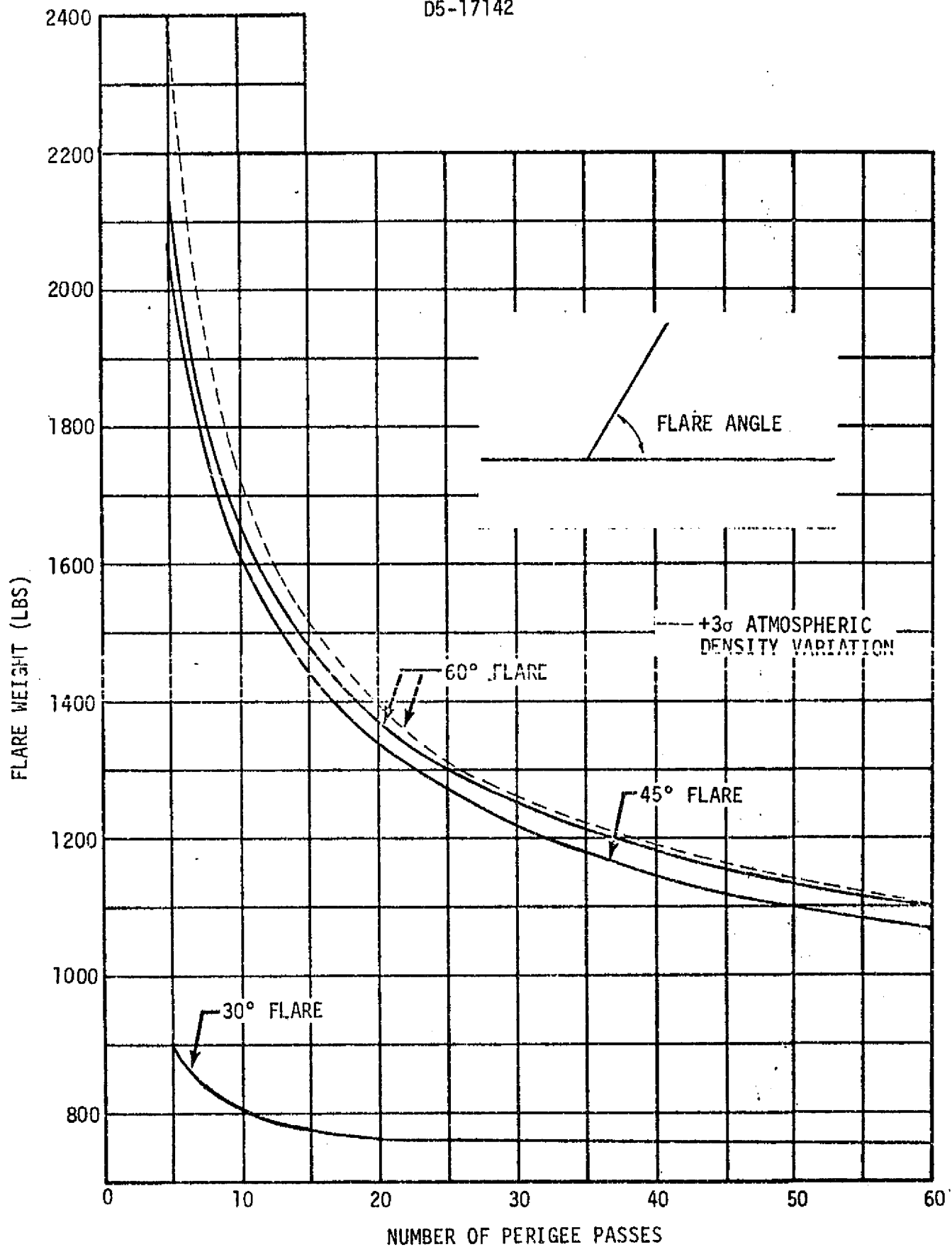


FIGURE 4.8.2.0-3 FLARE WEIGHT VS NUMBER OF PASSES

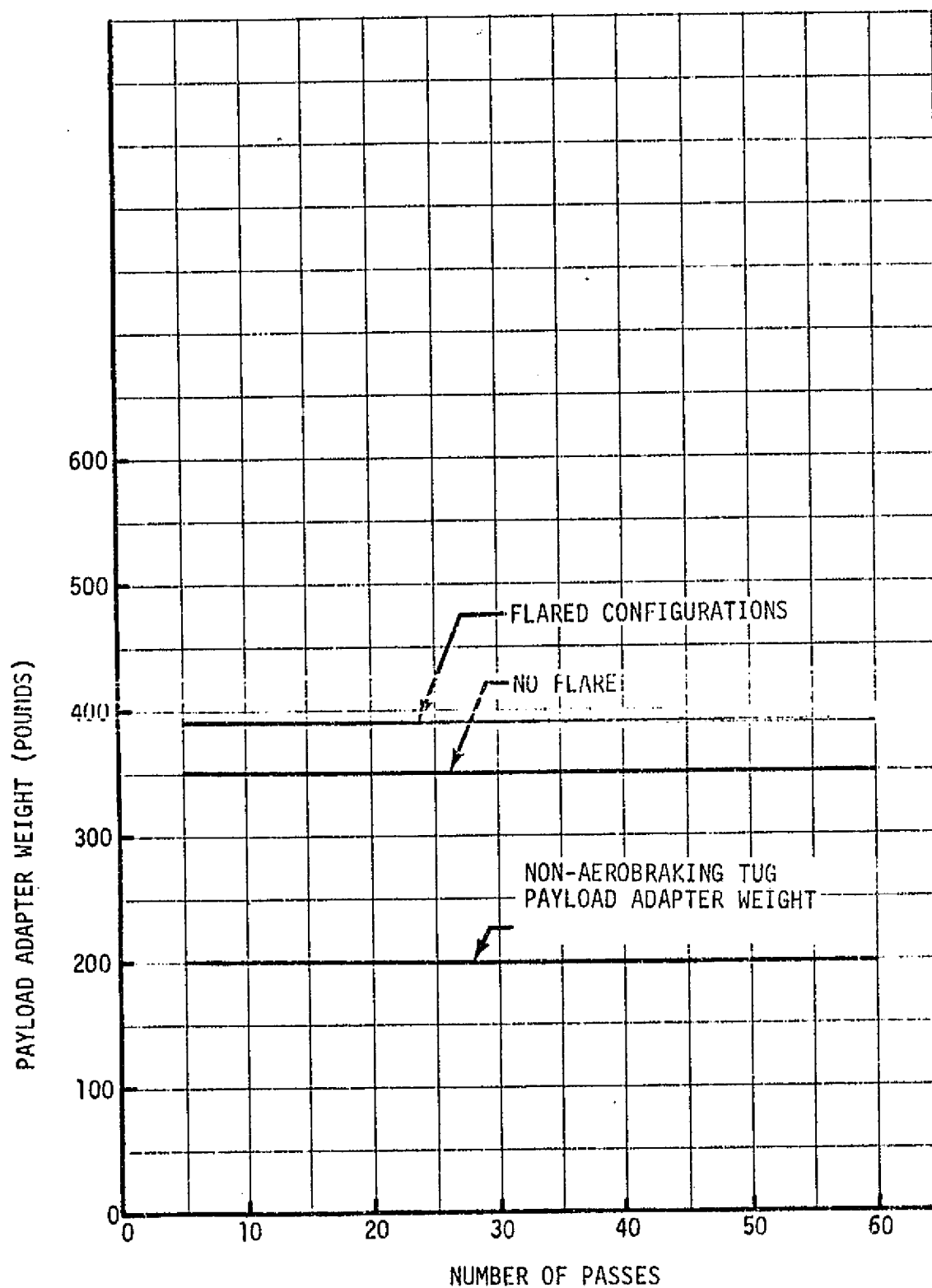


FIGURE 4.8.2.0-4 PAYLOAD ADAPTER WEIGHT VERSUS NUMBER OF PASSES

	NO FLARE CONFIGURATION (LBS)	FLARED CONFIGURATIONS (LBS)
SKIN/STRINGERS	200	200
RING-FRAMES	45	45
CROSS BEAMS	--	40
GUIDE TUBES	25	25
GUIDE CONE	30	30
PAYLOAD LATCHES & GUIDES	50	50
TOTAL	350	390

FIGURE 4.8.2.0-5 WEIGHT SUMMARY - PAYLOAD ADAPTER/FLARED SKIRT SUPPORT

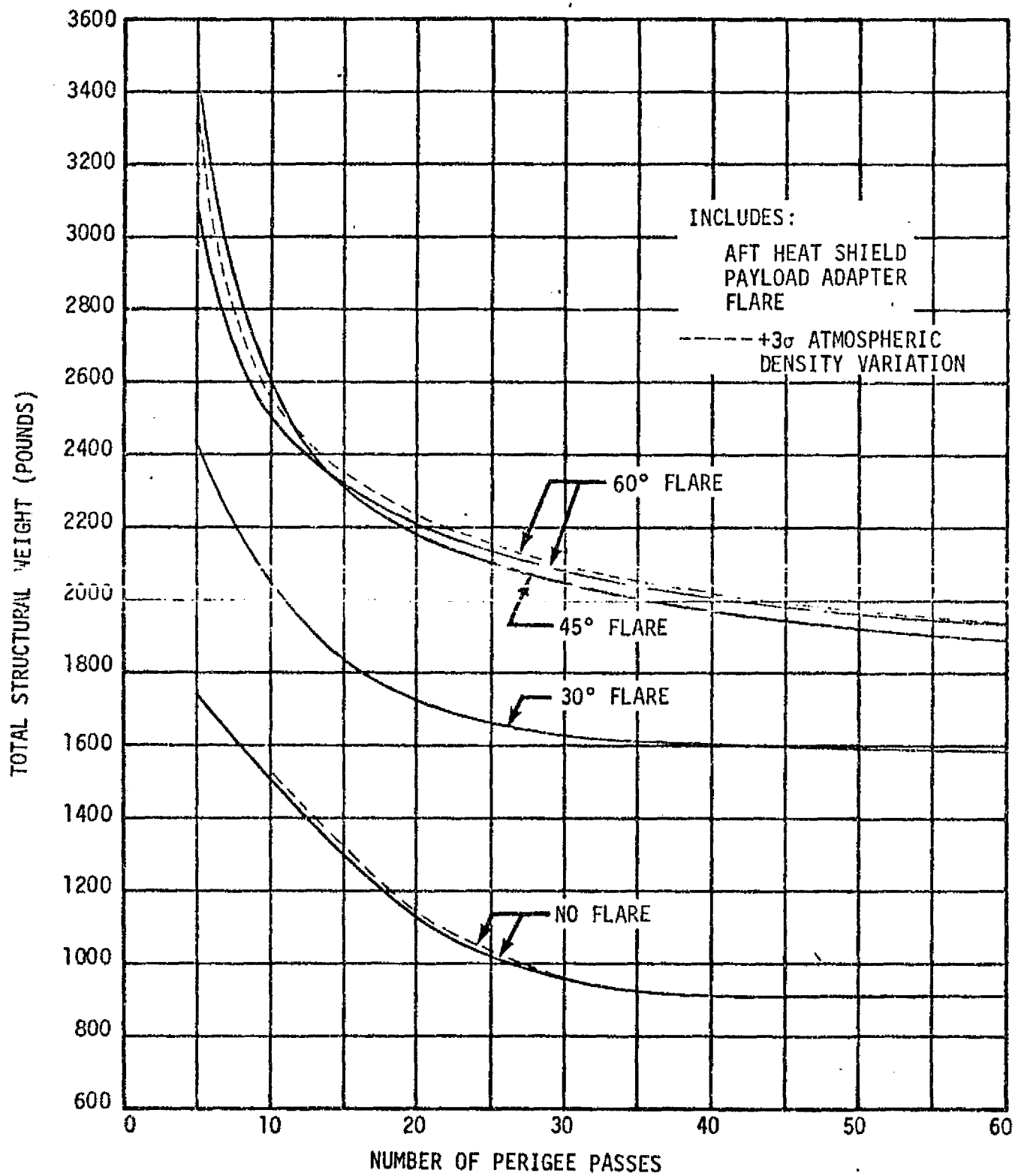


FIGURE 4.8.2.0-6 TOTAL STRUCTURAL WEIGHT VS NUMBER OF PASSES

4.8.2.1 Aft Heat Shield

The aft heat shield is required for protection of the primary propulsion system from aerodynamic effects during the aerobraking return mode. The basic configuration of the heat shield consists of a stiffened skin elliptical dome with a b/a ratio of 2:1. The base diameter of the shield is 168 inches. A 96 inch diameter removable hatch is included for operation of the primary propulsion system both before and after aerobraking. The aft heat shield was sized to react the pressure loadings given in Section 4.1. The materials used are those specified in Section 4.7 and were selected in accordance with the temperature environments of Section 4.5. The heat shield operates as a hot structure with no external thermal protection. Figure 4.8.2.0-1 gives a summary of the materials and equivalent monocoque thickness (\bar{t}) used in obtaining the shield weight. Figure 4.8.2.0-2 presents the aft heat shield weight as a function of the number of passes.

4.8.2.2 Flared Skirt

The flared skirt is designed as a stiffened frame covered with a thin facing sheet. The skirt is supported by 36 tubular struts and can be stowed within a 15 foot diameter mold line. Inconel 718 is used for the frame and facing sheets with titanium 6Al-4V being used for the support struts. The skirt will operate as a hot structure with no thermal protection being required. The skirt was sized to react the pressure loading given in Section 4.1 and the temperature environments of Section 4.5. Figure 4.8.2.0-3 shows the total weight of the flared skirts, including deploy/retract mechanisms, as a function of the number of passes.

4.8.2.3 Payload Adapter/Flared Skirt Support

The payload adapter is required for protecting the payload during aerobraking and, with flared configurations, for providing an attach point for the flared skirt support struts. The adapter is an aluminum stiffened skin structure 168 inches in diameter and 120 inches long. Three ring frames are employed; a lower bolt ring for attachment to the astronics module, an intermediate ring for support of the flare struts, and an aft ring for support of the payload guide. Figures 4.8.2.0-4 and -5 show the weight of the adapter, less external insulation, for the basic no-flare configuration and for the flared configurations. The higher adapter weight for the flared configuration is due to the addition of a cross beam for support of the skirt deploy/retract mechanism.

4.8.3 Thermal Protection System Weight

The thermal protection system (TPS) weight as a function of the number of passes is presented in Figure 4.8.3.0-1. The TPS weights for the no-flare configuration are for the Tug sidewall, astronics module, payload side, and payload base region. The 30°, 45°, and 60° flare configuration TPS weights are for the Tug sidewall and astronics module only.

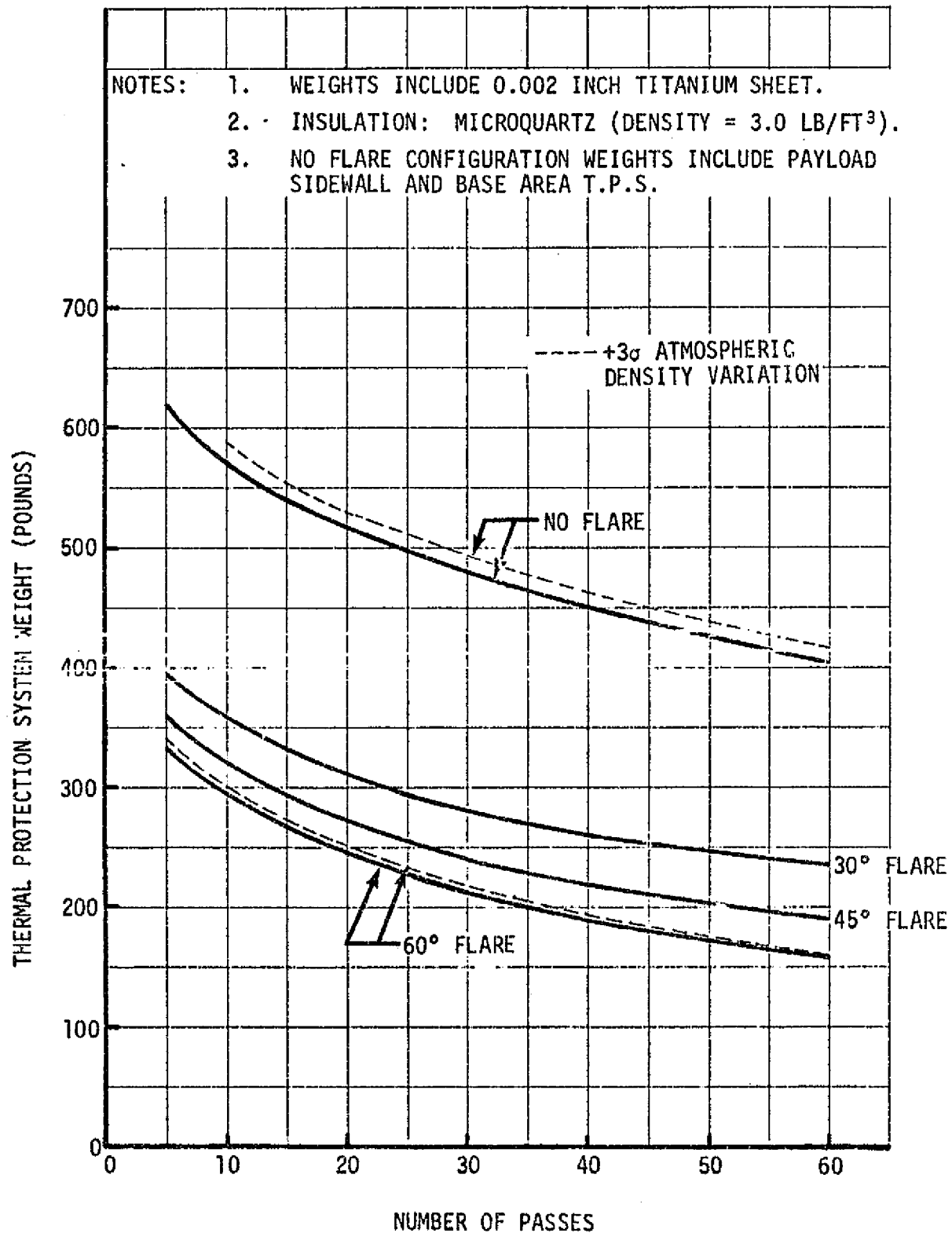


FIGURE 4.8.3.0-1 THERMAL PROTECTION SYSTEM WEIGHT VERSUS NUMBER OF PASSES

4.8.4 Astrionics System Weight

The weight of the astrionics system as a function of the number of passes is given in Figure 4.8.4.0-1. The astrionics system weight increase with the number of passes reflects the systems sensitivity to total operating time. An increase in total power supplied by the system, and in increased redundancy requirements, to maintain the same level of reliability, are reflected in added weight as the number of passes increase.

4.8.5 Control System Weight

Reaction control system weight for the different Tug configurations as a function of the number of passes is given in Figure 4.8.5.0-1. The total control system weight represents the hardware and consumable propellant required to maintain attitude control.

4.8.6 Total Tug Weight

The total weight of the Space Tug at start of aerobraking as a function of the number of passes is presented in Figure 4.8.6.0-1. This total was determined by adding the respective aerobraking weight penalties for each of the aerobraking kit elements (including RCS fuel) to the baseline Tug weight of 9,718 pounds, obtained by uprating the 39,800 pound capacity synchronous orbit primary propulsion module of prior Reference 1.1.0.0-1 to a 45,000 pound capacity propulsion module. The payload capability is the difference between this total and the 14,430 pound maximum allowable Tug weight at start of aerobraking based on available delta velocity capability.

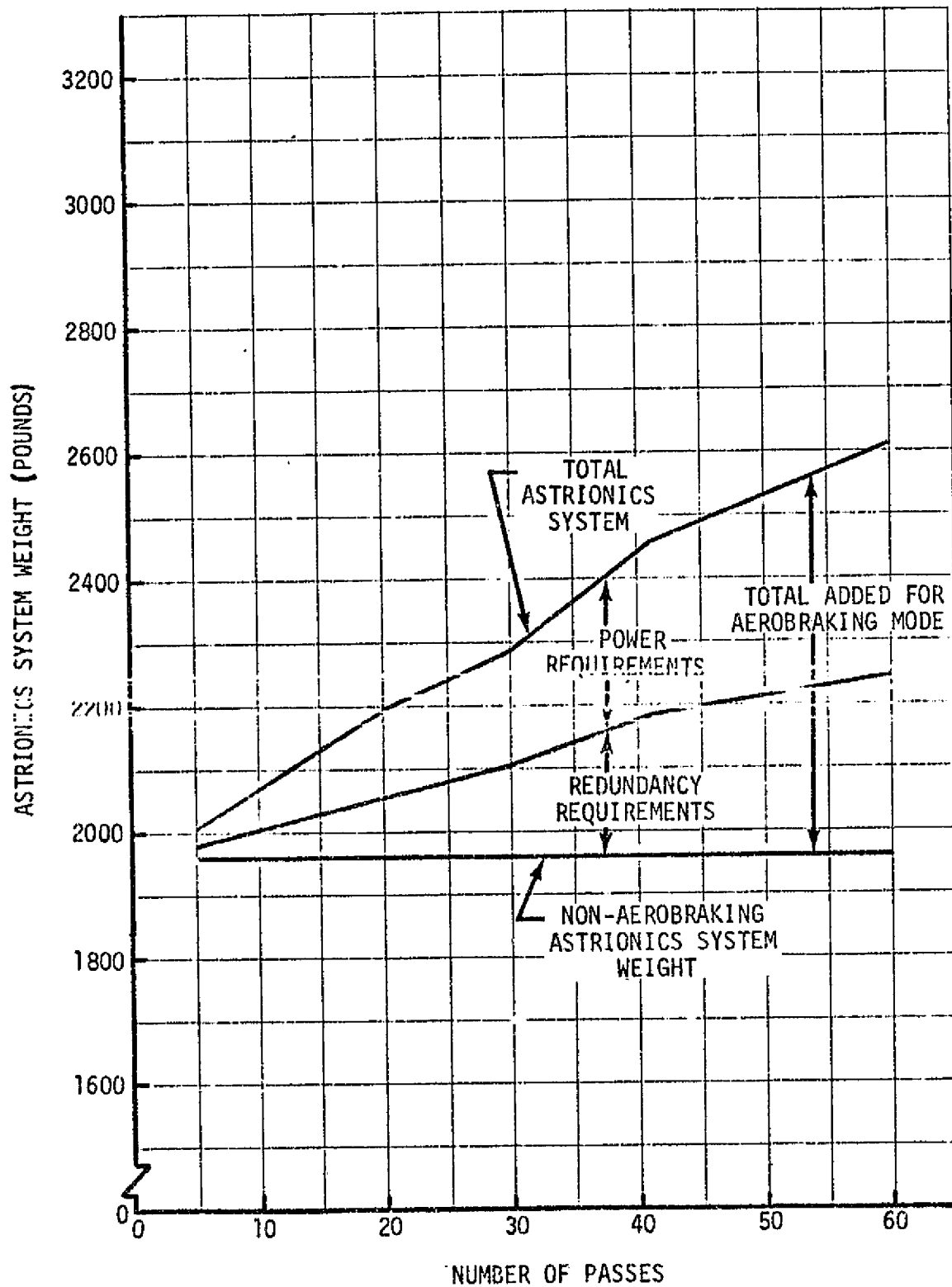


FIGURE 4.8.4.0-1 ASTRIONICS SYSTEM WEIGHT VERSUS NUMBER OF PASSES

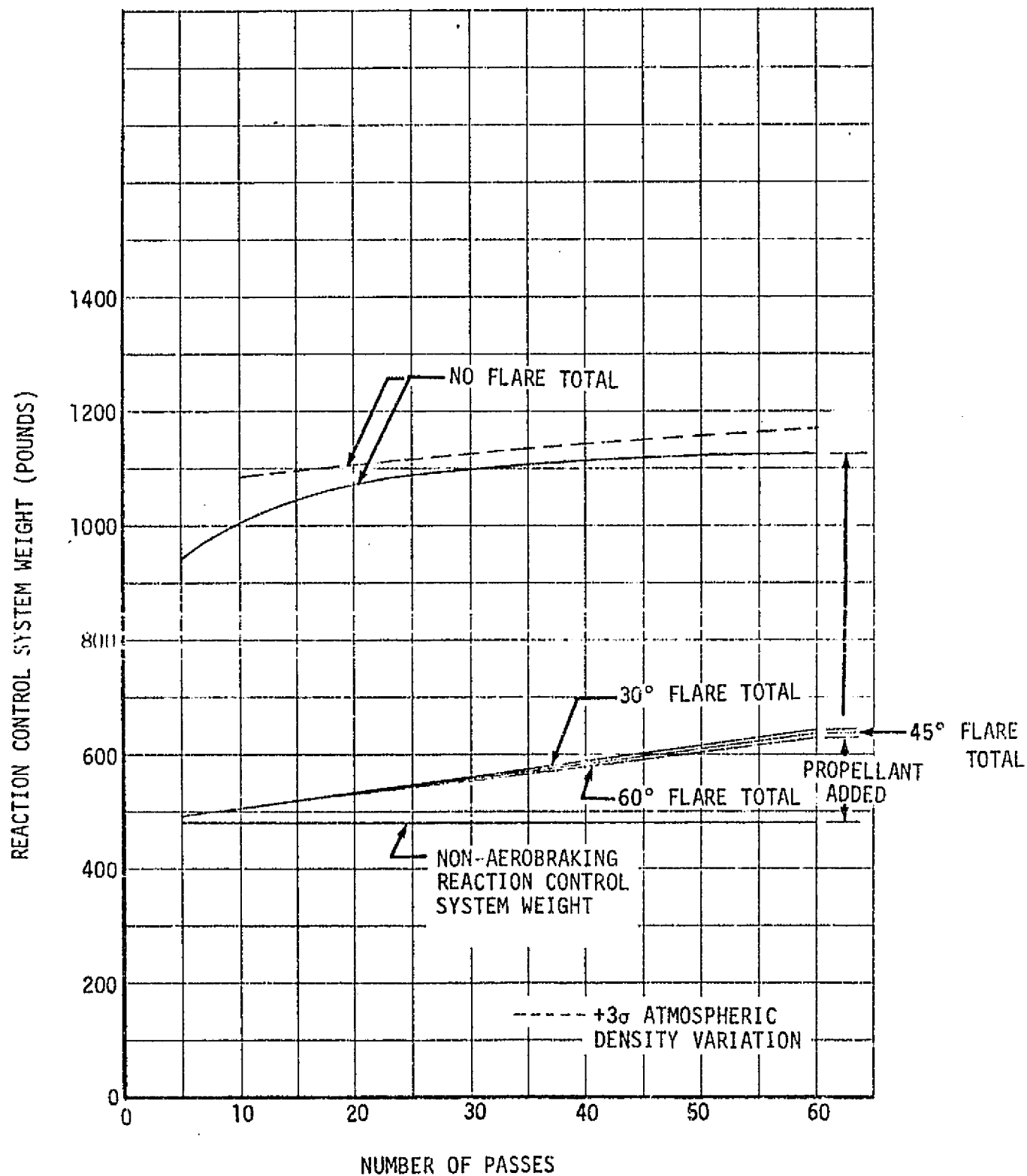


FIGURE 4.8.5.0-1 REACTION CONTROL SYSTEM WEIGHT VERSUS NUMBER OF PASSES

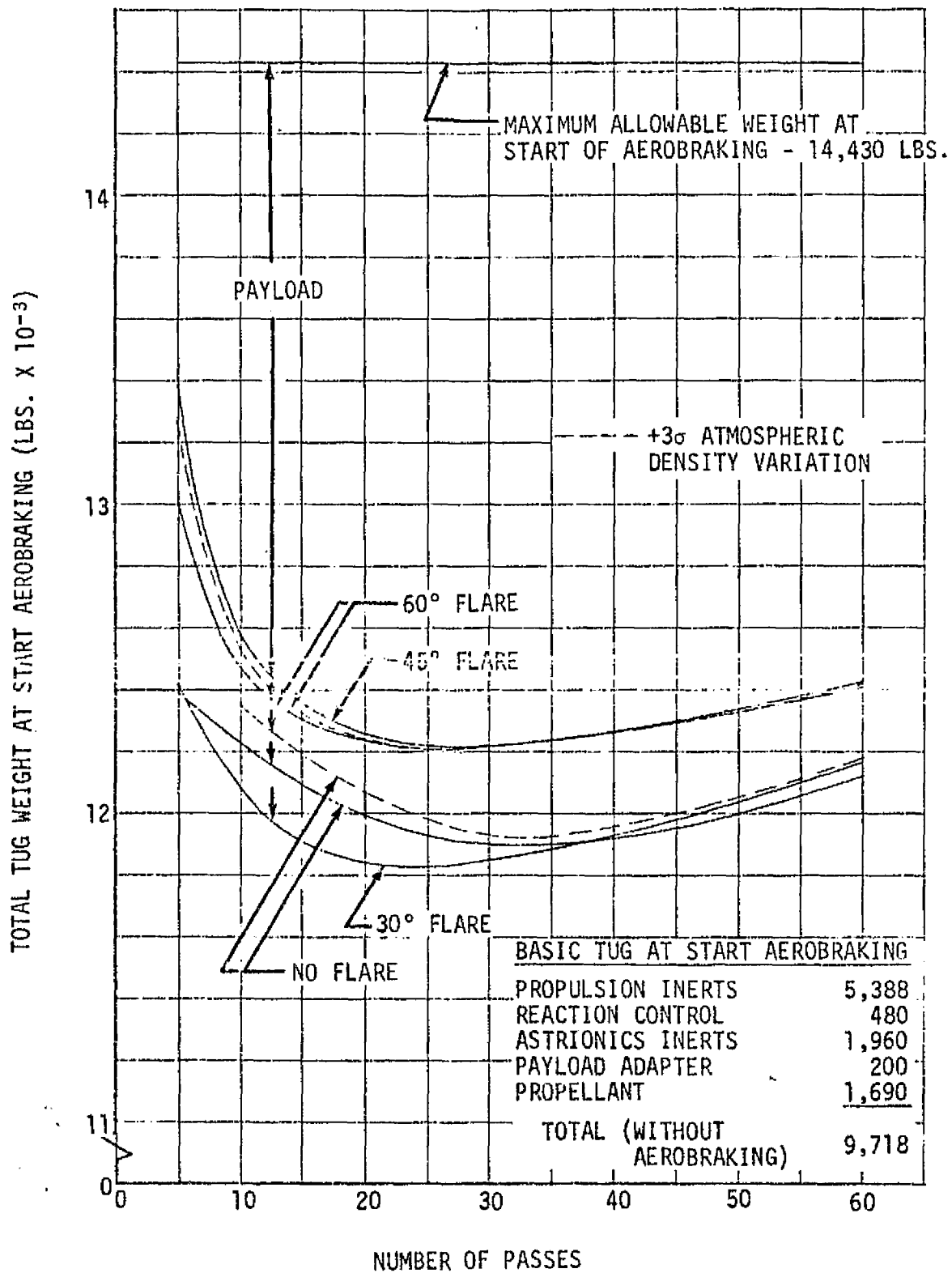


FIGURE 4.8.6.0-1 TOTAL TUG WEIGHT VERSUS NUMBER OF PASSES

5.0 SENSITIVITY ANALYSIS

The sensitivity analysis was performed to examine various parameters peculiar to aerobraking and to provide an overall impact assessment of the technical studies. In performing this analysis, data from Section 4 was utilized to determine the effects of the aerobraking kit inert weight penalties, delta velocity effects, reaction control system versus main engine operations, circularization altitude and Shuttle rendezvous effects. Operating modes were examined to define the payload capabilities of the four aerobraking Tug configurations (Section 5.1).

The effect of navigation uncertainties and atmospheric dispersions were defined to determine their impact on aerobraking Tug temperatures, materials, navigation accuracy, mission duration, operational modes and payload. The need for guidance schemes, better understanding of atmospheric variations and additional study of navigation and atmospheric effects was identified (Section 5.2).

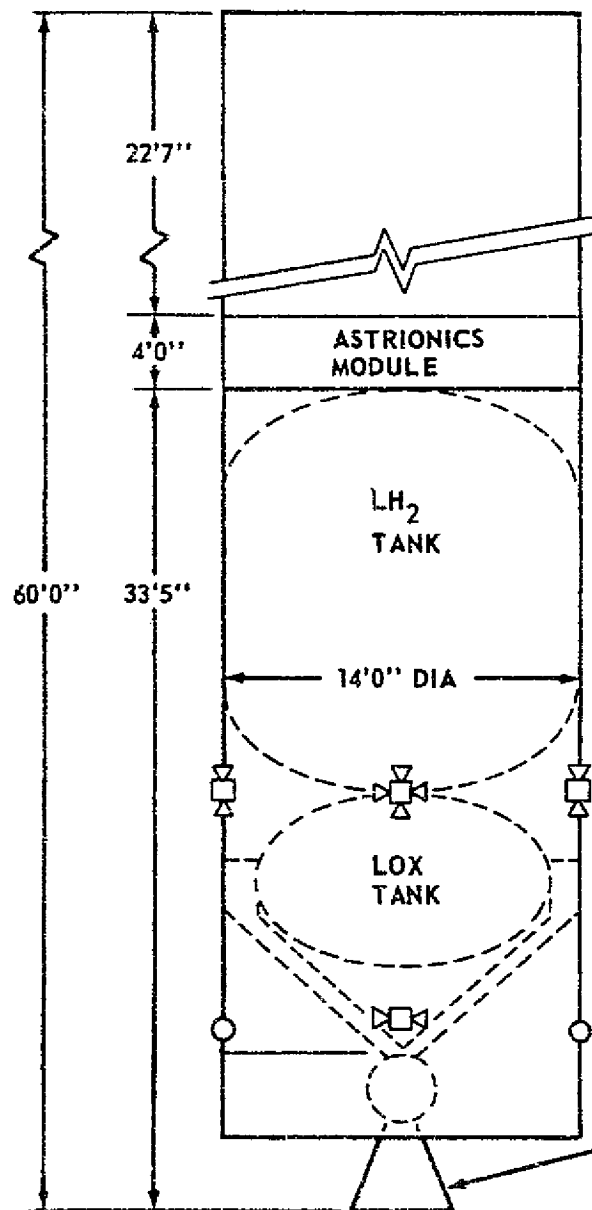
This analysis also compared the aerobraked Tug with the conventional trajectory single reusable stage Tug used in the geosynchronous role. Equivalent payload Tug sizes were computed and the performance parameter sensitivities were compared (Section 5.3).

The sensitivity analysis (1) indicated methods of increasing the payload capability of the aerobraking Tug, (2) defined the impact of atmospheric dispersions and navigation error on thermal protection requirements, mission operating mode and payload capability, and (3) evaluated the conventional and aerobraked Tug performance parameters and payloads. From the above analysis, conclusions and recommendations were developed to provide direction to technology and Space Tug follow-on studies (Section 5.4).

5.1 PAYLOAD/AEROBRAKING PERFORMANCE OPTIMIZATION

The round trip payload geosynchronous mission was the study's baseline mission. This mission requires that equal weight payloads be carried to and from geosynchronous orbit by the same Tug. Alternate missions (subject to cursory examination in the sensitivity analysis only) considered payload placement and retrieval. The conventional trajectory single reusable stage Tug used a starting point for this study (Figure 5.1.0.0-1), has no payload capability for placement, retrieval or round trip missions.

The aerobraking operational mode was examined in detail for the geosynchronous round trip mission, since this mission imposed the most stringent performance requirements on the Tug systems. In this mission profile, the Tug is deployed by the Shuttle in 100 NM, 28° inclination orbit. The Tug transfers the payload via Hohmann transfer to equatorial synchronous orbit with the 28° plane change being made at apogee. In synchronous orbit the payload is exchanged for an equal weight return payload. At the proper time the Tug and payload are placed on the aerobraking return ellipse by applying the deorbit and 28° plane change delta velocity. During the aerobraking return the



WEIGHT ESTIMATE (LBS)

● PROPULSION MODULE		50,868
● PROPELLANT	45,000	
● INERTS	5,868	
● ENGINE	639	
● PROP/MECH	801	
● THERMO/MICRO	573	
● STRUCTURE	2912	
● CONT. & RESID.	943	
● ASTRIONICS MODULE		2,526
● ELECTRICAL	841	
● AVIONICS	625	
● STRUCTURE	400	
● THERMAL	660	
● PAYLOAD ADAPTER		200
TOTAL SPACE TUG WEIGHT		53,594
MASS FRACTION		0.840

FIGURE 5.1.0.0-1: CONVENTIONAL (NON-AEROBRKING) SPACE TUG CONFIGURATION

5.1 (Continued)

apogee of the ellipse is reduced to 270 NM by drag dissipation of the orbital kinetic energy on one or more passes through the upper atmosphere. The orbit is circularized at 270 NM for phasing with the Shuttle at 100 NM and at the proper time a final Hohmann transfer is made to 100 NM for rendezvous with the Shuttle.

Using this mode, the four aerobraking configurations all have significant positive payloads in the baseline round trip mission. The payload capabilities for the two alternate missions (payload placement and retrieval) are more than double that of the round trip mission. The following subsections discuss the general parametric results (Section 5.1.1 - not configuration oriented) and the specific payload capability assessment (Section 5.1.2 - configuration oriented).

5.1.1 General Parametric Results (not configuration oriented)

This subsection discusses the parametric analysis results pertaining to the aerobraked geosynchronous mission. This analysis was used to provide early visibility of the effects of weight penalties, mission delta velocities, and specific impulse on payload capabilities. Alternate mission modes and the sensitivity of payloads to these mission modes were investigated to determine if the 100 NM departure orbit to geosynchronous orbit and back to a 270 NM circularization orbit followed by a 100 NM rendezvous with Shuttle sequence described above is near optimum.

5.1.1.1 Inert Weights and Delta Velocity Effects

The initial aerobraking delta velocity budget utilized in the sensitivity analysis was 14,100 ft/sec outbound and 8,000 ft/sec return (total mission budget of 22,100 ft/sec). With this velocity budget and the baseline Tug configuration shown in Figure 5.1.0.0-1, the aerobraking Tug round trip payload capability was computed. Figure 5.1.1.1-1 parametrically illustrates the payload capability as a function of aerobraking inert weight penalties. Assuming no aerobraking kit inert weight penalty, the maximum round trip payload would be approximately 4450 pounds. Because the round trip mission is, to a first order approximation, a direct one-to-one substitution of inert weight for payload, the payload is zero when the aerobraking penalty is 4450 pounds. The vertical bars on Figure 5.1.1.1-1 illustrate the percentages of the 287 synchronous missions that can be captured (accomplished). For example, with an aerobraking kit inert weight penalty of 1450 pounds and the associated 3000 pound payload capability, approximately 95% of all geosynchronous missions can be captured. The remaining 5% of the geosynchronous payloads in the mission model are heavy (7000-10,000 pounds) and are beyond the round trip payload capability of the aerobraked Tug. (Note: This payload may be accomplished in a placement or retrieval mode). Therefore, a 3000 pound round trip capability for the aerobraked Tug appears to be a desirable design goal.

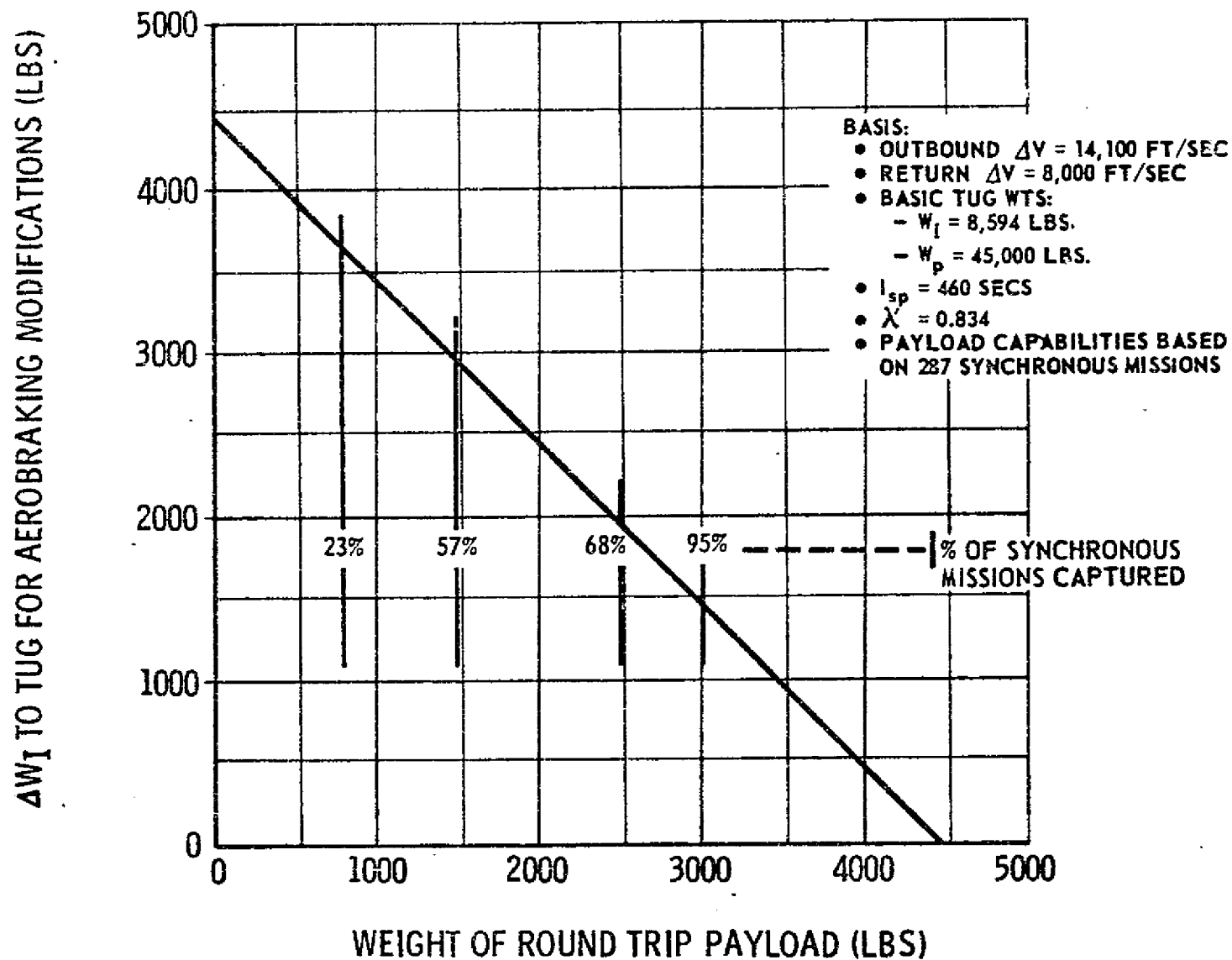


FIGURE 5.1.1.1-1. EFFECT OF AEROBRAKING MODIFICATION WEIGHTS ON ROUND TRIP PAYLOAD

5.1.1.1 (Continued)

Figure 5.1.1.1-2 extends the parametric investigation beyond that shown in Figure 5.1.1.1-1 above. The effects of both aerobraking inert weight penalties and return delta velocities are depicted. The return delta velocity of 8000 ft/sec with zero inert weight penalty results in a 4450 pound payload. However, if the return delta velocity were 7500 ft/sec (zero inert weight penalty), the payload capability is increased to 5000 pounds.

Linear interpolation can be used vertically (along equal return delta velocity lines) in Figure 5.1.1.1-2. The lines across the figure labeled with the inert weight penalties are not straight lines because of the natural logarithms involved. The slope of these lines varies from approximately 1.07 to 1.23 lbs/ft per second for the 8500-9000 and 7000-7500 ft/sec bands, respectively and indicates the payload sensitivity of the aerobraked Tug to changes in delta velocity.

As the delta velocity is dependent on the operational Shuttle/Tug mode used, Figure 5.1.1.1-2 provides insight to the effect on payload capability of the selected operating mode's delta velocity. For example, Figure 5.1.1.1-2 can be used to estimate round trip payload capabilities for various total mission delta velocities. To do this, add the 14,100 ft/sec outbound and a return velocity (e.g., 8000 ft/sec) and compare with the computed total mission delta velocity. The difference between these two values is used as a delta to move right or left from the same return velocity selected on the chart. Using the inert weight difference (penalty) associated with a particular configuration, the resulting payload can be estimated. An example of this is shown below:

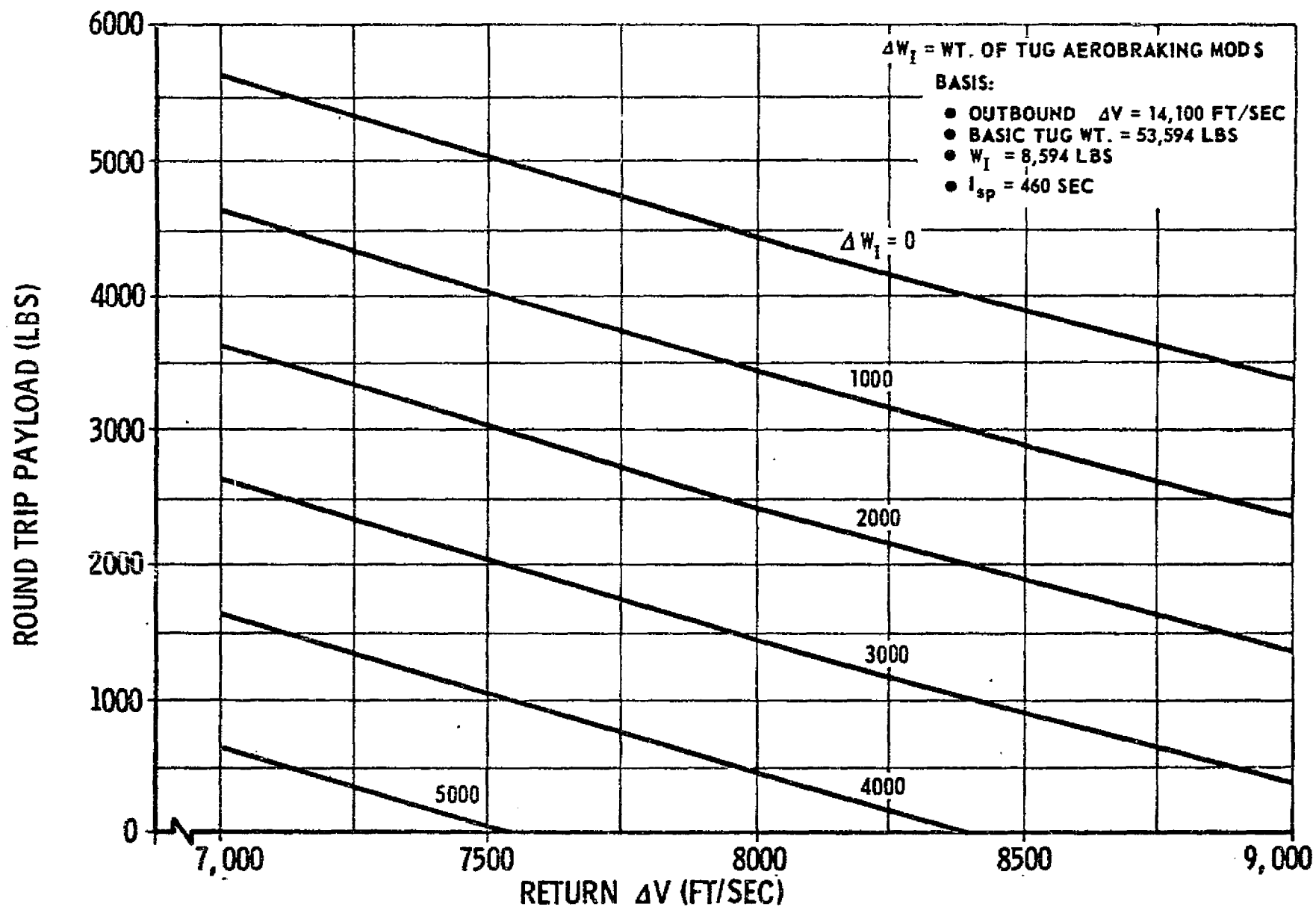
	<u>Configuration A (Computed)</u>	<u>Figure 5.1.1.1-2 Values</u>
Outbound ΔV (ft/sec)	14,500	14,100
Return ΔV (ft/sec)	8,100	8,000
Total Mission ΔV (ft/sec)	22,600	22,100
Total Inert Weight (Lbs)	9,594	8,594

Difference in total mission $\Delta V = 22,600 - 22,100 = +500$ ft/sec

Difference in total inert weight = 9594 - 8594 = 1000 lbs (ΔW_I)

Read up vertically from 8500 ft/sec (8000 + 500) to the $\Delta W_I = 1000$ line

The estimated round trip payload is 2900 pounds

FIGURE 5.1.1.1-2. EFFECT OF AEROBRAKED RETURN ΔV ON ROUND TRIP PAYLOAD

5.1.1.1 (Continued)

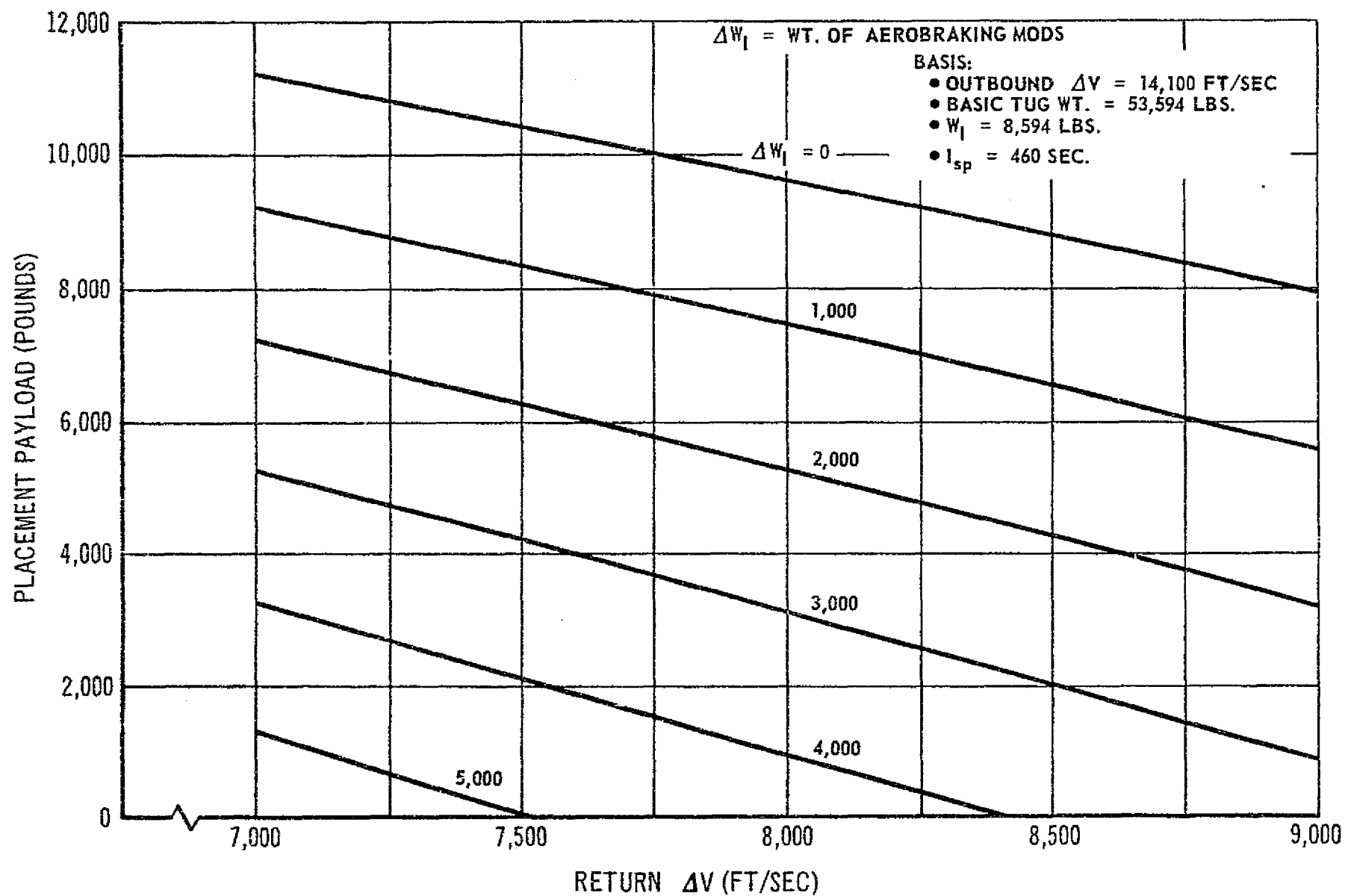
Figure 5.1.1.1-3 and -4 show the same type of data as Figure 5.1.1.1-2 for the two alternate missions, payload placement and retrieval, respectively. The interpretation and use of these two figures is similar to that of Figure 5.1.1.1-2. The maximum payload placement capability is approximately 9600 pounds (8000 ft/sec return delta velocity and zero inert weight penalty). With the same 8000 ft/sec return delta velocity and 2000 pounds inert weight penalty, approximately 5300 pounds of payload can be placed. Payload capabilities for the retrieval mission using the same velocity budget and aerobraking kit weight penalties are 8300 and 4600 pounds of payload, respectively. The retrieval mission, shown in Figure 5.1.1.1-4, is more sensitive to delta velocity than the placement mission but for return delta velocities of 7000-7200 ft/sec, the placement and retrieval payload capabilities are essentially equivalent.

5.1.1.2 RCS Isp Effects

The Tug's GO_2/GH_2 RCS system has an effective specific impulse (Isp) of 400 seconds compared to 460 seconds for the main RL-10A-3-8 engine (prior Reference 1.1.0.0-1). Because of this lower Isp value, there will be a payload reduction associated with extensive use of the RCS system during the aerobraking phase of the mission. In addition to the normal RCS functions of limit cycle operation and stabilization as discussed in Section 4.4 (Control Analysis), the RCS might substitute for the main engine in the final low earth circularization, phasing and rendezvous maneuvers.

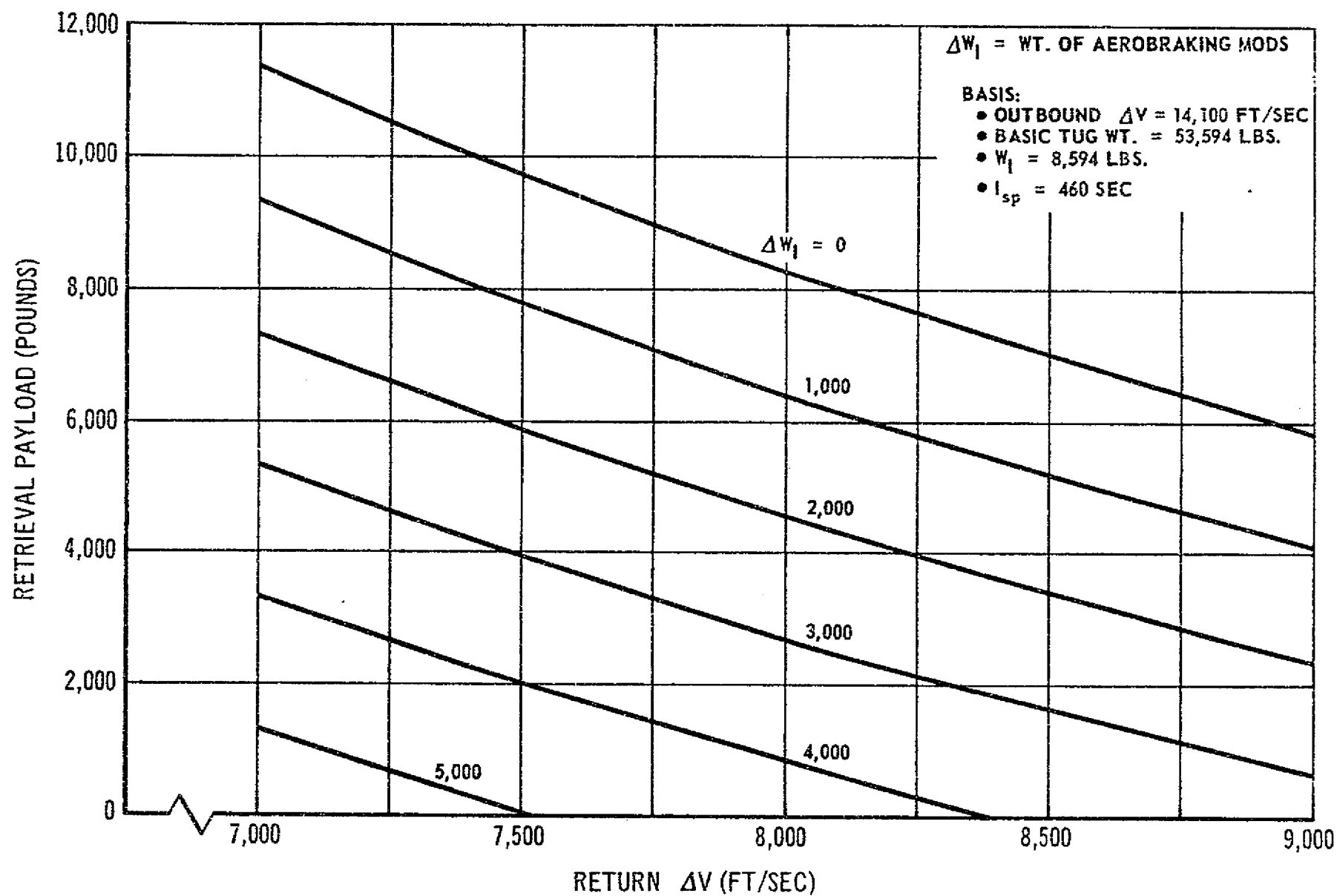
Figure 5.1.1.2-1 shows the effect on entry weight by using the RCS to provide all of the propulsive delta velocity requirements after the completion of the aerobraking phase. The change in Tug gross weight at the beginning of the aerobraking phase is shown on the ordinate. The abscissa represents a range of possible total mission propulsive delta velocity requirements. The trajectory analysis (Section 4.3) utilized a baseline delta velocity budget of 22,400 ft/sec. For this delta velocity value, the delta entry weight (using the main engine) is zero. With this same total budget (22,400 ft/sec) and using the RCS to provide all propulsive requirements after aerobraking, the Tug's gross entry weight is decreased approximately 75 pounds. The entry weight difference between the main engine and RCS curves is less for smaller velocity budgets because of the decreased velocity requirement imposed on the lower Isp RCS. Similarly, the entry weight difference is greater for the larger velocity budgets because of the increased demands on the RCS. The additional propellant required by the lower Isp RCS is included in the entry weights shown. Therefore, the entry weight deltas do not represent completely the payload penalties associated with using the RCS as a substitute for the main engine. These payload penalties are further discussed in the following paragraphs.

Figure 5.1.1.2-2 extends the parametric analysis of Figure 5.1.1.2-1 above. The effects of using the RCS for all propulsive maneuvers after the completion of aerobraking are plotted as a function of initial Tug and payload gross weight at 100 NM. The weight differences between the



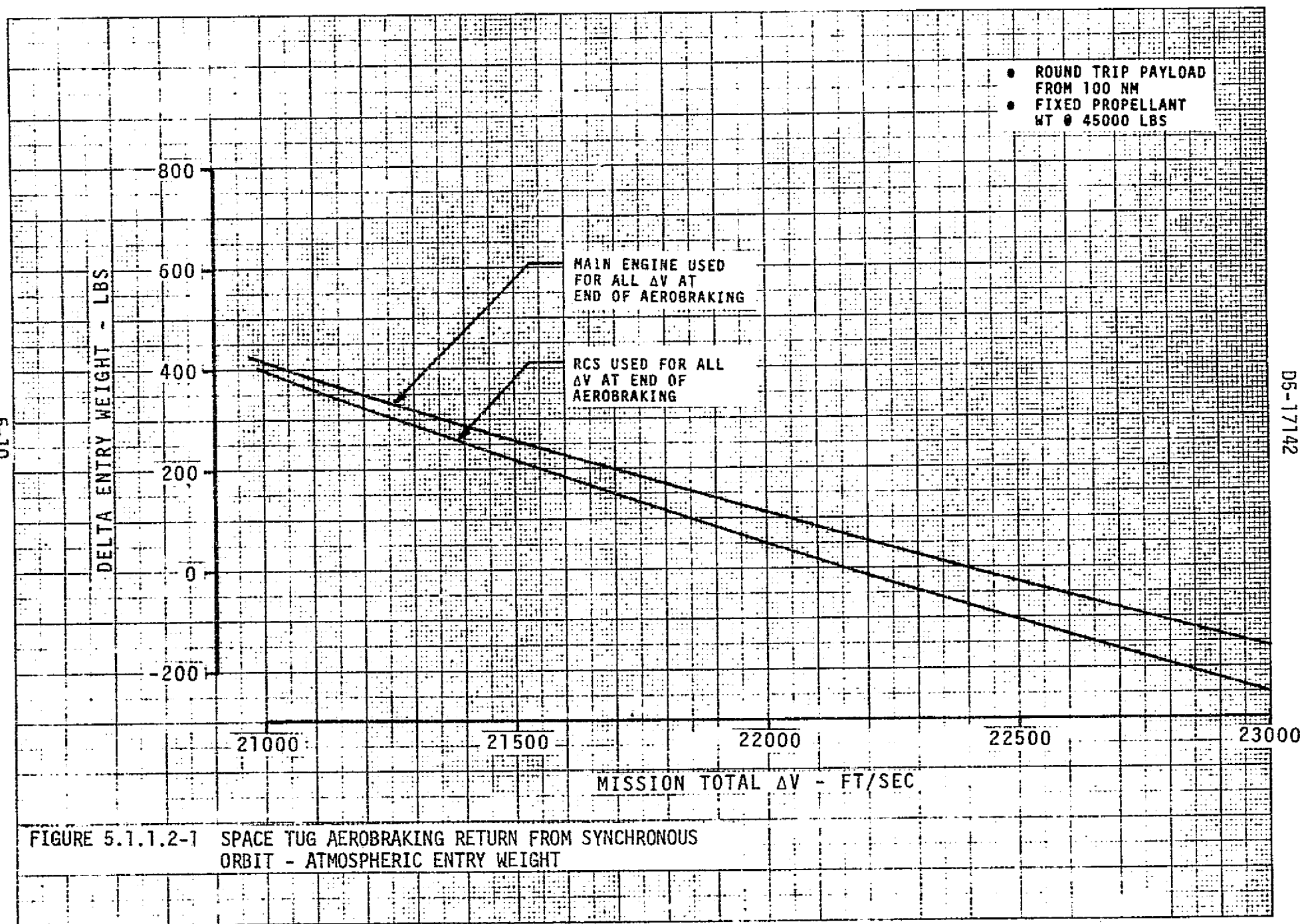
DS-17142

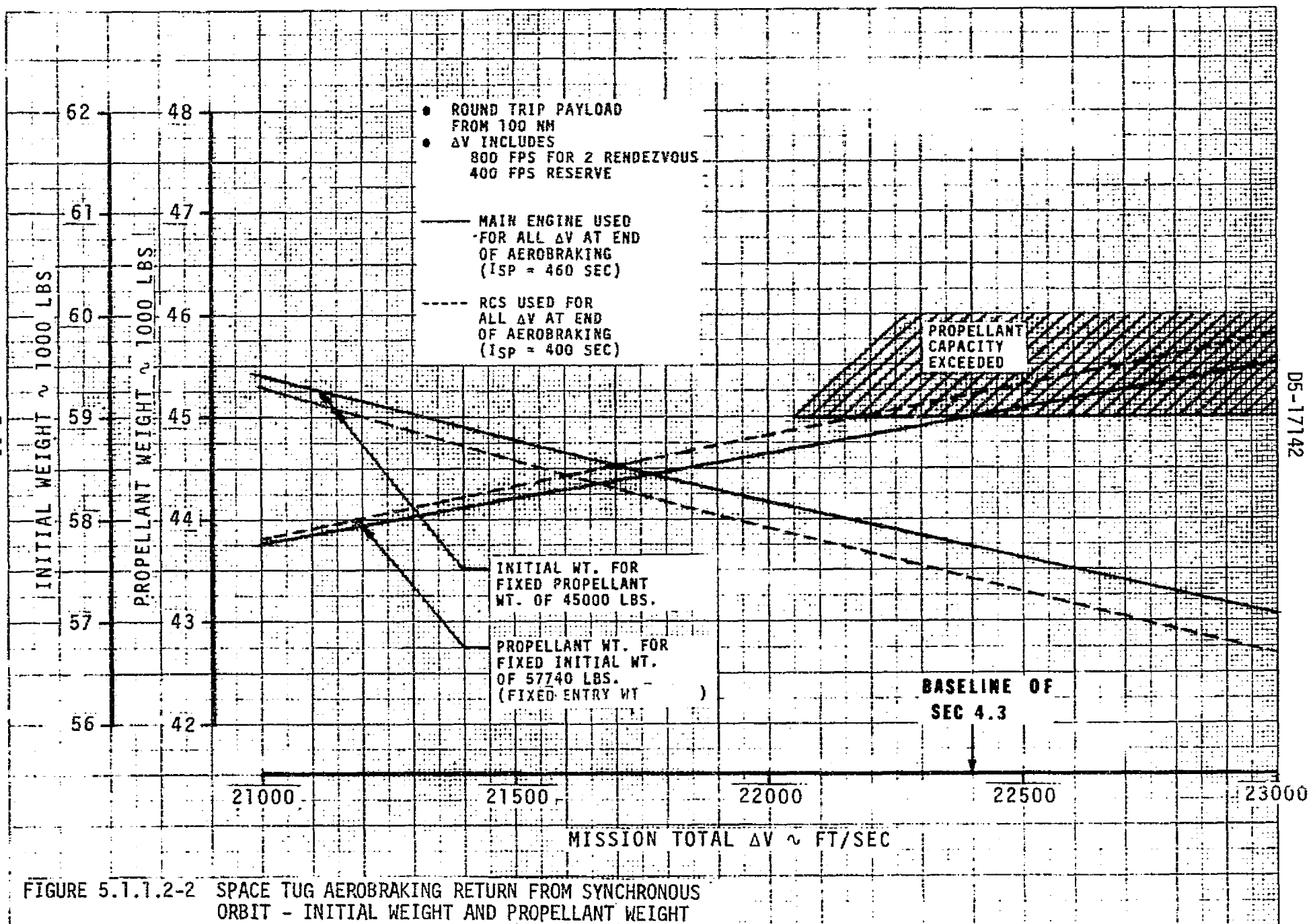
FIGURE 5.1.1.1-3. EFFECT OF AEROBRAKED RETURN DELTA VELOCITY ON PLACEMENT PAYLOAD



DS-17142

FIGURE 5.1.1.1-4. EFFECT OF AEROBRAKED RETURN DELTA VELOCITY ON RETRIEVAL PAYLOAD





5.1.1.2 (Continued)

main engine and RCS curves are identical to those of Figure 5.1.1.2-1. Also shown in Figure 5.1.1.2-2 is the effect of offloading propellant to maintain a fixed initial Tug and payload gross weight (57,740 pounds). With this fixed initial weight, the aerobraked Tug's maximum delta velocity capability is 22,400 ft/sec (main engine). Using the RCS for all propulsive maneuvers after the completion of aerobraking reduces the maximum capability to 22,170 ft/sec. Neither propellant loading technique (full nor offloading) depicted on the figure permits an initial Tug and payload gross weight greater than 59,500 pounds for the expected aerobraking delta velocity budget.

If the RCS were used to provide the propulsive delta velocity after aerobraking, there will be a reduction in round trip payload because of the lower specific impulse. This payload reduction (total mission delta velocity budget = 22,400 ft/sec) is approximately 300 pounds for a fixed initial propellant weight of 45,000 pounds. The maximum delta velocity capability is exceeded for the fixed initial weight approach. However, if this were not true, and to provide a comparative value, the payload reduction would be approximately 230 pounds.

The two approaches shown in Figure 5.1.1.2-2 (fixed initial propellant weight or fixed initial gross weight) were compared to determine the preferable operational mode. Fixing propellant weight is the most logical approach to take since using all available propellant for a fixed stage size is more efficient than offloading propellant. But, fixing propellant causes a change in entry weight which in turn causes a change in inert weight (due to heating and loads). These changes cannot be evaluated directly from the results of the technical studies (Section 4) since the trajectory, thermal, control and weights analyses were performed for a fixed entry weight. However, as will be shown in Section 5.1.2 below, the actual changes in entry weights are small. Therefore, any inert weight penalties would be very small and have an insignificant impact on the payload capabilities of the aerobraked Tug configurations.

Figure 5.1.1.2-3 shows the round trip payload penalties associated with using the RCS for various percentages of the return trip delta velocities. The notes on Figure 5.1.1.2-3 refer to Figures 5.1.1.1-1 and -2. For example, if the RCS accomplished 15% of the 8000 ft/sec return delta velocity (1200 ft/sec), the round trip payload penalty would be approximately 200 pounds. The payload penalties shown in this figure were used in the configuration oriented payload computations discussed in subsequent subsections.

5.1.1.3 Circularization Altitude and EOS Rendezvous Effects

One of the objectives of the sensitivity analysis was to investigate alternate mission modes that could enhance the payload potential of the aerobraking technique. As seen in prior Figure 5.1.1.1-2, the mission delta velocity budget is a critical payload parameter. Figure 5.1.1.3-1 shows the reductions in total mission delta velocity that can be obtained

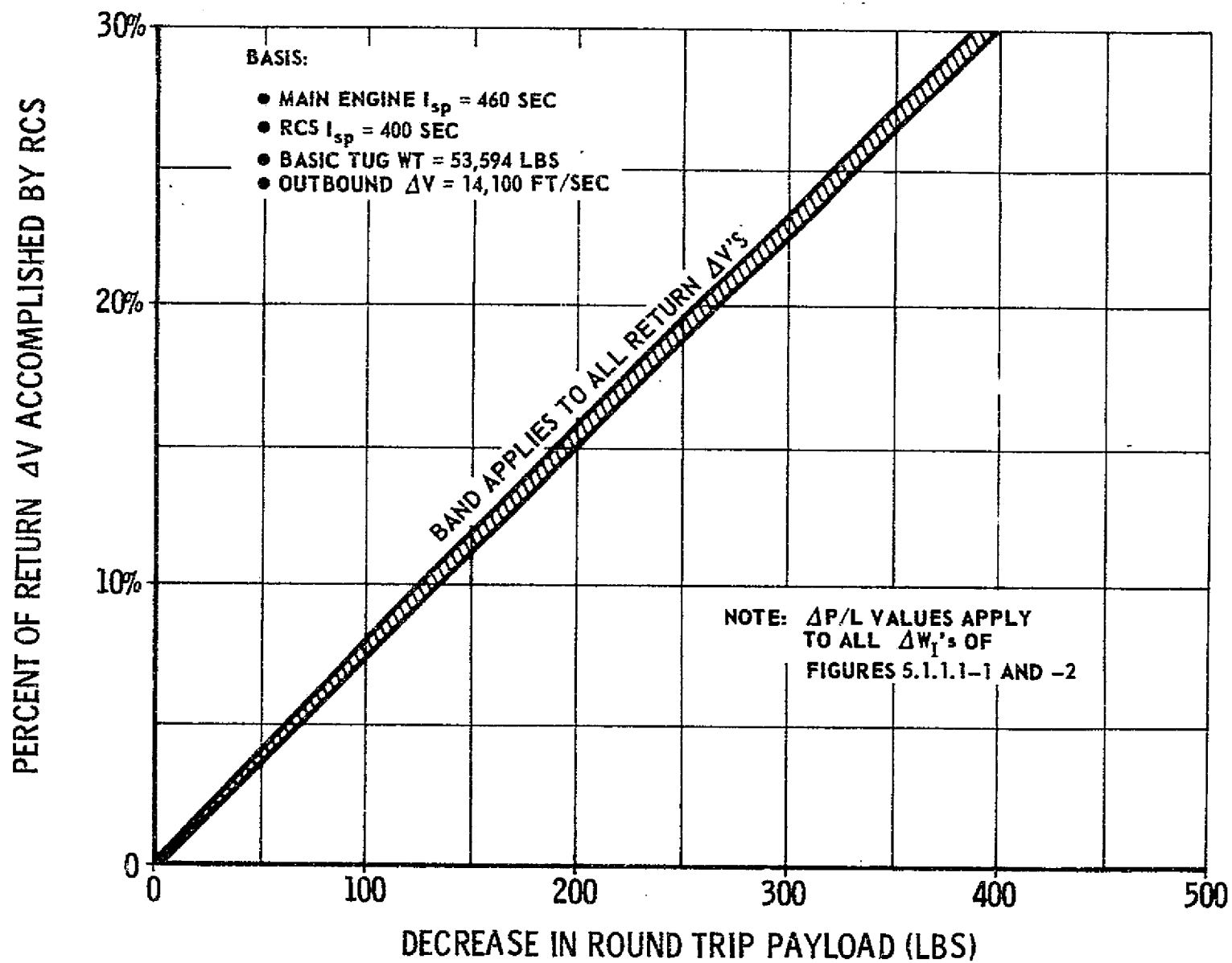


FIGURE 5.1.1.2-3. EFFECT OF RCS USAGE ON PAYLOAD

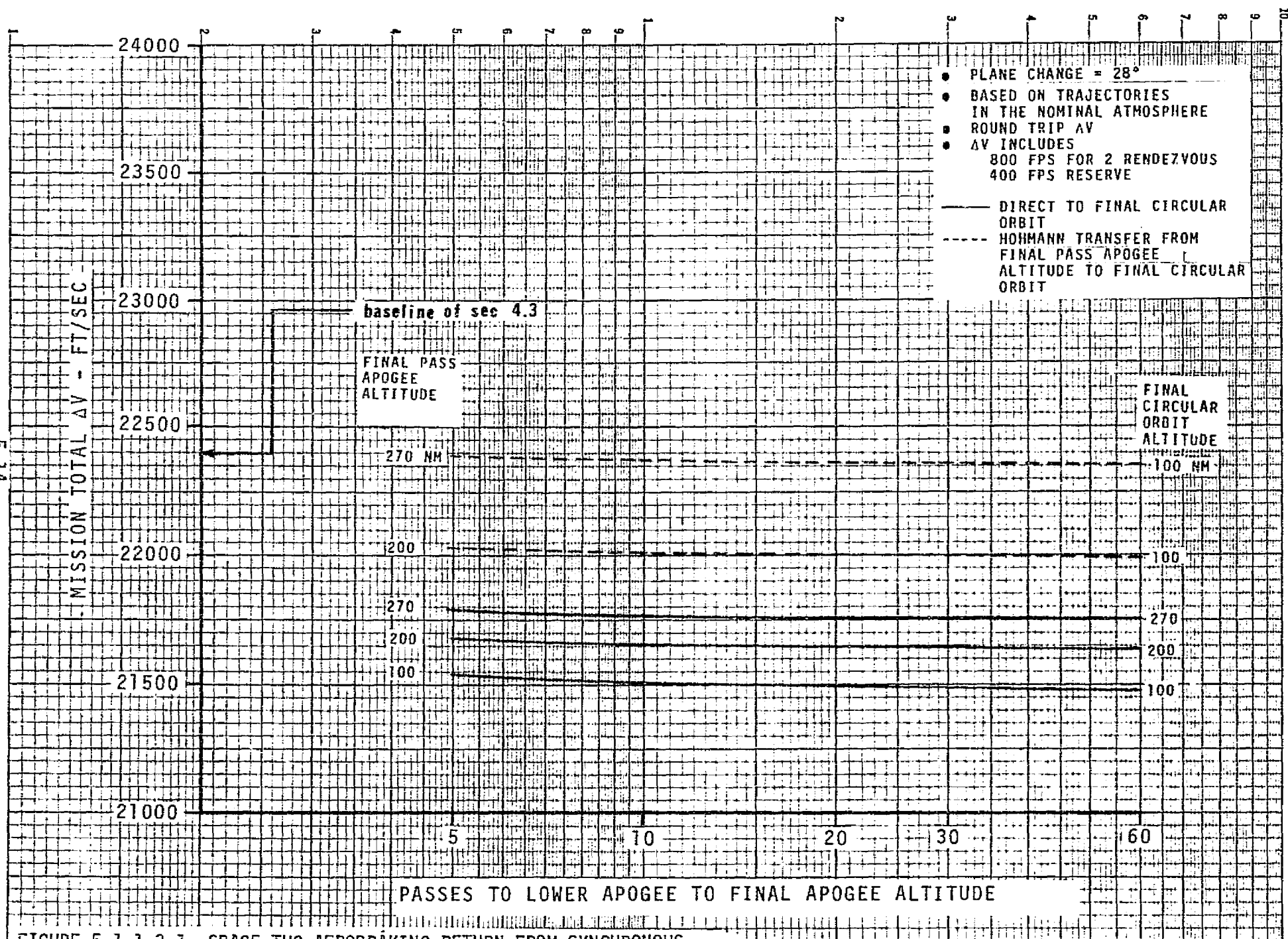


FIGURE 5.1.1.3-1 SPACE TUG AEROBRAKING RETURN FROM SYNCHRONOUS ORBIT - MISSION TOTAL DELTA VELOCITY SENSITIVITY TO FINAL ORBIT ALTITUDE

5.1.1.3 (Continued)

by using alternate Tug/Shuttle mission profiles for rendezvous. The top dotted curve on the figure illustrates the nominal Tug circularization at 270 NM followed by a propulsive transfer to 100 NM for Shuttle rendezvous (see prior Figure 1.2.0.0-1). The mission delta velocity budget for this mode could vary from 20,150 to 22,400 ft/sec dependent upon the rendezvous, docking, and reserve requirements (see notes on Figure 5.1.1.3-1). If a circularization altitude of 200 NM, followed by a transfer to 100 NM were selected, the delta velocity requirement is reduced approximately 360 ft/sec. The mission modes shown by the solid lines eliminate the transfers to 100 NM. The Tug circularizes at the altitude shown and awaits the Shuttle in that orbit. Significant decreases in the mission delta velocity budget are obtainable by using these direct rendezvous modes.

The trajectories for the alternate mission modes shown on Figure 5.1.1.3-1 were generated by varying the first pass vacuum perigee so that the final pass apogee decayed to the desired altitude. The maximum variation in the first pass perigee was approximately 230 feet to change the final pass apogee from 270 NM to 100 NM.

Figure 5.1.1.3-2 shows the results of the analysis of an alternate aerobraking mission mode. The mode depicted has the following sequence: (1) the EOS ejects the Tug and payload in 100 NM/28.5° circular orbit; (2) the Tug delivers the payload into geosynchronous orbit, picks up another payload and deorbits; (3) the aerobraking phase is completed with a circularization burn into a variable altitude shown on the ordinate of Figure 5.1.1.3-2; and (4) the Tug transfers to 100 NM/28.5° to meet the Shuttle for return to earth.

Figure 5.1.1.3-2 shows the effects of (1) circularization altitude selection, (2) jettisoning part of the aerobraking modification kit, and (3) use of the RCS to perform the circularization and transfer burns. For this example, an aerobraking kit inert weight penalty of 1000 pounds was assumed (800 pounds assigned to propulsion module and 200 pounds assigned to the avionics module). Referring to the top hatched area, with this inert weight penalty and an 8000 ft/sec return delta velocity, the basic payload would be 3450 pounds using the main engine to circularize at 270 NM and then to transfer the Tug from 270 to 100 NM. If the propulsion module aerobraking kit (800 pounds) were jettisoned immediately after the last atmospheric passage, the payload capability would increase about 100 pounds. Circularizing at higher altitudes (above 270 NM) with the main engine decreases the payload because of the higher propulsive requirements to circularize at the higher altitude and then to transfer to 100 NM. The impact on payload capability by jettisoning the propulsion module aerobraking kit at the higher circularization altitude is also small (~125 pounds) for a circularization altitude of 400 NM.

Circularizing at altitudes below 270 NM increases the payload capability because of the lower circularization propulsive requirements. The payload capability effect of retaining or jettisoning the aerobraking kit

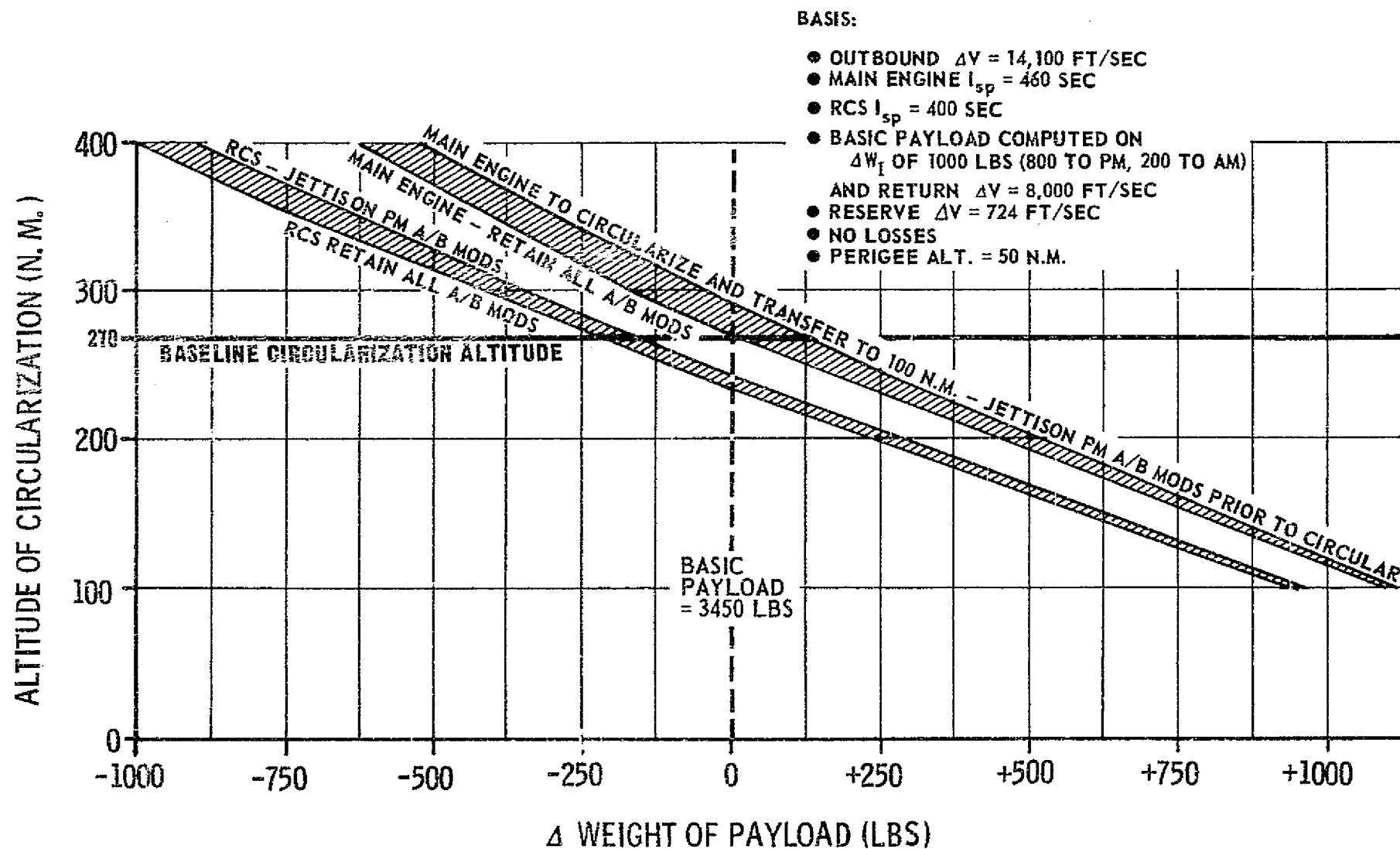


FIGURE 5.1.1.3-2. EFFECTS OF CIRCULARIZATION ALTITUDE ON PAYLOAD
(LIGHT WEIGHT AEROBRAKING KIT PENALTY-1000 POUNDS)

5.1.1.3 (Continued)

modifications becomes even less significant than the effect at higher altitudes. Circularizing at 200 NM rather than 270 NM will increase payload capability approximately 500 pounds.

The bottom hatched area presents similar data but utilizes the RCS as a substitute for the main engine to perform all return trip low earth burns. The same trends noted for the main engine are shown. The payload penalty using the RCS as a substitute for the nominal 270-100 NM burns is approximately 250 pounds.

Figure 5.1.1.3-3 has the same mission mode sequence as Figure 5.1.1.3-2 above but assumes a more severe inert weight penalty for aerobraking kit modifications. The propulsion module aerobraking kit was assumed to weigh 2400 pounds. This case was included to investigate the effect of jettisoning a heavier aerobraking kit (e.g., containing a large flare). Using the main engine and with the nominal post aerobraking operations, i.e., 270 → 100 NM transfer, approximately 225 pounds of payload increase can be obtained by jettisoning 2400 pounds of modifications. This payload capability increase varies from negligible (circularizing at 100 NM) to 300 pounds (circularizing at 400 NM).

Figure 5.1.1.3-4 examines the effect on round trip payload by using the Shuttle to accomplish more of the low earth orbit (circularization, phasing, rendezvous and docking) propulsive requirements. The mission mode (shown by the solid lines) includes the nominal 100 NM/28.5° departure, geosynchronous orbit, deorbit, and aerobraking phase. The Tug then circularizes at any altitude shown on the ordinate. If this circularization altitude is between 100 NM and 270 NM the Shuttle recovers the Tug in this circular orbit, thereby eliminating the requirement for any Tug transfer burn. If the Tug circularized above 270 NM, the Tug then transfers to 270 NM and is recovered by the Shuttle, thereby reducing the Tug's propulsive transfer requirement. The dotted lines on Figure 5.1.1.3-4 represent the mode (transfer to 100 NM for EOS recovery) shown in prior Figures 5.1.1.3-2 and -3 and are shown for comparative analysis.

Comparing the Tug payload capabilities of the two operational modes at a circularization altitude of 270 NM, an increase of approximately 700 pounds is gained by EOS/Tug rendezvous at 270 NM over the payload capability of the Tug transferring down to 100 NM. With a Shuttle/Tug rendezvous altitude of 200 NM, approximately 1000 additional pounds of payload can be achieved. This 1000 pound increase is 500 pounds more than is achieved by the Tug circularizing at 200 NM and transferring to 100 NM. These operational options are indicative of the many modes available and demonstrate the major impact that the circularization and rendezvous operation modes have on aerobraking payload capability. The payload performance associated with the use of the RCS as a substitute for the main engine in the return low earth burns are also shown.

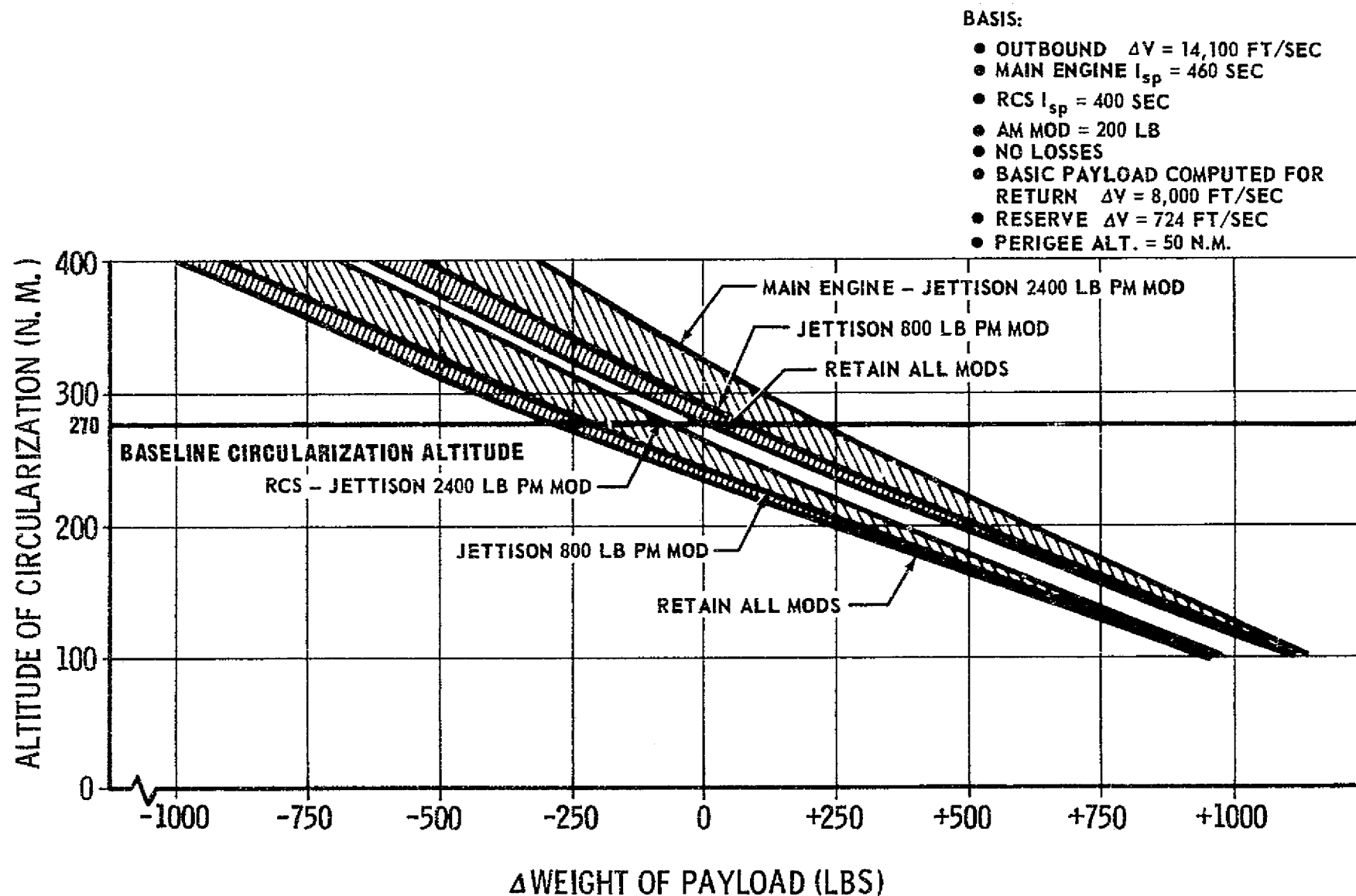


FIGURE 5.1.1.3-3. EFFECT OF CIRCULARIZATION ALTITUDE ON PAYLOAD

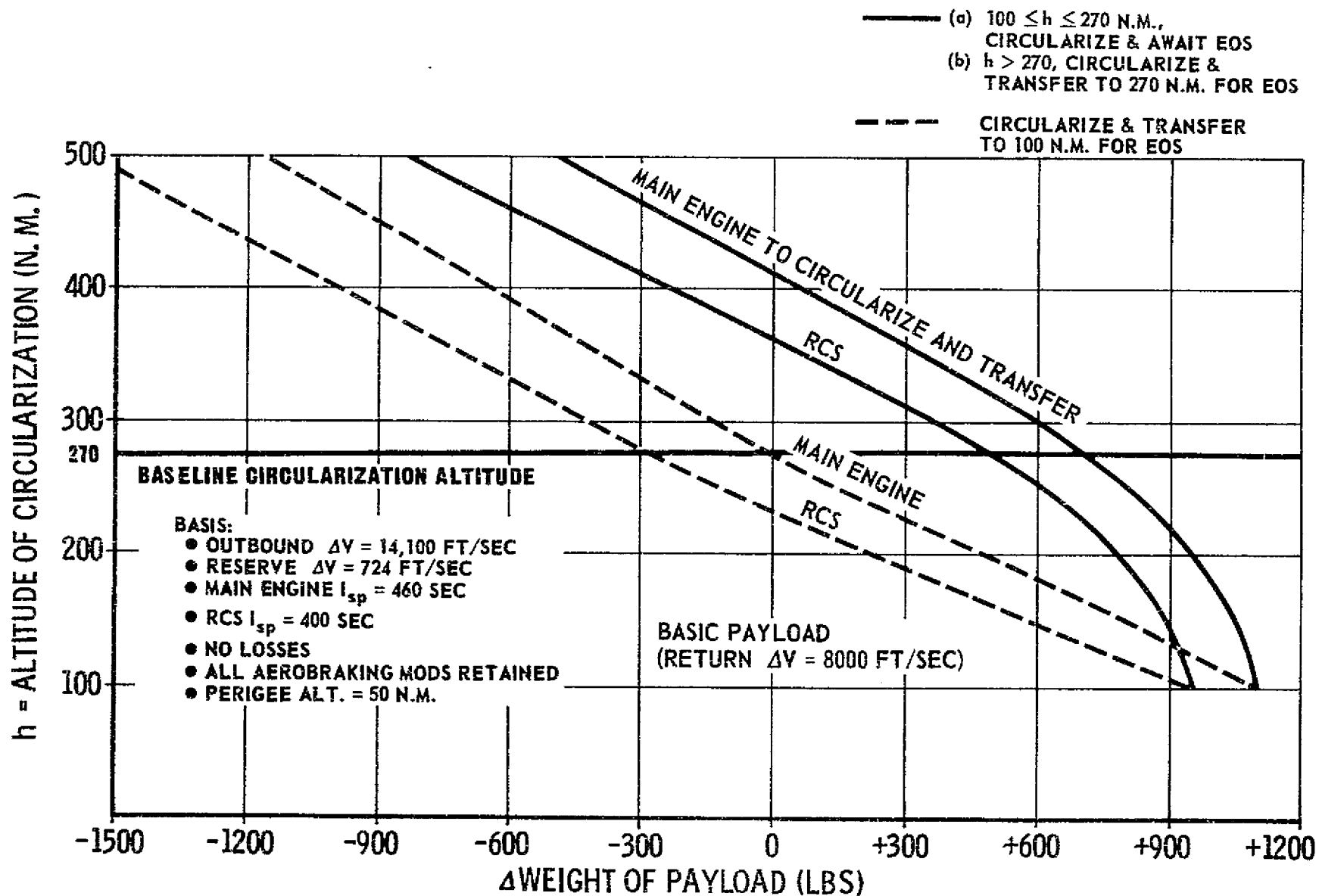


FIGURE 5.1.1.3-4. EFFECT OF TUG RECOVERY ALTITUDE AND RECOVERY METHOD ON DELTA PAYLOAD

5.1.1.4 General Parametric Conclusions

From the data presented, three conclusions were drawn.

- o Payload capability would be significantly increased by decreasing the nominal circularization altitude from 270 NM to approximately 200 NM. Very low circularization altitudes (e.g., 100 NM) have certain disadvantages including: (1) Orbital decay if the Tug must wait some significant period of time for EOS recovery; and (2) the lack of an altitude tolerance band in which to circularize after repeated passages through an unpredictable atmosphere.
- o Jettisoning the propulsion module aerobraking kit to gain payload should not be considered as the aerobraked Tug's baseline operational mode. The payload increase does not appear sufficiently significant (~ 250 pounds payload at 200 NM for 2400 pounds inerts) to justify the normal expenditure of the kit for this reason alone.
- o The combination Shuttle/Tug capability should be assessed to determine not only optimum recovery but also optimum departure orbits.

5.1.2 Specific Payload Capability Assessment (Configuration Oriented)

The four aerobraking configurations selected for analysis during this study are discussed in Section 4.2 and are shown in Figure 5.1.2.0-1. The fully fueled weight statements (standard atmosphere and no navigation errors) for these four configurations have been extracted from Section 4.8 and are shown in Figure 5.1.2.0-2. The inert weights of the basic propulsion module (5868 pounds) and astronics module (1960 pounds) are summed in the column labeled Tug Inert Weight.

The maximum gross Tug weight (less payload) shown in Figure 5.1.2.0-2 is 56,685 pounds for the 5 pass, 45° flare configuration. Using prior Figure 5.1.1.1-2, with an effective delta inert weight of 3091 pounds, a maximum round trip payload of 1000-2000 pounds could be expected. The total gross payload for the Shuttle would be approximately 58,500 pounds. Similarly, the minimum gross Tug weight of 54,643 pounds for the 30 pass basic (no flare) configuration would have an estimated maximum 3000-4000 pounds of payload for a total gross Shuttle payload of 58,500 pounds. Both of these gross weights are less than the Shuttle's 100 NM/28.5° payload capability of 65,000 pounds shown in Figure 5.1.2.0-3 (Reference 5.1.2.0-1).

From the general parametric studies of Section 5.1.1 above, a Tug circularization and recovery altitude of approximately 200 NM appeared attractive. Figure 5.1.2.0-3 indicates that a representative Shuttle payload capability to a 200 NM/28.5° orbit would be 60,000 pounds. Therefore, both operational modes were carried forward for further analysis. Within this subsection, the only exception to this is the payload placement mission where the Tug with payload has a gross weight greater than the

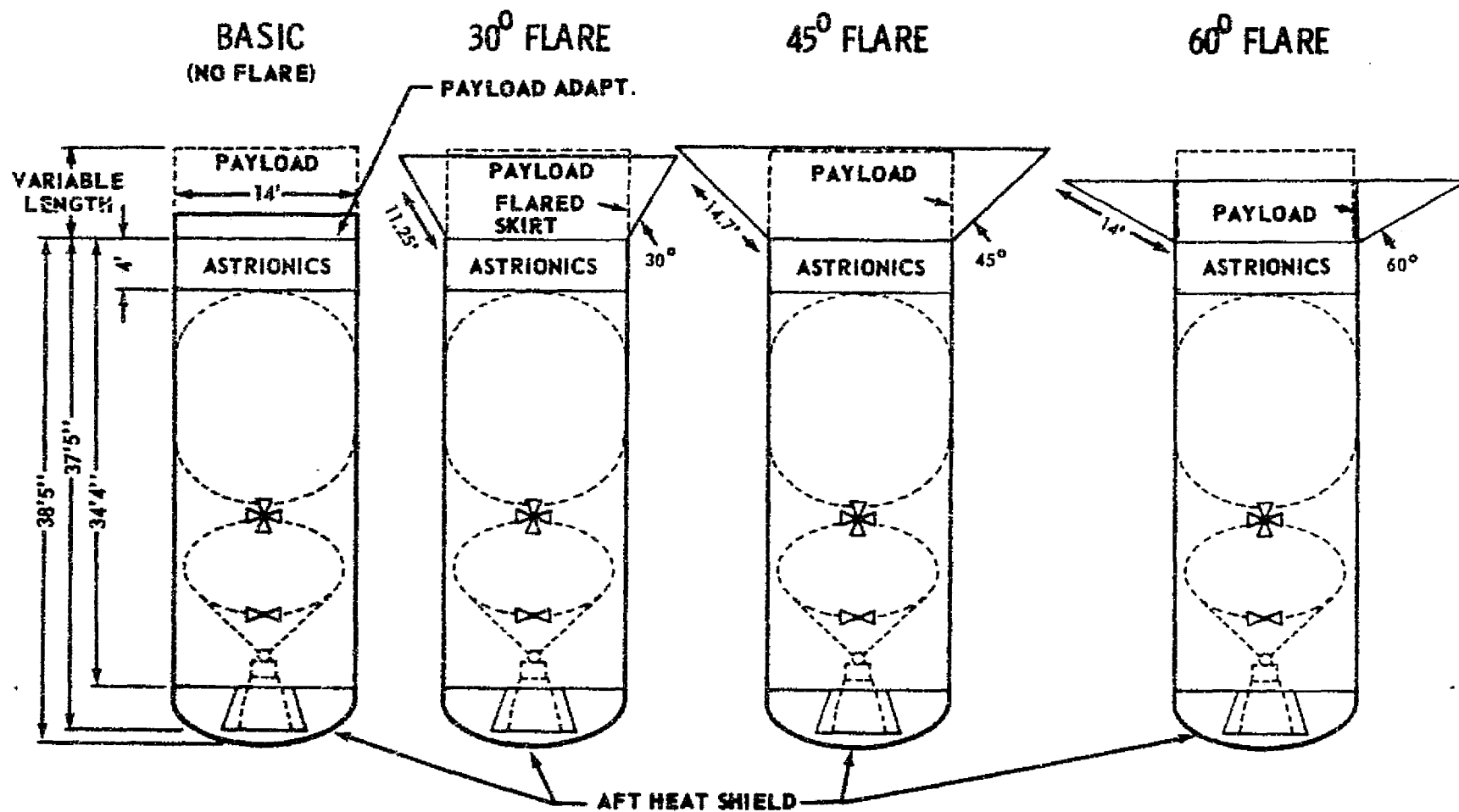


FIGURE 5.1.2.0-1: SELECTED SPACE TUG AEROBRACING CONFIGURATION CONCEPTS (1ST PHASE)

COMPONENT CONFIGURATION NO. OF MISSION PASSES	TUG INERT WEIGHT (LB)	PROPELLANT (LB)	* AFT HEAT SHIELD (LB)	*FLARE (LB)	*SIDEWALL INSULATION (LB)	PAYLOAD/FLARE ADAPTER (LB)	ASTRONICS MODULE PENALTY (LB)	GROSS TUG WEIGHT (LESS PAYLOAD) (LB)	MASS FRACTION (X)
<u>BASIC-NO FLARE</u>									
5	7828	45,000	1,395	----	419	**614	45	55,301	0.814
10	7828	45,000	1,160	----	386	**582	110	55,066	0.817
30	7828	45,000	610	----	328	**552	325	54,643	0.824
60	7828	45,000	560	----	298	**505	650	54,841	0.821
<u>30° FLARE</u>									
5	7828	45,000	1,155	900	398	390	45	55,721	0.808
10	7828	45,000	875	805	361	390	110	55,369	0.813
30	7828	45,000	480	760	283	390	325	55,066	0.817
60	7828	45,000	450	755	238	390	650	55,311	0.814
<u>45° FLARE</u>									
5	7828	45,000	990	2070	362	390	45	56,685	0.794
10	7828	45,000	585	1625	317	390	110	55,855	0.806
30	7828	45,000	450	1220	240	390	325	55,453	0.811
60	7828	45,000	440	1065	189	390	650	55,562	0.810
<u>60° FLARE</u>									
5	7828	45,000	575	2130	328	390	45	56,296	0.799
10	7828	45,000	455	1655	294	390	110	55,732	0.807
30	7828	45,000	440	1255	215	390	325	55,453	0.811
60	7828	45,000	440	1100	158	390	650	55,566	0.810

* STANDARD ATMOSPHERE AND NO NAVIGATION ERRORS

** INCLUDES PAYLOAD INSULATION AND PAYLOAD CAP ACTUATION DEVICE

FIGURE 5.1.2.0-2 FULLY FUELED WEIGHT STATEMENT

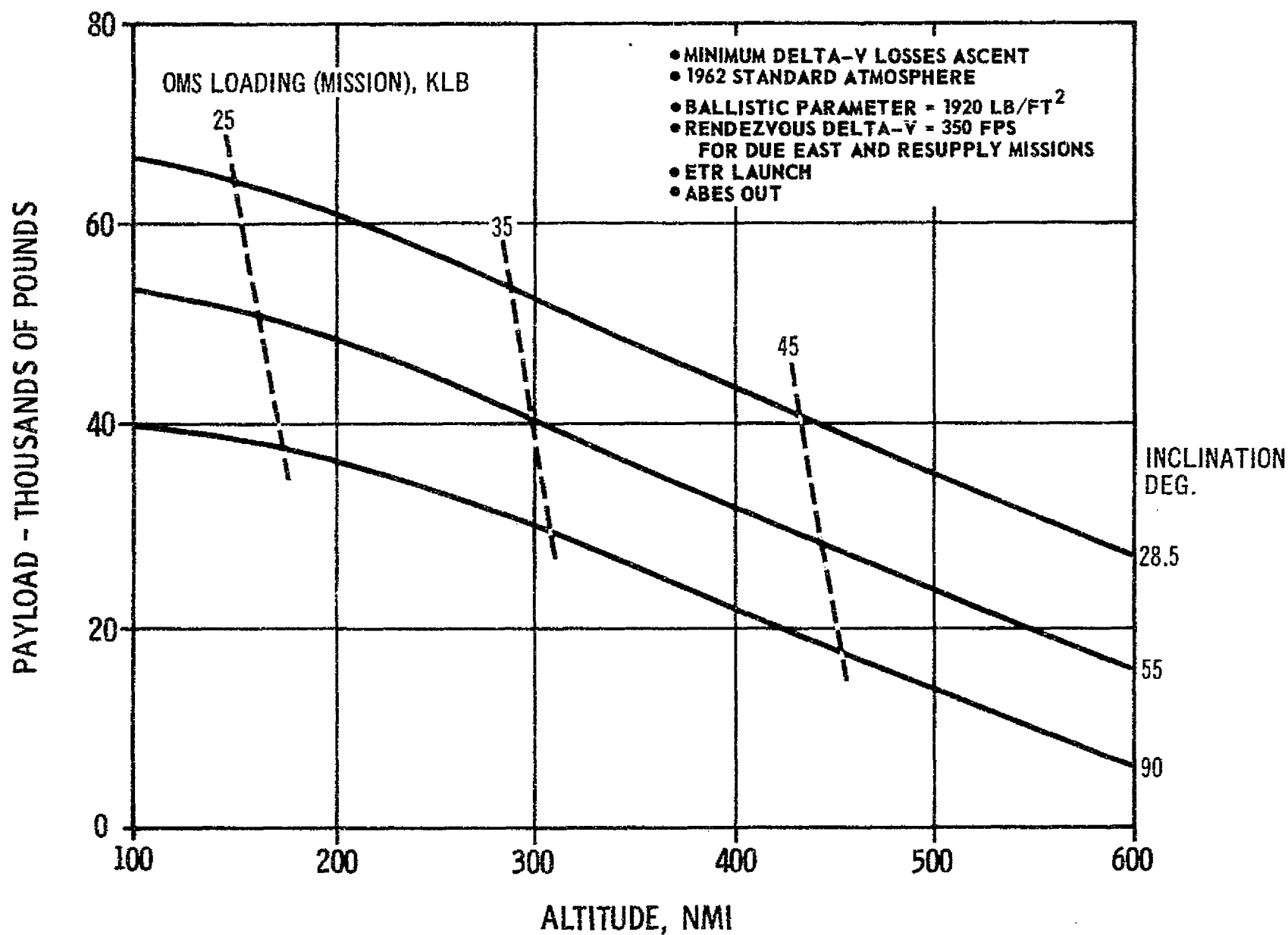


FIGURE 5.1.2.0-3: H-33 CONFIGURATION EXTERNAL H₂ TANK ORBITER
ALTERNATE MISSION CAPABILITY

5.1.2 (Continued)

Shuttle can deliver to 200 NM. For identification, the mode of departing from 100 NM, circularizing at 270 NM and transferring back to 100 NM, is denoted by "270-100 NM recovery". The 200 NM mode is denoted by "Depart and Recover at 200 NM".

The following subsections discuss the mission delta velocity budgets and the payload capabilities of the four aerobraked configurations under the standard atmosphere and zero navigation error conditions. The sensitivity of the payload capabilities to atmospheric perturbations and navigation errors is contained in Section 5.2.

5.1.2.1 Delta Velocity Budgets

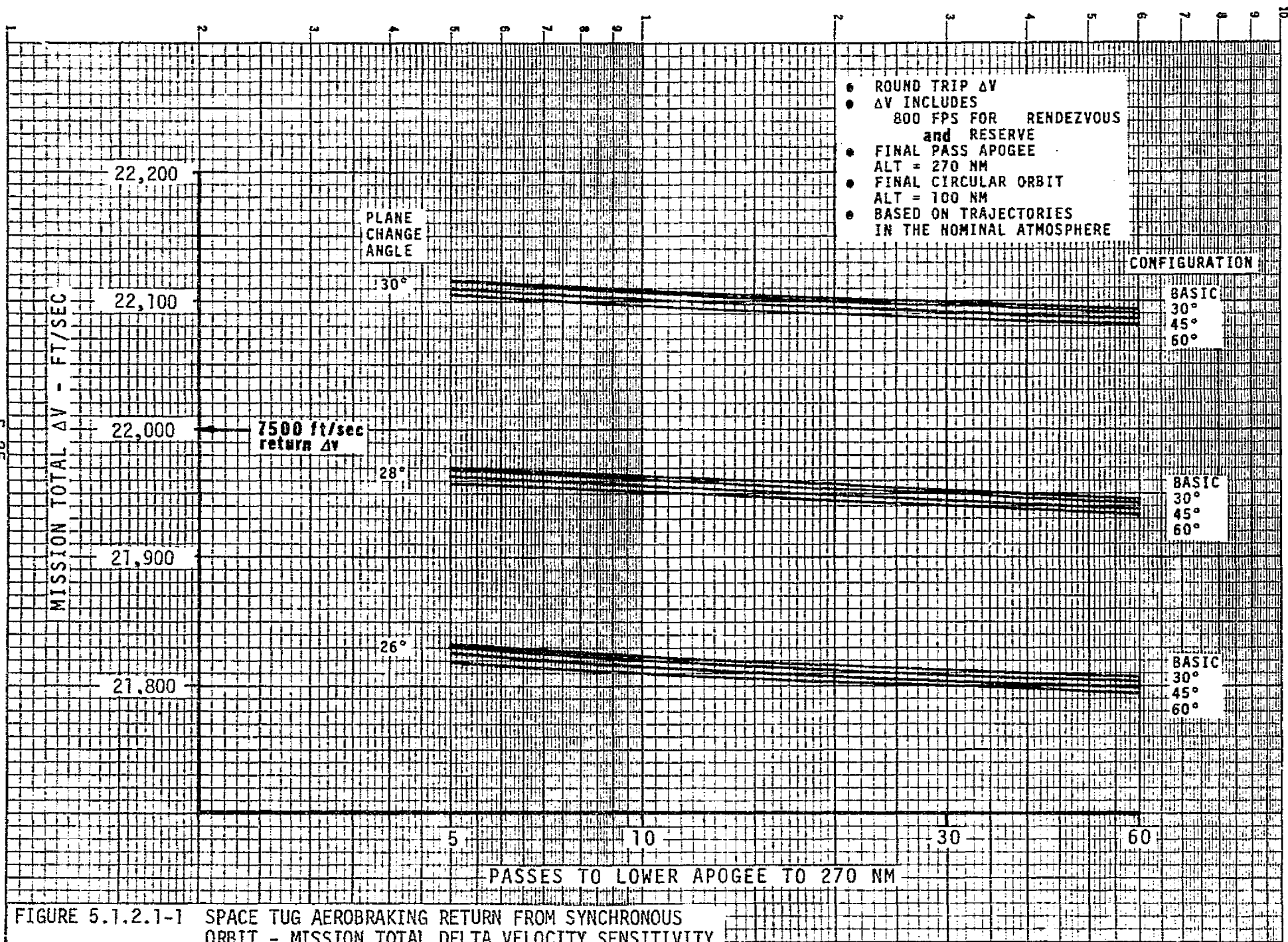
The total mission delta velocity budget for an aerobraked Tug configuration is the sum of (1) the normal main engine and RCS propulsive requirements for the non-aerobraking phases of the geosynchronous mission, and (2) the added RCS requirements for stability and control during the aerobraking phase. This subsection discusses both of these requirements in order to establish a total mission delta velocity budget for the payload computations to follow. The first two figures show the non-aerobraked propulsive delta velocity requirements for the four configurations and establish the operational mode dependent fixed base requirements. The last figure in this subsection shows the added aerobraking phase RCS delta velocity requirements and the total mission budget.

Figure 5.1.2.1-1 shows the sensitivity of the delta velocity budget to (1) the descent plane change angle, (2) the number of passes to lower the apogee to 270 NM, and (3) the aerobraked Tug configuration. Increasing the plane change requirement from the nominal 28° to 30° results in a delta velocity increase of 150 ft/sec. Similarly, a decrease in the plane change requirements of 2° to 26° results in a delta velocity decrease of 150 ft/sec. The sensitivity of delta velocity to the number of passes is relatively insignificant and is the result of varying the first pass perigee (see Paragraph 5.1.1.3 above).

All four of the aerobraked configurations have nearly identical delta velocity budgets (fixed plane change angle). The delta velocity budget difference between the basic (no flare) and the 60° flare configurations is approximately 13 ft/sec for all mission durations. The maximum difference in delta velocities (fixed plane change angle) is approximately 38 ft/sec (5 pass basic no flare to 60 pass 60° flare). These small differences can be absorbed within a rendezvous and reserve delta velocity budget of 800 ft/sec and are not considered payload significant.

Figure 5.1.2.1-2 illustrates the sensitivity of the 30° flared configuration's burnout weight (inerts plus payload) to the mission mode selected. The delta velocities shown on the abscissa include 1200 ft/sec for rendezvous and reserves. The delta velocity (using the main engine for post aerobraking propulsion) of 22,400 ft/sec (see prior Figure 5.1.1.2-2) has a zero delta burnout weight. This delta velocity, with the additional velocity allowances made, approximates the 270-100 NM mode (labeled "D"). Other mission

5-25



- ROUND TRIP ΔV
- ΔV INCLUDES 800 FPS FOR RENDEZVOUS and RESERVE
- FINAL PASS APOGEE ALT = 270 NM
- FINAL CIRCULAR ORBIT ALT = 100 NM
- BASED ON TRAJECTORIES IN THE NOMINAL ATMOSPHERE

DS-17142

FIGURE 5.1.2.1-1 SPACE TUG AEROBRACING RETURN FROM SYNCHRONOUS ORBIT - MISSION TOTAL DELTA VELOCITY SENSITIVITY TO PLANE CHANGE ANGLE AND CONFIGURATION

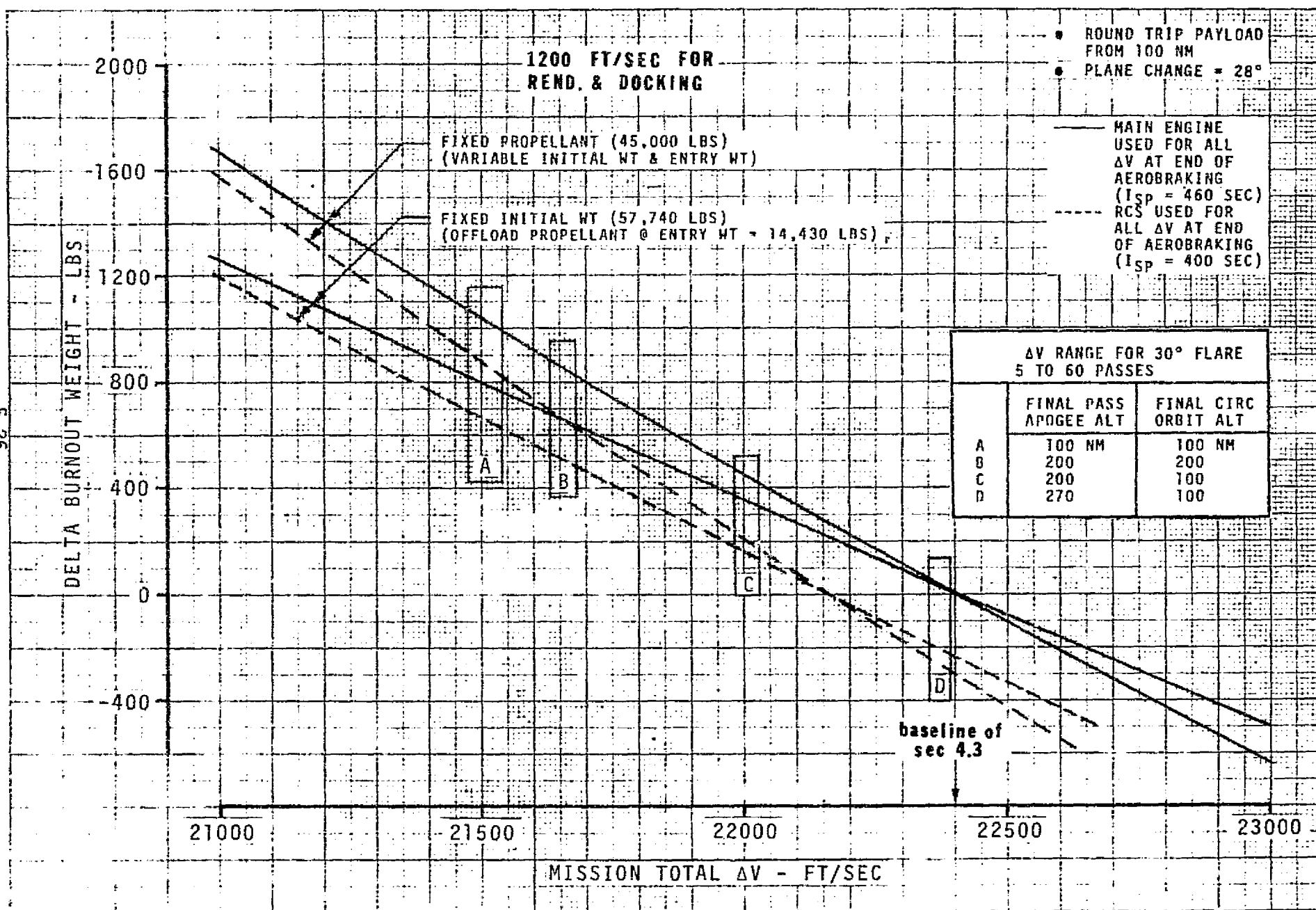


FIGURE 5.1.2.1-2 SPACE TUG AEROBRAKING RETURN FROM SYNCHRONOUS ORBIT - PAYLOAD SENSITIVITY TO DELTA VELOCITY

5.1.2.1 (Continued)

modes, all departing 100 NM, are similarly labeled. Also shown on Figure 5.1.2.1-2 are the effects of using the RCS to provide the post aerobraking propulsive requirements.

The data for the 30° flare configuration shown on Figure 5.1.2.1-2 confirms the general parametric conclusions of Section 5.1.1 above. For example, the 30° flare configuration's delta velocity budget can be reduced approximately 900 ft/sec by returning direct to 100 NM rather than using the 270-100 NM mode. This results in a round trip payload increase of 810 pounds (fixed initial or entry weight) or about 1000 pounds (fixed 45,000 pounds initial propellant weight). Without consideration of the RCS control requirements, all of the four aerobraked configurations will have approximately the same payload increase because the delta velocity budgets are nearly identical.

Section 4.4 contains data on the RCS propellant consumed by the various configurations during the aerobraking phase of the mission. This RCS propellant can be converted to an equivalent delta velocity by the relationship shown below:

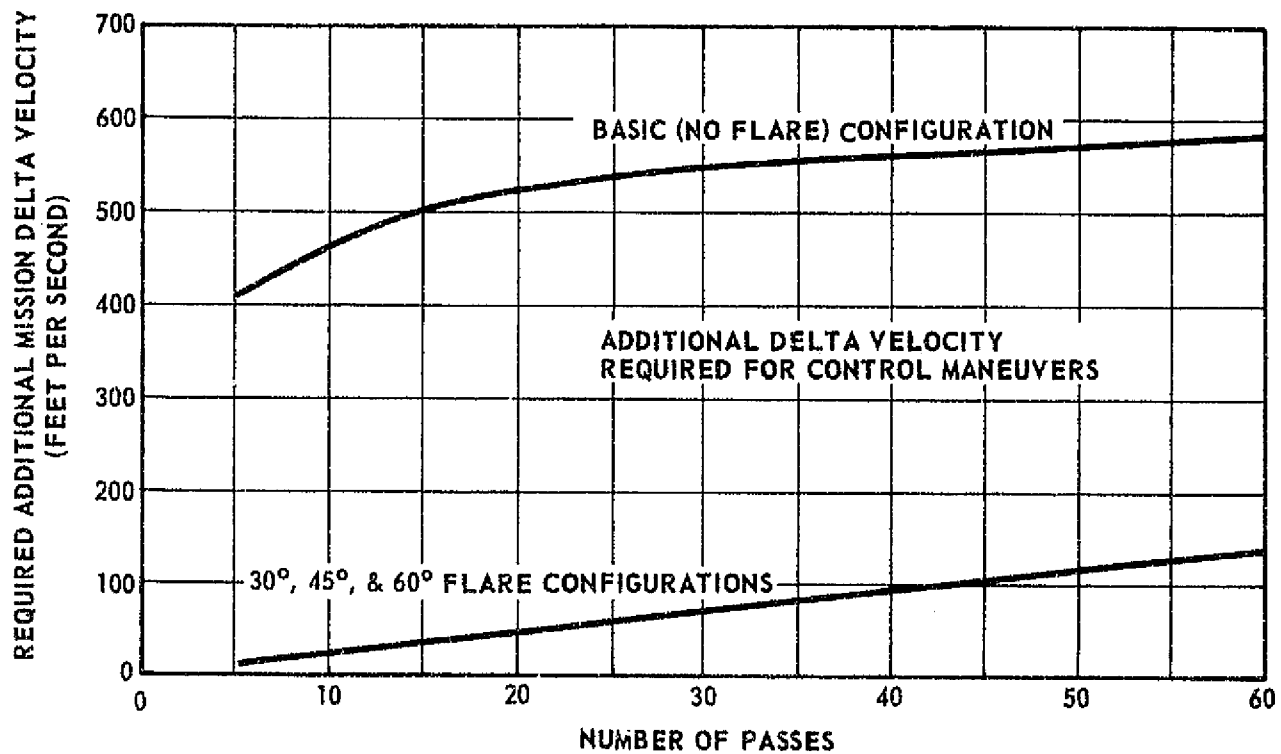
$$(1) \text{ Weight of Propellant } (W_p) = \frac{\text{Total Impulse } (I)}{\text{Specific Impulse } (Isp)}$$

$$(2) I = (\text{mass}) \times (\text{delta velocity})$$

These equivalent delta velocities were added to the nominal mission requirements. Also included was 400 feet per second for midcourse corrections due to navigational errors during the aerobraking phase. The resulting overall mission delta velocity budgets are shown in Figure 5.1.2.1-3. The top portion of this figure reflects the equivalent delta velocity required by the RCS during the aerobraking phase and are configuration dependent. The fixed base totals shown at the bottom of Figure 5.1.2.1-3 are operational mode dependent. Only one fixed base value was utilized for all configurations because of the insensitivity of configuration to delta velocity as shown in Figure 5.1.2.1-1. The total mission delta velocity for a specific configuration and number of passes and for an operational mode is the sum of the two values. For example, the basic (no flare) 30 pass configuration operating in the 270-100 NM transfer mode has a total mission delta velocity of 22,500 (21,950 + 550) ft/sec. The 60° flare 30 pass configuration in the same operational mode has a total mission delta velocity of 22,020 ft/sec. This decrease in total mission delta velocity for the flared configurations tends to compensate for their greater inert weights shown in the prior Figure 5.1.2.0-2.

5.1.2.2 Basic (No Flare) Configuration

Figure 5.1.2.2-1 shows the gross weight distribution of the basic (no flare) Tug configuration and its round trip payload at the start of the aerobraking phase (i.e., at the time of first atmospheric entry) using the 270-100 NM recovery mode. The Tug inerts are those shown previously in Figure 5.1.2.0-2. The aerobraking penalties are the sums of the inert weight



FIXED BASE TOTAL MISSION DELTA VELOCITY

	270-100 N.M. TRANSFER MODE	200 N.M. DEPARTURE & RECOVERY MODE
TO SYNC. ORBIT	14,100	13,810
DOCKING @ ORBIT	400	400
DEORBIT	5,993	5,993
CIRCULARIZATION(S) & TRANSFER	1,057	307
RESERVE FOR MANEUVERS	400	400
FIXED BASE TOTAL	21,950 FT/SEC	20,910 FT/SEC

FIGURE 5.1.2.1-3. TOTAL MISSION DELTA VELOCITY EQUIVALENT VS. NUMBER OF PASSES

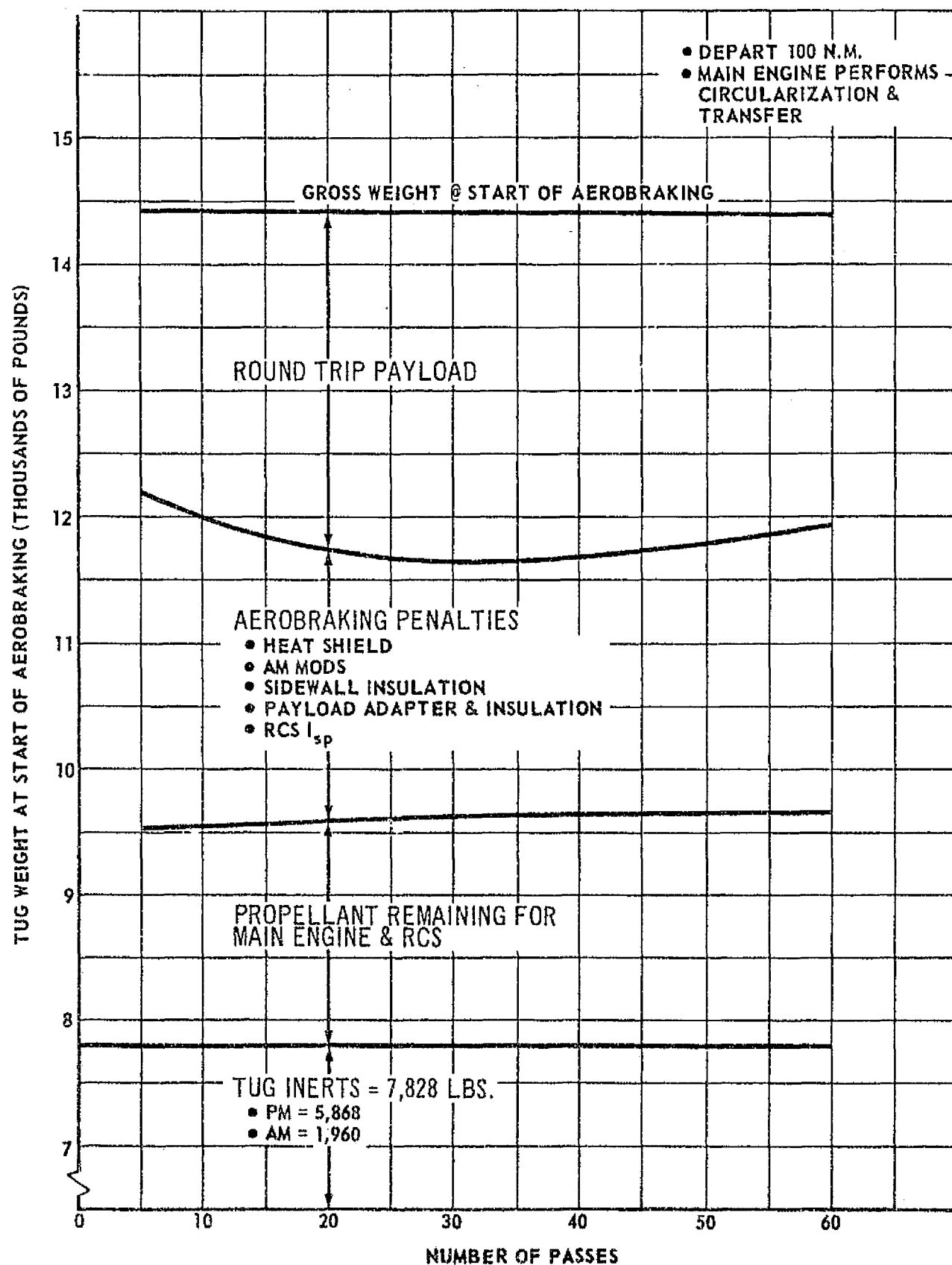


FIGURE 5.1.2.2-1: AEROBRAKING WEIGHT VERSUS NUMBER OF PASSES
 (BASIC - 270-100 N.M. RECOVERY)

5.1.2.2 (Continued)

penalties (Figure 5.1.2.0-2) and the penalty of using the RCS to provide part of the equivalent mission delta velocity (Figure 5.1.1.2-3). Since the main engine was utilized to circularize at 270 NM and to transfer from 270 to 100 NM, this RCS Isp penalty was relatively small (~ 200 pounds of payload). The propellant remaining for the main engine and the RCS is that usable propellant required to perform the remainder of the mission during and after the aerobraking phase.

As the number of passes in the mission increases, a small increase in the remaining propellant can be noted. This is caused by the increased equivalent total mission delta velocity shown in Figure 5.1.2.1-3. The bucket in the aerobraking penalty curve (~ 30 passes) represents that shown in tabular form in Figure 5.1.2.0-2. Because of the almost insignificant slope of the gross weight line, this aerobraking penalty bucket also represents the point at which the maximized round trip payload for the basic (no flare) Tug will occur.

Figure 5.1.2.2-2 shows similar data to that in Figure 5.1.2.2-1 but uses the operational mode of EOS delivery and recovery at 200 NM. As shown in Figure 5.1.2.1-3, the mission delta velocity for this operational mode is decreased approximately 1000 ft/sec from that of the 270-100 NM mode. The same trends are noted with this operational mode as with 270-100 NM mode. The round trip payload maximizes for missions having approximately 30 passes. The basic (no flare) configuration has approximately 1200 pounds more round trip payload capability in the 200 NM mode ($\sim 45\%$ more) than in the 270-100 NM mode (3950 pounds versus 2750 pounds).

5.1.2.3 30° Flare Configuration

The gross weight distribution at the start of aerobraking (270-100 NM mode) is shown in Figure 5.1.2.3-1. The rationale of the data shown is similar to that discussed for the basic (no flare) configuration in Figure 5.1.2.2-1 above. The 30° flare (as well as the 45° and 60° flares to follow) has a smaller total mission equivalent delta velocity than the basic (no flare) configuration. The RCS Isp penalty is also smaller and has lesser impact on the total aerobraking penalty. The bucket in the aerobraking penalty curve is not sharp or well defined. Therefore, the round trip payload capability is nearly constant for missions having 20-40 passes (3.7 to 7.4 days).

Figure 5.1.2.3-2 shows similar data for the 200 NM mode. The same trends as discussed in Figure 5.1.2.3-1 above are observed. In particular, the same relatively insensitivity of payload capability for missions of 20-40 passes is seen. The round trip payload capability for the 200 NM mode is approximately 1275 pounds greater than for the 270-100 NM mode. This increase in payload capability is slightly greater than for the basic (no flare) configuration because of the impact of the decreased delta velocity offsets the increased inert weights.

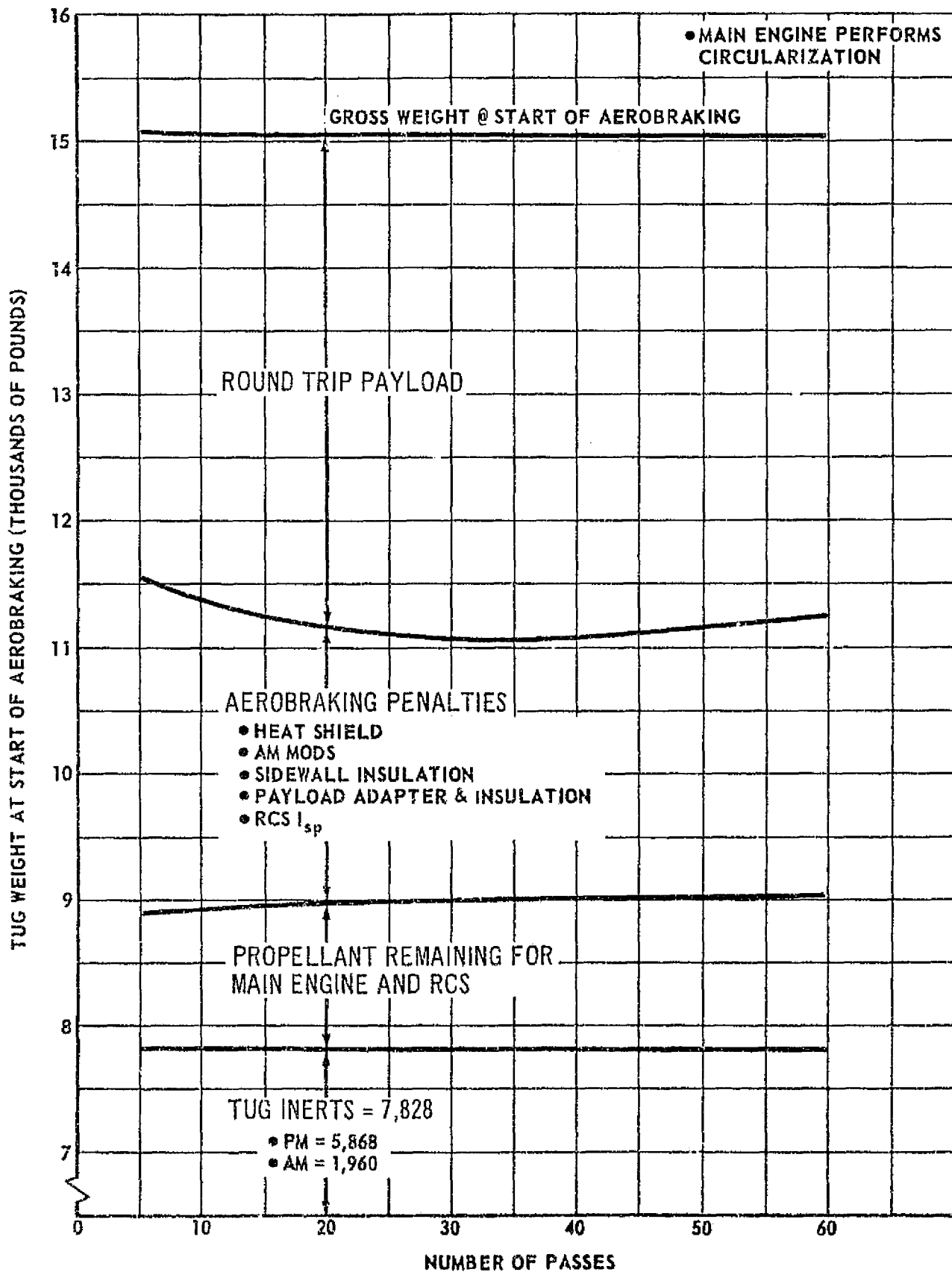


FIGURE 5.1.2.2-2: AEROBRAKING WEIGHT VERSUS NUMBER OF PASSES
(BASIC - DEPART AND RECOVER AT 200 N.M.)

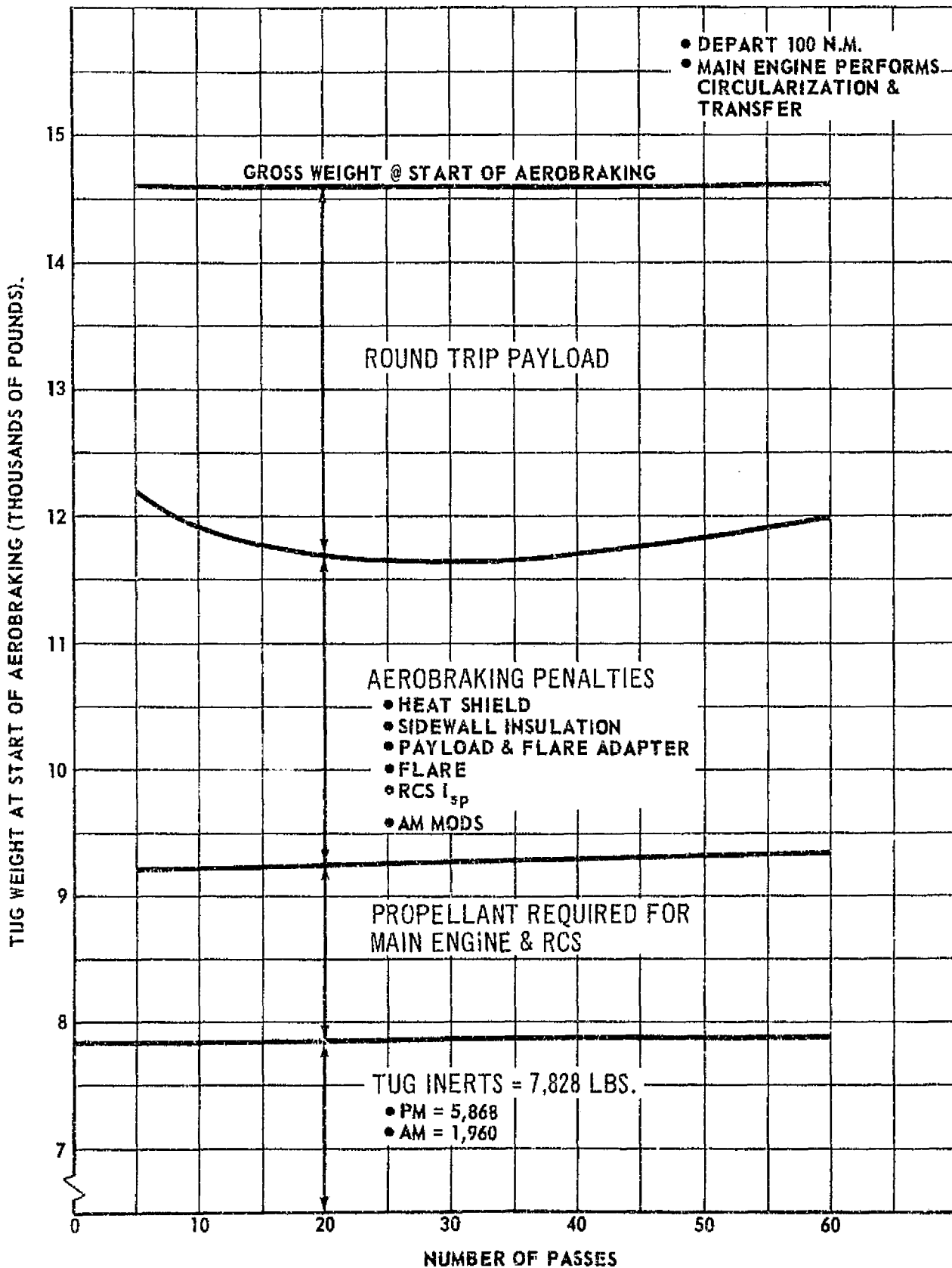


FIGURE 5.1.2.3-1: AEROBRAKING WEIGHT VERSUS NUMBER OF PASSES
 (30° FLARE - 270-100 N.M. RECOVERY)

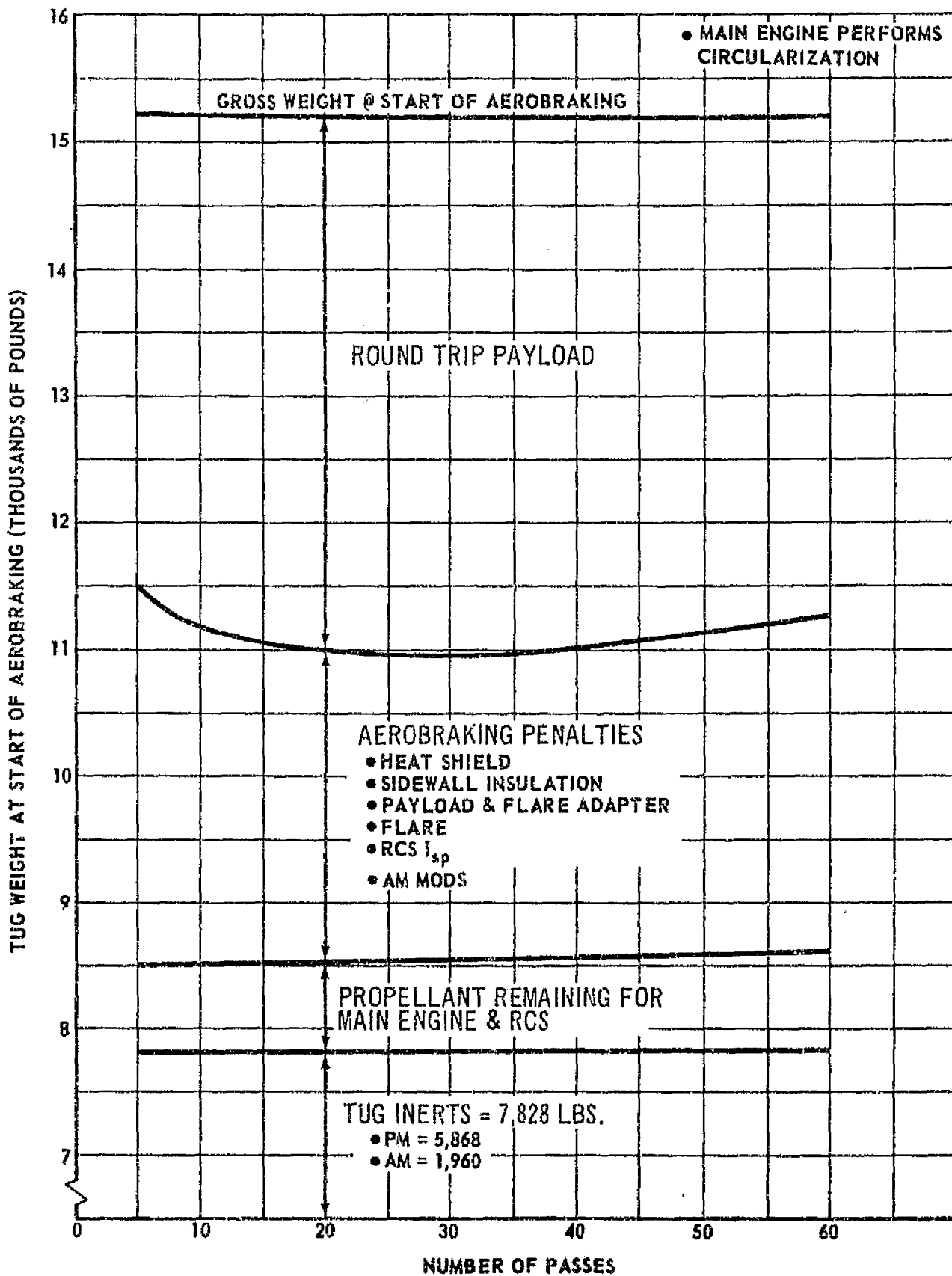


FIGURE 5.1.2.3-2: AEROBRAKING WEIGHT VERSUS NUMBER OF PASSES
(30° FLARE - DEPART AND RECOVER AT 200 N.M.)

5.1.2.4 45° Flare Configuration

The 270-100 NM mode 45° flare configuration gross weight distribution is shown in Figure 5.1.2.4-1. This configuration has a relatively heavy flare and heat shield for a 5 pass mission (see Figure 5.1.2.0-2). The 10 pass mission aerobraking inert weights significantly decreased and this fact is reflected in the sharp drop in the aerobraking penalty curve between 5 and 10 passes. Similar to the 30° flare configuration, the aerobraking penalty bucket is not sharp. Therefore, the round trip payload is relatively insensitive to trip times over 2 days (10 passes).

Figure 5.1.2.4-2 shows the 45° flare configuration in the 200 NM mode. The characteristics of the 45° flare curves are similar to the 30° flare configuration and the 200 NM mode provides the same increase in payload capability as did the 30° flare.

5.1.2.5 60° Flare Configuration

The 60° flare configuration in the 270-100 NM mode is shown in Figure 5.1.2.5-1. The major flare weight difference between the five and ten pass missions (Figure 5.1.2.0-2) has the greatest impact on the decrease in aerobraking penalty weights shown in that region. Similar to the other flares, the 60° flare configuration is relatively insensitive to mission duration (after about 10 passes or 2 days).

The 60° flare data for the 200 NM mode is shown in Figure 5.1.2.5-2. The same relative insensitivity of payload to mission time (missions of at least 10 passes) is demonstrated. The 200 NM mode provides about 1275 pounds of additional payload capability (approximately 50%) over that of the 270-100 NM mode (3875 pounds versus 2600 pounds).

5.1.2.6 Configuration Payload Comparison

Figures 5.1.2.6-1 and -2 compare the round trip payload capabilities of the four configurations in the 270-100 NM and 200 NM modes respectively. The 30° flare configuration has the greatest payload capability in both modes. Its maximum round trip payload capability in the 270-100 NM mode is 2950 pounds and 4225 pounds in 200 NM mode. (Note: The 45° and 60° flare payloads are comparable to the 30° flare payloads if flare lengths/weights are equivalent.)

The shape of the curves is similar in both figures but the reduction in mission delta velocity by using the 200 NM mode has affected the flare configuration more than the basic (no flare) configuration. This is shown by the difference in relative spacing among the curves on the two figures. The small payload difference between the 45° and 60° flares (25-60 passes) is due to the small difference in RCS requirements (equivalent delta velocity) because the total inert weights of these two configurations are almost identical.

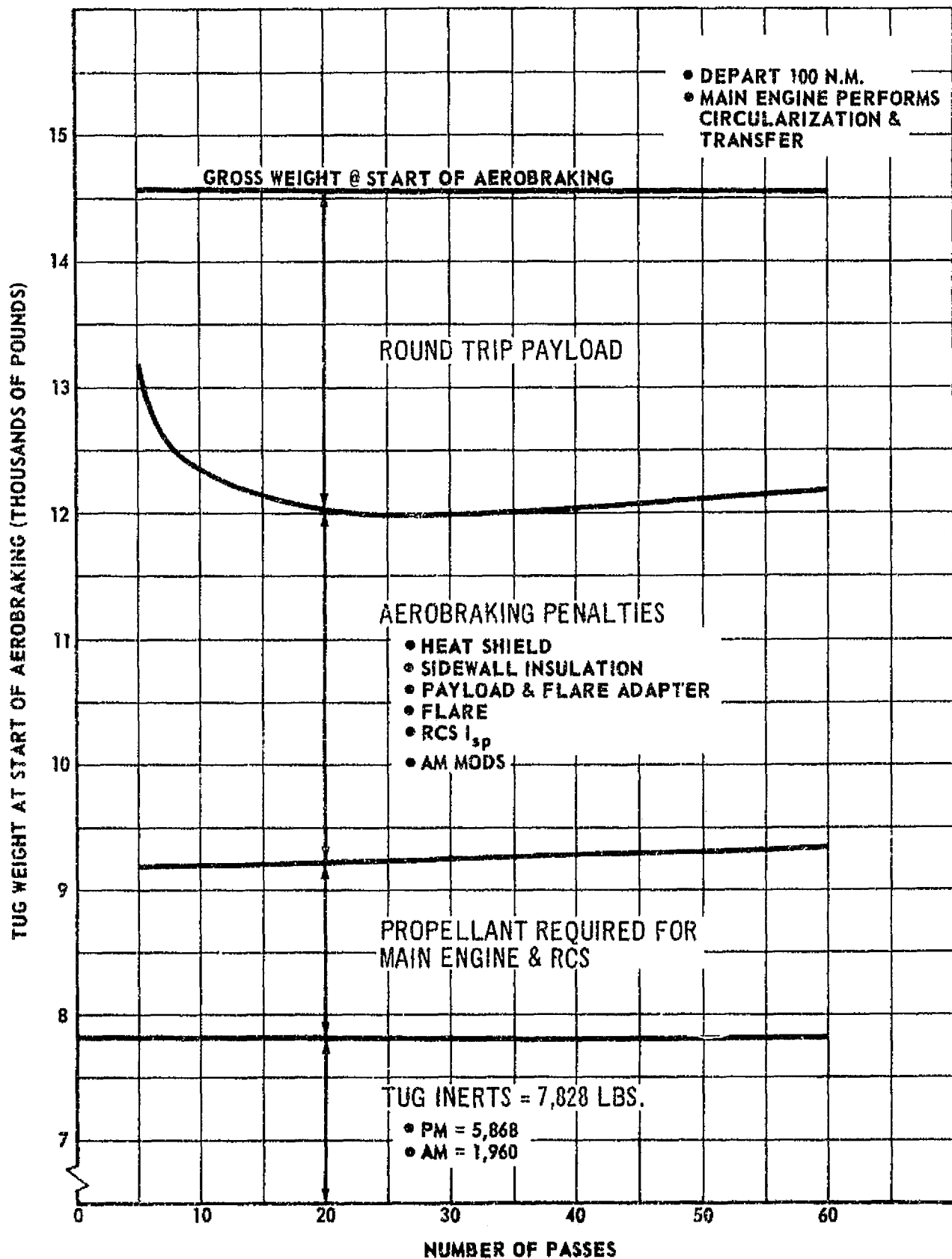


FIGURE 5.1.2.4-1: AEROBRAKING WEIGHT VERSUS NUMBER OF PASSES
(45° FLARE - 270-100 N.M. RECOVERY)

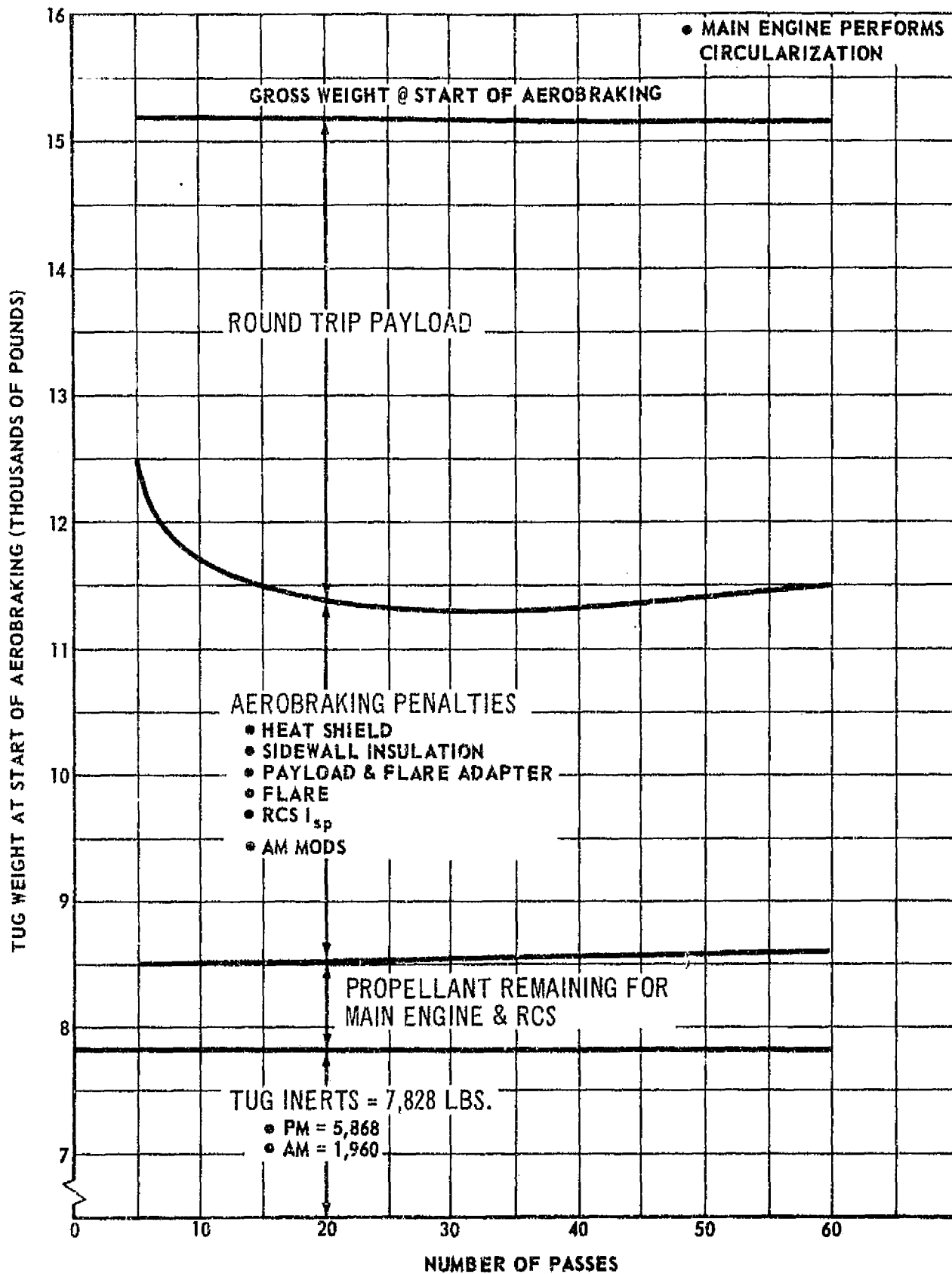


FIGURE 5.1.2.4-2: AEROBRAKING WEIGHT VERSUS NUMBER OF PASSES
(45° FLARE-DEPART AND RECOVER AT 200 N.M.)

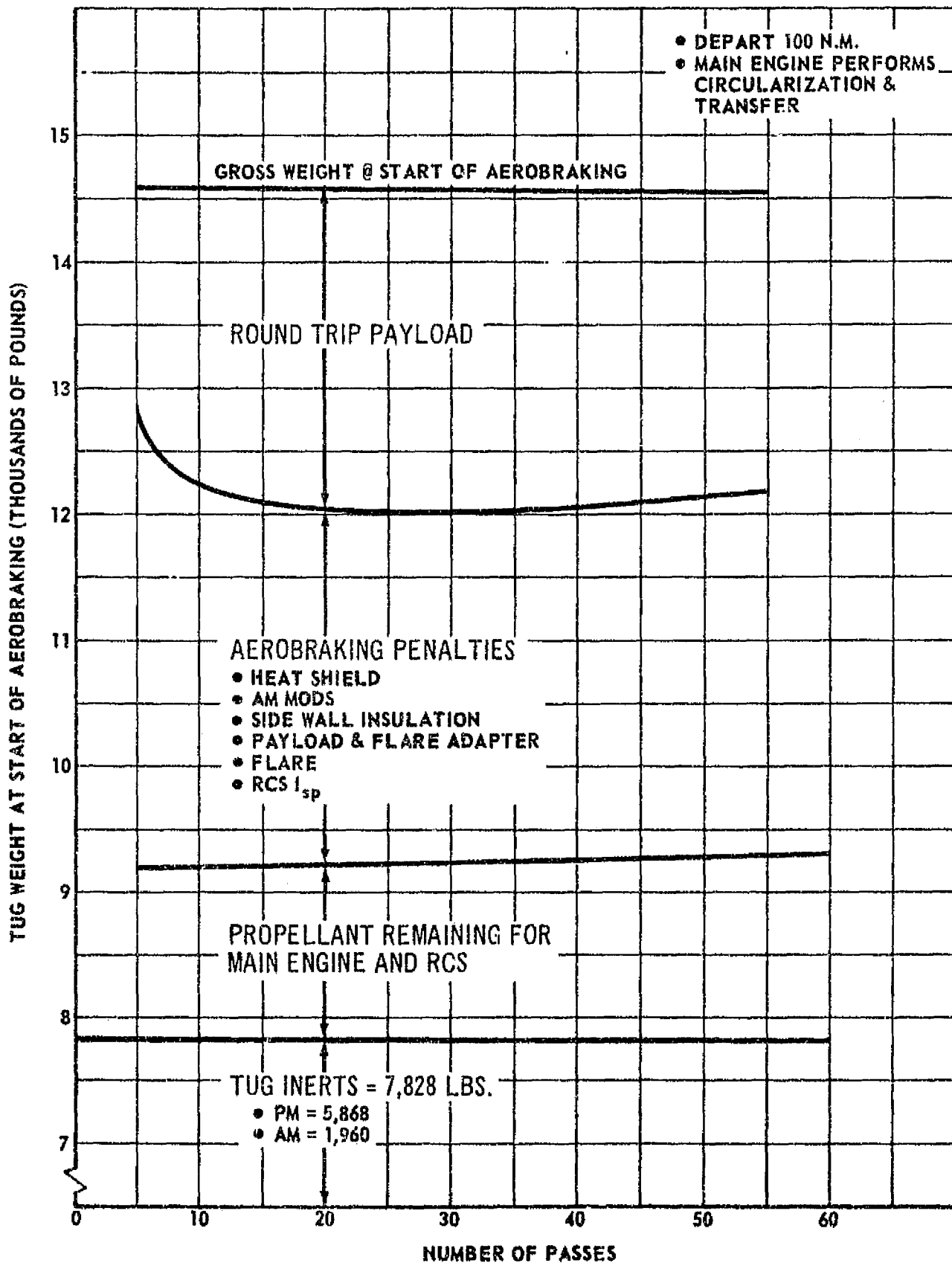


FIGURE 5.1.2.5-1: AEROBRAKING WEIGHT VERSUS NUMBER OF PASSES
 (60° FLARE - 270-100 N.M. RECOVERY)

D5-17142

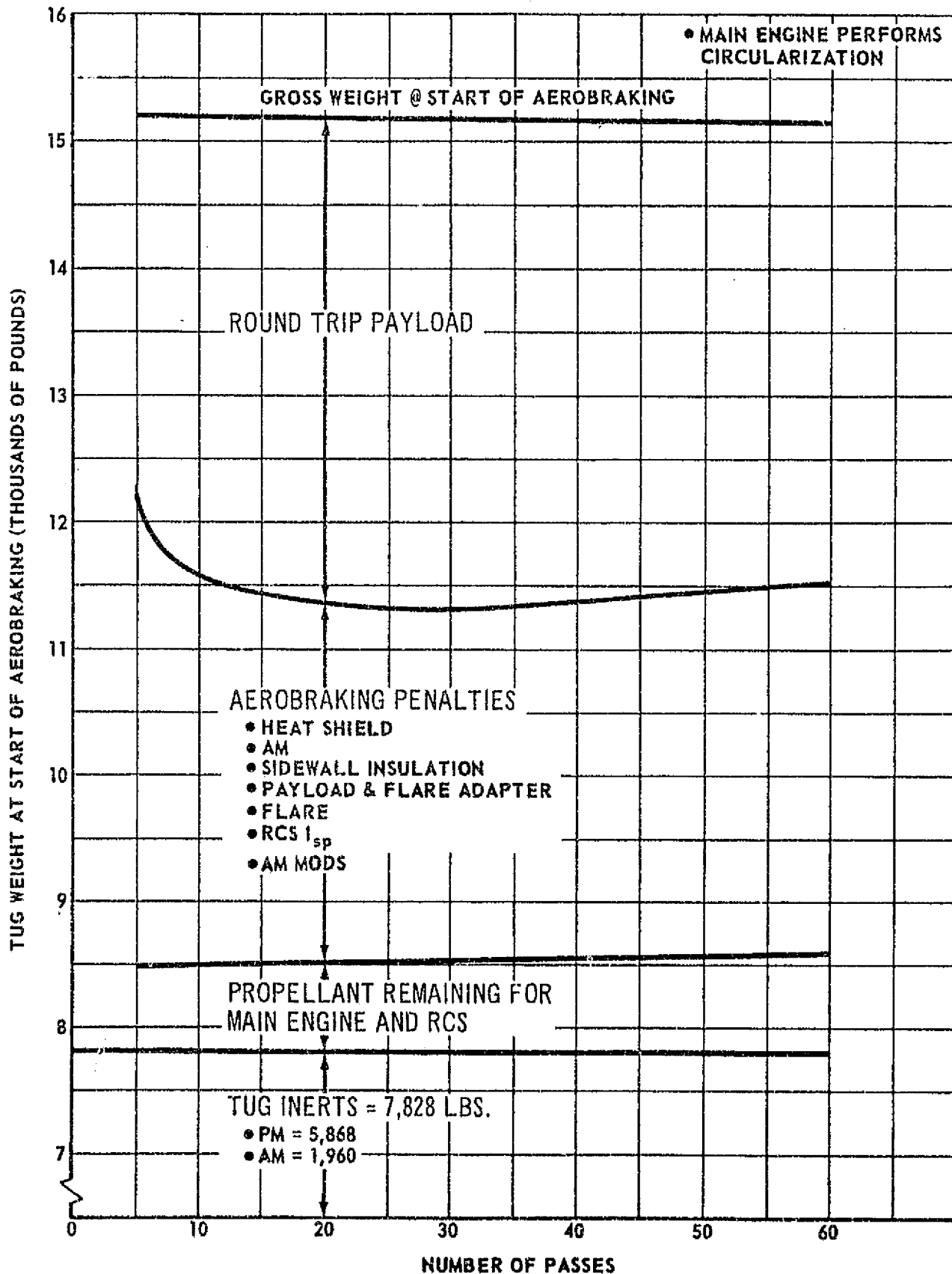


FIGURE 5.1.2.5-2: AEROBRAKING WEIGHT VERSUS NUMBER OF PASSES
(60° FLARE - DEPART AND RECOVER AT 200 N.M.)

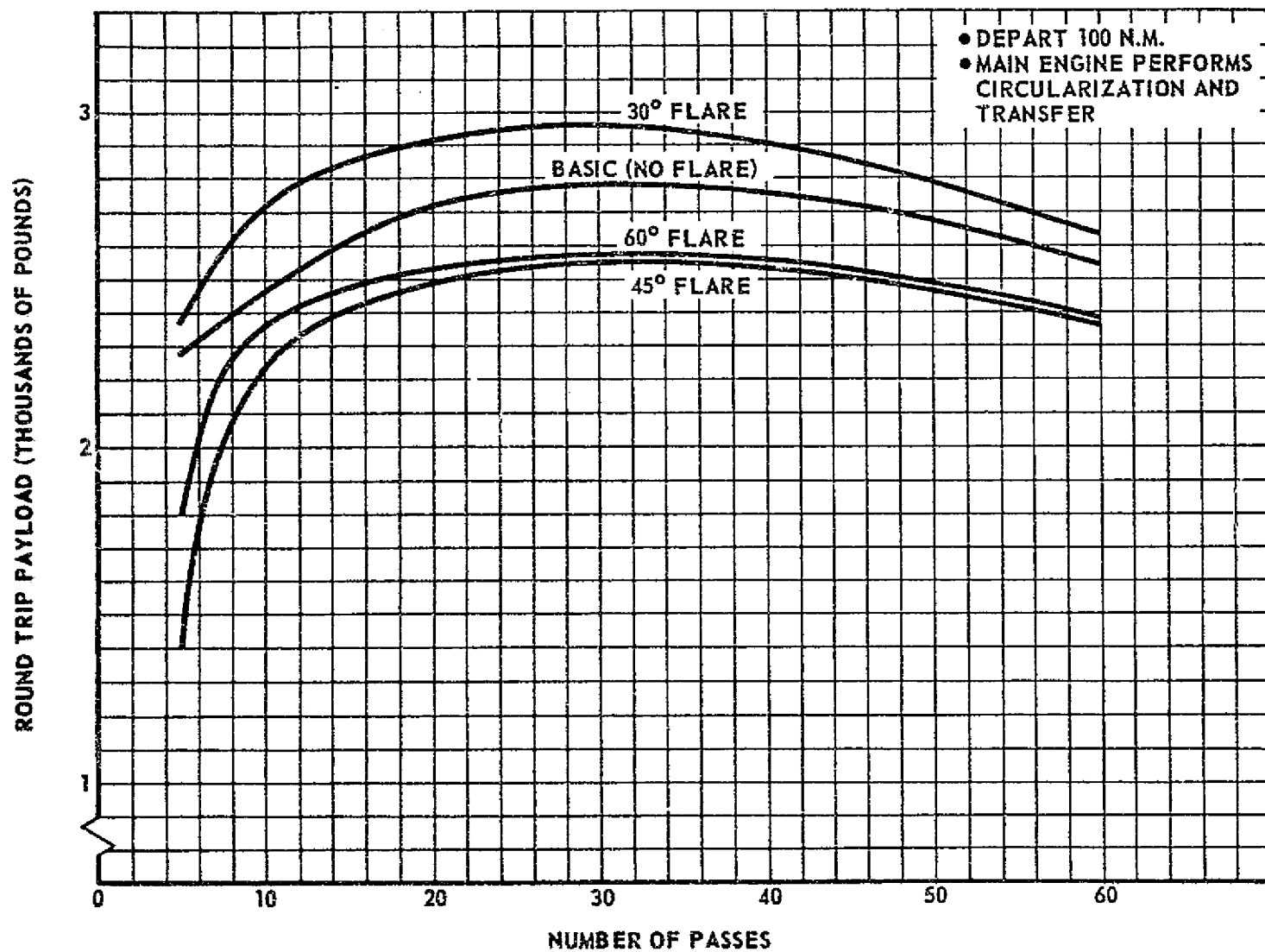


FIGURE 5.1.2.6-1: ROUND TRIP PAYLOAD VERSUS NUMBER OF PASSES
(270 - 100 N.M. RECOVERY)

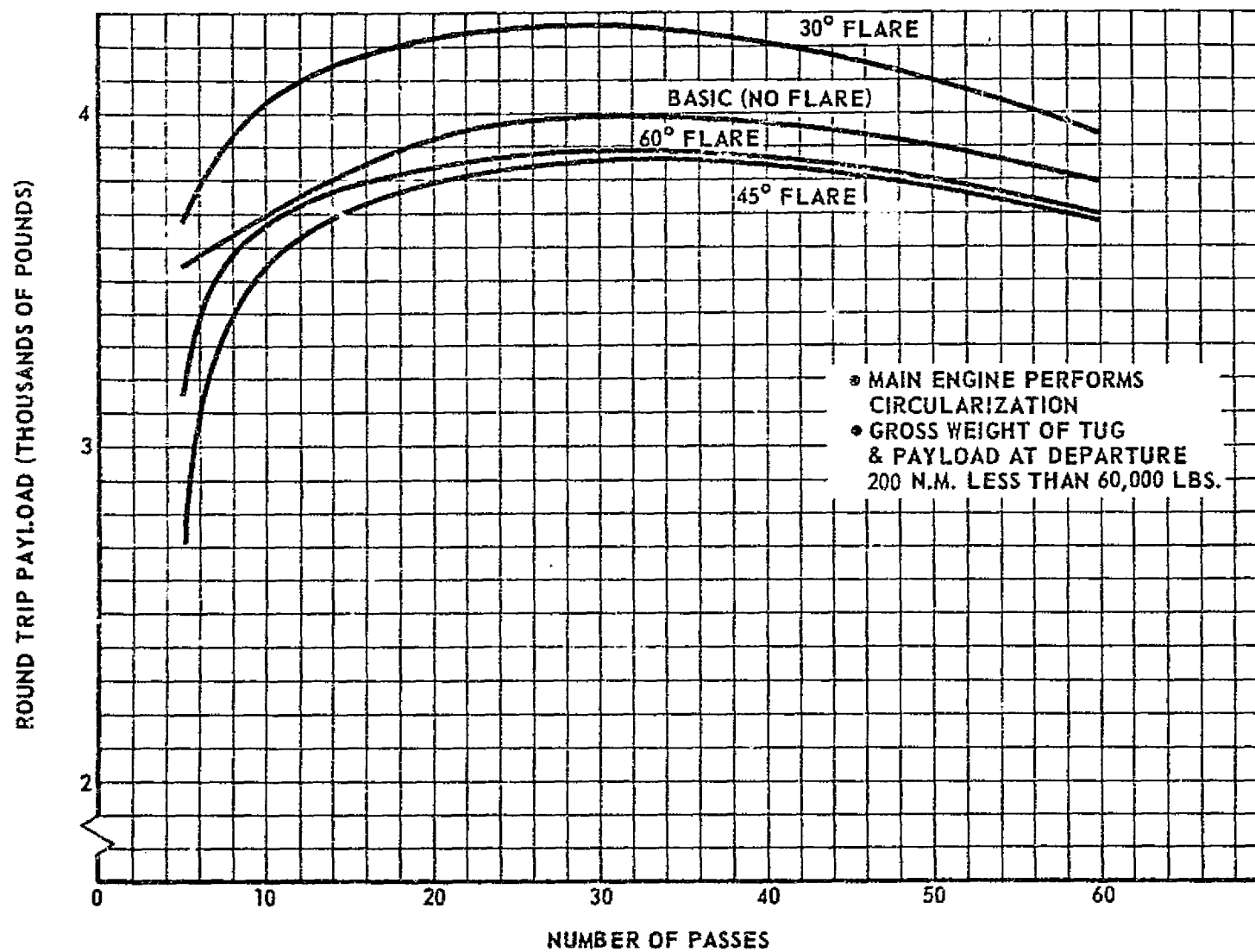


FIGURE 5.1.2.6-2: ROUND TRIP PAYLOAD VERSUS NUMBER OF PASSES
(DEPARTURE AND RECOVERY AT 200 N.M.)

5.1.2.6 (Continued)

For missions of greater than 20 passes, the 45° and 60° flares have slightly less payload sensitivity to mission time than do the other two configurations. However, for very short missions (5-10 passes), these two flares have the greatest sensitivities. The basic (no flare) configuration has the least payload sensitivity to mission time over the entire range studied (5-60 passes). The 30° flare configuration represents an intermediate case over the entire range.

Figures 5.1.2.6-3 and -4 are the same basic plots as 5.1.2.6-1 and -2 above. Overplotted are isotherm lines that correspond to the maximum heat shield nose steady state equilibrium temperatures developed in Section 4.5. These specific temperatures were selected because they represent the various selected material temperature ranges of Section 4.7. These materials and their temperature ranges are repeated below.

1200-1800°F	Rene 41
1800-2200°F	TD-nickel-chrome
2200-2500°F	Fansteel 85
2500-3500°F	Fansteel 60

The 2000°F line on these figures represents the state-of-the-art of radiative materials. Above this temperature, the new high temperature alloys of tantalum/columbium/titanium such as the Fansteels 85 and 60 are required. These require advances in the state-of-the-art.

Restricting the TD-nickel-chrome to 2000°F reduces the payload capability of the 30° flare about 100 pounds or 2-1/2%. The payload capability at 43 passes (2000°F temperature limit) is 2850 pounds. The other flares are not affected by this temperature limit since both maximize payload at temperatures less than 2000°F. Therefore, for this nominal case (standard atmosphere and no navigation errors), TD-nickel-chrome is a suitable material for the heat shield of the flared configurations for the maximized payload mission durations. Because the flared configurations sidewalls and flares have maximum temperatures less than the heat shield nose, TD-nickel-chrome and/or lesser temperature materials can be utilized.

The basic (no flare) configuration maximizes payload at approximately 2500°F steady state and requires more than 60 passes to reduce the temperature to 2200°F. This particular configuration was subjected to a transient analysis (Section 4.5). This analysis showed that the 2200°F limit was reached at approximately 35 passes and the 2000°F limit at 55 passes. These results were not shown on Figure 5.1.2.6-3 and -4 in order to provide a common basis for comparison of all configurations. The effect of this transient analysis on the basic (no flare) configuration's heat shield material is to reduce the requirement from Fansteel 60 to Fansteel 85 for maximum payload mission duration (30 passes).

The alternate payload placement mission capabilities for the four configurations are shown in Figure 5.1.2.6-5. This mission could not be flown from 200 NM (as with the payload retrieval and round trip missions)

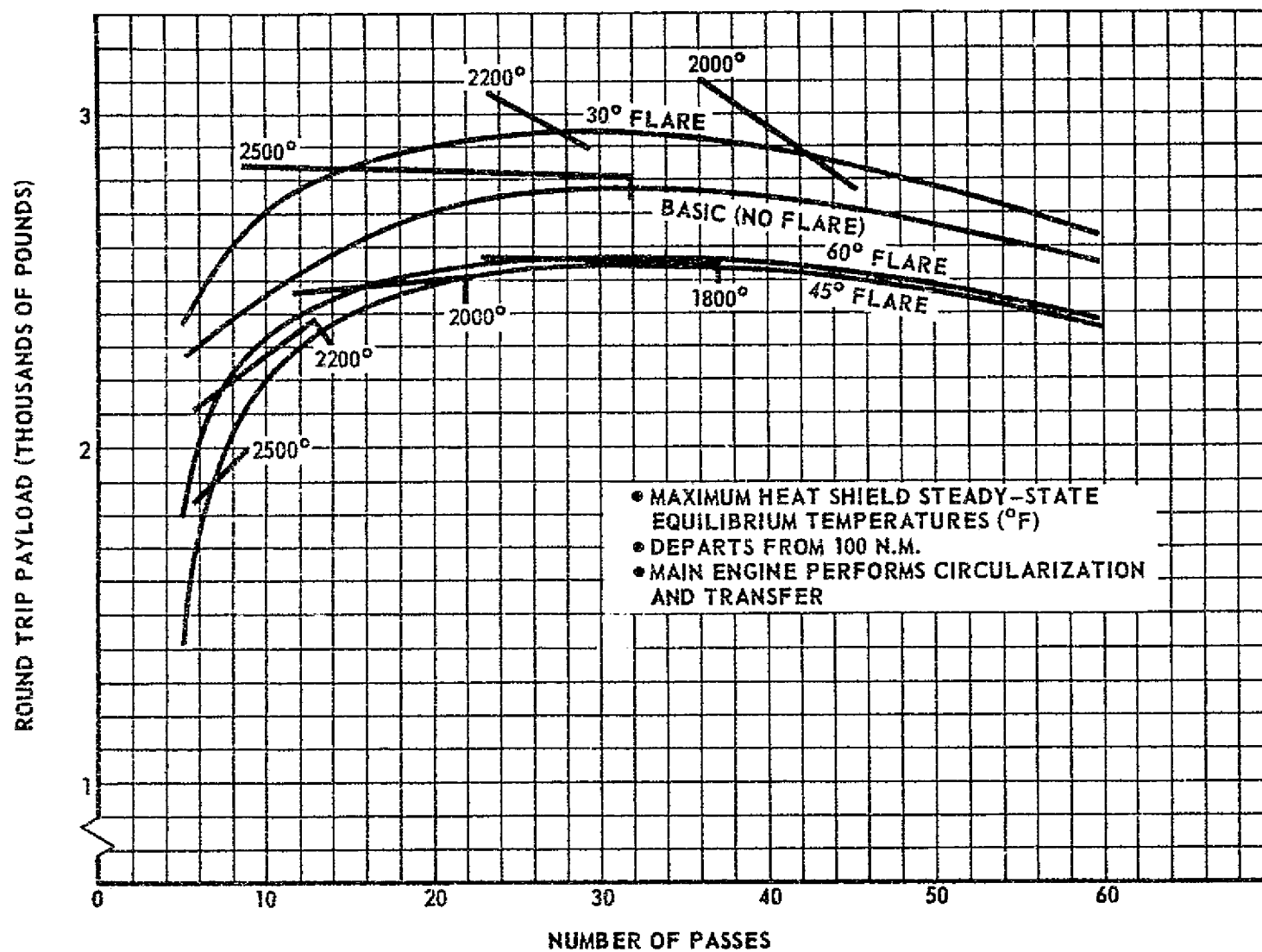
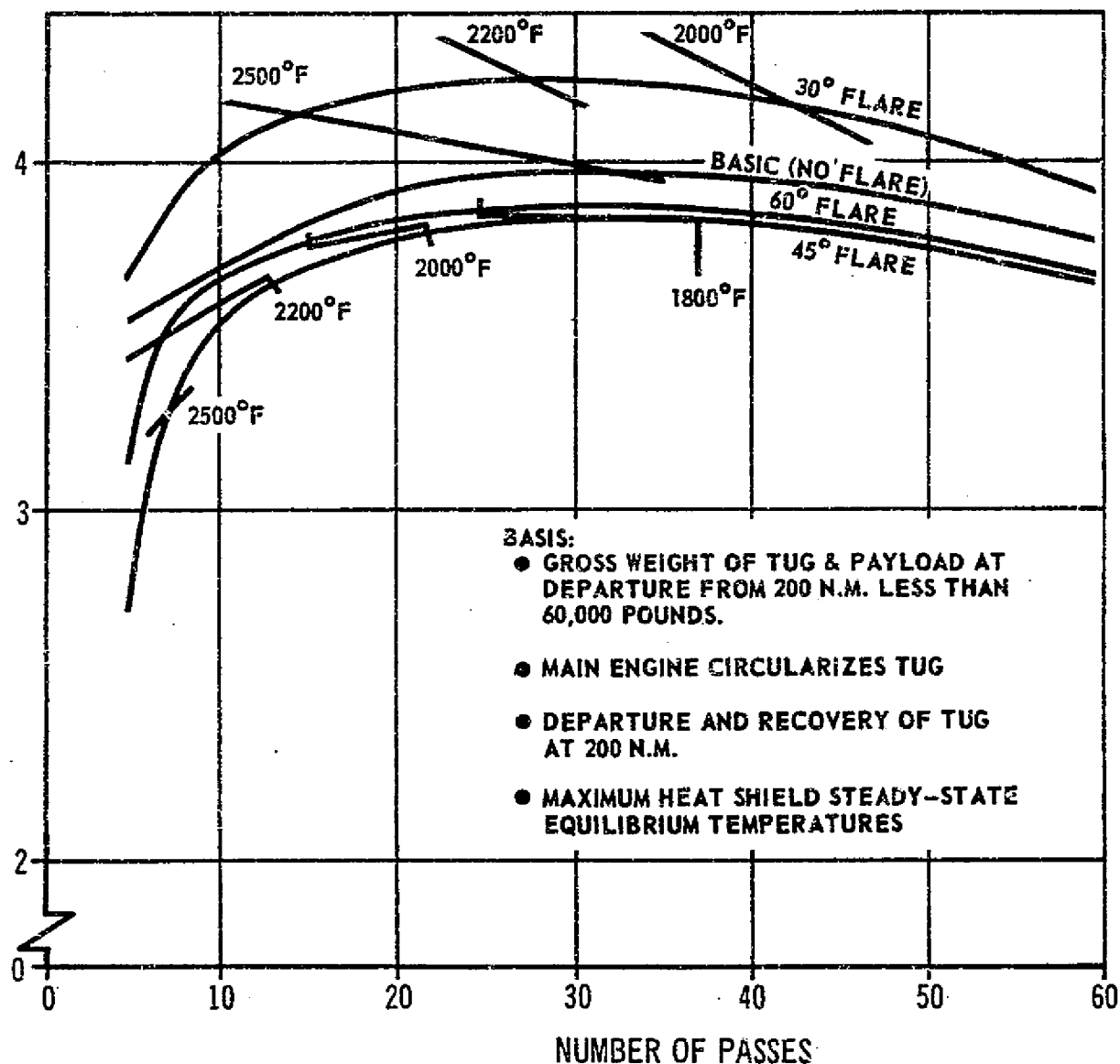


FIGURE 5.1.2.6-3: ROUND TRIP PAYLOAD VERSUS NUMBER OF PASSES
(270 - 100 N.M. RECOVERY)

ROUND TRIP PAYLOAD (THOUSANDS OF POUNDS)



DS-17142

FIGURE 5.1.2.6-4: SYNCHRONOUS ROUND TRIP PAYLOAD VERSUS NUMBER OF PASSES

D5-17142

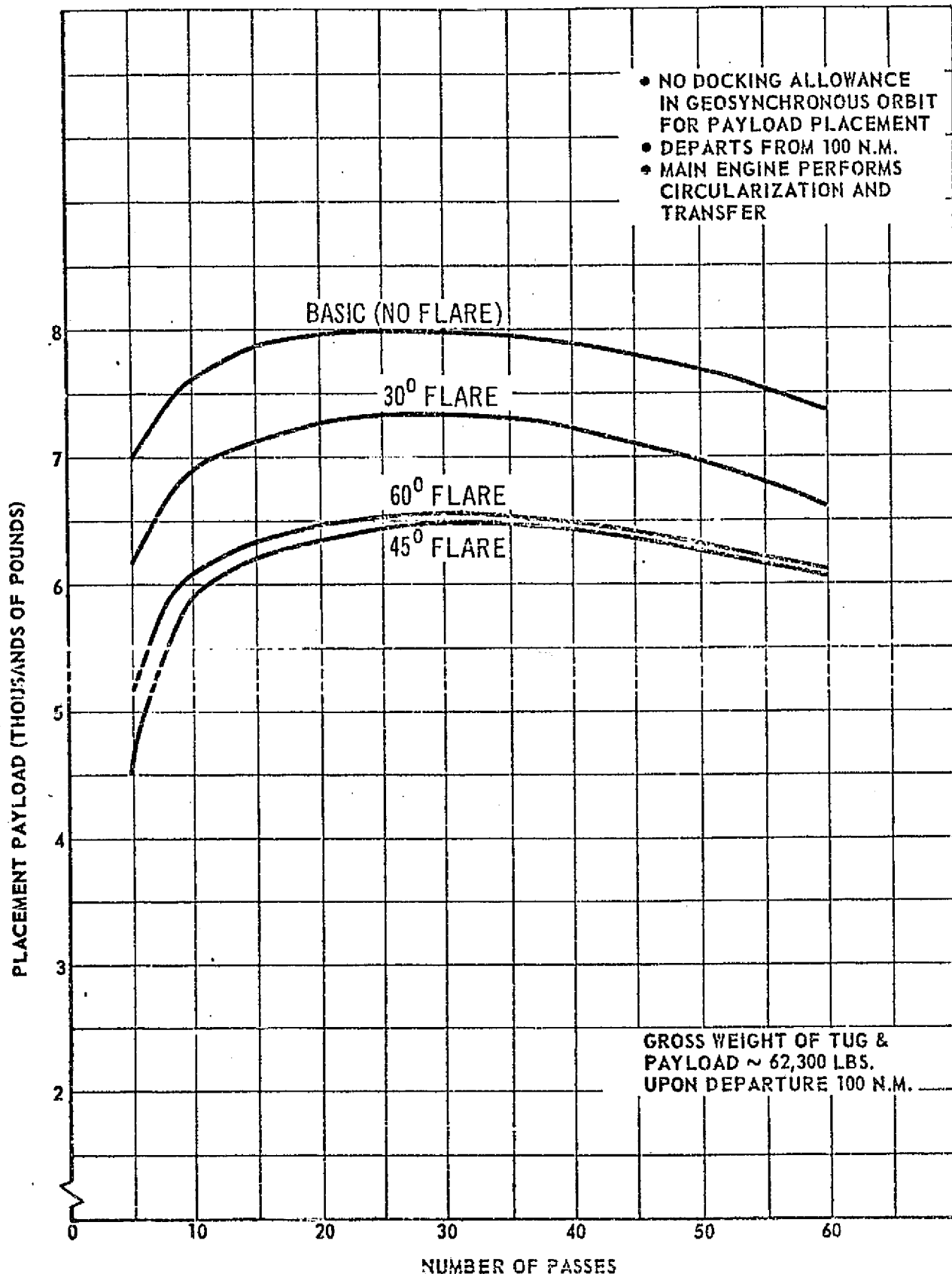


FIGURE 5.1.2.6-5: PLACEMENT PAYLOAD VERSUS NUMBER OF PASSES
(270 - 100 N.M. RECOVERY)

5.1.2.6 (Continued)

because the gross weight of the Tug and payload exceeded the EOS capability. Approximately 8000 pound placement payloads were easily achieved with the nominal 270-100 NM mode; however, the 10,000 pound payload placement missions could probably not be accomplished even with optimization of departure and recovery altitudes. The payload placement mission does not require a docking delta velocity allowance at geosynchronous orbit. Therefore, the outbound delta velocity budget was established at the nominal 14,100 ft/sec. In addition, this particular mission impacts the basic (no flare) configuration's aerobraking inert weights shown in prior Figure 5.1.2.0-2. There is no payload during the aerobraking phase so that only a fixed insulation cap was placed over the exposed end of astrion module. The conventional trajectory Tug's payload adapter was substituted for the aerobraking payload/flare adapter. The resulting payload placement mission basic (no flare) configuration weight statement is shown below and reflect changes in the ballistic coefficient:

	<u>5 Pass</u>	<u>10 Pass</u>	<u>30 Pass</u>	<u>60 Pass</u>
W_I	9,872	9,528	9,289	9,545
W_P	<u>45,000</u>	<u>45,000</u>	<u>45,000</u>	<u>45,000</u>
Gross Wt	54,872	54,520	54,089	54,545

The flared configurations require all components of the aerobraking kit and their weights are similar to those shown previously in Figure 5.1.2.0-2 but reflect the $W/C_D A$ changes. This flexibility in selection of aerobraking kit components is directly reflected in Figure 5.1.2.6-5 with the basic no flare configuration showing a relatively large payload advantage. The sensitivities to mission time and maximum equilibrium temperature constraints are similar to the round trip payload case.

The other alternate mission capability, that of payload retrieval, is shown in Figure 5.1.2.6-6. This mission could be flown using the 200 NM mode since only the fully fueled Tug required low earth orbit insertion.

As in the placement case, further payload increases by departure and recovery altitude optimization could be achieved. The payload retrieval capabilities are slightly greater than the placement capabilities. This is because: (1) A different operational mode was used; and (2) aerobraking reduces the delta velocity requirements of the heavier Tug and retrieved payload during the return trip. Carrying no payload to orbit (large propulsive requirement) with aerobraking return of a retrieved payload (small propulsive requirement) results in the basic (no flare), 45° flare and 60° flare configurations to be approximately equivalent for missions greater than 5.5 days (30 passes).

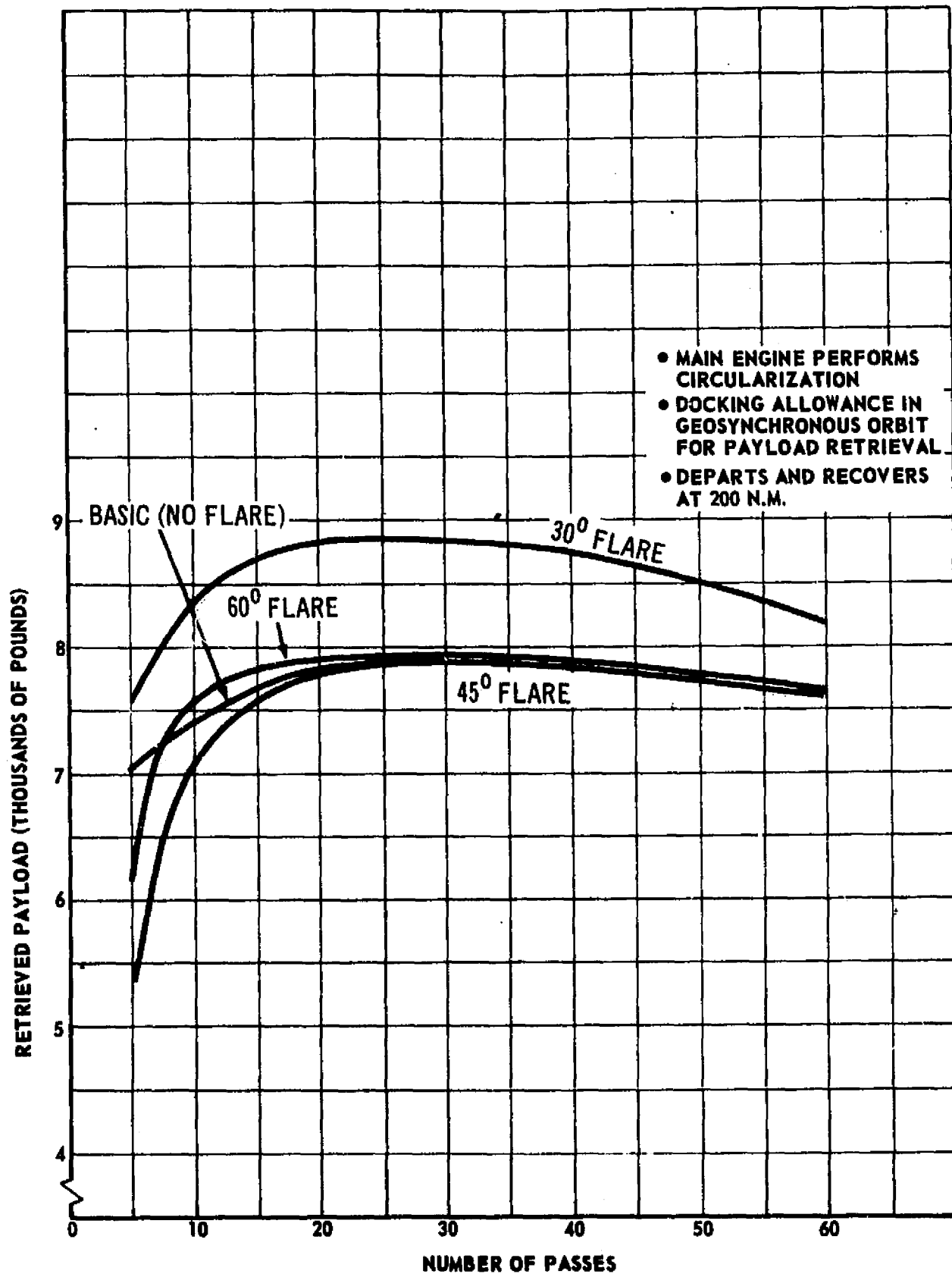


FIGURE 5.1.2.6-6: RETRIEVED PAYLOAD VERSUS NUMBER OF PASSES
(DEPART AND RECOVER AT 200 N.M.)

5.1.2.6 (Continued)

Figure 5.1.2.6-7 is a summary capture map illustrating the capabilities of aerobraking to accomplish the 287 geosynchronous missions contained in the mission model utilized. The shaded area in all three blocks shows the cumulative percent of the mission model within the payload weight increments. For example, 64% of all payloads weigh less than 3000 pounds and 95% weigh 3000 pounds or less. There is a large discontinuity beyond payload weights of 3000 pounds with the next level estimated to be approximately 7000-10,000 pounds.

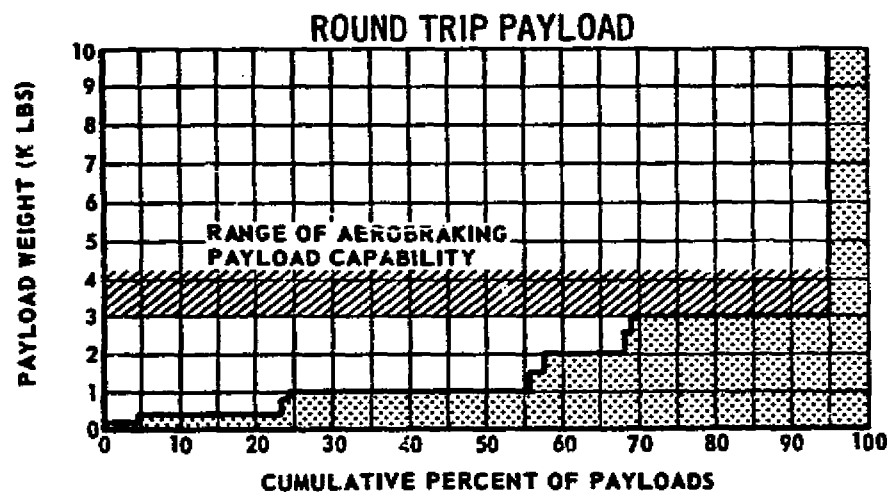
The round trip capability (200 NM mode) easily captures the 3000 pound payload class and below. The ~ 1000 pound excess payload capability margin is an indication that if the inert weights and/or delta velocities used in this analysis were optimistic by a significant amount, the 3000 pound round trip payload missions could still be accomplished. The placement (270-100 NM mode) and retrieval (200 NM mode) payload capabilities are approximately 8000 and 9000 pounds respectively. Neither of these capabilities capture the proposed 10,000 pound payloads. However, reduction of these payload weights to those matching the aerobraked Tug's capability would still provide for placing and retrieving relatively large payloads in geosynchronous orbit. The figure illustrates only the basic Tug and the 30° flare configuration. The 45° and 60° flare configuration will also capture 95% of the missions.

5.2 ATMOSPHERIC PERTURBATION AND NAVIGATION ERROR SENSITIVITIES

Sections 4.3, 4.5, and 4.8 (trajectory, thermal and weights analyses, respectively) contain data on the effects of atmospheric perturbations from the 1962 Standard Atmosphere used in this study. Section 4.6 (astrionics analysis) discusses the effects of state vector uncertainties, navigational errors, and midcourse correction burns. This subsection discusses the combination of the results of these previous analyses and the resulting payload sensitivities to these parameters. The sensitivities shown are for the high atmospheric density range and for 1 sigma (σ) or 3 sigma (σ) errors (or uncertainties) from the astrionics analysis. The study scope did not permit a more extensive analysis in this area.

5.2.1 Effects on Nominal Perigee Altitudes

Figure 5.2.1.0-1 shows the 1 σ radial perigee position uncertainties for various midcourse correction burn options. As discussed in Section 4.6, a corrective burn after the Horizon Sensor updates (at altitudes far from perigee altitude) actually increases the perigee error. With no burn correction applied, the 3 σ perigee uncertainty is approximately 5.1 NM (31,000 feet). Correcting to a lower error value, such as 0.5 NM, can be relatively inexpensive in terms of RCS propellant consumption (see prior Figure 4.6.4.6-2). Therefore, these two large error cases were eliminated from the analysis.

**BASIS:**

- EOS CAPABILITY ~ H-33 ORBITER
- 287 GEOSYNCHRONOUS MISSIONS
- 30 PASS MISSIONS

CONCLUSIONS:

- 95% OF ALL GEOSYNCHRONOUS MISSIONS CAPTURED

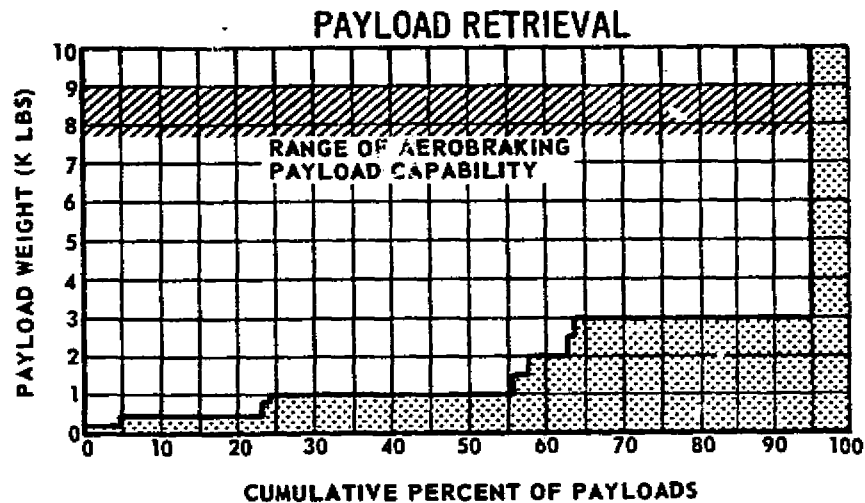
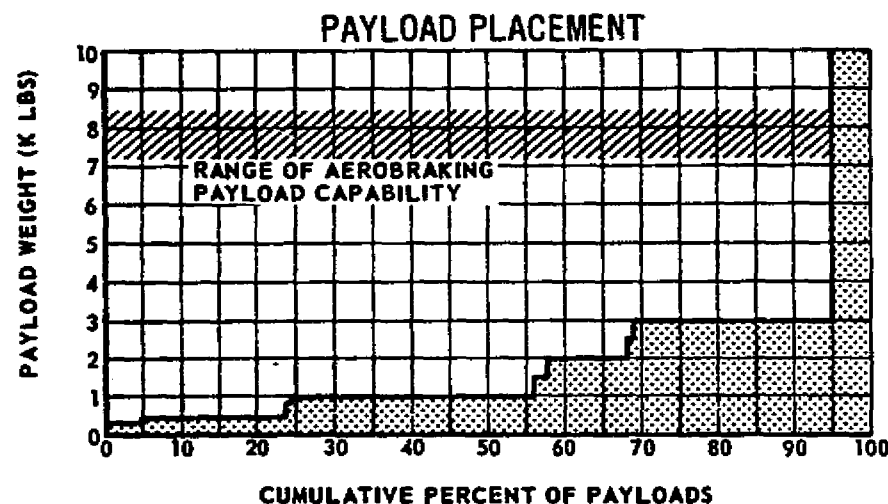


FIGURE 5.1.2.6-7: GEOSYNCHRONOUS PAYLOAD CAPABILITY OF AEROBRAKED TUG

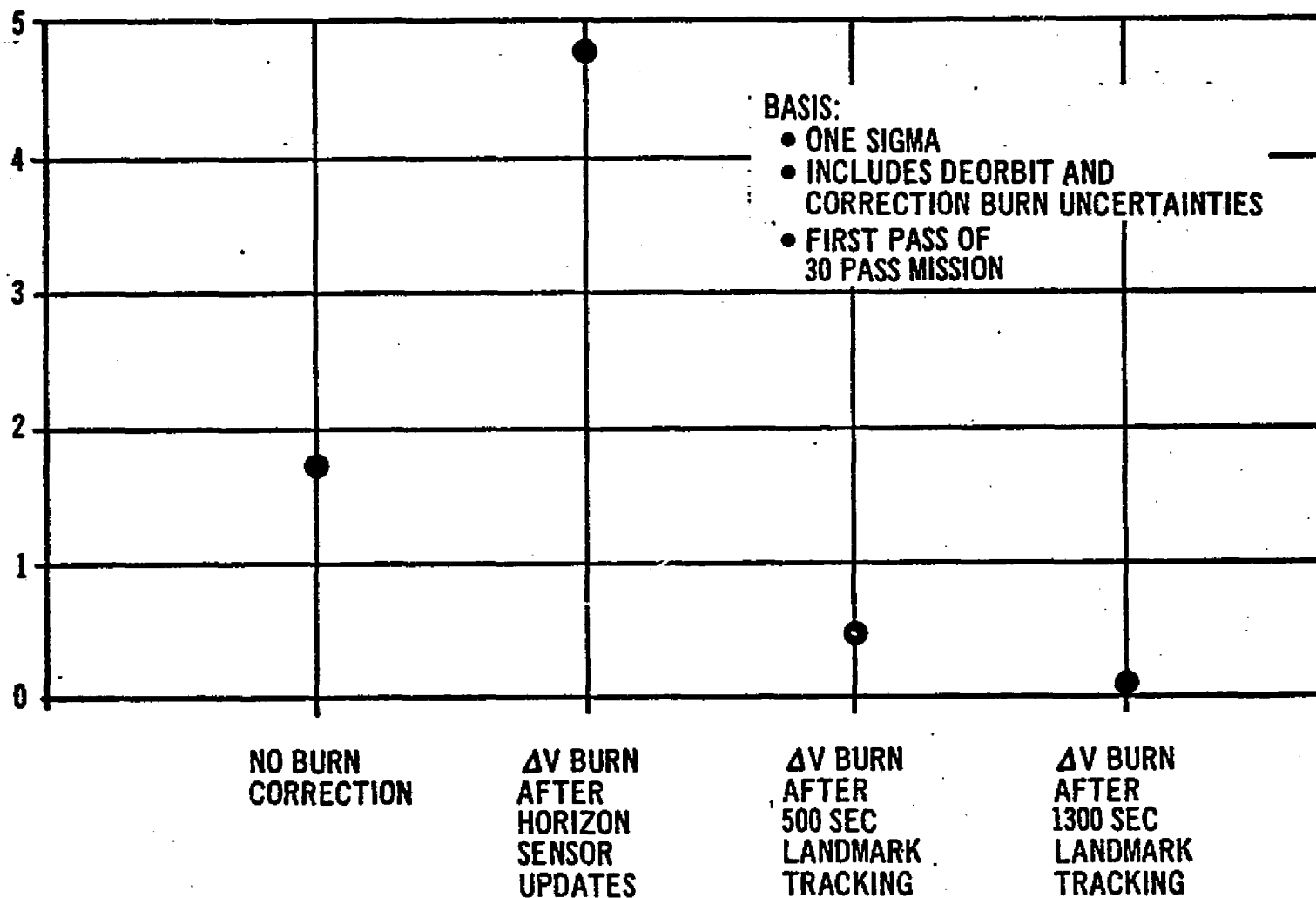
RADIAL POSITION UNCERTAINTY
AT PERIGEE (N.M.)

FIGURE 5.2.1.0-1: RADIAL POSITION UNCERTAINTY AT PERIGEE

5.2.1 (Continued)

Figure 5.2.1.0-2 shows the atmospheric perturbation data utilized for the high and low cases. This information was furnished by NASA/MSFC (prior Reference 4.3.4.0-1). The original data from MSFC included the expected range under both summer and winter conditions. Because the study limitations did not permit an investigation of each season independently, the two ranges were compared and the extreme high and low ranges selected. The selected limits are shown on Figure 5.2.1.0-2 as Winter Low and Summer High. This conservative approach then encompasses all cases with the exception of geomagnetic storms (not considered). The percentage of expected perturbation is greater at higher altitudes than at the aerobraking perigee altitude region where maximum equilibrium temperatures occur. In the perigee region, the highest densities expected vary from 140% to 165% of the 1962 Standard Atmosphere with the lowest densities varying from 50% to 65% of the nominal. The range of atmospheric perturbations (or anomalies) depicted in Figure 5.2.1.0-2 are unpredictable. Not shown in this figure are the mean perturbations (dependent on solar activity) which are predictable. Within the target perigee range, these mean values are near nominal. Because of these two facts (predictability and less variability), the mean values could be programmed into the mission sequence as nominal and as such, were not analyzed in this study.

Figure 5.2.1.0-3 shows the maximum equilibrium temperatures for the heat shield nose as functions of atmosphere density range and navigational errors. The solid lines indicate the temperatures experienced in the high density atmosphere and the dotted lines represent the Standard atmosphere. No transient (heat sink) effects are included so that the data shown will be conservative.

As discussed in the thermal analysis, Section 4.5, the impact of the high density atmosphere will result in an approximate 65 and 80°F rise in maximum equilibrium temperature for the 60° flare and basic (no flare) configurations, respectively, with no navigation errors.

The impact of only the high density atmosphere is shown along the ordinate of Figure 5.2.1.0-3. The 30 pass basic (no flare) configuration (atmosphere plus navigation error) will have a maximum ("worst case") temperature rise of approximately 360°F. This maximum increase is measured from the Standard Atmosphere with zero navigation error to the high density atmosphere with 3 σ_2 (500 seconds of landmark tracking) navigation error. The 60° flare configuration's maximum rise is approximately 225°F under the same conditions.

The 60° flare's maximum equilibrium temperature does not exceed 2000°F and therefore TD-nickel-chrome remains a suitable material for the "worst case" 30 pass mission. The basic (no flare) has a 30 pass "worst case" equilibrium temperature of 2850°F (steady state). Allowing for a possible transient analysis decrease of 250°F, this worst case would still necessitate advanced alloys such as Fansteel 60 (2500-3500°F).

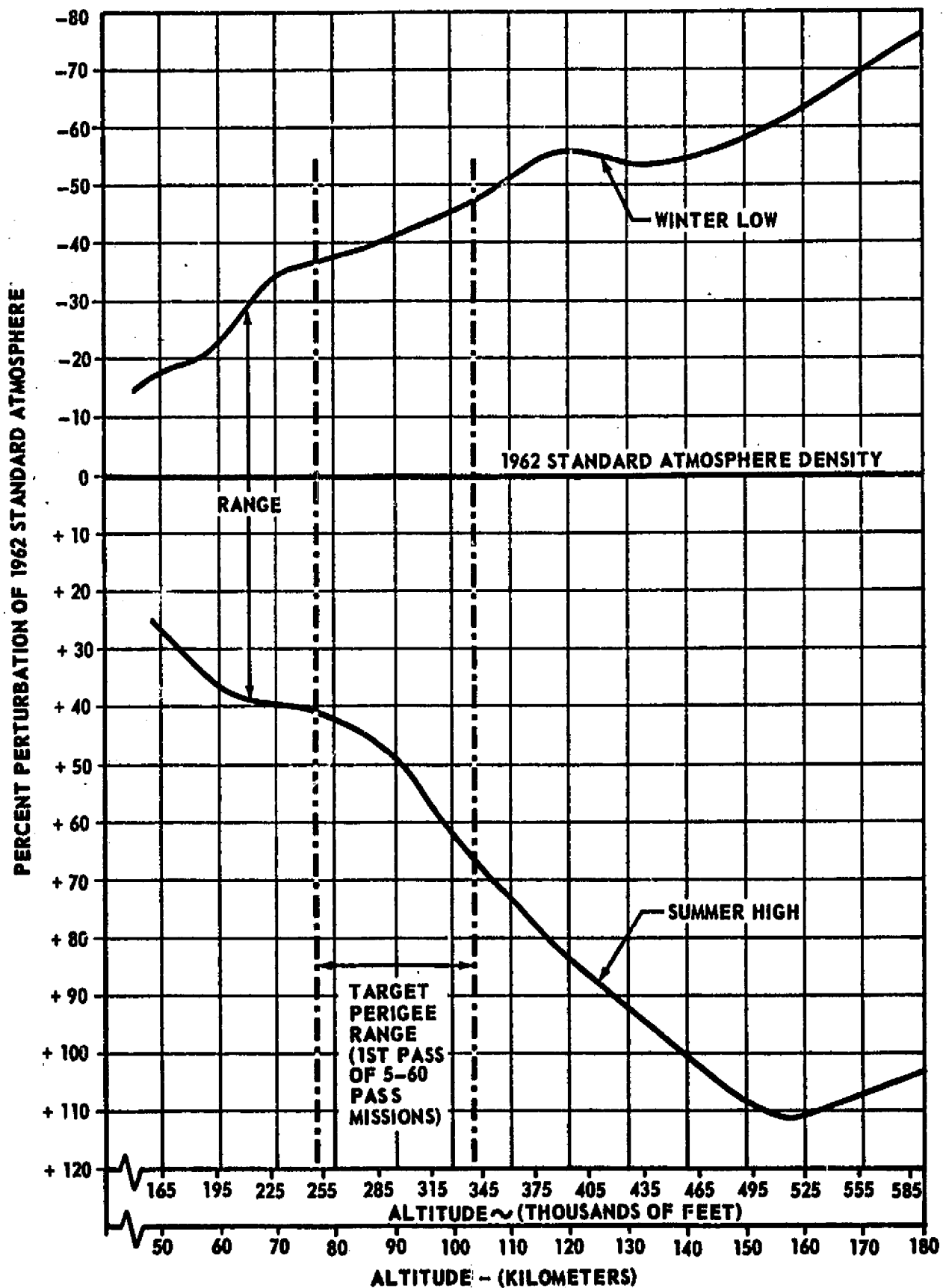


FIGURE 5.2.1.0-2. RANGE OF ATMOSPHERIC PERTURBATIONS

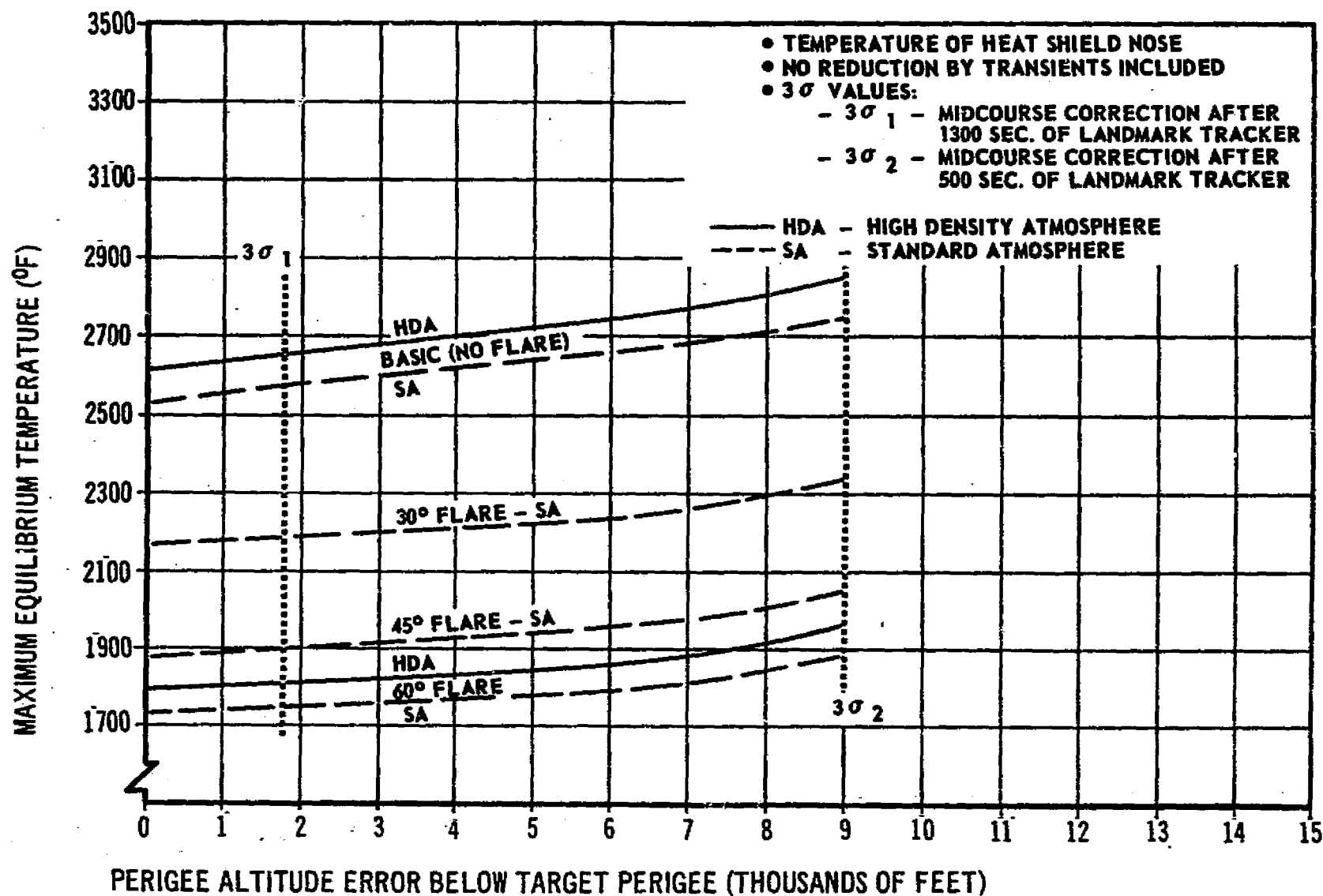


FIGURE 5.2.1.0-3. MAXIMUM EQUILIBRIUM TEMPERATURE VS. INITIAL PERIGEE ERROR (FIRST PASS OF 30-PASS MISSION)

5.2.1 (Continued)

The 30° and 45° flares are shown for the Standard Atmosphere case only. The high density atmosphere thermal analysis was not performed on these two configurations, but it is expected that the atmospheric density dispersion impact will be similar to that shown for the other two configurations and Figure 5.2.1.0-3 indicates the probable results. The 45° flare's maximum equilibrium temperature would be under 2200°F (TD-nickel-chrome). The 30° flare's maximum temperature would be approximately 2450°F and require advanced state-of-the art materials (Fansteel 60).

5.2.2 Payload Sensitivities

The trajectory analysis (Section 4.3) used a first pass target perigee based on the nominal Standard 1962 Atmosphere. This assumed, as discussed in Section 5.2.1 above, that the atmospheric perturbations were not predictable. The impact of the perturbed first pass was then utilized to adjust apogee decay on subsequent passes so that the number of mission passes (mission time) was held exactly at or approximately at the desired constant. In the high density atmosphere, the Tug experienced higher equilibrium temperatures and higher pressure loads. As discussed in Section 4.8 and shown in Figure 5.1.2.0-2, the temperatures and loads were major factors in the determination of the heat shield and flare weights. Figure 5.2.2.0-1 shows the basic (no flare) and 60° flare configuration aerobraking weights and delta velocities associated with the high density atmosphere. The delta velocities shown are based on "an impulse at entry" technique developed for this study. This technique was investigated to overcome the effects of the large navigational uncertainties encountered at either exit or apogee. The technique has several advantages including:

- o Correction burns are made based on the greatest knowledge of current position and velocity errors.
- o Atmospheric perturbation correction burns can be combined with the navigational error correction burns thereby simplifying the procedures and probably reducing the total propulsive impulse required.
- o Relative insensitivity of the required impulse to mission duration allowing for better mission planning.
- o Final apogee control sufficiently accurate to permit alternate circularization altitudes (e.g., 200 n.m.).

Figure 5.2.2.0-2 shows the effect of the high density atmosphere on the round trip capability of the basic (no flare) and 60° flare configurations. Both configurations easily maintain their 3000 pound plus capability but some have reduction in capability due to this environment. The reduction is mostly due to the added inert weights (short duration missions) and the added delta velocities (longer duration missions). The maximum payload capabilities (30 passes) are only decreased approximately 10-12% with

COMPONENT CONFIGURATION NO. OF MISSION PASS	TUG INERT WEIGHT (LB)	PROPELLANT (LB)	AFT HEAT SHIELD (LB)	FLARE (LB)	SIDEWALL INSULA- TION (LB)	PAYLOAD/FLARE ADAPTER (LB)	ASTRONICS MODULE PENALTY (LB)	GROSS TUG WEIGHT (LESS PAYLOAD (LB)	TOTAL MISSION DELTA * VELOCITY (FT/SEC)
<u>BASIC-NO FLARE</u>									
10	7828	45,000	1180	----	396	**587	110	55,101	21,663
30	7828	45,000	610	----	335	**555	325	54,653	21,704
60	7828	45,000	560	----	302	**506	650	54,846	21,806
<u>60° FLARE</u>									
10	7828	45,000	455	1715	300	390	110	55,798	21,171
30	7828	45,000	440	1260	219	390	325	54,462	21,255
60	7828	45,000	440	1100	158	390	650	55,566	21,387

- * DEPART AND RECOVER AT 200 N.M.
 ** INCLUDES PAYLOAD INSULATION AND PAYLOAD CAP ACTUATION DEVICE

FIGURE 5.2.2.0-1 FULLY FUELED WEIGHT STATEMENTS FOR HIGH DENSITY ATMOSPHERE

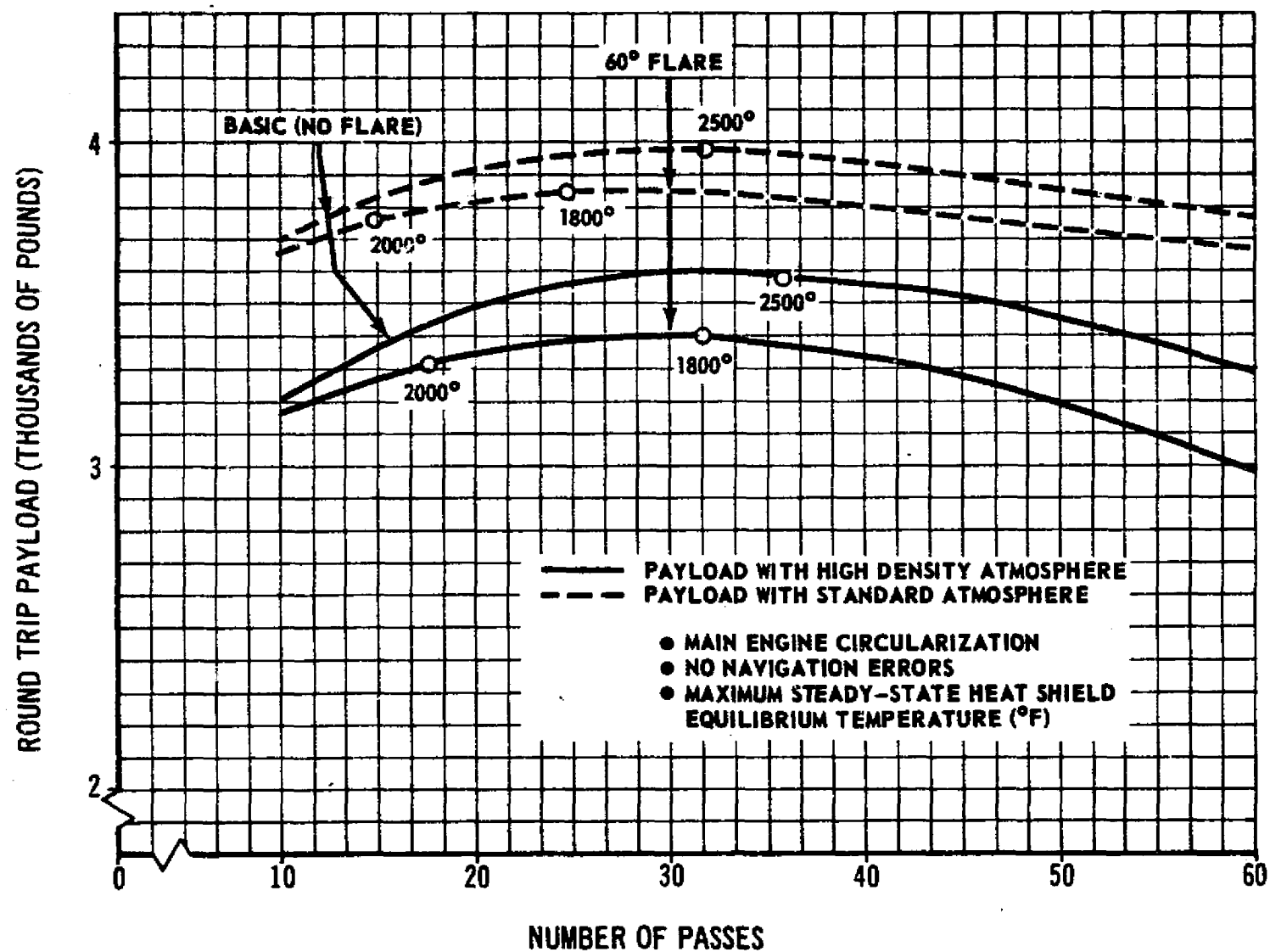


FIGURE 5.2.2.0-2: ROUND TRIP PAYLOAD VS. NUMBER OF PASSES
(DEPART AND RECOVER AT 200 N.M.)

5.2.2 (Continued)

somewhat greater decreases at the mission duration extremes shown. For the short duration missions (~10 passes), both configurations are impacted approximately the same. For mission durations of 20 passes or more, the 60° flare configuration is impacted by this atmospheric condition more than the basic (no flare) configuration.

The high density atmosphere's major mission impact is the decrease in the range of mission durations (and configurations) that will allow for 3000 pound round trip payload missions. Assuming materials such as Fansteel 60 were available and with a Standard Atmosphere, trip times of less than one day (5 passes) were feasible for the 3000 pound payload using either configuration. Long duration missions of 11 days (60 passes), again assuming a Standard Atmosphere, were easily accomplished by either configuration with state-of-the-art materials. With the high density atmosphere, the 5 pass 3000 pound payload mission may be marginal. The mission duration range is therefore between 10 and 60 pass mission region.

Also shown on Figure 5.2.2.0-2 are the steady state temperatures associated with the material limits discussed in Section 5.1.2.6. The high density atmosphere impact is an increase of approximately 4 or 5 passes to maintain equal maximum equilibrium temperatures. The basic (no flare) configuration's apparent requirement for a 2500°F plus material (e.g., Fansteel 60) is offset by the relative payload insensitivity to missions having between 30 and 40 passes and by considering transient (heat sink) effects.

Figure 5.2.2.0-3 shows the round trip payload sensitivities (10 pass mission) to atmospheric anomalies and navigational errors. Shown in the first two hatched columns of each configuration are the payloads and temperatures previously discussed (Figure 5.2.2.0-2). The third hatched column of each configuration shows the round trip payloads achievable under the combined effects of the high density atmosphere and the 3 sigma navigational errors (1300 seconds of landmark tracking). Because the prior payload analyses has reserved 400 ft/second delta velocity for navigation error corrections, including the navigational errors has a minimum impact on the round trip payload. Even for the relatively short duration 10 pass mission, the 3000 pound payload capability is retained under these "worst" conditions depicted. Further bounding of the atmospheric anomalies will result in increased payloads.

The temperatures shown in Figure 5.2.2.0-3 are the heat shield nose stagnation temperatures. The expected increases are only 110° for the 60° flare and 160° for the basic no-flare. These increases are nominal when the wide environmental variations encountered are considered.

5.2.3 Perturbation Summary and Conclusions

The study scope limited the analysis of the atmosphere density variations to the specific cases of a constant high density, standard, or low density atmosphere. Pass-to-pass unpredictable variations might be encountered in addition to the predictable variations that were considered nominal

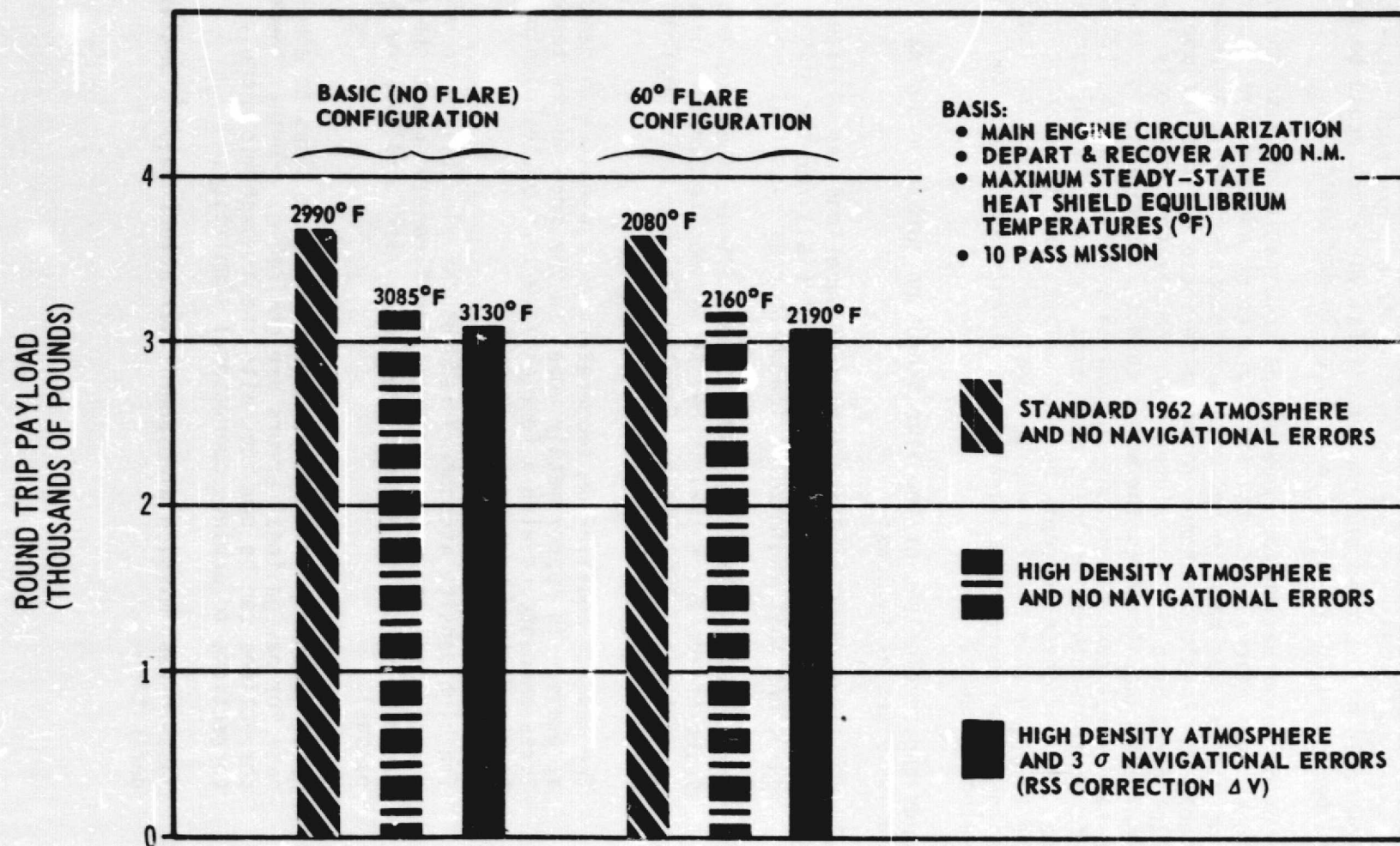


FIGURE 5.2.2.0-3: ATMOSPHERIC ANOMOLY AND NAVIGATION ERROR EFFECT ON ROUND TRIP PAYLOAD (10 PASS MISSION)

5.2.3 (Continued)

and pre-programmed into the flight trajectory. Prior to this type of detailed analysis, these pass-to-pass unpredictable variations should be bounded and rates of density changes defined (e.g., how much pass-to-pass variation could be expected and how much total variation could be expected from the beginning to the end of a 2, 5, or 10 day mission?).

Only a cursory examination was made of the combination of atmospheric variations, navigational uncertainties or errors, and midcourse corrections. No attempt was made to optimize a guidance scheme to accommodate these factors. Possible schemes to minimize these effects include: (1) Targeting the first pass perigee higher than nominal to insure only the nominal conditions are encountered as the worst case, (2) overdesign of the vehicle to withstand worst case conditions at nominal target perigees, (3) correcting with lift as temperatures or loads vary from nominal, and (4) combinations of these. All of these concepts have advantages and disadvantages. The approach taken in this section was to consider the aerobraking Tug to be overdesigned and require additional inert weights and impact the mission delta velocity budget.

The trends and conclusions of the atmospheric perturbation and navigational error analysis are as follows:

- o The large flare (45° and 60°) configurations can utilize state-of-the-art heat shield and flare materials for the mission durations that maximize payload ~ 30 pass missions.
- o The basic (no flare) and 30° flare configurations require advanced state-of-the-art materials having maximum temperature limits of approximately 2500° (e.g., Fansteel 85) for their maximum payload missions (30 passes).
- o The maximum equilibrium temperature of a n-pass high density atmosphere is approximately equal to the more severe temperatures encountered with a four or five less passes mission in a Standard Atmosphere.
- o The high density atmosphere reduces the flexibility in mission duration selection but does not significantly impact the payload capability for the maximum payload mission duration (~ 30 passes).
- o Prior to atmospheric entry, midcourse corrections to compensate for navigational errors are desirable. Further these corrections can be combined with the atmospheric anomaly corrections to achieve operational simplicity.
- o Pass-to-pass mission atmospheric variations require better definition.

5.2.3 (Continued)

- o An in-depth sensitivity analysis of the combination of navigation and atmospheric effects is required in a follow-on activity to define guidance schemes and to optimize the design and operational modes in a perturbed environment.

5.3 AEROBRAKING/CONVENTIONAL TRAJECTORY TUG COMPARISONS

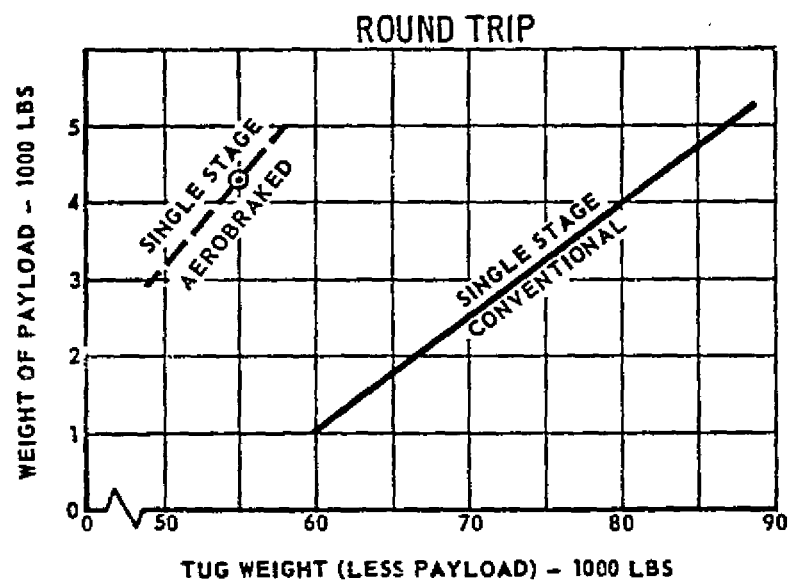
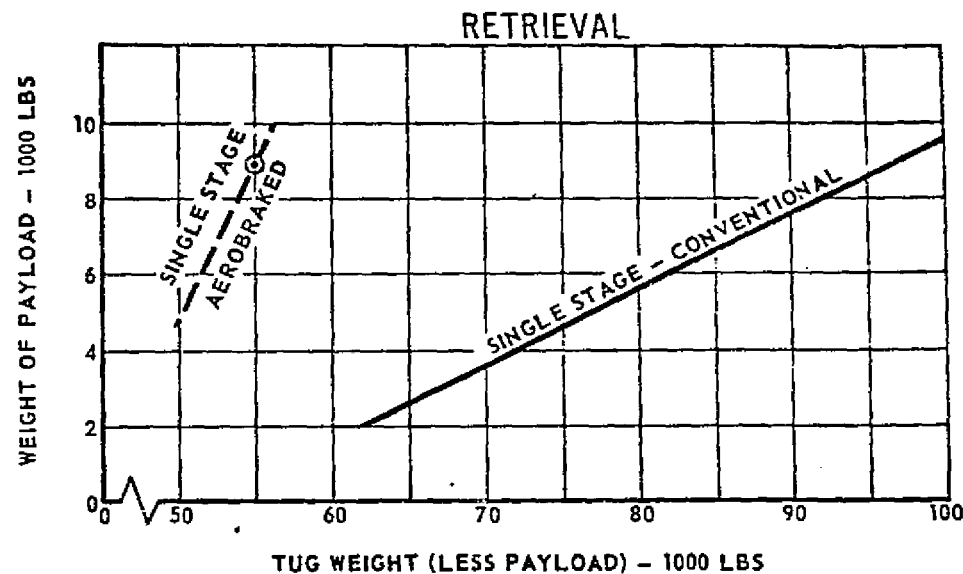
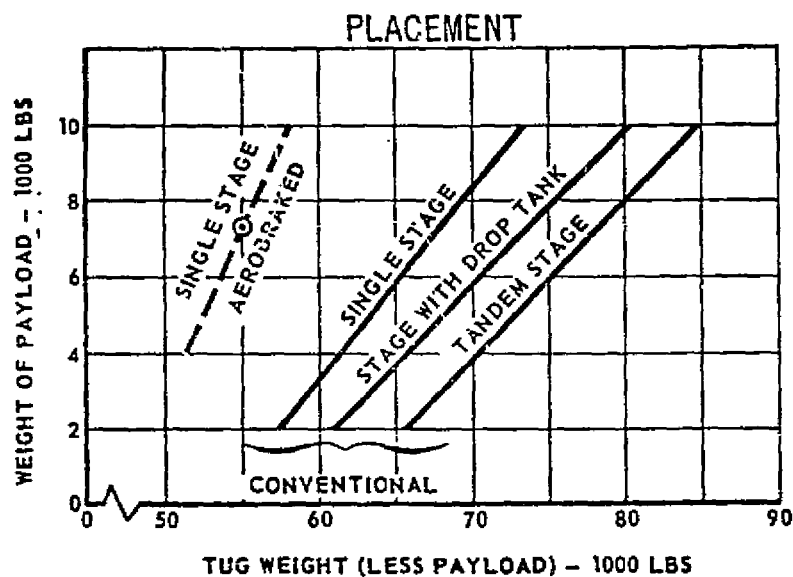
This section discusses the required conventional trajectory Tug sizes to deliver the equivalent aerobraked mode payloads and the sensitivities of the conventional and aerobraked Tugs to performance parameters. The comparisons, made between the aerobraking and conventional trajectory Tugs, used the same groundrules, i.e., identical (1) specific impulses, (2) departure and recovery altitudes, (3) docking delta velocity budgets, and (4) basic astrion module weights. Both the aerobraking and the conventional Tugs were considered to be single stage reusable configurations. The propulsion module weights for the conventional trajectory Tugs were derived from prior Reference 1.1.0.0-1.

5.3.1 Conventional Trajectory Tug Size Comparison

Figure 5.3.1.0-1 shows the conventional trajectory Tug weights as a function of geosynchronous payload weight. The zero payload capabilities are not identical because the departure and recovery altitudes were selected identical to those of the aerobraking mode (i.e., 270-100 NM placement and 200 NM retrieval and round trip). The 45,000 pound propellant conventional trajectory Tug (53,028 pounds gross) is slightly undersized for the zero payload placement case. For the retrieval and round trip payload missions, required conventional trajectory Tug weights rapidly increase with increased payload. Payload placement is a less demanding mission for the conventional trajectory and is reflected in the smaller Tug weight increase per payload increase.

Shown in Figure 5.3.1.0-1 are the maximum payload capabilities of the 30° flare aerobraked Tug (Section 5.1.2) and the gross weight of this Tug. The aerobraked 30° flare Tug's (gross 55,066 pounds) payload placement capability of 7250 pounds is matched by a conventional trajectory Tug having a gross weight of 68,000 pounds (less payload). For the retrieval mission, the 55,066 pound aerobraked 30° flare Tug is equivalent to a 96,000 pound (less payload) conventional trajectory Tug in payload capability. The 4425 pound payload round trip mission has a gross Tug weight difference of 26,000 pounds (55,066 pounds aerobraked 30° flare Tug, 81,000 pounds conventional). All three of the equivalent maximum payload capability conventional trajectory Tugs will require two Shuttle launches per mission in either the ground based or space based modes.

Used in the ground based mode (i.e., Tug begins and ends each mission on earth within the Shuttle's cargo bay), the gross weight of the conventional trajectory Tug is beyond one Shuttle's capability to deliver it to low earth orbit. For the larger conventional trajectory Tug stages, the 60' length limitation of the Shuttle's cargo bay and the Shuttle's payload

**BASIS:**

- PAYLOAD PLACEMENT MISSIONS
DEPART AND RETURN TO 100 N.M.
- PAYLOAD RETRIEVAL AND ROUND
TRIP PAYLOAD MISSIONS
DEPART AND RETURN TO 200 N.M.
- TANDEM STAGE VEHICLE IS TWO EQUAL
STAGES BOTH RECOVERED
- STAGE WITH DROP TANK HAS EQUAL
PROPELLANT IN STAGE AND DROP TANK
- DROP TANK IS EXPENDED IN SYNCHRONOUS
ORBIT
- ASTRIONICS MODULE WEIGHT - 1960#
- PAYLOAD ADAPTER WEIGHT - 200#
- STAGE ADAPTER AND STAGE
SEPARATION MECHANISM - 324#

FIGURE 5.3.1.0-1: PAYLOAD CAPABILITY COMPARISON - AEROBRAKED VERSUS CONVENTIONAL TUG

5.3.1 (Continued)

capability are dual constraints. Therefore, Tug in-orbit assembly and/or fueling is required prior to departing the low earth parking orbit for geosynchronous orbit.

Used in the space based mode (i.e., Tug remains on orbit and Shuttle delivers propellant and payload to Tug), the required propellant weights for the equivalent maximum payloads are beyond the single Shuttle capability. Using this mode, Tug in-orbit refueling is required prior to each geosynchronous mission.

5.3.2 Sensitivities to Performance Parameters

The conventional trajectory single reusable stage Tug was shown in Reference 1.1.0.0-1 to be sensitive to performance parameters. The performance sensitivity analysis of that previous study was accomplished by allowing stage weight to grow (shrink) so that the payload remained constant. Because of the scope of this aerobraking study, investigation of the aerobraking effects on larger (smaller) stages was not conducted. Extrapolating the aerobraking impact data (e.g., aerodynamic, thermal, and weights) to configure other aerobraked Tugs is not justified until follow-on in-depth analyses are made. Therefore, round trip payload was selected as the dependent variable for the performance sensitivity analysis and the propellant loading in the aerobraked and conventional trajectory Tugs was held constant. The 30 pass basic (no flare) configuration (45,000 pounds propellant) was utilized as the representative of the aerobraked configurations. The comparable conventional trajectory single reusable stage has a propellant loading of 71,500 pounds (~80,000 total Tug weight).

5.3.2.1 Mass Fraction (λ')

Figure 5.3.2.1-1 shows the round trip payload sensitivities to mass fraction. The conventional trajectory Tug (including astrion module and payload adapter) has a significantly higher mass fraction (0.892) than does the aerobraked Tug (0.824) for the baseline payload. Note: The large size of the conventional Tug (80,150 pounds) accounts for the high mass fraction. The aerobraked Tug is smaller (54,600 pounds) and therefore has a part of its lower mass fraction attributable to size effects.

Both Tugs maintain relatively constant exchange ratios ($\delta W_{pld} / \delta \lambda'$) over the range of mass fractions shown. The aerobraked Tug's payload capability is less sensitive to changes in mass fraction (lower exchange ratio). Dropping the mass fraction by 0.015 (-0.015 on the figure) decreases the aerobraked payload approximately 1000 pounds and the conventional trajectory payload decreases 1600 pounds. If the mass fractions were increased by 0.015 (+0.015 on the figure), the aerobraked payload increases 1000 pounds and the conventional trajectory payload increases 1300 pounds. Therefore, mass fraction changes will impact the conventional trajectory Tug more severely than the aerobraked Tug.

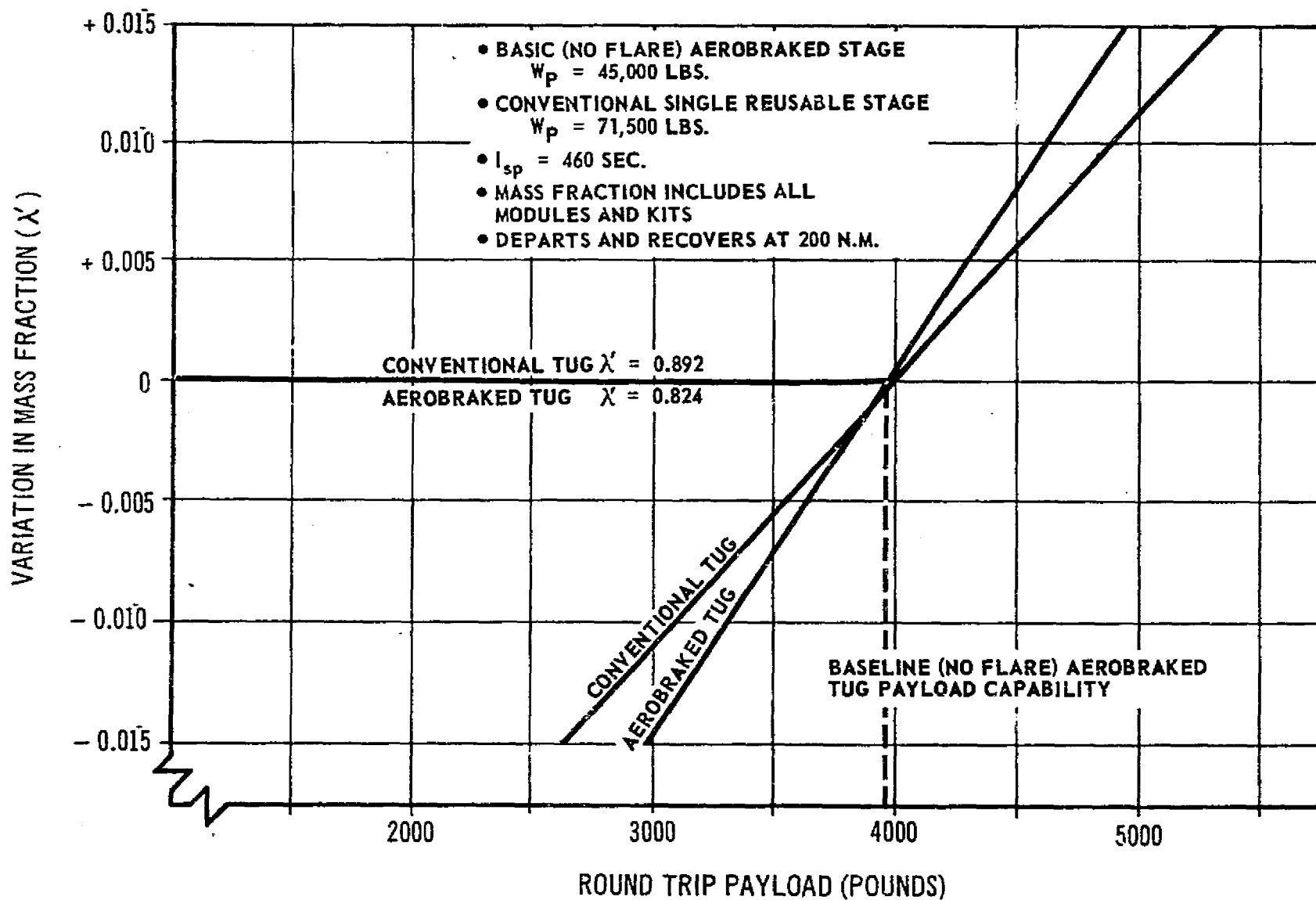


FIGURE 5.3.2.1-1: COMPARISON OF ROUND TRIP PAYLOAD SENSITIVITIES TO MASS FRACTION

5.3.2.2 Specific Impulse

Figure 5.3.2.2-1 compares the sensitivities to specific impulse. The data shown assumes that the variations in Isp could be achieved by equal engine weights and nozzle dimensions. (The nozzle's dimensions are important parameters in the aerobraked aft heat shield design and weight). For higher specific impulse than nominal values (461-470), both Tugs are about equally sensitive. Increasing the Isp from 460 to 450 seconds results in a small aerobraking advantage. However, the overall comparison is that nominal Isp variations affect both Tugs approximately the same.

5.3.2.3 Delta Velocity

Figure 5.3.2.3-1 compares the effects of mission delta velocity changes. The aerobraked Tug is somewhat more sensitive to delta velocity than the conventional trajectory Tug because of its lower mass fraction. Adding 1200 ft/sec to the mission's total delta velocity budget reduces both stage capabilities to less than 3000 pounds. The conventional trajectory stage essentially maintains its exchange ratio ($\delta W_{pld}/\delta \Delta V$) through the variations shown. The aerobraked stage's sensitivity to delta velocity increases with decreasing velocity requirements.

The round trip payload mission has been flown using the 200 NM departure and recovery mode and with one docking allowance. Therefore, it is anticipated that decreases in the baseline delta velocity budgets would be minor (800 ft/sec or less). As discussed in Section 5.2., the delta velocity budget for aerobraking Tug can increase to account for atmospheric variations and midcourse corrections. The conventional trajectory Tug could also have increased budgets due to long term space storage, docking with an orbital propellant depot, and in-orbit assembly operations. Probable delta velocity increases for both Tugs should be less than 1200 ft/sec. Within these upper and lower bounds, the aerobraked Tug is more sensitive to changes in delta velocity than the conventional trajectory Tug.

5.4 SENSITIVITY ANALYSIS CONCLUSIONS AND RECOMMENDATIONS

The sensitivity analysis has indicated certain definite trends, some of which require more comprehensive study in follow-on efforts. Most of these trends and follow-on efforts have been discussed in the previous sections. Following the tabulations listed below, a summary discussion of selected conclusions and recommendations is made. The sensitivity analysis conclusions are as follows:

- o The operational mode used by the aerobraked Tug should optimize the Shuttle capability to deliver and recover in low earth orbit.
- o An optimum aerobraked configuration should have a stabilization/drag device. (Assuming the 2000°F thermal constraint and a Shuttle recovery of the Tug within the seven day on-orbit Shuttle capability.)

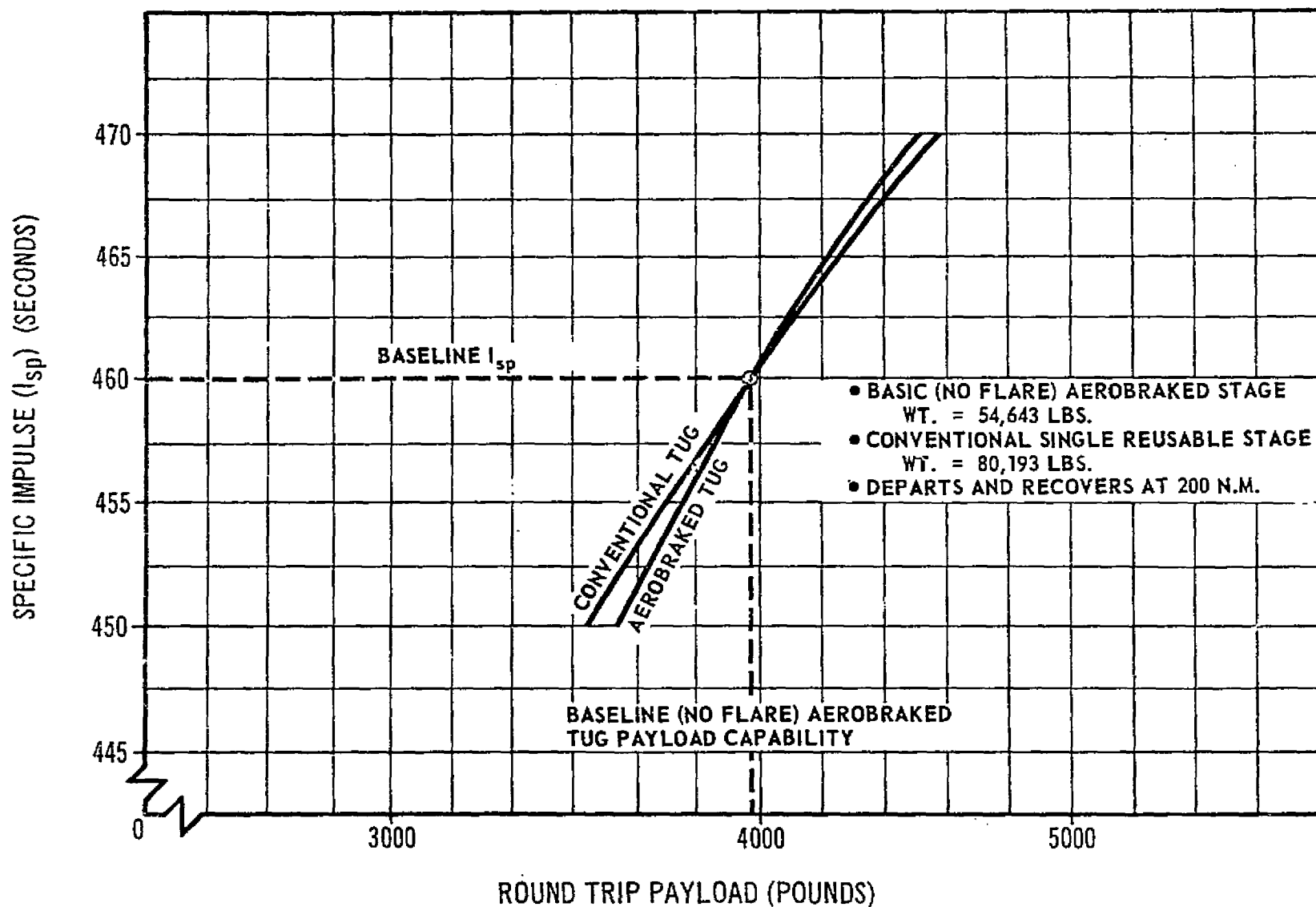


FIGURE 5.3.2.2-1: COMPARISON OF ROUND TRIP PAYLOAD SENSITIVITIES TO SPECIFIC IMPULSE

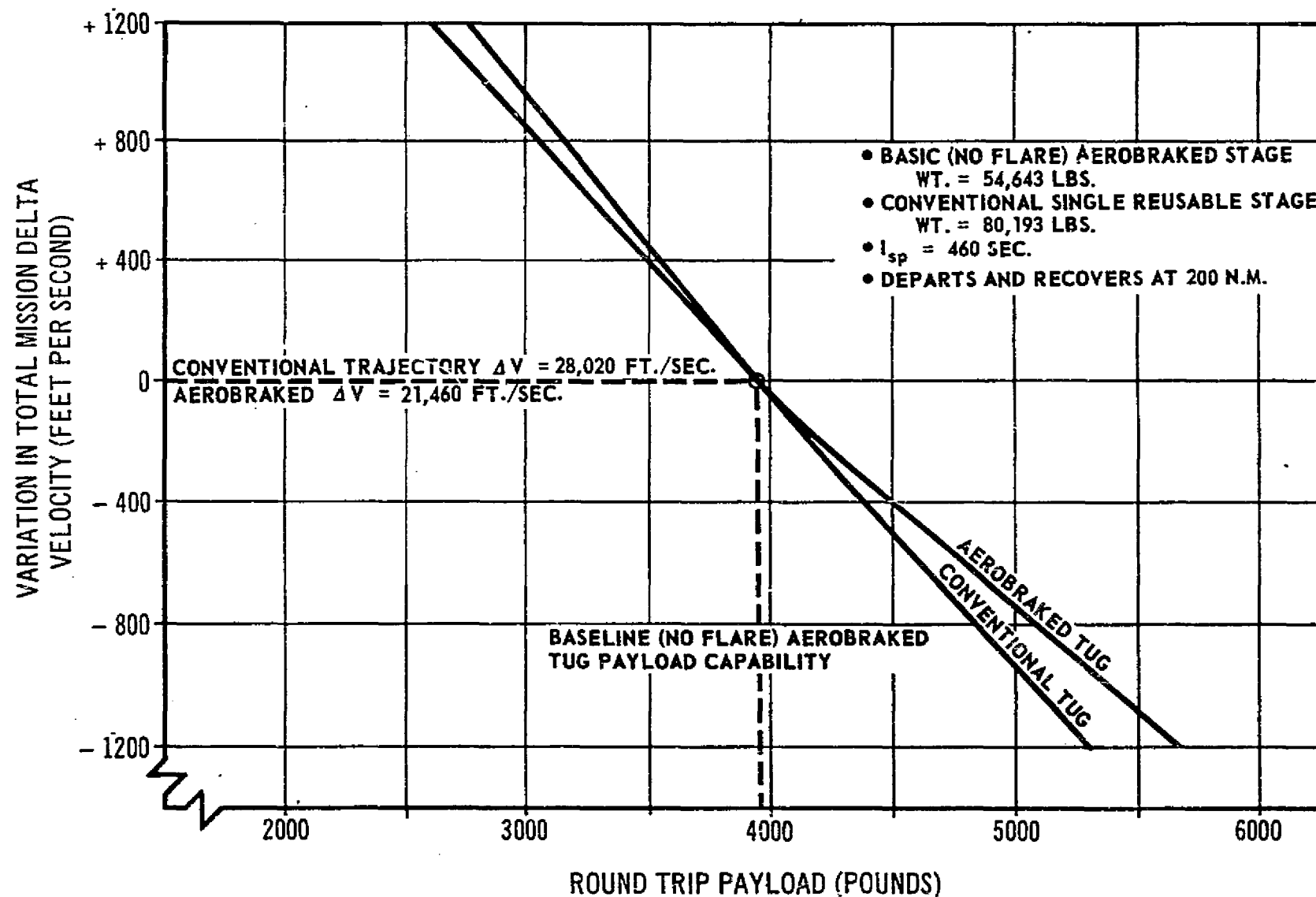


FIGURE 5.3.2.3-1: COMPARISON OF ROUND TRIP PAYLOAD SENSITIVITIES TO MISSION DELTA VELOCITY

5.4 (Continued)

- o Round trip geosynchronous payloads of 3000-4000 pounds are achievable by a 45,000 pound propellant aerobraked Tug.
- o Placement and retrieval of geosynchronous payloads of 7000-9000 pounds are within the capability of the 45,000 pound propellant aerobraked Tug.
- o The single Shuttle/Tug launch per geosynchronous mission is possible for 95% of the missions using Tug aerobraking.
- o Advanced state-of-the-art materials are required for configurations of less drag and/or shorter mission times.
- o Midcourse corrections can be made at an optimized time prior to reaching perigee to reduce the navigation and atmosphere uncertainty impact.
- o The equivalent round trip payload conventional trajectory Tug has a gross weight of approximately 26,000 pounds more than the aerobraked Tug (~45% heavier than aerobraking Tug).
- o The aerobraked Tug is less sensitive to changes in mass fraction than the conventional trajectory Tug. Sensitivities to specific impulse and delta velocity are less pronounced.

The following recommendations for advanced technology programs and follow-on aerobraking studies are made as a result of the sensitivity analysis:

- o Better definition of the short time-span atmospheric variations and their rate of change.
- o In-depth analysis of the combinations of atmospheric variations, navigational errors, and guidance/midcourse correction schemes.
- o Continued development of high temperature materials, particularly in the 2000-2500°F class.
- o Analysis of alternate drag device/stabilization configurations with a short high angle flare (near neutral stability) as one candidate.
- o Optimization of the Shuttle/Tug delivery and recovery orbits.
- o Impacts of possible Tug interim RCS propellant such as mono-propellants and bipropellants.

The Shuttle capabilities used as a reference in this analysis are subject to change as the Shuttle studies continue. As noted in the sensitivity analysis, changing the delivery and recovery mode to more nearly fully utilize the capabilities of both vehicles resulted in approximately 1000

5.4 (Continued)

pounds of additional round trip payload. This optimization should be continued in a follow-on Tug aerobraking study using the results of the current Shuttle extended Phase B studies.

The 30° flare had the maximum round trip payload because of its lighter flare weight and low equivalent delta velocity. Smaller physical size was the major factor in the weight and its stability resulted in lower delta velocities. It also had lower temperatures than the basic (no flare), because its increased drag permitted higher perigee altitudes. However, this configuration is probably not optimum for the aerobraked Tug. For example, a short 60° flare, with the same near-neutral stability as the 30° flare, could be superior.

The payload capabilities of all configurations studied maximized at approximately 30 passes (5.5 days). Using the Standard Atmosphere, a shorter mission (10 passes/2 days) or a longer mission (60 passes/11 days) did not greatly impact the payload capability. The high density atmosphere results indicated that a nominal mission should have 20-40 passes. The maximum equilibrium temperatures increased rapidly as the mission time shortened from 5.5 days and decreased slowly as mission time increased. The 30° flare configuration (30 passes) might experience steady state temperatures of approximately 2425° in the high density atmosphere - navigational error environment. Any configuration of similar drag coefficients could be expected to experience similar temperatures. To use the maximum payload potential of this configuration (or stability/drag) class, new materials to withstand the environment are required. With the transient effects considered, the temperature drops to approximately the upper limit of TD-nickel-chrome. Shorter mission times (e.g., 20 passes) would cause temperatures to exceed this TD-nickel-chrome limit but still be below 2500°F.

This study had the basic assumption that GO_2/GH_2 RCS development would be an integral part of the EOS program. The Tug inert weights, RCS performance, and payload capabilities were computed on this assumption. If it appears that this advanced system will not be available at the time the aerobraked Tug is to be placed into operation, an alternate system must be considered and the impacts on the aerobraking mode analyzed.

LIST OF REFERENCES

- 1.1.0.0-1 Technical Study for the Use of the Saturn V, INT-21 and Other Saturn V Derivatives to Determine an Optimum Fourth Stage (Space Tug), The Boeing Company, NAS8-5608, Schedule II, February 26, 1971

- 3.3.0.0-1 Astrionic System Optimization and Modular Astrionics for NASA Missions After 1974 - Preliminary Definition of Astrionic System for Space Tug Mission Vehicle Payload (MVP), Progress Report dated 16 June 1970 to 15 August 1970, IBM Number 69-K44-0006H, MSFC-DRL-008, Line Item Number 268

- 4.1.1.1-1 Keyes, J. W., "Aerodynamic Characteristics of Lenticular and Elliptic Shaped Configurations at a Mach Number of Six," NASA TN-D-2606, dated February 1965

- 4.1.1.1-2 Kinslow, Max, and Potter, J. L., "The Drag of Spheres in Rarefied Hypervelocity Flow", AEDC-TDR-62-205, December, 1962

- 4.1.1.1-3 Kussoy, M. I., et al, "Sphere Drag in Near Free Molecule Hypersonic Flow", AIAA Journal, Vol. 8, No. 11, November 1970

- 4.1.1.1-4 Mechanics of Rarefield Gases, Volume 5, Section 16 of Handbook of Supersonic Aerodynamics, NAVWEPS Report 1488 (Vol. 5, Section 16) dated 1961

- 4.1.1.1-5 Schaaf, S. A. and Chambre, P. L., Flow of Rarefield Gases, Princeton University Press, 1961

- 4.1.1.1-6 Cox, R. N. and Crabtree, L. F., Elements of Hypersonic Aerodynamics, Academic Press, 1965

- 4.1.1.1-7 Sentman, L. H., "Free Molecule Flow Theory and its Application to the Determination of Aerodynamic Forces," LMSC-448514, October 1961

- 4.1.1.1-8 Schlichting, H., Boundary Layer Theory, McGraw Hill, 1968

- 4.1.1.1-9 Nielson, J. N., Missile Aerodynamics, McGraw Hill, 1960

- 4.1.1.1-10 Patterson, G. N., Molecular Flow of Gases, J. Wiley & Sons, 1956

- 4.1.1.1-11 Hoerner, S. F., Fluid Dynamic Drag, Published by the Author, 1961

PRECEDING PAGE BLANK NOT FILMED

LIST OF REFERENCES (Continued)

- 4.1.1.2-1 Seiff, A. and Whiting, E. E., "Calculation of Flow Fields from Bow-Wave Profiles for the Downstream Region of Blunt-Nosed Circular Cylinders in Axial Hypersonic Flight," NASA-TN-D-1147
- 4.1.1.2-2 Seiff, A., "Secondary Flow Fields Embedded in Hypersonic Shock Layers," NASA-TN-D-1304
- 4.1.1.2-3 Seiff, A., and Whiting, E. E., "A Correlation Study of the Bow Wave Profiles of Blunt Bodies," NASA-TN-D-1148
- 4.1.1.2-4 Truitt, R. W., Hypersonic Aerodynamic, Ronald Press Co., 1959
- 4.1.1.2-5 Sentman, L. H., "Tables of Free Molecule Flow Functions," Appendix C to LMSC TR-448514, LMSC 448514-1
- 4.1.1.2-6 Blick, E. F., Aerodynamic Coefficients in the Slip and Transition Regime, AIAA Journal Vol. 1, No. 11, November 1963
- 4.1.1.2-7 Matting, F. W., "Approximate Bridging Relations in the Transitional Regime between Continuum and Free Molecule Flows," Journal Spacecraft and Rockets, Vol. 8, No. 1, January 1971
- 4.1.1.3-1 Wagner, R. D., and Watson, R., "Reynolds Number Effects on the Induced Pressures on Cylindrical Bodies with Different Nose Shapes and Nose Drag Coefficients in Helium at a Mach Number of 24," NASA TR-R-182
- 4.1.1.3-2 Henderson, A., "Investigation of Flow over Simple Bodies at Mach Numbers of the Order of 20," NASA TN-D-449
- 4.1.1.3-3 Van Hise, V., "Analytic Study of Induced Pressure on Long Bodies of Revolution with Varying Nose Bluntness at Hypersonic Speeds," NASA TR-R-78
- 4.1.1.3-4 Henderson, A., et al, "Fluid Dynamic Studies to $M = 41$ in Helium," AIAA Journal, Vol. 4 No.12, December 1966
- 4.1.2.1-1 DeRose, C. E., "Ballistic Range Tests of a Drag Ring Configuration at Mach Numbers Around 2," NASA TN-D-4291, December 1967
- 4.1.2.1-2 Ericsson, L. E., "Unsteady Aerodynamics of an Ablating Flared Body of Revolution Including the Effects of Entropy Gradient," AIAA Journal, Vol. 6 No. 12, December 1968

LIST OF REFERENCES (Continued)

- 4.3.1.1-1 "Space Shuttle System Natural Environment Design Requirements Document," NASA Document dated May 17, 1971
- 4.3.1.1-2 Terrestrial Environment (Climatic) Criteria Guidelines for Use in Space Vehicle Development, 1971 Revision, dated May 10, 1971, NASA TMX 64589
- 4.3.1.1-3 Space Environment Criteria Guidelines for Use in Space Vehicle Development, 1969 Revision, Second Edition, dated August 26, 1971, NASA TMX 53957
- 4.3.4.0-1 Private Communication with R. Smith/O. Smith, Aerospace Environment Division, Aero-Astrodynamics Laboratory, MSFC, January 27, 1971
- 4.5.1.0-1 Chapman, D. R., D. M. Kuehn and H. K. Larson, "Investigation of Separated Flows in Supersonic and Subsonic Streams with Emphasis on the Effect of Transition," NASA Report 1356, 1958
- 4.5.1.0-2 Larson, H. K., "Heat Transfer in Separated Flows," Journal of the Aero/Space Sciences, November 1959
- 4.6.4.4-1 "Astrionic System Study for Saturn S-II Expendable Second Stage," Phase B Study Report, dated 30 June 1971, IBM Number 71W-00225, MSFC-DRL-008A, Line Item Number 268
- 4.6.4.5-1 Toda, Schlee and Obsharsky, "The Region of Kalman Filter Convergence for Several Autonomous Navigation Modes," AIAA Paper Number 67-623, IBM Corporation
- 4.6.8.1-1 Vette, Lucero, and Wright, "Models of the Trapped Radiation Environment, Volume II Inner and Outer Zone Electrons," NASA SP-3024
- 4.6.8.1-2 Vette, "Models of the Trapped Radiation Environment," Volume I Inner Zone Protons and Electrons," NASA SP-3024
- 4.6.8.2-1 "ELBA - Electron and Bremsstrahlung Dose Rate Code," RSIC Computer Code Collection - CCG119, by Space Sciences Laboratory, Marshall Space Flight Center, Huntsville, Alabama
- 4.6.8.4-1 Burrell, M. O. and Wright, J. J., "Orbital Calculations and Trapped Radiation Mapping," NASA TMX-53406
- 4.7.2.0-1 Kostoff, R. N., "Aerobraking of the Space Tug from Synchronous Orbit into Low Circular Earth Orbit: Guidance and Heating Constraints on First Atmospheric Pass," Bellcomm Memorandum for File, July 15, 1971

LIST OF REFERENCES (Continued)

- 4.7.2.0-2 Kostoff, R. N., "Space Shuttle and Space Tug Peak Temperatures," Case 237, Bellcomm Memorandum for File, August 26, 1971
- 4.7.2.0-3 Pratt and Whitney Aircraft "Ascent and Re-Entry Heating RL-10/Space Tug," dated May 28, 1971
- 5.1.2.0-1 Alternate Space Shuttle Concepts Study, Final Report, Part II, Volume I, Grumman-Boeing, NAS9-11160, July 6, 1971

APPENDIX A

TWO PASS AEROBRAKING SPACE TUG ANALYSIS

A-1.0 INTRODUCTION AND SUMMARY

The original contracted activity for the Space Tug Aerobraking Study was accomplished from May 27, 1971 through November 27, 1971. This study activity was directed to determine the feasibility of aerobraking and to define the maximum payload capability aerobraking Tug concept as a function of mission duration. The successful completion of this activity identified the necessity to investigate short duration mission payload data and to impact the effect of flare length on aerobraking Tug payload capability.

This add-on contractual activity was initiated from January 12, 1972 through April 12, 1972. The three-month activity included two months for technical activity with one additional month for incorporation of results into the final documentation. This activity investigated the following concepts:

1. A basic (no flare) configuration - 2 pass mission.
2. A "short" 60° flare configuration - 2 pass mission.
3. A "short" 60° flare configuration - 30 pass mission.
4. A "large" 80° nose flare configuration - 2 pass mission.

The basic (no flare) Tug data (item 1. above) completed the spectrum of mission durations from the two pass (approximately nine hours aerobraking return time) to a 60 pass (approximately 11 days aerobraking return time). The "short" 60° flare configuration data (items 2. and 3. above) identified the performance and weights of low weight, high performance aerobraking configuration over the two pass to the 30 pass mission duration. The large nose flare configuration (item 4. above) was designed to achieve a low ballistic coefficient configuration which would result in significantly lower pressure loads and lower thermal environments than those experienced by the short flared configurations when performing the two pass mission.

The background for the add-on effort was based on the desirability of very short duration missions which will minimize the Shuttle's on-orbit stay time and which would minimize the monitoring and/or tracking operations of ground stations. The initial study effort was designed to maximize payload capability of the aerobraking Tug concept without considering mission on-orbit duration constraints.

Other constraints which increased mission duration included the ground-rule of 2000°F as state-of-the-art limit for radiative materials. As the temperatures for one to four pass missions were believed to exceed

A-1.0 (Continued)

any near-term improvement in radiative material capabilities, short duration missions were not investigated. The use of ablative materials were not considered due to the potential problems associated with multiple heating/cooling cycling during aerobraking, ablative out-gassing, hot spots, cold soak and surface recession. The add-on study activity considered the potential problems associated with ablatives to be controllable with the proper material selection criteria and design features.

The objectives of the add-on study were to:

- a. Determine the performance and round trip payload capability of a Space Tug utilizing a two pass aerobraking technique from synchronous orbit for the basic (no flare) Tug, the short 60° flare Tug and the large flare Tug.
- b. Determine the inert weight penalties associated with these configurations.
- c. Compare the Space Tug relative weights for conventional Tug with the new aerobraked Tug data points.
- d. Define the performance of a shortened 60° flare configuration to compare with the current 30° flare (30 pass mission).

Figure A-1.0.0-1 illustrates the concepts studied in the add-on effort. They include a basic (no flare) Tug with an ablative heat shield, a "short" 60° flare concept and a large nose flare concept. The basic (no flare) Tug for a two pass mission has the same configuration as the basic (no flare) Tug for the 30 pass mission. The heat shield, however, must use an ablative material rather than a radiative material as the temperatures encountered exceed the radiative materials' state-of-the-art capability. The sidewall insulation system requires the titanium outer foil be replaced by a L-605 material which has a higher thermal capability.

The "short" 60° flare Tug concept for the two pass mission also requires an ablative heat shield. The sidewall protection system is L-605 over microquartz insulation. The short Inconel 718 flare will not totally shield the payload and will allow the payload to experience temperatures above the desired 300°F. Therefore, the payload adapter must be insulated.

The large nose flare can be Inconel 718 or Rene' 41 as the flare will experience temperatures of 1300 to 1400°F. The sidewalls and payload are shielded by the flare and do not require insulation (see Appendix F).

The results of the follow-on activity are reflected in the payload capabilities of the various configurations are as shown in Figure A-1.0.0-2. The 2 pass basic (no flare) Tug will roundtrip five

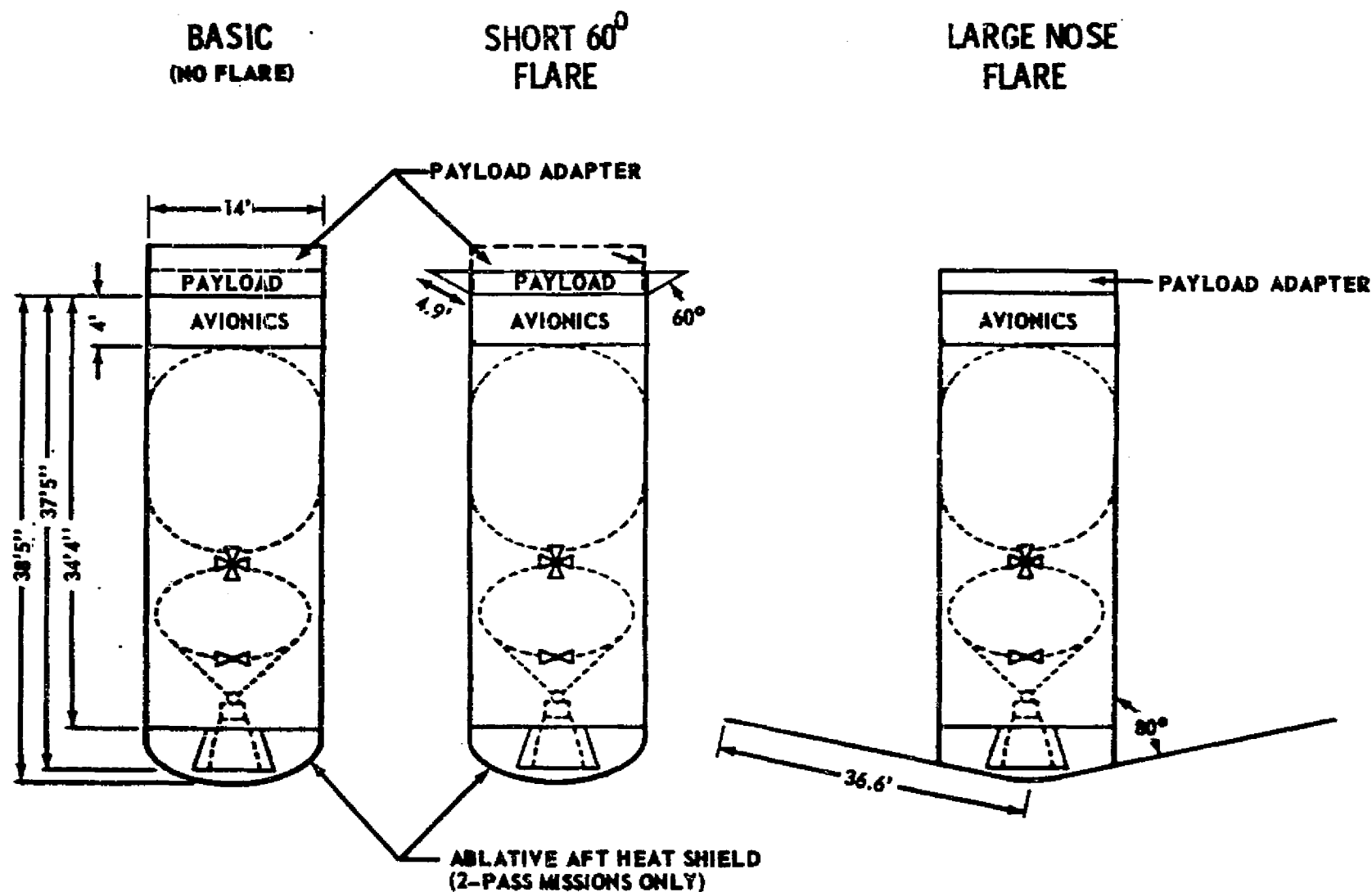


FIGURE A-1.0.0-1: SELECTED SPACE TUG AEROBRAKING CONFIGURATION CONCEPTS (ADD-ON ACTIVITY)

CONFIGURATION	ROUND TRIP PAYLOAD (LBS)	
	270-100 N.M. MODE	200 N.M. MODE
Basic (No Flare) - (2 Pass)	500	1700
Short 60° Flare - (2 Pass)	475	1700
Large Nose Flare - (2 Pass)	Negative	Negative
Short 60° Flare - (Same C_D as 30° Flare) (30 Pass)	2850	4100
Short 60° Flare (Neutrally Stable) - (30 Pass)	3100	4400
Light Weight Large Flare - (50' Diameter) (2 Pass)	1800 (See Appendix F)	3000

Figure A-1.0.0-2 Geosynchronous Round Trip Payloads

A-1.0 (Continued)

hundred pounds in the geosynchronous mission (assuming the Tug returns to a 270 n.m. orbit and then rendezvous with the Shuttle at 100 n.m. orbit). If the basic (no flare) Tug departs from and returns to a 200 n.m. orbit, this payload capability can be increased to approximately 1700 pounds. For the 2 pass, 9 hour basic Tug mission, the payload will be reduced approximately 2300 pounds from that obtained in the 30 pass mission due to the increased thermal protection required on the heat shield and the Tug sidewalls.

The short 60° flare has approximately the same small two-pass payload capability as does the basic (no flare). The use of a short flare did not reduce the thermal and pressure loads significantly. Therefore, the aerobraking kit components for the short 60° flare 2 pass concept were comparable in weight to that of the 2 pass basic Tug described above. As with the basic (no flare) Tug, increasing the rendezvous altitude to 200 n.m. orbit will increase the payload capability by an additional 1200 pounds to 1700 pounds.

The large nose flare for the two pass mission has a negative payload in either mission mode (270-100 n.m. or 200 n.m.). Approximately a 2000 pound inert weight reduction would be required to achieve a zero payload in the 270-100 n.m. mode or a 800 pound reduction in the 200 n.m. mode. The majority of the aerobraking kit weight for this concept is the large flare (approximately 99 percent of the weight). This design places the structure in compression. Alternative designs indicate that designing a tension flare configuration might significantly reduce weight and provide a positive payload capability as shown in Appendix F.

Also shown in Figure A-1.0.0-2 is the payload capability of the "short" 60° flare flown in a 30 pass mission mode. This configuration was designed to have the same drag coefficient as the 30° flare configuration. In the initial study effort, the 30° flare configuration had greater payload capabilities than the 45° and 60° flare configurations. This was believed to be due to the selection of the flare length rather than the flare angle selected. The 60° flare, when designed to the same drag coefficient as the 30° flare, will be 4.9 feet long compared to the 11.25 feet long for the 30° flare. This will decrease the 60° flare weight significantly. However, its flare weight saving is offset by the requirements for (1) increased RCS fuel (to provide static stability) and (2) payload adapter insulation (much higher temperatures behind the flare).

The 60° flare will be neutrally statically stable at 8.68 feet slant height. An assessment of payload capability indicated that the weight of the longer (8.68 feet) flare is less than the weight of RCS fuel and insulation required by the shorter flare (4.90 feet). The longer neutrally stable 60° flare's payload capability is shown for the 30 pass mission (Figure A-1.0.0-2). This neutrally stable 60° flare configuration will provide a slight improvement in the payload capability (approximately 180 pounds) over the 30° flared aerobraking Tug.

A-1.0 (Continued)

The results of the short mission duration analysis show that it is possible to return payloads within a day. However, the payload capability decreases significantly as the mission duration decreases. Some technology advances are required to improve the ablative materials. Further, the design of large aerodynamic decelerators need to be studied in greater depth to reduce the high weight penalties of the designs examined to date.

A-2.0 TRADE STUDIES

This section of the appendix presents the results of the add-on study activity including aerodynamics, configurations, trajectories, control, astronics, thermal, materials and weight analyses.

A-2.1 AERODYNAMIC ANALYSIS

Aerodynamic data was developed in accordance to the criteria shown in Section 4.1 (basic report). Data was developed to determine the drag coefficients for trajectory analysis, the static stability data for control analysis and the air loads for structural and weights analysis. This data was developed for the two pass missions with a basic (no flare) Tug, a Tug with a short 60° flare and a Tug with a large flare (low ballistic coefficient). Additional data was developed for the short 60° flare configuration flown in a 30 pass mission. This data was developed to provide comparable data to a similar 30 pass mission flown with a 30° flare configuration.

Figure A-2.1.0-1 is a representation of the payload capability trend versus ballistic coefficient ($W/C_D A$) illustrating the data points developed in the initial activity and identifies the recommended additional data points. The preliminary assessment indicated that the maximum payload capability may be obtained with a combination of a short steep angle flare and a moderate degree of static instability. One reason for this assessment was to determine the best short 60° flare configuration for analysis during the add-on effort (i.e., two choices were available; a neutrally stable 60° flare configuration or a 60° flare configuration with the same $W/C_D A$ as the 30° flare configuration).

Flow separation effects should be considered in detail for small, steep flare configurations. Flow separation should in general, (1) increase with increasing flare semi-vertex angle, (2) increase with decreasing perigee altitude (lower time to decay), and (3) increase, percentage wise with decreasing flare size. Follow-on in-depth study activity including wind tunnel testing must be performed to determine the optimum aerodynamic decelerator design.

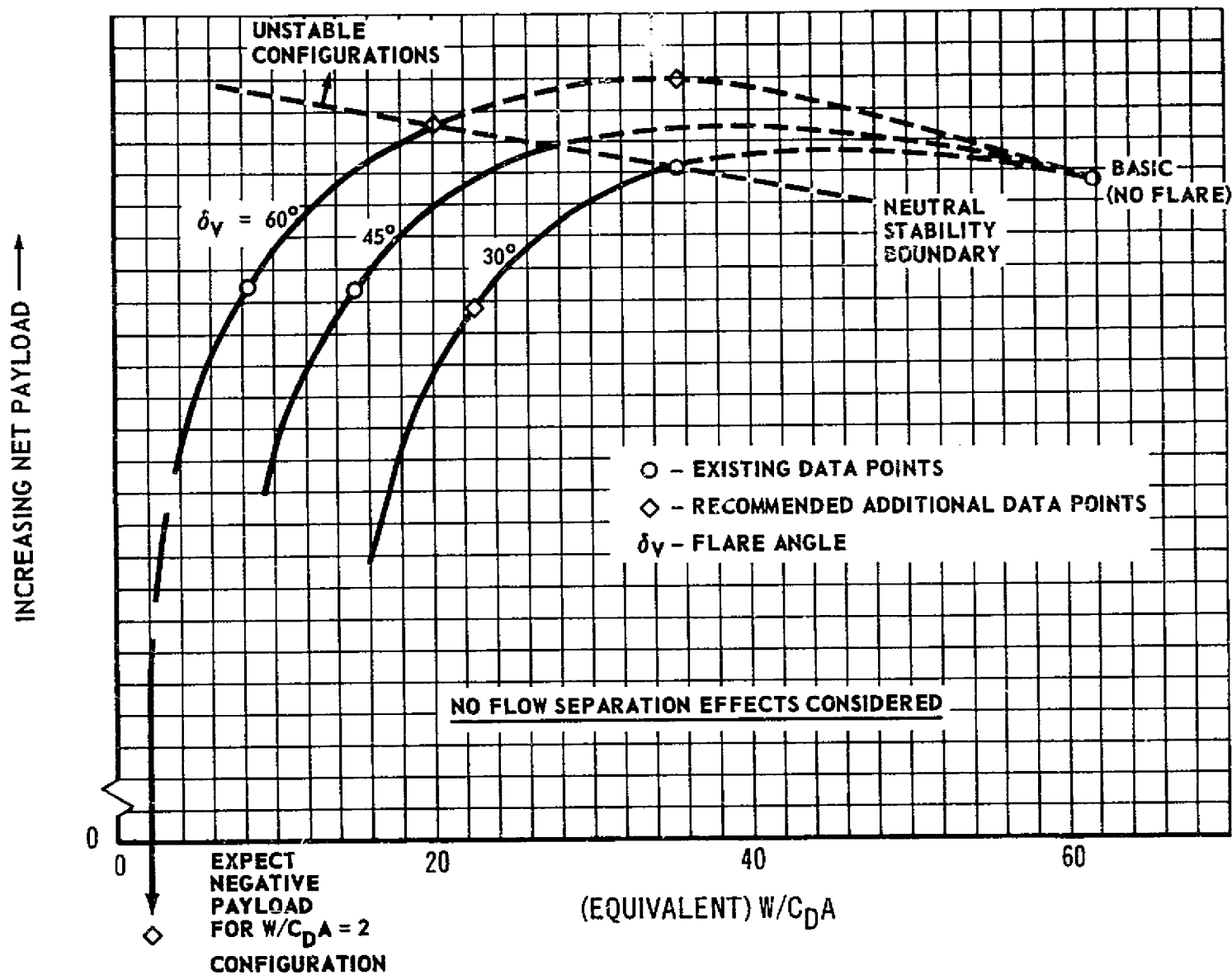


FIGURE A-2.1.0-1: PRELIMINARY FLARE CONFIGURATION/NET PAYLOAD SENSITIVITY ESTIMATE

A-2.1.1 Basic (No Flare) Two Pass Analysis

The possible ablation effects were not considered in the aerodynamics analysis of this configuration. The drag coefficients, normal force coefficients, and center of pressure data for the basic Tug are shown in Figures 4.1.1.1-2 and 4.1.1.2-1 (basic report).

The local pressure coefficient (C_{PLOCAL}) distribution for the basic (no flare) configuration over the range of 2 to 60 passes is shown in Figure A-2.1.1-1. The local pressure (P_L) for the two pass mission is more than double that for the five pass mission because of the 2 pass K_n^* factor. For example, the five pass maximum nose local pressure is less than 0.5 psi (Figure 4.1.1.3-2 of basic report) while the two pass value is slightly greater than 1.0 psi.

A-2.1.2 Short 60° Flare Analysis

Three short 60° flares of varying slant heights were defined as shown in Figure A-2.1.2-1. Short 60° flare #1, slant height = 0.26 caliber (3.64 feet) was sized to provide the same equivalent $W/C_D A$ as the 30° flare (the equivalent $W/C_D A$ for a given configuration is that constant $W/C_D A$ which would be required to result in the same initial target perigee altitude for the required time to decay). The drag characteristics of this configuration, presented in Figure A-2.1.2-2 appeared too low to result in the same equivalent $W/C_D A$ as the 30° flare configuration. Hence, the short 60° flare #2 was defined.

The short 60° flare #2 configuration (slant height = 0.35 caliber - 4.90 feet) resulted in approximately the same 30 pass initial perigee as the short 30° flare configuration. The drag characteristics of this configuration are presented in Figure A-2.1.2-3. This #2 configuration was selected as the baseline short 60° flare and was the configuration subjected to design, control, thermal, weights and payload analyses. This selection was based on the preliminary payload estimate (prior Figure A-2.1.0-1).

The static stability characteristics of the selected short 60° flare (#2) are shown in Figures A-2.1.2-4 ($C_{N\alpha}$) and -5 (CP/D). This configuration is statically unstable at altitudes below approximately 400,000 feet. The local pressure coefficients over the heat shield and cylinder are the same as those of the 30° flare (Figure 4.1.2.5-1 of basic report). The local pressure coefficients over the flare are shown in Figure A-2.1.2-6. This later figure also shows the K_n^* factors to be used to convert the local coefficients to local pressures.

The short 60° flare #3 configuration (slant height = 0.62 caliber - 8.68 feet) was sized to the neutral stability characteristics of the 30° flare. The drag coefficient data for this flare is shown in Figure A-2.1.2-7.

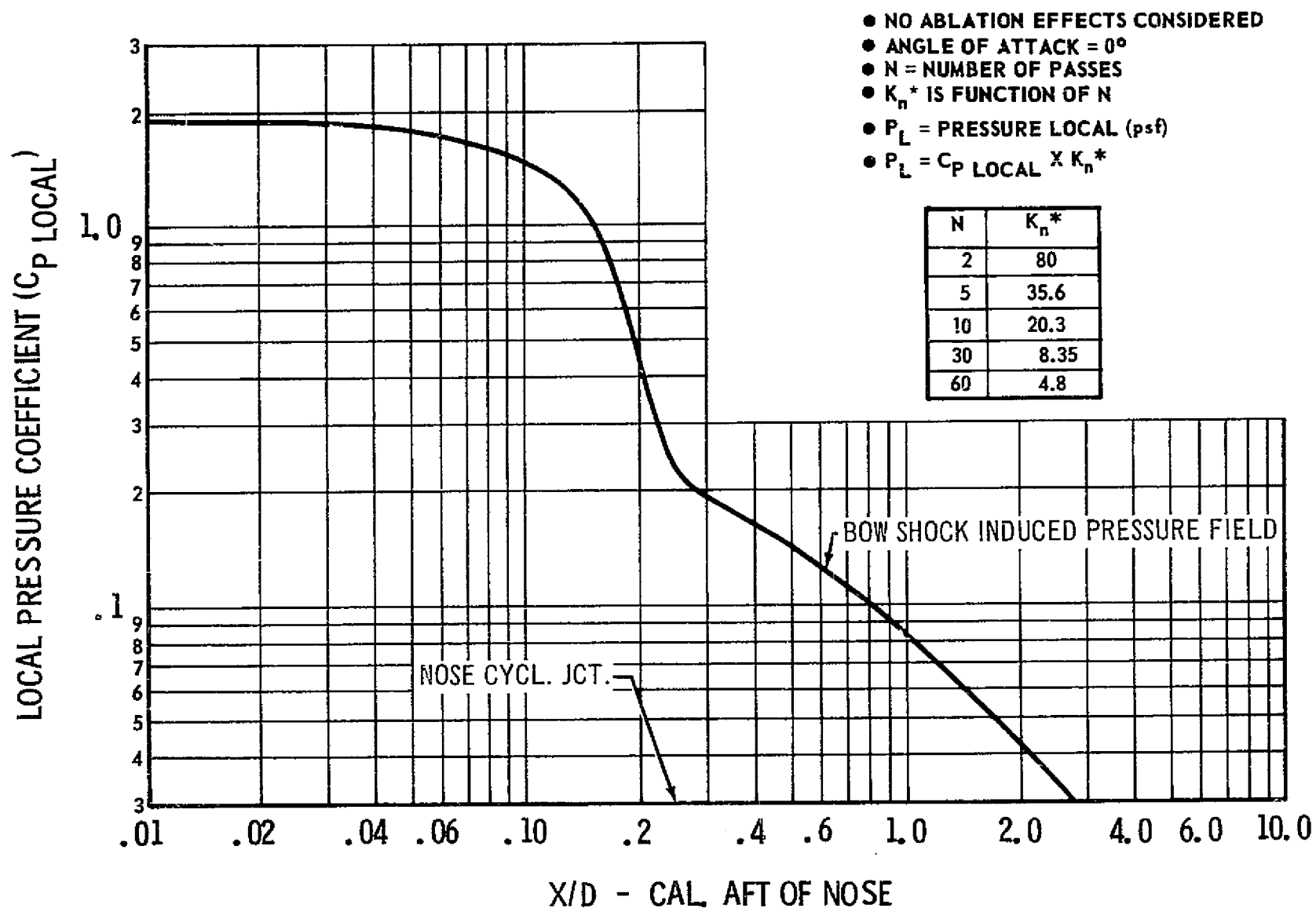


FIGURE A-2.1.1-1: BASIC (NO FLARE) PRESSURE COEFFICIENT DISTRIBUTION

NOTES:

- ① 2:1 ELLIPSOID NOSE COMMON TO ALL CONFIGURATIONS
- ① MAIN PROPULSION GIMBAL POINT
- ② ASTRONICS MODULE
- ③ PAYLOAD ADAPTER
- ④ PAYLOAD

TUG DIAM. = D_R = 14 FT.

CONFIG.	δ_v	SLANT LTH. - FT.
SHORT #1	60°	3.64
SHORT #2	60°	4.90
SHORT #3	60°	8.68

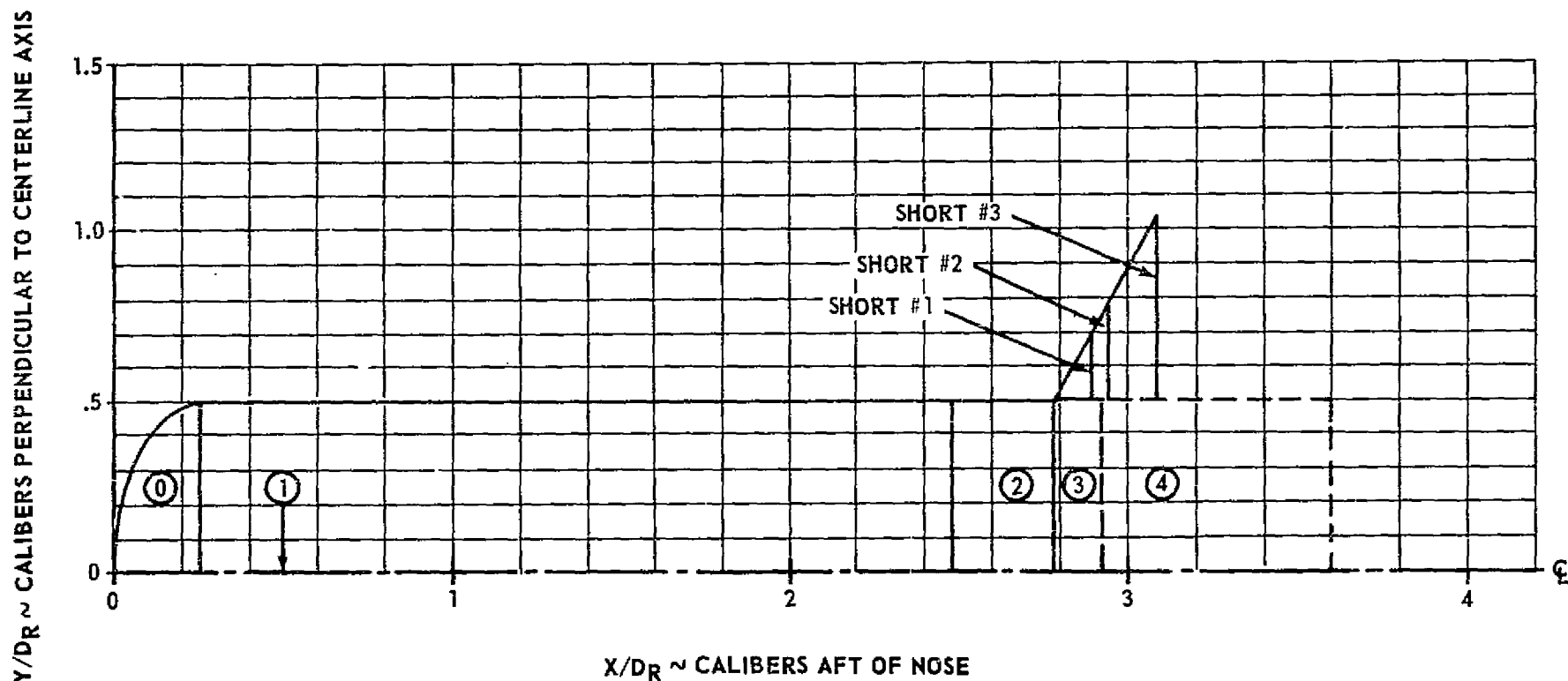


FIGURE A-2.1.2-1: SHORT 60° FLARED TUG CONFIGURATION(S) GEOMETRY

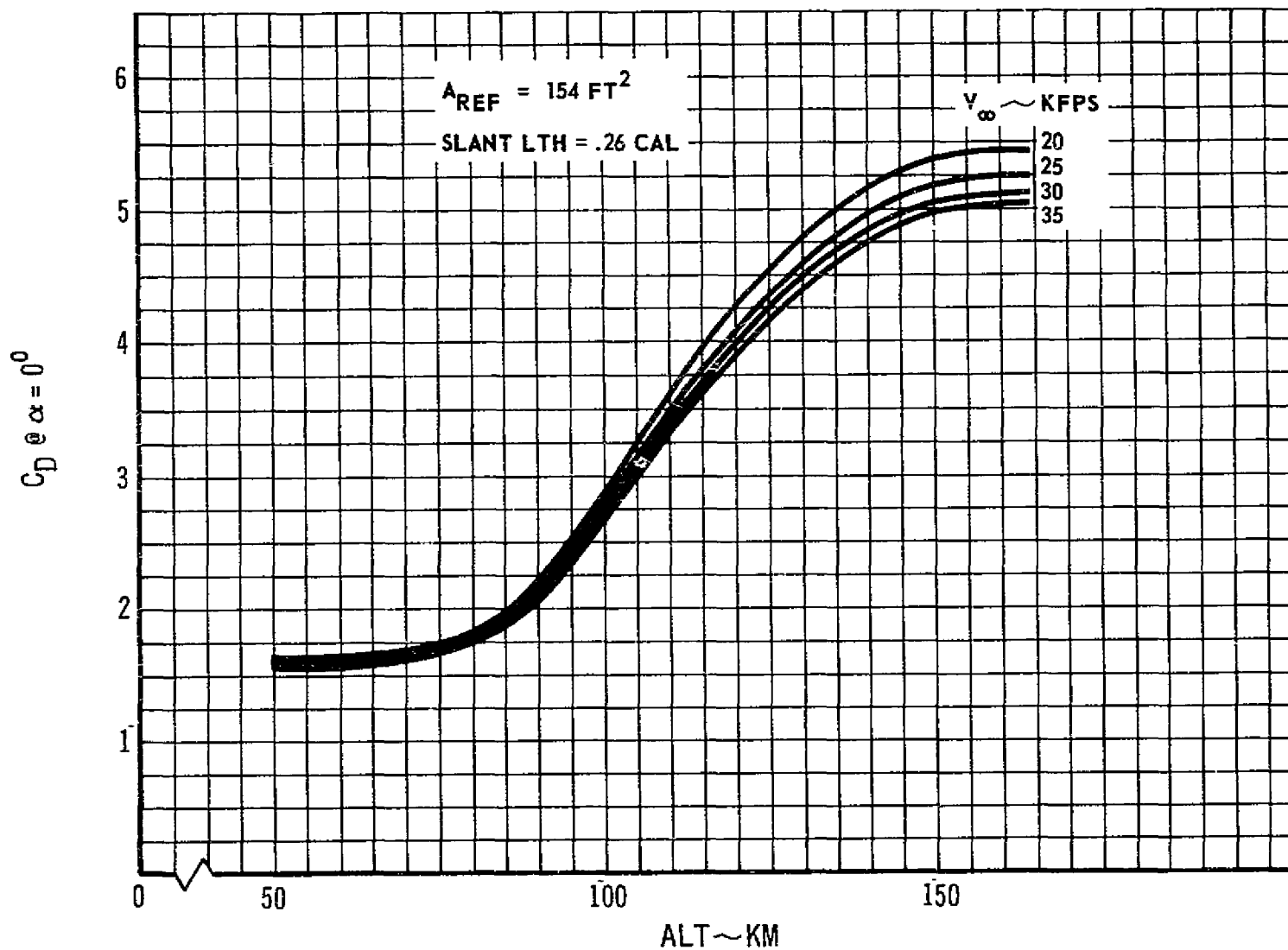


FIGURE A-2.1.2-2: DRAG COEFFICIENTS FOR SHORT 60° FLARE #1

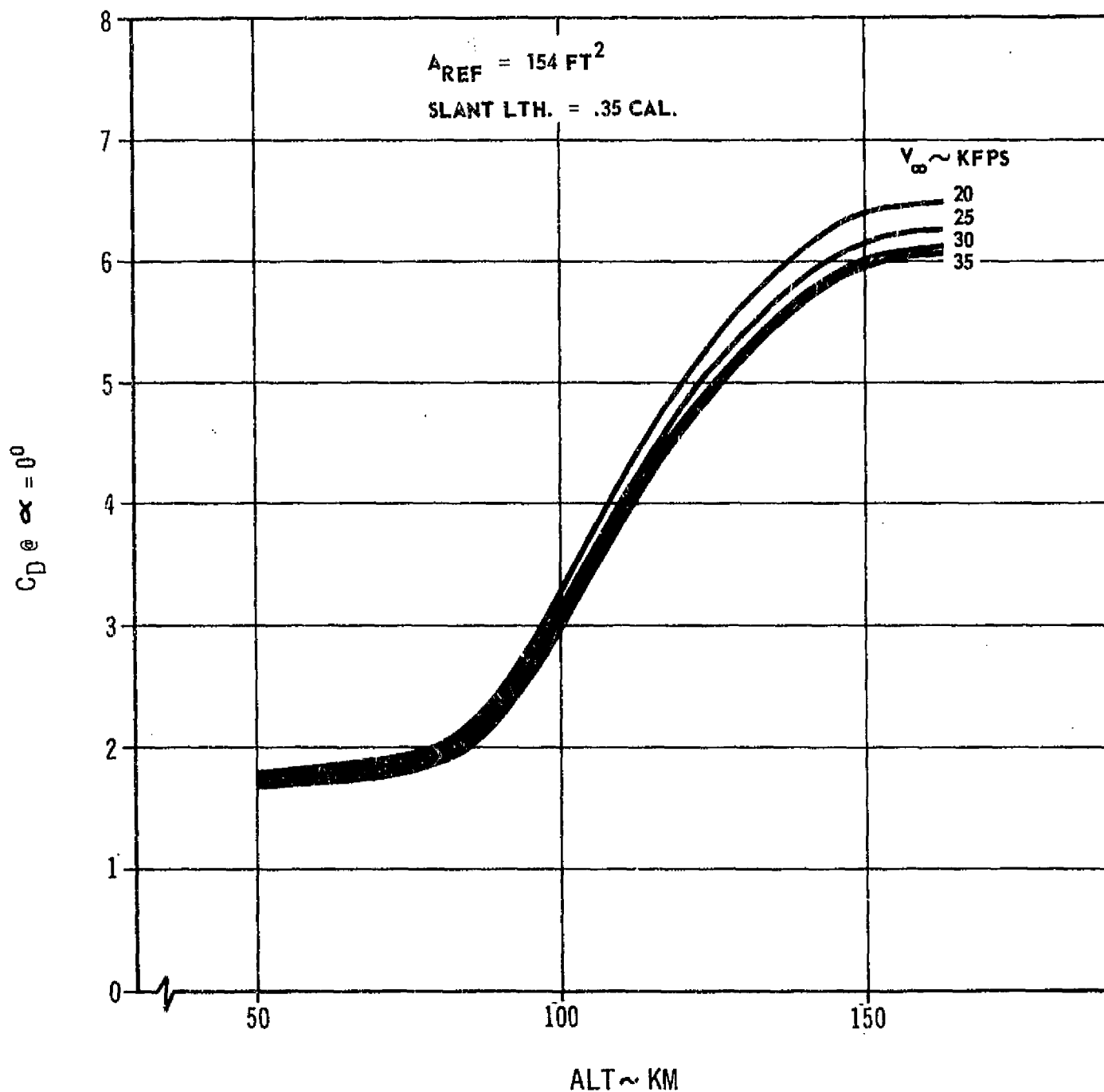


FIGURE A-2.1.2-3: DRAG COEFFICIENT FOR SHORT 60° FLARE #2
(SELECTED CONFIGURATION)

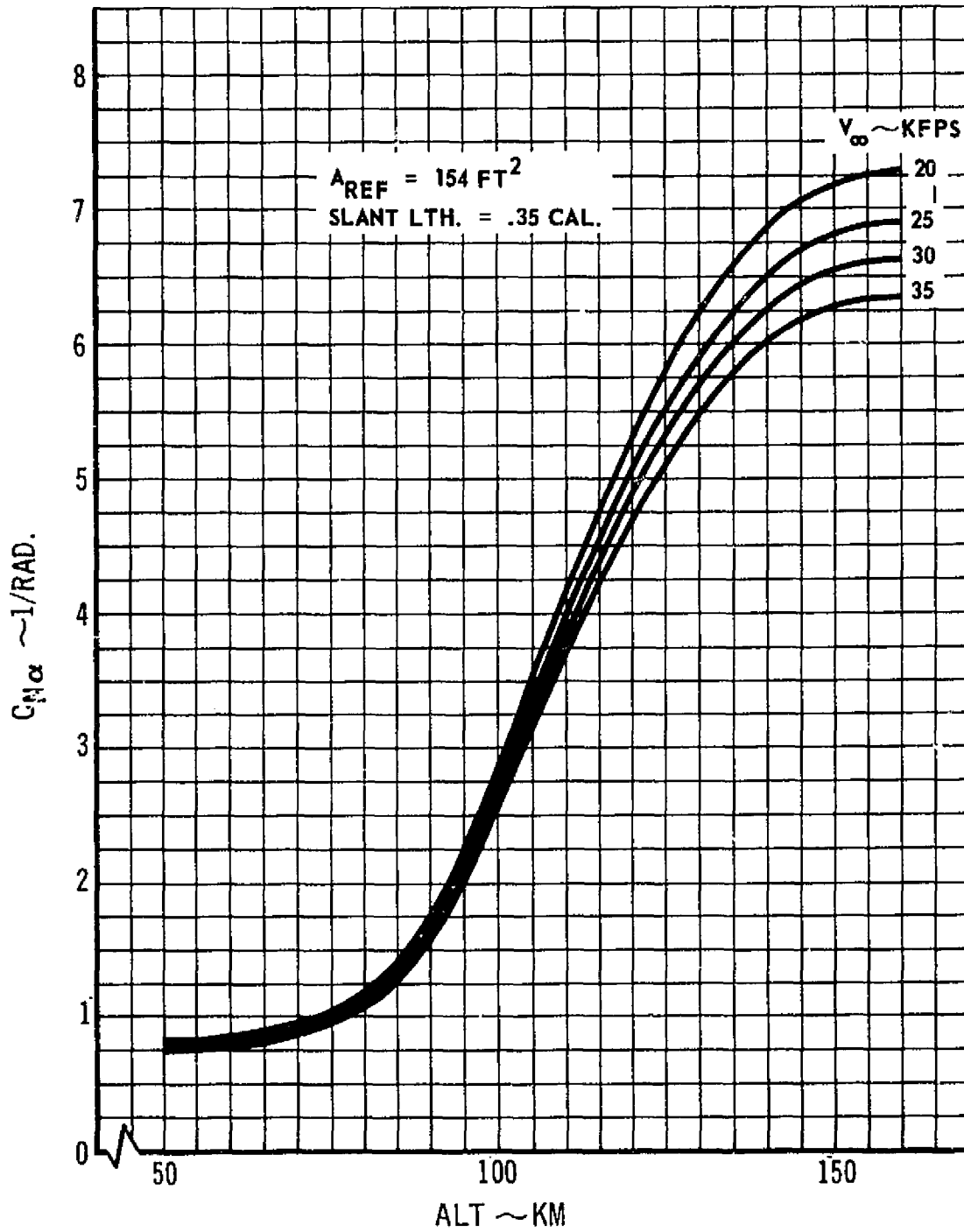


FIGURE A-2.1.2-4: COEFFICIENT OF NORMAL FORCE SLOPE FOR SHORT 60° FLARE #2

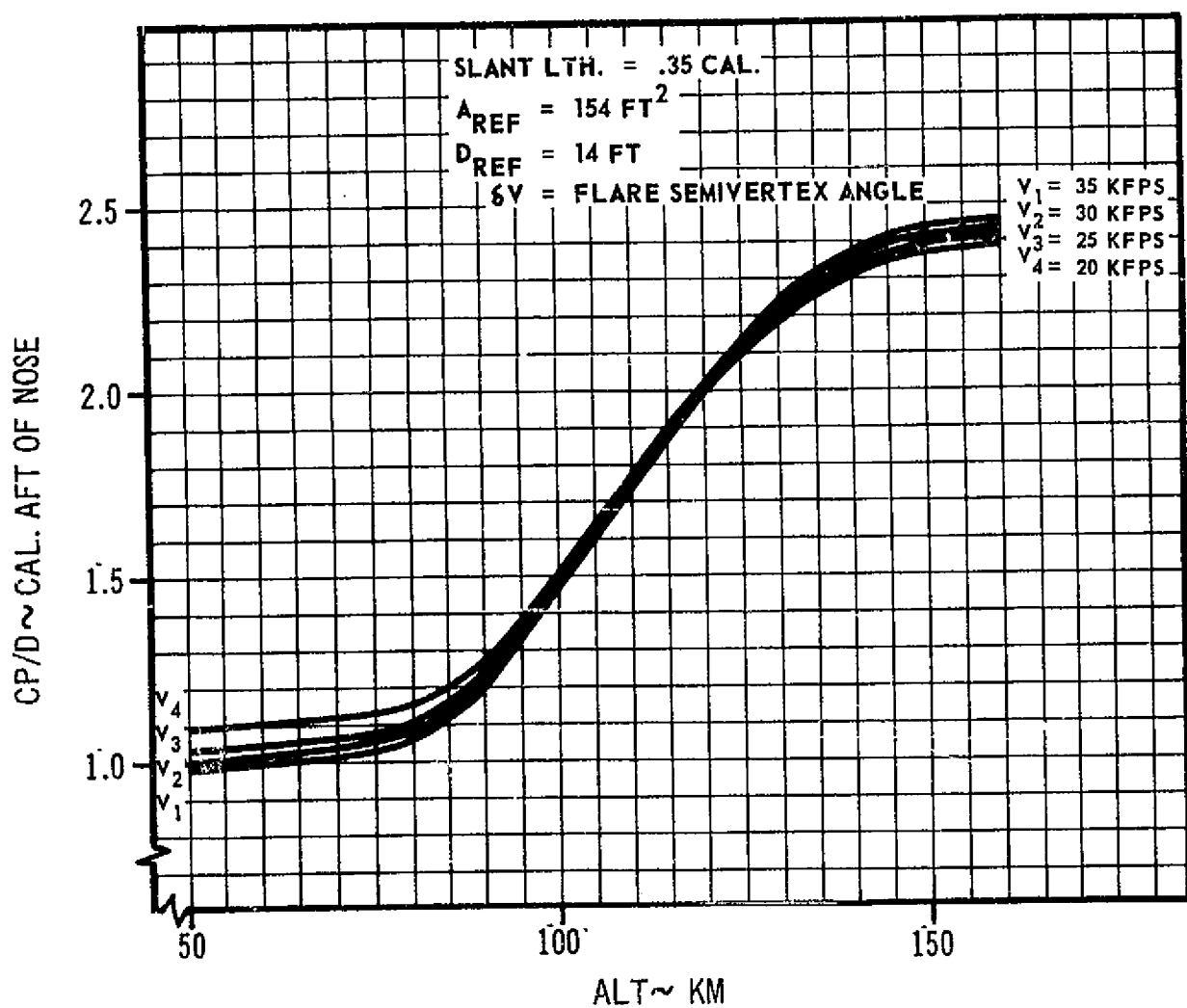
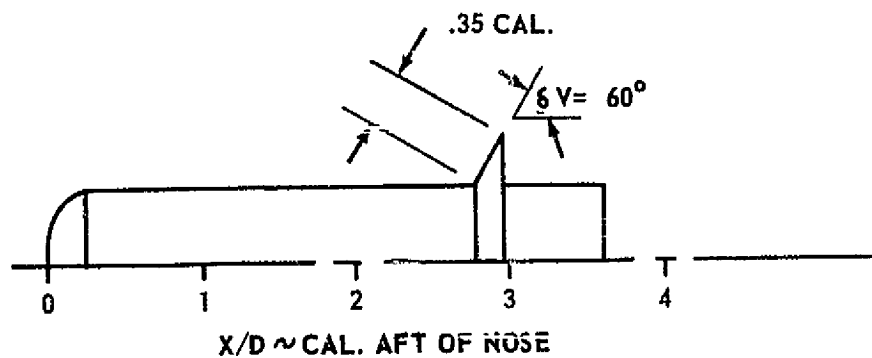


FIGURE A-2.1.2-5: CENTER OF PRESSURE FOR SHORT 60° FLARE #2

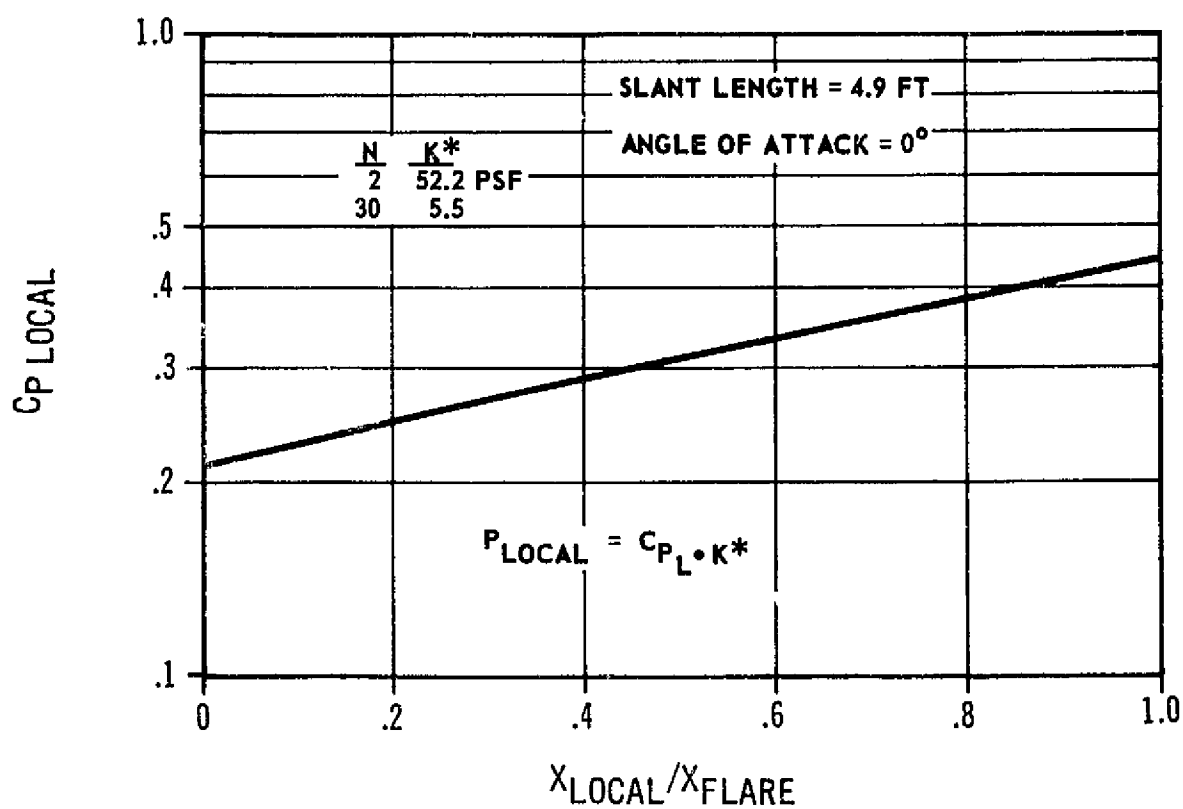
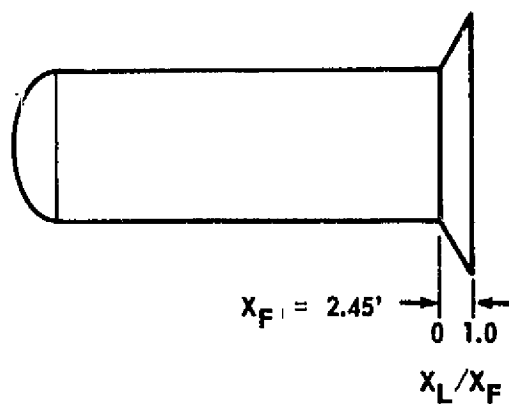


FIGURE A-2.1.2-6: LOCAL PRESSURE COEFFICIENTS OVER SHORT 60° FLARE #2

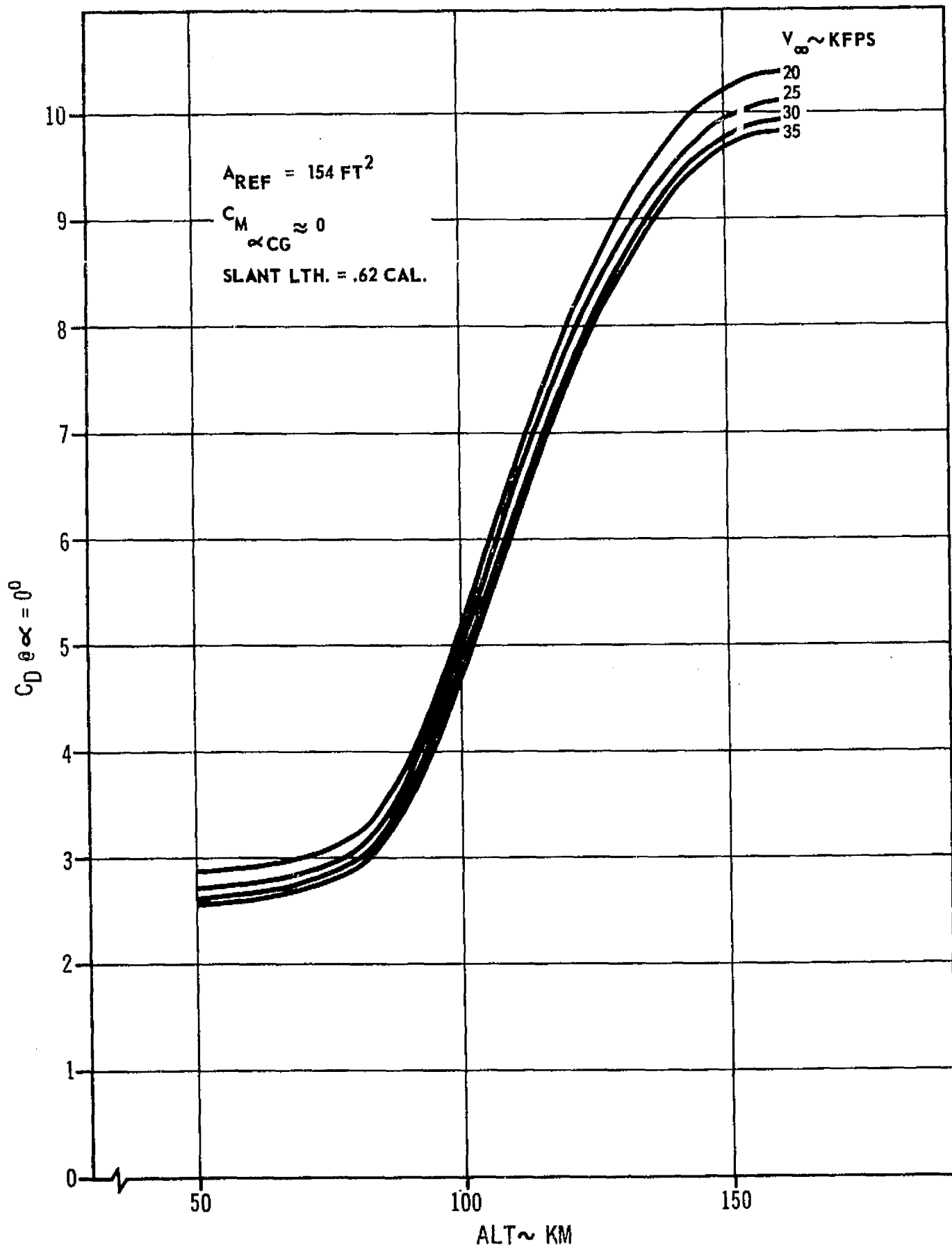


FIGURE A-2.1.2-7: DRAG COEFFICIENTS FOR SHORT 60° FLARE #3

A-2.1.3 Large Flare ($W/C_D A = 2$) Analysis

A spectrum of candidate configurations were sized to produce a ballistic coefficient of approximately 2 psf. The drag characteristics of a candidate $W/C_D A = 2$ psf "ring tail" flare configuration were estimated as a function of altitude in order to determine the importance of rarefied flow effects in increasing the effective configuration drag characteristics. The $C_D = f(h)$ for the candidate configuration is presented in Figure A-2.1.3-1. Based on a preliminary two pass trajectory analysis, a possible reduction in flare planform area of ≈ 10 percent was defined due to rarefied flow effects.

Other configurations were investigated and sized based on the preliminary data for the ring tail flare. Candidate configurations as shown in Figure A-2.1.3-2 above were subjected to a preliminary design analysis to determine the packaging, deployment and retraction feasibility and the astrionic sensors' field-of-view characteristics. The forward facing blunted cone with a flare angle (δv) of 80° was selected. Figure A-2.1.3-3 shows the drag coefficient data for this selected nose flare configuration. Velocity effects on the coefficients of drag were not considered because of the primary objective of determining realistic weights for this very low ballistic coefficient configuration. The local pressure loads are approximately 5.3 psf over the entire area. The nose flare configuration should provide satisfactory static stability over the flight regimes of interest.

A-2.2 CONFIGURATION OPTIONS

This section describes the aerobraking kit design modifications required for the additional missions investigated in the add-on activity. The add-on effort covered a two month technical activity and, therefore, was time restricted to define the feasibility and estimated performance of a few vehicle concepts for a few missions. The design activity was limited to defining reasonable configuration concepts, functional capabilities and weights. No attempt was made to optimize the weight or performance parameters.

The groundrules used for the design portion of the add-on effort are identical to those used in the initial portion of the study and are listed in Section 4.2, Aerobraking Configuration Concepts (basic report).

The aerobraking kit elements consist of:

- a. Aft Heat Shield (Section A-2.2.1)
- b. Sidewall Insulation (Section A-2.2.2)
- c. Reaction Control System (Section A-2.4)

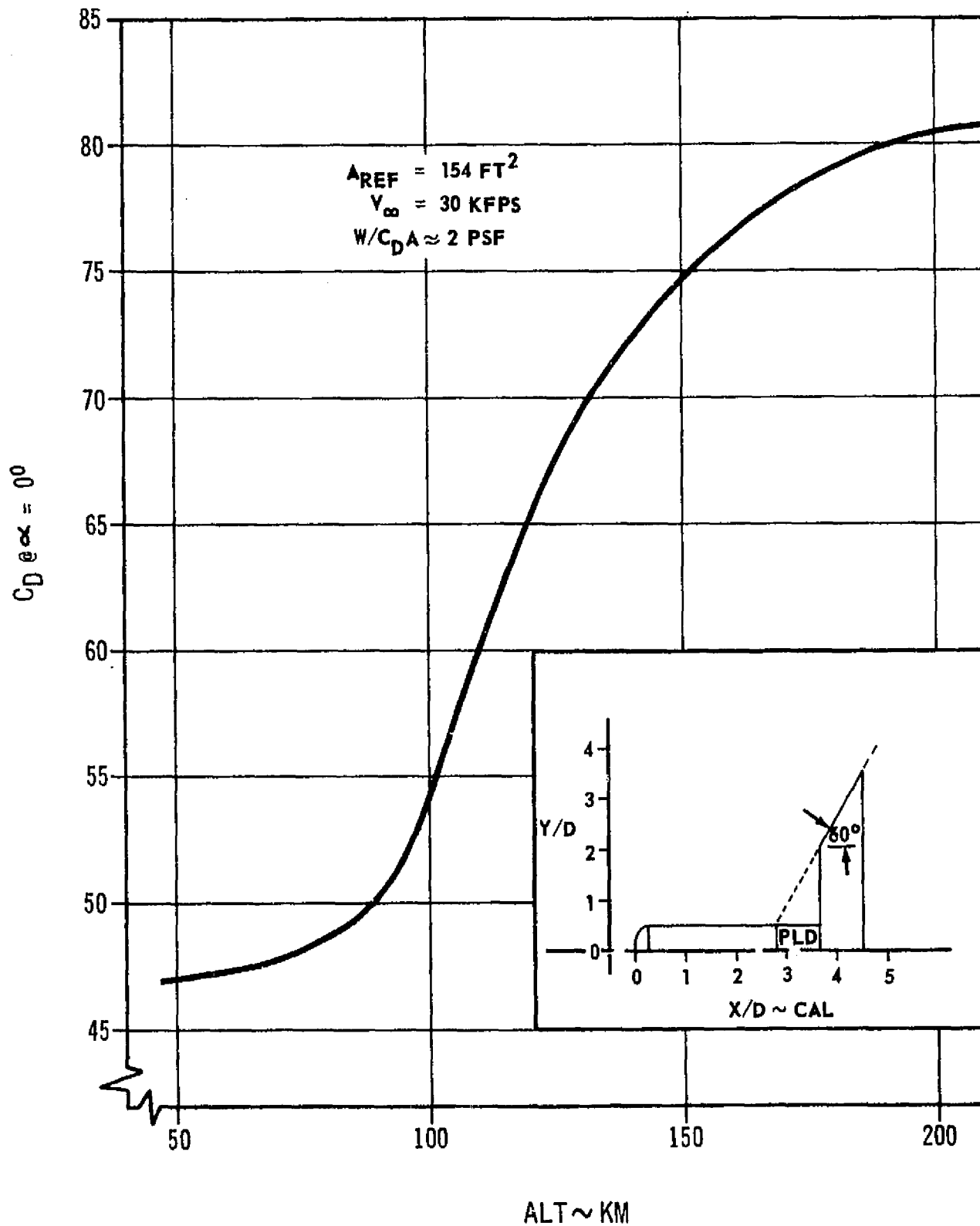
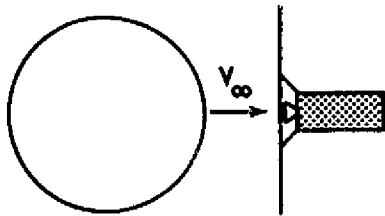


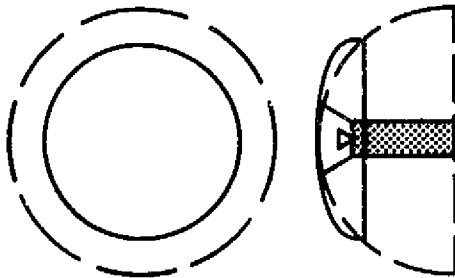
FIGURE A-2.1.3-1: DRAG COEFFICIENTS FOR "RING TAIL" FLARE

APPROX. CONFIG.

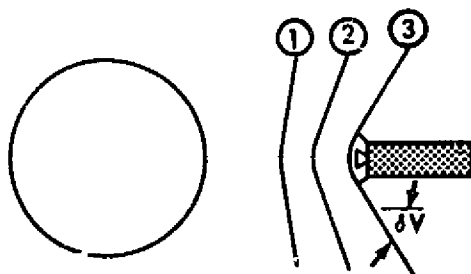
GEOMETRY: SHAPE & SIZE



FLAT DISC DIAM. $\approx 71' \rightarrow 75'$

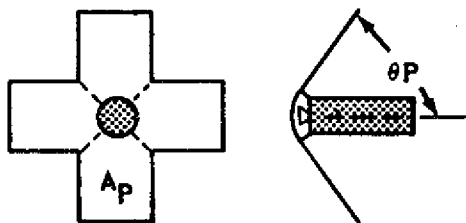


2:1 ELLIPSOID
HEMISPHERE DIAM. $\approx 81'$
DIAM. $\approx 95'$



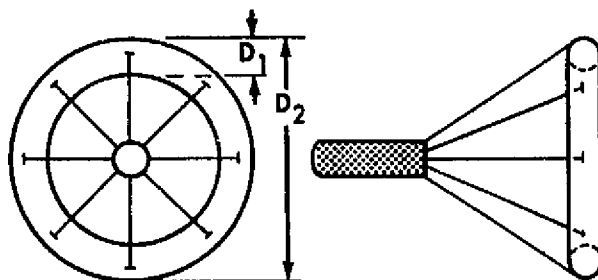
FORWARD
FACING
BLUNTED
CONES

θ	δV	DIAM.
1	80°	72'
2	70°	73'
3	60°	78'



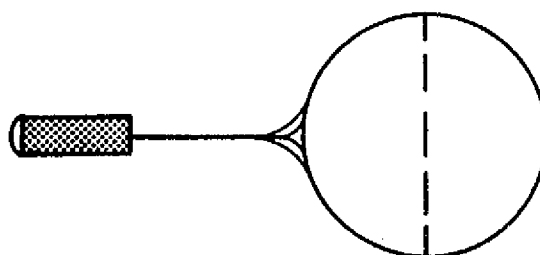
FORWARD
FACING
PANEL

θ_P	A_p RANGE
90°	1080-1200 FT^2
80°	1120-1240 FT^2
70°	1150-1280 FT^2
60°	1270-1410 FT^2



TRAILING
"DONUT"

D_1	$\approx D_2$
10'	192'
20'	96'
30'	64'



TRAILING
SPHERE
(OR HEMI-
SPHERE)

DIAM. $\approx 90'$

FIGURE A-2.1.3-2: CANDIDATE CONFIGURATIONS FOR $W/C_D A = 2 \text{ PSF}$

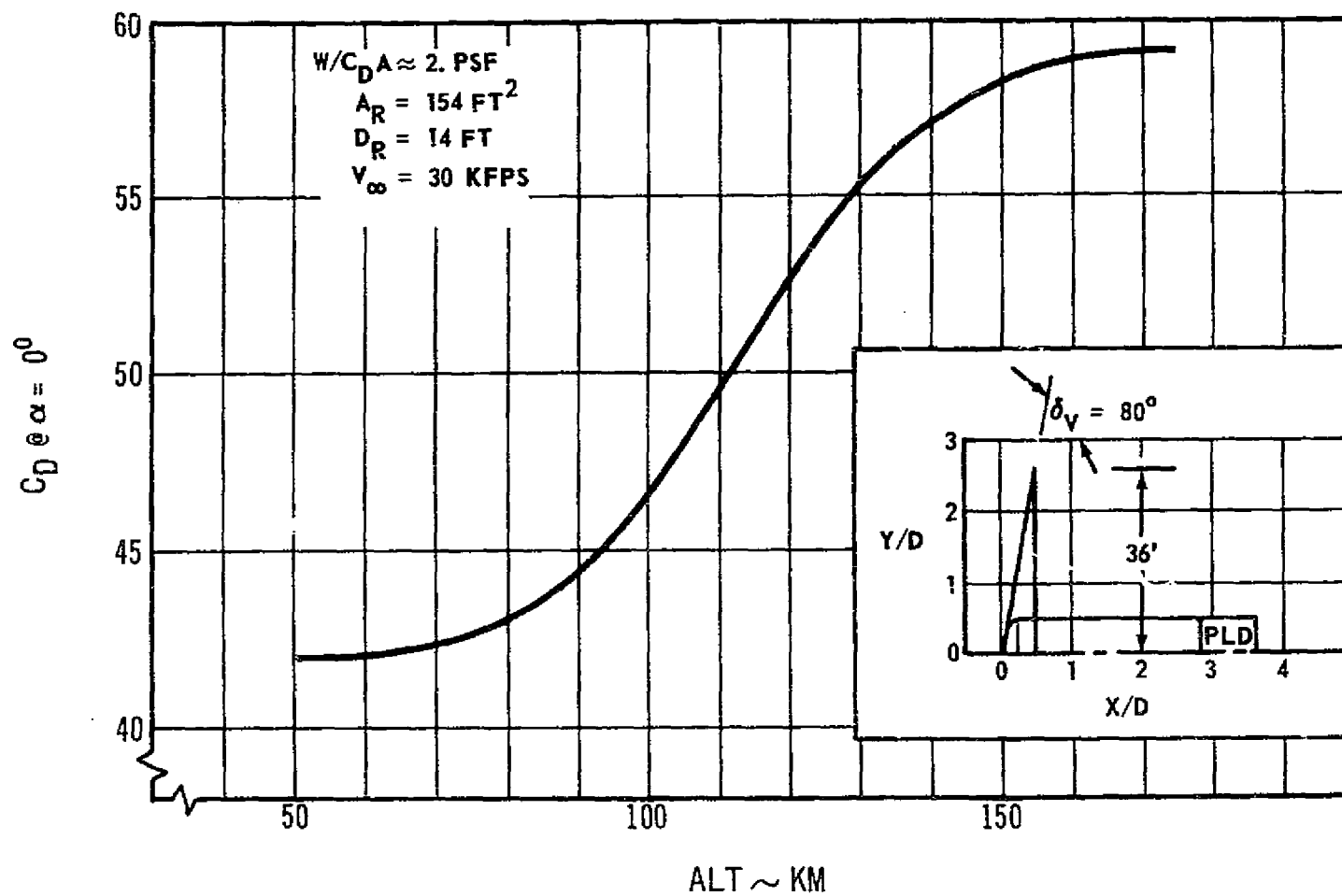


FIGURE A-2.1.3-3: DRAG COEFFICIENTS FOR NOSE FLARE (SELECTED CONFIGURATION)

A-2.2 (Continued)

- d. Astrionics System (Section A-2.6)
- e. Flare (Section A-2.2.3)
- f. Payload Adapters (Section A-2.2.4)

A-2.2.1 Aft Heat Shield

The aft heat shield is required to protect the engine nozzle and engine systems from aerodynamic heating and pressure loads during atmospheric braking. For the longer duration missions, radiative heat shields may be used. However, for short duration missions, an ablative heat shield is required due to the high temperatures encountered. For the three configurations investigated as a part of this add-on activity, the 2 pass mission basic (no flare) Tug and short 60° flare Tug will require an ablative heat shield. The large nose flare (2 pass mission) and the short 60° flare (30 pass mission) will use radiative heat shield concepts identical to that shown in Section 4.2.2, Aerobraking Configuration Concepts (basic report).

The ablative heat shield was designed to be a cold structure, i.e., the backside of the shield was designed to be limited to 300°F. Further, a review of the literature on ablative materials indicated that the fixed heat shield with a nine foot movable cap over the engine nozzle used with the radiative heat shield concept cannot be used for ablative heat shields due to the critical gas flow effects at the movable cap joint. Sealing at this joint appeared to present a difficult design problem. Therefore, the approach selected used a one piece heat shield which had the joint at the aft skirt extension interface. The joint now would be located in the less critical gas flow region and, therefore, the temperatures encountered would be lower.

The ablative heat shield concept is shown in Figure A-2.2.1-1. It consists of a silicon/epoxy ablative (Martin-Marietta ablative material 3560 IIA) over an titanium supporting structure. The ablative thickness varies from 3.3 inches at the center (stagnation point) to 1.0 inches at the interface with the sidewall. The titanium structure consists of, a ring frame at the sidewall joint, a 2:1 elliptical titanium skin .060" thick and 6 supporting titanium angle braces. The actuation system is supported by a set of "I" beam braces located 7.25 feet apart.

The heat shield is opened or closed by a signal to the electrical drive motor. Two driver gears mounted 7.25 feet apart on the drive shaft rotate the two hinge links approximately 82°. During this operation, the dome moves up and away from the ring frame at point C (see figure). The portion of the dome farthest from the hinge slides down the ring frame and disengages the 2 locking clips. After the hinge has rotated the 82°, the complete assembly then rotates about point A (see figure) until the dome can lock into the Tug sidewall at point B (see figure). A solenoid driven pin locks the dome to the sidewall during conventional Tug engine operations. The closure method reverses this process.

A-22

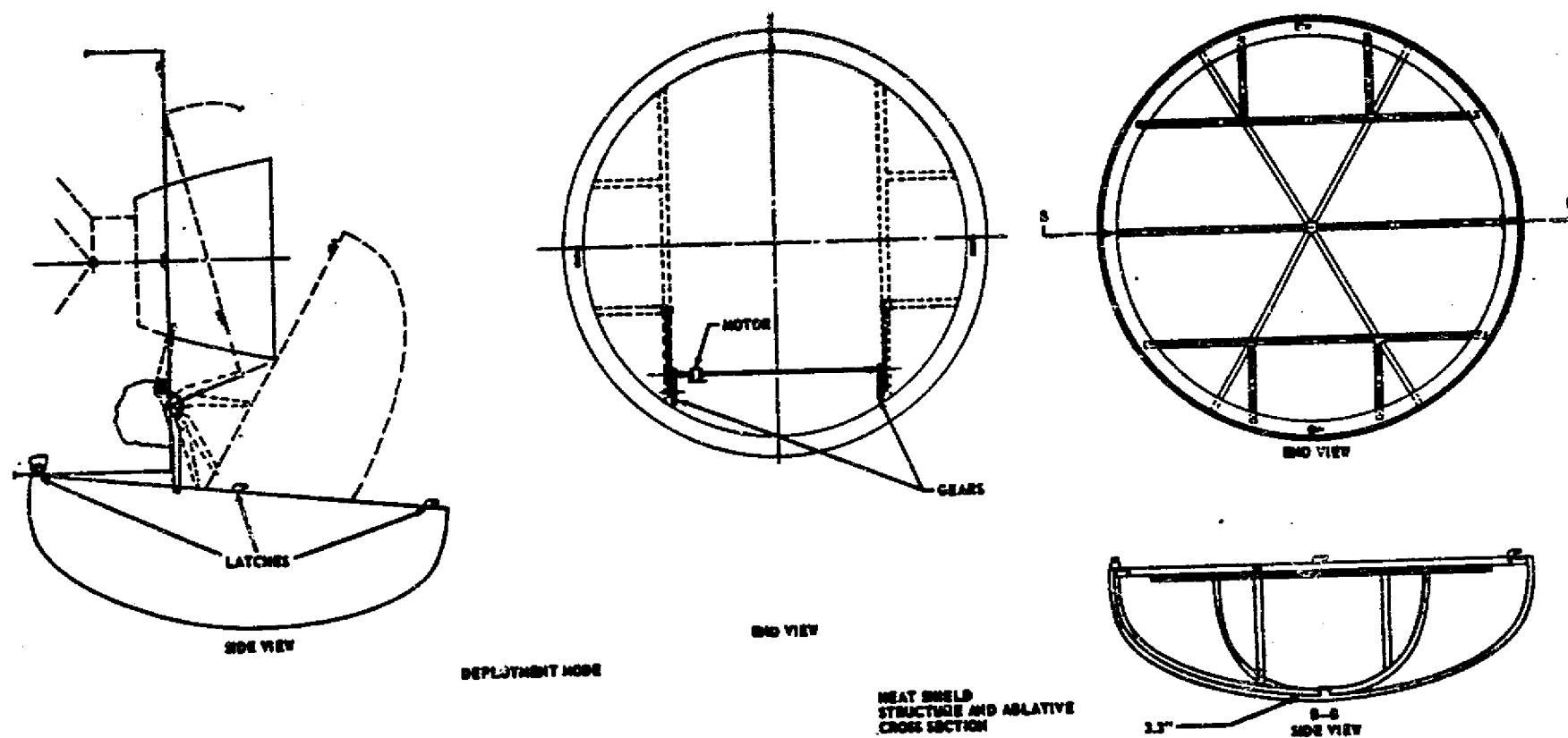


FIGURE A-2.2.1-1: ABLATIVE HEAT SHIELD CONCEPT

DS-17142

A-2.2.1 (Continued)

The location of the heat shield along the side of the Tug will impact the Tug c.g. location and must be compensated for during conventional Tug operations with the gimbaling of the main engine nozzle. This will result in some performance loss.

A-2.2.2 Sidewall Insulation

The sidewall insulation for the longer duration missions (i.e., short 60° flare 30 pass mission) consisted of a titanium outer skin over a microquartz insulation. The thickness of microquartz was designed to maintain 400°F at the micrometeoroid shield located under the microquartz. The temperature of the Tug sidewall decreases going from the heat shield/cylindrical wall joint toward the payload. The microquartz insulation thickness is tapered downward accordingly.

For the large nose flare, the flare shields the sidewall and no sidewall thermal protection is required.

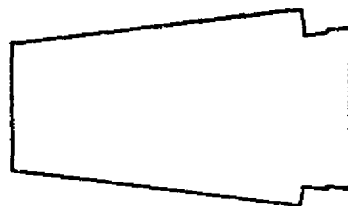
For the basic (no flare) Tug and the short 60° flare configuration (when used in a 2 pass mission mode), the sidewall temperatures exceed the titanium outer foil capabilities and L-605, a Haynes cobalt alloy replaces the titanium. The temperature on the payload exceeds 300°F and must be thermally protected. The sidewall TPS is extended to cover these areas. A payload aft closure must be provided also. A cover of aluminum (facing the payload) bonded to microquartz which in turn is covered by L-605 outer foil may be used.

A-2.2.3 Flare

Two of the three configurations investigated in this add-on study employed flares to increase the drag and to provide some improvement in static stability.

The short 60° flare used for the 2 pass and 30 pass missions were designed to use much of the flare concept proposed in Section 4.2.2.3 (basic report). The thermal environments range from approximately 850°F (30 pass mission) to approximately 1500°F (2 pass mission). The previously selected material, Inconel 718, may be used for both flare concepts as the inconel has temperature capabilities which exceed the temperatures encountered. The support struts may be titanium as the temperature directly beneath the flare will not exceed titanium's capability.

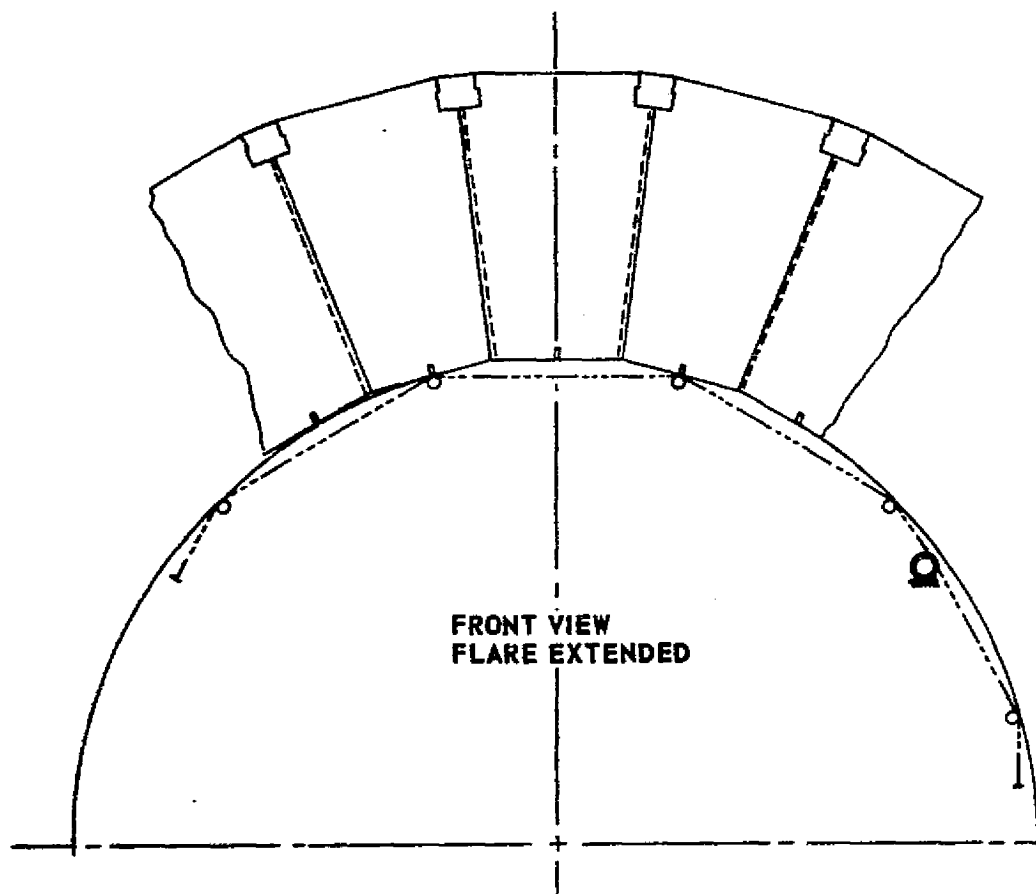
The short 60° flare concept, as shown in Figure A-2.2.3-1, will consist of 24 large panels (.020 inches thick) and 24 small panels. The 4.9 foot long flare is elevated to a 60° angle by the support strut. The 12 support struts are elevated in turn by threaded rods and followers. A reversible drive motor, a drive chain and 12 drive sprockets provide the actuation for the support struts. The flare is hinged at the payload adapter/astrionics module joint. Ring frames in the payload



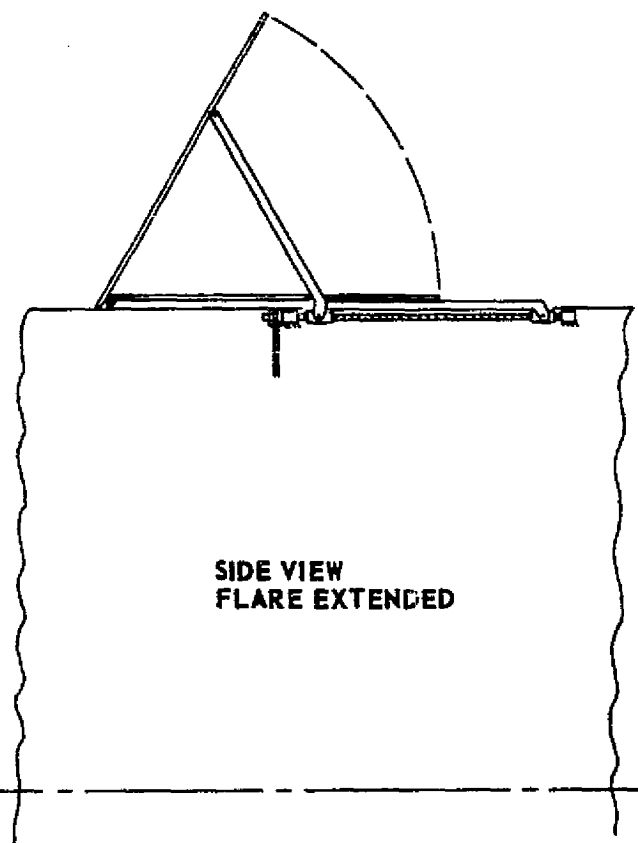
**FLARE PANEL
(24 REQ'D.)**



**FLARE INSERT
(24 REQ'D.)**



**FRONT VIEW
FLARE EXTENDED**



**SIDE VIEW
FLARE EXTENDED**

Figure A-2.2.3-1: SHORT 60° FLARE CONCEPT

A-2.2.3 (Continued)

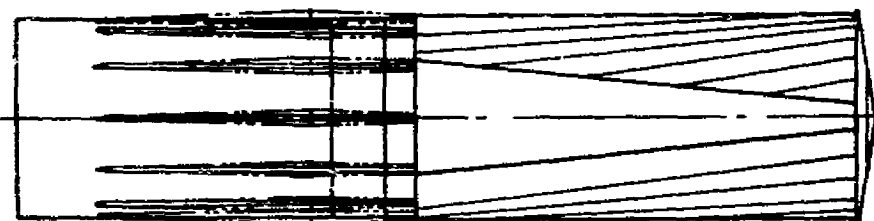
adapter and located at forward payload adapter face and at the support threaded rod act as "stops" to counteract flare loads. The flare when retracted will overlap the large panels. At the ends of the panels where the panel circumference is significantly larger than the Tug circumference, the smaller panels fold under the large panels to facilitate packaging of the Tug with flare into a 15 foot diameter Shuttle cargo bay constraint.

The large nose flare concept is a unique design to provide a ballistic coefficient of approximate 2 pounds per square foot. For this concept, the flare was placed forward of the propulsion module so that it could be combined with the heat shield to form a continuous forward aerodynamic flare as shown in Figure A-2.2.3-2. The temperatures encountered with the large flare are approximately 1350 to 1400°F and will permit the use of a radiative heat shield of Rene' 41. The large nose flare, however, does present a difficult packaging problem. When extended to its 80° angle, the flare is approximately 72 feet in diameter. This large flare must be folded (with considerable overlapping of panels) to allow it to fit within the Shuttle bay. The concept, as shown in Figure A-2.2.3-3, has 24 flare panels, 29 feet long. The panels are hinged to the Tug at the start of the cylindrical section of the propulsion module. The panels are tapered to provide minimum overlap at the forward end and sufficient surface to meet the large areas at the aft end of the flare. The flare panels are extended first and then the support system is positioned behind, but not connected to the flare panels. The nose section of the large nose flare corresponds to the radiative heat shields design. (See Section 4.2.2, Figure 4.2.2.1-1, Aft Heat Shield, basic report).

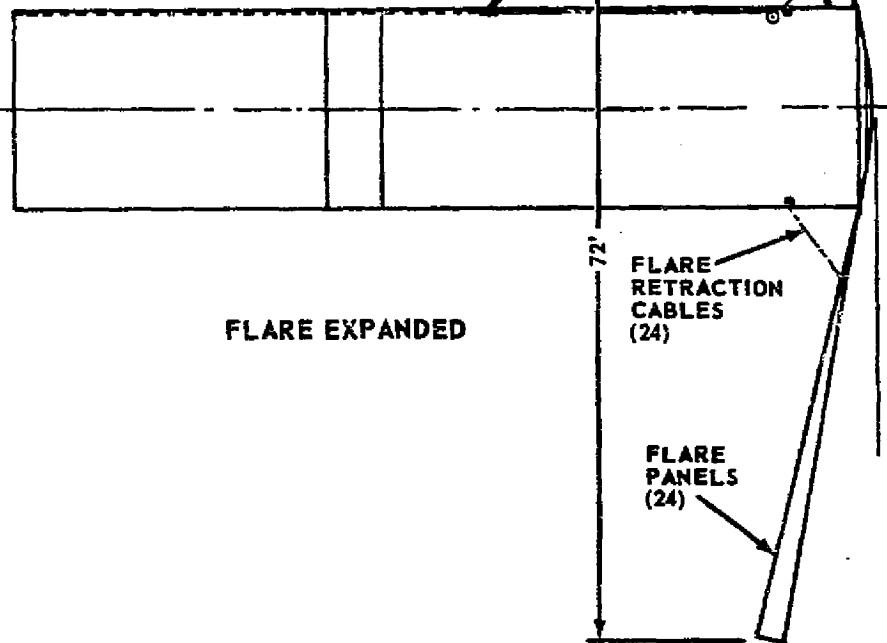
The flare panels are folded in 3 packets of 8 panels each (24 total). As shown in Figure A-2.2.2-3 on flare deployment sequence, three panels, 120° apart are deployed first. All of the panels have a lip along longitudinal edges which permit the panels to innerconnect. The lips also will facilitate the first set of panels to release the second set of panels, etc.

After all of the panels have been released, the support system is activated. The support system consists of 12 support rods equally spaced. Each rod extends down the length of the Tug sidewall when retracted. When extended, the aft portion of each of the 12 rods is pulled forward by a motor driven cable system. The aft rod is 30 feet long, 2" o.d. aluminum tubing. The forward leg is a 1-1/4" o.d. aluminum tubing rod. The upper hinge point between the forward and aft rod has a 1/16" diameter steel cable which is connected to each of the other support legs at their hinge point. The rods plus the cables thus provide support to the extended flare. Because of the loads, each of the 12 aft support legs will require a tripod support at their mid-point approximately 3 inches out from the center of the support rod. Steel cable will run over the tripod from the front to the back of the support rod.

A-26



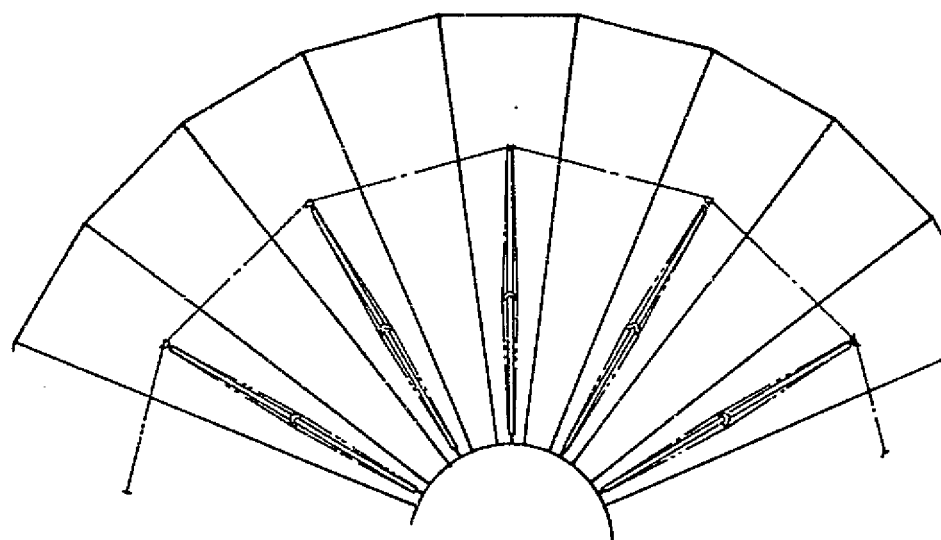
FLARE RETRACTED



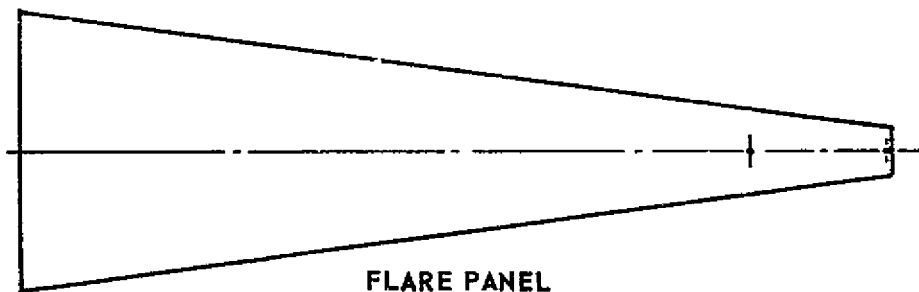
FLARE EXPANDED

FIGURE A-2.2.3-2: LARGE NOSE FLARE CONCEPT

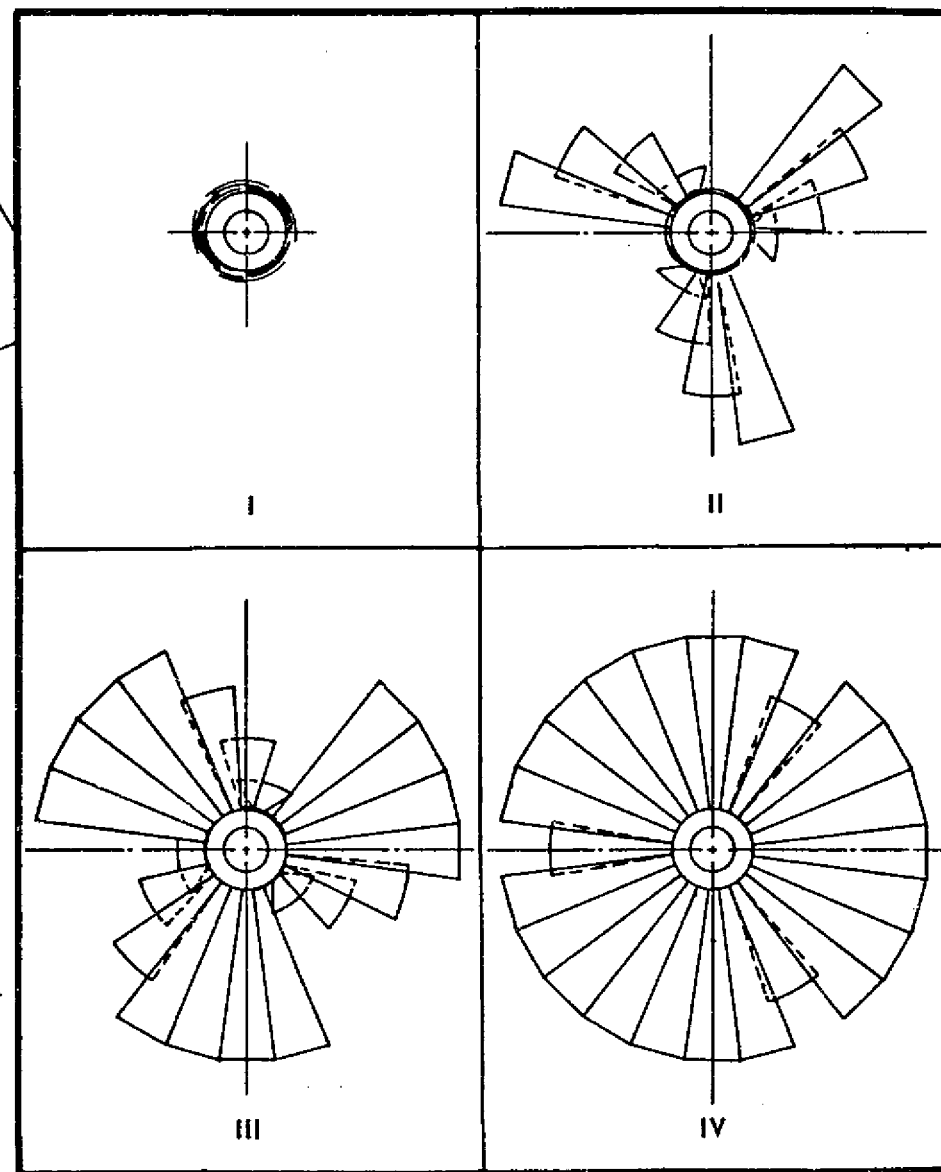
DS-17142



FLARE EXTENDED
AFT VIEW



FLARE PANEL
(24 REQ'D.)



FLARE DEPLOYMENT SEQUENCE

FIGURE A-2.2.3-3: LARGE NOSE FLARE DEPLOYMENT/RETRACTION

A-2.2.3 (Continued)

The retraction method is as follows. First, the support rods are retracted. The retracted rods can be spaced to fit between the astronics sensor system parts so as not to hamper guidance visibility requirements. After the support system has been retracted, the flare panels can be retracted. Each of the panels will have a steel cable connected to the back side of the panels. These cables are retracted sequentially which in turn retract the panels. The above design for a large nose flare for the Tug is only of several possible alternatives investigated to reduce the ballistic coefficient. Others may offer lower weight and should be investigated in future studies. One of these alternatives is the use of a large "doughnut" attached aft of the Tug and tied to the Tug by cabling. This mode permits a very large flare which can reduce the temperature on the flare to where light weight plastic and/or silicon rubber materials may be used. Two of the key problems associated with this concept are (1) packaging the flare within the Shuttle dimensional constraints and (2) providing rigidity to the "doughnut" flare during maneuvers.

Another concept which appears feasible is to employ a forward brake with an integrated dome concept. A very thin mesh material which can be extended into an umbrella like configuration provides a low weight drag structure. The material is held in place by the use of a torus shape inflatable ring located at the end of the umbrella mesh material. The end of the mesh material is wrapped over the ring and its interior is insulated to protect the ring. The ring is pressurized by helium or hydrogen to a pressure of approximately 9.2 psi. The ring is held in position by a series of cables extending from the ring to the Tug sidewall similar to the spokes on a bicycle wheel. This concept, while offering light weight, requires a complex retraction system. However, the reduced weight potential presents a valid reason for further investigation of this concept and a preliminary analyses of the data is shown in Appendix F.

A-2.2.4 Payload Adapter

The payload adapter configuration for the 2 pass missions is identical to that proposed in Section 4.2.2.4 (basic report). The thermal protection systems for the payload adapter were described in Paragraph A-2.2.2 above.

A-2.3 TRAJECTORY ANALYSIS

The trajectory data generated in the add-on activity consisted of the following:

- o Two and 30 pass trajectories for the short 60° flare (#2) configuration with the same W/C_DA as the 30° flare.

A-2.3 (Continued)

- o Two and 30 pass trajectories for the short 60° flare (#3) configuration sized for neutral static stability.
- o Two pass trajectories for the large "ring tail" and "nose" flares ($W/C_D A \approx 2$).

The assumptions, groundrules and methodology used were the same as reported in Section 4.3 (basic report). The effects of atmospheric and gravitational perturbations on the configurations or number of passes listed above were not considered in the add-on activity.

The two pass basic (no flare) trajectory data was generated during the initial study activity. Figure 4.3.3.0-1 (basic report) shows that the basic (no flare) initial target perigee altitude for the two pass mission is approximately 233,000 feet. The aerobraking return time is approximately 0.39 days (the same as other two pass configurations).

The drag coefficients used throughout the entire study (including the add-on activity) are not constant but depend on altitude and velocity. The equivalent $W/C_D A$ was defined to aid in the comparison of the configurations. Equivalent $W/C_D A$ of a configuration is that constant $W/C_D A$, not a function of altitude or velocity, which would produce the same initial perigee for a given number of passes as the actual $W/C_D A$.

A-2.3.1 Short 60° Flare Analysis

Figure A-2.3.1-1 shows the maximum dynamic pressures for the two short 60° flare configurations (#2 and #3). The two pass data is plotted as small circles (2nd pass values). The 30 pass data is plotted as solid lines and indicates the normal trend of maximum dynamic pressure occurring on the last pass. The two pass values are approximately ten times greater than the maximums experienced during the 30 pass mission.

The initial perigee altitude for these two configurations and the two mission durations are shown in Figure A-2.3.1-2 below.

CONFIGURATION/ NO. OF PASSES	INITIAL PERIGEE ALTITUDE (FEET)
<u>Short 60° #2</u>	
2	241,000
30	298,000
<u>Short 60° #3</u>	
2	251,000
30	308,000

Figure A-2.3.1-2 SHORT 60° FLARE INITIAL PERIGEE ALTITUDES

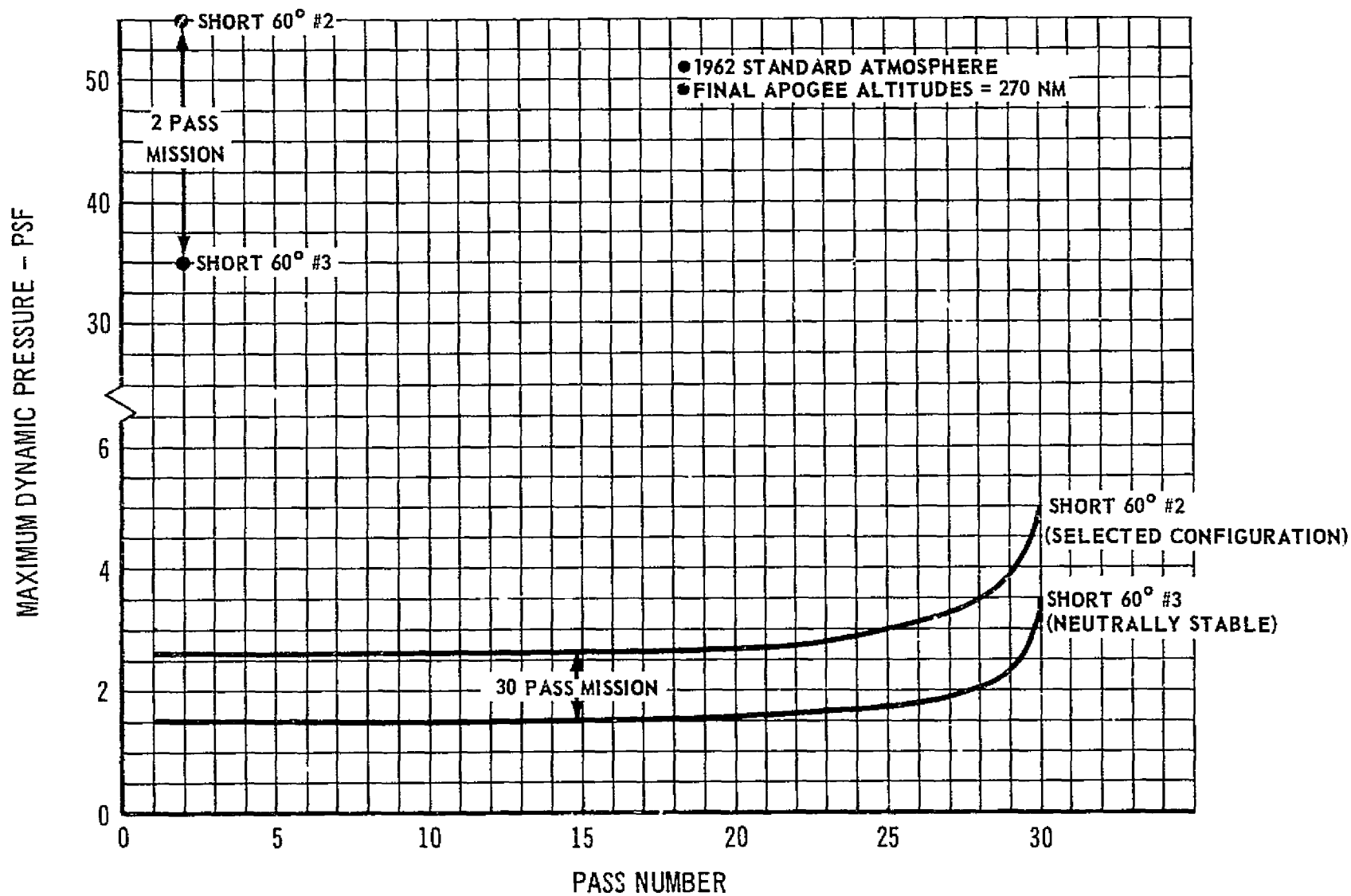


FIGURE A-2.3.1-1: SHORT 60° FLARE MAXIMUM DYNAMIC PRESSURE

A-2.3.2 Large Flare Analysis ($W/C_D A \approx 2$)

As discussed in Section A-2.1 above, the "ring tail" flare was used as the initial candidate large flare to determine the flow regime effects. This flare had an initial perigee altitude of approximately 302,000 feet (two pass mission). The maximum dynamic pressure encountered on the second pass was 2 psf. The "ring tail" flare had an actual equivalent $W/C_D A$ of 1.78 psf which indicated that the size of such a flare could be reduced to obtain the desired value of 2 psf.

The two pass nose flare configuration had an initial perigee altitude of 300,000 feet and a 2nd pass maximum dynamic pressure of 2.5 psf. The actual equivalent $W/C_D A$ value was 2.02 psf.

A-2.3.3 Equivalent Ballistic Coefficient Comparison

Figure A-2.3.3-1 shows a summation of the equivalent ballistic coefficients and the initial perigee altitudes for the configurations used in the overall study. Data from the main study is cross plotted with the new add-on activity data for comparison. The equivalent $W/C_D A$'s for any particular configuration are functions of the number of passes in the mission. In general, the equivalent $W/C_D A$ value for a configuration increases with decreased trip times. For example, the 45° flare has an equivalent $W/C_D A$ of 12.5 for 60 passes and 22 for two passes.

The short 60° flare (#2) and the 30° flare have nearly equivalent drag characteristics in terms of initial perigee altitude and equivalent $W/C_D A$ for the 2 and 30 pass missions. The selection of this short 60° flare conforms to the desired flare $W/C_D A$ comparison analysis activity planned for this study.

A-2.4 CONTROL ANALYSIS

A control analysis was conducted on the short 60° flare (#2) for the 2 and 30 pass missions, the basic Tug 2 pass mission, and on the large nose flare for the 2 pass mission. The assumptions, groundrules and methodology reported in Section 4.4 (basic report) were utilized in the add-on activity.

The short 60° flare is statically unstable. The Reaction Control System (RCS) was utilized to provide the required stability similar to that reported for the basic (no flare) configuration in Section 4.4 (basic report).

The basic (no flare) configuration's 2 pass maximum aeromoment was greater than the current 200 pound RCS thrusters could overcome. Therefore, the pitch/yaw RCS thrusters were resized to 250 pounds each (for the two pass basic configuration only). This increase in thrust level was sufficient to offset the aeromoment.

1962 US STAND. ATMOS.
 FINAL APOGEE ALTITUDE = 270 NM
 CONSTANT $W/C_D A$ RETURN FROM SYNC ORBIT

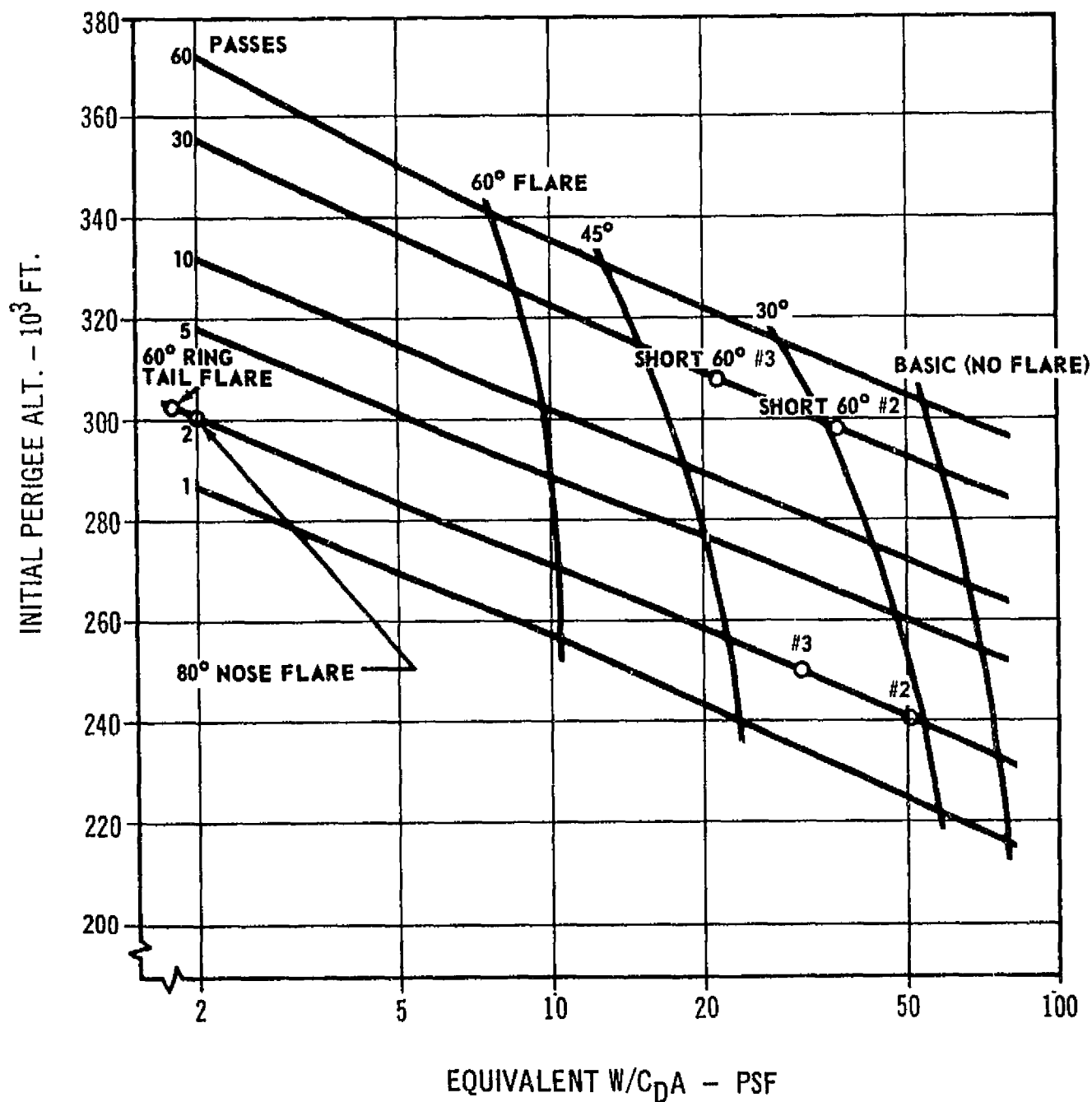


FIGURE A-2.3.3-1: EQUIVALENT $W/C_D A$ VALUES

A-2.4 (Continued)

The large nose flare configuration is statically stable. The RCS, for this configuration, was only required to provide the limit cycle and directional control impulses.

Figure A-2.4.0-1 shows the RCS propellant consumptions for the three configurations.

A-2.5 THERMAL ANALYSIS

The thermal analysis was conducted on the following configurations:

- o Basic (No Flare) - 2 passes
- o Short 60° Flare (#2) - 2 and 30 passes
- o Large Nose Flare - 2 passes

The assumptions, groundrules and methodology used in the add-on activity were extensions of those reported in Section 4.5 (basic report). The CHAP computer program also has the capability of accommodating ablative materials, such as the ESA-3560 IIA selected for the 2 pass mission basic (no flare) and short 60° flare aft heat shields.

A-2.5.1 Heating Rates

Figure A-2.5.1-1 shows the heating rate distribution for the 2 pass basic (no flare) configuration. Figures A-2.5.1-2 and -3 show similar data for the 2 and 30 pass short 60° flare. Figure A-2.5.1-4 illustrates the very low heating rates associated with the 2 pass low W/C_DA nose flare.

A-2.5.2 Maximum Equilibrium Temperatures

Figure A-2.5.2-1 shows the maximum equilibrium temperatures for the three configurations. The 2 pass basic (no flare) configuration's nose temperature (A) exceeds the limit for all re-radiative materials discussed in Section 4.7 (basic report). This high temperature, in conjunction with the high heating rates and total heat input shown in prior Figure A-2.5.1-1, established the criteria for the selection of the relatively dense ablative material for the aft heat shield. The sidewall and payload temperatures of the 2 pass basic (no flare) configuration are also higher, requiring more insulation and a heavier insulation outer foil (L605 Haynes rather than Titanium).

The short 60° flare has lower temperatures on the nose and along the sidewalls than the basic (no flare) configuration. The 2 pass short 60° flare has an ablative heat shield to withstand the 3290 degree temperature. It also uses the L605 Haynes alloy as the sidewall insulation outer foil (2 passes). This short 4.9 foot flare does not provide the environmental protection to the payload area that the other (larger) flares (basic report) provided. Therefore, insulation in this

CONFIGURATION	STATIC STABILITY	RCS PROPELLANT CONSUMED (LBS.)	
		2 PASS	30 PASS
Short 60° Flare	Unstable	256	271
Basic (No Flare)	Unstable	516 (250 lb. Thrusters)	620 (200 lb. Thrusters)
Nose Flare	Stable	6	----

Figure A-2.4.0-1 RCS Propellant Consumption

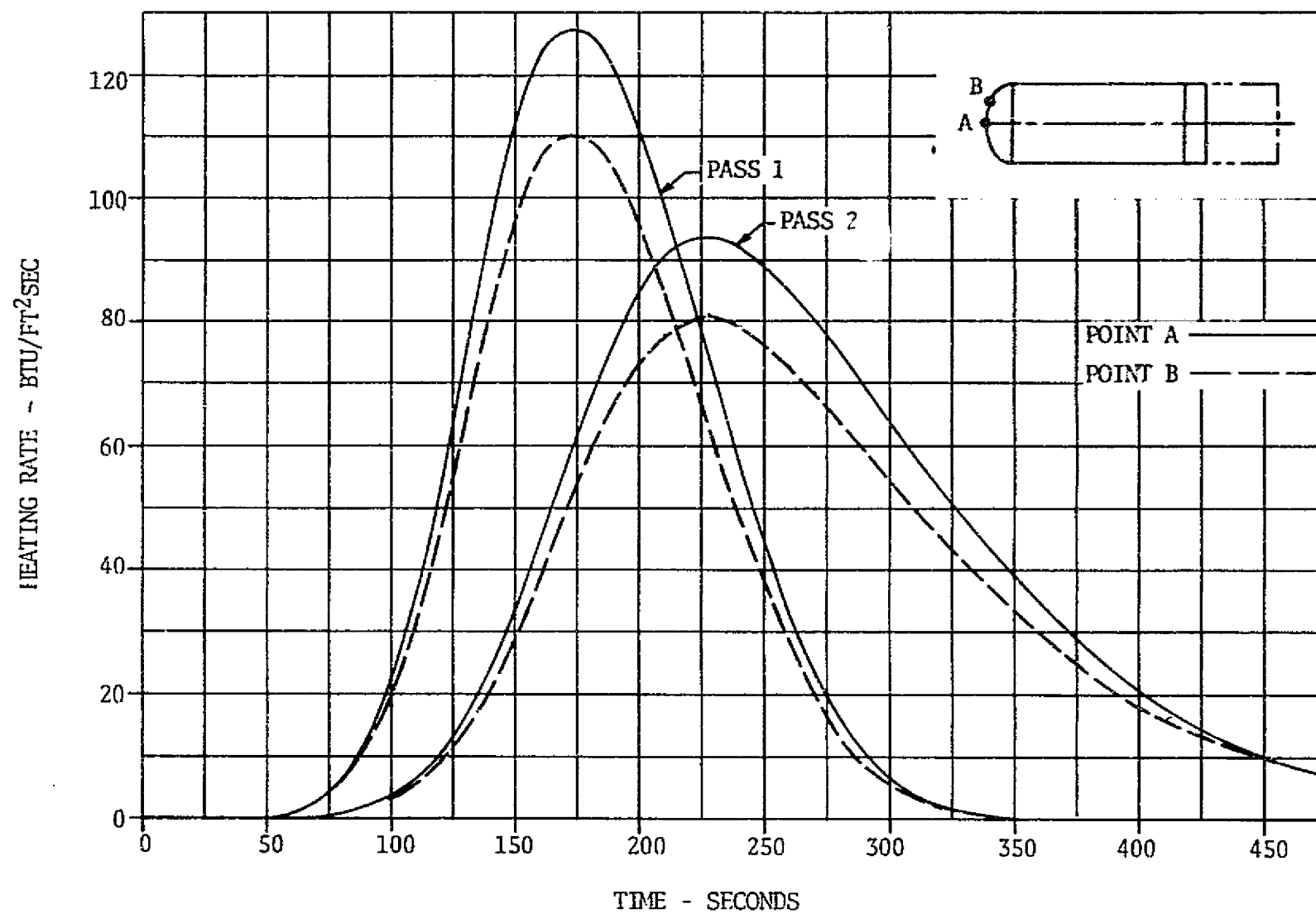


FIGURE A-2.5.1-1 HEATING RATE DISTRIBUTION - BASIC CONFIGURATION (2-PASS)

D5-17142

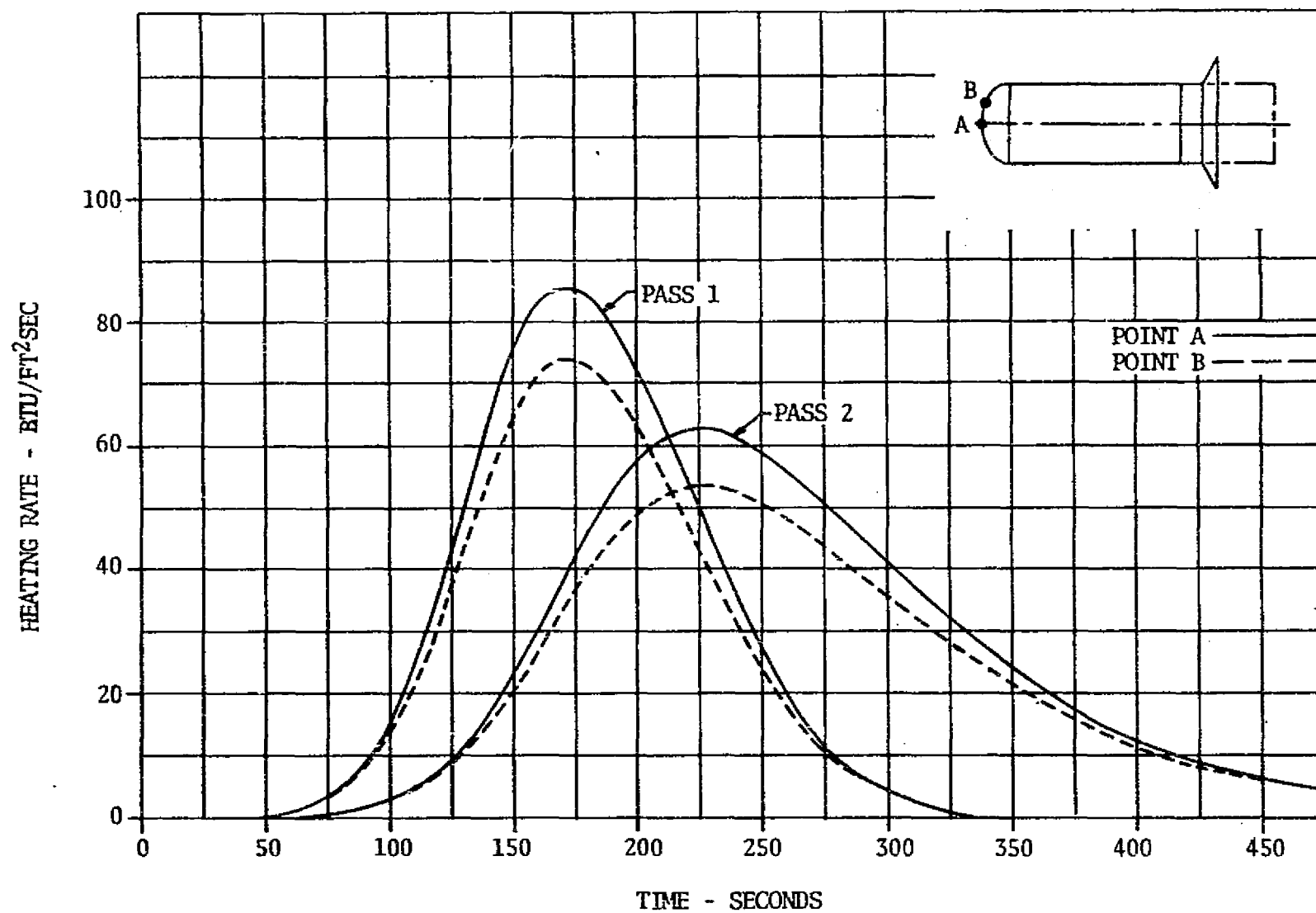


FIGURE A-2.5.1-2 HEATING RATE DISTRIBUTION - 60° SHORT FLARE (2-PASS)

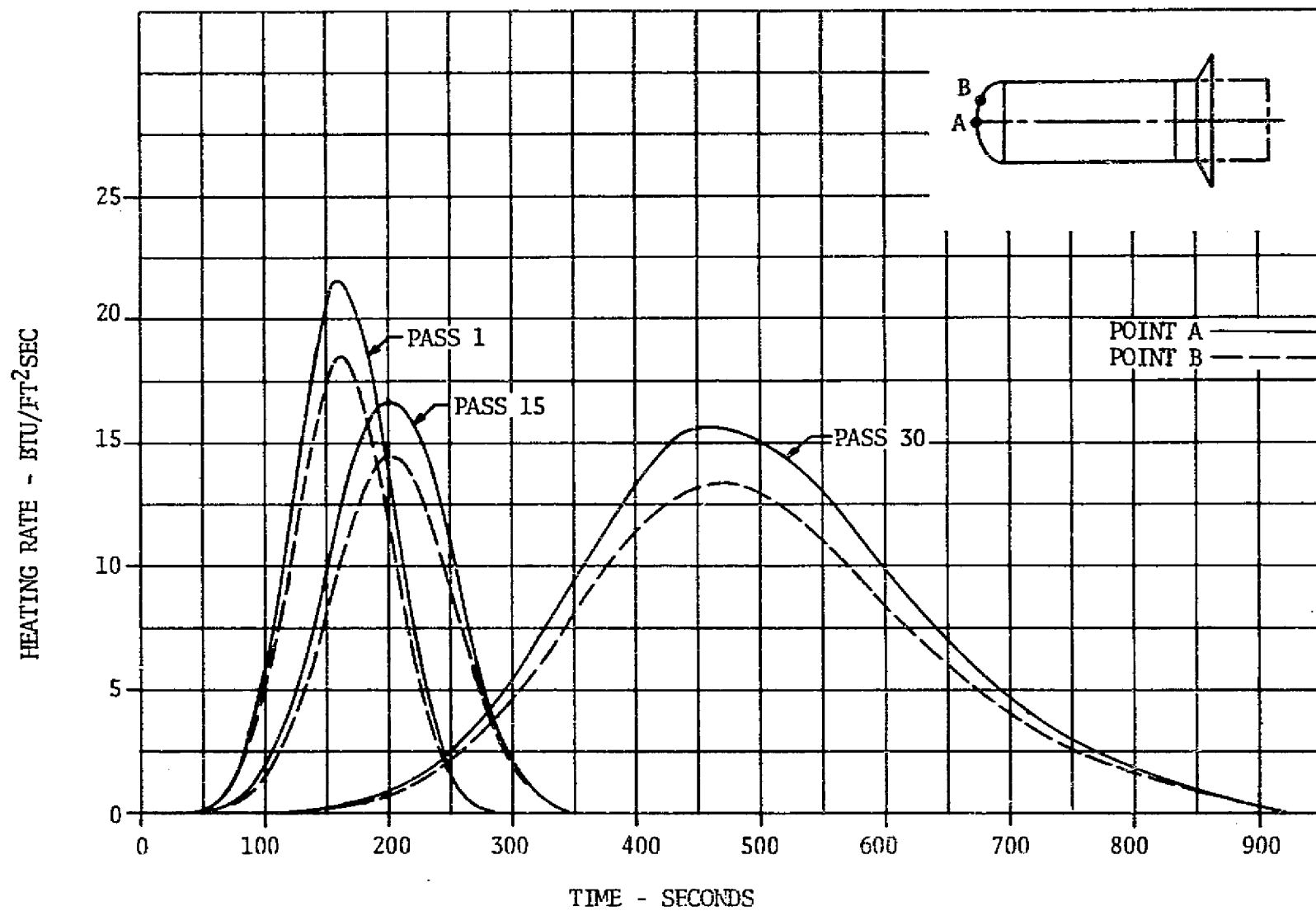


FIGURE A-2.5.1-3 HEATING RATE DISTRIBUTION - 60° SHORT FLAPE (30-PASS)

05-17142

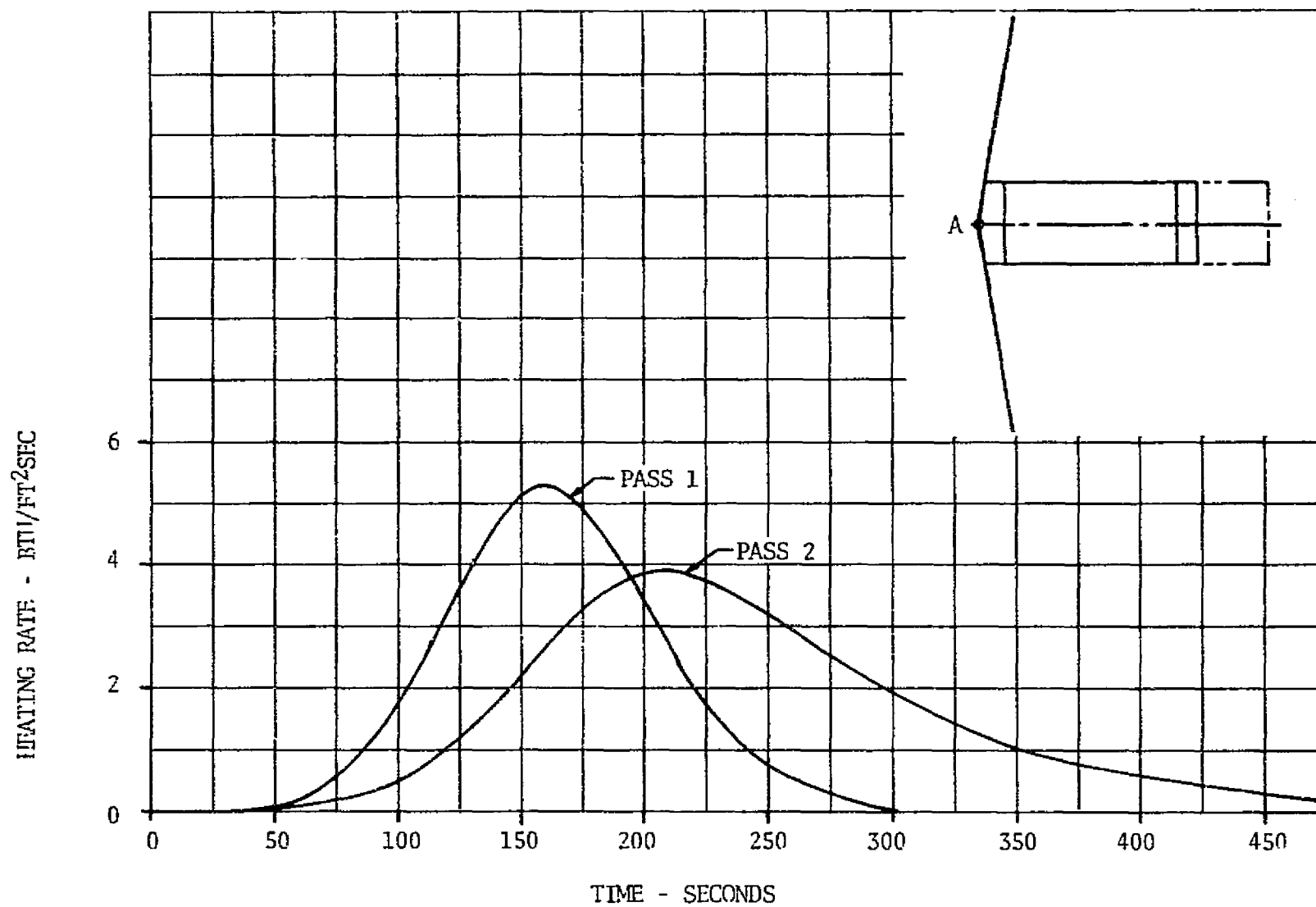
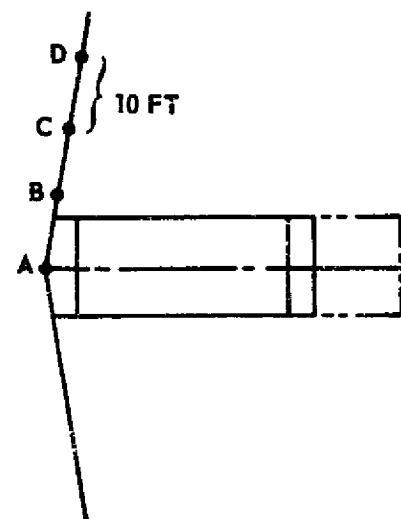
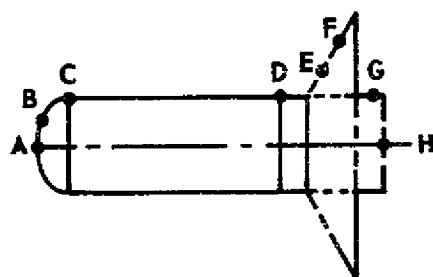


FIGURE A-2.5.1-4 HEATING RATE DISTRIBUTION - LARGE FLARE (2-PASS)



CONFIGURATION	TRAJECTORY	MAXIMUM EQUILIBRIUM TEMPERATURE (°F)							
		A	B	C	D	E	F	G	H
BASIC (NO FLARE)	2-PASS	3680	3520	1789	1275	—	—	1170	779
SHORT 60° FLARE	2-PASS	3290	3140	1570	1240	1490	1527	1138	758
SHORT 60° FLARE	30-PASS	2120	2070	980	748	856	889	687	458
LARGE NOSE FLARE	2-PASS	1410	1403	1380	1337	—	—	—	—

FIGURE A-2.5.2-1: MAXIMUM EQUILIBRIUM TEMPERATURES

A-2.5.2 (Continued)

region is provided similar to that described for the basic (no flare) in Section 4.2 (basic report).

A-2.5.3 Thermal Protection System

The aft heat shield ablative material thicknesses are shown in Figure A-2.5.3-1. The material thickness was based on 11,500 BTU's input on the first pass and 13,500 BTU's input on the second pass. To this, sufficient ablative material was used to obtain a 300°F temperature on the titanium support structure. The insulation was tapered to match the lower heat input on the dome as the contour matches the sidewall.

Figure A-2.5.3-2 shows the sidewall insulation thicknesses required for the 2 pass basic (no flare) and short 60° flare configurations. As discussed in A-2.5.2 above, the sidewall insulation extends the entire length of the Tug sidewall including the payload to ensure that the maximum payload temperature does not exceed 300°F. The micrometeoroid shield of the Tug stage is protected to 400°F. The insulation material utilized is the same microquartz as reported in Section 4.2 (basic report).

The weight statement for the thermal protection system is shown in Figure A-2.5.3-3. The 2 pass basic (no flare) and short 60° flare configurations required extensive thermal protection and this is reflected in their relatively heavy TPS weights of 3240 and 3125 pounds, respectively.

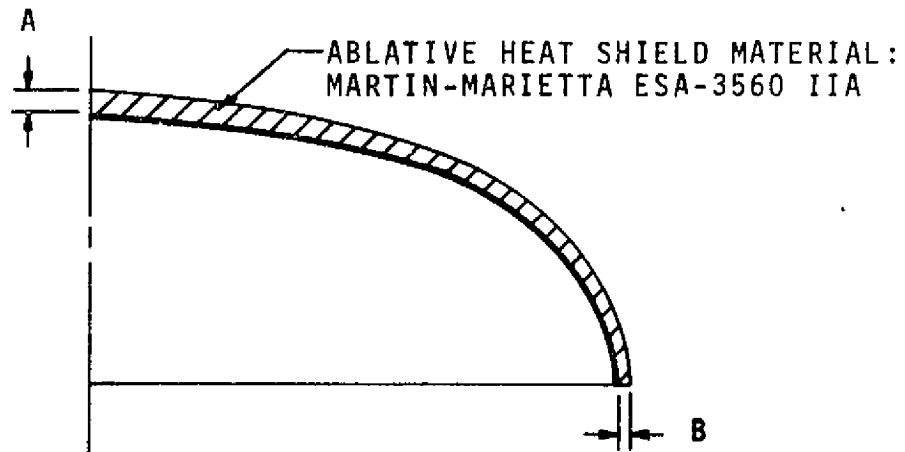
The large nose flare effectively protects the remainder of the Tug and payload and, therefore, no thermal protection system penalty is incurred for this configuration.

A-2.6 ASTRIONICS ANALYSIS

No additional astrionics analysis was accomplished during the add-on activity. The astrionic configuration and weights are shown in Section 4.6 (basic report). Section 4.6.4.5 (basic report) discusses a "quick-look" assessment of the one pass mission. The results of that assessment indicated that the perigee position uncertainties (approximately .35 NM) were similar to those of the longer mission durations. One major astrionics concern about the one pass mission was the apogee position uncertainty subsequent to the single atmospheric pass (approximately 5 NM with use of the horizon sensor). However, as indicated in Figures 4.6.4.5-4 and -5 (basic report), while the second apogee uncertainty is always greatest, the second perigee uncertainty is less than the first. Therefore, apogee uncertainty is not expected to significantly impact the 2 pass mission.

Another major concern was the sensitivity of deboost velocity error to initial perigee altitude. The sensitivity of initial perigee altitude to deboost velocity is approximately 2700 feet/ft./sec. For the 2 pass

D5-17142



CONFIGURATION	MATERIAL THICKNESS (INCHES)	
	A	B
BASIC (2-PASS)	3.32	1.0
60° SHORT FLARE (2-PASS)	3.20	1.0

FIGURE A-2.5.3-1 HEAT SHIELD ABLATIVE MATERIAL THICKNESS

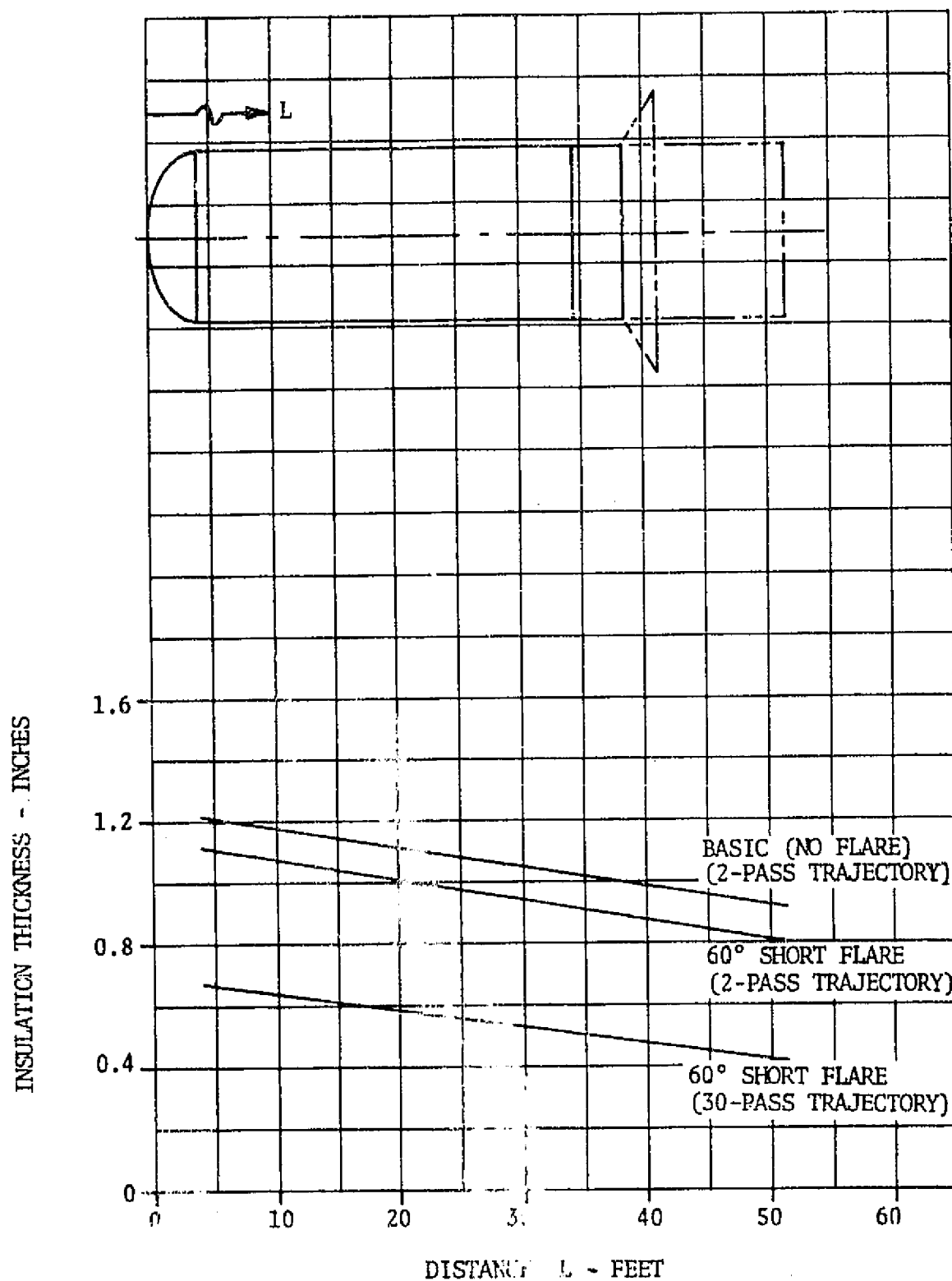


FIGURE A-2.5.3-2 SPACE TUG SIDEWALL INSULATION THICKNESS

CONFIGURATION	TRAJECTORY	SIDEWALL TPS WEIGHT (LBS)			HEAT SHIELD TPS MATERIAL WEIGHT (LBS)	TOTAL TPS WEIGHT (LBS)
		RE-RADIATION SHIELD	MICROQUARTZ INSULATION	TOTAL		
Basic (No Flare)	2-Pass	247 (1)	613	860 (3)	2380 (4)	3240
Short 60° Flare	2-Pass	247 (1)	573	820 (3)	2305 (4)	3125
Short 60° Flare	30-Pass	119 (2)	348	467 (3)	-	467
Large Nose Flare	2-Pass	0	0	0	-	-

- NOTES:
1. Re-radiation shield - L605 Haynes Alloy (0.002 inch thickness)
 2. Re-radiation shield - Titanium (0.002 inch thickness)
 3. Weights include re-radiation shield and microquartz insulation on Tug sidewall, astronics module and payload section.
 4. Heat shield material - ablative type, Martin-Marietta ESA-3560 IIA

FIGURE A-2.5.3-3 THERMAL PROTECTION SYSTEM WEIGHT SUMMARY

A-2.6 (Continued)

basic (no flare) configuration, the target perigee altitude is approximately 20,000 feet above the altitude resulting in a direct re-entry. The other 2 pass configurations have higher initial perigee altitudes. Therefore, it appears that velocity could be controlled sufficiently to avoid direct re-entry. As discussed in Section 4.6 (basic report), a detailed navigation and guidance analysis would be required in a follow-on activity to determine the full impact on the astronics system caused by very short duration missions.

A-2.7 AEROBRAKING KIT MATERIALS

The materials used for the two pass mission are the same as those defined in Section 4.7, Aerobraking Kit Materials Selection (basic report). The only differences are that the use of ablatives for heat shield applications and higher temperature outer foil materials for the sidewall insulation system were investigated.

The maximum stagnation point heating rates (thermal environment) for the 2 pass missions are shown in Figure A-2.7.0-1 below.

CONFIGURATION/PASS NO.	MAXIMUM HEATING RATE (BTU/ft ² /sec.)
<u>Basic (No Flare)</u>	
1	127
2	94
<u>Short 60° Flare</u>	
1	85
2	63
<u>Large Nose Flare</u>	
1	5.3
2	3.9

Figure A-2.7.0-1 2 Pass Maximum Heating Rates

The total heat input into the 2 pass basic (no flare) Tug is approximately 11,500 BTU's for the first pass and 13,500 BTU's for the second pass. These heat inputs are considerably higher than those encountered by the Space Shuttle. A low density ablator (approximately 20-40 pounds per cubic foot, such as those used on the Shuttle) would not be satisfactory for this application. Materials selected for further review included (1) ESA-3560 IIA, (2) SLA-561, (3) DC-93104, (4) DC-325, and (5) DC-93072.

A-2.7 (Continued)

The ESA-3560 IIA was selected for the ablative heat shield as it offered low density (56 pounds/ft³) compared to the 70 pounds/ft³ and 90 pounds/ft³ of the DC-93072 and DC-93104 silicon phenolics. The SLA-561 had the desirable low density of 14.5 pounds/ft³; however, its heating rate capability is not sufficient for the high heating rates encountered with two pass aerobraking. Figures A-2.7.0-2 and -3 illustrate the properties of the selected materials.

For the large nose flare, the temperatures encountered are approximately 1350 to 1400°F. A radiative heat shield material was used. Either Inconel 718 or Rene '41 are acceptable (Rene '41 was used as it has higher strength to density properties at the flare temperatures). The properties of these materials are shown in Section 4.7 (basic report). The short 60° flare configuration's heat shield will encounter temperatures of approximately 2000°F (30 pass mission). For this configuration and mission duration, the TD-nickel-chrome radiative heat shield material was used.

For the sidewall protection system, a microquartz insulation was used with a metallic outer foil. For the two pass basic (no flare) and short 60° flared Tugs, the sidewall temperatures are higher than encountered in the longer duration missions. These higher temperatures necessitate the use of a high temperature L-605, a Haynes Cobalt alloy to replace the titanium outer foil previously used. Figure A-2.7.0-4 lists the properties of the L-605. The short 60° flare configuration flown in a 30 pass mission can use the titanium outer foil to cover the microquartz.

The flare of the large nose flare configuration shields the body of the Tug and the temperatures on the micrometeoroid shield do not exceed the capability of the aluminum shield. Therefore, no thermal protection was required for the large flare configuration sidewalls.

The flare material for the short 60° flare does not exceed the capabilities of the Inconel 718 or Rene '41 for either the 2 pass (temperature-1400-1500°F) or the 30 pass (800-900°F). Either of these materials, therefore, can be used for the flare.

The payload adapter for the two pass mission used the same materials as the previous aerobraked configurations. Additional microquartz with the L-605 outer foil were required for the sidewall and payload for both the two pass basic (no flare) and short 60° flare Tug configurations.

A-2.8 WEIGHTS AND MASS PROPERTIES

The weights and mass properties for the three configurations studied in the add-on effort are presented in this section. The three configurations were (1) the basic (no flare) Tug (two pass mission), (2) the short 60° flare (two and 30 pass missions) and (3) the large nose flare (two pass mission).

	PROPERTY	VIRGIN MATERIAL @ 80°F	CHAR MATERIAL @ 1500°F	SHUTTLE APPLICABILITY
THERMOPHYSICAL	DENSITY (PCF)	56.0	21.3	REQUIRE TEST VERIFICATIONS FOR SHUTTLE ENVIRONMENT
	THERMAL CONDUCTIVITY (BTU/IN-SEC-°F)	1.9×10^{-6}	5.9×10^{-6}	
	SPECIFIC HEAT (BTU/LB-°F)	0.26	0.27	
	EMISSIVITY	0.75	0.67	
MECHANICAL	ULT. TENSILE STRENGTH (PSI)	245	---	APPLICABLE
	ULT. TENSILE STRAIN (IN./IN.)	0.062	---	
	MODULUS OF ELASTICITY (PSI)	5000	---	

PROJECT SOURCE: X-15A-2 FLIGHTS

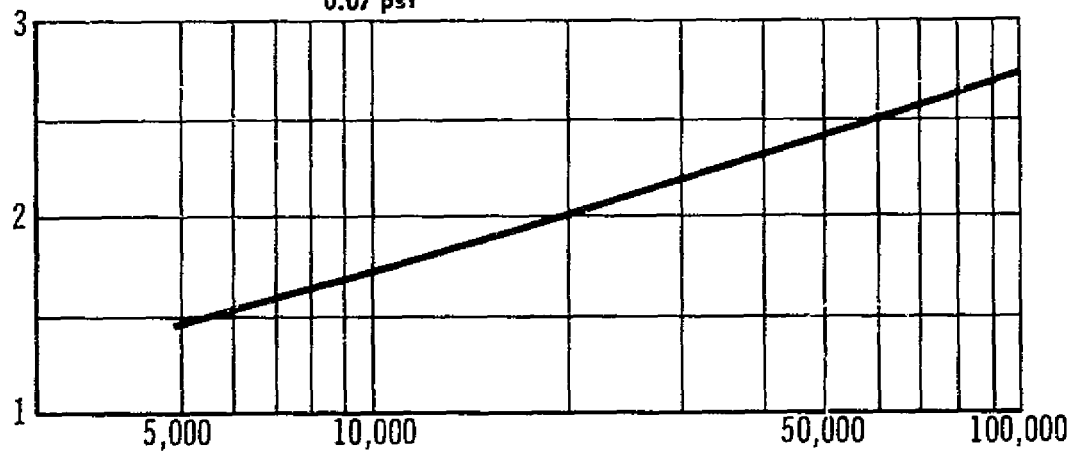
FIGURE A-2.7.0-2: ESA-3560 IIA PROPERTIES

LEADING EDGE LAMINAR FLOW
DIRECTLY BONDED ABLATOR
ABLATOR DENSITY = 56.0 LB/FT³

ADD:

0.02 psf HARDCOAT
0.05 psf BOND
0.07 psf

ABLATOR
THICKNESS
(INCHES)



MAXIMUM STRUCTURAL
TEMPERATURE = 300°F
BACKFACE SMEARED
THICKNESSES

ALUMINUM ~ .06"
TITANIUM ~ .05"

$Q_T \sim$ TOTAL LOCAL HEAT (ENTRY) (BTU/FT²)

FIGURE A-2.7.0-3: ESA-3560 IIA THICKNESS VS. HEAT INPUT

D5-17142

(L-605 ALLOY)

SPECIFICATION: L-605 Sheet and Bar.

CHARACTERISTICS: L-605 is a heat-resistant material similar to Stellite 31. It possesses high strength and oxidation resistance up to 2000°F. Ductility appears to be superior to the other high temperature alloys. Available as sheet bar, plate, wire and tubing.

APPLICATIONS: Primarily for afterburner parts requiring high strength up to 2000°F.

COMPOSITION: 0.15 C max, 19.0 - 21.0 Cr, 14.0 - 16.0 W,
9.0 - 11.0 Ni, 2.0 Fe, max, 1.0 Si max,
1.0-2.0 Mn, bal Co.

MECHANICAL PROPERTIES:

	<u>Sheet</u> <u>Annealed</u>	<u>Sheet</u> <u>As-rolled</u>
Condition		
Tensile, PSI	155,000	170,000
Yield, 0.2% offset	70,000	108,500
% Elongation in 2 inch	55.0	40.0
% Reduction of Area	40-45	
Brinell (3000 Kg)	218-228	305-330

PHYSICAL PROPERTIES:

Density	9.15 g/cc; 0.330 lb/cu. in.
Expansion Coef (70-600°F)	7.6×10^{-6} in/in/°F
Thermal Conductivity	100 BTU/sq.ft./hr/°F/in.
Scaling Temperature	2000°F

FABRICATION:

Forming,	Good
Welding,	Good
Machining,	Good

FIGURE A-2.7.0-4 L-605 COBALT ALLOY MATERIAL PROPERTIES

A-2.8 (Continued)

The mass properties used in the aerodynamic and the control analyses are shown in Figure A-2.8.0-1. The mass properties as shown in the figure were calculated for the conditions existing at the start of the aerobraking return from geosynchronous orbit.

The inert weight associated with the implementation of these aerobraking return modes of operation are summarized in Figure A-2.8.0-2. The structural weights for the aerobraking kit elements for the basic (no flare) Tug and for the short 60° flare Tug were determined by a detailed sizing analyses of the heat shield and flares for the pressure and thermal environments. The large nose flare was subjected to a less detailed sizing; however, the weight estimates were conducted in sufficient detail to determine that the large nose flare concept investigated has no geosynchronous payload capability.

The materials used for each of the four configuration aerobraking kits are as shown in Figure A-2.8.0-3.

The total Tug weight at the start of aerobraking for two of the three configurations are spotted on Figure A-2.8.0-4 for comparison with the previously reported weights data shown in Section 4.8 (Figure 4.8.6.0-1, basic report). Note that for the large nose flare, no payload was obtained so that this point was not plotted. The two pass mission data shows a rapid increase in aerobraking kit weight (and corresponding lower payload capability) with shorter duration missions. The short 60° flare configuration has approximately 40 pounds more aerobraking kit weight for the 30 pass mission than the 30° flare.

A-3.0 SENSITIVITIES AND PAYLOADS

This section discusses (1) the revised atmospheric dispersion targeting scheme and model, (2) a typical total mission navigation error correction burn sensitivity, (3) the payload capabilities of the configurations studies in the add-on activity, and (4) the performance sensitivity comparisons between the initial MSFC Point Design Tug and the Aerobraked Tug. The first two topics listed above are presented to provide initial insight into certain problem areas identified in Section 5 of the basic report. The third topic is a continuation of the add-on activity report. The fourth topic complements the conventional-aerobraked Tug comparisons of Section 5.3 of the basic report.

A-3.1 REVISED ATMOSPHERIC DISPERSIONS

Figure 5.2.1.0-2 of the basic report shows the range of atmospheric perturbations used in the main study. This density range was approximately +50% and -40% from the 1962 Standard Atmosphere. The expected variations during a mission or between individual passes were not given in the NASA Atmospheric Model. This gap in the atmospheric model data was discussed in the basic report and with the Space Environment personnel of MSFC. In response, the revised atmosphere model shown in Figure A-3.1.0-1 was

	<u>BASIC (NO FLARE)</u>	<u>SHORT 60° FLARE</u>	<u>LARGE FLARE</u>
WEIGHT (POUNDS)	14,430	14,430	14,430
CENTER OF GRAVITY \bar{X} (INCHES)	243.3	233.5	158.1
CENTER OF GRAVITY \bar{Y} (INCHES)	0	0	0
CENTER OF GRAVITY \bar{Z} (INCHES)	0	0	0
ROLL MOMENT OF INERTIA (SL.-FT ²)	10,388	12,700	64,000
PITCH MOMENT OF INERTIA (SL.-FT ²)	101,686	94,000	101,000
YAW MOMENT OF INERTIA (SL.-FT ²)	101,686	94,000	101,000

FIGURE A-2.8.0-1 MASS PROPERTIES FOR ADD-ON ACTIVITY

COMPONENT	CONFIGURATION WEIGHT (POUNDS)			
	BASIC (NO FLARE) 2 PASS	SHORT 60° 2 PASS	FLARE 30 PASS	LARGE NOSE FLARE 2 PASS
AFT HEAT SHIELD	2785	2700	480	400
FLARE	---	510	380	6580
*SIDEWALL INSULATION	925	881	513	---
PAYLOAD/FLARE ADAPTER	350	390	390	350
ASTRIONICS PENALTY	25	25	325	25
ADDED RCS INERTS	15	---	---	---
RCS PROPELLANT	516	256	271	6
TOTAL	4616	4762	2359	7361

* INCLUDES PAYLOAD INSULATION AND PAYLOAD CAP ACTUATION DEVICE

FIGURE A-2.8.0-2 AEROBRAKING KIT WEIGHTS

CONFIGURATION COMPONENT	BASIC	SHORT 60° FLARE		LARGE NOSE FLARE
	2 PASS	2 PASS	30 PASS	2 PASS
HEAT SHIELD STRUCTURE	TITANIUM	TITANIUM	TD-NICKEL CHROME	RENE' 41
HEAT SHIELD TPS	ESA-3560 IIA	ESA-3560 IIA	-	-
SIDEWALL, PAYLOAD ADAPTER AND CLOSURE TPS	MICROQUARTZ L-605 OUTER FOIL	MICROQUARTZ L-605 OUTER FOIL	MICROQUARTZ TITANIUM OUTER FOIL	-
PAYLOAD ADAPTER	ALUMINUM	ALUMINUM	ALUMINUM	ALUMINUM
ASTRIONICS	FUEL AND REDUNDANCY	FUEL AND REDUNDANCY	FUEL AND REDUNDANCY	FUEL AND REDUNDANCY
RCS SYSTEM	INCREASE THRUSTER SIZE AND FUEL	FUEL	FUEL	FUEL

FIGURE A-2.8.0-3 MATERIALS USED FOR AEROBRAKING KIT COMPONENTS

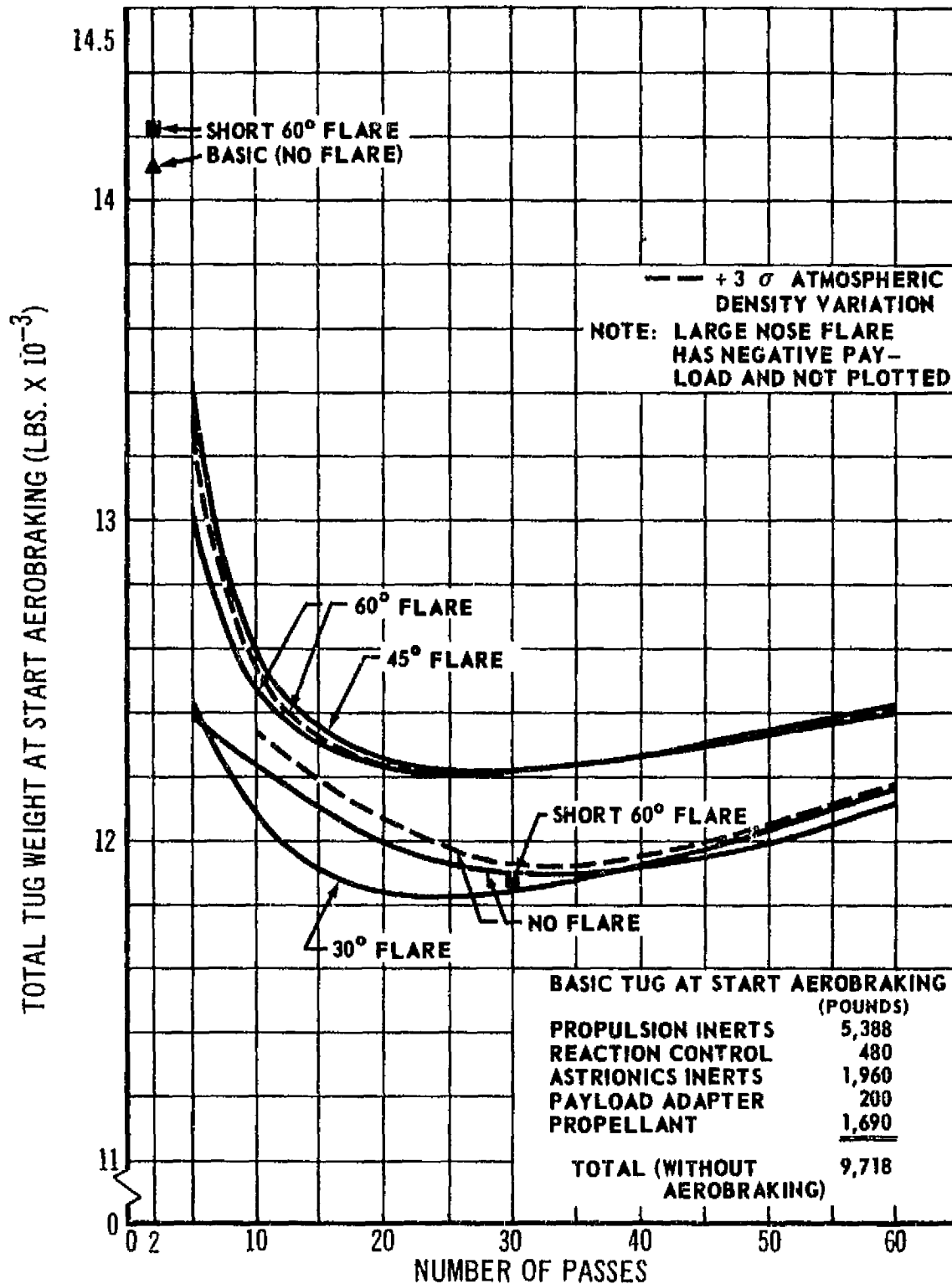


FIGURE A-2.8.0-4: TOTAL TUG WEIGHT VS. NUMBER OF PASSES

A-3.1 (Continued)

furnished by MSFC. This revised model is applicable to the equatorial regions in which the aerobraking perigees are expected to occur. The total variations are one-half or less of those in the original model. The maximum rate of change is 3% per hour of flight time for short time periods (approximately 4 hours). For comparison purposes, the 1962 Standard Atmosphere density values are approximately: (1) 85 KM - 7.96×10^{-6} kg/m³, (2) 90 KM - 3.17×10^{-6} kg/m³, and (3) 95 KM - 1.21×10^{-6} kg/m³.

The two preliminary targeting schemes discussed in Section 4.3 (basic report) were based on the invariability of the apogee decay rate and used either burns at apogee or burns at atmospheric exit to achieve the desired decay rates. The former scheme used apogee burns to up the perigee (assuming a constant high density atmosphere) for correction. The latter scheme used burns at exit to increase the apogee to the desired apogee.

The final targeting scheme was based on making the atmospheric correction burns at or near entry where better trajectory knowledge would be available. A series of trajectory were flown using atmospheric correction burns at entry to verify the feasibility of this scheme.

Figure A-3.1.0-2 shows the apogee decay rates for the 10 pass mission. The basic (no flare) was flown under four atmospheric conditions with the final targeting scheme utilized. The first atmospheric condition was the 1962 Standard Atmosphere to determine the nominal decay line (this nominal line is only dependent on mission duration and is identical to other 10-pass configurations). The effects of using a constant (+) or (-) density (initial atmosphere dispersion model) are shown and resulted in relatively large errors in the apogee subsequent to the first perigee pass. The apogee errors then rapidly converge to near-nominal for the remainder of the passes. Using the Varying Atmosphere of Figure A-3.1.0-1, the initial apogee error is greatly reduced. Although the decay rate convergence is not as rapid because of the time variance in the atmosphere, equivalent convergence occurs by the fourth pass.

Figure A-3.1.0-3 shows the final apogee error comparison between the two atmospheric models. This figure (at the 10-pass abscissa) is an expanded plot of the final pass decay rate data shown in Figure A-3.1.0-2 above. The Varying Atmosphere with the correction-at-entry technique resulted in an insignificant final apogee error of about 3 n.m. (10 pass mission). The 30 pass varying atmosphere mission had a final apogee error of 13 n.m. The constant atmospheres also had small final apogee errors (8-29 n.m.). This range of final apogee errors is less than those shown in Figures 4.3.4.1-7 and -8 (basic report) for the other targeting schemes.

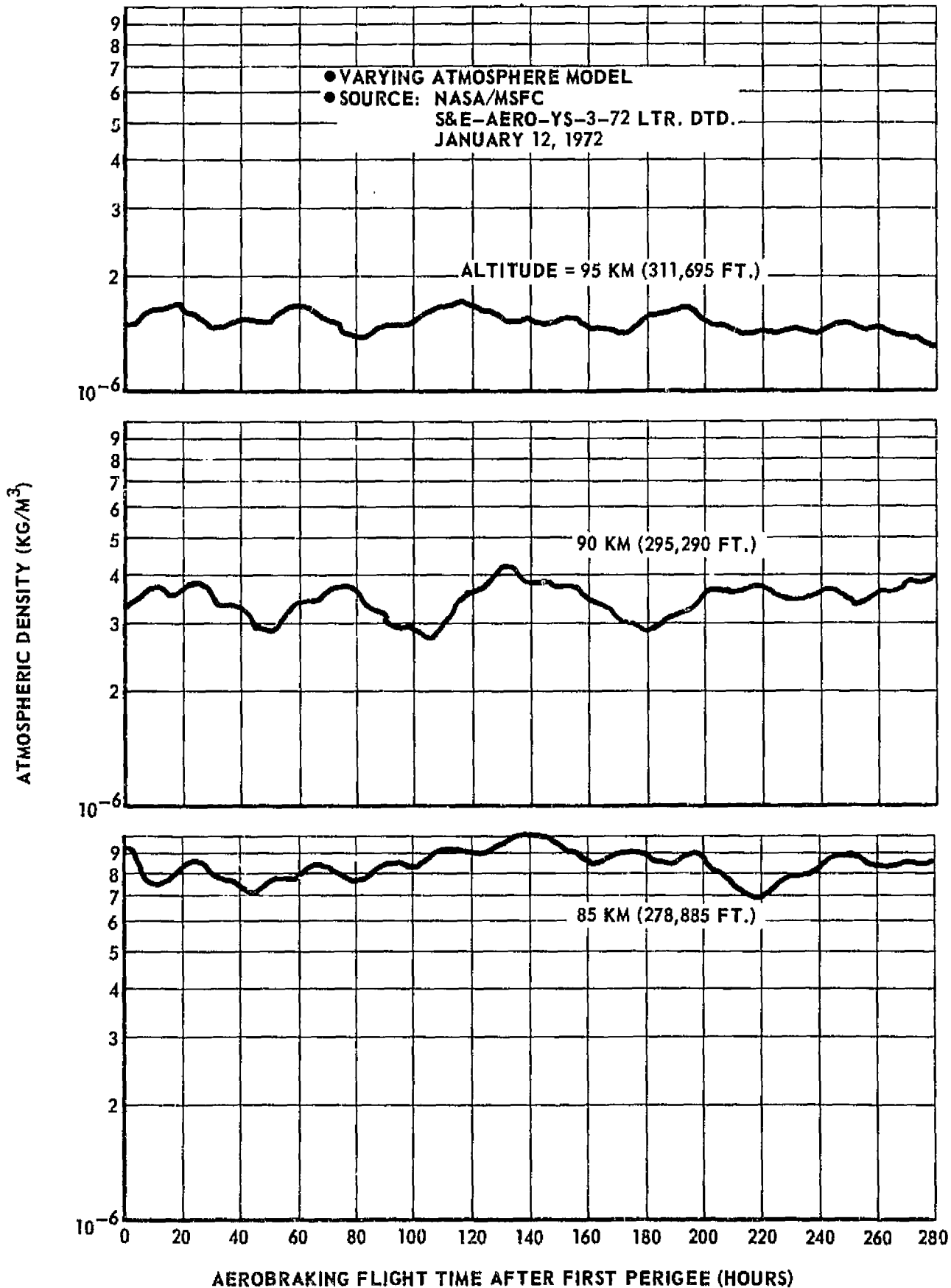


FIGURE A-3.1.0-1: ATMOSPHERIC DENSITY VARIATIONS FOR SPACE TUG AEROBRACING STUDIES

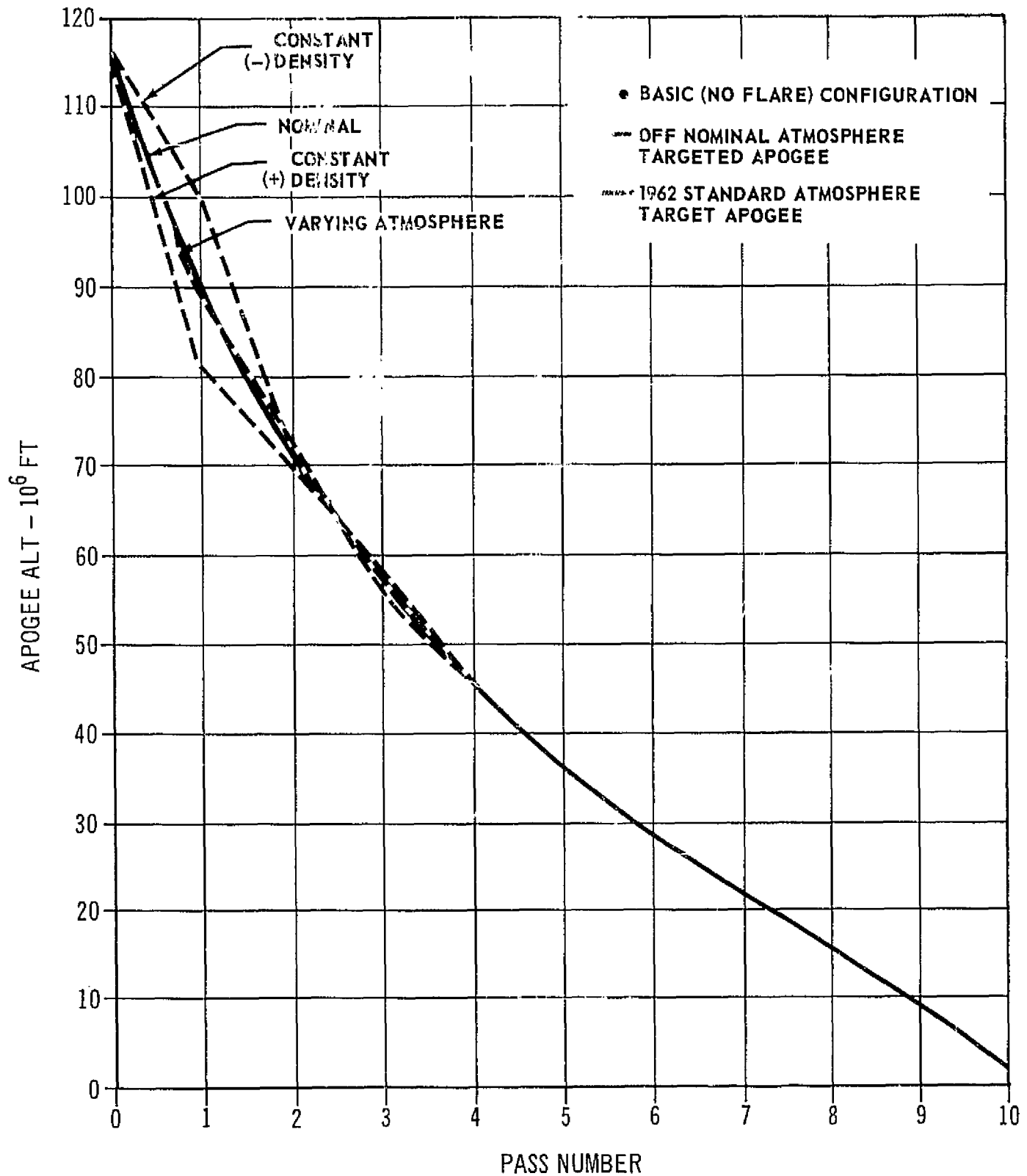


FIGURE A-3.1.0-2: SPACE TUG AEROBRAKING RETURN FROM SYNCHRONOUS ORBIT -
TEN PASS BASIC TUG - TARGET APOGEE VERSUS PASS NUMBER

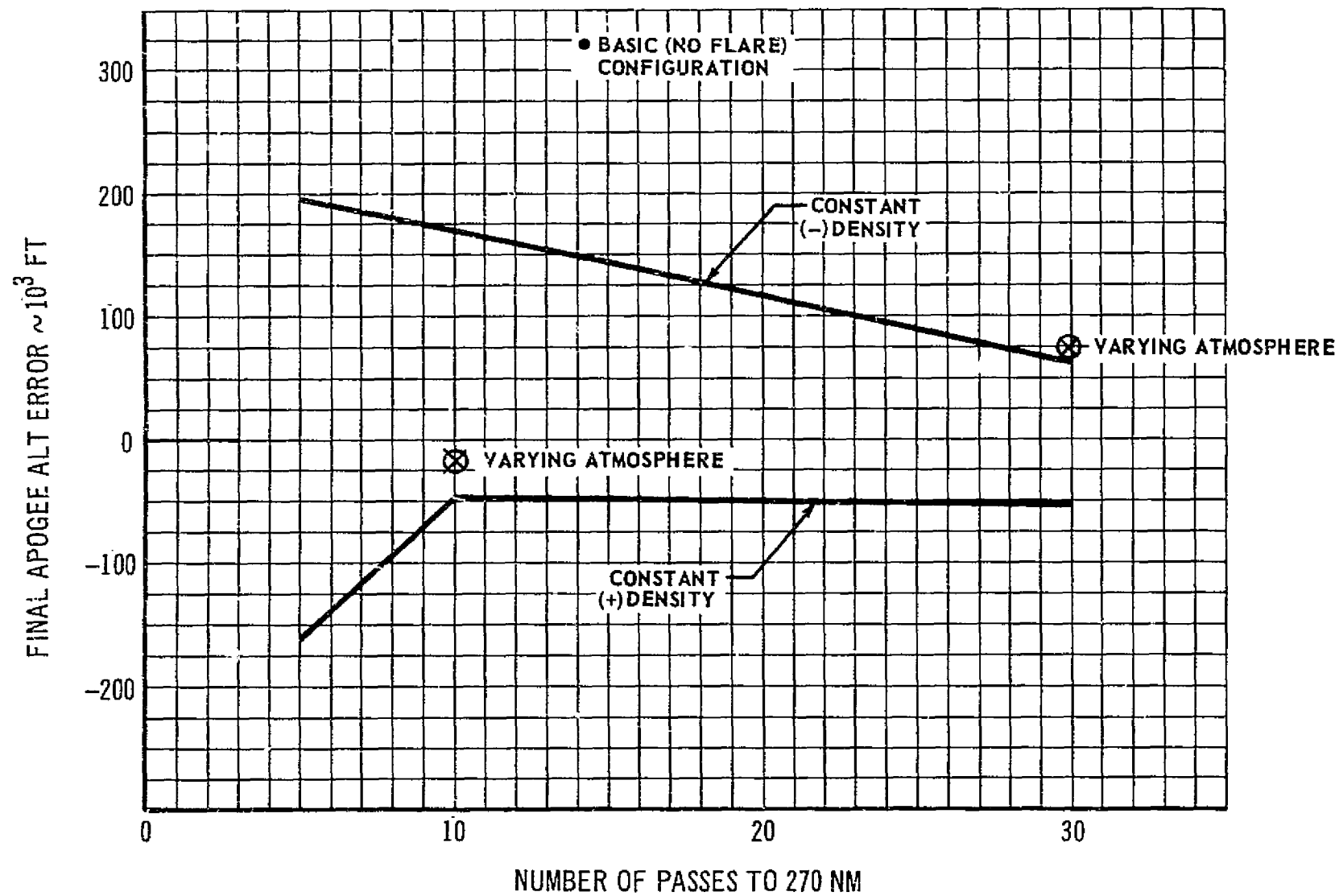


FIGURE A-3.1.0-3: SPACE TUG AEROBRAKING RETURN FROM SYNCHRONOUS ORBIT - FINAL APOGEE ERROR VERSUS NUMBER OF PASSES TO 270 NM

A-3.1 (Continued)

Figure A-3.1.0-4 compares the atmospheric correction delta velocities used to maintain the decay rates shown in Figure A-3.1.0-2 and to attain the desired final apogee. The constant atmospheres (+ and -) required approximately 200-225 ft/sec during the mission and this value is relatively insensitive to number of passes. This insensitivity is contrasted to the large delta velocities for the short duration missions using the other two targeting schemes (Figures 4.3.4.1-9 and -10 of basic report).

The Varying Atmosphere required approximately 100 ft/sec delta velocity for the 10 pass mission and less than 200 ft/sec for the 30 pass mission. The Varying Atmosphere trajectory was flown by correcting each pass back to the nominal apogee decay line. Because of the limited resources available during the add-on activity, no optimization concerning numbers of correction burns was made. The Varying Atmosphere has cyclic characteristics tending to equalize the high and low peaks during a mission. Therefore, the Varying Atmosphere may require no atmospheric corrections during the early passes since the atmosphere may provide decay rates approximating the desired rates. It is also probable that bounds or limits of deviations from the nominal decay rate could be established and burns made only when these limits are exceeded. These optimization studies would be performed in follow-on activities.

A-3.2 NAVIGATION ERROR CORRECTIONS

Sections 4.6 and 5 (basic report) discussed the requirement for and the timing of navigation error correction burns. The data showed the desirability of performing these burns after the landmark tracker had made sufficient readings to converge the navigation uncertainties to a relatively small value. This occurred after 500-1300 seconds of landmark tracker operation (just prior to entry). Using the navigational uncertainties (3 sigma values) during the total mission, one trajectory was flown to determine the optimum location of the navigational correction burns. The results for a basic (no flare) 10-pass mission are shown in Figure A-3.2.0-1. The minimum total mission navigation correction delta velocity occurs at a true anomaly of -30 degrees. However, making the navigation burns at entry each pass insignificantly increased the delta velocity requirement and is also compatible with the atmospheric correction burn location discussed in Section A-3.1 above. The possibility of combining these two independent burns to reduce the total delta velocity requirement should be investigated.

As discussed in Section 5 of the basic report, an in-depth analysis of this problem area is still required in a follow-on activity. However, this single test case has indicated a promising approach to achieve the desirable objectives of (1) maximizing perigee accuracies, (2) minimizing correction delta velocities, and (3) simplifying operational procedures.

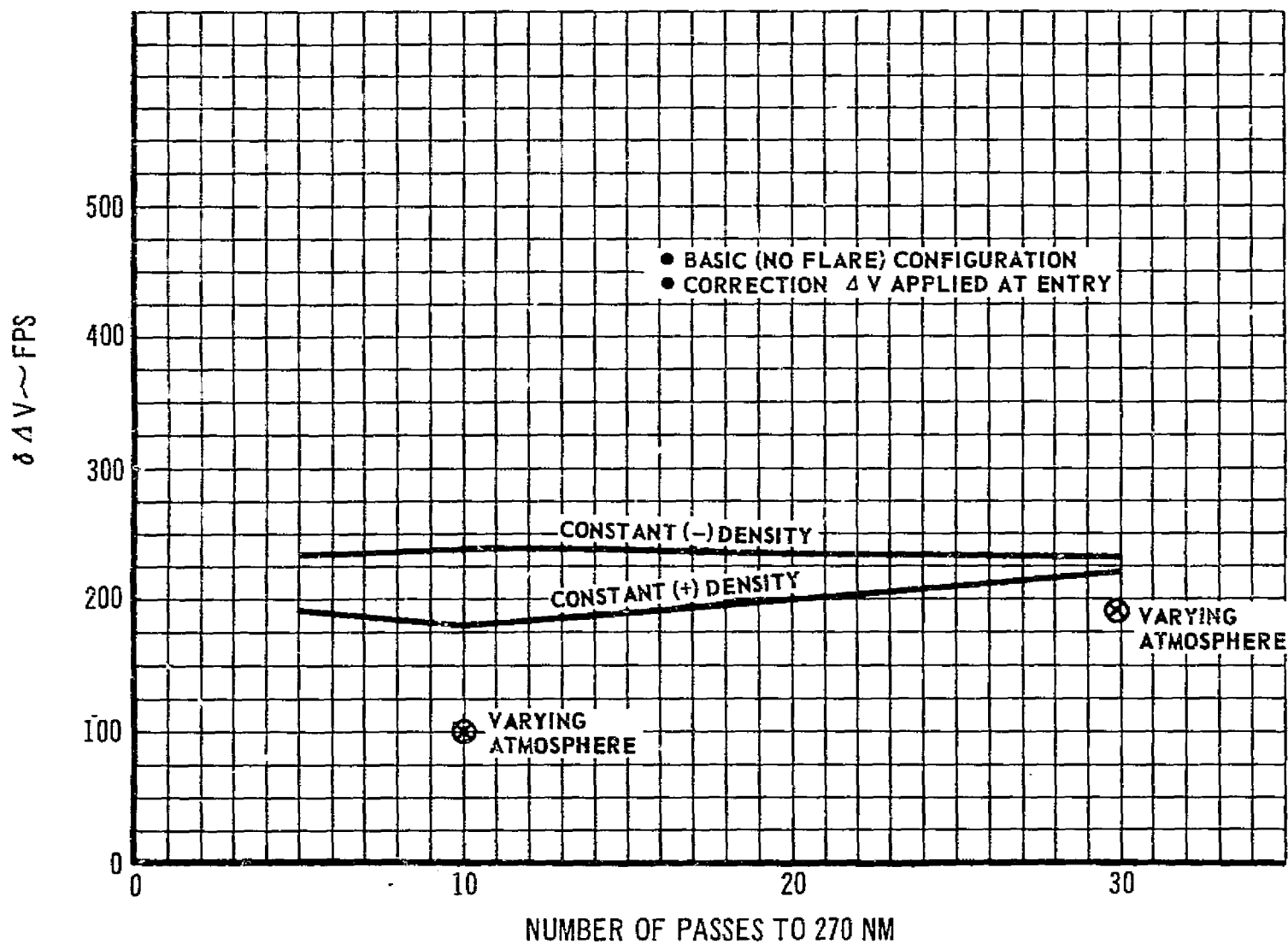


FIGURE A-3.1.0-4: SPACE TUG AEROBRAKING RETURN FROM SYNCHRONOUS ORBIT - INCREASE IN ΔV TO GO TO 270 NM FOR OFF NOMINAL ATMOSPHERE

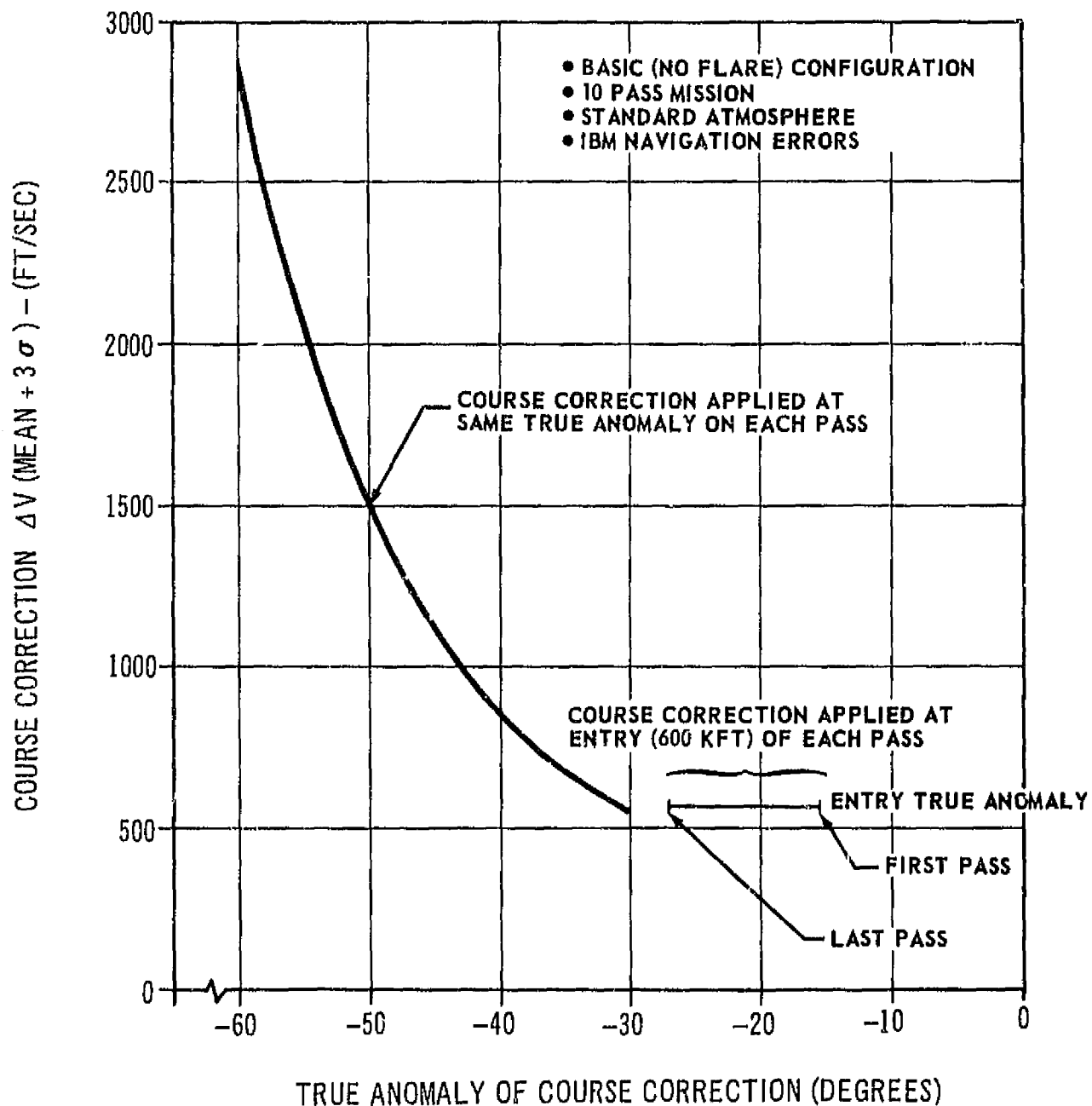


FIGURE A-3.2.0-1: SENSITIVITY OF TOTAL MISSION NAVIGATION ERROR CORRECTION DELTA VELOCITY TO CORRECTION BURN TIME

A-3.3 PAYLOAD CAPABILITIES

The payload capabilities of the two pass configurations and 30 pass short 60° flare configuration were computed in the same manner as discussed in Section 5 (basic report). The effects of atmospheric dispersions and navigational errors were not specifically addressed. However, a delta velocity budget of 800 ft/sec was allotted for docking in synchronous orbit and for making correction burns. This is the same budget utilized in Section 5.1.2 (basic report).

Figure A-3.3.0-1 shows the fully fueled weight statements for the selected add-on activity configurations. The aerobraking kit weights are the same as shown in prior Section A-2.8 (Weights and Mass Properties). The total mission delta velocities include the equivalent velocities furnished by the RCS. All three of the two pass configurations have low mass fractions due to their heavy thermal protection systems or large flare areas.

The geosynchronous round trip payload capabilities of these configurations are shown in Figure A-3.3.0-2. The two pass basic (no flare) and short 60° flare configurations have approximately equivalent capabilities. As discussed Section 5 (basic report), changing the mode from departing 100 n.m., circularizing at 270 n.m. and transferring back to 100 n.m. (270-100 n.m. mode) to a mode consisting of departing from and circularizing at 200 n.m. (200 n.m. mode) increases the payload capability approximately 1200 pounds. This increase is reflected in the two pass payloads shown in the figure.

The two pass large nose flare has a negative payload capability, even when flown from 200 n.m. The inert weights of this configuration would have to be reduced by approximately 600 pounds to have a zero payload on the 200 n.m. mode. Because the gross weight of this configuration is slightly over 60,000 pounds, little if any additional assistance could be expected from the Shuttle. Therefore, it was concluded that this particular configuration has little applicability in the geosynchronous mission role.

The 30 pass short 60° flare's payload capability is approximately 100 pounds less than the 30 pass 30° flare's capability (Figures 5.1.2.6-1 and -2, basic report). This is caused by two factors: (1) the equivalent mission delta velocity for the short 60° flare is 150 ft/sec greater (The short 60° flare is not stable. RCS fuel is required for stability); and (2) the short 60° flare configuration required a completely insulated payload which negated most of the decrease in flare weight.

The short 60° flare (flare slant height = 4.9') discussed above is the baseline #2 configuration (prior Section A-2.1). This flare has the same equivalent $W/C_D A$ as the 30° flare, however, it is statically unstable. The short 60° flare #3 configuration (flare slant height = 8.68') is neutrally stable. It has larger coefficients of drag and requires higher perigee altitudes (for same mission durations) as the

COMPONENT CONFIGURATION NO. OF MISSION PASSES	TUG INERT WT (LBS)	PROPELLANT (LBS)	AFT HEAT SHIELD (LBS)	FLARE (LBS)	SIDEWALL INSULATION (LBS)	PAYLOAD/FLARE ADAPTER (LBS)	ASTRONICS MODULE PENALTY (LBS)	GROSS TUG WEIGHT (LESS PAYLOAD) (LBS)	TUG MASS FRACTION (λ')	* TOTAL MISSION DELTA VELOCITY (FT/SEC)
<u>BASIC (NO FLARE)</u>										
2	7843**	45,000	2785	---	925***	350	25	56,928	0.790	21,369
<u>SHORT 60° FLARE #2</u>										
2	7828	45,000	2700	510	881***	390	25	57,334	0.785	21,138
30	7828	45,000	480	380	513***	390	325	54,916	0.819	21,151
<u>LARGE NOSE FLARE</u>										
2	7828	45,000	400	6580	---	350	25	60,183	0.748	20,915

- * DEPART AND RECOVER AT 200 N.M.
 ** INCLUDES RESIZED RCS THRUSTERS (250 LBS THRUST)
 *** INCLUDES PAYLOAD INSULATION AND PAYLOAD CAP ACTUATION DEVICE

FIGURE A-3.3.0-1 FULLY FUELED AEROBRAKING TUG WEIGHT STATEMENTS

CONFIGURATION/ NUMBER OF PASSES	ROUND TRIP PAYLOAD (LBS)	
	200 N. M. MODE	270-100 N. M. MODE
<u>BASIC (NO FLARE)</u> 2	1700	500
<u>SHORT 60° FLARE (#2)</u> 2 30	1700 4100	475 2850
<u>LARGE NOSE FLARE</u> 2	Negative	Negative

FIGURE A-3.3.0-2 ROUND TRIP PAYLOAD CAPABILITIES

A-3.3 (Continued)

#2 configuration. These configuration #3 characteristics could result in a larger payload capability.

Figure A-3.3.0-3 shows the fully fueled aerobraked Tug weight statement for the 30 pass short 60° flare configuration #3. The flare design concept is identical to that shown in Figure 4.2.2.3-1 (basic report) for the 30°, 45°, and 60° flare configurations. The other aerobraking kit elements are identical to those discussed in the basic report.

The #3 configuration mass fraction for the 30 pass mission is 0.820 while the #2 configuration mass fraction for the 30 pass mission is 0.819 (prior Figure A-3.3.0-1). The aerobraking kit element weight reduction was achieved by the decreased total sidewall insulation requirement of the #3 configuration. Therefore, without considering the decreased delta velocity requirements of the neutrally stable #3 configuration, this configuration has a greater payload capability than does the #2 configuration.

The 30 pass 30° flare configuration has a total aerobraking kit weight of 2238 pounds and a fully fueled mass fraction of 0.817 (Figure 5.1.2.0-2, basic report). The 30° flare has the same mission delta velocity requirements as the short 60° flare #3 because of their equivalent stability characteristics. Therefore, the short 60° flare #3 has a 30 pass round trip payload capability almost 200 pounds greater than the 30° flare. This neutrally stable short 60° flare Tug has the largest round trip payload potential of all the configurations examined in this study.

Prior Figure A-2.1.0-1 showed the preliminary flare configuration/net payloads sensitivity estimate. The preliminary estimate indicated that a moderately unstable configuration might maximize the payload capability. The short 60° flare payload analysis in this section indicates that a near-neutrally stable vehicle will maximize the payload. Based on these results, Figure A-3.3.0-4 shows a revised estimate. The data points computed in this study are shown as small circles. Except for the 80° large nose flare ($W/C_p A = 2$), these data points represent 30 pass data. The large nose flare's data point is for two passes.

The trend lines shown on Figure A-3.3.0-4 represent estimates from the study results. Follow-on activity is required to verify/modify these trend lines. These follow-on activities include flow separation effects, flare designs, and dynamic stability impacts. Completing the data for this figure would have several advantages including:

- o Establishment of flared configuration scaling laws
- o Optimization of flare size and stability characteristics
- o Establishment of configuration selection criteria based on allowable mission durations

D5-17142

<u>COMPONENT</u>		<u>WEIGHT (LBS)</u>
TUG INERTS		7,828
PROPELLANT		45,000
TOTAL AEROBRAKING KIT		2,045
AFT HEAT SHIELD	450	
FLARE	610	
SIDEWALL INSULATION	270	
PAYLOAD/FLARE ADAPTER	390	
ASTRIONICS MODULE PENALTY	325	
FULLY FUELED TUG		54,873
MASS FRACTION		0.820

FIGURE A-3.3.0-3 FULLY FUELED WEIGHT STATEMENT FOR 30 PASS
SHORT 60° FLARE TUG (#3)

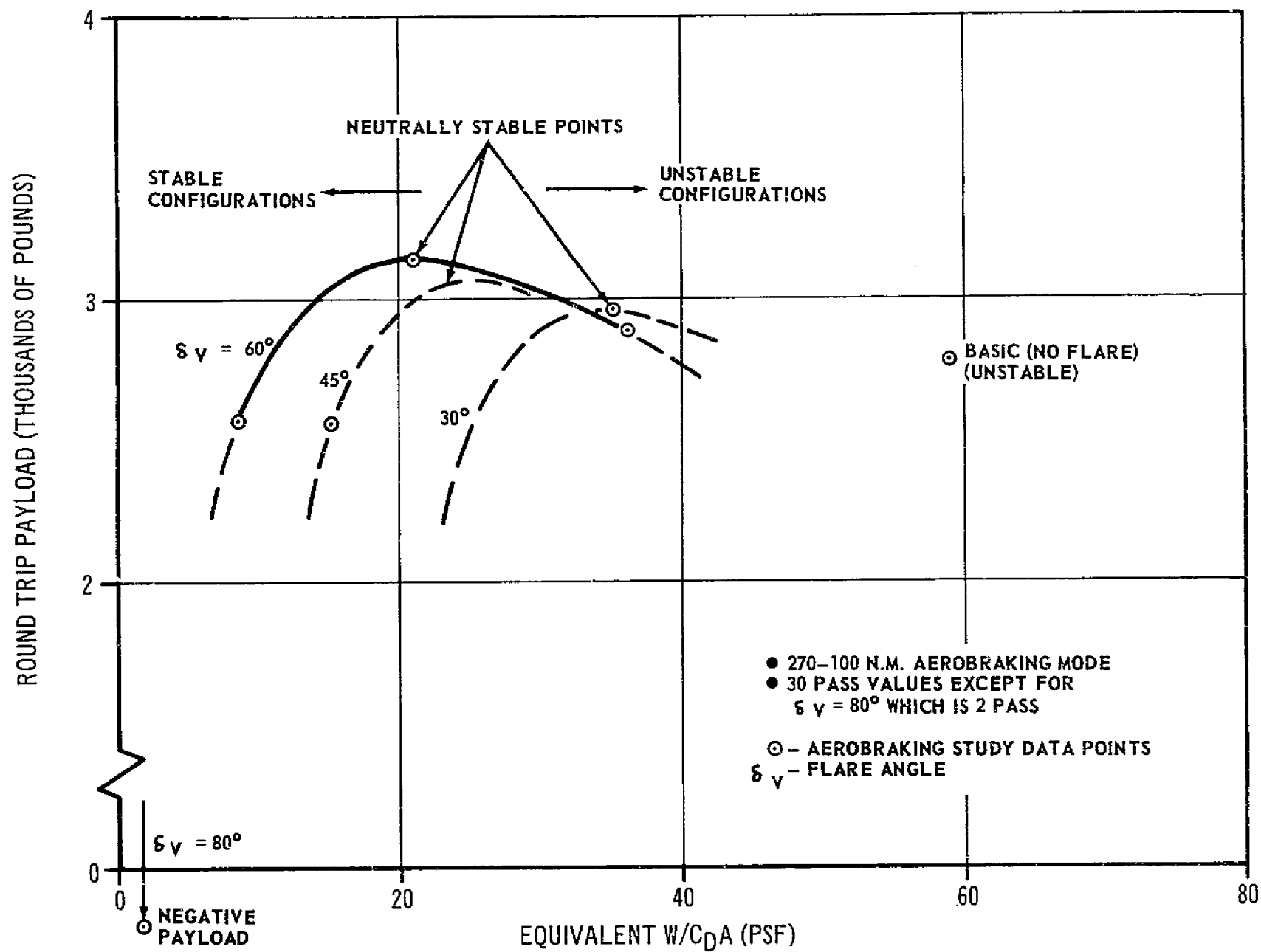


FIGURE A-3.3.0-4: FLARE CONFIGURATION/NET PAYLOAD SENSITIVITY ESTIMATE

A-3.4 CONVENTIONAL/AEROBRAKING TUG PERFORMANCE COMPARISON

The performance comparisons shown in Section 5.3 of the basic report were based on: (1) The conventional Tug's inert weight trends and mission delta velocity requirements developed in the prior Boeing Pre-Phase A Tug Study (Reference 1.1.0.0-1) and (2) the aerobraked Tug's inert weight penalties and mission delta velocity requirements developed in this study. Subsequent to the conclusion of the basic portions of this study, the MSFC Point Design Tug concept was developed under another set of groundrules. This section compares the payload sensitivities of the initial MSFC Point Design Tug with the aerobraked 30° flare configuration (30 pass mission). The groundrules used for this comparison were those established for the MSFC Point Design Tug Studies and differ in some respects to those used in either Boeing's Pre-Phase A Tug Study or in the Aerobraking Study. These groundrules were used in this section to provide a common basis for analysis. The reader should not make direct comparisons of the aerobraking results in this section with any other in the Aerobraking Study without first rationalizing the differences in groundrules utilized.

Figure A-3.4.0-1 shows the round trip payload capabilities of the conventional and aerobraked Tugs. The initial MSFC Point Design goal of 3000 pounds payload ($\lambda = 0.895$, $I_{sp} = 470$ sec, total usable propellant weight = 55,552 lbs.) is shown at the top of the figure. If the main engine I_{sp} were to be degraded to 460 seconds, approximately 500 pounds of payload capability would be sacrificed as evidenced by the $I_{sp} = 460$ line. As the conventional stage mass fraction is degraded (propellant loading constant), the payload capability is decreased until the capability is reduced to zero when the mass fraction is approximately 0.855 ($I_{sp} = 470$) or 0.861 ($I_{sp} = 460$).

The conventional Tug used as a "Starting Point" for this aerobraking study has a mass fraction of 0.852 without the payload adapter (total usable propellant weight = 45,000 lbs). The 3000 pound round trip payload could be achieved by the aerobraked 30° flare configuration (30 pass mission) with the current stage mass fraction (without the aerobraking kit) and with an uprated main engine having an I_{sp} of 470 seconds. Using the current engine ($I_{sp} = 460$ seconds), the stage would require a mass fraction of 0.862 to attain the 3000 pound payload capability. If the Aerobraked Tug stage were designed similar to the Point Design Tug and with a reasonable scaling factor to account for the differences in propellant loading (45,000 vs. 55,552 lbs.), the Aerobraked Tug might have a mass fraction of 0.875. This would provide a payload capability of approximately 4400 pounds ($I_{sp} = 470$ sec.).

The conventional Point Design Tug with 3000 pounds of payload, has a total gross weight in the Shuttle of 65,000 pounds, the maximum Shuttle capability at 28.5°/100 n.m. The Aerobraked Tug, with the same 3000 pounds of payload, has approximately 7000 pounds less gross weight in the Shuttle. Therefore, the Aerobraked Tug is not as sensitive to possible degradations in Shuttle payload capability.

cb

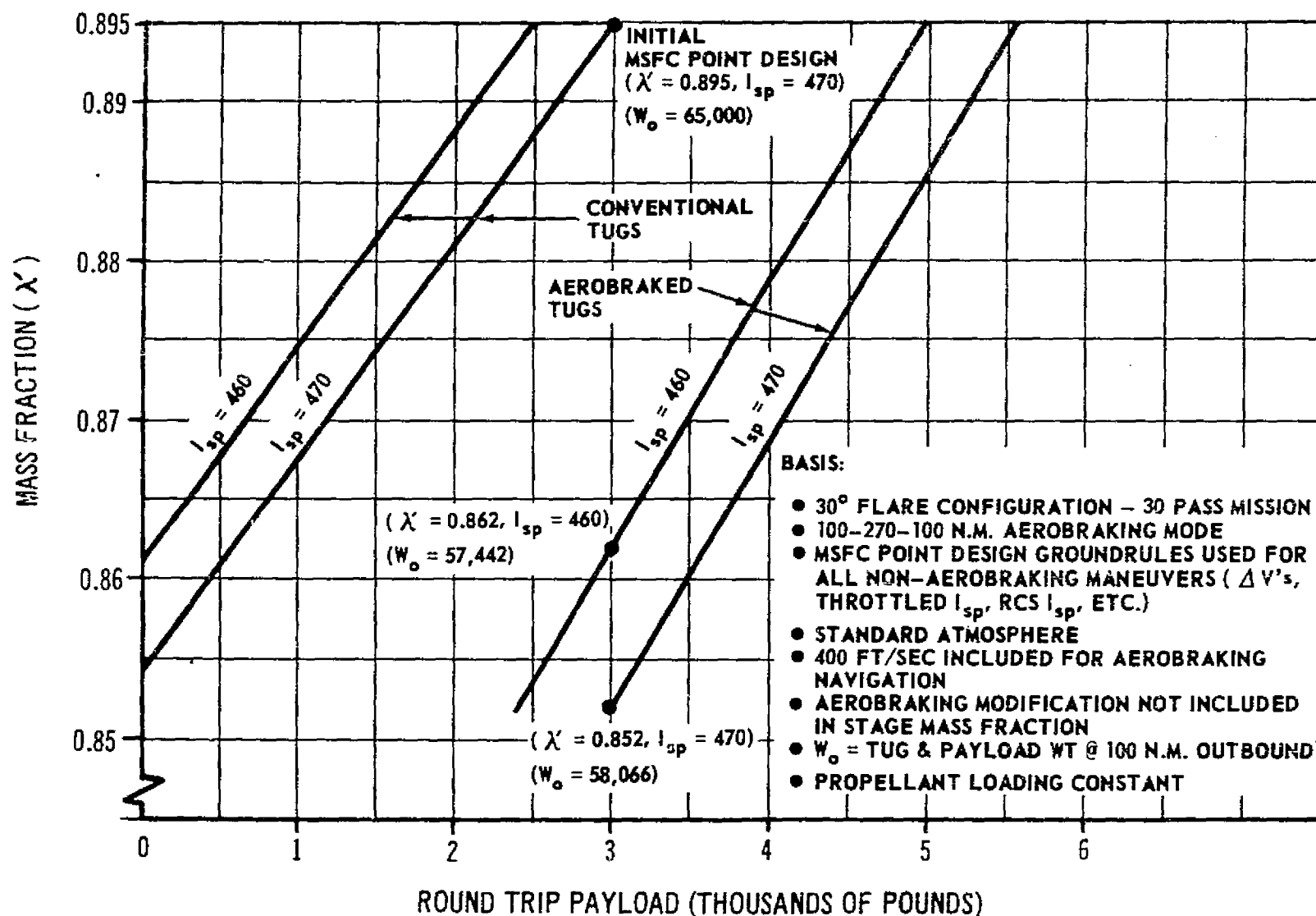


FIGURE A-3.4.0-1: ROUND TRIP PAYLOAD CAPABILITIES OF CONVENTIONAL AND AEROBRAKED TUGS

A-3.4 (Continued)

Figure A-3.4.0-2 shows similar data for the payload placement mission. The Initial Point Design Tug has a placement capability in excess of 8000 pounds. The Point Design Tug is constrained in the mission because of the 65,000 pound Shuttle limit. This limit forces the Point Design Tug to fly with approximately 5000 pounds of propellant off-loaded. The conventional Tug's payload sensitivities to possible degradations in both stage mass fraction and specific impulse are also shown.

The smaller Aerobraked Tug does not require propellant off-loading to remain within the Shuttle's 65,000 pound constraint. Therefore, the Aerobraked Tug again has a significant advantage over the larger conventional Tug even though this particular mission takes the least advantage of the aerobraking potential. To place the same 8000 pound payload, the Aerobraked Tug would require a stage mass fraction (without aerobraking kit) of 0.8605 (Isp = 470 seconds) or 0.869 (Isp = 460 seconds). The Aerobraked Tug's payload sensitivities to changes in stage mass fraction are less than for the conventional Tug because of the propellant off-loading factor. To achieve a placement capability of 10,000 pounds, the Aerobraked Tug would require technology similar to that of the Point Design Tug.

Figure A-3.4.0-3 shows the retrieval mission data. The Initial Point Design Tug has a payload retrieval capability of 4160 pounds as shown in the figure. This capability is decreased as the design parameters are degraded.

The aerobraking mode is most effective in the retrieval mission because the payload is carried only during the reduced propulsive requirement leg of the mission. Therefore, the Aerobraked Tug has a large retrieval potential as shown in the figure. Even with the current state-of-art technology as used in Boeing's Tug ($\lambda' = 0.852$, Isp = 460 seconds), the Aerobraked Tug significantly out performs the conventional Tug in this retrieval mission.

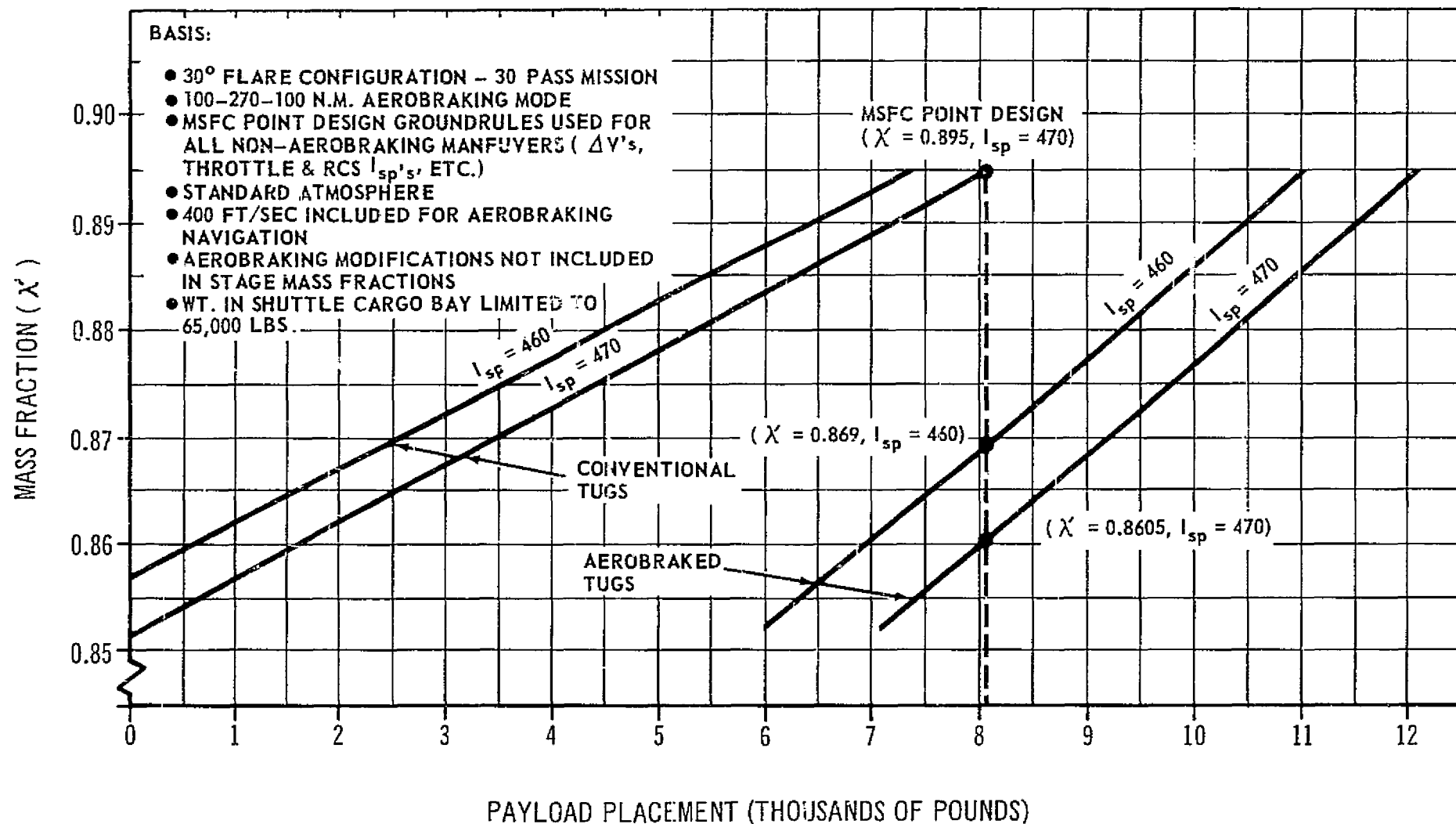


FIGURE A-3.4.0-2: PAYLOAD PLACEMENT CAPABILITIES OF CONVENTIONAL AND AEROBRAKED TUGS

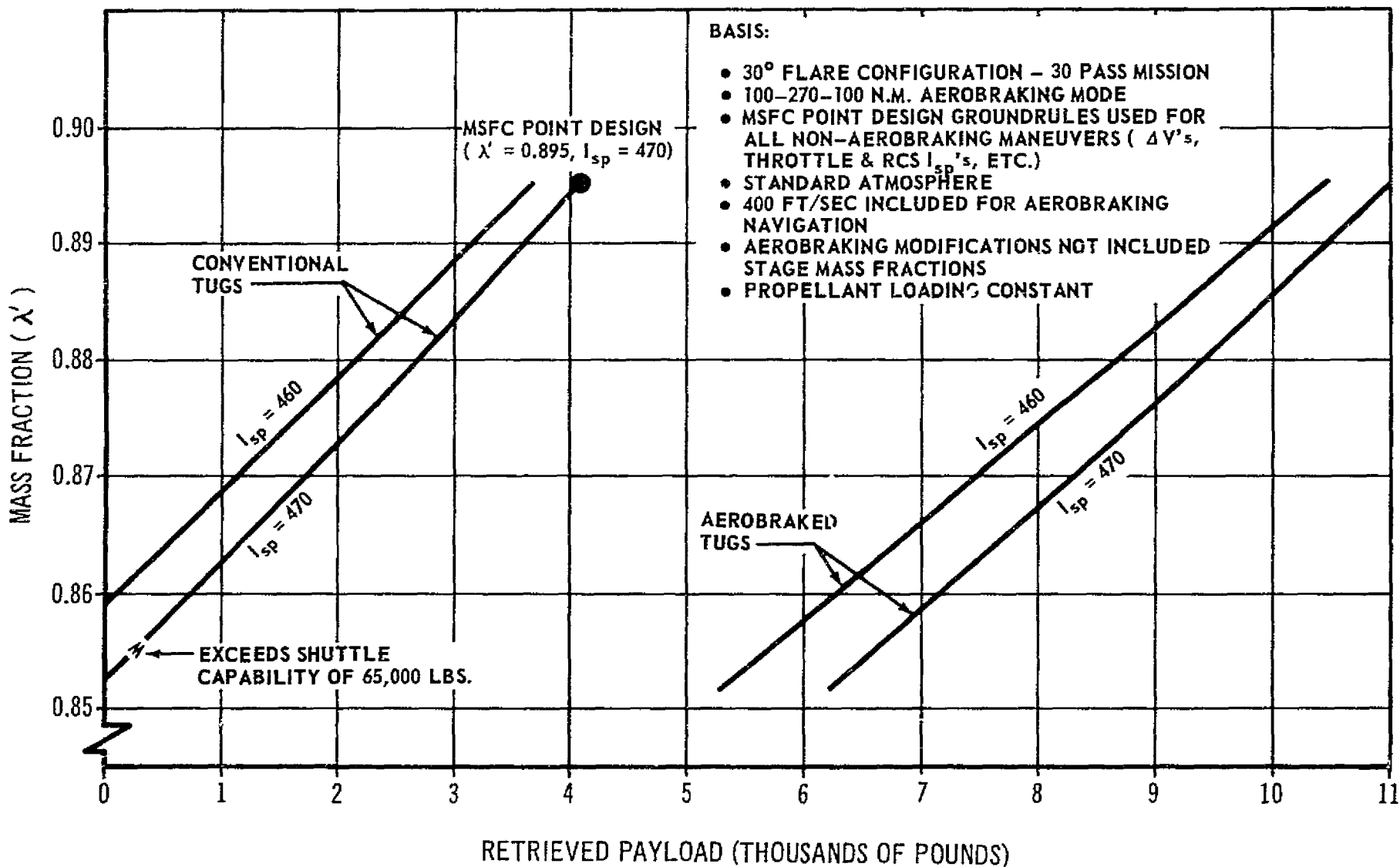


FIGURE A-3.4.0-3: PAYLOAD RETRIEVAL CAPABILITIES OF CONVENTIONAL AND AEROBRAKED TUGS

APPENDIX B
BRIEF DESCRIPTION OF KALMAN FILTERING

To understand the Kalman filter, it is helpful to examine the differences between two basic techniques for estimation. These are "least squares" and "maximum likelihood" methods.

Least squares estimation involves fitting a curve to the available data in such a way that the sum square of the residuals to the data points is minimized. The least squares curve fit is simply the average of measurement data readings. The RMS error in the estimate is σ/\sqrt{N} , where N is the number of readings. In general, no least squares curve fit is possible until there are at least as many equations as there are unknowns.

Maximum likelihood estimation introduces the new factor of "weighting" into the estimation process, in order to make allowances for the accuracy of the measuring instrument, as well as the variation in the quantity being measured. Thus, statistics concerning both the quantity being estimated and the errors in measurement are utilized.

The RMS error for both the Least Squares and Maximum Likelihood concepts is shown in Figure B-1.

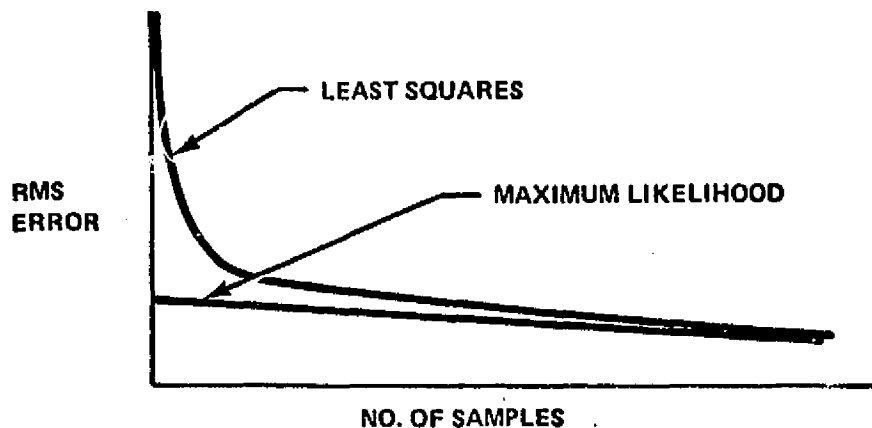


FIGURE B-1. COMPARISON OF LEAST SQUARES AND
MAXIMUM LIKELIHOOD ESTIMATION

PRECEDING PAGE BLANK NOT FILMED

A concept brought forth by Dr. R. E. Kalman in 1970, made feasible a practical maximum likelihood estimation technique for use on digital computers in a real-time application. Kalman developed a recursive or iterative procedure that applies a weighting factor b to measured data y , to yield a new estimate \hat{X} . The equation involved is summarized as shown.

$$b_n = \frac{M \sigma_{n-1}^2}{M^2 \sigma_{n-1}^2 + \sigma_\epsilon^2}$$

$$\hat{X}_n = \hat{X}_{n-1} + b_n (y_n - M \hat{X}_{n-1})$$

$$\sigma_n^2 = (1 - b_n M) \sigma_{n-1}^2$$

where

- y = measured data
- \hat{X} = estimated value of measurement
- M = scale factor
- σ_X^2 = variance or mean square deviation of estimate
- σ_ϵ^2 = mean square error in measurement
- b = weighting factor
- σ^2 = update mean square error in estimate

A comparison of navigation using a Kalman filter with navigation using straight position fixes is shown in Figure B-2. In the case where straight position fixes are implemented, the inertial navigation position is adjusted to agree with the externally indicated position. The position update is as accurate as the external position fix measurement. However, the navigation errors grow unabated between position fixes. On the other hand, the Kalman filter position fix updates continually improve the estimate of position and velocity so that the RMS position error gradually converges to a steady state error much smaller than that achieved using straight position fixes only.

In general, when properly mechanized, the Kalman filter will not introduce errors which are statistically larger than the errors which existed prior to making the estimate. This is true regardless of how poor the reference data are. It is definitely not true of least squares where one poor

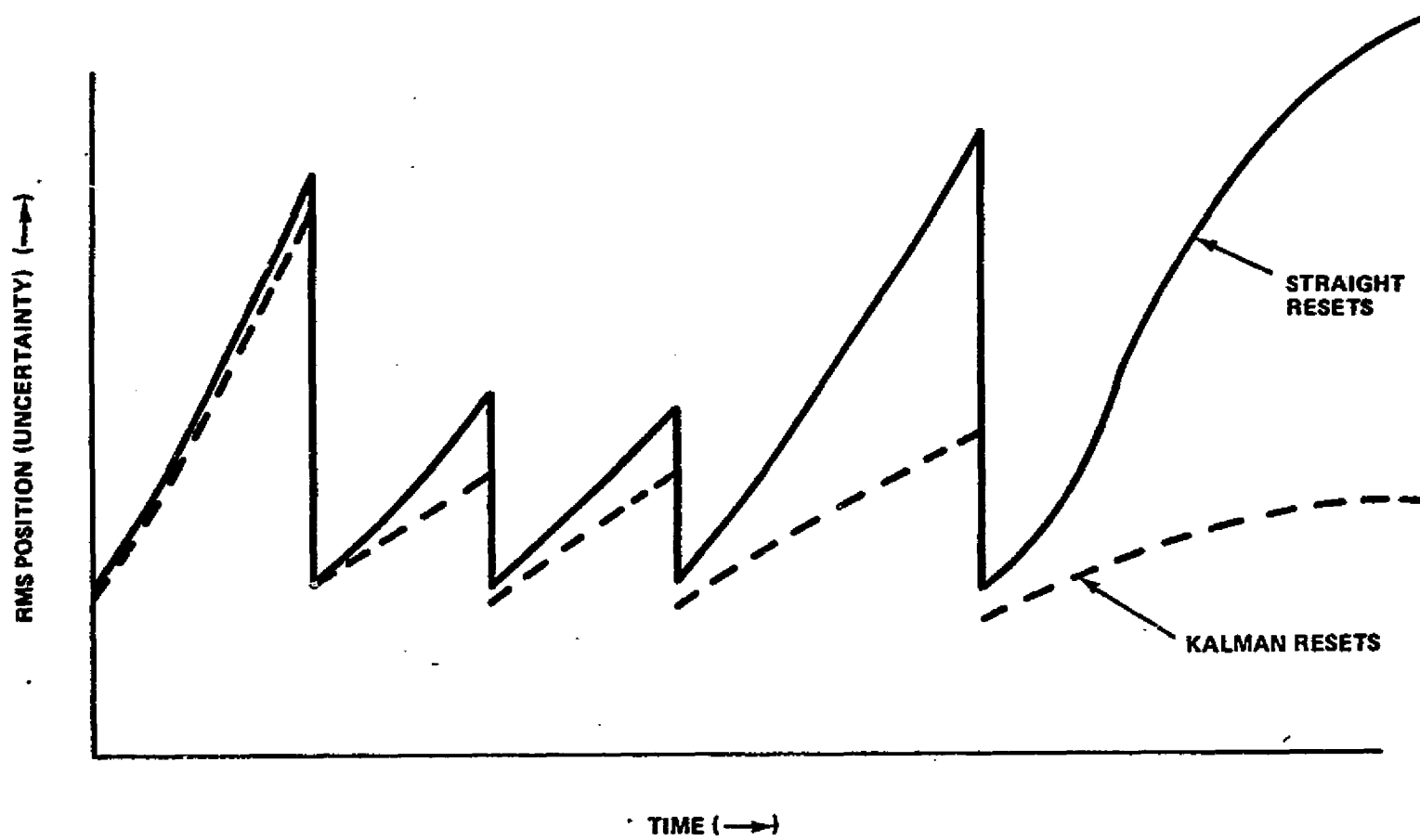


FIGURE B-2. COMPARISON OF STRAIGHT POSITION RESETS WITH KALMAN POSITION RESETS

measurement can greatly affect the mean average of the data.

In summary, a Kalman filter makes possible real-time on-board navigation. The filter accepts various external data and makes corrections to the system "state". This state vector estimate improves with each succeeding measurement, provided the accuracy of the measurement is better than the previous estimate of the state. The Kalman technique applies in a practical sense principally to linear systems and requires considerable computing capability.

APPENDIX C ANALYSIS PROGRAMS

1.0 TUG INTEGRATION PROGRAM

1.1 GENERAL DESCRIPTION

This program is a six dimensional orbital simulator that generates orbital trajectories by integrating a given set of initial conditions for as many orbits as required to satisfy one of three end conditions: Time of flight; flight-path-angle; or apogee altitude. Also, the program can calculate the required delta velocity to regulate perigee altitude and apply velocity increments at any point from apogee to the beginning of the atmosphere. The delta velocity is calculated as a function of semimajor axis, eccentricity, eccentric anomaly and velocity and is applied along the current velocity vector.

1.2 SUBROUTINE DESCRIPTION

- a. Main - The function of MAIN is to control the overall operation of the program. It first reads the input data and initiates the program by calling subroutine VAROP.
- b. VAROP - Subroutine VAROP monitors the steps necessary to perform an Encke integration of a near earth trajectory.
- c. EDITOR - EDITOR monitors the integration of the trajectory to determine when the desired terminal conditions have been met. Also, delta velocity corrections to adjust perigee are executed in this routine.
- d. MISC - This subroutine is a collection of entry points, each of which performs some calculation related to conic trajectories. The calculations that can be performed are as follows:
 - o Conic radius vector as a function of time
 - o Conic velocity vector as a function of time
 - o Coast time between two points on a conic
 - o Calculation of the elliptical or hyperbolic eccentric anomaly from the true anomaly
 - o Solution of Kepler's equation
 - o Calculation of the true anomaly of the desired altitude to perform a delta velocity correction
 - o Calculation of altitude as a function of latitude
 - o Calculation of argument of perigee and orbital period
- e. ORBITP - This subroutine utilizes the position and velocity vectors to calculate the orbital parameters needed for use in other subroutines. The quantities calculated are angular momentum, semi-latus rectum,

1.2 (Continued)

specific energy, eccentricity, true anomaly, semi-major axis, and eccentric anomaly.

- f. RUNKUT - This subroutine uses a 6th order Runge-Kutta integration formula, with step-size control, to calculate the disturbed velocity and position of the vehicle.
- g. FCALC - This subroutine calculates the disturbing acceleration acting on a vehicle with respect to an Earth centered coordinate system. In particular, this subroutine includes the second, third and fourth earth gravitational harmonics; calculation of the Encke acceleration; and calculation of drag accelerations.
- h. PARA62 - This routine is the 1962 standard atmosphere.
- i. INTRPT - Subroutine INTRPT is an iteration routine which calculates the current drag coefficient (C_D) as a function of current altitude and velocity.
- j. BLKDATA - Block data is an initialization routine for constants used in the Tug program.

2.0 ANS PROGRAM DESCRIPTION

2.1 GENERAL DESCRIPTION

2.1.1 Introduction

The Autonomous Navigation Simulation Program (ANS) simulates autonomous navigation along a Keplerian orbit as performed by a Kalman filter using data from selected combinations of horizon sensor, star tracker, landmark tracking telescope, radar altimeter and range (laser) measurements. Autonomous navigation is the process of determining the orbit of a spacecraft from on-board the space vehicle. The program simulates the use of a Kalman filter to process a sequence of stellar referenced or earth referenced measurements. The latest measurement data and the current best estimate of the orbit are processed by a Kalman filter to obtain a differential correction to the estimated orbit, i.e., a more accurate estimate of six orbit ephemeris parameters - three components of spacecraft position and three components of spacecraft velocity.

The program contains an environment simulation which generates true and estimated spacecraft position and velocity, landmark location and star sighting data. Given a set of initial conditions and an observation schedule, the program simulates the navigation process, producing a time history of RSS (root-sum-square) position error, RMS (root-mean-square) position error and other related quantities. The RSS position error, based on the difference between true and estimated spacecraft position, is a measure of the accuracy actually achieved by the Kalman filter estimation process. The RMS error, based on the estimation error covariance matrix, is an ensemble

2.1.1 (Continued)

statistic derived from a linearized model of the navigation process and is a measure of the theoretical or predicted accuracy. RSS position error is the length of the vector difference between true and estimated spacecraft position. RMS position error is the square root of the diagonal terms of the covariance matrix.

The program may be run in either of two modes: error analysis mode or full simulation mode. In the error analysis mode, which may be used if only navigation accuracy is of interest, the environment simulation generates true orbit parameters only. A time history of RMS position error and other covariance matrix-related quantities reflecting navigation accuracy is produced. The calculation of the estimated orbit and its correction, and RSS position error, which are features of the full simulation mode, are omitted for error analysis mode. Available options include the addition of earth oblateness and air drag effects upon spacecraft motion.

2.1.2 Navigation Systems Included

The following categories of navigation systems can be simulated (the observables measured by each system are indicated in brackets):

a. For known or unknown landmarks

- o Two star trackers and landmark tracking telescope [measures pitch and roll angle orientation of landmark line-of-sight in a known stellar orientation frame].

b. For known landmarks only

- o Range (laser) measuring device [range, which is the length of the line-of-sight vector from the spacecraft to the landmark].
- o Two star trackers, landmark tracking telescope, and range (laser) measuring device [pitch, roll, range].
- o Single star tracker and landmark tracking telescope [star-landmark angle].
- o Horizon sensor and landmark tracking telescope [landmark-vertical angle].

c. Other systems

- o Two star trackers and horizon sensor [star-vertical angle].
- o Radar altimeter [altitude, or the radial distance from spacecraft to earth's center].

For these modes, the Kalman filter estimates only the six orbit ephemeris parameters.

The categories of navigation systems and their combinations simulated in the ANS program are depicted in Figure C-1.

<u>Name of Mode</u>	<u>Navigation Sensors</u>	<u>Landmarks</u>	<u>Observable(s)</u>	<u>No. of States</u>
Star-Landmark: Submode 1	2 Star Trackers, Landmark Telescope	Known, Unknown	Pitch, Roll	9
Star-Landmark: Submode 2	Range (Laser) Measuring Device	Known	Range	9
Star-Landmark: Submode 3	2 Star Trackers, Landmark Telescope, Range (Laser) Measuring Device	Known	Pitch, Roll, Range	9
Star-Landmark: Submode 4	Single Star Tracker, Landmark Telescope	Known	Landmark- Single Star Angle	9
Landmark- Vertical	Horizon Sensor, Landmark Telescope	Known	Landmark- Vertical Angle	10
Star-Vertical	2 Star Trackers, Horizon Sensor	N/A	Star-Vertical Angle	6
Altimeter	Radar Altimeter	N/A	Altitude	6
Tracking	MSFN and/or DSNT Tracking Stations	N/A	Range Range Rate Azimuth Elevation	6

Figure C-1
AUTONOMOUS NAVIGATION MODES

2.1.3 Input Description

Program input consists of the initial conditions (initial time, true and estimated spacecraft position and velocity, and covariance matrix), information pertaining to the options to be included in the simulation, and the observation schedule. Specified for each observation are the time and type of observation, and the instrument pointing accuracy. For landmark tracking systems, landmark acquisition angle (pitch and roll) and the landmark survey accuracy, are also specified. For two systems, star acquisition angle(s) are additionally specified (star azimuth for the two star trackers - horizon sensor system; star azimuth and star elevation for the single star tracker-landmark tracking telescope system). For landmarks, a sequence of equally-spaced times of observations on the landmark, instead of a single observation time, is specified. For ground-based tracking systems, a sequence of equally-spaced times of observations by the tracker is specified.

2.1.4 Kalman Filter Operation

At each observation time, for each observable appropriate to the navigation system observation type, the Kalman filter equation sequence is used to generate updates to the estimated orbit (simulation mode only) and the covariance matrix.

The sequence of equations providing the weighting or gain matrix $\underline{W}(K)$, the updated estimated orbit $\hat{\underline{X}}(K+1)$ (simulation mode only), and the updated covariance matrix $\underline{P}(K+)$ at the K th observation time are:

- o $\underline{W}(K) = \underline{P}(K-) \underline{H}(K) [\underline{H}^T(K) \underline{P}(K-) + Q]^{-1}$
- o $\hat{\underline{X}}(K+) = \hat{\underline{X}}(K-) + \underline{W}(K) [\hat{\underline{A}}(K) - \underline{A}(K)]$
- o $\underline{P}(K+) = \underline{P}(K-) - \underline{W}(K) \underline{H}^T(K) \underline{P}(K-)$

$\hat{\underline{A}}(K)$ and $\underline{A}(K)$ are the actual and estimated observables, $\underline{H}(K)$ is the observable-related gradient vector, and Q is the variance of instrument noise errors.

The above update sequence is executed for each of the observables appropriate to the navigation system observation type (the observables, which are angles, or vector lengths, were listed above for the various navigation systems).

$\hat{\underline{X}}(K-)$ is the estimated orbit before update, for an observable under consideration. If this observable is the first or only observable for the navigation system, $\hat{\underline{X}}(K-)$ is the estimated orbit after propagation from the preceding $(K-1)$ observation time. If the observable is not the first in a set of more than one observable, $\hat{\underline{X}}(K-)$ is the estimated orbit after update for the preceding observable in the set.

Similarly, $\underline{P}(K-)$ is the covariance matrix before update. If the observable under consideration is the first or only observable for the navigation system $\underline{P}(K-)$ is the covariance matrix after map up from the preceding $(K-1)$ observation time. A state transition matrix (Jacobian matrix, computed in

2.1.4 (Continued)

closed form) along a Keplerian orbit is used to map up the covariance matrix. A program option is available which provides a machine noise modification to the Kalman filter to prevent filter divergence caused by modeling and computer round-off errors. The form of this filter modification is an additive term to the covariance matrix.

For landmark tracking systems a sequence of observations is made on the landmark (the sequence timing is specified in the observation schedule input data). The first sighting is used by the environment to compute landmark position coordinates from the acquisition time and acquisition pointing angles which form part of the input data. Subsequent sightings to this landmark are then treated as navigation observations, i.e., data is processed by the Kalman filter into updates of orbit and landmark parameters and of the corresponding covariance matrix.

Orbit propagation and covariance matrix map up occur between observations. Filter modification occurs only when the landmark is spotted.

2.1.5 Output Description

Three types of output are available:

- o Printout (one of three types, which include standard items plus varying amounts of additional items, may be selected).
- o Cal-Comp Plots (optional).
- o Punched Covariance Matrix (optional)

APPENDIX D NAVIGATION COMPONENTS

1.0 NAVIGATION COMPONENT DESCRIPTION

This section presents a description of all the hardware elements that were considered as candidates for the Space Tug aerobraking navigation.

1.1 IMU

The platform has four gimbals with appropriate synchros, resolvers and torque motors for each gimbal. The angular sequence starting with the inner gimbal is pitch, roll and yaw with the fourth gimbal providing redundant roll. The stable element (inner member) contains two-degree-of-freedom gyros with their spin reference axes directed along the pitch and yaw gimbal axes. One gyro controls the roll and yaw platform gimbals while the other controls the pitch gimbal axis. The platform baseline is typified by a Kearfott KT-70.

1.2 STAR TRACKER

The star tracker is a strapped down optical sensor using electronic gimbaling to determine star positions within the eight degree diameter field-of-view (FOV). The acquisition mode results in a scan of the entire FOV after which the brightness object is selected. The tracker then enters a tracking mode in which the selected object is scanned over a very small FOV, on the order of 16 arc minutes. The position of the object is measured in two axes with respect to the boresight of the tracker.

The star tracker baseline is typified by the ITT Dual Mode star tracker.

1.3 HORIZON SENSOR

Lockheed Missiles and Space Company (LMSC) has developed and qualified a high accuracy, horizon sensor for use at synchronous altitude. This sensor has two scanning mirrors, one in the pitch axis and one in the roll axis, and will operate over large displacements in either axis. The sensor is a 4 pound, 5 watt earth sensor which will perform for over 5 years in orbit with an accuracy of 0.05 degrees (3 sigma).

1.4 AUTOMATIC LANDMARK TRACKER

The automatic landmark tracker or automatic earth feature sensor (AEFS) is similar to the star tracker in that it consists of a sensor unit and an electronics unit. The entire sensor unit consisting of a vidicon and optics is gimballed in pitch and roll. Gimbaling and optical magnification is required to obtain the desired accuracy. Gimbaling is required for initial image motion compensation for acquisition and then final tracking; optical magnification of 2 or 3 power is required to overcome the TV line limitation for resolution. The gimbal angle readouts requirements are roughly 15 arc seconds requiring a simple inductosyn resolver and a 17 bit encoder.

1.4 (Continued)

Sequence of Operation

- o Known Target Mode - The field-of-view is directed to the estimated location and tracked with estimated image motion rates. The shutter is opened, exposure made, and the video readout examined to set the circuits and logic levels. A second exposure is made and the video readout is processed to compute the x value. A third exposure is made and read out with the scanning lines orthogonal to the previous readout. The video is processed to compute y. These values define the roll and pitch pointing errors. The gimbals are corrected by the distance of $x + y$ from boresight. A second sight is taken (two exposures) and a new x, y, value obtained. A succession of sights, taking two to four seconds per cycle will allow both pointing accuracy to one resolution element, and image motion compensation (IMC) to one resolution element per cycle time.

The only information which must be stored to identify a known landmark is the geodetic position. Target separation, size, contrast and other pertinent characteristics are accounted for in the selection process.

During all coasting phase navigation, an extrapolation of position and velocity by numerical integration of the equations of motion is required. The integration scheme implemented dictates the integration increment required. Therefore, the number and location of landmarks must be chosen to maintain the required integration accuracy.

- o Unknown Target Mode - The unknown mode of operation is the same as the known mode, except that the sensor is pointed maximum forward along track and the estimated IMC applied if necessary. The video is examined to determine if a trackable target is within the field-of-view. When a trackable target appears, the operation is identical to the known mode.

APPENDIX E RECOMMENDED AEROBRAKING FOLLOW-ON ACTIVITIES

E-1 FOLLOW-ON TUG AEROBRAKING PROGRAM ACTIVITIES

This initial program was conducted to determine the feasibility of aerobraking as applied to the Space Tug and to identify the technical considerations associated with the aerobraking mode. From this study, the significant potential advantages of Space Tug aerobraking entry were indicated. This study, however, did not examine the concept in sufficient depth to assess its full potential. Further studies are required to identify the missions and mission capabilities, the operational modes, Tug aerobraking economics and their impact on overall space program costs, Tug interfaces with other space transportation systems such as payloads, etc., and the impact of a Space Tug modified for aerobraking on the Space Shuttle. Each of these studies are discussed below.

The additional Tug aerobraking activities should be done in sufficient depth to bring the level of knowledge on Space Tug aerobraking to that obtained by the ongoing conventional Space Tug activities. Further, when these levels are comparable, comparisons should be made to fully assess the advantages and disadvantages of applying the aerobraking system as a major consideration for future Tug studies.

E-1.1 MISSIONS

This study primarily investigated round trip mission modes. Placement and retrieval modes were not considered in the technical trades. As the initial missions in the space program will most likely be placement only missions, it is desirable to determine the trajectory modes for payload placement and return of the empty Tug and their effect on the Shuttle and its operational modes. Further, this study investigated only synchronous orbit missions. Aerobraking should be investigated for other missions. For example, significant payload advantages may be obtained when aerobraking is applied to other high altitude earth orbital missions. Also, for interplanetary type missions, where recovery of the Tug is desirable, aerobraking may offer the potential for reducing the Space Tug propulsive requirements for the return mode and therefore increasing the interplanetary payload capability.

E-1.2 OPERATIONAL MODES

The primary operational mode examined in this study was an off optimum one wherein the Space Tug returns from synchronous orbit to a low (approximately 50 n.m.) perigee by 270 n.m. apogee orbit. The Tug then circularizes at 270 n.m. and after proper phasing between it and the Shuttle, in the lower 100 n.m. orbit, the Tug accomplishes propulsive burns to transfer from 270 n.m. to 100 n.m. The Tug circularizes at the 100 n.m. orbit. Then the Tug provides the necessary rendezvous and docking maneuvers. This mode of operation severely penalizes the Tug payload capability. The Space Shuttle has the capability to perform many of these operations including ascent to somewhat higher orbits with

E-1.2 (Continued)

little penalty to the Shuttle capability. Therefore, it is highly desirable that trades be accomplished on a mission by mission basis to identify (1) which of the interfacing vehicles should perform the various operations, (2) the Tug deployment and retrieval altitudes, and (3) the rendezvous and docking operations. The navigation timelines for performing all of these operations should be defined.

E-1.3 ECONOMICS

The economics of the Space Tug aerobraking has not been defined. R&D and operational costs for the aerobraking kits should be developed to define the impact on the overall Space Shuttle/Space Tug R&D and operational budgets. It is believed that the R&D costs for the aerobraking components will be small. Since the components may be designed for refurbishment and reuse during the operational phases, the overall costs of applying the aerobraking kit options can be minimal. An important economic consideration is the advantage of applying aerobraking to reduce the required number of Shuttle flights and to negate the requirements for orbital fuel transfer and assembly operations. This economic advantage is so significant that it should be defined as soon as possible in order to allow the aerobraking concept to have the required effect on the Space Shuttle/Space Tug design and operational planning.

E-1.4 INTERFACE ANALYSES

The Space Tug is designed to interface with all of the other space transportation systems including the Space Shuttle, satellites, interplanetary payloads, Space Stations, Nuclear Shuttles, etc. These interfaces will impose constraints on the configuration of the Space Tug and will impose further constraints on the operations that can be performed during aerobraking and on the environments which are permissible. An analysis of these interfaces should be undertaken to determine their impact on the Space Tug aerobraking concept.

E-1.5 SPACE SHUTTLE/AEROBRAKING SPACE TUG INTERACTIONS

The Shuttle and Tug must operate as a team for the majority of the space program missions. As a result, these two elements have a significant impact upon each other. The Shuttle has certain acceleration, thermal, handling, timeline, operational, and other constraints which will impact the aerobraking Tug design. Similarly, the aerobraking Tug will impose certain constraints upon the Shuttle, for example, the use of the aerobraking kit will impact hard points for stowage, deployment and retrieval mechanisms, etc. Investigation of these areas should be undertaken to minimize the aerobraking Tug impact on the Shuttle.

E-2 SUPPORTING RESEARCH AND TECHNOLOGY/ADVANCED RESEARCH AND TECHNOLOGY IMPLICATIONS

This study was specifically conducted to define the feasibility and practicality of the aerobraking return trajectory mode for the Space Tug. The baseline Tug configuration utilized for this activity was a scale-up of the Tug configuration developed by The Boeing Company for NASA under a prior contract (prior Reference 1.1.0.0-1). Groundrules for this previous study specified utilization of current and projected state-of-the-art technology for the Space Tug configurations. The previous study and this current study, therefore, did not consider advanced technology in the design of structures, components, engine systems, astronics, etc. As such, this study has presented the payload capabilities of the aerobraking mode conservatively. Increased payload capability for the aerobraking mode should therefore result from designs applying advanced technologies. Further, the limited scope of this study precluded in-depth investigation of the anticipated aerobraking environments, their impact and the optimal material and design solutions for overcoming the environments. Therefore, attractive advanced technology areas requiring further attention were defined and are outlined below.

E-2.1 AERONAUTICS

Aerodynamic Properties of Aerobraking Tug Options - The design of an optimum aerodynamic configuration cannot be adequately defined without a wind tunnel test program to ascertain the aerodynamic properties of potential configuration options. These options include nose bluntness, cylindrical length, flare angle, and angle of attack versus drag. The effects of real gas aerodynamics on drag is required as the flare is embedded in the flow field. The impact of angle of attack on lift coefficient, pitching moment coefficient and heat transfer rate distribution will provide substantiation for computation technique to be used in future studies.

Flow Field and Flow Separation - The effects of flow separation were not investigated within the limited scope of this study. Disassociated flow field effects will change the shock position and the boundary layer characteristics and can significantly alter the aerodynamic characteristics. Further, boundary layer height and separation effects were assumed to have a negligible influence on the aerodynamics characteristics. This needs verification by further analysis.

The effects of non-diffuse reflection and imperfect thermal accommodation in the free molecular flow regime have not been investigated and need analysis.

Rarefield flow field effects on the flared configurations depend on local flow field properties approaching the flare. These effects were approximated but need further analytical verification or experimental verification.

E-2 (Continued)

Aerodynamic Characteristics of Alternate Drag and Stability Configurations -

The aerobraking configurations investigated in this study were selected to provide a range of resulting data to establish feasibility and trends. They do not necessarily represent the more desirable systems. In future activities, consideration should be given to the aerodynamic characteristics of alternative configurations for drag and stability such as (1) split flares, (2) a forward drag brake, (3) different entry nose shapes, (4) forward facing engine exhausting parallel to the flow, (5) "lift" flare configurations, and (6) other options such as forward and entry (payload first), sideways entry, tumbling entry and use of extendable micrometeoroid shielding to provide drag brakes. The effect of flare semivertex angle and flare length should be parameterized.

Dynamic Stability Effects - No dynamic stability effects were included in the aerodynamics study. The dynamic instability may severely affect the reaction control system and therefore should be a part of follow-on studies.

Angle of Attack - The effects of angle of attack and lift-to-drag ratios were not investigated as part of this study. The use of applied angle of attack as a method of attaining the desired perigee altitude should be studied. The impact of angle of attack, in turn, upon the thermal environments, thermal protection system requirements and control (RCS fuel) requirements should be investigated. The maximum correction capability (planar and lateral) should be determined.

Flow Field Effects on Aerothermal Environments - Flow conditions behind the Space Tug payload section (basic no-flare configuration) and behind the aerodynamic flare (flare configurations) should be investigated in order to better define aerothermal environments in the area. This activity could be augmented by a series of wind tunnel tests.

Aerothermal Environmental Effects on Protuberances and Surface Discontinuities - The effects of protuberances and surface discontinuities should be investigated. Gaps occurring at the dome closure point and between adjacent hot structures must be evaluated for thermal design adequacy.

E-2.2 MATERIALS AND STRUCTURES

High Temperature Materials - This study generally assumed TD-nickel-chrome, with the maximum temperature capability of 2000°F, as an upper radiative temperature limit material. This restriction limited the configuration options and operational and mission modes significantly. The use of higher temperature materials in the 2000°F to 3500°F range, such as the various columbiums and Fansteels (tantalum alloys) may offer reduced trip times with equivalent payloads. These materials, however, may have physical properties, lack of availability, or cost which will restrict their use. A survey of potential materials, their characteristics and their potential availability and costs should be made and recommendations made as to which of these materials would enhance aerobraking and should therefore be pursued.

E-2.2 (Continued)

Alternative Thermal Protection Systems - The materials used for aerobraking kit components concentrated on the use of radiative type materials for the aft heat shield and the aerodynamic flare. Limited analyses of ablatives for the heat shield was undertaken in the add-on study effort. An investigation should be conducted considering alternative radiative materials and/or alternative thermal protection techniques which could, for example, utilize active cooling, transpiration cooling, exhaust gas cooling (with Tug engine operating in idle mode) and/or combinations of these systems.

Integrated Thermal/Structures/Micrometeoroid Systems - The use of an integrated structure offers a means of reducing the lug inert weights. The weight of the Tug sidewall structures may be substantially reduced by use of an integrated thermal/structure/micrometeoroid system. Analytical and experimental methods should be developed to verify the integrated design approach, e. g., dimensional analysis and modeling techniques can be developed for studying the effects of meteoroid impact.

Alternative Design Concepts - This study investigated point designs for the aft heat shield and the aerodynamic flare. Alternative design concepts should be investigated to determine ways of reducing aerobraking kit weights, simplifying the aerobraking kit actuation systems, improving reliability and reducing risk. Alternative design options could include forward drag flares, inflatable flares, split flares, "lift" flares, deployable micrometeoroid shielding for drag brakes, etc.

Materials Environmental Capabilities - The environmental design data and design criteria should be developed for potential missions. The capability of non-metallic materials that will be exposed to vacuum and radiation environments should be determined. For example, the application of advanced composites such as graphite-epoxy and boron-epoxy to integrated system design should be considered as a method of reducing Tug inert weight.

Materials Processing - Potential material and process problems associated with fabrication and/or refurbishment of aerobraking and thermal shielding components should be investigated.

E-2.3 ELECTRONICS AND CONTROL

Reaction Control System Operating Concepts and Modes - The reaction control system design and operating mode used for this aerobraking study were those developed for the Conventional Space Tug and are not considered as optimum for the aerobraking mode. The desirable sizing of the thrusters, the minimum and maximum operating times, accuracy, stabilization periods, the limit cycle requirements, and the specific type of reaction control system should be investigated in more depth. The impact of these requirements on RCS fuel consumption should be assessed. The use of gaseous hydrogen and oxygen which will result from boiling of the main tank residuals should also be considered for augmentation of the reaction control system.

E-2.3 (Continued)

Reaction Control System Requirements for Lift Trajectory Modes - The control system sizing and propellant requirements for configurations utilizing lift for atmospheric trajectory corrections should be evaluated.

Alternative Reaction Control Systems - The previous study selected a gaseous LOX/LH₂ RCS based upon the application of the then envisioned Space Shuttle technology. The current Space Shuttle RCS is based on the use of storables. The applicability of storables to the Space Tug both with and without aerobraking requires assessment. Criteria for evaluation should include performance, weight, mission life required, variation of impulse with pulse width, and funding requirements.

Stability Margin Effects - During the aerobraking missions, it may be desirable to employ lift to attain target perigees, to accomplish minor plane changes and/or to adjust perigee to compensate for the effects of atmospheric anomalies. The required controlling moments relative to the aerodynamic moments for the proper angle of attack for the desired lift-to-drag ratio, will require further study. Variable methods of achieving stability and the stability margins should be developed.

Update Capability Versus Control Requirements - An assessment should be made of the optimum sensors and update times to minimize RCS fuel requirements for error correction while at the same time minimizing perigee uncertainty. By proper selection of the time in which the guidance avionics are updated, the control fuel requirements may be reduced by a factor of 5 or more. Update timing which minimizes control requirements tends, however, to increase measurement uncertainty.

This recommended study effort would be an expansion of the effort included in the navigation analysis. The effort would perform detailed trades to determine the updating capability of onboard navigation components versus the required control penalties. This would include attitude control deadbands and requirements during sensor observations as well as the accuracy versus RCS penalties to perform navigation update burns for various times during the aerobraking orbit prior to perigee.

Astrionic System Configuration Analysis - The analysis performed for the present study was an updating of the initial Space Tug astrionic system design using the latest Shuttle concepts and components to perform only the synchronous mission instead of the broad spectrum originally studied. Present Shuttle emphasis appears to be in the area of low cost without weight being a pacing item. For the Space Tug, weight and cost would be pacing items. Therefore, additional effort should be expended to integrate Shuttle astrionic system concepts and components into the Tug while maintaining minimum weight where possible. Although this is not an aerobraking analysis per se, it is important to provide a well-defined baseline system configuration as a basis for future aerobraking study effort.

E-2.3 (Continued)

Redundancy Analysis - The redundancy effort to date has defined the typical redundancy weight deltas to be expected for aerobraking mission. Additional effort should be expended to provide a more detailed redundancy analysis using the updated astrionic system components, and to look individually at each component to determine methods of reliability and coverage enhancement. In addition, the risks associated with redundancy management for long duration missions should be addressed.

Navigation Timeline Analysis - The navigation analysis to date selected a typical navigation update timeline which provided satisfactory update accuracy. However, more analysis is required to perform a detailed operation analysis, using attitude constraints, sensor acquisition and reacquisition constraints, burn perturbations, length and frequency of updates, etc., to insure that the autonomous navigation during aerobraking is indeed feasible.

Advanced Sensors Systems - The ability to accurately predict the location of the Tug during the aerobraking operations is dependent upon the accuracy of the sensors systems. The present sensors systems have not been subjected to a detailed analysis as to their performance capabilities and/or reliabilities. The use of advanced sensors which represent Shuttle era technology should be likewise examined in detail for performance and reliability capabilities. The recommended study would look at existing and potential autonomous navigation sensors. One aspect of the study would be improvement of autonomous space navigation by using new technology sensors and/or concepts. A second part of the study would include indepth analysis of navigation sensor hardware to determine means of enhancing reliability and to determine operating modes and limitations of the hardware.

Redundancy Implementation - The successful completion of the Tug aerobraking mission depends on an operational astrionics system which in turn depends on "coverage" (failure identification) to "key-in" redundancy components at the proper time. Current technology depends heavily on BITE (Built-In-Test-Equipment), off-line dynamic response testing, voting or comparison or reasonableness testing to identify failed components. These methods have had limited success with electromechanical sensors and hence the development of a new component evaluation technology is desirable.

The basic evaluation limitations can be overcome by using random or pseudo-random noise input and correlation techniques. The advantages of using correlation identification techniques are (1) the system may be checked out "on-line", (2) test signals can be kept small and will not interfere with normal operation, (3) results can be obtained in the presence of random noise and parameter drifts, and (4) the technique can be easily applied to existing hardware as correlation is inherently a simple digital process.

The objective of such a new technology study would be to define the suitability and application of "on-line" system evaluation by digital methods.

E-2.3 (Continued)

Navigation Sensor Integration - The navigation analysis performed in this study utilized an optimal filter (Kalman) implemented on a general purpose floating point computer (IBM 360/75). In a space application, the sensor integration routines must be programmed in a limited memory machine in fixed point arithmetic. A new technology task is recommended to define a suboptimal filter routine in 16 bit fixed point arithmetic to provide integration of the landmark, horizon, and star sensors and the IMU.

Navigation and Guidance Analysis - The study effort to date has evaluated navigation uncertainties and preliminary evaluations of burn corrections and associated updates. To enhance the above effort, a study should be made considering the navigation system configuration, navigation accuracy, attitude pointing accuracy, targeting schemes and predictive problems associated with orbit disturbances that result from uncertainties in atmospheric density, navigation sensor, and vehicle dynamics. The study would involve development of a guidance law to predict future orbital variations based on past inputs (accelerations, state vectors), compute new orbit perigees to achieve mission objectives, and control vehicle forces during atmospheric braking to achieve the desired end conditions. The guidance law would then be tested using available simulations to verify its operation under a variety of disturbances from nominal performance. The midcourse velocity corrections would be defined and the subsystem weight penalties determined.

Radiation Analysis - The radiation analysis for this study was a "quick look" to identify any significant astrionic system impacts because of repeated passes through the Van Allen radiation belt. Additional study effort would include a more accurate determination of the elliptical orbit profiles using the Burrell Orbital Flux and Spectra (BOFES) code. The impacts of both single aerobraking missions and repeated aerobraking missions for a ground based Tug would be evaluated. Sensitivities of various components for various shielding and radiation doses would be addressed. Also, the effort could be expanded to include the impacts of artificial radiation environments if deemed desirable.

Astrionic System New Technology Component Analysis - As mentioned previously, weight is the pacing item for the Space Tug. The astrionic system weight can be reduced if new technology components (in lieu of Shuttle components) are considered. However, development costs and development risks would be associated with the new technology components. A study effort is required to evaluate the relative merits of using new technology components in the astrionic system of the Tug. This would include a survey of potential new technology components (such as LSI computers) and the relative development progress of each.

APPENDIX F

TWO PASS LIGHT WEIGHT LARGE FLARE

F-1.0 LIGHT WEIGHT LARGE FLARE CONCEPT

The large nose flare concept failed to have any payload capability due to the flare weight. One of the attractive alternative concepts investigated to decrease the flare weight employs an inflatable torus to extend the flare. This concept (see Figure F-1.0.0-1) integrates the radiative heat shield design (heat shield functions as described in Section 4.2.2.1 of basic report) with the forward flare. The flare attaches to the heat shield at the dome/cylindrical section interface as shown in the figure. The flare and torus would be fabricated of "AIRMAT," a "fabric" woven on the U. S. Air Force Loom operated by Goodyear Aerospace Corp. in Akron, Ohio. The Airmat "cloth" would be woven from Haynes 188 (Cobalt alloy) .0005 inch diameter wire and operate at a maximum temperature of 2000°F. This Airmat material has a porosity of 1% which means that 99% of the flare area would serve as a decelerator. When extended by the torus, the Airmat would result in a decelerator area of 50 feet in diameter. At the 50 foot diameter, the Airmat wraps around the torus. To reduce the torus temperatures from 2000 to 1500°F at the tip of the flare, a 1/16 inch thick coating of silicone rubber was used as noted. The torus is made from the same Airmat material and is sealed by a spray coating of silicone rubber. The torus is pressurized by helium from helium bottles housed under the LOX TANKS. The inflated torus shape is held rigid by 91 Rene' 41 cables spaced 20 inches apart. The cables are extended/retracted by electrically driven cable drums. Two methods were designed for packaging the retracted flare. If the Tug's diameter is fixed at 14 feet, then the flare would retract alongside the Tug sidewall as shown in the lower part of the figure. This approach would necessitate that the RCS system be moved aft into the astrionics module region. The other method would take advantage of the LOX tanks smaller size and would taper the Tug sidewalls to the smaller diameter. The flare could then retract into the recessed region as shown in the figure. This concept allows the RCS system to stay at the desired station. A protective door can be placed on the Tug to restrain the retracted flare.

The torus as shown consists of one large bag. A non-collapsible flexible hose would be used to supply/remove the helium from the torus. The configuration was designed for 20 missions, with creep-to-rupture at 2000°F as the design criteria. The weight of the system is 2703 pounds as compared to the 6580 pounds of the large nose flare. The two pass weight statement of this configuration is shown in Figure F-1.0.0-2.

<u>COMPONENT</u>	<u>WEIGHT (POUNDS)</u>
AFT HEAT SHIELD	450
FLARE	2703
FLARE CLOTH	1086
TORUS	801
SILICONE RUBBER	420
CABLES	45
PRESSURIZATION/DEPLOYMENT	105
CONTINGENCY	246
PAYLOAD/FLARE ADAPTER	390
ASTRIONICS PENALTY	25
RCS PROPELLANT	6
T O T A L	3574

FIGURE F-1.0.0-2 AEROBRAKING KIT WEIGHT STATEMENT
FOR TWO PASS AIRMAT FLARED CONFIGURATION

F-1.0 (Continued)

The candidate aerodynamic decelerator configurations considered in this appendix are shown in Figure F-1.0.0-3. As described above, design, stress and weight analyses were only performed for Configuration #1 (50' diameter, $W/C_D A \approx 4.2$). It is believed that the concept shown as Configuration #2 (120' diameter, $W/C_D A \approx 0.74$) would weigh less than that shown in Figure F-1.0.0-2 for Configuration #1 (AIRMAT Flare). The larger flare (#2) would have a maximum equilibrium temperature of approximately 800°F. Therefore, a polyimide film could be used instead of the high temperature Haynes 188 cloth used in the design shown in Figure F-1.0.0-1. The polyimide film has approximately the same strength at 800°F as the Haynes 188 alloy has at 2000°F while the polyimide's density is approximately 1/7th that of the Haynes. An estimated weight savings of approximately 1300 pounds might be achieved by using the larger polyimide flare. This potential weight savings is directly convertible into round trip payload. Therefore, it is recommended that further large polyimide flare design analysis be conducted in follow-on activities.

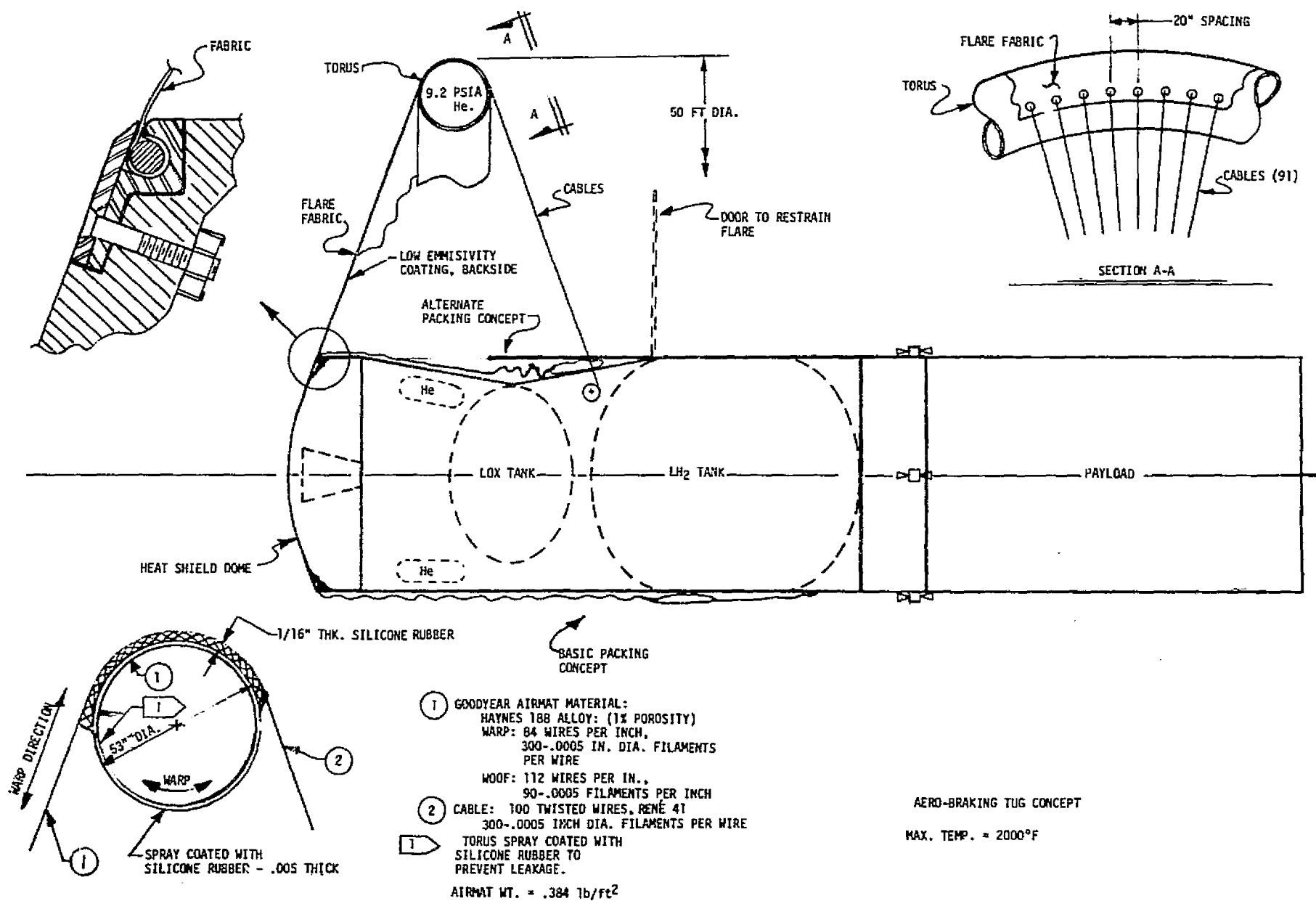


FIGURE F-1.0.0-1 LIGHT WEIGHT LARGE FLARE CONCEPT

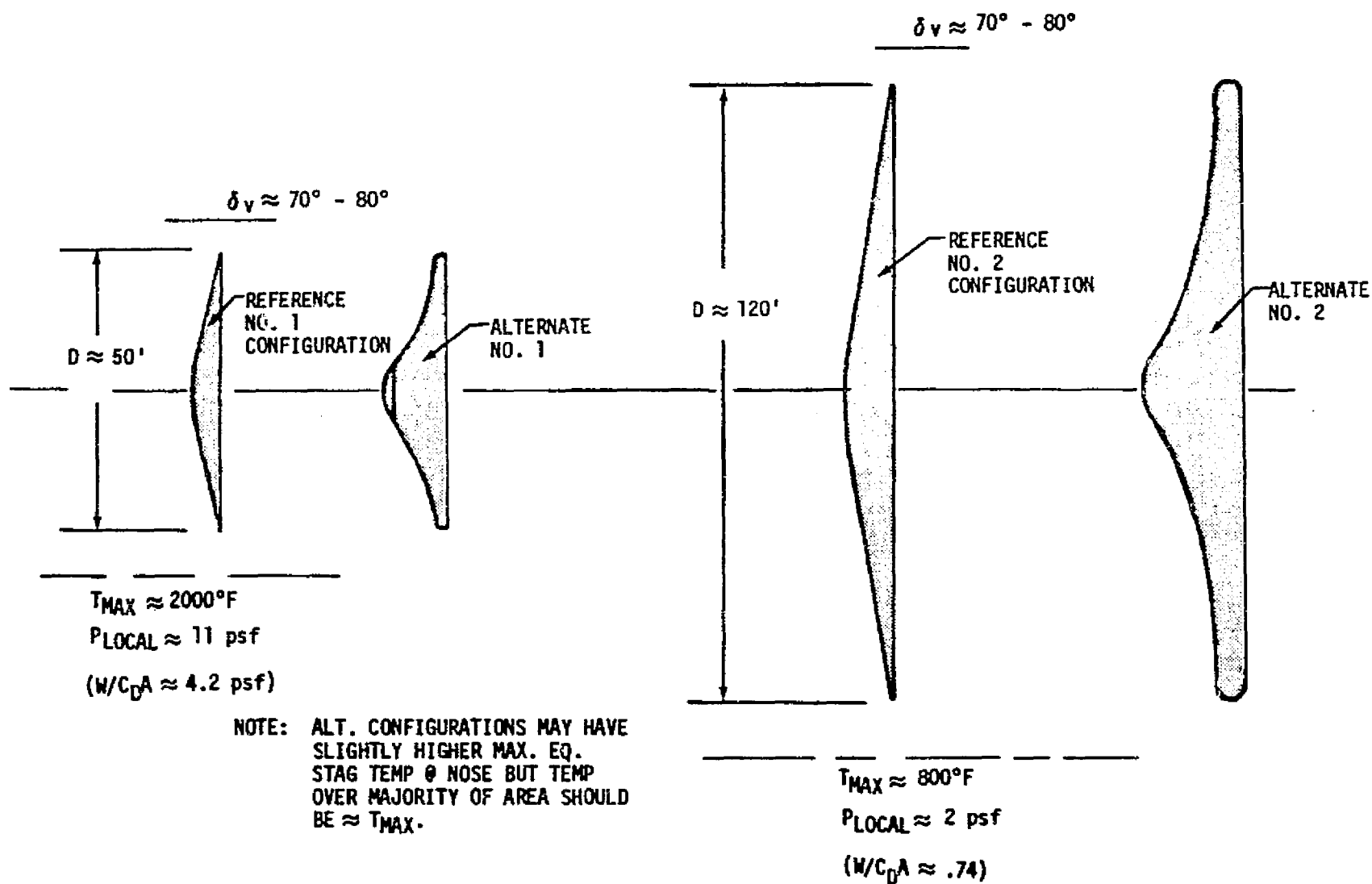


FIGURE F-1.0.0-3. CANDIDATE LIGHT WEIGHT LARGE FLARE CONCEPTS

F-2.0 TWO PASS LIGHT WEIGHT LARGE FLARE PAYLOAD CAPABILITIES

The two pass payload capability of the AIRMAT flare (50' diameter) was computed with the same groundrules utilized for the large nose flare (Appendix A). In addition, the estimated payload capability of the larger polyimide flare (120' diameter) was computed in the same manner. Figure F-2.0.0-1 shows the capabilities in both the nominal 270 n.m. recovery mode and the Shuttle assisted 200 n.m. recovery mode.

CONFIGURATION	ROUND TRIP PAYLOAD (POUNDS)	
	270 n.m. Mode	200 n.m. Mode
AIRMAT Flare (50')	1800	3000
Polymide Flare (120')	3100	4300

FIGURE F-2.0.0-1 ROUND TRIP PAYLOAD CAPABILITIES

In either operational mode, these large flares have significant payload capabilities when used in the two pass mission. Compared to those payload capabilities shown in Appendix A for the other two pass configurations, this general concept is far superior. Follow-on study activities should investigate this type of aerodynamic deceleration in detail in order to determine all of its ramifications and potential.